Peril and promise for Afghans *pp. 715, 722, & 725*

Managing our crumbling sewer systems *pp. 734 & 812*

Captured dust particles return from space *p. 786*

# Science

$10
15 AUGUST 2014
sciencemag.org

AAAS

SPECIAL ISSUE

## *Parenting*

A legacy that transcends genes

*p. 742*

# CONTENTS

15 AUGUST 2014 • VOLUME 345 • ISSUE 6198

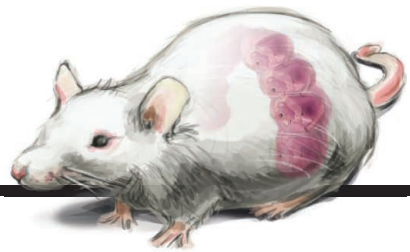

733 & 785
Transgenerational effects of prenatal undernutrition

INTRODUCTION
742 A legacy that transcends genes

NEWS
744 Unsettled questions trail IVF's success *By K. Servick*

747 Nature's first functional food *By T. Gura*

750 The taste of things to come *By E. Underwood*

752 An experiment in zero parenting *By E. Marshall*

OPINION
755 Maternal mental illness *By K. B. Kozhimannil and H. Kim*

REVIEWS
756 Parenting from before conception *M. Lane* et al.

760 Preterm labor: One syndrome, many causes *R. Romero* et al.

765 Neural control of maternal and paternal behaviors *C. Dulac* et al.

771 The biology of mammalian parenting and its effect on offspring social development *J. K. Rilling and L. J. Young*

776 The evolution of flexible parenting *N. J. Royle* et al.

**ON THE COVER**

Babies are produced by contributions from both parents. More and more we are beginning to realize that such contributions go well beyond mere genes, with nurture, environment, and even the parents' own physiology and experiences shaping offspring and their preparedness for life ahead. See page 742. *Photo: © imageBROKER/Alamy*

SEE ALSO ▸ PERSPECTIVE P. 733 ▸ PODCAST ▸ RESEARCH ARTICLE P. 785 ▸ sciencemag.org/special/parenting ▸ *SCIENCE TRANSLATIONAL MEDICINE* RESEARCH ARTICLE BY R. DIAO *ET AL.*

# NEWS

## IN BRIEF

716 Roundup of the week's news

## IN DEPTH

718 **DEBATE ERUPTS ON 'REPURPOSED' DRUGS FOR EBOLA**
With experimental treatments in short supply, some researchers think existing medicines might help stem the epidemic *By M. Enserink*

719 **FIRING OF LOS ALAMOS RESEARCHER DRAWS CRITICISM**
Officials claim paper that challenged the doctrine of nuclear deterrence contained classified information
*By J. Mervis*

720 **A BOOM IN BOOMLESS SEISMOLOGY**
Densely packed sensors use Earth's background noise to image fine details of the crust *By E. Hand*

## FEATURES

**AFGHANISTAN: PERIL AND PROMISE**
As foreign troops head home, researchers assess the toll and size up the country's future prospects

722 **The rising toll**
Newly released data reveal mounting civilian casualties *By J. Bohannon*

725 **Mother of all lodes**
The United States is putting scientific boots on the ground in Afghanistan to assess its mineral riches
*By R. Stone*

▸ EDITORIAL P. 715

# INSIGHTS

## PERSPECTIVES

728 **TECHNOLOGY'S LIMITED ROLE IN RESOLVING DEBATES OVER DIGITAL SURVEILLANCE**
Teasing apart technical issues from social and political issues *By H. Lin*

730 **LETTING GO OF MUCUS**
Defective release of mucus from airway glands is present at birth in cystic fibrosis *By J. J. Wine*
▸ REPORT P. 818

732 **SELF-ASSEMBLED RNA NANOSTRUCTURES**
RNA structures have been designed that self-assemble and are programmable and scalable *By N. B. Leontis and E. Westhof*
▸ REPORT P. 799

733 **YOU ARE WHAT YOU EAT, BUT WHAT ABOUT YOUR DNA?**
Parental nutrition influences the health of subsequent generations through epigenetic changes in germ cells
*By M. Susiarjo and M. S. Bartolomei*
▸ PARENTING SECTION P. 742; RESEARCH ARTICLE P. 785

734 **REPLACE CONTAMINATION, NOT THE PIPES**
Rethinking water treatment additives can have synergistic benefits for urban water management systems
*By W. Rauch and M. Kleidorfer*
▸ REPORT P. 812



Published by AAAS

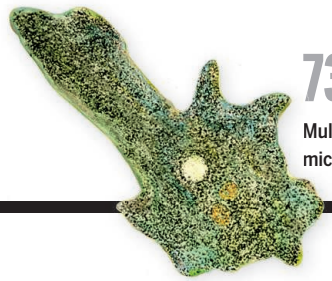

738
Multitudinous microscopic life

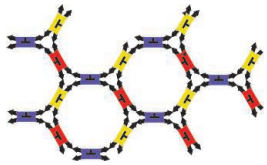

732 & 799
Building hexagonal lattices from RNA strands


736 **ONE STEP CLOSER TO $O_2$**
A crucial step in photosynthesis is becoming clearer
*By R. D. Britt and P. H. Oyala*
▸ REPORT P. 804

**BOOKS *ET AL.***

737 **WALDEN WARMING**
*By R. B. Primack, reviewed by A. C. Schneider*

738 **THE AMOEBA IN THE ROOM**
*By N. P. Money, reviewed by M. Shen*

**LETTERS**

739 **HIV COVER ILL-ADVISED**
*By R. Diamond*

739 **RESPONSE**
*By M. McNutt*

739 **CLIMATE CHANGE: TIME TO NAVIGATE**
*By G. H. Rau*

739 **FOSSIL FUELS' FUTURE**
*By B. Mackey and D. Lindenmayer*

740 **SHARING IDEAS TOO SOON**
*By P. de Souto Barreto*

740 **OUTSIDE THE TOWER: KIDS' QUESTIONS TRANSCEND CONFLICT**
*By L. Perié* et al.


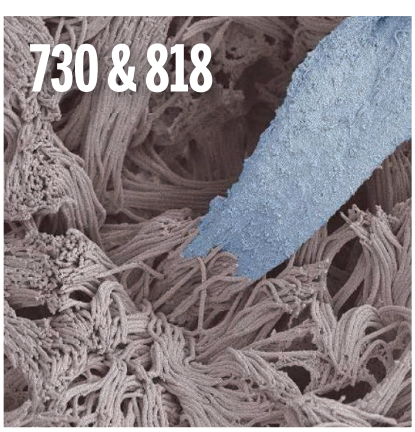


# RESEARCH


**IN BRIEF**

782 From *Science* and other journals

**RESEARCH ARTICLES**

785 **IN UTERO EFFECTS**
In utero undernourishment perturbs the adult sperm methylome and intergenerational metabolism
*E. J. Radford* et al.
RESEARCH ARTICLE SUMMARY; FOR FULL TEXT: dx.doi.org/10.1126/science.1255903
▸ PERSPECTIVE P. 733; PARENTING SECTION P. 742

786 **INTERSTELLAR DUST**
Evidence for interstellar origin of seven dust particles collected by the Stardust spacecraft *A. J. Westphal* et al.

**REPORTS**

791 **INTERSTELLAR MEDIUM**
Pseudo–three-dimensional maps of the diffuse interstellar band at 862 nm
*J. Kos* et al.

795 **ROBOTICS**
Programmable self-assembly in a thousand-robot swarm
*M. Rubenstein* et al.

799 **RNA NANOSTRUCTURES**
A single-stranded architecture for cotranscriptional folding of RNA nanostructures *C. Geary* et al.
▸ PERSPECTIVE P. 732

804 **PHOTOSYNTHESIS**
Electronic structure of the oxygen-evolving complex in photosystem II prior to O-O bond formation *N. Cox* et al.
▸ PERSPECTIVE P. 736

808 **PLANT SCIENCE**
Genomic-scale exchange of mRNA between a parasitic plant and its hosts *G. Kim* et al.

812 **WATER ENGINEERING**
Reducing sewer corrosion through integrated urban water management
*I. Pikaar* et al.
▸ PERSPECTIVE P. 734

814 **PLACE CELLS**
Large environments reveal the statistical structure governing hippocampal representations
*P. D. Rich* et al.

818 **CYSTIC FIBROSIS**
Impaired mucus detachment disrupts mucociliary transport in a piglet model of cystic fibrosis
*M. J. Hoegger* et al.
▸ PERSPECTIVE P. 730

822 **CELL REPROGRAMMING**
Histone chaperone ASF1A is required for maintenance of pluripotency and cellular reprogramming
*E. Gonzalez-Muñoz* et al.

826 **TRANSDIFFERENTIATION**
Sequential histone-modifying activities determine the robustness of transdifferentiation *S. Zuryn* et al.

829 **SYNTHETIC BIOLOGY**
Programmable on-chip DNA compartments as artificial cells
*E. Karzbrun* et al.

**DEPARTMENTS**

715 **EDITORIAL**
Science for lasting peace
*By Marcia McNutt*
▸ NEWS STORY P. 725

842 **WORKING LIFE**
Outside my comfort zone
*By Blaise J. Arena*

*Science* Staff ..... 714
New Products ..... 833
*Science* Careers ..... 834



**SCIENCE (ISSN 0036-8075) is published weekly on Friday, except the last week in December, by the American Association for the Advancement of Science, 1200 New York Avenue, NW, Washington, DC 20005.** Periodicals mail postage (publication No. 484460) paid at Washington, DC, and additional mailing offices.


Copyright © 2014 by the American Association for the Advancement of Science. The title SCIENCE is a registered trademark of the AAAS.


Domestic individual membership and subscription (51 issues): $153 ($74 allocated to subscription). Domestic institutional subscription (51 issues): $1282; Foreign postage extra: Mexico, Caribbean (surface mail) $55; other countries (air assist delivery) $85. First class, airmail, student, and emeritus rates on request. Canadian rates with GST available upon request, GST #1254 88122. Publications Mail Agreement Number 1069624. **Printed in the U.S.A.**
**Change of address:** Allow 4 weeks, giving old and new addresses and 8-digit account number. **Postmaster:** Send change of address to AAAS, P.O. Box 96178, Washington, DC 20090–6178. **Single-copy sales:** $10.00 current issue, $15.00 back issue prepaid includes surface postage; bulk rates on request.


**Authorization to photocopy** material for internal or personal use under circumstances not falling within the fair use provisions of the Copyright Act is granted by AAAS to libraries and other users registered with the Copyright Clearance Center (CCC) Transactional Reporting Service, provided that $30.00 per article is paid directly to CCC, 222 Rosewood Drive, Danvers, MA 01923. The identification code for *Science* is 0036-8075. *Science* is indexed in the *Reader's Guide to Periodical Literature* and in several specialized indexes.


PHOTO: (BOTTOM LEFT) MICHAEL J. WELSH




*Published by AAAS*

EDITORIAL

# Science for lasting peace

Thomas Barnett, a U.S. military geostrategist, has argued that we have leviathan armies that quickly win wars, only to lose the peace. To change that outcome, stability must be established by rebuilding the infrastructure, institutions, and economy of a war-torn nation. An outstanding example of science applied to nation rebuilding is the hyperspectral survey of Afghanistan by the U.S. Geological Survey (USGS) in 2007. This survey quantified 24 world-class mineral deposits (including iron, cobalt, gold, copper, and rare earth elements), positioning Afghanistan to become a major supplier of minerals (see the News story on p. 725), most of which are in demand for the manufacture of cell phones, computers, and renewable energy technologies.

Soviet-era geologic reports on Afghanistan hinted at a nation as rich in minerals as Saudi Arabia is in petroleum. However, in such rugged terrain with few roads, approximately 25 years of boots-on-the-ground fieldwork would be required to bring the maps up to the standards necessary for resource development. Furthermore, the safety of mapping parties was a concern. The USGS suggested instead to survey from the air using remote sensing. Spectacular results were achieved from a hyperspectral survey that uses the spectrum of reflected sunlight to identify economically important mineral assemblages. Over 70% of the country was mapped in just 2 months, avoiding only regions close to the border with neighbors.

Data collection was just the start. The Afghan Geological Survey (AGS) was an empty shell of a building. The USGS set about rebuilding the AGS, teaching staff and students modern techniques such as remote sensing, digital data processing, and geophysical techniques through distance-learning methods. With this mentoring, the first woman Afghan scientist joined the ranks of the AGS employees. Together, the USGS and the reconstituted AGS interpreted the hyperspectral data and verified the discoveries with ground truth, converting the information to "treasure maps" for what eventually might be a trillion-dollar payday for Afghanistan.

Other resource-rich countries, such as Botswana, Chile, and Norway, provide good models for Afghanistan to emulate in order to avoid the social unrest, graft, corruption, and environmental degradation that can often accompany natural resource development. Important factors contributing to peace, prosperity, and improved quality of life are equitable redistribution of revenues; strong public institutions; and investment in local capacity-building, environmental planning, and transparency.

Copper deposits in Afghanistan

***"...the USGS and...AGS... [converted] the information to 'treasure maps' for what...might be a trillion-dollar payday for Afghanistan."***

As director of the USGS in the summer of 2012, I presented to Ambassador Eklil Hakimi at the Afghan Embassy the two newly created hyperspectral mineral maps for his nation. At that point, there were innumerable challenges ahead in transforming those maps into jobs and economic development: from the lack of a single functioning cement plant in the entire country to the need for modern mining law. The ambassador, however, believed that the promise of future mines would attract immediate foreign investment in transportation, telecommunications, manufacturing, education, scientific institutions, and human resources, propelling a largely agrarian nation into the 21st century. In actual fact, it is the investment in education, scientific institutions, and human resources that sustains a nation's economy long after nonrenewable natural resources are depleted. The leaders of Afghanistan will have many important decisions to make in the coming years and decades. Science has opened the door to a new, more prosperous future. May they use this opportunity wisely.

**– Marcia McNutt**

*Marcia McNutt is Editor-in-Chief of* Science.

Downloaded from www.sciencemag.org on August 15, 2014

PHOTOS: (INSET) MATTHEW C. RAINS/MCT VIA GETTY IMAGES; (RIGHT) STACEY PENTLAND PHOTOGRAPHY

10.1126/science.1259611



Published by AAAS

# NEWS

> “The international community was comfortable in allowing two relief agencies to provide all of the clinical care for the Ebola victims in three countries.”
>
> **Ken Isaacs** of Samaritan’s Purse, one of those agencies, criticizing the response to the Ebola threat at a House of Representatives subcommittee hearing on 7 August.

## IN BRIEF

### Comet chaser arrives at quarry

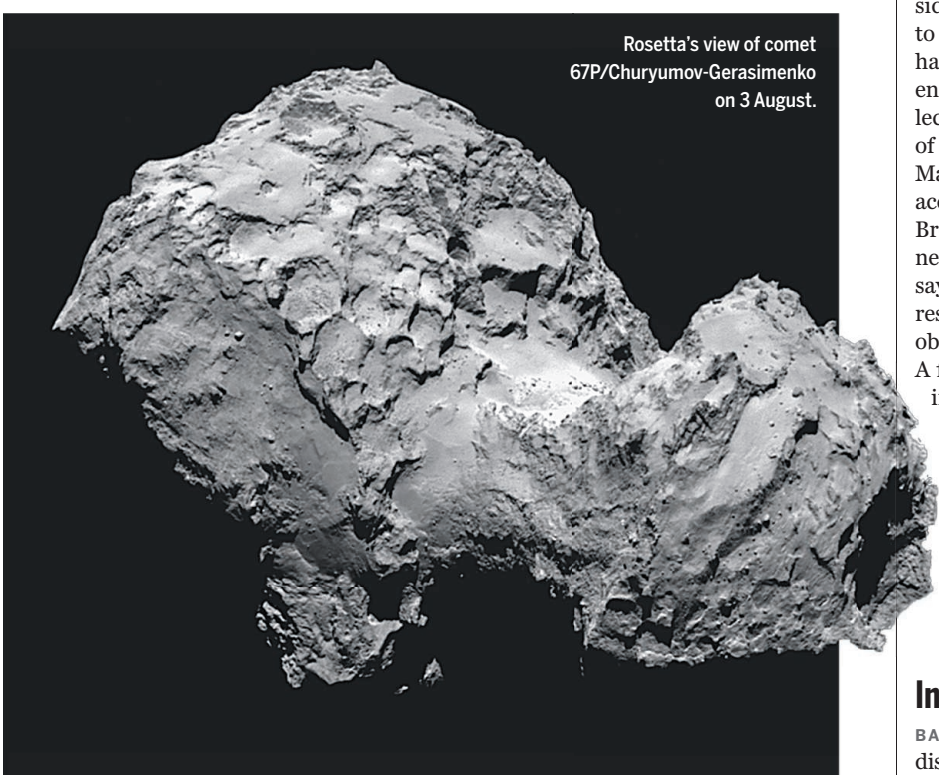

Rosetta’s view of comet 67P/Churyumov-Gerasimenko on 3 August.

Rosetta has finally met its cometary match. Last week, after a 10-year journey, the European Space Agency’s spacecraft arrived at comet 67P/Churyumov-Gerasimenko, a lopsided, bilobed lump of dust and ice sometimes likened to a 4-kilometer-long rubber duckie. The duo will now take a lap around the sun, and Rosetta will watch as the comet heats up and releases ice in a halo of gas and dust (*Science*, 1 August, p. 502). The spacecraft is now flying triangles in front of the comet, staying 100 kilometers away; in several weeks, Rosetta will settle into a 30-kilometer orbit around the comet. Mission scientists are gearing up to map the comet’s surface in hopes of finding a smooth area on which to drop Philae, a lander the size of a washing machine, this November. To help it stick the landing in the comet’s feeble gravity field, Philae will use two harpoons. Then, it will drill into the comet to gather surface material for analysis.

AROUND THE WORLD

### Patent or perish?

BRISBANE, AUSTRALIA | A suggestion by Australia Minister for Industry Ian Macfarlane that the government may consider tying science funding for universities to the number of patents they generate has drawn sharp criticism. “We need to ensure that commercialisation of [intellectual property] … is part of the process of giving taxpayers’ money to researchers,” Macfarlane said in a 6 August speech, according to a transcript by the Australian Broadcasting Corporation. Political opponents and researchers decried the idea, saying it could shift funding from basic research, particularly in areas with no obvious potential for commercialization. A focus on patents could create “perverse incentives,” Aidan Byrne, chief of the Australian Research Council, told *The Australian*. But several commentators note that Macfarlane’s ministry may have little impact on university research funding policy, which is primarily the responsibility of the education ministry.

http://scim.ag/Ausminpatents

### India bans dissections

BANGALORE, INDIA | A campaign to bar dissections in India’s university classes has scored a major victory. India’s University Grants Commission, which sets India’s standards for university education, has banned the dissection of animals in zoology and life science university courses. That follows a

India’s Western Ghats bullfrog.

PHOTOS: (LEFT TO RIGHT) ESA/ROSETTA/MPS FOR OSIRIS TEAM MPS/UPD/LAM/IAA/SSO/INTA/UPM/DASP/IDA; AJITH U/FLICKR

Downloaded from www.sciencemag.org on August 15, 2014



Published by AAAS

Resin on fibers from Predynastic Egypt, viewed in polarized light.

## Mummification's origins pushed back

In prehistoric Egypt, between 4500 and 3100 B.C.E., the hot, dry desert did the work of mummification by desiccating bodies naturally. It wasn't until much later, around 2200 B.C.E., that artificial embalming using resins began—or so scientists thought. New evidence pushes back the origin of artificial mummification in ancient Egypt by 1500 years, researchers at the University of York in the United Kingdom and Macquarie University in Sydney, Australia, reported online this week in *PLOS ONE*. The researchers examined funeral wrappings dating to between 4300 and 2900 B.C.E. and excavated pit graves in cemeteries dating to between 4500 and 3350 B.C.E. in the Badari region in Upper Egypt. The team identified embalming agents on the linen wrappings made from ingredients such as pine resin, gum, aromatic plant extract, and natural petroleum. Some 3000 years later, the researchers note, Egyptians at the height of the Pharaonic period used recipes with the same ingredients in similar proportions to produce more famous mummies.

decision in March by the Medical Council of India to prohibit animal dissection in undergraduate medical courses; it may extend the ban to postgraduate courses. The group People for the Ethical Treatment of Animals has argued that computer models and simulations can replace dissection and that several frog species are now endangered due to large numbers of zoology students collecting them for experiments. But some educators contend that university classrooms aren't prepared to offer alternatives.
http://scim.ag/Indiadissect

## Wolverine protection withdrawn

WASHINGTON, D.C. | Citing scientific uncertainty in climate change models, the U.S. Fish and Wildlife Service (USFWS) on 12 August decided not to list the wolverine as threatened. The decision is controversial because the agency's scientists and two independent review panels had previously endorsed the listing proposal, only to be overruled in May by a regional director. Once hunted, trapped, and poisoned nearly to extinction, the wolverine has bounced back in the mountain west. But global warming threatens their snowy dens. In May, a regional official decided that climate change models could not predict a lack of dens precisely enough to justify the listing. USFWS Director Dan Ashe defended the decision: "Reasonable professionals can look at the same information and come to a good but different conclusion," he said.
http://scim.ag/_wolver

NEWSMAKERS

## Three Q's

A draconian antigay law enacted in Uganda in February (and struck down on a technicality on 1 August) generated worldwide censure—and the scientific community's response has been a trial by fire for the Uganda National Academy of Sciences' president, **Nelson Sewankambo**, 62. Sewankambo spoke with *Science* about the controversy.
http://scim.ag/Sewankambo

**Q: What were the origins of the antigay law?**
**A:** The international community tends to think that intolerance for gays started after Christian activists visited Uganda in 2009. [But] intolerance for gays has been going on for years. [The Christian] group may have accelerated antigay feelings within the government.

**Q: After Parliament passed the antigay legislation last December, when was your academy asked to weigh in?**
**A:** We were brought into the picture very late, a week or so before the report was required. I said, this academy … has to use evidence and produce a credible report. I also knew that this report would define the reputation of this academy. So we declined.

**Q: Is the law shelved for now?**
**A:** The government is free to appeal. They are still thinking through it. Members of Parliament are free to reintroduce it.

BY THE NUMBERS

**5**

Hours of sleep per night that astronauts got aboard the International Space Station and the space shuttle, according to a study of 85 crew members in *The Lancet Neurology*. An official flight schedule mandates 8.5 hours.

**60%**

Fraction of plants, in a study of 300 species across the United States, that moved downhill over the last 40 years—likely seeking wetter regions despite warmer temperatures at lower elevations, according to a study in *Global Change Biology*.

PHOTOS: (TOP TO BOTTOM) © RON OLDFIELD; R. STONE/*SCIENCE*



Published by AAAS

IN DEPTH

A health official checks the temperature of an airport worker in Lagos, Nigeria.

PHOTO: AP PHOTO/SUNDAY ALAMBA, FILE

INFECTIOUS DISEASES

# Debate erupts on 'repurposed' drugs for Ebola

## With experimental treatments in short supply, some researchers think existing medicines might work

*By* **Martin Enserink**

Eleanor Fish is frustrated. The immunologist at the University of Toronto in Canada thinks she knows how to help save the lives of people battling Ebola—but nobody seems interested. Fish believes health care workers and people exposed to the virus should take Infergen, a synthetic interferon α that she has studied extensively and that has been used widely to treat hepatitis C and several other diseases. Pharmunion BSV Development, the Ukrainian company that makes it, has offered to ship 60,000 vials to Africa for free.

But as *Science* went to press this week, Fish had tried in vain to get the attention of the World Health Organization (WHO) or Doctors Without Borders, two organizations that might help distribute it. And other scientists are skeptical of the plan, because monkey studies have not clearly shown that Infergen is effective against Ebola. That should be the threshold for trying any drug or vaccine in the current outbreak, says Thomas Geisbert, a longtime Ebola researcher at the University of Texas Medical Branch in Galveston.

Fish's plan—and several others to use existing drugs that weren't approved specifically for Ebola—are a new twist on a debate that has rocked the scientific and public health community for the past couple of months: whether to use promising experimental, but unapproved, Ebola drugs and vaccines in the four African nations with Ebola cases.

Just a month ago, WHO said it would be unethical and unwise to use such interventions at this time (*Science*, 25 July, p. 364). But the treatment of two U.S. patients who contracted Ebola in Liberia with an experimental antibody cocktail called ZMapp has shifted public perceptions, says Armand Sprecher of Doctors Without Borders in Brussels. And on Tuesday, a special ethics panel convened by WHO said that, if certain criteria are met, it's ethical to use unapproved vaccines or drugs (http://scim.ag/Ebolaethics). "The shoe is on the other foot now," Sprecher says. "It's not that we would inflict horrible things on [patients], but that we failed to inflict good things on them."

The problem is that none of the experimental therapies and vaccines appears to be available in quantities large enough to treat the thousands in need. That's where Food and Drug Administration (FDA)–approved drugs like Infergen might come in. The advantages of these "repurposed" drugs are clear: They have been tested for safety, there is plenty of experience with them, and they are often readily available in large quantities.

Fish has long studied the antiviral action of interferon and, in 2003, used it with some success on patients infected with another epidemic virus, SARS. Attached to an e-mail that she sent to WHO and Doctors Without Borders officials on Monday were two papers from a team at the Public Health Agency of Canada showing that interferon, delivered by an adenovirus and combined with an antibody cocktail, saved nonhuman primates from an otherwise fatal Ebola dose. But Geisbert says the efficacy of the mix may have been due to the antibodies; past studies he and others have done have shown no effect on Ebola from interferon itself, he says.

Other scientists are promoting the use of drugs that might modulate the immune system's reaction to Ebola, such as statins—known primarily as cholesterol-lowering drugs—ACE inhibitors, and angiotensin receptor blockers. Steven Opal of Brown University and David Fedson, a retired pharma executive living in France, argue that the problem in Ebola is not so much the virus infection itself, but a runaway immune reaction that also happens in sepsis. Some drugs, including statins, dampen that response; a 2012 trial in sepsis patients showed that atorvastatin reduced the risk of progressing to severe sepsis by 83%. The

Downloaded from www.sciencemag.org on August 15, 2014



Published by AAAS

drugs haven't been tried against Ebola, but there is reason to think they can save lives, Fedson says.

Fedson says he has written to WHO Assistant Director-General Marie-Paule Kieny about the idea; she replied with a detailed letter about the agency's reservations, he says. Determined to get the matter on the international agenda, he and Opal circulated the draft of an op-ed for *The New York Times* to some 80 prominent scientists on 8 August. The letter created a "firestorm" over the weekend, says Geisbert, who didn't sign it because there is no evidence in nonhuman primates that the strategy would work.

"I completely understand that people mean well, and we all want to do something," Geisbert says. "But I have seen so many things that inhibit Ebola in cell culture and didn't work in rodents, or that worked in rodents but didn't protect monkeys. … We shouldn't just grab anything on the back burner that's FDA-approved." Ineffective drugs could spoil the prospects for more promising candidates, he worries, and compounds that change the immune response could actually make Ebola infection worse.

Fedson counters that virologists like Geisbert have yet to catch on to the idea of treating the immune response. "All they can think about is hammering the virus," he says. As *Science* went to press, it was unclear whether the letter would be published. Among the almost 30 supporters are prominent researchers such as Hans-Dieter Klenk, who studies filoviruses such as Ebola at the University of Marburg in Germany. But another Ebola researcher at Marburg, Stephan Becker, says he opposes the plan for reasons similar to Geisbert's.

Several other ideas have been floated, and Fish realizes that she's not the only one trying to get WHO's attention. "I imagine people are probably falling out of the trees with all kinds of garlic therapies and who knows what," she says. Indeed, whether WHO has time and resources to look at all the ideas is unclear. At an 8 August press conference, WHO Director-General Margaret Chan said that her organization is "extremely stretched," as is Doctors Without Borders.

Meanwhile, the outbreak shows no signs of abating. On Tuesday, WHO reported 1848 cases so far and 1013 deaths; the real numbers almost certainly exceed official tallies because many patients don't seek medical help. Also on 8 August, WHO declared the situation a Public Health Emergency of International Concern, an official designation that allows it to recommend travel restrictions but also serves as a global plea for resources and money. "This is an urgent call for international solidarity," Chan said. ■

PHOTO: APIC/GETTY IMAGES

NUCLEAR WEAPONS

# *Firing of Los Alamos researcher draws criticism*

## Officials claim paper contained classified information

*By* **Jeffrey Mervis**

A political scientist at Los Alamos National Laboratory has been fired after authoring a scholarly article that questions the dogma of nuclear deterrence. Congressional staff had raised concerns that the article contained classified information, and lab officials subsequently decided that it did. Although the reasons James Doyle's 17-year career at the Department of Energy (DOE) weapons lab in New Mexico ended last week may never be clear, many nuclear security experts are sharply criticizing the lab's actions.

"It sends a chilling message not just to employees, but also those beyond the lab, that their ability to work on topics subject to classification could be restricted if they become too critical of policies that the lab holds dear," says Frank von Hippel, a physicist at Princeton University. "It's a very disturbing situation," adds Daryl Kimball, executive director of the Arms Control Association in Washington, D.C. "DOE leadership needs to reverse this decision."

Scholar's paper questioned value of nuclear weapons for deterrence.

The affair, first reported by the Center for Public Integrity, an investigative news service in Washington, D.C., began after Doyle's article "Why Eliminate Nuclear Weapons?" appeared in the February-March 2013 issue of *Survival: Global Politics and Strategy*, published by the London-based International Institute for Strategic Studies. The article, which Doyle wrote on his own time and which includes a disclaimer clarifying that he was speaking for himself, opens with President Barack Obama's 2009 call for "a world without nuclear weapons." It goes on to argue that nuclear deterrence is not effective and that nuclear weapons should be eliminated for a host of political, military, humanitarian, and environmental reasons.

Doyle's arguments are squarely in the mainstream of nuclear security debates, says George Perkovich, an arms control specialist at the Carnegie Endowment for International Peace in Washington, D.C. "The only thing unusual about [the article] was that it came from somebody at a weapons lab," which typically touts the merits of nuclear deterrence, he says. Nor does it represent a change of heart for Doyle, who until his dismissal was one of the few political scientists at a 10,000-person laboratory dedicated to maintaining the U.S. stockpile. "I probably decided that nuclear weapons didn't make sense by the age of 21," says Doyle, 55.

Despite that belief, Doyle had become steeped in nuclear issues. Working in the mid-1990s for SAIC, a major defense contractor, he helped draft a U.S. government plan to track and safeguard nuclear material in the former Soviet Union. He then earned his Ph.D. from the University of Virginia and came to Los Alamos as a postdoc in 1997. Within a year, he was hired to work on nonproliferation.

Over the past decade, Doyle has published numerous papers, opinion pieces, and a textbook, as well as spoken at conferences, without causing a stir. His *Survival* article, however, caught the eye of a staffer on the Armed Services Committee of the U.S. House of Representatives. The staffer was concerned that it contained classified information and asked lab officials if it had been cleared for publication, according to a committee aide.

Soon after that inquiry, lab managers asked Doyle for copies of his other articles; he gave them about 20 publications. Shortly after that, security officials told him that the *Survival* article contains classified material, eventually searching his home computer for copies. Doyle says he thought



Published by AAAS

he had followed the proper rules for prior review and that he had received approval from a classification analyst before submitting the article. But Daniel Gerth, the lab's chief classification officer, ultimately decided to classify the article.

For Doyle, that reversal began a 17-month ordeal. Lab officials revoked his top-level security clearance, and he says he became persona non grata within his division. His formal complaints of retaliation and loss of academic freedom were rejected, and he says that on 8 July, lab officials told him he was being laid off because of budget cuts.

In a statement, the Los Alamos lab said officials "do not publicly discuss" personnel matters. But in a 7 August e-mail to lab staff obtained by *Science*, Doyle's boss denies that Doyle was fired as a result of the article. "I would like to assure you that this is not the case," wrote division leader Michael Baker. He urged lab employees to continue publishing "thoughtful, articulate and technically sound work in the public domain, to the extent we can do so within laboratory policy."

In a Catch-22, neither lab officials nor Doyle will discuss the paper, which is still on *Survival*'s website, because it is now classified. Reviews by lab officials backed the classification decision. But one concluded that the lab's classification rules were "vague and confusing," lacked "consistency and transparency," and noted that reviewing officials had disagreed on whether Doyle disclosed secrets.

Outside experts—including several who have handled similar classified material—say they see nothing problematic in Doyle's paper. But they speculate that two sections might have caught the attention of classification officers. One lists Israel as possessing nuclear weapons, which the United States has never officially confirmed. The other discusses documents related to a Cold War misunderstanding that some historians believe could have led to nuclear war.

Former Los Alamos Director Siegfried Hecker thinks that lab officials overreacted. "Is it typical to fire someone who has made a classification mistake?" he says. "The answer is no."

Hecker and others worry that the lab may be turning its back on contributions from political scientists like Doyle, who can bring a different perspective to the lab's work. "I think his writing about these issues is beneficial to both the laboratory and the country," says Hecker, a professor of engineering and management sciences at Stanford University in Palo Alto, California. "But the question is whether Los Alamos, in today's world, still values their input." ■

*With reporting by David Malakoff.*

EARTH SCIENCE

# A boom in boomless seismology

## Densely packed sensors eavesdrop on Earth's hum

*By* **Eric Hand**

Last week, geoscientists in Washington state finished the largest ever seismological survey of Mount St. Helens, burying 2500 seismometers on its flanks to listen for reverberations as 23 blasts sent seismic waves deep under the volcano. But tucked within the megasurvey was a second one—denser, quieter, and, in its long-term implications for the field of seismology, potentially more important.

Brandon Schmandt, a seismologist at the University of New Mexico, Albuquerque, and a small crew had boot-stomped into the ground 920 other recorders, called ZLands—state-of-the-art instruments that can record continuously for 2 weeks. As a result, Schmandt's array caught not only the 23 blasts, but also ambient noise: an incessant murmuring that can "passively" image the subsurface as if Earth itself were the sound source—no explosions needed.

Schmandt's Mount St. Helens experiment is just one of several dense, passive array surveys that have been conducted this summer. Cheap, long-lasting sensors play a role in the boom in boomless seismology, as does regulatory reality: Passive arrays are relatively easy to set up. Alan Levander, a principal investigator of the main Mount St. Helens survey, spent a year getting permits for the explosive shots—from nine counties, four timber companies, the state of Washington, and the U.S. Forest Service. Schmandt's array was put together on the fly in a few months for less than $100,000. "You can put out a lot more instruments and put in a lot less effort," says Levander, a seismologist at Rice University in Houston, Texas, of Schmandt's array.

The result, enthusiasts predict, will be unprecedented imaging of Earth's crust. Academic geologists, who have long envied the detailed survey data of their industrial peers, will be able to see magma chambers and pipes underneath volcanos, map the geometry of faults, and pinpoint earthquake ruptures as never before. "There is about to be a major turning point in earthquake and volcano seismology," says Florent Brenguier, a seismologist at the Institute of Earth Sciences in Grenoble, France, who last month completed a 300-seismometer passive survey of the active volcano on the island of Réunion in the Indian Ocean.

Earth's ambient noise arises largely when ocean waves and wind sweep the planet's surface like brushes on an enormous cymbal. For more than a decade, geoscientists have used its lower frequencies to answer questions about the mantle-

PHOTO: STEVE HANSEN

Downloaded from www.sciencemag.org on August 15, 2014



Published by AAAS

Seismometers (yellow) have recorded ambient noise around the Mount St. Helens volcano.

PHOTO: E. HAND/SCIENCE

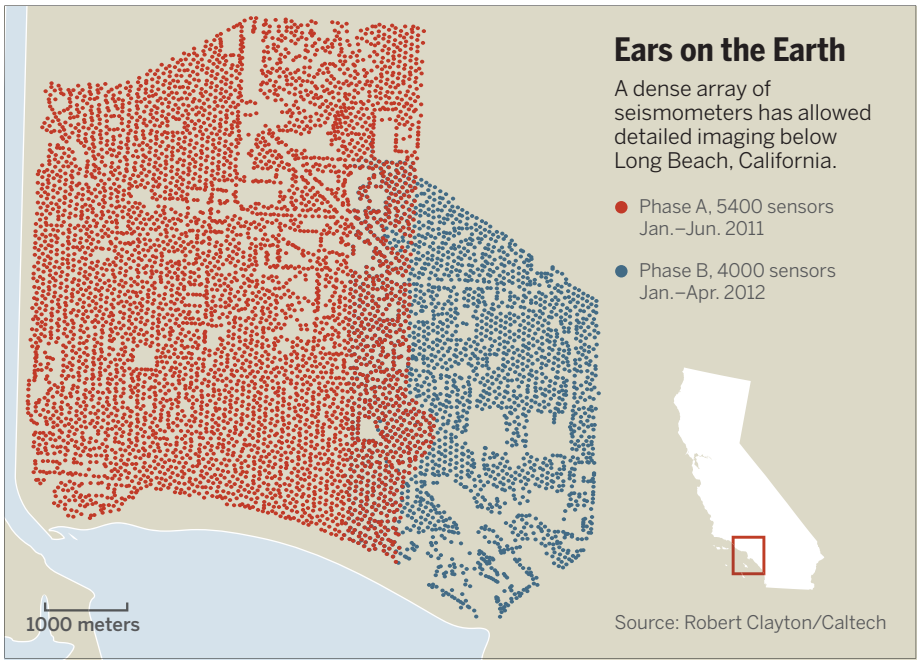


crust boundary. Probing such deep regions, tens or hundreds of kilometers down, requires arrays with sensors spaced similar distances apart—such as the U.S. Transportable Array, a system of 400 seismometers, spaced at intervals of 70 kilometers, that has been marching eastward across the continent over the past decade (*Science*, 14 June 2013, p. 1283).

Much denser arrays, however, can sample higher frequency ambient noise to answer questions about the upper 10 kilometers of crust. "The potential to put out thousands of sensors over a very small area lets you resolve structure in ways you couldn't before," says Robert Detrick, president of the Incorporated Research Institutions for Seismology (IRIS) in Washington, D.C., which operates the Transportable Array. Until recently, only oil and gas companies could afford to deploy such arrays. "We in the academic community thought a big experiment was putting out a few dozen sensors or maybe a hundred sensors," Detrick says.

Robert Clayton with sensor.

Robert Clayton, a seismologist at the California Institute of Technology in Pasadena, was in the right place at the right time to take advantage of an industry-scale array. In 2011, an oil company, Signal Hill Petroleum, surveyed a small oil field in Long Beach, California, deploying 5300 ZLands and a fleet of "thumper trucks" to generate seismic signals. In between thumps, however, the seismometers also caught the sounds of cars on the Los Angeles freeways and the Pacific surf. The data would have normally been tossed out as junk, but Clayton thought he could make use of it, and the company shared it with him.

Ambient noise, Clayton realized, makes strong surface waves—waves confined to shallow rock layers, in contrast to the deep-diving body waves associated with earthquakes and active shots. Analyzing the Signal Hill data, he found that he could use these surface waves to image the top kilometer of crust. The result was valuable to the company, serving as a sort of corrective lens for the deeper part of the company's survey, he says. And because the upper kilometer of crust has an outsize effect on ground shaking in an earthquake, the information should also be extremely useful for the city of Long Beach and its engineers. "I think it's going to revolutionize how we do seismology in urban areas," he says.

Clayton's success has sparked wide interest: A half-dozen other universities have asked for the Signal Hill data. In the past 3 months, IRIS and the American Geophysical Union have each hosted workshops on the new techniques. New data, from a 5400-node survey of shale and limestone formations near Sweetwater, Texas, will be uploaded to IRIS databases later this month, freely available for scientists wanting to experiment with the passive techniques. In June, Yehuda Ben-Zion of the University of Southern California in Los Angeles packed 1100 ZLand sensors into less than a square kilometer along an active portion of the San Jacinto fault, a major offshoot of the San Andreas fault. With sensor spacings as little as 10 meters, Ben-Zion hopes for insights into how earthquakes get started and how properties of the rock along the fault change before and after an earthquake.

Oil and gas companies are getting more comfortable with the passive techniques, and they too would like to avoid some of the hassles of permitting shots and thumps, says Dan Hollis, vice president of marketing and technology at Nodal Seismic in Signal Hill, California, which performs dense surveys for industry clients. "I see this as the way that the oil exploration industry is going to go."

As industry money pours in, sensors like the ZLand are getting better and cheaper. For now, Hollis is happy to lend his collection of ZLands to scientists like Schmandt when they aren't being used by industry. And Schmandt is happy to take advantage. "If someone like me can scrap this thing together in the past few months, we should be capable of some cool things as a community in the next few years," he says. ■



Published by AAAS

The aftermath of a suicide bomb attack in Kabul on 6 December 2011 that claimed several dozen lives.

PHOTO: MASSOUD HOSSAINI/AFP/GETTY IMAGES

# The rising toll

## Newly released data reveal that the war in Afghanistan is becoming more dangerous for civilians

*By* **John Bohannon**

As troops head home from the war in Afghanistan, the longest in U.S. history, the growing death toll for Afghan civilians is coming into focus. Last year, the occupying military coalition—the International Security Assistance Force (ISAF)—recorded 1685 Afghans killed and 3554 wounded. It is the highest number of civilian casualties since rigorous counting began in 2008. Those figures come from a previously undisclosed data set, drawn from reports from ISAF soldiers, that details the past 4 years of civilian casualties.

The death toll for ISAF troops is public information: As this issue went to press, 3465 coalition soldiers have died on duty in Afghanistan since the war against al-Qaida and the Taliban began in October 2001. Similar clarity exists for the civilians who died in the 11 September 2001 terrorist attacks on U.S. soil that ignited the war: Those 2977 names are now inscribed in bronze plaques where the World Trade Center once stood. But for Afghan civilians, the human cost of the war has been more elusive.

The number of Afghan civilians killed between 2001 and 2006 will never be known—no one was counting. Starting in 2007, the United Nations Assistance Mission in Afghanistan (UNAMA) has noted an annual figure of civilian deaths. But beyond that, says Danielle Bell, a UNAMA human rights officer, "we only release detailed data sets when it serves a precise humanitarian purpose. [And] in such cases, the detailed information is not made public."

UNAMA's reports offer little to researchers who study asymmetric warfare, in which a traditional army is pitted against a weak but highly adaptable insurgency. "What do you do with national yearly numbers?" asks Nils Weidmann, a political scientist at the University of Konstanz in Germany. To study the relationship between civilian casualties and the ebb and flow of an insurgency, he says, "you need variation both in space and in time."

Researchers received just such a windfall 3 years ago, when *Science* obtained data from three organizations tracking Afghan civilian casualties: ISAF, UNAMA, and the nongovernmental organization Afghanistan Rights Monitor (*Science*, 11 March 2011, p. 1256). It was the first data release of its kind, and it seemed to be the last. ISAF and UNAMA have refused to publicly divulge more civilian casualty data, and Afghanistan Rights Monitor has since folded.

But some ISAF partners have set their own rules on data sharing. In January, Neil Shortland, a research psychologist at the Center for Terrorism and Security Studies at the University of Massachusetts, Lowell, obtained ISAF's civilian casualty data—known as CIVCAS—from the U.K. Ministry of Defence. The ministry authorized Shortland to openly use the data, covering January 2010 through December 2013, for research and to share with collaborators, enabling *Science* to make them available at http://scim.ag/Afghandata.

The data trace the war's trajectory through

Downloaded from www.sciencemag.org on August 15, 2014



Published by AAAS

## Civilian casualties in Afghanistan

This graph shows the monthly tally of civilian casualties in Afghanistan caused by insurgents and coalition military forces (ISAF). It is based on data released by the U.K. Ministry of Defence for a study conducted by Neil Shortland of the Center for Terrorism and Security Studies at the University of Massachusetts, Lowell. The entire data set is available at http://scim.ag/Afghandata.

*By* **Neil Shortland** *and* **John Bohannon**

**May 2009** ISAF airstrike in Granai

**July 2009** General Stanley McChrystal, ISAF commander, declares the civilian population the "center of gravity" in Afghanistan

**May 2011** Osama bin Laden killed by U.S. Special Forces raid

**June 2011** President Barack Obama announces schedule for troop withdrawal

**November 2011** Mullah Mohammed Omar calls on Taliban to "take every step to protect the lives" of civilians

**December 2011** Suicide bombing in Kabul

**June 2012** General John Allen, ISAF commander, limits aerial bombings

**September 2012** The Afghan government is leading over 80% of security operations

**May 2013** Double IED attacks in Kabul

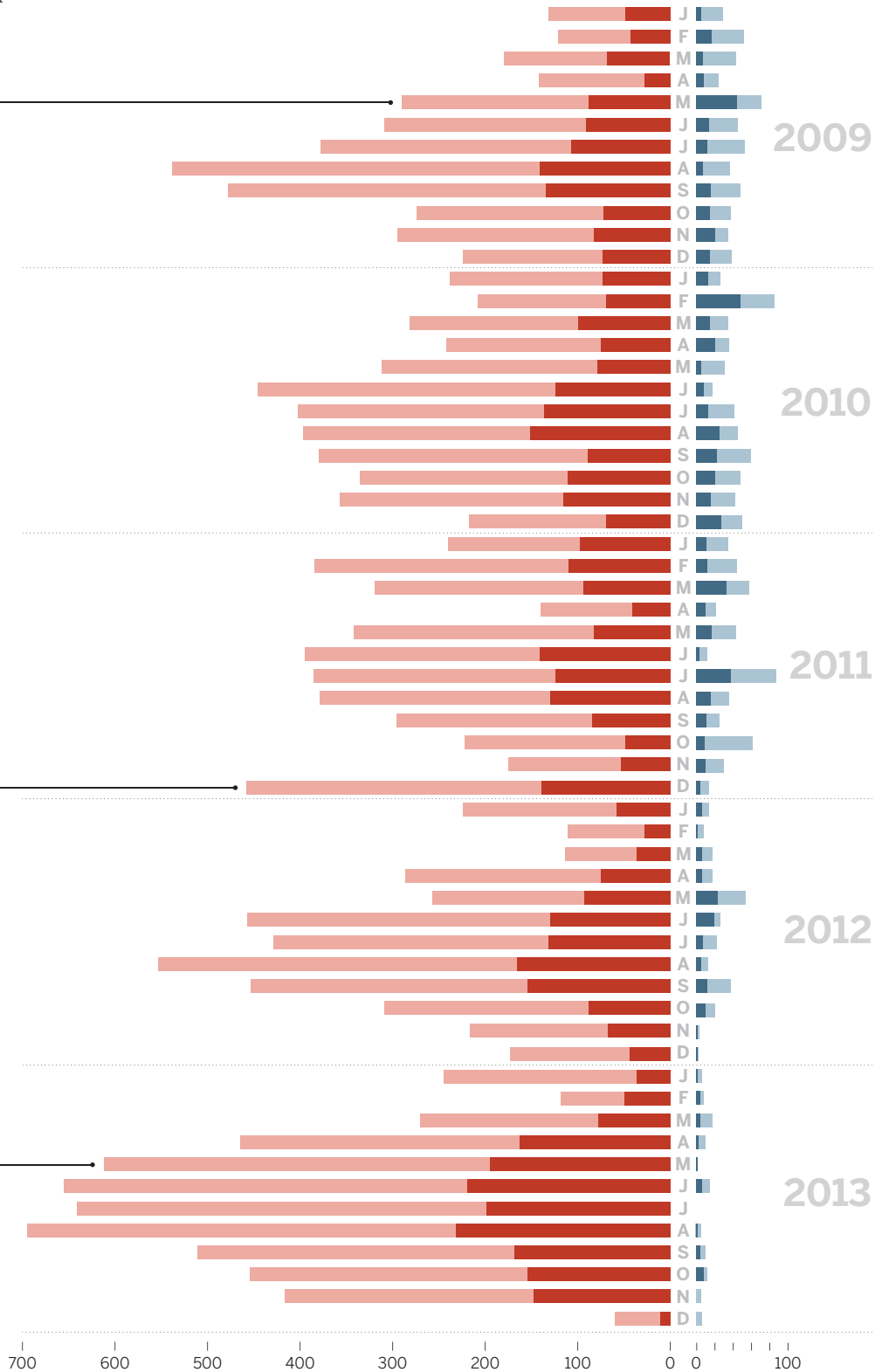


PHOTOS: (TOP TO BOTTOM) JOAO SILVA/*THE NEW YORK TIMES*/REDUX; S. SABAWOON/EPA/CORBIS; REUTERS/OMAR SOBHANI



Published by AAAS

the lens of civilian death and injury. The original military mission of ousting the Taliban, a fundamentalist regime that harbored the al-Qaida terrorists, expanded to a full military occupation of Afghanistan with the goal of providing security to its civilians.

By 2011, many analysts believed that the tide was turning in this war against a protean enemy, which melts in and out of the civilian population. A surge in troop numbers was yielding palpable gains, raising hopes that the insurgency would be weakened long enough for Afghanistan's fragile government and its forces to take over security. In June 2011, U.S. President Barack Obama announced plans for a phased troop withdrawal. (In May of this year, Obama said that the current force would be reduced to fewer than 10,000 by the end of 2014.) According to the newly released CIVCAS data, 1320 Afghan civilians were killed in the conflict in 2011, 7% fewer than in 2010 and a promising reversal of the upward spiral in casualties.

That decrease was ephemeral. An ill omen came in December 2011, when insurgent bombings killed 115 civilians and wounded 301. The massacres happened well outside the "fighting season"; as the CIVCAS data show, the Taliban tend to lie low over the harsh Afghan winter (see p. 723). And since then, casualties have grown year by year.

As UNAMA has long noted, insurgents are responsible for the majority of deaths and injuries, accounting for two-thirds of the civilian casualties last year. Improvised explosive devices (IEDs) are largely to blame. Analyzing incident counts in the new data—these were not part of the 2011 release—Shortland learned that IEDs have become more numerous and more lethal. Insurgents launched 868 IED attacks last year: 50% more than in 2010. And they have conducted more complex attacks, often with multiple coordinated explosions that compound the toll.

The newly released data also suggest that recent ISAF airstrikes have caused less collateral damage, in contrast to costly mistakes earlier in the war. In 2008, for example, ISAF jets mistakenly targeted at least two wedding parties, killing dozens of women and children and prompting Afghan President Hamid Karzai to demand an end to airstrikes. ISAF never halted them, but the newly released CIVCAS data recorded 16 civilian deaths caused by jets, helicopters, and drones last year, compared with 89 in 2010. And the number of deaths per airstrike declined by half.

The latest CIVCAS data offer a window on how the military revises its casualty counts as investigations play out. Comparing casualty numbers for the year 2010 in the data released in 2011 and in the new data shows that final casualty counts for individual events can change dramatically. This is especially true for IED attacks, with monthly totals revised up or down by dozens of deaths. On balance for 2010, ISAF-caused casualties increased by 15% and insurgent-caused decreased by 7%.

Today's release more than doubles the amount of casualty data available for researchers. "The big question is how civilian casualties trigger withdrawal of support from the population," says Konstanz's Weidmann. Anger at civilian deaths caused by the military may be driving an increase in "green-on-blue" incidents in which men in Afghan army uniforms attack ISAF personnel, including last week's slaying of a U.S. two-star general. And though most civilian casualties are caused by insurgents, the nature of their attacks—an ambush of a military convoy versus an IED exploding in front of a mosque—may have vastly different effects on popular support for the Taliban. Far from being simply a tragic byproduct of the conflict, civilian casualties also perpetuate it, says Neil Johnson, a physicist at the University of Miami in Florida who models asymmetric warfare. "We definitely find the causal arrow goes both ways."

The data made public today end in December 2013, but the civilian casualties continue. On 15 July, a car bomb exploded near a busy market and mosque in Paktika province, near Afghanistan's border with Pakistan. Eighty-nine people were killed, making it the single deadliest attack by insurgents on record. ■

An elderly man prays at his son's grave in Kabul.

PHOTO: SHAH MARAI/AFP/GETTY IMAGES

## How to count the dead

From old-fashioned surveys to Twitter scraping, researchers who tally civilian casualties have more options than ever for data sources. Each technique has its pluses and minuses.

### Real time

The coalition in Afghanistan was the first military force to count civilian casualties systematically. U.N. informants and journalists report what they observe.

**From soldiers**
**Pro:** Most casualties are at the front lines
**Con:** Data treated with suspicion

**From informants**
**Pro:** Data viewed as trustworthy
**Con:** Methods opaque

**From journalists**
**Pro:** Rapid; open
**Con:** Biased toward the largest casualty events

### After the fact

Surveys and interviews in the wake of conflicts have been a mainstay for approximating the death toll. But the information evaporates as people migrate.

**Household cluster surveys**
**Pro:** Rigorous
**Con:** Dangerous for researchers; huge error bars because of sampling

**Refugee interviews**
**Pro:** Safer for researchers
**Con:** Difficult to extrapolate results to whole country

### A future of counting

The body count is climbing in Iraq, Syria, and Ukraine. They are becoming grim natural experiments for new casualty tracking methods.

**Crowdsourcing**
Online mapping platforms like Ushahidi are being adapted for war zones, with casualties reported almost immediately on social media.

**Collaboration**
The group everycasualty.org is improving casualty recording by standardizing methods for researchers and promoting transparency.



Published by AAAS

Making every second count, Robert Tucker liberates a chunk of rare earth minerals from the Khanneshin volcano complex.

PHOTO: TFBSO PHOTO BY TINA HAGER

Downloaded from www.sciencemag.org on August 15, 2014

# Mother of all lodes

## The United States is putting scientific boots on the ground in Afghanistan to assess its mineral riches

*By* **Richard Stone**

In February 2011, Robert Tucker went prospecting in southern Afghanistan's Helmand province, a region dominated by Taliban insurgents. It was not a leisurely field trip. U.S. Marines first arrived at the site to secure a perimeter, then a team of U.S. and Afghan scientists including Tucker, a research geologist with the U.S. Geological Survey (USGS) in Reston, Virginia, swooped in on two Black Hawk helicopters. Weighed down by flak jackets in the searing heat, the group had just a few hours to scale a "very, very steep" volcano, Tucker says, collect samples, and hustle back to the choppers. One of his colleagues collapsed from heat prostration.

"I've never experienced anything like it," says Tucker, who has been clambering over rugged topography ever since his grad school days in the early 1980s, when he studied rock formations along Norway's coastal fjords. But the risky, arduous work in Afghanistan paid off. Tucker's team confirmed that Helmand's Khanneshin carbonatite deposit, last surveyed in the early 1970s by Soviet geologists, is as rich as they suspected. The deposit, chock-full of rare earth elements—highly sought components of lasers and magnets—and niobium, used to temper steel and in superconducting alloys, is now valued at $89 billion.

Khanneshin is only a thimbleful of Afghanistan's mineral wealth. Based in part on USGS-led aerial surveys, the U.S. Department of Defense's (DOD's) Task Force for Business and Stability Operations (TFBSO), charged with rebuilding Afghanistan, in 2010 valued the country's mineral resources—everything from gold and



Published by AAAS

## Afghanistan in a new light

USGS's hyperspectral survey revealed a vivid panoply of nonferrous mineral formations. Boxes indicate approximate locations of confirmed major mineral reserves.

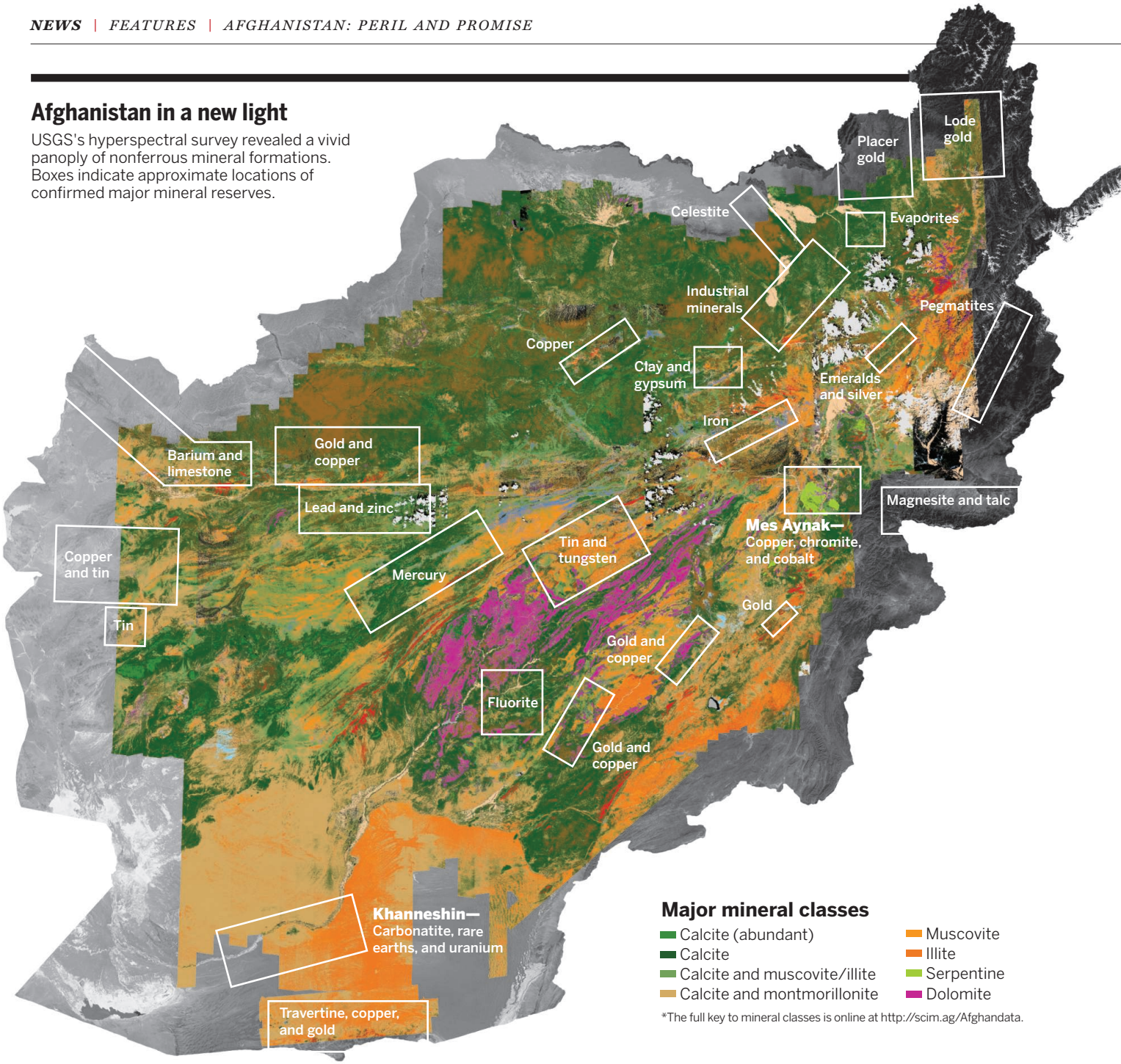


MAP: ADPATED FROM USGS

copper to lithium and petroleum—at $908 billion. (The Afghan government's preferred figure is $3 trillion.) That bounty is a product of a tortured tectonic history: Afghanistan is an amalgam of at least four pieces of crust squashed together by the collision of the Indian subcontient with Asia. "This is a very, very mineral-rich country," says Jack Medlin, a USGS geologist who leads the agency's work in Afghanistan. Over the past 4 years, USGS and TFBSO have been putting scientific boots on the ground to acquire more data.

The goal, says James Devine, senior adviser for science applications at USGS, is to show mining companies "not only that the minerals are there, but where they are, how much is there, and what you can do about it." As *Science* went to press, the final scoping mission was about to get under way. A team will drill into a dry lakebed about 100 kilometers south of Kabul to sample a potential reserve of lithium, an element used in ceramics and batteries.

As the flood of foreign aid that has buoyed Afghanistan's economy for more than a decade recedes, the country's prosperity may well depend on its prodigious mineral resources. "The conversation has changed from agriculture and opium to minerals and sophisticated development," Devine says. Already, the Afghan government has awarded contracts to a Chinese company to exploit the Mes Aynak copper deposit and to an Indian consortium to tap a massive iron ore lode. A major impediment to developing these and other reserves was removed last month, when Afghanistan's parliament passed the country's first mining law. "Now we have the rules of the game," says Said Mirzad, co-coordinator of USGS's Afghanistan program.

But Afghanistan faces huge challenges in shifting to a minerals-based economy. "The



Published by AAAS

area is basically screwed," says geologist John Shroder, a longtime Afghanistan expert and professor emeritus at the University of Nebraska, Omaha. It lacks roads, railroads, and electrical lines—and is also short of energy and water. Another formidable challenge is security, which will depend on the nation's fledgling army and police forces after the U.S.-led coalition withdraws its last combat troops by the end of this year. "Many of the mineral resources are located in areas where the security situation is very bad," says Hamidullah Waizy, a geologist at Kabul Polytechnic University.

After U.S.-led forces drove the Taliban from power at the end of 2001, the U.S. Agency for International Development (USAID) enlisted a USGS team to size up Afghanistan's natural resources and the condition of its geological facilities and expertise. What they found after arriving in Kabul in April 2004 "was a real downer," Medlin says. The headquarters of the Afghanistan Geological Survey (AGS) was a looted shell with most of its windows blown out during Taliban rule.

But during those bleak years, AGS staff had taken home for safekeeping something precious: Soviet geological maps and reports. Perusing the musty materials, some a half-century or more old, the USGS team found hints of a geological wonderland. But "we had our doubts," Medlin says. Many reports were based on antiquated views of ore-forming processes, from before the advent of plate tectonic theory. And the Soviet maps were filled with deliberate errors such as imaginary roads and villages placed miles from their true locations. "The idea was that an invader would be misled," Medlin says. Still, the data and maps helped USGS identify 24 potentially blockbuster deposits.

USGS wanted to use pricey remote sensing to probe further. "Everybody—USAID, the World Bank, the U.N., the Asian Development Bank—was against it. They said it was better to spend money on education," says Mirzad, who served as the U.S. Interior Department's representative in the U.S. embassy in Kabul from 2004 to 2006. Mirzad could speak with authority on Afghanistan's mineral potential. As a field geologist in the 1960s, he says, he crisscrossed the country on "foot, horseback, donkeyback, camelback, and yakback." He rose to become AGS director, but after Afghanistan's last king was deposed in 1973, Mirzad was imprisoned several times and left for the United States in 1981.

Mirzad still had powerful connections. As a young man in Kabul, he had played bridge on Thursday nights at the home of Hamid Karzai, the future Afghan president. Mirzad persuaded Karzai that mining would "bring life to the country" through job creation and tax revenues. Tapping a fund from payments made by airlines for the right to fly over Afghanistan, Karzai in 2004 gave USGS $8.86 million for an airborne geophysics campaign.

In 2006, USGS and the U.S. Naval Research Laboratory flew a 35-person team into Kandahar to conduct magnetic and gravity surveys aboard a U.S. Navy NP-3D Orion surveillance plane. Magnetism reveals iron-bearing minerals up to 10 kilometers below the surface, whereas gravimeters identify deep, sediment-filled basins. "Sediments mean oil and gas," Mirzad says. Although the Orion flew higher than optimal for such surveys to stay out of range of shoulder-fired missiles, the data haul was superb, Medlin says.

Next, the geologists set out to map the bare rock and sediment that cover much of the country using an airborne hyperspectral imager. "Every mineral reflects the sun's rays with a different color," Mirzad says. A prized tool in the mining industry since it was introduced about 20 years ago, the technique had never before been carried out on such a broad scale. To do the survey, DOD offered up an old B-57 bomber that "went like a lawn mower back and forth across the country," Medlin says.

> ***"You're not so much worried about whether you will get shot or not, but whether you can get samples in the 20 minutes or so you have on the ground."***
>
> **James Devine,** USGS

USGS has released two hyperspectral maps of Afghanistan, one depicting iron-bearing minerals and a second (see p. 726) showing nonferrous minerals. "The hyperspectral stuff is really cool. The data are so detailed," Shroder says. "Every time you process it differently, you see other things," Devine adds. The survey corroborated all the major Soviet finds and pointed to several anomalous areas that Afghan geologists intend to check out. Among the highlights: 60 million tons of copper; 2.2 billion tons of iron ore; 1.4 million tons of rare extractable minerals; and untapped lodes of aluminum, gold, silver, zinc, mercury, and lithium.

USGS expected USAID to leap at the chance to follow up on the survey findings. But for more than 2 years, the data "just sat gathering dust," Medlin says. "No one was interested." A turning point came in January 2010, when TFBSO Director Paul Brinkley was briefed on the USGS surveys. "He saw a great opportunity to move the mineral development forward," Medlin says. But both the military and USGS doubted that industry would venture into Afghanistan based on the airborne geophysics data and decades-old fieldwork.

So over the last 4 years, USGS geologists, with security and logistics provided by TFBSO, have made several dozen hasty forays into the war zone to collect and analyze samples from the major deposits and confirm the mineralization patterns mapped from above. "You're not so much worried about whether you will get shot or not, but whether you can get samples in the 20 minutes or so you have on the ground," Devine says.

USGS brass got what they needed: The data on mineral types and ages of formations were critical to "information packages"—covering everything from roads and population figures to topography and geophysical data—that the agency has put together to entice companies to bid on the rights to deposits.

The next step is creating realistic expectations among Afghan leaders. Members of Afghanistan's parliament have clamored for royalties on extracted minerals of up to 50%—10 times the normal rate paid in countries with far better infrastructure and far less risk to life and limb. The upfront investment at a single site is huge: "You're talking 5 to 10 billion dollars before you extract anything," Medlin says. Last year, the Colorado School of Mines started training Afghan engineers and mining officials in such basics as mineral law, economics, and environmentally sustainable mining—and laying out the path to a vibrant mining industry. "In good circumstances, that's between 5 and 8 years," Medlin says. "In Afghanistan it could take 20 to 25 years."

In the meantime, USGS is helping build Afghan scientific expertise. Every Monday to Wednesday from 3 a.m. to 5 a.m., bleary-eyed scientists in Reston run training courses by video link for AGS scientists, who are now working in comfortable new digs in Kabul. Shroder is leading an effort to update the geology curricula at Kabul Polytechnic University. USGS and partner agencies have provided instruments for three modern seismic stations in Afghanistan, and DOD installed a data center at AGS that should be connected to the Internet by the end of the year. The shift to a minerals-based economy, meanwhile, will not happen overnight. But it promises to transform the conflict-ravaged country. Mining, Devine argues, "will get Afghanistan out of the 14th century." ■



Published by AAAS

An overly tight mucus grip in cystic fibrosis *p. 730*

Getting to $O_2$ in photosynthesis *p. 736*

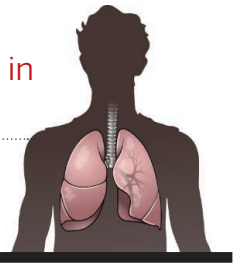

PERSPECTIVES

INFORMATION TECHNOLOGY

# *Technology's limited role in resolving debates over digital surveillance*

## Teasing apart technical issues from social and political issues

*By* **Herbert Lin***

Although it has been known for many years that the U.S. National Security Agency (NSA) has engaged in electronic surveillance, its scope and scale were not widely understood in the United States or abroad before the revelations of the past year based on documents obtained from former NSA contractor Edward Snowden. Today, an important public debate is over how policy-makers balance between two goals: identifying evildoers and thwarting their activities without unduly intruding on the rights and lives of law-abiding people who pose no threat to society.

POLICY

Scientists and engineers can make an important contribution to this policy discussion. It is not that they have a privileged position to address these issues but rather that they are uniquely qualified to tease apart technical aspects of these issues from social and political ones. I outline some important questions that arise and suggest some limitations of technology in solving what are essentially problems of public policy.

**DATA VERSUS METADATA.** In 1979, the U.S. Supreme Court ruled in *Smith* v. *Maryland* that certain information about phone calls (specifically, the phone numbers involved in a call) was worthy of less privacy protection than "content" information, what the parties to a phone call actually said to each other. The theory was that called phone numbers were being furnished to a third party, the phone company, and thus, the caller had a lesser privacy interest in that information than in the content of the call.

The proliferation of cell phones since 1979 has altered the foundation on which *Smith* v. *Maryland* was based. For example, cell phone numbers are much more closely associated with specific individuals than are landline numbers. Also, the cell phone infrastructure makes it possible to generate geo-

PHOTO: © KACPER PEMPEL/REUTERS/CORBIS

Downloaded from www.sciencemag.org on August 15, 2014



Published by AAAS

graphic tracking information for a particular cell phone.

In 1979, information about phone calls apart from content could only include numbers dialed and time and duration of those calls. The theory under which *Smith* v. *Maryland* was decided suggested that any data apart from content—namely, metadata—are less worthy of privacy protection than content information—namely, data. Should this be true, for example, of location information?

Evolution of technology may call into question legal concepts formulated in an earlier technological context. What counts as data and metadata in e-mail? Is a buddy list on an instant messenger client or information posted to Facebook or Google+ data or metadata? Such questions arise because of new technology, but the answers depend on what society regards as the proper policy outcome. Do we want greater privacy for data vis-à-vis metadata for new technologies, or should they be equally protected?

National security and law enforcement agencies tend to answer such questions in ways that maximize their legal authority to obtain as much information as they can. Advocates for civil liberties tend to answer the same questions in ways that circumscribe the legal authority of these agencies to obtain information. Any given interpretation of existing law in new and unanticipated technological circumstances may be valid legal reasoning, but the fundamental issue is whether that result offers the correct policy outcome. If not, perhaps the laws themselves need to change.

**SEARCH AND SEIZURE.** When the Fourth Amendment to the U.S. Constitution was adopted in 1792, outlining individual protections against search and seizure, human beings were the instrument of search. Today, computers can search for information, with vastly greater efficiency through much larger volumes. Does a "search" refer to the moment of data collection? The moment a computer is instructed to scan a corpus of collected data? The moment that a human being examines the results of the scan? What privacy is compromised when a computer examines information, decides it to be irrelevant, and passes it over without further attention? Is it a seizure when the government copies a data stream or a file without human examination? Some federal magistrates are demanding greater technical specificity from law enforcement agencies that seek to obtain electronic information (*1*). When upheld, such requirements narrow the scope of information these agencies may collect.

*Chief Scientist, Computer Science and Telecommunications Board, National Research Council, Washington, DC 20001, USA.*The views expressed here do not necessarily reflect those of the NRC, the CSTB, or any other organization. E-mail: hlin@nas.edu.*

***"Evolution of technology may call into question legal concepts formulated in an earlier technological context."***

More generally, the U.S. government has advocated an interpretation that querying a database is the threshold event that defines a search. Privacy advocates strenuously disagree, arguing that capturing data should be regarded as search. Such questions arise because computer-based searches are different from human searches, but their answers are judgments about the formulation of national policy.

**LOCAL VERSUS INTERNATIONAL STORAGE OF DATA.** As U.S. companies increasingly store data abroad for a variety of business reasons, how and to what extent, if any, does U.S. government access to such data require legal assent of the nations where data are stored? The U.S. government asserts that only a properly directed U.S. government action against a U.S. company is required. Companies seeking to protect data privacy argue that any U.S. demand for data must be legally authorized under domestic law of the nation in which the data are held.

In one recent case, a federal magistrate held that a search of e-mail would take place only when e-mail was opened, and if the e-mail (held by Microsoft in Ireland) was opened in the United States, only U.S. law was relevant. A federal judge upheld this decision, rejecting Mircosoft's argument that the search for relevant data would take place in Ireland and that it could not comply if the demand for data did not comport with Irish law (*2*).

**COLLECTION VERSUS USE.** Restrictions on data collection address whether certain data should be collected at all, and once collected, how long they may be retained. Restrictions on data use address the purposes for which data, once collected, may be used and/or the parties that may legitimately use that data; such restrictions for protecting privacy are endorsed in a 2014 White House report (*3*). Notably, the report does little to address issues raised by government surveillance, which has fueled speculation that the report may be intended to divert public attention to private-sector use of data.

The distinction is important because people will often consent to the gathering of information for one purpose but not for another. Few people object to the phone company's collecting metadata for billing purposes. But they may object to bulk collection of such information by government agencies.

Data that are not collected provide the maximal degree of privacy protection but are, by definition, unusable. Use-based privacy provides more flexibility in using data, but the degree of privacy protection depends on the scope of approved uses and on compliance to rules governing use. Perfect compliance with use-based protections cannot be assured, and thus, policy-makers must determine what level of noncompliance would make such protections ineffective.

**SECURING VERSUS SURVEILLING.** The U.S. government has sought to promote a global Internet that is safe, secure, and reliable. To this end, it undertakes many efforts, e.g., developing global standards to ensure secure communications. But it has been suggested that some parts of the U.S. government have sought to weaken standards for secure communication and to penetrate seemingly secure data communications pathways and storage facilities.

Whether or not the allegations about U.S. activities are true, a tension still exists. How, if at all, and to what extent should the United States seek to weaken security of products and services used in other nations to facilitate access for national security purposes (*4*) or attempt to penetrate the operational security of these products and services to obtain intelligence? How does it reconcile its own activities in international forums with complaints about other nations that also claim the right to monitor Internet traffic in the name of national security?

**NECESSARY VERSUS USEFUL.** Critics of U.S. collection efforts have argued that information derived from many surveillance programs has not been necessary in thwarting any terrorist plot. Less has been voiced about whether a given piece of information, even if not absolutely necessary, may still be useful. Intelligence analysis does not seek to reach a conclusion that might be possible from a minimal set of information but rather conclusions that are supported as much as possible. Although analysts may be swamped with so much information that crucial information is overlooked, it is hard to decide what information will be unnecessary before analysis is complete.

A more constructive debate would focus on the potential trade-off—if certain information is unavailable, what would be the impact on the analytical process? Does making certain information available enable reaching valid conclusions faster? With higher confidence? With a lower error rate?



*Published by AAAS*

How and to what extent, if any, are we willing to live with constraints on intelligence-gathering if their consequence is a less effective intelligence process?

**THE LIMITED ROLE OF TECHNOLOGY.** Fundamental scientific and technological realities underlie these issues, and it is tempting to think that problems originating in technology can be solved by judicious application of more technology. For example, the technology of information accountability has been proposed as a way to enforce use-based privacy restrictions. Data-mining systems based on this technology capture the logic underlying queries and inferences and record who is making such queries (*5*). Similarly, homomorphic encryption—a method for performing operations such as "sort" and "find" on encrypted data—is sometimes offered as a way to protect privacy of those whose data are stored in searchable databases (*6*).

If and when these technologies become available on a large scale, they may reassure some who are skeptical of U.S. government intentions. But to do so, appropriate policies and procedures must be in place to govern their use. For example, audits of query logs must actually be performed and users held accountable if transparent accountable data mining is to enhance privacy. Whether such policies and procedures will be followed is another matter entirely. Technologies, always embedded within a broader milieu of policy and procedures, will never be the sole—or necessarily most important—element of a solution to such dilemmas.

In January 2014, President Obama said that the United States would reduce the scope of phone metadata collection and called for explicit judicial authorization for nonemergency queries to the existing database of metadata information. He also extended some privacy protections to non-U.S. persons and forbade eavesdropping on the leaders of friendly nations. Legislation is pending in the U.S. Congress that would bar government collection of phone metadata in bulk. But these and other changes, adopted or proposed, leave many important issues unaddressed, and thus the policy debate is far from over. ■


**REFERENCES**

1. A. E. Marimow, C. Timberg, *Washington Post*, 24 April 2014; http://wapo.st/1o8L3Zf.
2. N. Wingfield, New York Times, 31 July 2014; http://bits.blogs.nytimes.com/2014/07/31/judge-rules-that-microsoft-must-turn-over-data-stored-in-ireland/.
3. President's Council of Advisors on Science and Technology, *Big Data and Privacy: A Technological Perspective* (White House, Washington, DC, 2014); http://1.usa.gov/1s79RBo.
4. E. Nakashima, *Washington Post*, 26 July 2014; http://wapo.st/1rTh2Qc.
5. D. J. Weitzner *et al.*, *Commun. ACM* **51**, 82–87 (2008).
6. C. Gentry, *Commun. ACM* **53**, 97 (2010).


10.1126/science.1251485

MEDICINE

# Letting go of mucus

## Defective release of mucus from airway glands is present at birth in cystic fibrosis

*By* **Jeffrey J. Wine**

The genetic disease cystic fibrosis (CF) results from mutations that disable an anion channel called cystic fibrosis transmembrane conductance regulator (CFTR). Loss of CFTR's anion channel functions triggers a cascade of defects that reduces the lung's innate mucosal defenses, including the critical component of mucus clearance (*1*, *2*). The lungs of individuals with CF, which appear grossly normal at birth, quickly become infected with bacteria and fungi localized within the lung mucus, which, like mucus in other CF organs, is thicker and more difficult to clear (*3*). The pathogenesis of CF airways has been difficult to determine because appropriate animal models have been lacking. On page 818 in this issue, Hoegger *et al.* (*4*) find that lung disease in a piglet model of CF is caused by abnormal tethering of mucus to the submucosal glands that produce it.

> ***"Maybe we will fix cystic fibrosis before we fully understand it."***

Hoegger *et al.* used computed tomography imaging of intact, anesthetized pigs to track the movements of 0.35-mm tantalum disks (which are visible with this type of imaging) in trachea and mainstem bronchi of pigs with and without CF. Imaging showed normal basal clearance by beating cilia. Columnar epithelial cells that line pulmonary airways bear cilia that sweep mucus out of the trachea and bronchi. By contrast, strong cholinergic stimulation, which elicits mucus secretion, accelerated clearance in normal pigs but not in pigs with CF, where many disks stopped moving, even though beating of cilia increased normally. No difference in the depth of periciliary liquid (which contacts the surface epithelial cells and lies below the superficial mucus layer) was detected.

In another approach, Hoegger *et al.* removed the tracheas from piglets, cut them along their ventral surface, and pinned them out so that mucociliary clearance over the dorsal mucosal surface could be imaged. CFTR, which conducts chloride ($Cl^-$) and bicarbonate ($HCO_3^-$) ions to mediate fluid secretion (*5*), is apically localized in both surface epithelia and in submucosal glands. To disrupt ion and fluid transport by surface epithelia, the authors submerged the tracheas in saline and then tracked mucus transport in the flooded airways.

The key finding was that in flooded CF tracheas, many tantalum disks were still immobile. To observe mucus movements more directly, Hoegger *et al.* dispersed fluorescent nanospheres in the saline, which stick to mucus. In submerged tracheas, even from piglets without CF, the nanospheres revealed strands of mucus emanating from submucosal gland ducts and stretching for hundreds of micrometers before they broke free and were transported up the airway. Sometimes the mucus strands broke apart, and the portion that remained tethered to the glands contracted back toward the duct.

Because some tethering of mucus to gland ducts occurred even in non-CF tracheas, Hoegger *et al.* employed another clever method to quantify it. A series of 32 images of a 10.2-$mm^2$ field were taken over a 4-s period and averaged, so that static beads produced bright signals whereas moving beads did not. A scanning stage was used to image tracheal areas of 163 to 358 $mm^2$. In submerged, non-CF tracheas, fewer than 6 "adherent entities" accumulated on average over a 45-min period, versus 15 to 50 entities in CF tracheas. Importantly, all of the adherent strands could be traced to submucosal gland ducts.

To assess the contributions of $HCO_3^-$ and $Cl^-$ anions to mucus secretion, Hoegger *et al.* used the same visualization methods to study mucus accumulation in submerged tracheas of pigs without CF after transport of each anion was blocked individually and together. Blocking either $Cl^-$ or $HCO_3^-$ alone, which reduces gland volume secretion by about half (*5*), had no appreciable effect on the amount of mucus tethering in submerged airways, whereas blocking both anions, which reduces volume secretion by >90% (*6*), resulted in tethering as severe as in the CF tracheas. This result fits neatly with the finding that mucin accumulation



Published by AAAS

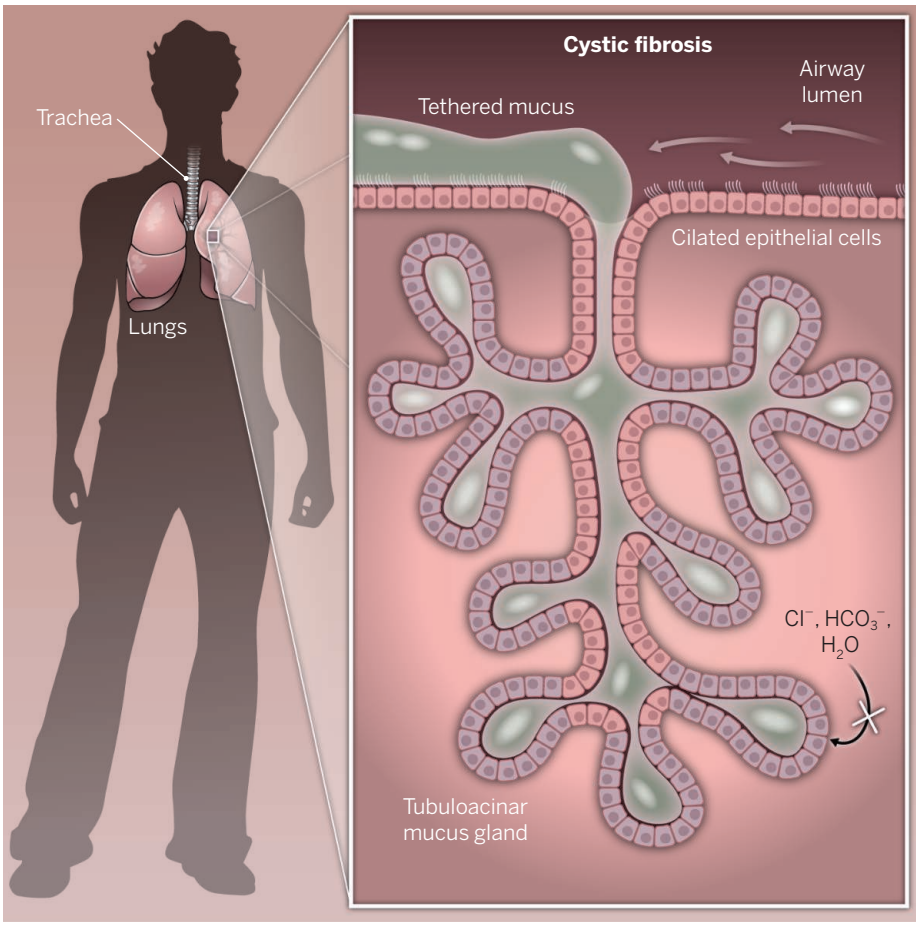


**Clearance.** Mucus-producing glands that line the human airway are multiply branched tubuloacinar structures. In cystic fibrosis, mucus remains anchored in the gland and is not swept out of the airway by ciliated epithelial cells.

ILLUSTRATION: C. BICKEL/*SCIENCE*

in gland ducts following cholinergic stimulation required blocking of both anions (*7*, *8*).

The finding of Hoegger *et al.* reveals a new aspect of airway submucosal gland dysfunction in CF. It has long been hoped that the contentious problem of how CF lung disease starts could be addressed in CF animal models. Indeed, when five pigs with CF were kept alive for up to 5 months, they developed CF pulmonary disease with infection, inflammation, and mucus obstruction similar to that seen in humans with CF (*9*). These experiments are unlikely to be repeated widely because exhaustive effort is required to raise pigs with CF-related disruptions of their digestive systems (*10*). This has enforced a focus on newborn piglets, but this constraint has had the salutary effect of producing abundant new evidence about the chicken-and-egg questions that have bedeviled the CF field for decades; that is, whether, defective airway mucus clearance is a primary cause of the disease or is a secondary consequence of infection and inflammation. The findings of Hoegger *et al.* suggest that it is a primary cause.

By calling attention to mucus tethering in CF airways and supplying new methods to study it, Hoegger *et al.* initiate a new paradigm with new questions. These include the mechanisms by which mucus is normally released from glands (see the figure); why cholinergic stimulation of fluid secretion, which occurs mainly by non-CFTR pathways (*11*, *12*), produces such profound consequences in pigs with CF; and whether physiological amounts of acetylcholine from the vagus nerve will produce the same result as the strong specific stimulus (for the muscarinic acetylcholine receptor) that was used in their study.

Observing mucus transport in submerged airways was a brilliant stroke that effectively clamped the surface composition and volume. But could this approach have allowed the scant (*6*), high-solids mucin aggregates (*7*) that form when anion secretion is blocked to expand in the bathing fluid, as they do normally in other organs and on the surfaces in aquatic animals? If so, this may have amplified the subtle differences in clearance between CF and control animals in vivo. A more precise estimate of the tethering phenomenon should prove useful going forward. Hoegger *et al.* used a four-point "tethered mucus score" because fluorescence from beads attached to mucus from regions outside the imaged field made more exact measurement difficult; so an average of "2" for pigs with CF means that 15 to 50 adherent entities accumulated over 163 to 358 $mm^2$. With ~10 glands per $mm^2$ in newborn pig tracheas (*12*), this would represent tethering to 0.4 to 3% of the ducts.

Most individuals with CF eventually succumb to chronic pulmonary infections. Pathogens are localized in the mucus, so increased mucus tethering could trigger CF pulmonary disease and would exacerbate it. Do the findings of Hoegger *et al.* suggest new ways in which CF lung disease should be treated? Submucosal glands are an abundant source of the mucin MUC5B in human upper airways. Reducing the amount of mucus secreted seems ill advised, given the devastating effects of eliminating MUC5B from mouse airways (*13*). But strategies to improve the release of mucus from glands might be considered.

The exciting findings of Hoegger *et al.* bolster evidence that mucus clearance, submucosal glands, anion secretion, and mucus maturation are worthy of the attention being devoted to them by CF researchers. As the evidence mounts that these defects are seen within hours of birth, failure to intervene early is increasingly indefensible. However, the study also underscores the complexities of airway innate defenses and the multiple defects that follow loss of CFTR function. Given the recent progress in attacking CF at its source, it may be time to resurrect a saying that has been out of fashion since the early heady days of gene therapy: Maybe we will fix cystic fibrosis before we fully understand it. ■

*CF Research Laboratory, Department of Psychology, Stanford University, Stanford, CA 94305–2130, USA. E-mail: wine@stanford.edu*

## REFERENCES

1. M. R. Knowles, R. C. Boucher, *J. Clin. Invest.* **109**, 571 (2002).
2. J. J. Wine, N. S. Joo, *Proc. Am. Thorac. Soc.* **1**, 47 (2004).
3. P. M. Quinton, *Am. J. Physiol. Cell Physiol.* **299**, C1222 (2010).
4. M. J. Hoegger *et al.*, *Science* **345**, 818 (2014).
5. R. A. Frizzell, J. W. Hanrahan, *Cold Spring Harb. Perspect. Med.* **2**, a009563 (2012).
6. N. S. Joo, Y. Saenz, M. E. Krouse, J. J. Wine, *J. Biol. Chem.* **277**, 28167 (2002).
7. S. K. Inglis, M. R. Corboz, S. T. Ballard, *Am. J. Physiol.* **274**, L762 (1998).
8. S. T. Ballard, D. Spadafora, *Respir. Physiol. Neurobiol.* **159**, 271 (2007).
9. C. S. Rogers *et al.*, *Science* **321**, 1837 (2008).
10. D. A. Stoltz *et al.*, *J. Clin. Invest.* **123**, 2685 (2013).
11. R. J. Lee, J. K. Foskett, *Am. J. Physiol. Lung Cell. Mol. Physiol.* **298**, L210 (2010).
12. N. S. Joo, H. J. Cho, M. Khansaheb, J. J. Wine, *J. Clin. Invest.* **120**, 3161 (2010).
13. M. G. Roy *et al.*, *Nature* **505**, 412 (2014).

10.1126/science.1258493



*Published by AAAS*

CHEMISTRY

# Self-assembled RNA nanostructures

## RNA structures have been designed that self-assemble and are programmable and scalable

*By* **Neocles B. Leontis**[1] *and* **Eric Westhof**[2]

The aim of nanobiotechnology based on nucleic acids is to make three-dimensional objects with both precise architecture and function that can be programmed via their sequence. The ultimate goal is to build self-assembling, biologically active nanostructures within targeted cells by harnessing the cellular nucleic acid synthesis and assembly machineries. On page 799 of this issue, Geary *et al.* (*1*) move us closer to this goal by designing RNA "tiles" that can fold into modular units as they are transcribed.

DNA nanotechnology relies on double-stranded base-paired helices and on the recurrent use of a small number of structural motifs (*2*). Multiple DNA strands are combined in a precise order in vitro to build programmed subassemblies through complementary Watson-Crick base pairing, thereby achieving complex hierarchical structures. A major challenge facing the field is how to extend this engineering approach in vivo, where complex objects must form entirely by self-assembly without the help of a deus ex machina. No technology currently exists to routinely synthesize short DNA strands within cells. However, cells can be readily programmed to synthesize RNA molecules of arbitrary sizes, which makes the report of Geary *et al.* all the more noteworthy.

Work on immobile four-way junctions (where four helices meet) marked the beginning of DNA nanotechnology (*2*, *3*). The inherent flexibility of four-way and three-way junctions made them suitable for constructing a variety of polyhedra in which DNA double helices formed the edges and junctions formed the vertices (*3*, *4*). To construct repeating planar arrays, the four-way junctions needed to be combined with each other to form more rigid planar tiles. The next major advance was marked by the design of programmable antiparallel, double-crossover tiles. This was followed by the invention of "DNA origami"—a method to make arbitrary planar shapes by folding a long, single strand of DNA using hundreds of short "staples" made of complementary DNA strands (*5*). The origami method was adapted to make 3D shapes, first as surfaces, leading to polyhedra having faces as well as edges of DNA, and then to build DNA programmable "bricks" composed of parallel layers of helices that can be combined to create DNA arrays (*6*) or 3D tubular (*7*) or waffle-like structures (*8*).

Unlike DNA, the inherent architectural potential of RNA extends far beyond RNA double-stranded helices. RNA can form a variety of distinct base pairs having at least two hydrogen bonds. The various types can be grouped into 12 main families, including the canonical Watson-Crick family (*9*). The 11 families of non–Watson-Crick base pairs enable RNA to form a large number and variety of recurrent structural modules that serve as the building blocks of the tertiary architecture of folded RNA transcripts. RNA nanotechnology can draw on these naturally occurring 3D modules and their predictable interactions (*10*), many of which are now known at atomic resolution from large biologically active RNA structures, notably ribosomes, ribozymes of various kinds, and natural RNA aptamers embedded in riboswitches.

One of the holy grails of RNA nanotechnology has been to rationally design objects comparable in size and complexity to natural RNA machines like the ribosome and spliceosome, as well as current highly sophisticated DNA nanostructures. However, a general blueprint has been lacking for the construction of complex RNA-based objects that rival those already achieved for DNA-based objects. The aim is to take advantage of the unique assembly properties of RNA manifest in natural RNA complexes. Such a goal is also subject to the limitations imposed by in vivo synthesis, namely, continuous transcription from a DNA template using a processive RNA polymerase enzyme.

In the cellular environment, RNA molecules are synthesized under essentially isothermal conditions by transcription in the 5′ to 3′ direction. The rate of synthesis is much slower than the rate at which the newly formed RNA strands fold to form local hairpin structures, generally organized by multiway junctions, to yield functional subdomains. Because of the favorable ionic conditions of the cellular environment (i.e., moderate ionic strength and an ample concentration of $Mg^{2+}$ ions), as soon as local structures form,

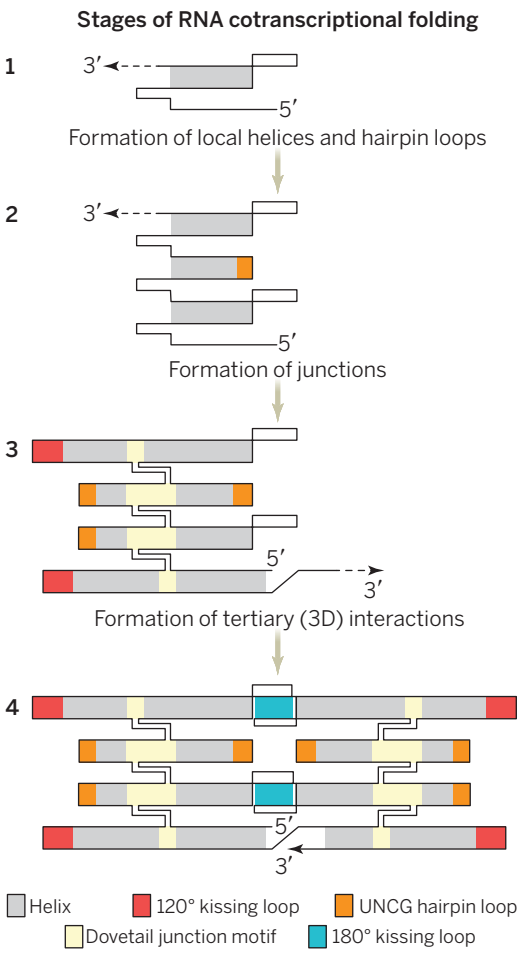


**RNA origami in real time.** The proposed stages of RNA cotranscriptional folding for an RNA tile. (**1**) The first hairpin stem-loop folds upon synthesis (gray box). (**2**) More hairpin loops form, some of which are capped by stable UNCG loops. (**3**) The first domain of the tile is completed with the right number of modules in the sequence to interact with the second domain, once it is made. Finally, in (**4**), the tertiary contacts (blue) between the two subdomains are established through kissing-loop interactions, completing the synthesis and self-assembly of the tile, which can assemble with other tiles using the preformed hairpin loops (red).

[1]*Chemistry Department, Bowling Green State University, Bowling Green, OH, USA.* [2]*Institut de biologie moléculaire et cellulaire du CNRS, Architecture et Réactivité de l'ARN, Strasbourg, France. E-mail: leontis@bgsu.edu; e.westhof@ibmc-cnrs.unistra.fr*



Published by AAAS

they can begin to assemble to form tertiary structures. In the case of designed RNAs, once modular building blocks (i.e., tiles) fold, they can join with other units to form larger repeating structures using stereochemically precise long-range interactions programmed into the sequence.

Geary *et al.* have artfully used these principles of RNA architecture, modularity, and folding to design planar, extensible RNA tiles that can be synthesized as continuous strands and can fold cotranscriptionally to form modular units. The tiles themselves are programmed to fold through the formation of modules. The modules are carefully positioned in the secondary structure to mediate internal tertiary interactions (see the figure) taking the place of the staple strands used in DNA origami. Self-assembly of tiles into supramolecular structures is achieved by positioning sequences on the periphery of individual tiles that form addressable and programmable "kissing hairpin" interactions, the RNA equivalent of DNA "sticky ends."

The work of Geary *et al.* is particularly timely because it provides a valuable new tool for the rapidly growing field of synthetic biology, which seeks to develop and apply new engineering principles to modify and improve existing forms of life. Up to now, developments in synthetic biology have been mostly limited to sequence-based tinkering with gene expression programs, with only rare forays into explicit use of 3D architectural modules (*11*, *12*). Many new types of RNAs have been discovered in just the last few years, but understanding of their roles and mechanisms of action has lagged behind because of lack of adequate tools to manipulate RNA in vivo. The approach of Geary *et al.* should allow nanotechnologists and synthetic biologists to apply much of what has been learned working with DNA to RNA to create tools to move this technology into living cells and organisms. These tools should revolutionize our understanding of the cell, and perhaps of life itself. ■


**REFERENCES**

1. C. Geary, P. W. K. Rothemund, E. S. Andersen, *Science* **345**, 799 (2014).
2. N. C. Seeman, N. R. Kallenbach, *Biophys. J.* **44**, 201 (1983).
3. E. Winfree, F. Liu, L. A. Wenzler, N. C. Seeman, *Nature* **394**, 539 (1998).
4. J. Zheng *et al.*, *Nature* **461**, 74 (2009).
5. P. W. Rothemund, *Nature* **440**, 297 (2006).
6. B. Wei, M. Dai, P. Yin, *Nature* **485**, 623 (2012).
7. M. Endo *et al.*, *Angew. Chem. Int. Ed. Engl.* (2014)
8. T. Yamazaki, J. G. Heddle, A. Kuzuya, M. Komiyama, *Nanoscale* **6**, 9122 (2014).
9. N. B. Leontis, E. Westhof, *RNA* **7**, 499 (2001).
10. A. Chworos *et al.*, *Science* **306**, 2068 (2004).
11. T. Hara, H. Saito, T. Inoue, *Chem. Commun. (Camb.)* **49**, 3833 (2013).
12. Y. Krishnan, F. C. Simmel, *Angew. Chem. Int. Ed. Engl.* **50**, 3124 (2011).


10.1126/science.1257989

ILLUSTRATION: V. ALTOUNIAN/*SCIENCE*

EPIGENETICS

# You are what you eat, but what about your DNA?

## Parental nutrition influences the health of subsequent generations through epigenetic changes in germ cells

*By* **Martha Susiarjo** *and* **Marisa S. Bartolomei**

Human and animal studies have demonstrated that the prenatal environment affects adult health and disease. Epidemiological studies have shown that gestational exposure to maternal starvation or overnutrition of the paternal grandfather is linked to increased risks for cardiovascular diseases and diabetes (*1*, *2*). In both cases, adverse metabolic health outcomes can be transmitted multigenerationally. As well, pregnant rats fed low-protein diets produced two sequential generations of offspring that became diabetic as adults (*3*). Nevertheless, despite considerable research efforts elaborating the phenotypic consequences of in utero insults to adult offspring and to their progeny, the mechanisms mediating multigenerational effects are unclear. On page 785 of this issue, Radford *et al.* (*4*) undertook an in-depth, genome-wide approach using a mouse model of undernutrition. This model has been linked to low birth weight, glucose intolerance, and reduced pancreatic function in two subsequent generations (*5*). Radford *et al.* not only provide convincing mechanistic insights about the transmission of phenotypes to later generations, their findings also suggest a path forward for pursuing these types of detailed studies.

Because prenatal exposures are associated with adverse phenotypes much later in life, it is postulated that epigenetic mechanisms are involved. That is, heritable changes in DNA that are not accompanied by a change in DNA sequence could be responsible for remembering the insult. Epigenetic mechanisms include DNA methylation and changes in chromatin structure, noncoding RNA, and nuclear organization. The epigenetic mechanism commonly implicated in heritable transmission of a phenotype is DNA methylation. Other fetal exposure models have been associated with altered DNA methylation at the *IGF2* gene in humans (*1*) and the *PPARα* gene in rats (*6*). As such, in the absence of further environmental insults, one potential mechanism of how fetal perturbation influences the health of the subsequent generations is through germline epigenetic inheritance. Thus, the epigenetic signature of the sperm or oocyte from individuals who were reprogrammed in utero (i.e., the $F_1$) is transmitted to the next generation (i.e., the $F_2$).

To test the hypothesis that altered DNA methylation mediates the phenotypes of the undernutrition mouse model, Radford *et al.* used methylated DNA immunoprecipitation (MeDIP)–sequencing and bisulfite pyrosequencing and show that in utero caloric restriction in parent mice affects locus-specific DNA methylation patterns in the sperm from their offspring (adult $F_1$ mice) (see the figure). The nutritional stress occurred during late

gestation when primordial germ cells are epigenetically reprogrammed and are reacquiring DNA methylation specifically in the male germ line. Two independent pools of sperm derived from four representative litters per pool (one mouse per litter) were compared between control and undernutrition groups. A total of 111 hypomethylated regions from the nutritionally restricted $F_1$ males were identified. Of 24 randomly selected hypomethylated regions, 17 were validated, indicating that ~70% of hypomethylated candidate sequences were true differentially methylated regions. Although hypermethylated regions were also identified, none were validated when assayed by bisulfite pyrosequencing, demonstrating the importance of validation of candidate sequences by an alternative method on independent samples.

The presence of novel hypomethylated regions suggested that primordial germ cells from nutritionally restricted fetuses did not completely remethylate their DNA. These hypomethylated regions were sequences that remethylate later in normal primordial germ cells (*7*); hence, adverse fetal environment

*Department of Cell and Developmental Biology, Perelman School of Medicine, University of Pennsylvania, Philadelphia, PA 19104, USA. E-mail: bartolom@mail.med.upenn.edu*



*Published by AAAS*

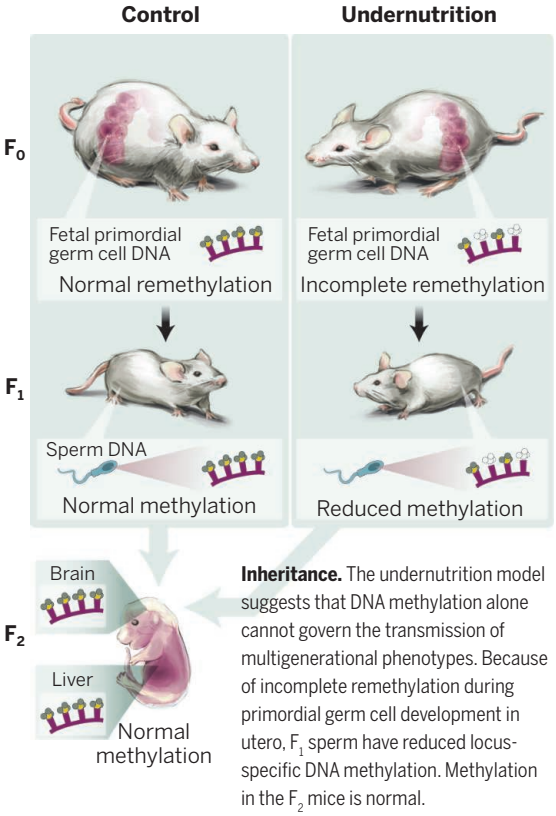


**Inheritance.** The undernutrition model suggests that DNA methylation alone cannot govern the transmission of multigenerational phenotypes. Because of incomplete remethylation during primordial germ cell development in utero, $F_1$ sperm have reduced locus-specific DNA methylation. Methylation in the $F_2$ mice is normal.

perturbed the epigenome nonrandomly. Furthermore, 21% of the hypomethylated regions overlapped with regions previously shown to be nucleosome-enriched (*8*), which is striking, because 99% of histones are normally replaced by protamines in mature sperm to facilitate packaging. The observation suggested that nutritional restriction in utero may have altered chromatin architecture of the sperm.

To determine whether the altered $F_1$ sperm epigenetic state could be transmitted to the $F_2$ generation, Radford *et al.* mated young, prediabetic $F_1$ males with control females and then assessed DNA methylation in $F_2$ liver and brain at embryonic day 16.5 (E16.5). The use of a paternal transmission strategy excluded maternal effects during pregnancy. Analysis of late embryonic $F_2$ tissues demonstrated that DNA methylation at the differentially methylated regions was reset and reprogrammed such that, by E16.5, methylation between control and food-restricted $F_2$ offspring was similar. However, a few genes in close proximity to the differentially methylated regions still displayed differential expression at E16.5. Together, the data suggest that DNA methylation may not be the primary epigenetic mechanism underlying the inherited gene expression profile and phenotypes in the $F_2$ offspring, although this remains to be determined. These observations are in contrast to results from a study that used a similar undernutrition mouse model in which a slight differential methylation at the *Lxra* locus was maintained in the $F_2$ generation (*9*). That study, however, used a candidate approach by first identifying transcriptional differences between control and undernutrition groups and then assaying candidate sequences. Differences in mouse chow ingredients and husbandry conditions could also contribute to the discrepancies between studies.

How nutritional deficiency in utero leads to multigenerational phenotype transmission remains unclear. The presence of hypomethylated regions in the $F_1$ sperm suggests that DNA methylation initially mediates environmental perturbation–induced developmental changes, but secondary epigenetic mechanisms must be involved. DNA methylation changes at other regions not detected by MeDIP sequencing may also be relevant to the affected developmental loci. Alternatively, other epigenetic modifications operate at these loci and mediate the inheritance of phenotypes. Histone H3 $Lys^4$ and $Lys^{27}$ trimethylation (H3K27me3 and H3K4me3, respectively) are found in nucleosome-enriched developmental loci in sperm (*8*), implicating histone modifications as a potential mechanism for paternal transmission to the next generation. Another possible mechanism could involve small RNAs, as shown in a *Caenorhabditis elegans* caloric restriction model (*10*).

Radford *et al.* provide a model of how whole-genome approaches followed by independent validation should be conducted in analogous studies. Although DNA methylation plays an important role in nutritional restriction–induced developmental changes, other epigenetic mechanisms mediating multigenerational inheritance should be investigated. ■


**REFERENCES**

1. T. J. Roseboom *et al.*, *Mol. Cell. Endocrinol.* **185**, 93 (2001).
2. G. Kaati, L. O. Bygren, S. Edvinsson, *Eur. J. Hum. Genet.* **10**, 682 (2002).
3. K. A. Lillycrop, E. S. Phillips, A. A. Jackson, M. A. Hanson, G. C. Burdge, *J. Nutr.* **135**, 1382 (2005).
4. E. J. Radford *et al.*, *Science* **345**, 1255903 (2014); 10.1126/science.1255903.
5. J. C. Jiménez-Chillaron *et al.*, *Diabetes* **58**, 460 (2009).
6. H.-J. Park *et al.*, *J. Clin. Invest.* **118**, 259 (2008).
7. S. Seisenberger *et al.*, *Mol. Cell* **48**, 849 (2012).
8. S. Erkek *et al.*, *Nat. Struct. Mol. Biol.* **20**, 868 (2013).
9. D. Martínez *et al.*, *Cell Metab.* **19**, 941 (2014).
10. O. Rechavi *et al.*, *Cell* **158**, 277 (2014).


10.1126/science.1258654

WATER TREATMENT

# Replace contamination, not the pipes

## Rethinking water treatment additives can have synergistic benefits for urban water management systems

*By* **Wolfgang Rauch** *and* **Manfred Kleidorfer**

Wastewater from urban settlements contains—among a multitude of other substances—sulfate ($SO_4^{2-}$). Under anaerobic conditions, $SO_4^{2-}$ can be biologically converted into toxic hydrogen sulfide gas ($H_2S$) and further to corrosive sulfuric acid ($H_2SO_4$), which results not only in noxious odors but also health issues and damage to sewer systems. This "sulfide problem" in sewers has long been recognized, but until recently, efforts have focused only on mitigation strategies for sulfide emissions in sewers. On page 812 of this issue, Pikaar *et al.* (*1*) provide an alternative to current technical measures—source control. They argue that by using substitutes for $SO_4^{2-}$, which is often used as a coagulant in the treatment of water, the $SO_4^{2-}$ concentration in the wastewater can be reduced such that $H_2S$ no longer affects sewer infrastructure.

Traditional urban water management usually involves the following (illustrated in the figure). After the uptake and treatment of raw water, drinking water is distributed to the end users. Waste and stormwater are then collected from the end users and surrounding environment and treated for release. An observer may see this as one technical system for managing water, but in reality, it is segmented into the subsystems of water supply and sanitation. Such partitioning into "clean" and "dirty" water is not only administrative but fundamental and is found at all levels, from operators to research. The advantages of taking a more integrated view of the urban water cycle have been noted (*2*), but barriers to implementation remain.

*Institute of Infrastructure Engineering, University Innsbruck, Technikerstrasse 13, 6020 Innsbruck, Austria. E-mail: wolfgang.rauch@uibk.ac.at*

ILLUSTRATION: V. ALTOUNIAN/*SCIENCE*



Published by AAAS

This network-based water system is commonly seen as a technological success story and as a main contributor to improved human health. For example, for sanitation, around 64% of the world population lives in a dwelling connected to sanitation systems (*3*). However, the underground sewer system comes at a price. Assuming typical replacement values for sanitation systems at ~$3000 per capita (without wastewater treatment), we can assess global investments of more than $10 trillion for sewer networks that need to be maintained. This amounts to 10 to 20% of the annual global gross domestic product (*4*).

rates on the order of several millimeters per year.

Although the mechanism is undisputed (*6*), it is relevant to ask about the sources for this "sulfide problem." Sulfate is found in all types of urban wastewater. It originates from geologically induced background concentration in source water, from municipal waste products, and, when applied, from the use of aluminum sulfate or ferric sulfate as a coagulant in treatment of raw water. Hydrogen sulfide emission in sewers is favored by oxygen-limited conditions and warm temperature. Such circumstances are found in many

There are many other examples that outline the benefits of a holistic view to urban water management. For the past three decades, the phosphate content of laundry detergents has been steadily reduced by switching to substitutes, thus decreasing the phosphorus concentration in the wastewater. Because this source control measure is successfully mitigating eutrophication in inland waters (*8*), it is a commonly cited successful intervention. One could even ask whether decentralized solutions in water management (*4*) could avoid the sulfide problem altogether. This is certainly true when all wastewater is treated or reused

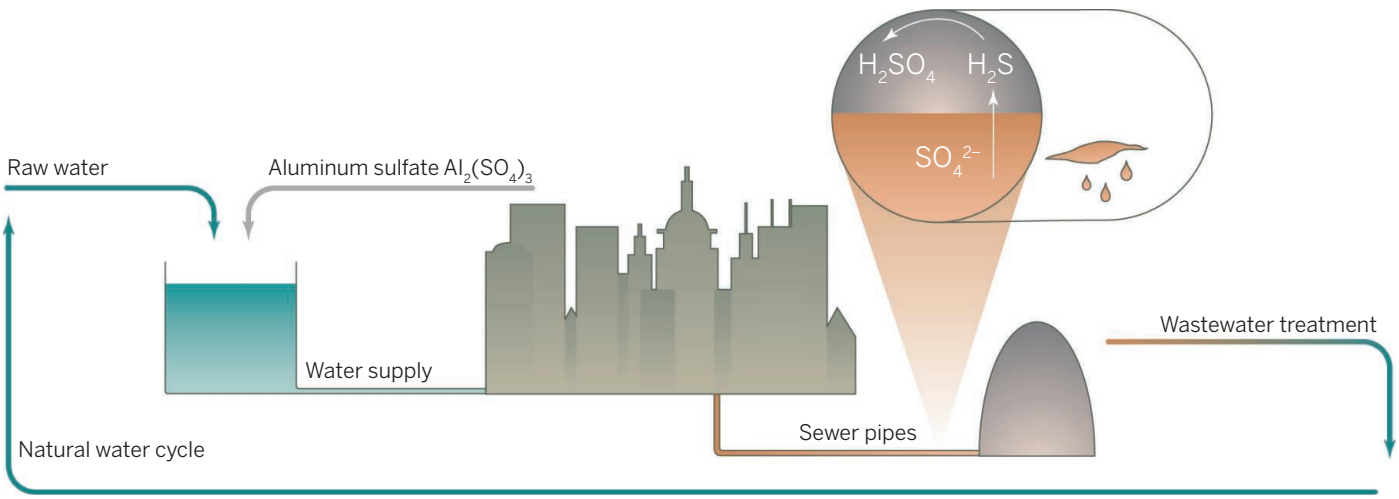


**Breaking the link.** Pikaar *et al.* show that substitution of aluminum sulfate as a coagulant prevents $H_2S$ formation and resulting corrosion by $H_2SO_4$ in downstream sewer pipes.

More than a century after the implementation of modern sewer systems, the age of much of this infrastructure already makes their maintenance a challenge. The deterioration of sewer pipes depends mainly on factors such as type and quality of construction material, soil and sewage quality, and external impacts such as traffic loads or climate. Typically, engineers estimate the average life span of sewers at 50 to 100 years, which leads to necessary annual investments of 1 to 2% of the replacement values. Thus, any technological improvement that helps to increase the service life of sewers by 1 year would save globally more than $1 billion per year.

For concrete pipes, the reduction of sulfide can be seen as such a technology. The detrimental effect of $SO_4^{2-}$ to sewer pipes was first described in 1900 (*5*). $SO_4^{2-}$ in the wastewater is reduced by anaerobic bacteria (primarily *Desulfovibrio* in biofilm and sediments) to $H_2S$. Once emitted to the sewer atmosphere, $H_2S$ is not only a health and odor issue but also oxidized to $H_2SO_4$ by aerobic bacteria from the family *Thiobacillus*. In concrete pipes, $H_2SO_4$ leads to concrete corrosion with deterioration

sewer systems, particularly in pressurized pipe sections after pumping stations. Combined systems (which collectively discharge stormwater and sewage) are generally less affected because of sufficient ventilation in dry weather and elevated flow during rain conditions. The corrosion caused by $H_2SO_4$ is essentially limited to concrete pipes that prevail in highly urbanized areas as being the dominant material for large-diameter pipes.

Because none of the influencing factors stated above is seemingly easy to control, mitigation measures have usually focused on $H_2S$ removal after formation (*7*). The costs arising from such technical interventions are on the same order as the loss in asset value caused by sulfide-induced deterioration. Pikaar *et al.* took a wider look at the problem and identified the obvious link between water supply and sanitation. Replacing the $SO_4^{2-}$ in water treatment by sulfate-free coagulants (e.g., ferric chloride or polyaluminum chloride) or alternative measures (e.g., membrane-based nanofiltration) is a simple source control measure that can at least counteract if not solve the sulfide problem.

on site, thus completely avoiding the piped sanitation system. However, a combination of decentralized solutions and existing sewers will most likely prevail. The resulting decrease in sewage flow can exacerbate $H_2S$ problems in existing systems.

There is a long history of making wrong decisions in complex technical systems if the components are viewed in a segregated way. Understanding processes, interlinkages, and consequences in the complete urban water cycle allows identification of optimal solutions. ■

## REFERENCES


1. I. Pikaar *et al.*, *Science* **345**, 812 (2014).
2. P. M. Bach, W. Rauch, P. S. Mikkelsen, D. T. McCarthy, A. Deletic, *Environ. Model. Softw.* **54**, 88 (2014).
3. World Health Organization, *Progress on Drinking Water and Sanitation: 2014 Update* (WHO and UNICEF, WHO Press, Geneva, 2014).
4. T. A. Larsen, K. M. Udert, J. Lienert, Eds., *Source Separation and Decentralization for Wastewater Management* (IWA Publishing, London, 2013).
5. F. H. Olmsted, H. Hamlin, *Eng. News* **44**, 19 (1900).
6. T. Hvitved-Jacobsen, J. Vollertsen, A. H. Nielsen, *Sewer Processes: Microbial and Chemical Process Engineering of Sewer Networks* (CRC Press, Boca Raton, FL, ed. 2, 2013).
7. L. Zhang *et al.*, *Water Res.* **42**, 1 (2008).
8. A. W. Maki *et al.*, *Water Res.* **18**, 893 (1984).


10.1126/science.1257988

ILLUSTRATION: P. HUEY/*SCIENCE*



*Published by AAAS*

BIOCHEMISTRY

# One step closer to $O_2$

## A crucial step in photosynthesis is becoming clearer

*By* **R. David Britt** *and* **Paul H. Oyala**

Photosynthetic organisms such as plants use the protein complex photosystem II (PS II) to split water using the energy of photons, generating molecular oxygen as a by-product. This photon-powered chemistry is a paradigm for developing catalysts for solar-generated fuels. Recent x-ray structures (*1*) have provided a detailed picture of the water-splitting 4 Mn–1 Ca cluster of PS II (see the figure); this cluster goes through a number of states during photosynthesis. On page 804 of this issue, Cox *et al.* (*2*) present electron paramagnetic resonance (EPR) results providing details of the state that is only one photon away from producing $O_2$. The results get us closer to understanding this key reaction.

Oxidation of two bound water molecules in PS II requires transfer of four electrons. This transfer occurs one electron at a time, starting with chlorophyll-based photooxidation of a tyrosine. The resulting tyrosine radical, $Y_Z^{\bullet}$, in turn oxidizes the Mn cluster in a series of intermediates, $S_0$ to $S_4$. $O_2$ is released 1 ms after the highly oxidized $S_4$ state is formed. All but the short-lived $S_4$ state have been trapped at low temperatures, allowing detailed study of these states (*3*, *4*).

EPR spectroscopy is most commonly performed on chemical systems with an odd number of unpaired electrons, as in the $S_0$ and $S_2$ states. Species with an even number of electrons—such as the $S_3$ state—are more difficult to study with EPR, because they may be either diamagnetic (total spin $S = 0$) and hence invisible to EPR, or have a nonzero integer spin ($S = 1$, 2, etc.). In the latter case, the interactions of multiple electron spins (zero field splitting, ZFS) may broaden or even eliminate transitions. The effects of ZFS may be mitigated by using higher microwave resonance frequencies. To study the integer-spin ($S = 3$) $S_3$ state, Cox *et al.* use a frequency 10 times that previously used. Instead of the very broad EPR signal previously assigned to the $S_3$ state (*5*), they obtain a very well resolved signal centered nearer the free electron resonance.

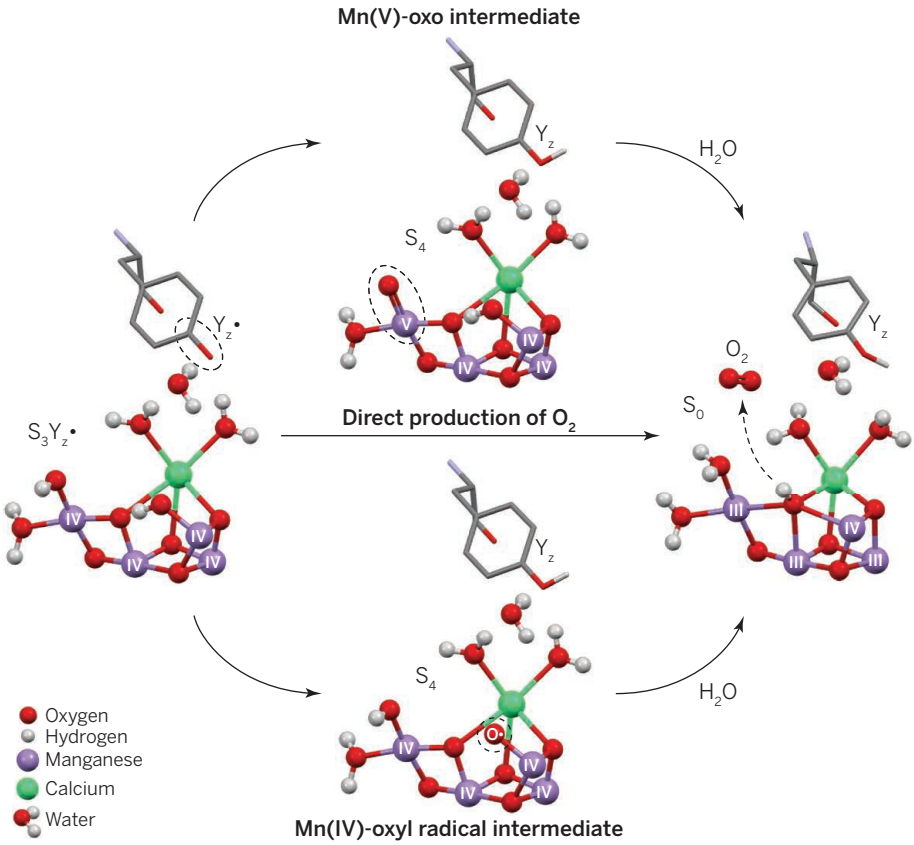


**Three possible paths.** Starting from the $S_3$ state characterized by Cox *et al.* and the tyrosine radical, $Y_Z^{\bullet}$, there are three possible mechanisms for the final step of $O_2$ evolution. Dashed lines denote the location of the electron hole.

Analysis of the line shape of the $S_3$ signal reveals a small ZFS, comparable to that of a synthetic $Mn(IV)_3CaO_4$ complex (*6*) and less than would be observed if $S_3$ contained one or more Mn(III) ions. High-resolution pulse EPR experiments confirm a six-coordinate Mn(IV) assignment for all four Mn ions. Computational modeling supports an "open cubane" structure in the $S_3$ state (see the figure). This structure closely matches that proposed by Siegbahn (*7*).

The all-Mn(IV) assignment of the $S_3$ state has important implications for the mechanism of $O_2$ formation (see the figure). $S_3$ and the tyrosine radical $Y_Z^{\bullet}$ may be the immediate precursors to $O_2$, as described in the H-atom abstraction model (*8*). This simple model fell out of favor when high-resolution x-ray structures showed that $Y_Z^{\bullet}$ forms hydrogen bonds with water molecules of the redox-inert $Ca^{2+}$ rather than a redox-active Mn ion. Alternatively, further oxidation of one Mn atom would give an $S_4$ state, generating a single Mn(V) species that could form an O-O bond with a $Ca^{2+}$-bound water or hydroxide (*9*). Such a high-spin Mn(V)-O species is unknown in other biological contexts but has been synthesized (*10*). Finally, in the transient $S_4$ state, the electron hole may be localized on a substrate O atom, as in the water-splitting mechanism in (*7*).

It may be possible to discriminate between these mechanisms with time-resolved x-ray spectroscopy and diffraction (*11*, *12*). With Cox *et al.*'s study giving a new description of the structure of the $S_3$ state, only one step removed from $O_2$ formation, we are rapidly closing on a detailed picture of this crucial water-splitting reaction. ■

*Department of Chemistry, University of California, Davis, CA 95616, USA. E-mail: rdbritt@ucdavis.edu*

### REFERENCES

1. Y. Umena, K. Kawakami, J. R. Shen, N. Kamiya, *Nature* **473**, 55 (2011).
2. N. Cox *et al.*, *Science* **345**, 804 (2014).
3. J. Yano, V. Yachandra, *Chem. Rev.* **114**, 4175 (2014).
4. N. Cox, D. A. Pantazis, F. Neese, W. Lubitz, *Acc. Chem. Res.* **46**, 1588 (2013).
5. A. Boussac, M. Sugiura, A. W. Rutherford, P. Dorlet, *J. Am. Chem. Soc.* **131**, 5050 (2009).
6. S. Mukherjee *et al.*, *Proc. Natl. Acad. Sci. U.S.A.* **109**, 2257 (2012).
7. P. E. M. Siegbahn, *Biochim. Biophys. Acta* **1827**, 1003 (2013).
8. C. W. Hoganson, G. T. Babcock, *Science* **277**, 1953 (1997).
9. J. Limburg, V. A. Szalai, G. W. Brudvig, *J. Chem. Soc., Dalton Trans.* **1999**, 1353 (1999).
10. T. Taguchi *et al.*, *J. Am. Chem. Soc.* **134**, 1996 (2012).
11. J. Kern *et al.*, *Science* **340**, 491 (2013).
12. C. Kupitz *et al.*, *Nature* 10.1038/nature13453 (2014).

10.1126/science.1258008



Published by AAAS

CLIMATE CHANGE

# *Does springtime feel extra early?*

*By* **Adam C. Schneider**

Henry David Thoreau spent much of 23 August 1853 walking the environs of Concord, Massachusetts. He noted the advancing of summer to autumn in no fewer than 27 species of plants and six species of animals while exhorting "Live in each season as it passes; breathe the air, drink the drink, taste the fruit, and resign yourself to the influences of each" (*1*).

A century and a half later, in *Walden Warming: Climate Change Comes to Thoreau's Woods*, Richard Primack finds that the seasons Thoreau lived in no longer match the ones we encounter. Primack uses the extensive and meticulous phenological observations (periodic natural phenomena that are influenced by climate and season) made by Thoreau and nearly two dozen subsequent naturalists and organizations, including himself, to illustrate climate-induced changes in seasonal biotic and abiotic events over the past 150 years. These changes are already profoundly evident in New England. Primack shows that a wide variety of seasonal events—including ice breakup on Walden Pond, the first flowering time of native plants, and animal migrations—happen up to several weeks earlier today then during the mid-1800s. In addition to conveying the impressive conclusions of over a decade of research, *Walden Warming* is part memoir and part call to action to become more engaged with nature and combat climate change.

The chapters are organized thematically and arranged chronologically by when Primack and his colleagues became aware of the various sets of phenological records. In this way, the book follows the natural flow of Primack's research program, from plants to birds, insects, fish, and even people. Accordingly, claims made earlier in the book, such as the extent of climate-induced changes in plant flowering times, are more convincing, as they are supported by a larger legacy of scrutiny and analysis.

*The reviewer is at the Department of Integrative Biology and University and Jepson Herbaria, University of California, Berkeley, CA 94720, USA. E-mail: acschneider@berkeley.edu*

**Walden Warming**
**Climate Change Comes to Thoreau's Woods**
*Richard B. Primack*
University of Chicago Press, 2014. 265 pp.

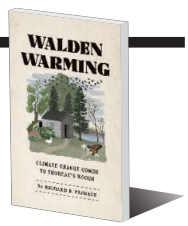


Not only did Thoreau and Primack each record phenophases from hundreds of species over about a decade, but a third botanist, Alfred Hosmer, collected 16 years of chronologically and phenologically intermediate data in the late 19th century. Recently, Primack and his students have gone beyond merely describing these phenomena by using laboratory experiments to reveal sources of interspecific variation in phenological response.

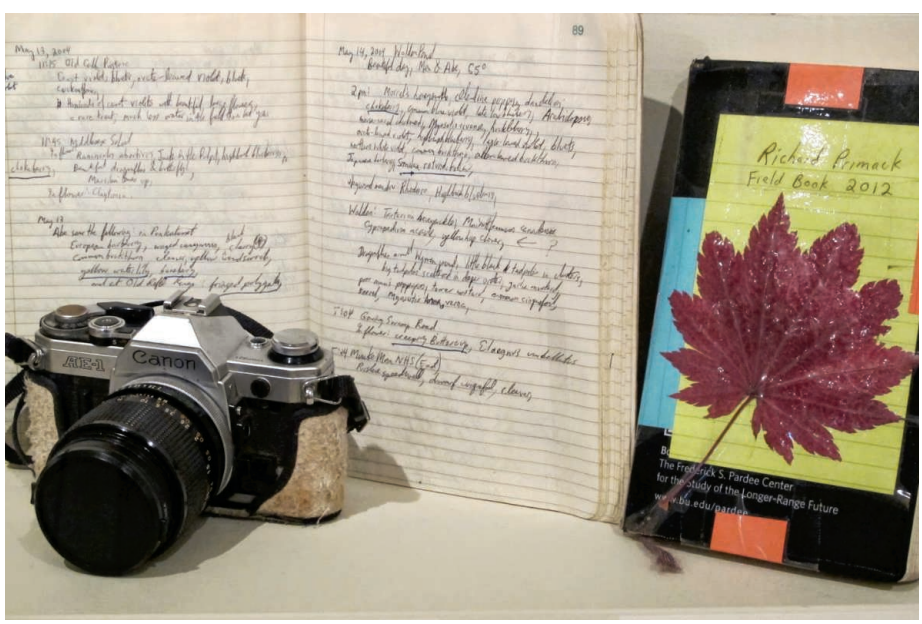


Richard Primack's 2012 field notebook and equipment.

Primack intersperses these scientific results with anecdotes, quotes, and sometimes biographical information to emphasize the main points of the research. For example, the weather of certain days in the 1850s is contrasted with those same days in modern times. While such accounts do emphasize the dramatic changes indicated by Primack's research, they also may perpetuate confusion in distinguishing long-term climatic trends from interannual variation.

Later chapters are somewhat more incomplete or speculative. For example, after hearing of "enormous amounts of mosquito data" collected over 50 years and several compelling hypotheses of the relationship between mosquito populations, increased temperatures, and public health, the reader may be disappointed to find that the data have not yet been analyzed. Regarding spotted salamanders, Primack concludes little more than it's "hard to know whether they're responding to climate change at this time." In the penultimate chapter, discussion of variation in Boston Marathon race times as an attempt to look at the effects of climate change is an interesting thought experiment, but the data are limited to showing that people run slower on warmer days. In fact, any potential trend due to climate change is swamped out by increased competition and training methods leading to faster race times toward the present. To Primack's credit, these and other confounding issues, such as changes in population sizes of target organisms and the difficult task of attributing biotic shifts to climate change, are explicitly and clearly discussed.

Although Primack risks overreach in his broad taxonomic coverage (plants, birds, insects, amphibians, fish, and humans), it does facilitate a discussion of phenological mismatches, a research area limited by the paucity of long-term data but quickly

CREDIT: RICHARD B. PRIMACK

Downloaded from www.sciencemag.org on August 15, 2014



Published by AAAS

becoming important as ecological interactions are disrupted due to differences in species' sensitivities to climate change. Moreover, including humans alongside other affected species rightly emphasizes that, in spite of our technology, we are far from immune to climate change, socially or physiologically.

Geographically, the breadth of coverage is limited to the Massachusetts area, one of the world's best-studied areas phenologically. A passing mention that comparisons of historic and modern data sets have led to similar conclusions in many other places, such as California (*2*), Wisconsin (*3*), North Dakota (*4*), and the United Kingdom (*5*), would have emphasized the ubiquitous effects of climate change and perhaps served as an inspiration for scientists to uncover historic data sets from their own localities.

In an Afterword, Primack encourages the reader to engage in citizen science using the same tools as Thoreau (pencil, paper, and sturdy walking shoes) or, at the very least, to reconnect with nature. After all, past efforts of amateur naturalists, who Primack is consistently eager to credit, have been indispensable to the research and conclusions put forth in the book. He writes, "If you are reading this book, chances are you are already a member of the choir for this particular sermon." However, this volume is best suited for a nonspecialist audience, for whom such a book is sorely needed given the large fraction of people skeptical of climate change or its relevance. Those looking for the data, analyses, and results without an ambling narrative or anecdotes may be better served by an equally readable but more concise and academic review by Primack and his former graduate student Abe Miller-Rushing (*6*) as well as the references therein.

Yet this book is more than a clarion testament to the real and present effects of climate change. It is an exhortation to become more engaged in the natural world whether through citizen science or observation and, in so doing, recognize and limit our own impacts on the earth. A constant presence throughout this book, Thoreau would be pleased to read this volume, which weaves together science, nature, ethics, and human action as parts of a single whole. ■


**REFERENCES AND NOTES**

1. *The Journal of Henry David Thoreau*, B. Torrey, Ed. (Houghton Mifflin, Boston, 1906), vol. 5, p. 394.
2. G. Rapacciuolo *et al.*, *Glob. Change Biol.* **20**, 2841 (2014).
3. N. L. Bradley, A. C. Leopold, J. Ross, W. Huffaker, *Proc. Natl. Acad. Sci. U.S.A.* **96**, 9701 (1999).
4. K. L. Dunnell, S. E. Travers, *Am. J. Bot.* **98**, 935 (2011).
5. E. M. Wolkovich *et al.*, *Am. J. Bot.* **100**, 1407 (2013).
6. R. B. Primack, A. J. Miller-Rushing, *Bioscience* **62**, 170 (2012).


10.1126/science.1255970

MICROBIOLOGY

# Spotlight on the small

*By* **Michael Shen**

**The Amoeba in the Room**
**Lives of the Microbes**
*Nicholas P. Money*
Oxford University Press, 2014. 246 pp.

Just how well do we know the world around us? And just how important is it for us to understand our smaller, less-readily-seen neighbors? In *The Amoeba in the Room*, mycologist Nicholas Money addresses these questions. Claiming that "we have been misled by our brains to exaggerate the importance of elephants," he argues that the scientific community is merely beginning to appreciate the stunning diversity among microorganisms and their impact.

Money opens with a survey of eukaryotes, organized not in the rudimentary tree of life taught to schoolchildren but in a wheel. Eight genetically distinct eukaryotic supergroups are rooted at the wheel's hub, symbolizing a common (unknown) eukaryotic ancestor. Just one of these contains the entirety of animals and fungi. As he uses examples from his backyard pond to illustrate each supergroup, Money contends that "the way that we teach biology is no more sensible than evaluating all of English Literature by reading nothing but a Harry Potter book."

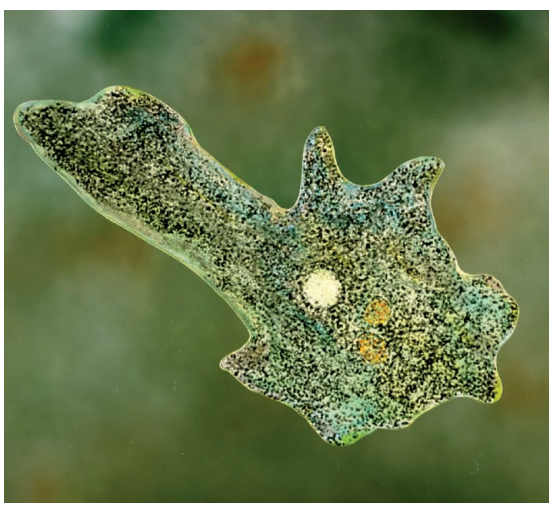

Photomicrograph of *Amoeba proteus*.

Money holds that through most of our history, humans have viewed the world with a scientific narcissism, primarily concerning ourselves with that which we can see with the naked eye. (Of course, we must consider the historical lack of tools that would permit us to observe and understand the Lilliputian inhabitants of our environments.) In a chapter ostensibly devoted to lenses and the history of light microscopy, Money also dives into the "history of biological thought," noting contributions such as Robert Hooke's *Micrographia* (with a subsequent parody by Thomas Shadwell) and Carl Woese's genetic inquiries.

Advances in genomic analysis and development of culture techniques for heretofore uncultivable microbes will go far toward establishing the identity and features of an organism that lives in the soil, drifts in the water, or floats through the air. The much more complex challenge, Money implies, is to understand "what it does, where precisely it operates, or with whom it associates." In enumerating some of the organisms that trap carbon dioxide in the sea, fix nitrogen from the air, or digest food products in the human gut, Money articulates a powerful case for changing how we introduce aspiring scientists to the natural world. He champions the view that "the charismatic megafauna are very distracting, and the popularization of microbial beauty will require a shift in thinking, a subtlety of news coverage, a new genre of wildlife documentary." Of great interest are the extremophiles, organisms adapted to extremes of temperature, pH, hydration, and radiation. The potential application of their particularly suited enzymes to industrial or pharmaceutical processes reminds us that there is also great practical benefit to acquainting ourselves with as large a slice of microbial diversity as we can manage.

Scientists are often encouraged to "think big." *The Amoeba in the Room* reminds us that perhaps we would be well served to do just the opposite. ■

*The author is at the NYU Medical Scientist Training Program, New York, NY 10016, USA. E-mail: michael.shen@med.nyu.edu*

10.1126/science.1255863

CREDIT: GRANT HEILMAN PHOTOGRAPHY/ALAMY

Downloaded from www.sciencemag.org on August 15, 2014



Published by AAAS

# LETTERS

*Edited by* **Jennifer Sills**

## HIV cover ill-advised

I AM CHAIR OF THE Board of Directors of the National Organization of Gay and Lesbian Scientists and Technical Professionals (NOGLSTP) that encompasses lesbian, gay, bisexual, transgender, queer, and questioning (LGBTQ) people in science, technology, engineering, and mathematics. On behalf of NOGLSTP, an AAAS affiliate since 1994, I wish to register our indignation with the 11 July cover of *Science* showing transgender sex workers from Jakarta. The cover, a misguided attempt to pique interest in reading the special section on HIV/AIDS, has provoked many readers, including many members of our organization, to express their dismay at *Science*'s lack of decorum and lack of sensitivity to a much maligned and misunderstood community. The scant attention the magazine paid to the transgender sex worker community makes these omissions all the more important. With one inappropriate picture, you have managed to stereotype all transgender women as sex workers and vectors of disease, as well as hyper-sexualize women of color in general. NOGLSTP applauds the articles presented in this issue, but we question why the cover explicitly shows transgender sex workers when there is no actual content in the articles about HIV prevention, care, or treatment efforts in these transgender communities.

To avoid the kind of hurtful misunderstanding and atmosphere of disrespect that has been generated by this dehumanizing and insensitive decision, NOGLSTP leadership would have been happy to facilitate discussion between science and engineering leaders in the trans community and the editorial staff of *Science* regarding appropriate content as it relates to transgender sex workers and the struggles they face, of which HIV infection is but one.

This incident should be used as a teachable moment to correct the prejudices of those who are insufficiently familiar with LGBTQ communities and their concerns. We exist in all cultures, ethnicities, and walks of life. We are proud scientists, engineers, mathematicians, doctors, and technologists who are part of the *Science* readership. The cover photo is unworthy of *Science* and AAAS. The LGBTQ communities, including in particular the trans community in this instance, deserve more respect than you have offered. The ethic of science demands that we regard all minds and people equally. Prejudice has no place in our endeavors.

***Rochelle Diamond***

Chair, NOGLSTP Board of Directors, Pasadena, CA 91109, USA. E-mail: rd-chair@noglstp.org

### Response

WE DEEPLY REGRET the harm done by the ill-considered choice of cover. Dr. Diamond, in her letter, has made constructive suggestions to help our organization prevent further misunderstandings with the LBGTQ communities, become more sensitive to their issues, and repair damaged relations. We are already in discussions on how to follow up on those recommendations. Many thanks to other leaders in the LBGTQ and other communities who have also graciously stepped forward with offers of help.

***Marcia McNutt***

Editor-in-Chief

PHOTO: PESKY MONKEY/GETTY IMAGES

## Climate change: Time to navigate

THANK YOU FOR the enlightening 4 July Policy Forum set exploring how the Intergovernmental Panel on Climate Change's (IPCC's) AR5 WGIII "Summary for Policymakers" (SPM) reached its final version ("IPCC lessons from Berlin," B. Wible, p. 34). With scientists as the "mapmakers" and policy-makers as the "navigators" ("Mapmakers and navigators, facts and values," p. 37), O. Edenhofer and J. Minx describe how the former had to acquiesce to the latter's demands that certain data depictions and analyses in the original SPM be removed, allegedly because they were politically "toxic" ("Getting serious about categorizing countries," D. G. Victor *et al.*, p. 34). Yet if the SPM is to provide an accurate if abbreviated map for the navigators to guide us to a low-carbon future, how is it that the navigators also get to modify this influential map by deleting the mapmakers' work? Shall we also allow judges to change the testimony of witnesses, or doctors to modify the charts of patients?

In any case, thanks to the exemplary work by the IPCC and many other scientific organizations, maps of where we've been and depictions of the landscape that we now face regarding climate change (and in parallel, ocean acidification) are not what is lacking. Rather, it is now time for the "navigators" to act on this information and finally do their job.

***Greg H. Rau***

Institute of Marine Sciences, University of California, Santa Cruz, CA 95064, USA. E-mail: ghrau@sbcglobal.net

## Fossil fuels' future

THE 27 JUNE SPECIAL SECTION on The Great Gas Boom ("The gas surge," D. Malakoff, p. 1464) about natural gas from hydraulic fracturing provided a useful update on a range of important environmental, social, and economic issues, with the exception of the elephant in the room: Natural gas is a fossil fuel. While a natural gas–fired power station has fewer $CO_2$ emissions per unit energy produced compared with a coal-fired power station (up to 50% if fugitive emissions are captured or ignored) ("Hunting a climate fugitive," News, E. Kintisch, p. 1472), this is largely irrelevant to solving the climate change problem. What matters is the long-term accumulated stock of carbon in the atmosphere, not the short-term rate of emissions (*1*).

The relationship between cumulative emissions and peak warming is insensitive to timing of emissions or peak emission rate (*2*). The lifetime of the airborne fraction of a pulse of fossil fuel–derived $CO_2$ is much longer than the centuries some authors still believe (as stated in the News story by Kintisch). Modeling reveals that 20 to 35% of the $CO_2$ emitted now will still be in the atmosphere after 2 to 20 millennia (*3*). To have a greater than 66% chance of limiting global warming to less than 2°C above the pre-industrial average surface temperature (*4*), humanity can emit only a further 275 Gt C, or about 34 years of "business-as-usual" emissions (*5*). The harsh reality is that $CO_2$ emissions must decrease to zero before the end of this century or we will likely exceed the 2°C guard rail. In these circumstances, it is difficult

Downloaded from www.sciencemag.org on August 15, 2014



Published by AAAS

to envisage a future where both the climate change problem is resolved and today's fossil fuel industry persists.

***Brendan Mackey[1]* and David Lindenmayer[2]***

[1]Griffith Climate Change Response Program, Griffith University, Southport, QLD 4222, Australia. [2]Fenner School of Environment and Society, The Australian National University, Canberra, ACT 0200, Australia.

*Corresponding author. E-mail: b.mackey@griffith.edu.au

**REFERENCES**

1. B. Mackey *et al.*, *Nat. Clim. Change* **3**, 552 (2013).
2. M. R. Allen *et al.*, *Nature* **458**, 1163 (2009).
3. D. Archer *et al.*, *Annu. Rev. Earth Planet. Sci.* **37**, 117 (2009).
4. United Nations Framework Convention on Climate Change, Copenhagen Accord (2009); http://unfccc.int/meetings/copenhagen_dec_2009/items/5262.php.
5. T. F. Stocker *et al.*, Eds., IPCC, 2013: Summary for Policymakers in Climate Change 2013: The Physical Science Basis, Contribution of Working Group I to the Fifth Assessment Report of the Intergovernmental Panel on Climate Change (Cambridge Univ. Press, Cambridge, 2013).

# *Sharing ideas too soon*

THE IN DEPTH ARTICLE "A radical change in peer review" (J. Mervis, 18 July, p. 248) suggests asking grant applicants to review their competitors. This initiative from the National Science Foundation (NSF) may save time and money, and the NSF's "novel scoring system aimed at dissuading a reviewer from downgrading a competitor's proposal in order to boost their own" may represent an advance in the peer-review procedures. However, this "radical alternative" to the traditional peer review system raises questions about intellectual property.

In the new peer-review system, grant applicants will share their novel ideas, which have not yet been scientifically tested, with their competitors for the grant. Although the "reviewers of grant applications are expected to maintain confidentiality and avoid using ideas in those applications without permission in their own research and for their own gain" (*1*), stealing ideas occurs in the research field (*2*). This unethical behavior might increase with the proposed system. The peer-review process certainly needs to evolve, but changes should be accompanied by mechanisms that minimize the risk of unethical behavior.

***Philipe de Souto Barreto***

Gérontopôle de Toulouse, Institut du Vieillissement, Centre Hospitalo-Universitaire de Toulouse (CHU Toulouse), 31000 Toulouse, France. E-mail: philipebarreto81@yahoo.com.br

**REFERENCES**

1. InterAcademy Council and IAP (The Global Network of Science Academies), "Responsible conduct in the global research enterprise: A policy report" (2012); www.interacademies.net/10878/19787.aspx.
2. L. C. Rodrigues, *Br. Med. J.* **317**, 857 (1998).

Workshop in Nablus (An-Najah National University, West Bank).

OUTSIDE THE TOWER

# Kids' questions transcend conflict

"Are nails growing at the same speed on each finger?"

"Is there a volcano in our land?"

"Why does the moon walk with us at night, while stars stay still?"

These questions were asked by children last November, during the Science Days of Palestine, an event we initiated in 2010. This time, in several Palestinian cities in the West Bank and Gaza, we introduced 300 kids aged 8 to 12 to the questioning process of scientific research.

First, to their surprise, instead of the gray-haired men they expected, the children met young scientists, both men and women. We explained the role of questions in science. Then, through games and observation of their environment, pupils raised a hundred questions, genuine, profound, poetic, and meaningful to their lives (*1*). Their surprise grew when we did not provide answers. Instead, we invited them to ask peers, teachers, and parents to search books and Web sites, or to set up simple observations and experiments. Kids were thus left positively frustrated, keen to learn and explore further.

We held similar activities in Israel, Egypt, former Yugoslavia, and impoverished suburbs of Western cities (*2*–*4*). These costless activities (a pen and a paper suffice) can substantially change the attitude of students, and indirectly, teachers. They are encouraged to collectively explore the unknown, in close connection with their daily experience, thereby allowing them to find unexpected solutions. We hope more scientists will join us in sharing with children the very first step of their research practice, which is to ask open questions. In particular, in difficult situations where conflict lies too close, curiosity may spark enthusiasm, divert from violence, and lead toward innovative and pragmatic answers, which may eventually contribute to peace.

***Leïla Perié,[1,2]* Livio Riboli-Sasco,[3] Claire Ribrault,[3] Ewa Zlotek-Zlotkiewicz[4]***

[1]Netherlands Cancer Institute, Amsterdam, 1066CX, Netherlands. [2]Utrecht University, 3584 CH Utrecht, Netherlands. [3]Atelier des Jours à Venir, 75006 Paris, France. [4]Institut Curie/CNRS UMR 144, 75005 Paris, France.

*Corresponding author. E-mail: l.perie@nki.nl

**REFERENCES**

1. L. Perié, L. Riboli-Sasco, C. Ribrault, Workshop tools: Detailed protocol of the workshop to stimulate questions (http://tinyurl.com/kpkkz9q).
2. L. Perié, L. Riboli-Sasco, C. Ribrault, *J. Commun.* **13**, C05 (2014).
3. L. Riboli-Sasco, L. Perié, *Science* **332**, 1503 (2011).
4. L'Atelier des Jours à Venir (www.joursavenir.org).

*Outside the Tower is an occasional feature highlighting science advocacy projects led by scientists and citizen scientists. How do you advocate for science? Tell us at submit2science.org.*

PHOTO: ATELIER DES JOURS À VENIR



Published by AAAS

Downloaded from www.sciencemag.org on August 15, 2014

Published by AAAS

# Parenting

## A legacy that transcends genes

*By* **Beverly A. Purnell**

Parents of any species pass on their DNA, but the biology of parenting and its impacts on the offspring don't end there.

Animal parenting behaviors, which can include providing food, shelter, protection, and instruction, rely on sensory cues and hormone activation of neural pathways in males and females (Dulac *et al.*, p. 765; Rilling and Young, p. 771). Faced with a changing environment and the need to adapt, parents may scale back care or defense (Royle *et al.*, p. 776). The molecular legacy extends beyond gene transfer to include mitochondria and epigenetics (Lane *et al.*, p. 756). Finally, the gestation and birthing processes also shape offspring, and preterm birth is now a focus of research (Romero *et al.*, p. 760).

Assisted reproduction has helped millions become parents, but in vitro procedures expose the early embryo to highly unusual conditions, with possible long-term health consequences as the child ages (Servick, p. 744). In the womb, mothers can unwittingly shape their children's taste and smell preferences (Underwood, p. 750), and when a newborn begins to nurse, components of breast milk nourish an ecosystem of beneficial gut bacteria (Gura, p. 747). As a child grows, a lack of parental care can have devastating consequences for brain development (Marshall, p. 752).

Such insights will help us understand how parenting equips offspring to grow, thrive, and become parents themselves.

*This special issue was edited by Beverly A. Purnell, Sacha Vignieri, and Laura M. Zahn (Editorial) and Elizabeth Culotta, Elizabeth Pennisi, John Travis, and Tim Appenzeller (News).*

PHOTO: JAMI TARRIS/CORBIS

INSIDE

**NEWS**

Unsettled questions trail IVF's success *p. 744*

Nature's first functional food *p. 747*

The taste of things to come *p. 750*

An experiment in zero parenting *p. 752*

**OPINION**

Maternal mental illness *p. 755*

**REVIEWS**

Parenting from before conception *p. 756*

Preterm labor: One syndrome, many causes *p. 760*

Neural control of maternal and paternal behaviors *p. 765*

The biology of mammalian parenting and its effect on offspring social development *p. 771*

The evolution of flexible parenting *p. 776*

**SEE ALSO**

- PERSPECTIVE P. 733
- RESEARCH ARTICLE P. 785
- *SCIENCE TRANSLATIONAL MEDICINE* RESEARCH ARTICLE BY R. DIAO *ET AL.*
- PODCAST
- sciencemag.org/special/parenting

Published by AAAS

# Unsettled questions trail IVF's success

## Researchers are still struggling to understand the potential long-term effects of assisted reproduction

*By* **Kelly Servick**

Back in 2001, developmental biologist Richard Schultz stood before a meeting of reproductive clinicians in New York City to present some uncomfortable results. Adult mice that had developed in vitro as early embryos, he reported, showed subtle differences from controls, including poorer spatial memory. He thought that his audience of experts on human in vitro fertilization (IVF)—extracting and combining sperm and egg in a culture medium, then transferring the embryo back into the mother's uterus—would be interested. "I was naive," he says.

Several attendees pounced on the idea that IVF could have long-term effects, and one asked how he dared to conduct such an experiment. Clinicians seemed to fear that his finding would threaten the fertility industry, or even provoke litigation from patients, Schultz says. "I have never been attacked ad hominem in a public summit such as this."

> ***"What will happen to these kids when they are middle-aged?"***
>
> **Paolo Rinaudo**, University of California, San Francisco, Medical Center

In the audience that day was Paolo Rinaudo, then a medical fellow looking for his first research project. He, for one, took Schultz's results to heart. "This was really a key moment for me," Rinaudo says. "I was completely flabbergasted" by the suggestion that IVF could have consequences in adulthood. He now studies possible metabolic effects of IVF in mice and also performs the procedures for couples at the University of California, San Francisco, Medical Center.

Based on existing research, he's able to tell patients that the known risks of assisted reproductive technologies (ART), which include variations on in vitro fertilization, are relatively small: a slight increase in pregnancy complications, preterm birth, and low birth weight, and possibly an increased, though still very low, risk of birth defects.

But as Rinaudo and others learn more about the sensitivity of early embryos, they have begun to wonder if the manipulations of IVF may have additional subtle effects that appear as children grow. So far the evidence is equivocal. IVF boosters can point to more than 5 million children conceived this way, most apparently healthy. But the track record is short: The oldest IVF baby, Louise Brown, is just 36. "What will happen to these kids when they are middle-aged?" Rinaudo wonders. Animal studies hint that these people may be at higher risk of age-related disorders, such as heart disease, diabetes, or hypertension, though these effects haven't been confirmed in people. A few other studies suggest subtle cognitive differences in ART children, but sample sizes are small.

No researchers are suggesting that ART shouldn't be done. But some argue that to inform parents accurately about risks, they need more and larger studies. Rinaudo and clinician-researchers like him straddle two worlds: a multibillion-dollar industry full of eager patients, and a contradictory scientific literature full of vague concerns. Most fertility researchers are trying to improve success as measured by a single, clear standard—the birth of an apparently healthy baby. Only a few are trying to discern whether IVF leaves a subtle legacy in children.

**TWO EVENINGS A MONTH,** the conference room in Aberdeen Maternity Hospital in the United Kingdom fills with couples planning to start fertility treatments. At these get-togethers, they realize that "there are plenty of other people in the same boat," says Abha Maheshwari, a gynecologist at the hospital who also studies the possible consequences of ART. Worldwide, more than 45 million couples face the same painful situation.

Driven by the urgent desires of these couples, scientists have turned ART into one of medicine's dramatic success stories. In the United States, the odds of a live birth with the method have risen from the low teens in the 1980s to roughly 40% today for women under 35. That's largely due

An empty petri dish awaits an egg for in vitro fertilization.

Downloaded from www.sciencemag.org on August 15, 2014



Published by AAAS

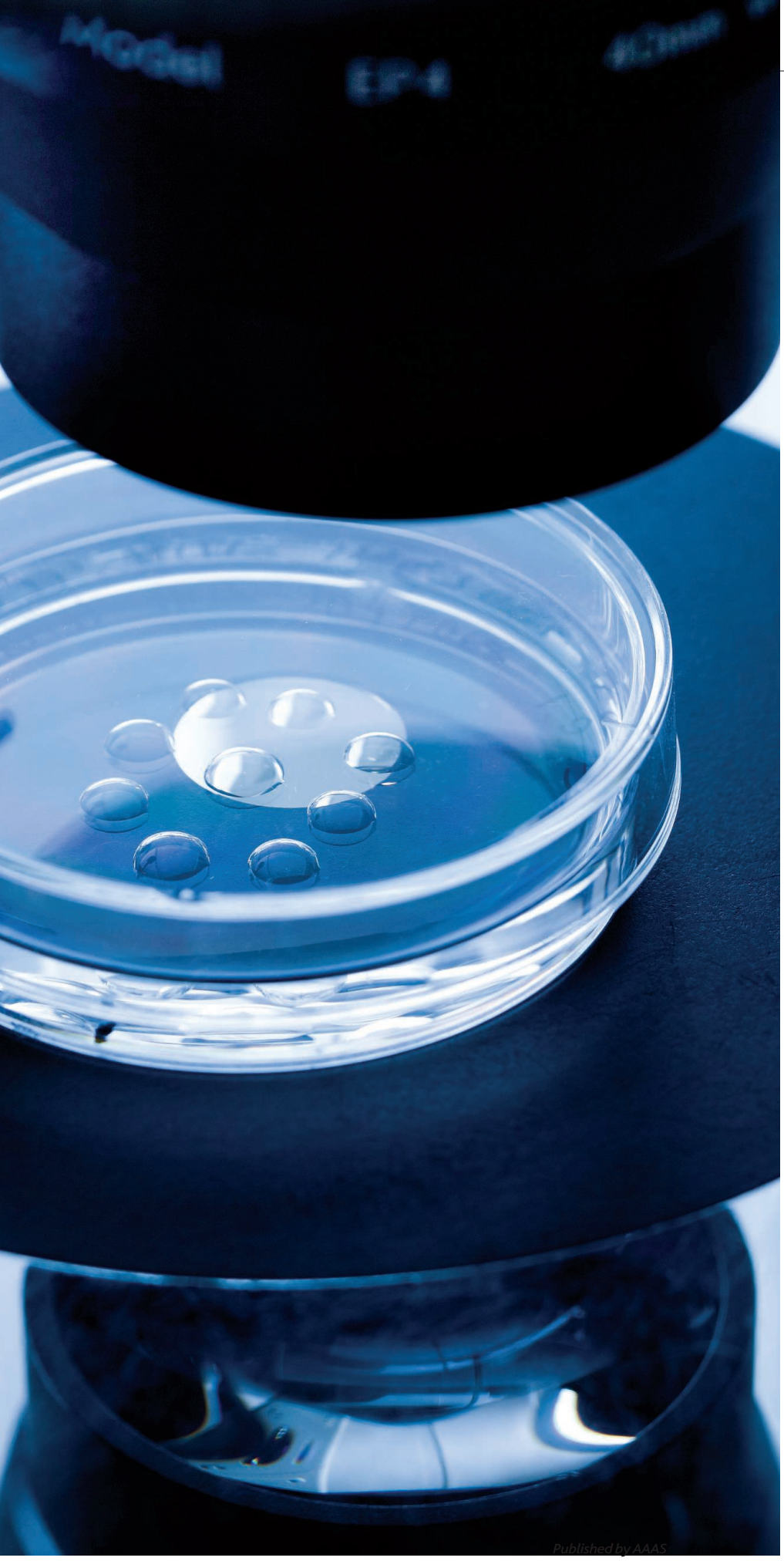

PHOTO: SCIENCE PHOTO LIBRARY

to lab conditions that more closely mimic a mother's body, and to new technology—notably, the use of intracytoplasmic sperm injection (ICSI), in which a sperm is inserted directly into the egg to make up for defects in sperm.

But as ART took off in the clinic, some basic scientists remained wary. "It didn't rest upon a solid foundation of experimental work," says Schultz, citing the lack of animal research documenting physiology, behavior, longevity, and susceptibility to disease later in life. "There really weren't any solid data in terms of 'Were these children at risk?' "

When asked why they suspect ART might have long-term effects, most researchers start by citing one name: David Barker. In landmark studies in the 1980s, the physician and epidemiologist linked chronic diseases like diabetes and heart disease to malnourishment in the womb, as measured by low birth weight.

As Barker's ideas gained popularity in the mid-1990s, some wondered whether the formative effects of fetal development reached further "upstream," to the period before a drifting clump of embryonic cells nestles itself into the uterine wall to become a fetus. In 2000, developmental biologist Tom Fleming and his colleagues at the University of Southampton in the United Kingdom showed that pregnant rats that were malnourished during this preimplantation stage gave birth to offspring with high blood pressure and abnormally sized organs, even if the mothers resumed a normal diet for the rest of pregnancy. Apparently, the early embryo's struggle for resources in nutrient-poor surroundings led to irreversible changes in development. "The embryo needs to fight for itself," Fleming says.

That raised a new question: Are embryos that develop in the foreign environment of a petri dish and undergo physical manipulation in the lab compelled to "fight for themselves" in particular ways? The question spurred Schultz's animal studies, and a few labs have begun to explore these issues with human embryos—the surplus from IVF procedures, donated by parents.

In vitro embryos are not malnourished—quite the opposite. Compared with the relatively weak, watery solution in a mother's fallopian tube, commercially available cell culture medium, which is sometimes enriched with growth factors, is "a little bit like rocket fuel," says reproductive biologist Helen Picton of the University of Leeds in the United Kingdom, who is exploring the effects of the medium. "You really set [the embryos] off at a great speed."

Picton adds that in human embryo research, with only a few donated embryos

Published by AAAS

of a handful of cells each, "the hard work is characterizing what's normal." Adding growth factors to the medium appears to alter the expression of certain genes known in mice to be associated with cell fate—which cells survive, and which will develop into part of the placenta or part of the fetus. But researchers are far from linking these gene expression patterns to any health risks.

In the years since Schultz presented his results, Rinaudo says most evidence from animal models has been reassuring—the procedure doesn't seem to affect longevity, for example. But ART-conceived animals do appear more likely to have problems metabolizing glucose, and this effect may be transmitted to subsequent generations, probably through epigenetic changes—alterations in inherited chemical markers that attach to DNA and affect its expression. Two rare disorders related to epigenetic marks, Beckwith-Wiedemann and Angelman syndromes, also appear to be more common in ART children, although the absolute risk is still extremely low, with fewer than 100 cases of either disorder reported in these children.

Perhaps because of all the uncertainty, Rinaudo says that most of his clinical colleagues remain focused on improving the numbers of live births with ART, rather than exploring its possible consequences. "We haven't been able yet to metabolize this information," he says, "because there are not really studies in humans that show long-term problems."

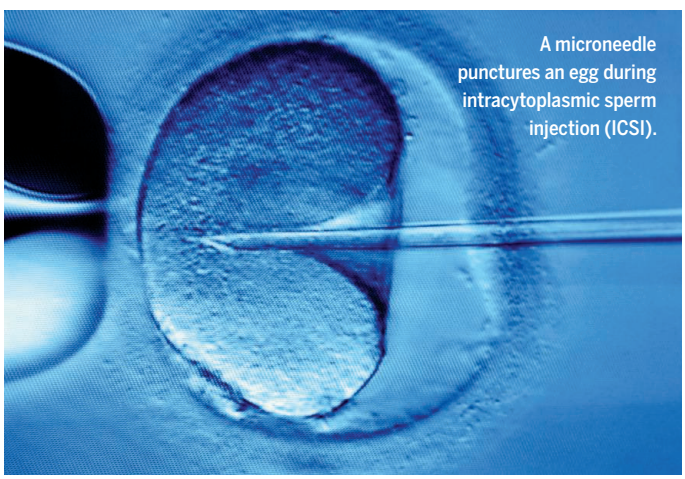

A microneedle punctures an egg during intracytoplasmic sperm injection (ICSI).

PHOTO: MAURO FERMARIELLO/SCIENCE PHOTO LIBRARY/CORBIS

**HUNTING FOR SUCH PROBLEMS** among the millions of ART children is far from straightforward. Easiest to spot are negative outcomes early in life, and studies have repeatedly shown small increases in low birth weight, preterm birth, cerebral palsy, and other birth defects in ART children. "They have higher risk of all the anomalies, all the complications in pregnancy you can name," Maheshwari says. The best estimates put their overall risk of a major birth defect at about 30% higher than the general population. That's a modest increase in a small risk: 4% to 5% versus 3% to 4%.

But Maheshwari adds that with any increased risk, researchers have to ask: "Is it because of IVF processes, or is it because we are treating a different population?" Couples who seek ART tend to be older, and for some, the difficulty conceiving may be related to abnormalities in sperm or eggs that also affect embryos. The procedures also increase the odds of multiple births as much as 20-fold in women under 35, according to a paper Rinaudo and colleagues published in *Molecular Human Reproduction* in 2013. And however they are conceived, twins and triplets face increased risks of all kinds, from pregnancy complications and low birth weight to cognitive and behavioral problems.

A control group of fertile couples willing to undergo ART for no reason could resolve such questions, but that's not practical. But there's a natural control group: children born to couples diagnosed as infertile who then waited long enough for ART that they conceived spontaneously. In 2006, researchers in the Netherlands used a national database to find 6343 Dutch women diagnosed with infertility who conceived without IVF or the ovulation-stimulating drugs that usually precede it. Compared with these controls, babies born after both fertility drugs and IVF were more likely to have very low birth weight and to be born very preterm—before 32 weeks. Another group used the same database to conclude that the ART children, aged 8 to 18 at the time of testing, had slightly higher blood pressure and blood glucose levels than their spontaneously conceived counterparts—potential indicators of risk for heart disease or diabetes later in life.

Those findings hint that ART carries an extra overlay of risk. Still, most studies to date are relatively small and lack statistical power, says reproductive epidemiologist Michael Davies of the University of Adelaide in Australia. "People are dragging their feet somewhat," he says. "They've yet to find the utterly compelling body of data."

Early reports of mild cognitive differences in very young ART children, for example, have been criticized for small sample size and other biases. Davies recently submitted a grant for a study that would link 11,000 IVF births to school records and census data measuring sight, hearing, and disability, in part to follow up on controversial suggestions that IVF children have more contact with disability services.

His group also did a large analysis of data from South Australian clinics and birth defect registries, published in 2012 in *The New England Journal of Medicine*, showing that the direct sperm-into-egg injection method of ICSI appeared to increase the risk of birth defects, but only when embryos were transferred to the uterus while fresh, not preserved by freezing and rethawed for later use.

Such efforts to pick apart the risks of different ART techniques are critical, Maheshwari says. ICSI, which accounts for more than half of ART procedures in both the United Kingdom and the United States, can increase the chance of a live birth, but the Aberdeen clinic recommends against it unless defective sperm make it absolutely necessary. The dilemma highlights the tension between offering parents the best odds of conceiving and the least risk to the embryo, Maheshwari says. National registries that list live birthrates at different IVF centers heighten the pressure to demonstrate efficiency, she says. "This is what drives the market, and that's what drives your practices."

A more dramatic and controversial example is the practice, still relatively common in the United States but increasingly discouraged in most developed countries, of returning multiple embryos to a woman's uterus simultaneously. This reduces the chance a couple will have to go through (and pay for) another round of IVF to get pregnant, but raises the chance of multiple pregnancies and their associated risks.

A newer technique in which an embryo is allowed to develop in culture for 5 days rather than three presents another trade-off. The practice appears to boost the odds of pregnancy, but Maheshwari thinks it may also increase the risk of preterm delivery. Rinaudo also worries about lengthening the exposure of early embryos to an unusual environment, but he says, "It's very difficult to make a recommendation when the evidence is not there."

He's still not sure how many vague concerns about long-term health to share with hopeful parents-to-be. For now, he tells couples that some animal studies suggest subtle adverse effects later in life, but it's too early to draw firm conclusions. He keeps animal studies, like Schultz's mouse work, on hand, should patients want to see them.

Usually, he says, they don't ask. ■



Published by AAAS

Breast milk supplies more than just nutrition for babies.

PHOTO: KIDSTOCK/BLEND IMAGES/CORBIS

Downloaded from www.sciencemag.org on August 15, 2014

# *Nature's first functional food*

## Breast milk feeds helpful microbes, fights harmful ones, provides immunity, and jump-starts a newborn's life

*By* **Trisha Gura**

Blood, urine, saliva, and spinal fluid. Those are the human bodily fluids most explored by scientists over the decades. Yet any woman who has ever nursed a newborn will cite a major omission: breast milk. Researchers long ago unraveled the basics of this maternal liquid. But until recently, few have given it serious attention with sophisticated analytical techniques. Breast milk was "ignored as not modern," for the last half-century, says epidemiologist Ardythe Morrow of Cincinnati Children's Hospital Medical Center in Ohio. But now, it's "an exploding area of science."

The resurgence has its origins in a long-standing conundrum: Breast milk abounds with complex carbohydrates called oligosaccharides that humans can't digest but beneficial bacteria can thrive on. Fifty years ago, when the oligosaccharides were discovered, investigators lacked the technology to deduce their structure and determine their effect on what is now called the infant gut microbiome (the myriad bacteria that naturally reside in human intestines, beginning at birth). Unable to progress significantly, scientists lost interest in milk-microbe connections.

Now, thanks to breakthroughs in analytical chemistry and a growing interest in the microbial fauna in the human body, as well as a movement touting the benefits of breast-feeding, those connections are being explored once again. Some researchers have focused on making better use of the microbiome fostered by milk, while others have documented how breast milk does more than feed a newborn and its "good" bacteria. Mother's milk also contains an evolving stockpile of compounds that thwart pathogens, foster a robust immune system, and perform other functions. Most recently, researchers have discovered that mom provides inactive enzymes in her milk that turn on in the infant gut and clip out bioactive molecules from other milk proteins. "Milk is really a genius fluid that was outrageously understudied," says microbial ecologist David Mills of the University of California (UC), Davis. "If we can identify components of human breast milk that are important, then we can understand the wisdom of milk—and take advantage of them."

**AT FIRST BLUSH, BREAST MILK** is a buffet of fats, proteins, and sugars, in a ratio of about 1-to-3-to-7. Until recently, scientists viewed the fluid mainly as food for a rap-



*Published by AAAS*

idly growing newborn. Yet, mother's milk also teems with immune cells, such as macrophages, stem cells for regeneration, and hundreds to thousands of bioactive molecules—some fatlike, others protein in nature, and still others that are indigestible oligosaccharides. These bioactive molecules can protect against infection, ward off inflammation, spur immune system and organ development—and, in the case of oligosaccharides, shape the infant microbiome, scientists have found. Milk "is not primarily about nutrition," Morrow says. "Rather [it's about] immune protection."

Signs of that protection began to emerge almost 130 years ago with the discovery that breast-fed infants survived more often than bottle-fed ones. In searching for reasons why, pediatricians and microbiologists analyzed the bacterial composition of the feces of both types of infants, which reflects their gut microbiome, and found significant differences. Meanwhile, chemists at the turn of the 20th century noted that human breast milk contained "a different type of lactose" than cow's milk did. Then, in the 1950s, Nobel Prize winner Richard Kuhn and physician Paul György showed that this "different type" consisted of hundreds of oligosaccharides that promoted the growth of microbes called bifidobacteria. But the work paused, as chemists spent the next 50 years advancing techniques necessary to sort out the complexity of the oligosaccharides.

In 2006, a team at UC Davis led by food chemist Bruce German and his graduate student Robert Ward helped reignite interest in the milk-microbiome connection. The group enlisted analytical chemist Carlito Lebrilla, who used mass spectrometry and a sophisticated chromatographic technique to characterize the oligosaccharide repertoire. Lebrilla identified nearly 200 unique human milk oligosaccharides (HMOs) and handed the mix to Mills, who, along with German, assumed a plethora of bacterial species would feast on the sugary cocktail.

"But they didn't." German says. "It was a jaw-smacking moment."

Only one type grew robustly: *Bifidobacterium longum biovar infantis* (*B. longum* bv. *infantis*). Scientists are not yet certain exactly how the bacteria first enters the infant's intestinal tract—possibly when a fetus begins swallowing amniotic fluid and later as the infant passes through the vaginal tract. Breast milk, which contains small numbers of the bacteria, is another possible route. Assisted by the HMOs in breast milk, the organism eventually multiplies to dominate the breast-fed baby's microbiome, making up as much as 90% of it. After weaning, it eventually drops to 3% of the adult microbiome. The UC Davis team wondered: Why did *this* organism so rule the budding infant microbiome?

A year later, Mills came up with an answer. After sequencing the genome of *B. longum* bv. *infantis*, he learned that it carries the precise genes for all the enzymes needed to digest the milk's oligosaccharides—other bacteria, even closely related ones, don't share all of those genes. "Clearly this bacterium coevolved" with humans, German says.

Why would a new mother expend energy producing food for an organism other than her offspring? German says it's pretty clear. "Mother is recruiting another life form to babysit her baby."

> ***"Milk is really a genius fluid that was outrageously understudied. If we can identify components of human breast milk that are important, then we can understand the wisdom of milk–and take advantage of them."***
>
> **David Mills,** UC Davis

By babysitting, German refers to the growing list of protective functions in a newborn that *B. longum* bv. *infantis* appears to orchestrate. For example, the bacterium consumes the oligosaccharides whole before other nasty microbes can digest them, starving out the bad bugs. *B. longum* bv. *infantis* also produces molecules called short-chain fatty acids that serve as favorite food for other beneficial bacteria and help guide the cells that line the infant intestine in how to use energy and mount an immune defense.

Apart from promoting good bacteria, human milk oligosaccharides themselves can ward off dangerous bacteria such as *Salmonella*, *Listeria*, and *Campylobacter*, causes of diarrhea and infant mortality. The HMOs closely mimic carbohydrate structures on the infant's gut cells. Because many pathogens typically attach to these cell-bound structures to infiltrate the gut, mother's milk, in essence, floods the infant's gastrointestinal tract with decoys that bind the pathogens and keep them off the intestinal wall.

**NEONATOLOGISTS ARE NOW HOPING** to turn the growing understanding of *B. longum* bv. *infantis* to their advantage, most immediately by ameliorating, or preventing, an often deadly disease called necrotizing enterocolitis (NEC) that tends to develop in premature infants. Starting as a serious bacterial infection, NEC overwhelms the gut several weeks after birth. The intestinal tissue dies; surgeons try to remove it; and the baby often suffers severe and permanent disability, neurological damage, and—in 20% to 30% of cases—death.

NEC can strike just when it seems a premature infant is out of the initial dangers of being born too early. "I can think of a baby," says neonatologist Mark Underwood of UC Davis, "who one day was looking good and on the next day was pooping blood. By that night was dead. You see that in a kid who you thought was past the worst of it, and it is just so devastating."

Theories abound to explain the condition: Premature infants have a leaky gut that lets bacteria through, or cells lining their intestine exhibit an overreactive inflammatory response. Premature infants may also not get enough breast milk: Studies show that the risk of NEC plummets six- to 10-fold if preemies are given breast milk rather than formula.

Yet, even when mother's milk is provided in a feeding tube, NEC can still take hold. The problem may not be a lack of milk, but rather a deficient microbiome—one lacking enough *B. longum* bv. *infantis*, for example. Simply, premature infants carry premature intestinal fauna, Underwood and others say.

In some studies, attempts to speed the maturation of the microbiome, just as physicians give substances to preemies to promote lung development, have shown little success. In one recent effort involving preterm infants, the UC Davis team tried out different combinations of formula and breast milk with and without the right oligosaccharides. The researchers discovered that none of the interventions changed the microbiota of the preemies. By contrast, some studies in full-term infants indicate that adding HMOs to formula or breast milk promotes beneficial microbes. So why are preemies not responding similarly?

"It's a different environment that premature infants live in," notes neonatologist Barbara Warner of Washington University School of Medicine in St. Louis. Catheters, breathing tubes, and other instrumentation breed infections by microbes not normally in an infant. Also, preemies get antibiotics for long periods of time, wiping out beneficial bacteria.



Published by AAAS

**DESPITE MIXED RESULTS,** clinicians trying to help premature infants and other newborns now view mother's milk and its promotion of a good microbiome as so key that many are developing and testing supplements containing probiotics (the bacteria) and prebiotics—food that will stimulate the beneficial bacterial growth. Clinical researchers in Europe, Canada, and elsewhere have completed nearly 40 studies using pre- or probiotics, some containing *B. longum* bv. *infantis*, in premature infants, estimates Allan Walker of Boston's Massachusetts General Hospital and Harvard School of Public Health. The most recent, published online in January in *The Journal of Pediatrics*, showed that a probiotic product that contains *B. longum* bv. *infantis*, one readily available in North America, substantially reduced the frequency of NEC in a Montreal, Canada, neonatal intensive care unit.

Few such studies have been done in the United States, however. Although for adults probiotics are considered supplements and go unregulated, introducing microbes into premature infants falls under the same U.S. Food and Drug Administration regulations as vaccines or new drugs. Anticipating increased development costs and time, U.S. researchers have either pursued other strategies or partnered with collaborators elsewhere.

For example, Walker's group is working with neonatologists in Chile to test a specific sugar-containing molecule, or glycan, found in mother's milk. Studies in newborn mice, as well as in a tissue model of the human premature gut, show that the glycan damps down proinflammatory factors, while boosting anti-inflammatory ones. Chilean researchers will supplement mother's breast milk with the glycan and look for a reduction in the incidence of infection and death in premature infants.

While also pursuing the idea of introducing *B. longum* bv. *infantis* or its food in preemies, the UC Davis researchers have gone back to basic studies of mother's milk for further inspiration. They began by analyzing the fluids taken from the gastric tubes of premature infants after feeding. To their surprise, the researchers learned that the infant stomach is not wildly acidic and stocked with aggressive enzymes, as previously thought. The group reported online in April in *The Journal of Nutrition* that the infant stomach seems geared to digest very few proteins, mainly β-casein, but also lactoferrin, lysozyme, and α-lactalbumin. All are found in breast milk. The enzymes that were present were not chopping up proteins randomly, but rather were clipping them at very specific sites in their sequence, generating 603 peptides. Some of these are known to inhibit the growth of pathogenic bacteria or regulate the immune system.

What's more, the UC Davis team recently discovered that some of the digestive enzymes they found in infants' guts after feeding are actually produced by the mother and delivered, inactive, in her milk. Something in the infant's stomach later turns them on so they can free up the active peptides from the full milk proteins. The UC Davis team theorizes that supplementing milk with the latent enzymes will promote the formation of the beneficial peptides in premature infants.

Industry is watching this and the oligosaccharide developments closely. "It is a rat race," says nutritional scientist Lars Bode of UC San Diego. "Whatever formula company comes out with the first oligosaccharide to add to their product, that will make a huge shift in the market. Everyone is working on it."

For example, German, Mills, and the UC Davis team started a company called Evolve Biosystems Inc. to advance their own combination of prebiotics and probiotics. Because scientists cannot get enough donor human milk to isolate enough prebiotics, German's group is working instead with bovine milk, which contains small amounts of HMOs. Infants have been drinking dairy-based formulas for decades—without apparent harm—the researchers reason. Hence, the approach should get around some regulatory hurdles.

But the sugars in cow's milk often differ substantially in their structure and abundance from those in human breast milk. Thus, investigators such as biochemist David Newburg of Boston College have set out to synthesize HMOs. In 2004, Newburg showed that an oligosaccharide found in breast milk called 2'-fucosyllactose is effective in warding off the pathogenic bacteria that cause cholera, a diarrheal disease. With his own money, he co-founded Glycosyn LLC to test the oligosaccharide and its derivatives. The company makes them by inserting the genes for various sugar-building enzymes into yeast and bacteria. Newburg predicts he is about a year away from marketing a nutritional supplement.

This intense rush of research and commercial development only highlights the remarkable complexity and powers of the milk every mom naturally makes for her newborn. "Evolution has delivered *the* functional food," Mills says. "We just need to understand it." ■

*Trisha Gura is a science writer in Boston.*

## Breast milk's hidden gifts

A complex mixture of proteins, fats, and sugars, mother's milk does far more than nourish the growth of a newborn. Some of its components enlist helpful bacteria.

### In the milk

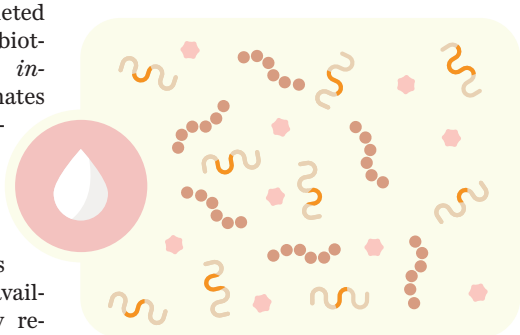

Milk transfers complex carbohydrates called oligosaccharides ( ), proteins ( ), and inactive enzymes ( ) to the baby.

### In the stomach

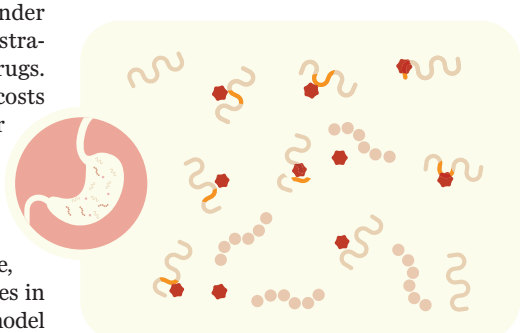

Activated enzymes ( ) cut useful peptides ( ) from proteins. The peptides aid the immune system.

### In the gut

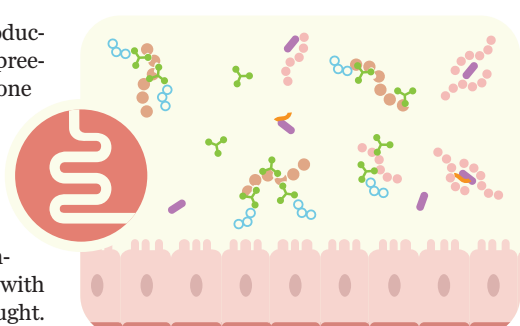

Good bacteria ( ) thrive on oligosaccharides, which, along with peptides, also mop up bad bacteria ( ) to keep the gut healthy. The good bacteria make beneficial fatty acids ( ).

Illustration: G. Grullón/*Science*



*Published by AAAS*

Babies form flavor preferences as early as in the womb.

# The taste of things to come

## Early postnatal, and even prenatal, experiences shape culinary tastes

*By* **Emily Underwood**

Everything about the newborns was normal, except for their pungent aromas of fenugreek, curry, and cumin. At first, the physicians who delivered the four unrelated babies at a Tel Aviv hospital were worried—some strong smells at birth signal disease. But soon they discovered the apparent source of the odors. Hours before labor, the mothers said, they had eaten *skhug* and *amba*, spicy traditional Yemeni and Israeli foods.

The obscure case study—described in a 1985 issue of the *European Journal of Pediatrics*—caught Julie Mennella's attention in the early 1990s. A biopsychologist at the Monell Chemical Senses Center in Philadelphia, Pennsylvania, Mennella studies why we like the foods that we do—what she describes as one of the "biggest mysteries of human behavior." The Israeli study "was a great 'aha!' moment," Mennella says, because it supported her hunch that infants can perceive—and perhaps even learn to love—the distinct flavors of their culture's foods while still in their mothers' wombs.

When Mennella began her career, relatively little was known about how and when humans form their preferences for different flavors. Despite a large literature on how maternal diet influences the overall nutrition and health of offspring, few researchers were looking at whether flavor preferences derive from what the mom consumes during pregnancy or soon after birth. Mennella recalls that doctors used to tell women still nursing their child to avoid spicy or pungent foods, based on "folklore" that infants inherently prefer bland foods.

Over the past several decades, however, a convergence of findings from psychologists and neuroscientists, including Mennella, has shown that infants' tastes are malleable. Although our cravings for salt, sugar, and fat do have a genetic basis, new evidence shows that the majority of our food preferences are "not inborn," Mennella says. Instead, the taste for a variety of flavorful foods, including bitter vegetables, is "part of culture, and something you have to learn." Through creative experiments with newborns, Mennella and others have shown such learning can begin as early as in the womb.

**FOLLOWING YOUR NOSE** is more than a figure of speech in Mennella's lab. An Italian-American for whom food is "very important," she made pungent garlic the focus of her first attempts to pin down some of the origins of our flavor preferences. Working with Gary Beauchamp, director of the Monell research program, Mennella asked pregnant women to consume either plain-flavored or garlic capsules during the last weeks of their pregnancy. By that point, a fetus clearly has both the ability to taste and to smell—around the 24th week of gestation, for example, mucus plugs blocking the nasal passages dissolve, allowing amniotic fluid to bathe a fetus's newly formed olfactory receptors (see p. 751).

Mennella then asked volunteers, recruited from around the university, to sniff unlabeled bottles of amniotic fluid and breast milk from both groups of mothers. If these amateur sommeliers could smell the garlic in a blind test, it was likely that the fetuses could, too, Mennella reasoned—and the volunteers easily sniffed out which came from the garlic consumers. Mennella next videotaped and documented how babies born to both maternal groups behaved when they were offered garlicky milk. Contrary to the old folk wisdom, the babies whose mothers had eaten garlic sucked their milk down with relish. In contrast, infants with garlic-free mothers grimaced and writhed to avoid it.

Downloaded from www.sciencemag.org on August 15, 2014

PHOTO: WENDELL/DAMBROSIA/WEESTOCK/CORBIS



Published by AAAS

Since that series of studies in the 1990s, Mennella and Beauchamp have obtained similar results with other flavors such as vanilla and carrot. Familiarity seems to breed affinity for substances such as alcohol, too, Mennella says. In one study, she and Beauchamp found that 1-year-olds with heavy-drinking or alcoholic parents prefer to mouth toys scented with ethanol over unscented or vanilla-scented toys.

Research in mice hints at a potential neurobiological basis for these early associations, says Diego Restrepo, a developmental biologist at the University of Colorado School of Medicine in Aurora. In 2010, he fed cherry- or mint-flavored chow to pregnant mice, then studied which flavor their offspring preferred at 20 days old. Like the human infants, the young mice preferred to eat the chow flavor they'd been exposed to in utero.

Neurons that relay information about smell from the nose to the brain respond individually to thousands of odorant molecules, allowing mice and humans to distinguish a vast array of different smells—possibly as many as 1 trillion odors in humans (*Science*, 21 March, p. 1370). On examining the brains of the two groups of rodents, Restrepo found that in mice exposed to the mint flavor in utero, the junctions between the olfactory sensory neurons that can detect mint and those that relay a mint signal to the amygdala, a brain region that processes emotion, were significantly enlarged. In mice exposed to cherry, those junctions between neurons relaying the cherry signal were bigger, suggesting that experience with the smell in utero had strengthened those connections, he says.

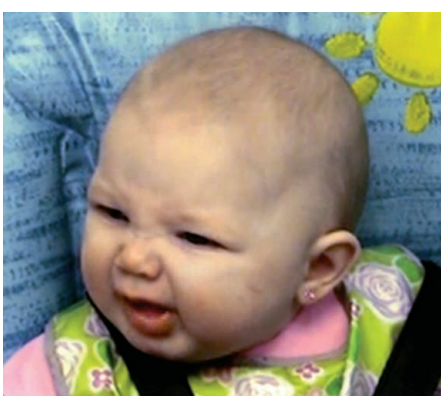

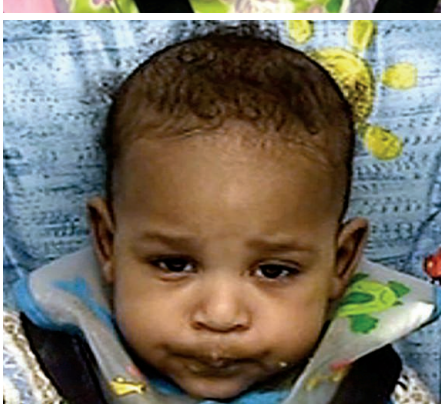

A baby rejects a novel flavor (*top*), while another exposed to a flavor in utero accepts it (*bottom*).

PHOTOS: (BOTTOM LEFT) CATHERINE FORESTELL AND JULIE MENNELLA/MONELL (2); (TOP RIGHT) NESTLE/PETIT FORMAT/SCIENCE SOURCE

More evidence that maternal diet can influence the developing brain's flavor processing came from a study published last year in *The FASEB Journal* by researchers at the University of Adelaide in Australia. They fed pregnant rats either a monotonous diet or a smorgasbord of tempting treats, including hazelnut spread, peanut butter, chocolate biscuits, sweetened cereal, and a lard and chow mix. Then they observed how the offspring behaved around those foods. Mice whose mothers had a junk food diet developed abnormal neural reward circuitry resembling that seen in addiction.

**SOME RESEARCHERS DOUBT** that prenatal or early postnatal experiences with flavor have much long-lasting effect. Adults are clearly capable of learning to love and hate new flavors, as anyone who's lost their taste for a favorite food after a bout of nausea can attest. And if you compare foods that college students enjoy with those they ate under their parents' watchful gazes, the correlation "is not zero, but it's very low," says Paul Rozin, a psychologist at the University of Pennsylvania.

But Mennella and others believe that there are sensitive periods for flavor learning, just as there are for the development of sight and other senses. At 3.5 months old, many babies will refuse to drink Nutramigen, a sour, bitter-tasting formula often prescribed to underweight infants who can't digest cow's milk. She and Beauchamp have shown that if the infants start the formula before that age, most will happily drink the nasty-tasting stuff, and even prefer it. Understanding why infants learn to accept different flavors could help guide treatment for premature babies, who frequently spend their first months of life being tube-fed and often gag when they first taste milk or formula, Mennella says.

From an evolutionary point of view, infants need to be receptive to new flavors early in life in order to survive, says Regina Sullivan, a psychiatrist at New York University Langone Medical Center in New York City. Because baby mammals depend so much on their parents, it makes sense that a mechanism exists to ensure that newborns learn to eat what mothers can provide no matter how it tastes, she explains.

Mennella hopes that understanding early-life influences on diet in children will help parents buffer children from an environment increasingly filled with sugar- and salt-laden foods. That is challenging because, as she and Beauchamp have found, infants are more sensitive than adults to both sweet flavors and bitter ones, making it harder for them to resist sugary foods and to eat vegetables.

A handful of correlational studies suggest that children eat more fruits and vegetables later in life if their mothers did the same while pregnant or breast-feeding. Rozin notes, however, that it is difficult to determine how much those early experiences affect long-term outcomes because the foods we're exposed to at a very young age often continue to surround us up until we leave the nest.

The most potent aspect of early flavor experiences may be their emotional power, Mennella says. Our first flavors are among "the oldest, most enduring memories that take us to our past," she says. "Food is much more than a source of calories—it provides us with an identity." ■

## Training the fetal palate

A fetus learns to recognize the flavors of mom's diet through her amniotic fluid.

### Taste

By 16 weeks old, the fetus begins to respond to flavors in amniotic fluid, swallowing and smacking its lips if it tastes sweet, and grimacing and swallowing less fluid if it tastes bitter.

### Smell

At 24 weeks, olfactory receptor cells that respond to different odors begin to function, when plugs obstructing the nasal passages dissolve and allow the fetus to inhale and smell amniotic fluid.



Published by AAAS

# An experiment in zero parenting

## A controversial study of Romanian orphans reveals long-term harm to the intellect

*By* **Eliot Marshall**

An unnerving sight greeted U.S. scientists a decade ago at an orphanage in Bucharest. The institution housed "many children rocking back and forth while sitting or on all fours, turning their head from side to side, or repeatedly bringing their hand to their face, often slapping themselves," write neuroscientists Charles Nelson and Nathan Fox and psychiatrist Charles Zeanah in their book *Romania's Abandoned Children*, published in January. The children's empty motions, or "stereotypies," are like the pacing of a tiger or elephant in the zoo. They are one of the abnormalities under scrutiny in a study of child neglect Nelson and his team launched in 2000.

What the researchers saw was the legacy of a tragic scheme to boost Romania's population. Former dictator Nicolae Ceaușescu decided in the late 1960s that Romania needed to grow; the government taxed women who had fewer than five children, regardless of what they could afford. To care for thousands of unwanted children, the government filled orphanages. They weren't designed or funded to mimic family life, but they were busy.

At their peak in the late 1980s, the orphanages housed nearly 170,000 children. Most grew up in a stunningly blank and unresponsive environment. Caregivers came and went in three shifts, and a single staffer might watch over 10 to 15 children. Infants spent time staring at the walls and ceiling, and a child might come in contact with 17 different caregivers in a single week. Nelson, a professor of pediatrics and neuroscience at Harvard Medical School in Boston, calls it an experiment in zero parenting.

After Ceaușescu's fall and execution in 1989, people from around the world adopted thousands of the orphans. (Romania later put a brake on this.) Researchers have studied these early international adoptees—some with serious emotional problems—for 2 decades now, examining how child rearing can go wrong, how it alters behavior, and how foster parenting can rescue lives. The Nelson group, known as the Bucharest Early Intervention Project (BEIP), saw a chance to answer an additional, specific question: How does neglect in early childhood change neurological development?

The researchers launched a radical and, at the time, controversial study. Using U.S. and private foundation funding, they teamed with Romanian officials to run a controlled study comparing a group left in orphanages with a group randomly selected for high-quality foster care in Romania. In a stream of reports since 2003, they have shown that children reared in institutions suffer an array of setbacks, some reflecting long-term changes in the brain (*Science*, 21 December 2007, p. 1937). The team is now analyzing data from the 12th year, measuring things like disparities in brain structure.

Findings from the Bucharest project have buttressed those from smaller and less controlled studies, many based on U.S. children in troubled homes. "We are all reporting the same effects," says Megan Gunnar, a clinical psychologist at the University of Minnesota (UMN), Twin Cities, who is not part of BEIP. "The brain needs stimulation to develop," and when it doesn't get it, cognitive and emotional growth are stunted.

Today, Nelson is convinced that early life without parenting can be "more disastrous for brain development" than living with an abusive caregiver. But the Romanian work also confirms that many children can bounce back to something like normality, if placed in a supportive environment. No country should be complacent, Nelson adds, noting that what he saw in Romania is "not all that different from the kind of neglect that many kids in the United States experience."

> ***"Children are learning: 'Why should I cry, or gesture, or make eye contact if no one is responding?' "***
>
> **Seth Pollak**, University of Wisconsin, Madison

### CHILD NEGLECT IS "A HUGE PROBLEM"

and probably "the most common form of child maltreatment in the world," says Seth Pollak, a clinical psychologist at the

PHOTO: WILLIAM SNYDER

Downloaded from www.sciencemag.org on August 15, 2014



Published by AAAS

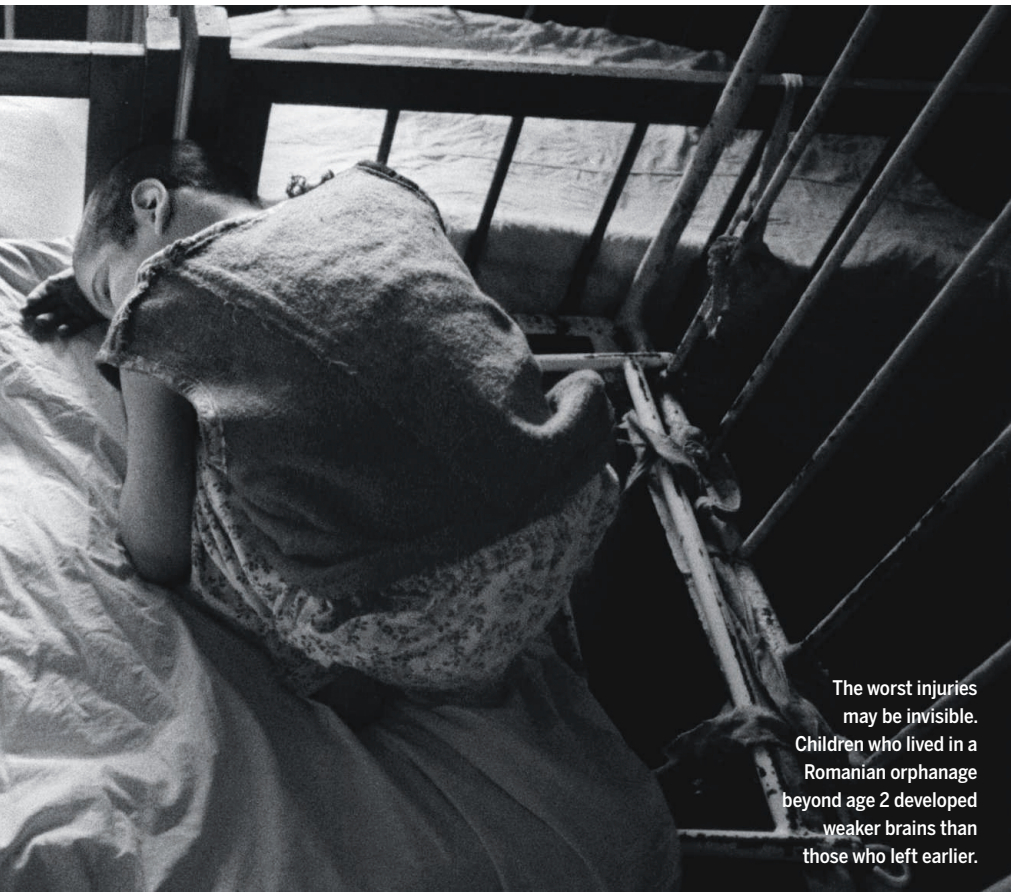

The worst injuries may be invisible. Children who lived in a Romanian orphanage beyond age 2 developed weaker brains than those who left earlier.

University of Wisconsin, Madison. Each year, the U.S. National Child Abuse and Neglect Data System tracks about 3 million case reports of maltreatment. These data suggest that neglect is nearly three times as prevalent as physical and sexual abuse combined. And the numbers may understate the problem because it's so difficult to see: "It's the absence of something happening between a parent and child when nobody else is around," Pollak says: "How do you measure it?"

Yet the consequences are haunting. The "creepiest thing" about the Romanian orphanages and other places where young children suffer chronic neglect is that "they're quiet," Pollak says. In most U.S. elementary schools or child care centers, he says, "you hear talking and screaming and crying … it's just raucous." But in "an environment where children are not being attended to, there is this kind of dead silence. … Children are learning: 'Why should I cry, or gesture, or make eye contact if no one is responding?' "

The problem is insidious because neglected children often don't have injuries and don't get the attention that victims of physical or sexual abuse receive. "They wind up coming to the emergency room when they're 5 years old and weigh 20 pounds," Nelson says, long after the damage is critical.

Neglect is difficult to study. Researchers normally can't control a child's environment, and they usually don't know what harm a child has experienced before he or she appears in the clinic. This is especially true for children living in poverty, says Gunnar, who sees many of them. "We can use fancy statistics to try to isolate the early effects from continuing and ongoing adversity," but the results are uncertain.

## Types of maltreatment

Percent of U.S. child-harm reports in 2010

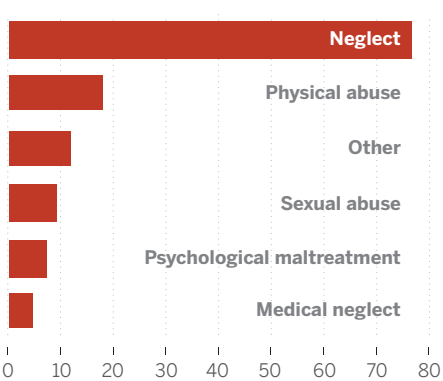


Source: U.S. Dept. of Health and Human Services

The opening of Romanian orphanages after Ceaușescu provided a rare chance to do well-controlled studies. A U.K. group then led by pediatric psychologist Michael Rutter at King's College London undertook the first, a large observational study. The English and Romanian Adoptee (ERA) project, as it was known, spent 2 decades comparing the development of children adopted by U.K. families with children who had not been institutionalized.

The BEIP group chose a more direct approach: It partnered with Romanian officials to conduct research within the orphanage network. BEIP offered to finance foster care for a small group of children who would exit the institutions; in return, Romania opened the doors and helped with a testing program.

BEIP came under fire in Europe for including *any* children still in an institution. Such vulnerable kids were incapable of giving consent, critics argued. Zeanah, a pediatrician and psychiatrist at Tulane University in New Orleans, Louisiana, involved in designing BEIP protocols, claims that the furor was based on "a misunderstanding" about the project's link to international adoption efforts, and European Commission officials ultimately dismissed concerns. BEIP investigators still hear from critics who "just cannot accept randomization" of children to a group that may not benefit, Zeanah says, but it was essential to make the trial work.

After screening to exclude children with genetic or neurological abnormalities, study leaders selected 136 children for the trial, ranging in age from 6 to 31 months. By random assignment, 68 went into a group that received BEIP-funded foster care and 68 were left to continue with "usual" care—that is, they lived in an institution. Foster caregivers were screened, trained, and paid a "living wage," Nelson says. It was deluxe care even by U.S. standards. BEIP experts monitored and consulted with the caregivers, who also had 24-hour pediatric medical backup. As controls, BEIP included a group of 72 children from Romanian communities who had never lived in an institution. Researchers gathered test results at 30 months, 42 months, 54 months, 8 years, and 12 years. They have been funded to return at 15 years.

Children in the institutional care group showed dramatic deficits on a variety of measures when compared with the community group. In an age-adjusted system that converts test results from young children into IQ-comparable scores, known as the developmental quotient (DQ) scale, the institutionalized kids at the outset earned an average DQ score of 74 compared with



Published by AAAS

103 for the community group. This was "two standard deviations below the mean" for children of that age, according to BEIP, suggesting "profound intellectual delay."

In time, the kids placed into foster care advanced toward the normal DQ and IQ ranges, though they continued to lag behind the community group. When BEIP tested children at 42 months, researchers found that the older a child was when placed into foster care, the lower the cognitive score was likely to be. Those who left the institution by 18 months scored above 90 on the DQ scale, whereas those who left at 24 to 30 months scored just over 80. Those who remained in institutions up to age 8 exhibited a "progressive decrease in IQ with age," the BEIP authors wrote.

Strangely, as they reached 8 years of age, the foster care children began to slow their climb into higher DQ and IQ scores and came to rest on a par with the children in the institutionalized group, with IQ scores hovering near 80. Both ranked "far below" children who had never lived in an institution, according to BEIP, perhaps because their recovery from the effects of early neglect had reached a ceiling.

Meanwhile, the gradual dissolution of study categories and the start of regular schooling may have helped boost scores in the institutionalized group. By 8 years of age, only 14 of the 68 kids originally assigned to institutional care remained in place; most had settled with relatives or foster families. Yet, as planned, the analysis treated them as belonging to their initial group. As children bailed out of orphanages, their experience of family life may have boosted DQ and IQ scores.

The good news is that IQ does seem to rebound in children who leave institutional care—the sooner they leave, the better, according to Nelson's group. BEIP found that children who left an institution by 24 months seemed to recover best. Other researchers agree about the need to get out early, but differ about timing. For example, the United Kingdom's ERA study found that children adopted into British families seemed to score just as well as community kids if they left the institution by 6 months of age. Both BEIP and ERA have found that certain behavioral problems, such as poor attention and hyperactivity, persist among kids who were in institutions for any period.

BEIP also showed that the longer children lived in an institution before going into foster care, the more likely specific neurological changes would appear. The thesis underlying all of this work is that a baby's brain "expects" regular stimulation, the kind that comes from an attentive caregiver. If this doesn't occur, neurons don't grow properly. This leads to abnormalities that show up in neural activity and brain structure.

BEIP researchers used small, sensor-laden caps to take snapshots of brain electrical activity, known as electroencephalography (EEG) readings, when children first joined the trial and at several intervals over the years. At the start, children living in institutions had lower EEG output than did children living in the community in the high-frequency alpha and beta EEG ranges, and larger output in the low-frequency theta range. This pattern, considered a sign of brain immaturity, persisted into the eighth year. Children placed in foster care before 24 months of age, however, developed EEG patterns with elevated alpha signals by 8 years of age that were "indistinguishable" from those of community children.

Institutional care also seems to have left a mark on the children's brain structure. In a 2012 paper in the *Proceedings of the National Academy of Sciences*, members of the BEIP group reported on an imaging study of Romanian children 8 to 11 years old. Using magnetic resonance imaging, Margaret Sheridan of Boston Children's Hospital and others found that Romanian kids raised in an institution had significantly less brain tissue, especially gray matter (a mix of various cell bodies), than those who had never lived in an institution. But children who had been placed in foster care showed a smaller deficit. "These reflect profound effects on the brain," Nelson says.

Like other studies, the BEIP project suggests that brain development passes through critical periods. The first 24 months of life seem especially important for cognitive development, and Nelson says that the critical period for healthy attachment to a parent lasts through the first 20 to 22 months. For language, the window appears to be up to 16 months. But there are no sharp lines, says UMN's Gunnar. "The general story seems to be that the brain is remarkably plastic" and can find many ways around obstacles. But neglect makes things harder.

The BEIP team is likely to retain its status as the only randomized controlled study of child neglect and its effects. Back when the trial began, some Romanian leaders were arguing that foster care would be worse than institutional care. But now that BEIP has demonstrated the opposite, the study most likely will never be repeated.

Romania has changed its own policies, according to Zeanah. It began a foster care system when BEIP's results started coming out. Later, he says, it banned the placement of children younger than 2 in institutions. The number of children in Romanian institutions today has dropped to below 20,000; many, according to Zeanah, are severely handicapped children in group homes.

Nelson says that his work and other Romanian studies have had global impact by, for instance, helping the United Nations Children's Fund in its efforts "to convince governments around the world to stop putting kids in institutions." There's plenty of convincing to be done: Orphanages around the globe still house an estimated 8 million children. ■

## Early foster care linked to stronger brain development

EEG readings from Romanian 8-year-olds

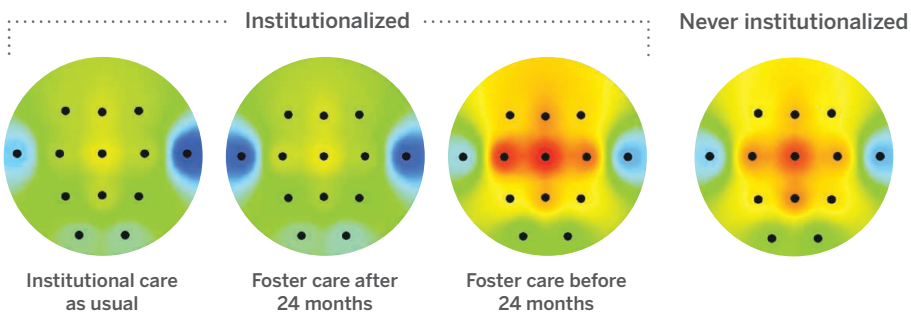


Source: Charles A. Nelson III

**Scalp EEG readings from 8-year-olds reveal big differences in the alpha (high-frequency) range. The institutionalized group (*far left*) and those assigned to foster care after 24 months had statistically similar, weak results (cool colors). Those assigned to foster care before 24 months (*third from left*) or never in an institution had strong alpha results. The two leftmost groups appear to have significant delays in brain development.**



Published by AAAS

OPINION

# Maternal mental illness

In the United States, more than half a million women experience postpartum depression every year; among teens and low-income mothers, the rate is one in four. For many depressed mothers, symptoms begin during pregnancy and may also include disabling anxiety. In addition, maternal mental illness adversely affects infant brain development and subsequent social and emotional health as a result of inadequate prenatal care, poor birth outcomes, and impaired parenting practices. The broad implications of these disorders have led several states to require perinatal depression screening and/or education. Also, a provision of the U.S. Affordable Care Act calls for further research on screening and treatment. These policies are a good start, but laws already on the books must be adequately funded and evaluated. In addition, there are immediate policy actions that can be taken to improve the well-being of mothers and families.

The pathogenesis of perinatal depression is not yet fully understood, but human and animal studies have highlighted possible interconnected contributors, including hormonal dysregulation, abnormalities of the hypothalamic-pituitary-adrenal axis, genetic vulnerability, and epigenetic effects. Social and behavioral research has revealed sociodemographic predictors of perinatal depression, including history of depression, lower socioeconomic status, poor social support, and stressful life events. In 2006, New Jersey became the first U.S. state to mandate universal screening for postpartum depression. Unfortunately, this legislation did not improve detection and treatment for low-income mothers. This is because the law, and others like it, are undermined by challenges at three levels: the patient level (e.g., mental health stigma), the provider level (e.g., lack of awareness, time, and reimbursement for screening and treatment), and the system level (e.g., inadequate insurance systems and lack of care integration). It is at the system level where policy changes can have the largest effects.

Each year, up to 1 million U.S. women move in and out of health insurance coverage shortly after giving birth. State Medicaid programs finance 48% of U.S. births, but women with incomes above $32,000 (for a family of four) lose this coverage 60 days after giving birth when their "pregnancy" eligibility ends. The timing of this insurance disruption is especially cruel because anxiety and depression symptoms often worsen in the 2 to 3 months after childbirth. Policy-makers could help by requiring consistency in mental health benefits across the perinatal period and overlap of provider networks between Medicaid and private insurance plans.

In addition, screening must be bridged with coordinated, comprehensive treatment and support. The idea of "treatment" is often narrowly thought of as psychiatric medication or talk therapy, leaving out important community, peer, and family support. This is particularly important for women who frequently fall through the cracks: those who are low-income, drug-addicted, rural, racial/ethnic minorities, or immigrants. Increasing the use of patient-centered medical homes could bring together diverse teams (including doctors, social workers, nurses, community health workers, doulas, etc.) to meet these patients' needs. In the United Kingdom, for example, a coordinating health care professional is identified for each woman, routine services include both clinic and home visits, and all patient information is shared among the providers involved in her care, before and after childbirth.

*"...U.S. families...deserve screening and comprehensive treatment for perinatal depression and anxiety..."*

Beyond the realm of health insurance and care delivery systems, families with babies are further strained by the lack of paid maternity leave and affordable high-quality childcare. As President Obama recently commented, "...the United States is the only developed country in the world without paid maternity leave." Policies to reduce family financial stressors contribute to maternal and child well-being. The 4 million U.S. families who will welcome a new baby this year deserve screening and comprehensive treatment for perinatal depression and anxiety, clinicians who embrace system-level change, and legislators who stand up for improved health for women and families.

**– Katy B. Kozhimannil and Helen Kim**

*Katy B. Kozhimannil is an assistant professor in the Division of Health Policy and Management at the University of Minnesota School of Public Health, Minneapolis, MN 55455. E-mail: kbk@umn.edu*

*Helen Kim is a perinatal psychiatrist in the Mother-Baby Program, Department of Psychiatry, Hennepin County Medical Center, Minneapolis, MN 55415. E-mail: kimxx237@umn.edu*

10.1126/science.1259614

PHOTOS: (INSET) CARLOS DOMINGUEZ/GETTY IMAGES; (TOP RIGHT) UNIVERSITY OF MINNESOTA SCHOOL OF PUBLIC HEALTH; (BOTTOM RIGHT) SHEILA RYAN PHOTOGRAPHY

Downloaded from www.sciencemag.org on August 15, 2014



Published by AAAS

REVIEW

# Parenting from before conception

Michelle Lane, Rebecca L. Robker, Sarah A. Robertson*

**At fertilization, the gametes endow the embryo with a genomic blueprint, the integrity of which is affected by the age and environmental exposures of both parents. Recent studies reveal that parental history and experiences also exert effects through epigenomic information not contained in the DNA sequence, including variations in sperm and oocyte cytosine methylation and chromatin patterning, noncoding RNAs, and mitochondria. Transgenerational epigenetic effects interact with conditions at conception to program the developmental trajectory of the embryo and fetus, ultimately affecting the lifetime health of the child. These insights compel us to revise generally held notions to accommodate the prospect that biological parenting commences well before birth, even prior to conception.**

Our constitution at birth informs how we respond to stressors and challenges, and the risk of disease, in childhood and through adult life. Experience in utero is a major determinant (*1*), but earlier life phases, commencing with oocyte and sperm, are also important. At conception, the gametes deliver the genetic material to form an embryo, plus a legacy of additional information, reflecting the exposures and experiences of both parents—not just mother, but father, too. If emerging concepts in transgenerational epigenetic inheritance (*2*, *3*) are correct, the early embryo is exquisitely sensitive to signals from gametes and the environment. Here, we explore how events before and at conception shape our development and life-course trajectory.

The Robinson Research Institute and School of Paediatrics and Reproductive Health, The University of Adelaide, Level 3, Medical School, South Adelaide, SA, 5005 Australia.
*Corresponding author. E-mail: sarah.robertson@adelaide.edu.au

## The sensitive and adaptable early embryo

Strategies to discern how different pregnancy stages affect infant health reveal a crucial window in early embryonic development (*2*). During fertilization and the first zygotic divisions, the embryo is highly sensitive to signals from the mother's reproductive tract (Fig. 1). The oviductal fluid surrounding the embryo varies according to maternal nutritional, metabolic, and inflammatory parameters (*4*), providing a microcosm that reflects the outside world. In responding to these environmental cues, the embryo exerts a high degree of developmental plasticity and can, within a discrete range, modulate its metabolism, gene expression, and rate of cell division. In this way, the maternal tract and the embryo collaborate to generate a developmental trajectory adapted to suit the anticipated external environment, to maximize survival and fitness of the organism (*2*). But if the resulting phenotype is a poor match for conditions after birth, or if adaptation constrains capacity to withstand later challenges, offspring are at risk (*1*).

Maternal diet at conception has a major impact on the developmental program (*5*). Reduced protein content for just the first 3 days of embryogenesis retards cell proliferation and skews the balance of cell lineage differentiation in the blastocyst (*6*). The effect of nutritional disturbance at conception persists through implantation and influences placental development and nutrient transfer capacity (*7*), then after birth, the neonate gains weight more rapidly, developing higher systolic blood pressure and elevated anxiety (*6*).

Maternal inflammation at conception also can influence adult phenotype. Female mice given bacterial lipopolysaccharide (LPS) on the first day of pregnancy, mimicking a mild infection, deliver pups that develop abnormally increased body fat and reduced exploratory behavior (*8*). Offspring have reduced sensitivity to LPS challenge in adulthood, with a blunted cytokine response (*8*). This suggests that infection, or even noninfectious causes of inflammation in a mother, could lead to altered immune function in her child.

In vitro fertilization (IVF) techniques further illustrate the impact of physiochemical manipulation of the conception environment, since the embryo is exposed to physical conditions not encountered in vivo. Mice conceived by IVF display

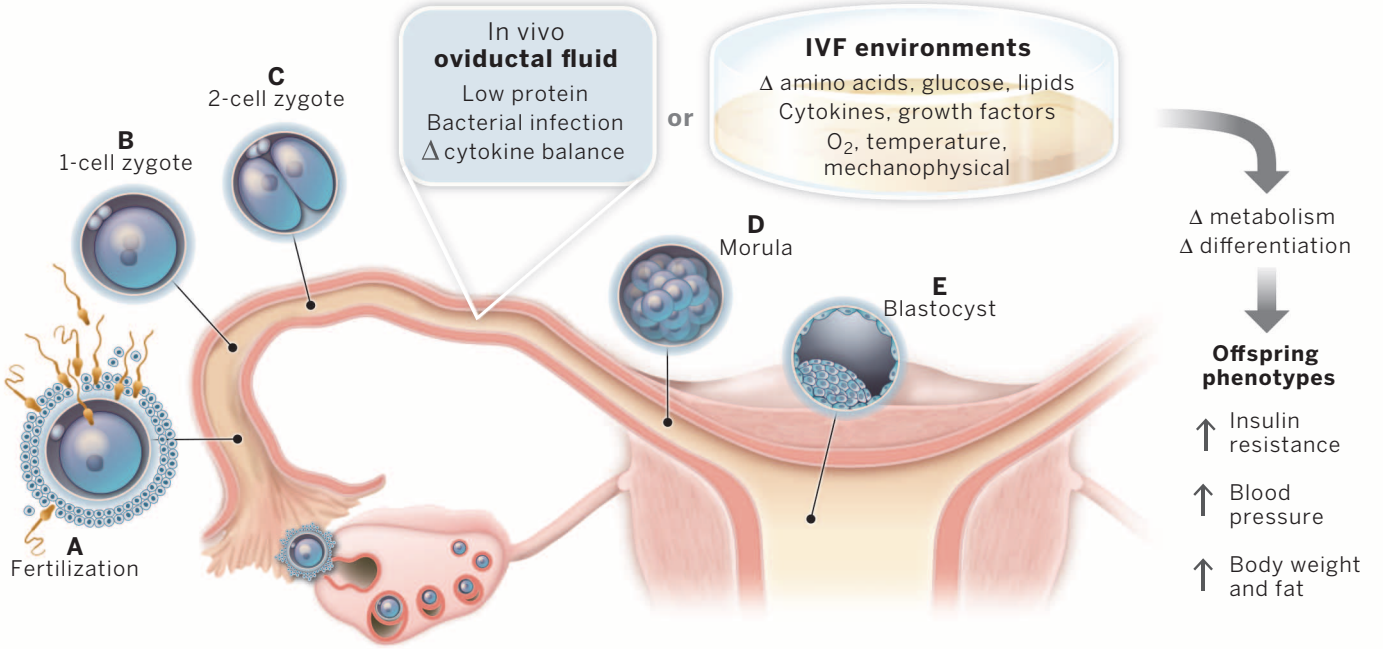


**Fig. 1. Environmental effects on embryogensis.** During progression from conception, through first cleavage to morula and blastocyst stages [(**A**) to (**E**), respectively], a preimplantation embryo is vulnerable to perturbations in its nutritional, biochemical, and physical environment. Influences exerted in the oviduct in vivo, or the culture dish in vitro, operate via epigenetic pathways to program embryo developmental trajectory, resulting in an altered adult phenotype.

increased fasting glucose, impaired glucose tolerance, and altered insulin signaling compared to naturally conceived controls (*9*). More rapid postnatal growth and fat deposition after IVF conception are associated with altered gene expression in liver, adipose tissue, pancreatic islets, and muscle (*10*), plus vascular stiffness, higher arterial blood pressure, and signs of endothelial dysfunction (*11*). Notably, adverse effects are retained if embryos are transferred to healthy recipients at the two-cell stage, implicating disruption of very early developmental events. Thus, at least in mice, conception by IVF alters later placental and fetal development, growth trajectory after birth, and metabolic parameters and behavior in adult life. In vitro–cultured embryos show changes to blastocysts and fetal growth that mimic many aspects of in vivo dietary and inflammatory insults (*12*), suggesting that endogenous cell stress may be a common pathway driving adverse impacts on offspring. Although the protocols implemented in animals are more aggressive than clinical IVF, emerging data suggest that in IVF-conceived children, blood pressure and fasting glucose are higher (*13*), and vascular dysfunction can be evident (*14*).

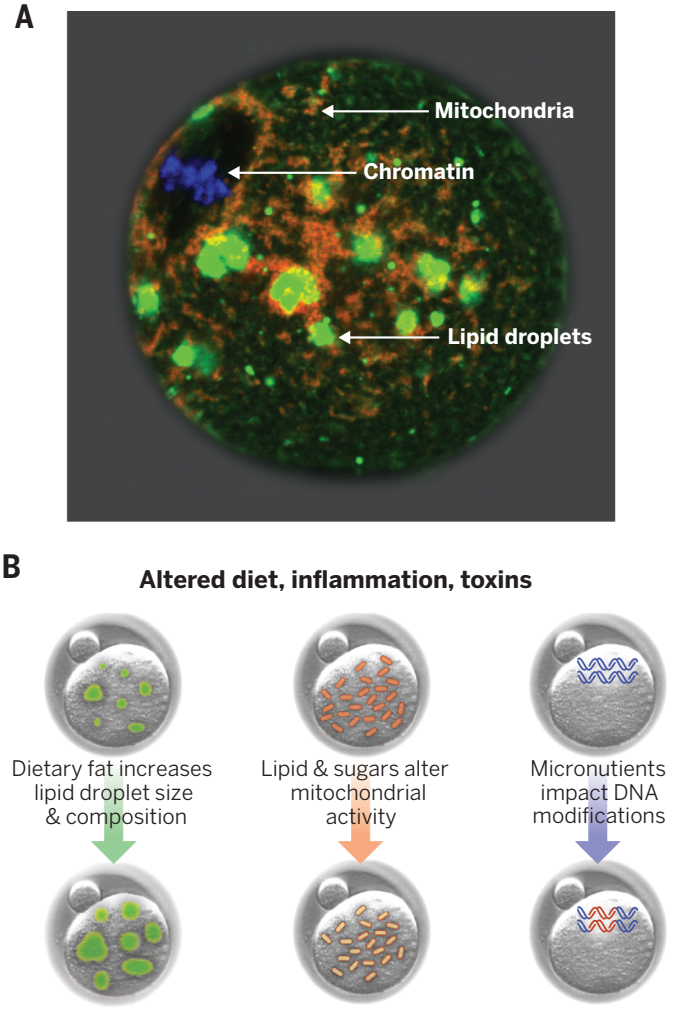


**Fig. 2. Maternal nutrition affects oocyte provisioning.** (**A**) The maternal environment influences oocyte stores of mitochondria and metabolites. Lipid droplets are stained green with BODIPY 493/503 in a mouse oocyte, and mitochondria are stained with MitoTracker Orange. Chromosomal DNA aligned at metaphase II is stained blue with Hoescht dye. (**B**) Cytoplasmic constituents respond to maternal nutrition and in turn alter conceptus development.

## Epigenetic reprogramming at conception

The periconception influences on development are believed to occur through environment-induced modification of the embryo's epigenome. A dynamic phase of epigenetic remodeling begins at fertilization, when most epigenetic marks are cleared from the oocyte and sperm genomes before fusion of the chromatin at syngamy, and is completed just before implantation when remethylation of the embryonic genome occurs (*15*). Altered methylation of cytosine residues, or loss of parental-specific imprinted marks, may be attenuated by the chromatin structure, including nucleosome positioning, and altered histone acetylation or assembly, which modulate the availability of DNA for transcription. Epigenetic marks are carried forward into daughter cells, where despite further modification by the developmental program, they permanently affect gene expression in resulting adult tissues (*15*).

Maternal nutrition at conception is a major influence on resetting of the epigenome in the early embryo—a compelling example is epigenetic control of the agouti viable yellow ($A^{vy}$) locus, which determines coat color in mice and is highly sensitive to methyl groups in the diet (*3*, *16*). DNA methylation in human infants was recently associated with seasonal variation in diet (*17*); similar epigenetic marks were present in different tissues, indicating that persistent systemic changes were established at conception.

Altered methylation patterns are also evident in embryos conceived by IVF or exposed to stress-inducing culture conditions (*16*, *18*, *19*). After IVF, mouse blastocysts show disrupted expression of the epigenetic regulator *Txnip* and enriched histone acetylation at its promoter, which are maintained into adulthood (*10*). Vascular dysfunction evident in IVF-conceived mice is associated with altered methylation of genes in the aorta (*11*)—but causal relationships between epigenetic changes and phenotypic alterations have not been demonstrated and are difficult to prove.

Specific classes of elements in the genome appear particularly sensitive to epigenetic dysregulation, including transposons (which control expression of the $A^{vy}$ locus) and genomically imprinted genes, which normally survive the global erasure of epigenetic marks at conception (*16*). Although the impact of IVF on transposons is not known, there is an increased incidence of imprinting disorders in IVF children, suggesting that maintenance of imprinted genes may be disturbed (*20*). However, genome-wide analysis of methylation shows no epigenetic changes attributable to IVF (*21*).

Intriguingly, males are consistently more vulnerable to most dietary, culture-induced, and physiochemical models of metabolic programming (*2*, *5*, *6*, *8*, *12*). Female embryos consume relatively more glucose, and male embryos develop more quickly to the blastocyst stage (*22*). Sex-dependent transcriptional differences in molecular pathways controlling glucose metabolism, protein metabolism, DNA methylation, and epigenetic regulation (*23*) likely cause sex-specific differential responses to environmental insults.

## Ex ovo omnia: All things come from eggs

Effects on oocytes contribute to the effects of maternal environment on offspring phenotype. Studies to isolate preconception effects from later pregnancy demonstrate that maternal nutrition during oocyte maturation influences offspring phenotype (Fig. 2). In sheep, maternal overfeeding generates offspring that accumulate fat (*24*), while in mice, a protein-deficient diet for 3.5 days before conception leads to hypertension (*25*).

Developing oocytes are suspended in follicular fluid that provides a unique nutritional environment which reflects maternal physiological states—for instance, adiposity (*26*). As the oocyte matures, it accumulates epigenetic marks, both on histones and DNA, until the final phases of maturation before ovulation. Although generally these marks are erased at conception, there is evidence that at some loci, oocyte epigenetic marks are not cleared, allowing the possibility of transgenerational inheritance. As well as maternally imprinted loci, epigenetic marks established in response to environmental cues may also be resistant (*3*, *27*). This is difficult to definitively demonstrate, because the complexity of the human genome makes it impossible to clearly distinguish genetic and epigenetic heredity (*27*).

Attributing effects to transgenerational inheritance requires experiments in inbred genetic backgrounds, and the use of oocyte transfer or cross-fostering to ensure that effects are truly transmitted through the germ line (*28*). Evidence from mice exposed to preconception zinc

deficiency is convincing, because embryos from mice fed a zinc-deficient diet for just 5 days before conception generated smaller fetuses prone to neural tube defects even after embryo transfer (*29*), and methylation of histones and chromatin was decreased in oocytes and retained in the maternal pronucleus after fertilization (*30*). Increased oocyte lipid content and cellular stress are also evident in mouse studies showing poor embryo and fetal development after maternal preconception diabetes or obesity (*31*, *32*).

Maternal nutritional influences on oocyte mitochondria are emerging as a pathway of lasting consequence to offspring (*33*). Embryogenesis is an energy-demanding process, and oocyte-derived mitochondria are required to support blastocyst formation (*34*). Alterations in maternal dietary protein affect mitochondrial localization and dampen mitochondrial activity in two-cell embryos (*35*) associated with later disturbances to fetal brain gene expression (*36*). In diabetic or obese mice, oocyte mitochondria fail to support normal embryo development (*31*, *32*). Promisingly, these defects are modifiable by diet—oocyte quality, mitochondrial function, and fertility in aged mice can be restored by caloric restriction (*37*) or an omega-3–enriched diet (*38*).

## Paternal programming—a new consideration

Paternal smoking, age, and occupational chemical exposure are well known to be linked with increased risk of cancer and neurological disorders in children (*39*, *40*). It is less well appreciated that the father's body mass has a greater impact than the mother's on body fat and metabolic measures in prepubertal children (*41*). As well as sperm DNA damage, in some instances there is accumulating evidence for pathways of paternal transgenerational epigenetic effects, attributable to sperm and seminal fluid (*42*, *43*). Interest in paternal epigenetic contributions stems from human epidemiological studies, relating a grandfather's food availability to mortality in grandsons (*44*) and associating paternal smoking with increased body mass index in male children (*44*). Paternal obesity is associated with changes to methylation in cord blood from offspring, at the demethylated region of *IGF2* and possibly other imprinted genes (*45*). Although this can be interpreted as evidence for an epigenetic pathway, as for all human cohort studies, the possibility of shared genetic or nongenetic programming contributions cannot be discounted (*27*).

Rodent models have been developed to assess epigenetic transmission of metabolic and other phenotypes via the paternal line (*42*). For example, male mice fed a low-protein diet fathered offspring with decreased hepatic cholesterol esters and altered hepatic expression of lipid and cholesterol biosynthesis genes, associated with altered epigenetic marks (*46*). Male mice born to undernourished mothers sired offspring with reduced birthweight and impaired glucose tolerance (*47*). Other rat studies showed that nutritional cues from the father result in female offspring with impaired metabolic health (*48*), associated with altered gene methylation and transcriptome changes within pancreas and adipose tissues (*48*, *49*). Rats exposed to the environmental toxin vinclozolin during development in utero have impaired spermatogenesis, which is transferred to male offspring (*50*). When male mice were conditioned to respond to a specific odor associated with a fear stimulus and then mated, their offspring inherited increased behavioral responses to the same odor (*51*). Similar transmissible effects are seen in the offspring of fathers exposed in early life to stress imposed by maternal separation (*52*). These intriguing studies raise the exciting prospect of specificity in paternal transmission and the possibility of targeted transmission of acquired characteristics; but to date, no biologically plausible mechanism has emerged.

## Fathers transmit DNA modifications to offspring

Genetic and epigenetic transmission mechanisms may be intertwined in sperm to transmit environmental exposures to the next generation (Fig. 3). Sperm development involves extensive DNA strand repair and chromatin remodeling in which histones are largely, but not completely, replaced by protamines (*43*). Both sperm nucleosome and histone-bound regions are conserved among mammalian species at loci of developmental importance—including promoters for early embryo development and imprinted regions (*53*). Compared with protamine-bound regions, genes in histone-bound regions appear more susceptible to DNA damage (*54*) due to smoking, obesity, and aging (*55*), compounded by the incapacity of sperm to repair DNA damage due to oxidative stress (*56*).

Histone-bound regions appear vital for paternal DNA replication following fertilization as well as activation of paternal genome transcription in the early embryo. Whereas the paternal protamines are replaced by maternal histones in the first 4 to 6 hours after fertilization, the retained paternal histones are not replaced; therefore, epigenetic marks to these histones are likely inherited by the embryo (*57*). Expression of SIRT6, a class III histone deacetylase, is regulated by metabolic state and is decreased in the testes germ cells of mice with diet-induced obesity, associated with increased DNA damage in transitional spermatids as well as mature sperm (*58*). This may explain why sperm from obese fathers can alter the developmental capacity of the embryo in vitro, altering rates of mitosis and early differentiation events (*59*), resulting in reduced pluripotency and metabolic function.

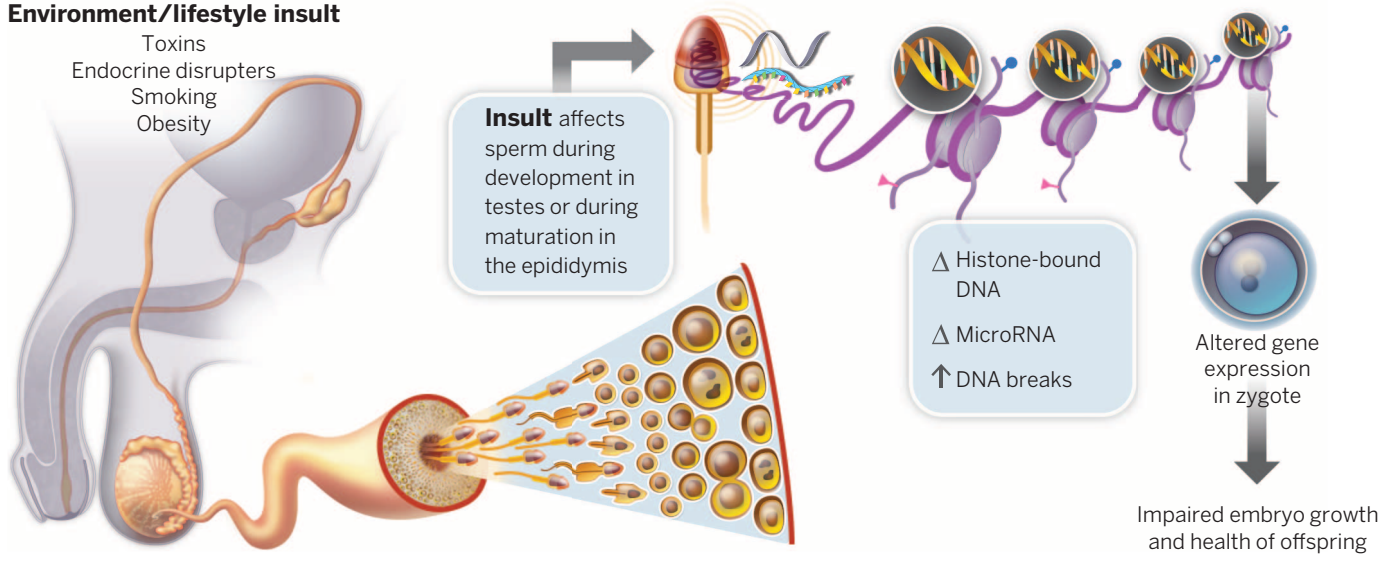


**Fig. 3. Environmental effects on paternal nongenetic contributions.** Postulated modes of action of environment or lifestyle factors on sperm function, imparted either during spermatogenesis or epididymal transit, and pathways for impact on the development of the embryo.

Although the sperm chromatin is substantially erased after conception, epigenetic marks are not completely reset. Mouse models of diet-induced paternal obesity produce sperm that are hypomethylated (*60*). When mothers are nutritionally restricted for the period of gestation in which reacquisition of methylation occurs in primordial germ cells of male fetuses, subsequent analysis of sperm from the adult $F_1$ offspring shows an altered germline DNA methylome, with hypomethylation of discrete loci associated with differential expression of genes involved in lipid oxidation in the fetal liver (*61*). Accompanying retention of nucleosomes instead of protamines in hypomethylated regions shows germline transmission in a chromatin context (*61*). Exposure in utero of male fetuses to environmental toxins alters the differentially methylated regions of sperm DNA (*62*) whereas in men, exposure to endocrine disruptor bisphenol A alters methylation of sperm DNA (*63*). An epigenetic pathway is implicated in transmission of paternal behavioral conditioning to offspring—in the case of the olfactory stimuli, both the father and his male offspring displayed hypomethylation of the *Olfr151* gene in sperm (*51*).

## Novel roles for sperm noncoding RNA

In addition to their tightly packaged DNA, sperm carry microRNAs, endogenous small interfering RNAs, and piwi-interacting RNAs (*64*). These noncoding RNAs can mediate epigenetic inheritance in lower organisms (*65*) and have the potential to influence developmental trajectory in mammalian embryos. Because each microRNA potentially regulates hundreds of mRNA transcripts, small shifts in microRNA profiles can be amplified through the molecular signaling cascades that regulate embryogenesis (*66*). Microinjection of miR-124 microRNA into the mouse pronuclear embryo can alter resultant offspring phenotype, causing cardiac hypertrophy and increased growth trajectory (*67*). The microinjected microRNAs persist only briefly, but altered gene expression is evident days later at the blastocyst stage, and change in chromatin structure in the promoter region of *Sox9* is inherited by the next two or three generations. In humans, smoking alters the microRNA profile in sperm, and in mice diet-induced obesity and early-life stress both alter sperm microRNA, persisting in the sperm of male offspring (*68*).

That oocytes with a null mutation in *Dgcr8*, a key subunit of the microRNA processing complex, generate normal blastocysts (*69*) initially suggested that microRNAs are unimportant in early embryo development. Although maternal microRNAs may be dispensable, some sperm-borne microRNAs appear capable of modulating embryo development. Most notably, psychosocial stress in early life altered mouse sperm microRNA, and injection of sperm RNAs from traumatized males into fertilized wild-type oocytes reproduced the behavioral and metabolic alterations in the resulting offspring (*52*). Sperm microRNA-34c was reported to be essential for the first cell division in mouse, through suppressing induction apoptosis (*70*), but a more recent report claims no change to male fertility in miR-34 null mutant mice (*71*).

## A contribution by seminal fluid?

As well as the sperm epigenome, information may be transmitted to offspring via the non-sperm fraction of the seminal fluid. Seminal plasma can alter offspring phenotypes through postejaculatory effects on sperm survival and functional competence, plus indirect actions on female factors that in turn regulate embryo development (*72*). Surgical excision of male accessory glands producing seminal plasma causes reduced fertility and is associated with impaired embryo development, largely attributable to sperm DNA damage due to oxidative injury in the female tract (*73*, *74*). An unexpected result of accessory sex gland excision seen in hamsters was altered postnatal growth and elevated anxiety in offspring (*73*). An epigenetic mechanism may be involved, as reduced acetylation in male pronuclei and retarded kinetics of demethylation and remethylation in cleavage-stage embryos were associated with dysregulated expression of paternally expressed *Igf2* and *Dlk1* in offspring of sex gland–excised males (*75*).

Even more surprising is the observation that seminal plasma may affect offspring independently of sperm. Seminal fluid directly stimulates the female reproductive tract to produce embryotrophic cytokines and growth factors that protect embryos from cell stress, and to suppress production of embryotoxic signals (*72*). When this cytokine balance is disrupted by ablation of seminal fluid signaling, altered programming of future fat deposition and metabolic phenotype occurs in offspring (*74*). The effect was particularly evident in male progeny, which showed a substantial increase in central fat and other hallmark characteristics of programmed metabolic syndrome. Given that infection and other exposures can alter seminal fluid signals (*76*), the prospect exists that male-to-female seminal fluid signaling can transmit information about paternal experiences.

## Summary

These emerging observations support the conclusion that parental influences begin before conception and compel us to further explore preconception pathways by which parents contribute more than genetic material to offspring. As well as effects of parental exposures on the genomic integrity of gametes, there is now clear evidence of epigenetic parental impact. From animal models allowing the temporal isolation of insults, we can confidently attribute outcomes on offspring of nongenomic effects mediated during maturation of the gametes, as well as effects of reproductive tract mediators on the preimplantation embryo.

Key questions to resolve are how exposures at specific stages of gamete development influence epigenetic marks in oocytes and sperm, just how early in development this begins, and the means by which these epigenetic marks survive zygotic reprogramming to be retained within the embryo. Investigating the extent to which epigenetic pathways are established and affected by interactions with noncoding RNA will likely be informative. Several questions are now pressing: Can programming conferred at or before conception be further modulated in offspring by later life events and insults? Or can it be influenced by the parents' or fetal genetics? What factors confer susceptibility or resilience to these interactions? Is this compounded or diluted in subsequent generations? Most excitingly, can acquired characteristics be transmitted by epigenetic pathways? These questions require careful analysis in appropriate models, with due consideration of confounding factors. Ultimately, once pathways are defined and prioritized according to importance for health outcomes, it will be possible to define how prospective parents can attenuate their lifestyle choices and adopt interventions to protect children from adverse outcomes.

### REFERENCES AND NOTES


1. K. M. Godfrey, P. D. Gluckman, M. A. Hanson, *Trends Endocrinol. Metab.* **21**, 199–205 (2010).
2. Z. Hochberg *et al*., *Endocr. Rev.* **32**, 159–224 (2011).
3. L. Daxinger, E. Whitelaw, *Nat. Rev. Genet.* **13**, 153–162 (2012).
4. H. J. Leese *et al*., *Reprod. Fertil. Dev.* **20**, 1–8 (2008).
5. T. P. Fleming, E. S. Lucas, A. J. Watkins, J. J. Eckert, *Reprod. Fertil. Dev.* **24**, 35–44 (2011).
6. C. Sun *et al*., *Development* **141**, 1140–1150 (2014).
7. A. L. Fowden, A. J. Forhead, P. M. Coan, G. J. Burton, *J. Neuroendocrinol.* **20**, 439–450 (2008).
8. C. L. Williams, J. L. Teeling, V. H. Perry, T. P. Fleming, *BMC Biol.* **9**, 49 (2011).
9. M. Chen *et al*., *Diabetes* (2014).
10. S. K. Feuer *et al*., *Endocrinology* **155**, 1956–1969 (2014).
11. E. Rexhaj *et al*., *J. Clin. Invest.* **123**, 5052–5060 (2013).
12. C. Sjöblom, C. T. Roberts, M. Wikland, S. A. Robertson, *Endocrinology* **146**, 2142–2153 (2005).
13. M. Ceelen, M. M. van Weissenbruch, J. P. Vermeiden, F. E. van Leeuwen, H. A. Delemarre-van de Waal, *J. Clin. Endocrinol. Metab.* **93**, 1682–1688 (2008).
14. U. Scherrer *et al*., *Circulation* **125**, 1890–1896 (2012).
15. W. Reik, *Nature* **447**, 425–432 (2007).
16. R. A. Waterland, R. L. Jirtle, *Nutrition* **20**, 63–68 (2004).
17. P. Dominguez-Salas *et al*., *Nat. Commun.* **5**, 3746 (2014).
18. A. S. Doherty, M. R. Mann, K. D. Tremblay, M. S. Bartolomei, R. M. Schultz, *Biol. Reprod.* **62**, 1526–1535 (2000).
19. T. Stojanov, C. O'Neill, *Biol. Reprod.* **64**, 696–705 (2001).
20. G. Lazaraviciute, M. Kauser, S. Bhattacharya, P. Haggarty, S. Bhattacharya, *Hum. Reprod. Update* (2014).
21. V. F. Oliver *et al*., *Fertil. Steril.* **97**, 147–53.e7 (2012).
22. D. K. Gardner, M. G. Larman, G. A. Thouas, *Mol. Hum. Reprod.* **16**, 539–547 (2010).
23. P. Bermejo-Alvarez, D. Rizos, D. Rath, P. Lonergan, A. Gutierrez-Adan, *Proc. Natl. Acad. Sci. U.S.A.* **107**, 3394–3399 (2010).
24. L. Rattanatray *et al*., *Endocrinology* **151**, 5195–5205 (2010).
25. A. J. Watkins, E. S. Lucas, A. Wilkins, F. R. Cagampang, T. P. Fleming, *PLOS ONE* **6**, e28745 (2011).
26. R. L. Robker *et al*., *J. Clin. Endocrinol. Metab.* **94**, 1533–1540 (2009).
27. J. H. Nadeau, *Hum. Mol. Genet.* **18**, R202–R210 (2009).
28. S. Chong, N. A. Youngson, E. Whitelaw, *Nat. Genet.* **39**, 574–575 (2007).
29. X. Tian, K. Anthony, T. Neuberger, F. J. Diaz, *Biol. Reprod.* **90**, 83 (2014).

30. X. Tian, F. J. Diaz, *Dev. Biol.* **376**, 51–61 (2013).
31. K. M. Luzzo *et al.*, *PLOS ONE* **7**, e49217 (2012).
32. L. L. Wu *et al.*, *Endocrinology* **151**, 5438–5445 (2010).
33. T. Wai *et al.*, *Biol. Reprod.* **83**, 52–62 (2010).
34. R. Dumollard, M. Duchen, J. Carroll, *Curr. Top. Dev. Biol.* **77**, 21–49 (2007).
35. M. Mitchell, S. L. Schulz, D. T. Armstrong, M. Lane, *Biol. Reprod.* **80**, 622–630 (2009).
36. T. Fullston, M. Mitchell, S. Wakefield, M. Lane, *Reprod. Fertil. Dev.* **23**, 691–701 (2011).
37. K. Selesniemi, H. J. Lee, A. Muhlhauser, J. L. Tilly, *Proc. Natl. Acad. Sci. U.S.A.* **108**, 12319–12324 (2011).
38. D. Nehra *et al.*, *Aging Cell* **11**, 1046–1054 (2012).
39. K. M. Lee *et al.*, *Leuk. Res.* **33**, 250–258 (2009).
40. I. D. van Balkom *et al.*, *PLOS ONE* **7**, e45090 (2012).
41. R. Figueroa-Colon, R. B. Arani, M. I. Goran, R. L. Weinsier, *Am. J. Clin. Nutr.* **71**, 829–834 (2000).
42. O. J. Rando, *Cell* **151**, 702–708 (2012).
43. J. R. Gannon, B. R. Emery, T. G. Jenkins, D. T. Carrell, *Adv. Exp. Med. Biol.* **791**, 53–66 (2014).
44. M. E. Pembrey *et al.*, *Eur. J. Hum. Genet.* **14**, 159–166 (2006).
45. A. Soubry *et al.*, *BMC Med.* **11**, 29 (2013).
46. B. R. Carone *et al.*, *Cell* **143**, 1084–1096 (2010).
47. J. C. Jimenez-Chillaron *et al.*, *Diabetes* **58**, 460–468 (2009).
48. S. F. Ng *et al.*, *Nature* **467**, 963–966 (2010).
49. S. F. Ng *et al.*, *FASEB J.* **28**, 1830–1841 (2014).
50. M. D. Anway, A. S. Cupp, M. Uzumcu, M. K. Skinner, *Science* **308**, 1466–1469 (2005).
51. B. G. Dias, K. J. Ressler, *Nat. Neurosci.* **17**, 89–96 (2014).
52. K. Gapp *et al.*, *Nat. Neurosci.* **17**, 667–669 (2014).
53. S. S. Hammoud *et al.*, *Hum. Reprod.* **26**, 2558–2569 (2011).
54. A. Noblanc *et al.*, *Free Radic. Biol. Med.* **65**, 719–723 (2013).
55. A. Kong *et al.*, *Nature* **488**, 471–475 (2012).
56. R. J. Aitken, T. B. Smith, M. S. Jobling, M. A. Baker, G. N. De Iuliis, *Asian J. Androl.* **16**, 31–38 (2014).
57. W. S. Ward, *Mol. Hum. Reprod.* **16**, 30–36 (2010).
58. N. O. Palmer, T. Fullston, M. Mitchell, B. P. Setchell, M. Lane, *Reprod. Fertil. Dev.* **23**, 929–939 (2011).
59. M. Mitchell, H. W. Bakos, M. Lane, *Fertil. Steril.* **95**, 1349–1353 (2011).
60. T. Fullston *et al.*, *FASEB J.* **27**, 4226–4243 (2013).
61. E. J. Radford *et al.*, *Science* 1255903 (2014).
62. M. Manikkam, C. Guerrero-Bosagna, R. Tracey, M. M. Haque, M. K. Skinner, *PLOS ONE* **7**, e31901 (2012).
63. M. Miao *et al.*, *Andrology* **2**, 138–144 (2014).
64. R. P. Yadav, N. Kotaja, *Mol. Cell. Endocrinol.* **382**, 498–508 (2014).
65. J. Brennecke *et al.*, *Science* **322**, 1387–1392 (2008).
66. G. C. Ostermeier, D. Miller, J. D. Huntriss, M. P. Diamond, S. A. Krawetz, *Nature* **429**, 154 (2004).
67. V. Grandjean *et al.*, *Development* **136**, 3647–3655 (2009).
68. A. Soubry, C. Hoyo, R. L. Jirtle, S. K. Murphy, *BioEssays* **36**, 359–371 (2014).
69. N. Suh *et al.*, *Curr. Biol.* **20**, 271–277 (2010).
70. W. M. Liu *et al.*, *Proc. Natl. Acad. Sci. U.S.A.* **109**, 490–494 (2012).
71. C. P. Concepcion *et al.*, *PLOS Genet.* **8**, e1002797 (2012).
72. S. A. Robertson, *Cell Tissue Res.* **322**, 43–52 (2005).
73. C. L. Wong *et al.*, *Theriogenology* **68**, 654–662 (2007).
74. J. J. Bromfield *et al.*, *Proc. Natl. Acad. Sci. U.S.A.* **111**, 2200–2205 (2014).
75. H. K. Poon, K. H. Lee, C. L. Wong, W. S. O, P. H. Chow, *Theriogenology* **71**, 1367 (2009).
76. J. K. Kafka *et al.*, *AIDS* **26**, 27–36 (2012).

**ACKNOWLEDGMENTS**

M.L., R.L.R., and S.A.R. are funded by the National Health and Medical Research Council (Australia). We thank L. Wu for the oocyte image in Fig. 2, and R. Richards and J. Thompson for critical comments. M.L. is an employee of Repromed Ltd. (Australia), and S.A.R. receives royalties on a patent describing use of granulocyte-macrophage colony-stimulating factor in IVF, licensed to Origio A/S (Denmark).

10.1126/science.1254400

REVIEW

# Preterm labor: One syndrome, many causes

**Roberto Romero,[1,2,3]* Sudhansu K. Dey,[4] Susan J. Fisher[5]**

**Preterm birth is associated with 5 to 18% of pregnancies and is a leading cause of infant morbidity and mortality. Spontaneous preterm labor, a syndrome caused by multiple pathologic processes, leads to 70% of preterm births. The prevention and the treatment of preterm labor have been long-standing challenges. We summarize the current understanding of the mechanisms of disease implicated in this condition and review advances relevant to intra-amniotic infection, decidual senescence, and breakdown of maternal-fetal tolerance. The success of progestogen treatment to prevent preterm birth in a subset of patients at risk is a cause for optimism. Solving the mystery of preterm labor, which compromises the health of future generations, is a formidable scientific challenge worthy of investment.**

Preterm birth, defined as birth before 37 weeks of gestation, affects 5 to 18% of pregnancies. It is the leading cause of neonatal death and the second cause of childhood death below the age of 5 years (*1*). About 15 million preterm neonates are born every year, and the highest rates occur in Africa and North America (*2*). Neonates born preterm are at an increased risk of short-term complications attributed to immaturity of multiple organ systems as well as neurodevelopmental disorders, such as cerebral palsy, intellectual disabilities, and vision and hearing impairments (*3*). Preterm birth is a leading cause of disability-adjusted life years [the number of years lost because of ill health, disability, or early death (*4*)], and the annual cost in the United States is at least $26.2 billion per year and climbing (*5*).

Two-thirds of preterm births occur after the spontaneous onset of labor, whereas the remainder is medically indicated because of maternal or fetal complications, such as preeclampsia or intrauterine growth restriction (*6*). Herein, we propose that preterm labor is a syndrome caused by multiple pathologic processes, summarize important strategies in the prevention of spontaneous preterm birth, and highlight promising areas for investigation.

## Preterm labor: Not just labor before term

A tacit assumption underlying the study of parturition is that preterm labor is merely labor that starts too soon. In other words, the main difference between preterm and term labor is when labor begins. This is perhaps understandable given that both involve similar clinical events: increased uterine contractility, cervical dilatation, and rupture of the chorioamniotic membranes (*7*). These events represent the "common pathway" of labor. The current understanding of this process is that the switch of the myometrium from a quiescent to a contractile state is accompanied by a shift in signaling from anti-inflammatory to pro-inflammatory pathways, which include chemokines [interleukin-8 (IL-8)], cytokines (IL-1 and -6), and contraction-associated proteins (oxytocin receptor, connexin 43, prostaglandin receptors). Progesterone maintains uterine quiescence by repressing the expression of these genes. Increased expression of the microRNA-200 (miR-200) family near term can derepress contractile genes and promote progesterone catabolism (*8*). Cervical ripening in preparation for dilatation is mediated by changes in extracellular matrix proteins, which include a loss in collagen cross-linking, an increase in glycosaminoglycans, as well as changes in the epithelial barrier and immune surveillance properties (*9*). This decreases the tensile strength of the cervix, key for cervical dilatation. Decidual or membrane activation refers to the anatomical and biochemical events involved in withdrawal of decidual support for pregnancy, separation of the chorioamniotic membranes from the decidua, and eventually membrane rupture. Increased expression of inflammatory cytokines [tumor necrosis factor–α (TNF-α) and IL-1] and chemokines, increased activity of proteases [matrix metalloprotease 8 (MMP-8) and MMP-9], dissolution of extracellular matrix components such as fibronectin, and apoptosis have been implicated in this process (*10*, *11*) (Fig. 1).

In our view, the common pathway is activated physiologically in the case of labor at term, whereas several disease processes activate one or more of the components of the common pathway in the case of preterm labor. This conceptual framework has implications for the diagnosis, treatment,

[1]Perinatology Research Branch, Program for Perinatal Research and Obstetrics, Division of Intramural Research, Eunice Kennedy Shriver National Institute of Child Health and Human Development (NICHD), National Institutes of Health, Bethesda, MD, Wayne State University/the Detroit Medical Center, Detroit, MI, USA. [2]Department of Obstetrics and Gynecology, University of Michigan, Ann Arbor, MI, USA. [3]Department of Epidemiology and Biostatistics, Michigan State University, East Lansing, MI, USA. [4]Division of Reproductive Sciences, Perinatal Institute, Cincinnati Children's Hospital Medical Center, Cincinnati, OH, USA. [5]Department of Obstetrics, Gynecology and Reproductive Sciences, Department of Anatomy, and Center for Reproductive Sciences, University of California San Francisco, San Francisco, CA, USA.
***Corresponding author. E-mail: romeror@mail.nih.gov**

and prevention of spontaneous preterm labor. For example, interest in myometrial contractility, the most recognizable sign of preterm labor, has led clinical and translational research to focus on the use of pharmacologic agents to arrest or decrease uterine contractility (i.e., tocolytics) with the goal of preventing preterm delivery. Yet, after decades of investigation, there is no persuasive evidence that inhibiting or arresting uterine contractility per se decreases the rate of preterm delivery or improves neonatal outcome, although these agents can achieve short-term prolongation of pregnancy for steroid administration and maternal transfer to tertiary care centers. We consider that, in most cases, tocolytic agents address a symptom and not the underlying cause(s) that activate the parturitional process. The extent to which the physiologic signals that mediate labor at term can be co-opted in the context of pathologic processes in preterm labor remains to be elucidated.

## Preterm labor as a syndrome associated with multiple mechanisms of disease

Spontaneous preterm labor is often treated implicitly or explicitly as if it were a single condition. Accumulating evidence suggests that it is a syndrome attributable to multiple pathologic processes (*7*). Figure 2 illustrates the mechanisms of disease implicated in spontaneous preterm labor. Of these, only intra-amniotic infection has been causally linked to spontaneous preterm delivery (*12*). The others largely have their bases in associations reported by clinical, epidemiologic, placental pathologic, or experimental studies.

### *Microbial-induced inflammation*

One of every four preterm infants is born to mothers with an intra-amniotic infection that is largely subclinical (*12*). Microorganisms isolated from the amniotic fluid are similar to those found in the lower genital tract, and, therefore, an ascending pathway is considered the most frequent route of infection. Bacteria involved in periodontal disease have been found in the amniotic fluid, suggesting that hematogenous dissemination with transplacental passage can also occur (*13*). Microbial-induced preterm labor is mediated by an inflammatory process. Microorganisms and their products are sensed by pattern recognition receptors, such as toll-like receptors (TLRs), which induce the production of chemokines [e.g., IL-8, and C-C motif ligand 2 (CCL2)], cytokines (e.g., IL-1β and TNF-α), prostaglandins, and proteases leading to activation of the common pathway of parturition (*12*, *14*, *15*) (Fig. 3A).

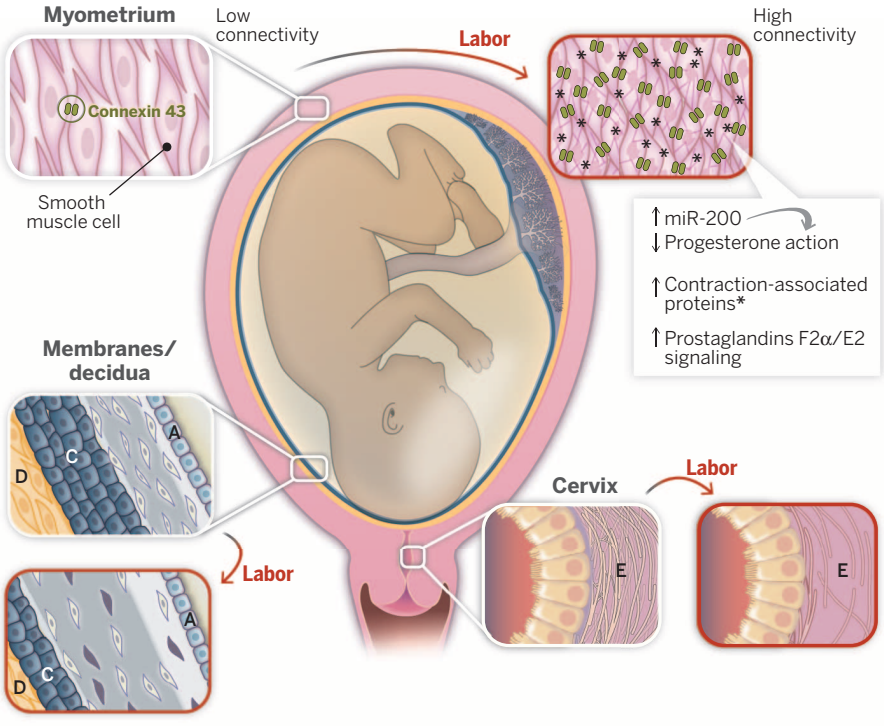


**Fig. 1. Labor (term and preterm) is characterized by increased myometrial contractility, cervical dilatation, and rupture of the chorioamniotic membranes.** Collectively, these events have been referred to as the common pathway of parturition. The switch of the myometrium from a quiescent to a contractile state is associated with a change in nuclear progesterone receptor isoforms and an increase in the expression of the miR-200 family, as well as an increase in estrogen receptor α signaling. Cervical ripening is mediated by changes in extracellular matrix proteins, as well as alterations in epithelial barrier and immune surveillance properties. Decidual or membrane activation, in close proximity to the cervix, occurs in preparation for membrane rupture and to facilitate separation of the chorioamniotic membranes and placenta from the uterus. E denotes extracellular matrix; M, mucus; Os, cervical os.

In 30% of cases of intra-amniotic infection, bacteria are identified in the fetal circulation (*16*), resulting in a fetal systemic inflammatory response (*17*). Such fetuses have multiorgan involvement and are at risk for long-term complications, such as cerebral palsy and chronic lung disease, underscoring that complications of infants born preterm are not only due to immaturity but also to the inflammatory process responsible for preterm labor. This has important implications because recent evidence suggests that down-regulation of congenital systemic inflammation in the neonatal period using nanodevices coupled with anti-inflammatory agents can reverse a cerebral palsy–like phenotype in an animal model (*18*).

From an evolutionary perspective, the onset of preterm labor in the context of infection can be considered to have survival value, because it allows the mother to expel infected tissue and maintain reproductive fitness. In a remarkable example of evolutionary co-option, the molecular mechanisms developed for host defense against infection in primitive multicellular organisms (e.g., pattern-recognition receptors in sponges) have been deployed in viviparous species to initiate parturition. This unique mechanism of maternal host defense comes at a price: prematurity. In terms of the fetus, inflammation may also have survival value near term, contributing to infant host defense against infection and accelerating lung maturation (*19*).

A central question is why some women develop an ascending intra-amniotic infection, whereas most do not. The relationship between the mucosa of the lower genital tract (vagina and cervix) and the microbial ecosystem appears key. Bacterial vaginosis, a change in the microbial ecosystem in which there is proliferation of anaerobic bacteria, confers risk for intra-amniotic infection and spontaneous preterm delivery. However, antibiotic treatment of asymptomatic women with bacterial vaginosis has not reduced the rate of preterm delivery. A comprehensive understanding of microbial ecology and genetic factors that control susceptibility to infection and the inflammatory response is required, particularly in light of evidence that gene-environment interactions may predispose some women to preterm labor (*20*). Viral infection has recently been shown to alter mucosal immunity in the lower genital tract and to predispose one to ascending bacterial infection (*21*).

Early studies of the vaginal microbiota in normal pregnancy using sequence-based techniques suggested that this ecosystem, which is different from that of the nonpregnant state, is more stable (*22*). Whether the vaginal microbiota and the local immune response of the vagina are different between women who subsequently deliver preterm and those who deliver at term are important unanswered questions (*23*, *24*). The factors responsible for changes in the vaginal microbiota during pregnancy remain to be established. Sex steroid hormones are attractive candidates, given that estrogens can induce the accumulation of glycogen in the vaginal

epithelium and also modify glycosylation (*25*). Carbohydrate structures are key for bacterial adherence to mammalian cells; therefore, sex steroid hormones could alter the microbiota of the lower genital tract.

At a mechanistic level, little is known about how preterm labor-related infections occur. On the pathogen side, the Group B *Streptococcus* pigment plays a role in the hemolytic and cytolytic activity required for ascending infection related to preterm birth (*26*). Further work is required to elucidate the role of the host. One intriguing possibility involves the "glyco-code," specific aspects of human carbohydrate structures that mediate the binding of bacteria via lectins and, subsequently, adherence. For example, *Helicobacter pylori* adhere via the Lewis b blood group glycan, making participants that express this antigen more susceptible to infection. Conversely, blood group O provides a selective advantage for surviving malaria (*27*). Whether similar mechanisms may help explain the increased frequency of spontaneous preterm birth in some ethnic groups is a question for in-depth exploration.

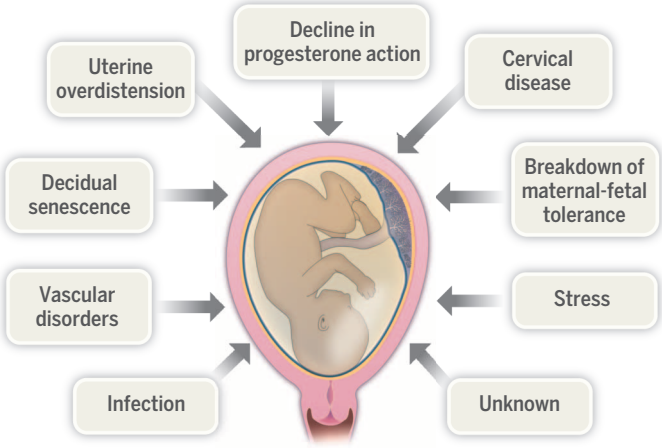


**Fig. 2. Proposed mechanisms of disease implicated in spontaneous preterm labor.** Genetic and environmental factors are likely contributors to each mechanism.

Although the maternal-fetal interface has traditionally been considered sterile, bacteria and viruses have been identified in first- and second-trimester decidua (*28*). Moreover, a placental microbiota has been described by using sequence-based techniques (*29*), along with differences reported between patients who delivered preterm and term (*29*). Large studies, such as those under consideration by the Human Placenta Project initiated by NICHD/NIH (*30*), are required to clarify the role of a putative placental microbiota and the maternal and fetal immune responses in normal pregnancy and spontaneous preterm labor. Recent studies using a combination of cultivation and molecular techniques suggest that intra-amniotic inflammation associated with spontaneous preterm labor occurs in the absence of demonstrable microorganisms, indicating a role for sterile intra-amniotic inflammation (*31*).

Extrauterine infections are also associated with spontaneous preterm delivery (e.g., malaria, pyelonephritis, and pneumonia). Indeed, from a global health perspective, malaria may be a major contributor to preterm birth in endemic areas. The mechanisms whereby malaria leads to preterm labor remain to be determined.

### Decidual hemorrhage and vascular disease

A subset of patients with preterm labor with intact membranes and preterm prelabor rupture of membranes have vaginal bleeding attributed to defective decidual hemostasis. Thrombin generated during the course of decidual hemorrhage can stimulate myometrial contractility and degrade the extracellular matrix in the chorioamniotic membranes, predisposing to rupture (*32*, *33*). Mothers with evidence of increased thrombin generation are at greater risk for spontaneous preterm labor. Uterine bleeding has also been observed with vascular lesions of the placenta. During normal pregnancy, cytotrophoblast invasion physiologically transforms uterine spiral arteries—small-diameter, high-resistance vessels—into large-diameter, low-resistance conduits that perfuse the chorionic villi of the placenta (Fig. 4, A, B, and D). About 30% of patients with preterm labor have placental lesions consistent with maternal vascular underperfusion, and a similar number have failure of physiologic transformation of the myometrial segments of the spiral arteries (*34*). In these cases, the vessel lumen fails to expand (Fig. 4, C and E), a pathological feature that is commonly associated with preeclampsia (maternal high blood pressure and protein in the urine) (*35*). An abnormal maternal plasma antiangiogenic profile in the midtrimester, which predates the symptoms of preeclampsia (*36*), has also been reported in a subset of patients who deliver preterm and have placental vascular lesions of underperfusion (*37*). Understanding why some women with these vascular lesions and an abnormal angiogenic profile develop preeclampsia and others preterm labor can provide insight into the pathophysiology of both conditions.

### Decidual senescence

Around the time of implantation, the endometrium undergoes anatomical and functional changes to become the decidua, which is crucial for successful implantation, pregnancy maintenance, and parturition. Decidualization is characterized by extensive proliferation and differentiation of uterine stromal cells into specialized cell types called decidual cells. The tumor suppressor protein p53 plays an important role in decidual growth, and its deletion causes implantation failure or, if pregnancy is established, inadequate decidualization. Premature decidual senescence has been implicated in implantation failure, fetal death, and preterm birth. In mice, conditional deletion of uterine *Trp53* leads to spontaneous preterm birth in 50% of cases (*38*), which is associated with decidual senescence demonstrated by increased mammalian target of rapamycin (mTOR) complex 1 signaling, p21 levels, and β-galactosidase staining but without progesterone withdrawal (*38*, *39*). The administration of rapamycin (an mTOR inhibitor) and/or progesterone attenuates premature decidual senescence and preterm birth. Evidence of decidual senescence has been demonstrated adjacent to the basal plate of the placenta (placental surface in direct contact with the uterine wall) in cases with preterm labor but not in women who delivered at term (*39*). Whether other mechanisms of preterm labor (e.g., infection and uterine bleeding) converge on decidual senescence is an open question. Additionally, it would be interesting to determine whether tissue stiffness, measured by atomic force microscopy, is a proxy for decidual senescence and therefore a biomarker (*40*).

### Disruption of maternal-fetal tolerance

The fetus and placenta express both maternal and paternal antigens and are therefore semiallografts (*41*). Immune tolerance is required for successful pregnancy (*42*, *43*), and a breakdown in tolerance can lead to a pathologic state (Fig. 2) with features of allograft rejection. Chronic chorioamnionitis, the most common placental lesion in late spontaneous preterm birth, is characterized by maternal T cell infiltration of the chorioamnion with trophoblast apoptosis and resembles allograft rejection (*44*). Maternal sensitization to fetal human leukocyte antigens is frequently found in patients with chronic chorioamnionitis and is accompanied by C4d deposition in umbilical vein endothelium (*45*, *46*). A novel form of fetal systemic inflammation characterized by overexpression of T cell chemokines (e.g., C-X-C motif ligand 10) (*47*) has been observed in chronic chorioamnionitis. Breakdown of maternal-fetal tolerance may be particularly relevant to preterm labor occurring after fetal surgery or stem cell transplantation, interventions that increase in the number of maternal T cells in the fetal circulation (*48*). The mechanisms linking disorders in tolerance and spontaneous preterm labor remain to be defined.

### Decline in progesterone action

Progesterone is key to pregnancy maintenance, and a decline in its progesterone action precedes labor in most species, which can be mediated by a reduction in serum levels of progesterone, local changes in metabolism, and/or alterations in receptor isoforms/coactivators (*49*, *50*). The administration

of progesterone receptor antagonists, such as mifepristone (RU-486), induces cervical ripening, spontaneous abortion, and labor in both animals and humans—hence the concept that a decline in progesterone may be responsible for some cases of preterm labor. Indeed, progesterone has effects on each component of the common pathway of parturition. Throughout gestation, progesterone promotes myometrial quiescence by reducing the expression of contraction-associated proteins (*51*) and inflammatory cytokines/chemokines (e.g., IL-1, IL-8, and CCL2) (*50*). Near term, increased myometrial expression of miR-200 family members counteracts many actions of progesterone, increasing its catabolism and inducing expression of proinflammatory cytokines/chemokines and prostaglandin synthase 2 (*8*). Progesterone's effects on the decidua and chorioamniotic membranes include inhibition of basal- and TNF-α–induced apoptosis, which protects the component cells from calcium-induced cell death and attenuates cytokine-induced MMP expression and activity (*52*). Progesterone has been implicated in the control of cervical ripening by regulating extracellular matrix metabolism (*9*). It is possible that the efficacy of progesterone in reducing preterm birth is due to a pharmacological effect rather than treatment of a progesterone deficiency.

### Other mechanisms of disease

Uterine overdistension has been implicated in spontaneous preterm birth associated with multiple gestations and polyhydramnios (an excessive amount of amniotic fluid). In nonhuman primates, inflation of intra-amniotic balloons can stimulate uterine contractility, preterm labor, and an "inflammatory pulse," which is characterized by increased maternal plasma concentrations of IL-1β, TNF-α, IL-8, and IL-6 (*53*). This finding is consistent with the observation that stretching human myometrium results in the overexpression of inflammatory cytokines.

Maternal stress is also a risk factor for preterm birth. Stressful stimuli range from a heavy workload to anxiety and depression, occurring at any time during the preconceptional period and/or pregnancy. Stress signals increase the production of maternal and fetal cortisol, which in turn could stimulate placental production of corticotropin-releasing hormone and its release into the maternal and fetal circulations (*54*).

### Cell-free fetal DNA

Cell-free fetal (cff) DNA has recently been proposed as a signal for the onset of labor (*55*). In pregnant women, cffDNA is normally present in the plasma, and concentrations increase as a function of gestational age—peaking at the end of pregnancy just before the onset of labor. cffDNA (in contrast with adult cell-free DNA) is hypomethylated, can engage TLR-9 (*56*, *57*), and induce an inflammatory response. The downstream consequences could include activating the common pathway of labor. Interestingly, patients who have an elevation of cffDNA in the midtrimester are at increased risk for spontaneous preterm delivery later in gestation (*58*), and those with an episode of preterm labor and high plasma concentrations of cff DNA are also at increased risk for preterm delivery (*59*, *60*). The concept that cff DNA can mediate a fetal/placental/maternal dialogue to signal the onset of labor in normal pregnancy, as well as preterm labor after insult, is a fascinating hypothesis worthy of investigation.

### Progress in the prevention of spontaneous preterm birth

After decades of clinical and basic investigation, major progress has been made toward the prediction and prevention of spontaneous preterm birth. The two most important predictors of spontaneous preterm birth are a sonographic short cervix in the midtrimester (*61*) and spontaneous preterm birth in a prior pregnancy. As for prevention, vaginal progesterone administered to asymptomatic women with a short cervix in the midtrimester reduces the rate of preterm birth at <33 weeks by 45% and decreases the rate of neonatal complications, including neonatal respiratory distress syndrome (*62*). In women with a previous spontaneous preterm birth, the administration of 17-alpha hydroxyprogesterone caproate reduces the rate of preterm birth at <37 weeks by 34% and decreases the need for oxygen supplementation in singleton gestation (*63*). Cervical cerclage in patients with a previous spontaneous preterm birth and a short cervix reduces the rate of preterm birth at <35 weeks by 30%, as well as composite perinatal mortality and morbidity. However, vaginal progesterone is as efficacious as cervical cerclage in these patients and does not require anesthesia or a surgical procedure.

The combination of transvaginal ultrasound in the midtrimester to identify women with a short cervix and treatment with vaginal progesterone represents an important step in reducing the rate of preterm birth. This approach is anchored in the knowledge that progesterone plays a role in cervical ripening and has the potential to save the U.S. health care system $500 million to $750 million per year.

### Looking forward

Progress in the understanding and prevention of preterm labor will require recognition that preterm parturition has multiple etiologies and further elucidation of the mechanisms underlying each. The definition of pathologic processes, identification of specific biomarkers, and implementation of therapeutic interventions within the unique complexity of pregnancy are particularly challenging. In pregnancy, two individuals with different genomes and exposomes coexist, largely with overlapping interests but occasionally in potential conflict. Inaccessibility

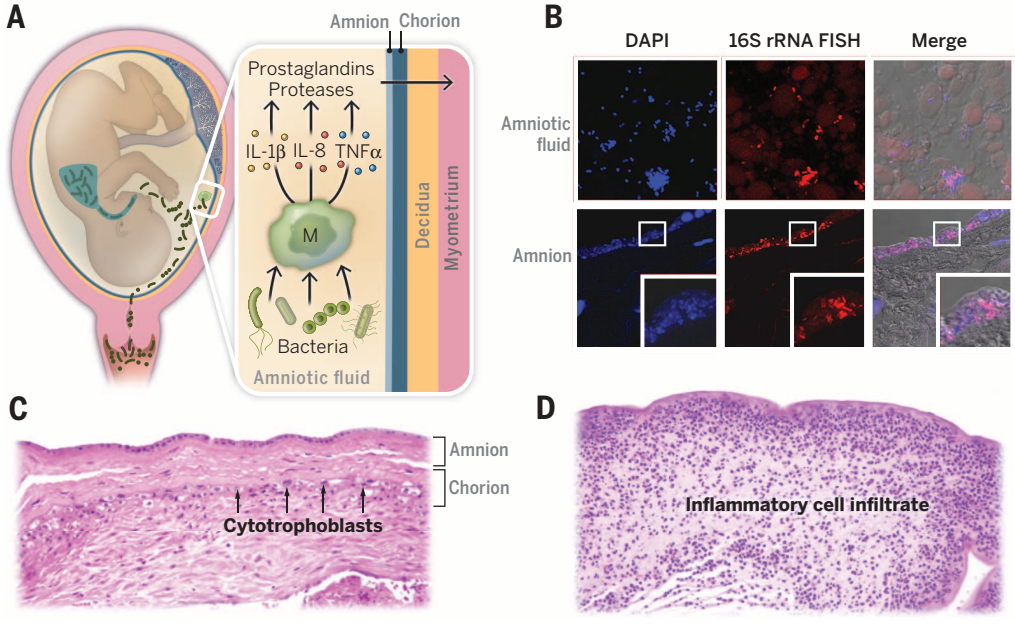


**Fig. 3. Mechanisms of microbial-induced preterm labor.** (**A**) Bacteria from the lower genital tract gain access to the amniotic cavity and stimulate the production of chemokines (IL-8 and CCL2) and cytokines (IL-1α and TNF-α), as well as other inflammatory mediators (prostaglandins and reactive oxygen radicals) and proteases. These products can initiate myometrial contractility and induce membrane rupture. (**B**) (Top left) Amniotic fluid containing bacteria that was retrieved by amniocentesis from a patient with preterm labor. Bacteria and nuclei stained with DAPI (4′,6-diamidino-2-phenylindole) (blue). (Top middle) Bacteria identified with a probe against 16S ribosomal RNA (rRNA) using fluorescent in situ hybridization. (Bottom left and middle) Bacteria invading the amnion epithelium. Note the absence of bacteria in the subepithelial part of the amnion, suggesting that the pathway of microbial invasion is ascending into the amniotic cavity (*74*). (**C**) Chorioamniotic membranes without evidence of inflammation. Amnion and chorion are identified. (**D**) A similar membrane section as (C) from a patient with intra-amniotic infection. Inflammatory cells from the mother infiltrate the chorion and amnion.

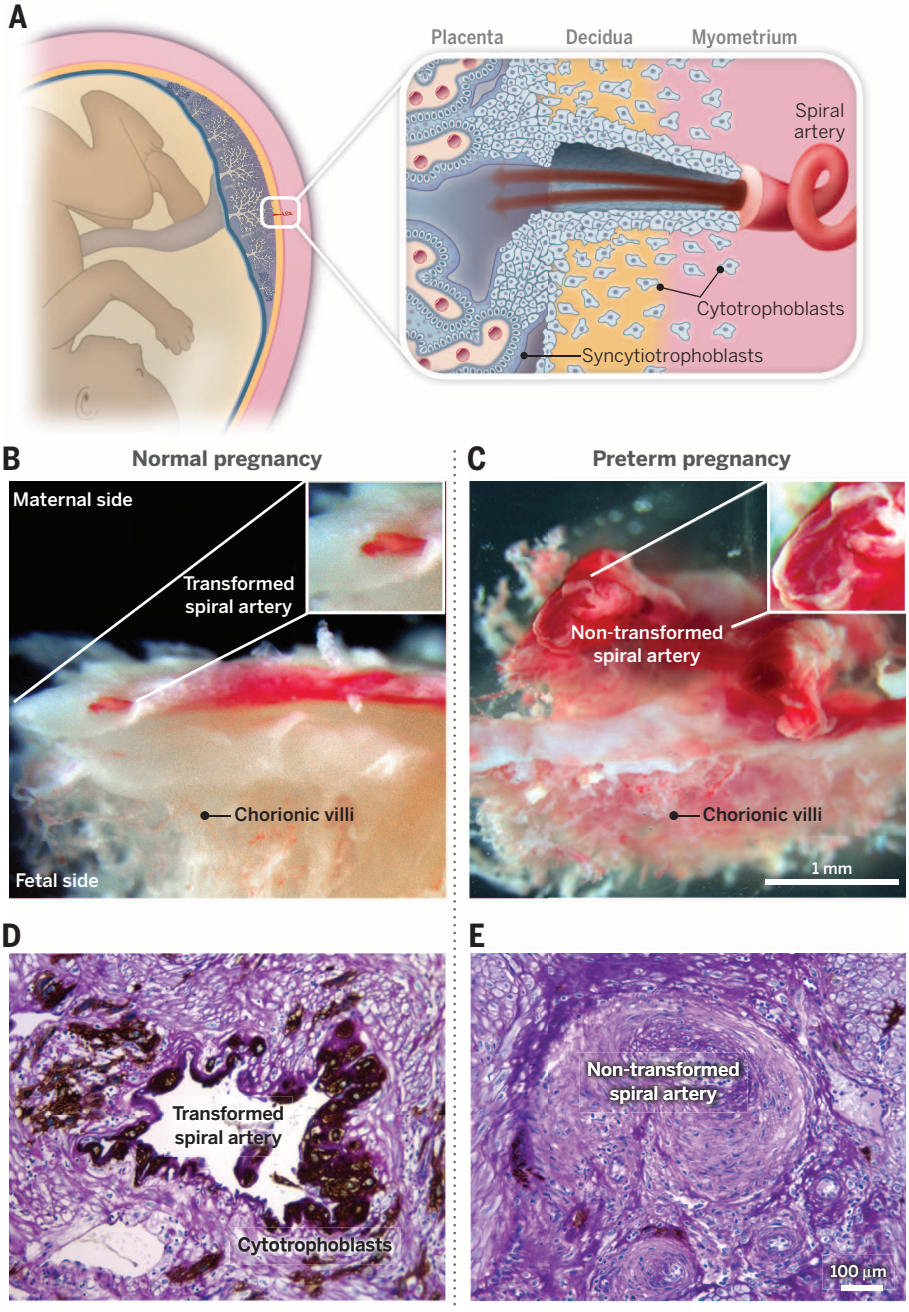


**Fig. 4. A subset of patients with preterm labor has placental vascular lesions, including failure of physiologic transformation of the uterine spiral arteries.** (**A**) Schematic drawing of the maternal-fetal interface in normal pregnancy. A physiologically transformed uterine spiral artery with a wide lumen delivers blood to the chorionic villi of the placenta. (**B**) A spiral artery with an expanded ostium that normally enables adequate perfusion of the chorionic villi. (**C**) Ostium of a narrow spiral artery with failure of physiologic transformation in a patient with spontaneous preterm labor. (**D**) Periodic acid–Schiff staining of a histological section of the maternal-fetal interface in normal pregnancy shows a spiral artery transformed by cytokeratin 7–positive cytotrophoblasts (brown) that line the lumen. (**E**) Failure of physiologic transformation of a spiral artery in a patient with preterm labor. The lumen is narrow, and cytotrophoblasts have not invaded the muscular wall.

of the human fetus also poses a formidable obstacle to elucidating the physiology of fetal development, maternal responses to this process, and the changes in both when pathologic processes arise.

High-throughput techniques and systems biology can be used to improve the understanding of the preterm labor syndrome. Early studies using unbiased genomic/epigenomic (*64*–*66*), transcriptomic (*67*, *68*), proteomic (*69*, *70*), and metabolomic approaches (*71*) have been informative yet require verification and validation. Progress will also depend on the generation and availability of multidimensional data sets, with detailed phenotypic characterization of disaggregated patient groups according to the mechanisms of disease. Longitudinal studies are required to determine whether any of the discriminators, at molecular or pathway levels, can serve as biomarkers during the preclinical disease stage and enable risk assessment and/or noninvasive monitoring of fetal health and disease. In vivo monitoring of cell-free RNA during human pregnancy can provide information about fetal tissue-specific transcription is an exciting development (*72*, *73*). Since a stereotypic blood transcriptome has been identified in fetuses with acute and chronic placental inflammatory lesions, there are opportunities to determine whether and when, during the course of pregnancy, these changes can be detected in maternal blood. This information could have enormous diagnostic and prognostic value to inform the selection of therapeutic interventions. Thus, we envision that the goal of reducing the rate of spontaneous preterm birth will be grounded in a deeper understanding of the mechanisms of disease responsible for this syndrome.

## REFERENCES AND NOTES


1. L. Liu *et al.*, *Lancet* **379**, 2151–2161 (2012).
2. H. Blencowe *et al.*, *Lancet* **379**, 2162–2172 (2012).
3. M. K. Mwaniki, M. Atieno, J. E. Lawn, C. R. Newton, *Lancet* **379**, 445–452 (2012).
4. C. J. Murray *et al.*, *Lancet* **380**, 2197–2223 (2012).
5. National Research Council, in *Preterm Birth: Causes, Consequences, and Prevention*, R. E. Behrman, A. S. Butler, Eds. (National Academies Press, Washington, DC, 2007), p. 400.
6. R. L. Goldenberg, J. F. Culhane, J. D. Iams, R. Romero, *Lancet* **371**, 75–84 (2008).
7. R. Romero *et al.*, *BJOG* **113** (suppl. 3), 17–42 (2006).
8. N. E. Renthal, K. C. Williams, C. R. Mendelson, *Nat. Rev. Endocrinol.* **9**, 391–401 (2013).
9. M. Mahendroo, *Reproduction* **143**, 429–438 (2012).
10. R. Menon, S. J. Fortunato, *Best Pract. Res. Clin. Obstet. Gynaecol.* **21**, 467–478 (2007).
11. R. M. Moore, J. M. Mansour, R. W. Redline, B. M. Mercer, J. J. Moore, *Placenta* **27**, 1037–1051 (2006).
12. R. Romero *et al.*, *Paediatr. Perinat. Epidemiol.* **15** (suppl. 2), 41–56 (2001).
13. P. N. Madianos, Y. A. Bobetsis, S. Offenbacher, *J. Periodontol.* **84** (suppl.), S170–S180 (2013).
14. M. A. Elovitz, Z. Wang, E. K. Chien, D. F. Rychlik, M. Phillippe, *Am. J. Pathol.* **163**, 2103–2111 (2003).
15. V. Agrawal, E. Hirsch, *Semin. Fetal Neonatal Med.* **17**, 12–19 (2012).
16. S. G. Carroll *et al.*, *Arch. Dis. Child. Fetal Neonatal Ed.* **72**, F43–F46 (1995).
17. R. Gomez *et al.*, *Am. J. Obstet. Gynecol.* **179**, 194–202 (1998).
18. S. Kannan *et al.*, *Sci. Transl. Med.* **4**, 130ra46 (2012).
19. A. H. Jobe, *Pediatr. Neonatol.* **51**, 7–13 (2010).
20. G. A. Macones *et al.*, *Am. J. Obstet. Gynecol.* **190**, 1504–1508, discussion 3A (2004).
21. K. Racicot *et al.*, *J. Immunol.* **191**, 934–941 (2013).
22. R. Romero *et al.*, *Microbiome* **2**, 4 (2014).
23. R. W. Hyman *et al.*, *Reprod. Sci.* **21**, 32–40 (2014).
24. R. Romero *et al.*, *Microbiome* **2**, 4 (2014).
25. O. Genbacev, Y. Zhou, J. W. Ludlow, S. J. Fisher, *Science* **277**, 1669–1672 (1997).
26. C. Whidbey *et al.*, *J. Exp. Med.* **210**, 1265–1281 (2013).
27. D. J. Anstee, *Blood* **115**, 4635–4643 (2010).
28. S. McDonagh *et al.*, *J. Infect. Dis.* **190**, 826–834 (2004).
29. K. Aagaard *et al.*, *Sci. Transl. Med.* **6**, 237ra65 (2014).
30. Eunice Kennedy Shriver NICHD, The Human Placenta Project: Placental Structure and Function in Real Time (2014); www.nichd.nih.gov/about/meetings/2014/Pages/052814.aspx.
31. R. Romero *et al.*, *Am. J. Reprod. Immunol.* 10.1111/aji.12296 (2014).
32. M. A. Elovitz, T. Saunders, J. Ascher-Landsberg, M. Phillippe, *Am. J. Obstet. Gynecol.* **183**, 799–804 (2000).

33. C. S. Han, F. Schatz, C. J. Lockwood, *Clin. Perinatol.* **38**, 407–421 (2011).
34. Y. M. Kim *et al.*, *Am. J. Obstet. Gynecol.* **189**, 1063–1069 (2003).
35. I. Brosens, R. Pijnenborg, L. Vercruysse, R. Romero, *Am. J. Obstet. Gynecol.* **204**, 193–201 (2011).
36. R. J. Levine *et al.*, *N. Engl. J. Med.* **350**, 672–683 (2004).
37. T. Chaiworapongsa *et al.*, *J. Matern. Fetal Neonatal Med.* **22**, 1122–1139 (2009).
38. Y. Hirota *et al.*, *J. Clin. Invest.* **120**, 803–815 (2010).
39. J. Cha *et al.*, *J. Clin. Invest.* **123**, 4063–4075 (2013).
40. P. Lu, V. M. Weaver, Z. Werb, *J. Cell Biol.* **196**, 395–406 (2012).
41. A. Erlebacher, *Nat. Rev. Immunol.* **13**, 23–33 (2013).
42. J. E. Mold *et al.*, *Science* **322**, 1562–1565 (2008).
43. J. H. Rowe, J. M. Ertelt, L. Xin, S. S. Way, *Nature* **490**, 102–106 (2012).
44. C. J. Kim *et al.*, *Mod. Pathol.* **23**, 1000–1011 (2010).
45. J. Lee *et al.*, *PLOS ONE* **6**, e16806 (2011).
46. J. Lee *et al.*, *Am. J. Reprod. Immunol.* **70**, 162–175 (2013).
47. J. Lee *et al.*, *Am. J. Reprod. Immunol.* **70**, 265–284 (2013).
48. M. Wegorzewska *et al.*, *J. Immunol.* **192**, 1938–1945 (2014).
49. J. C. Condon, D. B. Hardy, K. Kovaric, C. R. Mendelson, *Mol. Endocrinol.* **20**, 764–775 (2006).
50. H. Tan, L. Yi, N. S. Rote, W. W. Hurd, S. Mesiano, *J. Clin. Endocrinol. Metab.* **97**, E719–E730 (2012).
51. O. Shynlova, P. Tsui, S. Jaffer, S. J. Lye, *Eur. J. Obstet. Gynecol. Reprod. Biol.* **144** (suppl. 1), S2–S10 (2009).
52. J. F. Strauss 3rd, *Reprod. Sci.* **20**, 140–153 (2013).
53. K. M. Waldorf *et al.*, *Reprod. Sci.* **21**, 96A (2014).
54. F. Petraglia, A. Imperatore, J. R. Challis, *Endocr. Rev.* **31**, 783–816 (2010).
55. M. Phillippe, *N. Engl. J. Med.* **370**, 2534–2536 (2014).
56. J. E. Thaxton, R. Romero, S. Sharma, *J. Immunol.* **183**, 1144–1154 (2009).
57. A. Scharfe-Nugent *et al.*, *J. Immunol.* **188**, 5706–5712 (2012).
58. T. R. Jakobsen, F. B. Clausen, L. Rode, M. H. Dziegiel, A. Tabor, *Prenat. Diagn.* **32**, 840–845 (2012).
59. T. N. Leung, J. Zhang, T. K. Lau, N. M. Hjelm, Y. M. Lo, *Lancet* **352**, 1904–1905 (1998).
60. A. Farina *et al.*, *Am. J. Obstet. Gynecol.* **193**, 421–425 (2005).
61. R. Romero *et al.*, *J. Perinat. Med.* **41**, 27–44 (2013).
62. R. Romero *et al*, *Am. J. Obstet. Gynecol.* **206**, 124.e1 (2012).
63. P. J. Meis *et al.*, *N. Engl. J. Med.* **348**, 2379–2385 (2003).
64. H. Wang *et al.*, *Hum. Mol. Genet.* **17**, 1087–1096 (2008).
65. L. J. Muglia, M. Katz, *N. Engl. J. Med.* **362**, 529–535 (2010).
66. K. Y. Bezold, M. K. Karjalainen, M. Hallman, K. Teramo, L. J. Muglia, *Genome Med* **5**, 34 (2013).
67. Y. J. Heng, C. E. Pennell, H. N. Chua, J. E. Perkins, S. J. Lye, *PLOS ONE* **9**, e96901 (2014).
68. R. Haddad *et al*, *Am. J. Obstet. Gynecol.* **195**, 394.e1 (2006).
69. M. G. Gravett *et al.*, *JAMA* **292**, 462–469 (2004).
70. M. S. Esplin *et al*, *Am. J. Obstet. Gynecol.* **204**, 391.e1 (2010).
71. R. Romero *et al.*, *J. Matern. Fetal Neonatal Med.* **23**, 1344–1359 (2010).
72. W. Koh *et al.*, *Proc. Natl. Acad. Sci. U.S.A.* **111**, 7361–7366 (2014).
73. D. W. Bianchi, *Nat. Med.* **18**, 1041–1051 (2012).
74. M. J. Kim *et al.*, *Lab. Invest.* **89**, 924–936 (2009).

**ACKNOWLEDGMENTS**

The authors regret that, because of page limitations, the contributions of many investigators to the study of parturition could not be credited in this article. The authors thank S. Curtis for editing the manuscript. The work of R.R. is supported by the Division of Intramural Research of the Eunice Kennedy Shriver NICHD, NIH/Department of Health and Human Services. Studies from S.K.D.'s lab were supported in part by grants from the NIH (HD068524 and DA06668) and March of Dimes (21-FY12-127 and 22-FY14-470). The work of S.F. is supported by R37 HD076253 and U54 HD055764. We thank M. Gormley for assistance preparing the figures.

10.1126/science.1251816

REVIEW

# Neural control of maternal and paternal behaviors

**Catherine Dulac,[1]* Lauren A. O'Connell,[2] Zheng Wu[1]**

**Parental care, including feeding and protection of young, is essential for the survival as well as mental and physical well-being of the offspring. A large variety of parental behaviors has been described across species and sexes, raising fascinating questions about how animals identify the young and how brain circuits drive and modulate parental displays in males and females. Recent studies have begun to uncover a striking antagonistic interplay between brain systems underlying parental care and infant-directed aggression in both males and females, as well as a large range of intrinsic and environmentally driven neural modulation and plasticity. Improved understanding of the neural control of parental interactions in animals should provide novel insights into the complex issue of human parental care in both health and disease.**

Parental behavior aims at caring for conspecific young and increasing their survival. Among oviparous animals, parenting can include behaviors such as egg-laying site selection, nest building, burrowing, egg attending, and brooding and carrying the young; among viviparous animals, it can include food provisioning, nursing, defense of offspring, and even teaching of skills. Parenting occurs in a surprisingly large variety of vertebrates and invertebrates, including insects, arachnids, mollusks, fishes, amphibians, reptiles, birds, and mammals. In mammals, mothers commonly take the primary responsibility of parental care, whereas fathers often ignore or even attack the young. However, in many species, direct engagement of fathers has been observed; in some species, fathers participate equally or even exclusively in parental duties (Fig. 1).

Nurturing and affiliative behavior toward infants is sensitive to physiological and environmental factors such as stress and hormone levels. In humans, the quality of parental care is affected by stress and mental illnesses such as postpartum depression (PPD), which affects more than 10% of mothers in the United States (*1*). How is the diversity of parental behavior generated in males and females, across different species, and in various physiological or pathological conditions? Recent studies have begun to uncover the nature and function of circuits underlying parental interactions with young. Here, we review data suggesting the existence of highly conserved and antagonistic circuits controlling affiliative and aggressive behavior toward offspring, respectively. Circuits underlying these opposing behaviors are present in both male and female brains irrespective of the normal expression of parenting displays and are modulated by intrinsic and environmental factors.

## Diversity in parental care

Parental care has evolved repeatedly across vertebrate and invertebrate taxa (*2*). The involvement of males and/or females in the care for offspring varies across taxa and even between populations within a species (Fig. 2). In many systems, the parent that cares for offspring can be partially correlated with certainty in parentage and/or adult sex ratio. In mammals, male involvement is rare because internal fertilization ensures maternity but not paternity, and because only females lactate (*3*). In some rodents, canids, and primates, males assist and invest substantially in the care of offspring (*4*–*8*), whereas closely related species are exclusively maternal (*9*–*12*). For example, prairie voles and California mice are biparental, with males showing all female-typical parental displays except nursing (*4*, *5*), but closely related species in the same genus—such as the montane vole, meadow vole, or deer mouse—are female uniparental (*9*–*12*). Cross-fostering experiments showed that meadow vole males reared by biparental prairie voles exhibited significantly more paternal care to their offspring than in-fostered counterparts (*13*). This result demonstrates the influence of early social environment, in addition to genetic differences between congeneric species, on parental behavior.

Male involvement in offspring care is common in many taxa other than mammals. In teleost fish species, males provide care more often than females, including nest building and egg attendance (*14*). In the well-known case of the three-spined stickleback, males set up the territory, build nests, and defend their offspring (*15*). In birds, 90% of the species are biparental, with both parents sharing the responsibilities of building a nest, incubating eggs, and defending and feeding the young (*16*). The sex ratio of individuals available to mate in a bird population largely determines which parent cares for offspring. For example, male shorebirds are more likely to care for offspring in populations where males are more abundant than females (*17*).

Amphibians display striking diversity in parental care. Many species of anurans and salamanders display care for offspring beyond egg laying, with roughly 50 independent evolutionary transitions to parental care (*18*). These behaviors include preparation of foam nests (*19*), egg guarding, transport of offspring piggyback

[1]Howard Hughes Medical Institute, Department of Molecular and Cellular Biology, Center for Brain Science, Harvard University, Cambridge, MA 02138, USA. [2]FAS Center for System Biology, Harvard University, Cambridge, MA 02138, USA.
*Corresponding author. E-mail: dulac@fas.harvard.edu

style (*20*), and egg incubation in dorsal pouches, vocal sacs, or the stomach. South American poison frogs (*Dendrobatidae*) show particularly striking diversity in which sex cares for offspring within closely related species (*21*).

Such natural diversity in parental care strategies across large evolutionary distances—as well as in related species and in individuals within a species—suggests the existence of conserved neural pathways underlying parental care that are differentially regulated in males and females, and in different species.

## Sensory cues that drive parental interactions

Neuroethologists have long recognized intriguing differences in the nature and complexity of signals driving parental behaviors. In fish and birds, social behaviors including care of young were often seen to be triggered by simple cues (*22*). The domestic hen, for example, comes to the immediate rescue of a chick after hearing its distress call, but the sight of a struggling chick without sounds leaves the fowl indifferent (*23*). In turn, the reliance on simple visual signals in some species of birds generates the so-called "supernormal" stimulus effect, in which artificial eggs with exaggerated features (such as higher-contrast pigmentation or giant sizes) are even more effective at eliciting parental behavior than natural eggs (*22*).

In mammals, multiple sensory modalities have been shown to trigger maternal responses. Early studies in rats (*24*) found that blind, anosmic, or anaptic lactating females each retrieve pups in a fashion not significantly different from controls. However, the combination of anosmia and tactile deprivation results in more pronounced defects in retrieving than does the loss of either sensory system alone, and the defects are even more severe when all three sensory inputs were eliminated. Different sensory modalities appear to often synergize with each other, as they perform critical roles in different steps of the parental response.

In rodents, low-frequency wriggling calls emitted by pups when they struggle in the nest induce licking, change of suckling position, and nest building by the mother (*25*). By contrast, ultrasonic vocalizations produced by pups lost outside the nest trigger immediate search for the pups and retrieval to the nest (*26*), with retrieval occurring even if the ultrasonic vocalizations have ceased. Intriguingly, mouse fathers can be induced to display fast pup-retrieving behavior by 38-kHz ultrasonic vocalization from their female partners (*27*).

Chemosensory cues are extensively used to elicit or inhibit parental care according to the sex and physiological status of the animal. Many amphibians, fish, birds, and insects, such as ants or the burrowing bug, were shown to use olfactory cues to recognize offspring (*28*–*31*). In many mammals, the vomeronasal pathway, in conjunction with the olfactory system for some species, inhibits parental behavior and drives pup-mediated aggression in virgin animals, whereas olfactory cues are often seen facilitating the care of offspring in parents or primed animals (*29*). Virgin rats initially find foreign pups aversive but exhibit parental

**Fig. 1. Paternal care can be observed in many different taxa.** (**A**) Giant water bug (*Abedus herberti*). (**B**) Los Tayos rocket frog (*Hyloxalus nexipus*). (**C**) Silverback mountain gorilla (*Gorilla beringei beringei*) father with infants. [Photos by Ivan Phillipsen (A), Adam Stuckert (B), Lubert Stryer (C)]

care after continuous exposure to the pups (*30*). Surgical removal of the vomeronasal organ (VNO) reduces infanticidal behavior and induces faster paternal behavior (*31*); however, olfactory cues emitted by pups appear to facilitate parental care (*29*, *32*). Recent studies in mice confirmed that surgical or genetic VNO loss of function leads to a marked reduction in pup-directed aggression and to the emergence of parental care in virgin males (*33*, *34*). In humans, one study documented a much higher rating of infant body odors by postpartum mothers than by nulliparous women (*35*), and odors have been proposed as important cues in early interactions between mothers and infants (*36*, *37*).

A fascinating example of multisensory interaction comes from the mother-infant bonding in sheep (*38*). Olfactory cues are responsible for both inhibiting maternal responsiveness of ewes before parturition and for attraction to amniotic fluid immediately after parturition (*39*). Shortly after pregnant ewes give birth, a selective bonding between the mother and the infants rapidly develops, such that ewes nurse only their own offspring and behave aggressively toward alien young. However, artificial vaginocervical stimulation that mimics the expulsion of the lamb resets the ewe's olfactory preference toward an alien lamb, likely through oxytocin release.

The sensing of infant cues is remarkably enhanced in parents, and parturition and maternal care have been associated with multisensory facilitation and extensive cortical plasticity. Recordings of ultrasonic calls played to lactating female rodents showed that searching behavior is facilitated by pup vocalizations in the presence of olfactory cues (*40*, *41*). Neuron responses and population dynamics in the auditory cortex undergo significant changes in mothers relative to virgin female mice, likely facilitating the representation of pup vocalizations and enhancing their behavioral relevance (*42*–*45*). Moreover, a significant modulation of sound-evoked responses by pup odors has been shown in the primary auditory cortex of lactating female mice shortly after parturition, with neurons from lactating mothers displaying more sensitivity to sounds than virgins (*44*). In the olfactory system, mitral cells in the olfactory bulb of female ewes have been shown to undergo marked changes in sensory responses to lamb versus food odors after parturition (*46*, *47*). Moreover, in vivo time-lapse imaging of adult newly born granule cells in mice showed an enhanced integration of these neurons into the olfactory circuit of lactating mothers (*46*).

## Switching between parental care and aggression

Infant-directed aggression is prevalent in animals that are not rearing offspring (such as virgin animals) and in sexually mature stranger males (*48*), and it is often seen to switch into affiliative behavior after birth of offspring or habituation to the young. Thus, adult animals may display

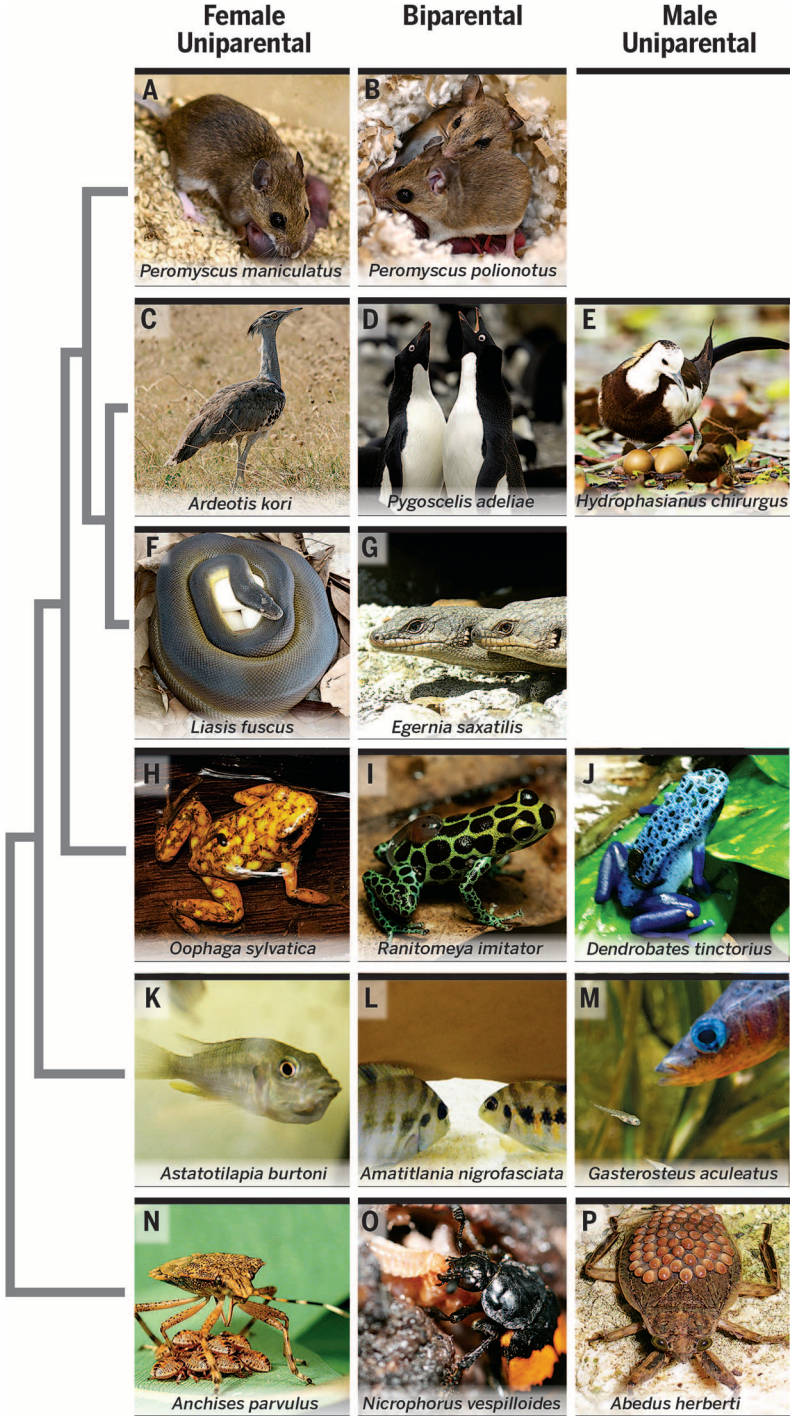


**Fig. 2. Evolution of diverse and distinct parental cares strategies across the animal kingdom.** Examples of different parental care strategies are shown across vertebrates and invertebrates. Male uniparental care is lacking only in the mammalian and reptilian lineages, although there are male-biased parental care systems in few canids and primates. (**A**) Common deer mouse (*Peromyscus maniculatus*). (**B**) Oldfield mouse (*Peromyscus polionotus*). (**C**) Kori bustard (*Ardeotis kori*). (**D**) Adélie penguin (*Pygoscelis adeliae*). (**E**) Pheasant-tailed jacana (*Hydrophasianus chirurgus*). (**F**) Water python (*Liasis fuscus*). (**G**) Black rock skink (*Egernia saxatilis*). (**H**) Diablito frog (*Oophaga sylvatica*). (**I**) Mimic poison frog (*Ranitomeya imitator*). (**J**) Dyeing poison frog (*Dendrobates tinctorius*). (**K**) Burton's mouthbrooder (*Astatotilapia burtoni*). (**L**) Convict cichlid (*Amatitlania nigrofasciata*). (**M**) Three-spined stickleback (*Gasterosteus aculeatus*). (**N**) Golden brown stink bug (*Anchises parvulus*). (**O**) Burying beetle (*Nicrophorus vespilloides*). (**P**) Giant water bug (*Abedus herberti*). [Photos by Andrés Bendesky (A and B), Tamas Szekely (C), Oliver Kruger (D), Ghulam Rasool (E), Zachary Stahlschmidt (F), Alan Couch (G), Elicio E. Tapia (H), Evan Twomey (I), Lauren A. O'Connell (J), Rayna Harris (K), Bryan J. Matthews (L), Dwight Kuhn (M), Peter Chew at www.brisbaneinsects.com (N), Allen Moore (O), Michael Bogan (P)]

parental care or aggression according to their physiological and environmental state, and the regulation of affiliative versus agonistic behavior circuits raises an important and fascinating question in the study of parental interactions.

In laboratory mice, infanticide is commonly observed in virgin males (*49*). Males stop committing infanticide and become paternal toward pups in a transient period after mating with a female, starting at the approximate time of birth and continuing until the weaning of pups (Fig. 3) (*50*). The coincidence of the suppression of infanticide in males and the birth of their own pups likely provides an adaptive mechanism that prevents a male mouse from killing its own pups, but successfully eliminates pups sired by competing males. Parental males and females, however, do not appear to differ in the overall incidence of retrieving, nest building, licking, and huddling over the pups (*51*). Wild-caught female mice are typically infanticidal, and they follow a similar transition to parental care associated with parturition and lactation, with a surprising elevation of infanticide throughout pregnancy (*52*, *53*). The drastic difference between laboratory and wild female mice suggests that infanticide was selected out by colony breeding in females.

Time-dependent synaptic or transcriptional change triggered by mating, as well as the chemical cues released by females during pregnancy (*54*), have been hypothesized to drive the radical behavior shift from infanticide to parental behavior (*50*, *55*–*57*). The timing and mechanism of the mating-induced behavioral switch in mice has been assessed by two recent studies (*33*, *34*). After pup exposure, neurons in the vomeronasal pathway appear more strongly activated in virgin males than in fathers (*33*), and impairment of VNO sensing results in decreased pup-directed aggression and induction of parental care (*33*, *34*). These results raise the intriguing possibility that the transition of attack to parenting could be due to a time-dependent reduction of vomeronasal activation by pup cues in males.

The intriguing temporal switch in offspring recognition associated with mating is not restricted to rodents; it has been observed and characterized in a variety of species including isopods, burying beetles, African cichlids, and birds (*58*).

## Neural circuits underlying parental interactions

Much of our knowledge about neural circuits underlying parental behavior comes from studies in rats, with recent insights provided by genetic studies in mice. In contrast to lactating females, which are highly maternal, virgin male and female rats usually avoid physical contact with foreign pups. Nonetheless, after continuous exposure to pups, virgin males and females approach, interact with them, and eventually exhibit parental care, in a process termed "sensitization" (*30*).

The changes in levels of female hormones such as estrogen, progesterone, and prolactin through pregnancy have long been implicated in the regulation of maternal behavior (*59*). Treatment of virgin females with a regimen of hormones mimicking this pattern facilitates the display of maternal behavior (*60*). Moreover, recent genetic studies have shown that the prolactin receptor is essential for the normal display of maternal behavior (*61*). Prolactin is also an important regulator of parental care in nonmammalian vertebrates, most notably in birds and teleost fish, where prolactin rises during egg laying/spawning and remains elevated throughout the duration of parental care (*62*, *63*).

Male interaction with infants is also influenced by hormonal changes (*64*). In many vertebrate species where males are involved in offspring care, testosterone levels decrease during fatherhood, such as in humans, frogs, and fish (*65*–*67*). The intrauterine position of mouse fetuses, and therefore the early exposure to different levels of sex hormones, has been proposed to influence pup-directed aggression in adulthood (*68*). In addition, progesterone receptor knockout virgin male mice were shown to exhibit little aggression but elevated parental care toward foster pups (*69*).

The contrast between caring by parents and aversion by virgin animals has led to searches for brain areas involved in the stimulation and inhibition of maternal behavior (*70*) (Fig. 4). Classical mapping experiments have demonstrated the essential role of several brain areas in the control of maternal behavior, including the medial

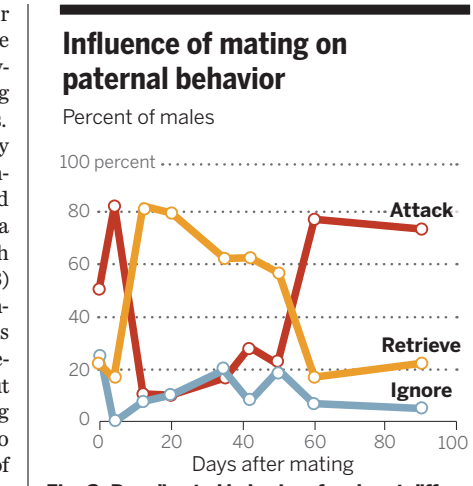


**Fig. 3. Pup-directed behavior of males at different days after mating [replotted from (50), table 2].** Adult male mice of the CF-1 strain were mated with females, randomly assigned into groups, and tested at different days after mating. Control virgin males are plotted at day 0. After a significant increase in pup-directed aggression at day 4, there is a transient suppression of attack and increase in paternal care in the males from day 12 to day 50, which approximately corresponds to the birth of and the weaning of their own pups. This experiment illustrates a remarkable influence of mating on male parental behavior.

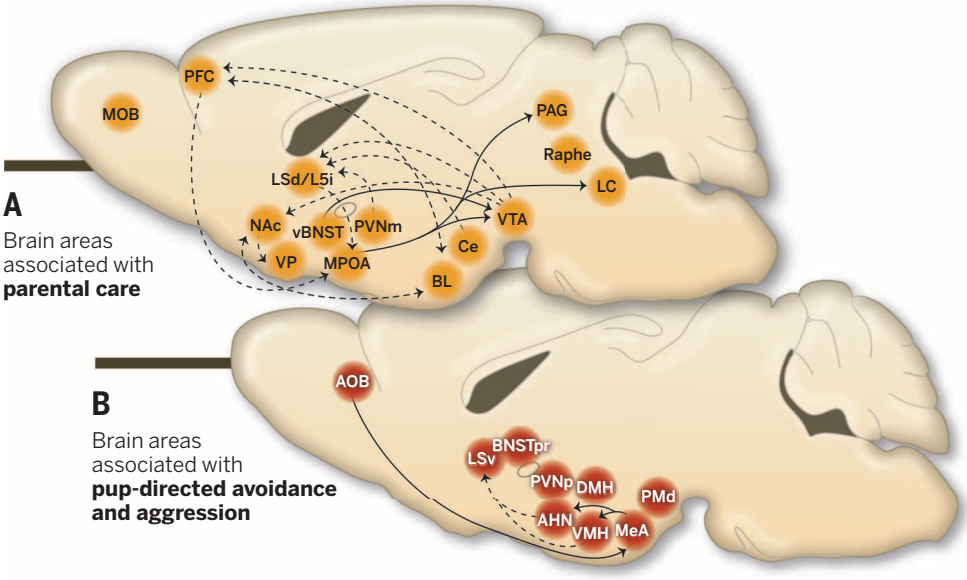


**Fig. 4. Schematic presentation of brain areas associated with parental care (A) and pup-directed avoidance and aggression (B).** Solid lines denote projections that are involved in the regulation of pup-directed behavior, as supported by direct evidence. Dashed lines denote known connections that exist between these areas and are potentially involved in the behavior. The lines and arrows simply denote origins and targets and do not represent actual axon path or excitatory inputs. Not all the known connections are shown. Abbreviations of brain areas: MOB, main olfactory bulb; PFC, prefrontal cortex; NAc, nucleus accumbens; VP, ventral pallidum; LSd, lateral septum, dorsal part; LSi, lateral septum, intermediate part; vBNST, bed nucleus of stria terminalis, ventral part; MPOA, medial preoptic area; PVNm, paraventricular nucleus, magnocellular part; BL, basolateral amygdala; Ce, central amygdala; VTA, ventral tegmental area; PAG, periaqueductal gray; Raphe, Raphe nucleus; LC, locus coeruleus; AOB, accessory olfactory bulb; LSv, lateral septum, ventral part; BNSTpr, bed nucleus of stria terminalis, principal nucleus; PVNp, paraventricular nucleus, parvocellular part; DMH, dorsomedial hypothalamic nucleus; VMH ventromedial hypothalamic nucleus; MeA, medial amygdala; PMd, premammillary nucleus, dorsal part.

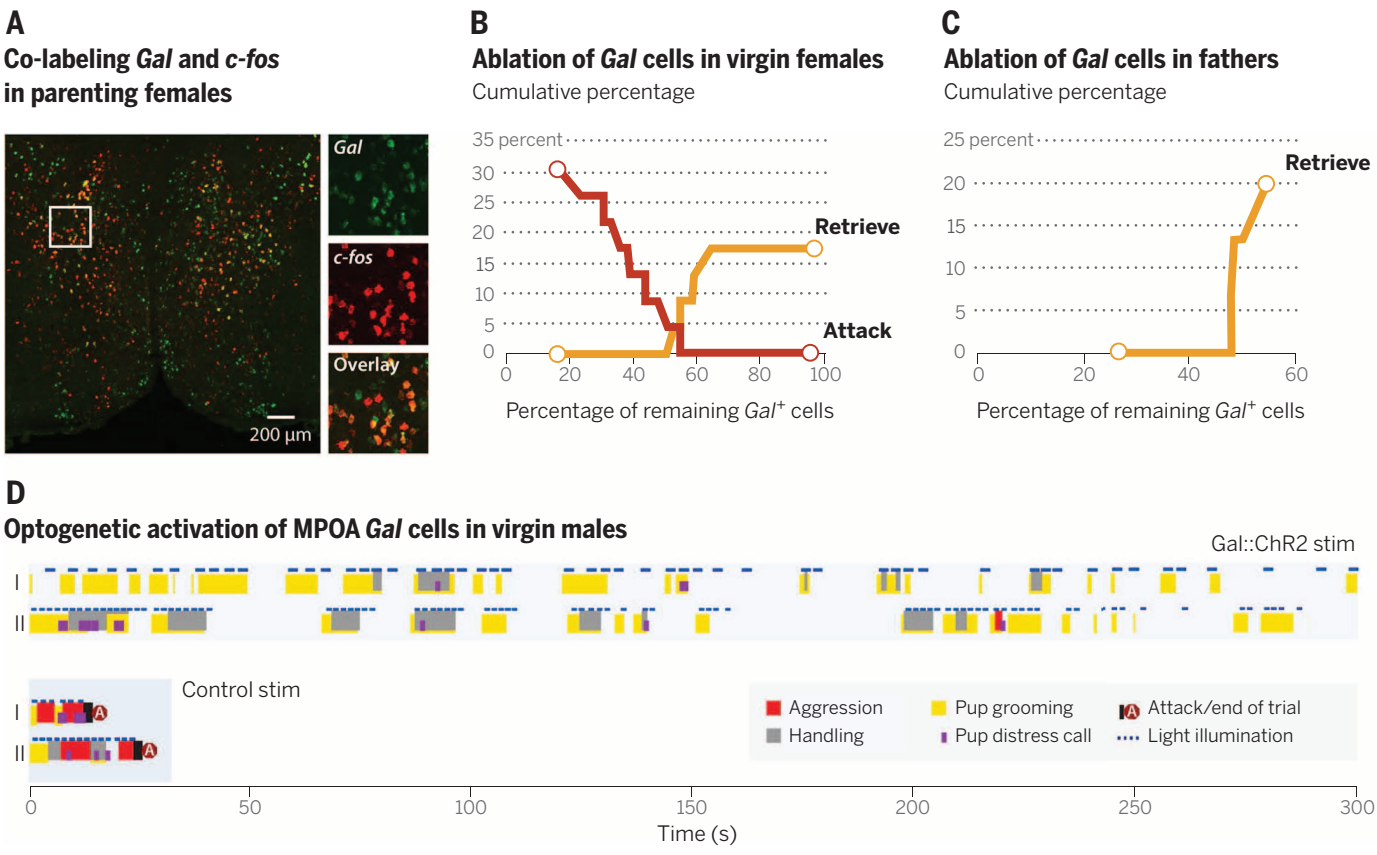


**Fig. 5. MPOA *Gal* neurons serve as an essential regulatory node for parental care in both male and female mice.** (**A**) Co-labeling of *c-fos* and *Gal* in the MPOA of parenting females. (**B**) Cumulative percentages of virgin females that retrieved or attacked pups as a function of the percentage of remaining *Gal* cells after *Gal* cell ablation. Reference cell number (100%) is the average MPOA *Gal* cell number in the control group. (**C**) Cumulative percentages of fathers that retrieved pups as a function of remaining *Gal* cells after *Gal* cell ablation. (**D**) Behavior raster plots after optogenetic activation of *Gal* cells in virgin males interacting with pups. The control group consisted of littermates that do not express light-activated channelrhodopsin-2. Different behavior elements are color-coded and could occur simultaneously.

preoptic area (MPOA) and the adjacent ventral bed nucleus of stria terminalis (vBNST) (Fig. 4A) (*70*, *71*). A combination of immediate early gene (IEG) mapping and tracing further mapped the projection sites of the active MPOA/vBNST neurons (Fig. 4A) (*72*). In addition to the preoptic area, the lateral septum is also involved in the regulation of parental care (*73*), and both areas have been implicated by IEG studies in the paternal care of biparental rodents (*74*) and biparental cichlid fish (*67*). Electrical stimulation of the preoptic area in male bluegill sunfish also elicits paternal care (*75*). These results suggest that highly conserved circuits and neuroendocrine mechanisms may be repeatedly recruited to mediate similar social behaviors (*2*, *76*). What specific information is carried by these brain regions and how they encode the various components of parental care remain to be determined.

A similar set of experiments uncovered a parallel neural system that inhibits maternal behavior, thus opposing the function of the parental pathways described above (Fig. 4B). In particular, the medial amygdala, which receives direct projection from the accessory olfactory bulb, was shown to mediate the suppression of maternal care and the initial avoidance responses in virgin female rats (*77*). A number of other brain areas, many of them interconnected and involved in defensive social encounters, were also shown to inhibit maternal responses (*78*, *79*); such findings suggest that pup aversion may share common circuitry with defensive behavior.

From these studies, a hypothetical neural model of the control of parental behavior in rats has been proposed, according to which two competing pathways mediate active maternal responses and aversive behavior toward pups, respectively (*80*, *81*). In male and most female virgin rats, the aversive circuit, primarily innervated by vomeronasal inputs, is dominant and suppresses parental care, whereas in postpartum and "sensitized" females, hormonal, neuromodulatory, and experience-dependent factors activate the facilitative circuit and silence the avoidance circuit. Uncovering how these two conflicting circuits are differentially modulated in different physiological or environmental conditions is therefore central to the understanding of the control of parental care in males and females of various species.

The ventral tegmental area (VTA) is a major dopaminergic area that is involved in reward and reinforcement learning. Pups are known to be a reinforcing stimulus to postpartum females (*82*), and MPOA lesions were found to disrupt the performance of an associative learning task using pups as positive reinforcement (*83*). Moreover, inactivation of VTA projections disrupts maternal behavior in postpartum rats (*84*), and depletion of dopamine in the ventral striatum or lesion of dopamine neurons in the VTA causes a persistent deficiency in pup retrieval (*85*, *86*). These results suggest that the dopaminergic system helps initiate and maintain maternal behavior in rats, likely by engaging the MPOA (*71*).

Targeted disruption of the dopamine β-hydroxylase (*Dbh*) gene, which synthesizes noradrenaline and adrenaline, leads to severe defects in maternal behavior (*87*). Intriguingly, providing noradrenaline precursor at the time of parturition is sufficient to restore maternal behavior in *Dbh* mutant females and maintain maternal care toward their future litters; this finding suggests that noradrenaline is critical at birth for the formation of a stable behavioral memory, which in turn is responsible for the maintenance of maternal care (*87*, *88*).

The role of the serotonergic system was recently demonstrated by the maternal defects

of Pet-1 (an ETS transcription factor whose brain expression is limited to serotonin neurons) knockout mice, in which serotonergic gene expression and serotonin synthesis are greatly reduced (*89*). The MPOA and the BNST are innervated by serotonin-immunoreactive fibers (*90*), which suggests that the maternal deficiency may result from impaired serotonin inputs to these areas.

The highly conserved neuropeptide oxytocin is also an essential regulator of parental care across animals (*91*). Female mice deficient in oxytocin are unable to nurse, although they display largely normal maternal behavior (*92*). Studies using oxytocin receptor knockout females found no obvious deficits in their maternal care (*93*), but a recent reexamination of their behavior suggested that oxytocin is involved in the initiation but not the maintenance of maternal behavior (*94*). In addition to mammals, the function of oxytocin appears to also extend to other vertebrate systems including birds (*95*) and fish (*67*).

The brain regions involved in the control of parental behavior are highly heterogeneous structures, and newly designed molecular and genetic tools make it possible to identify and functionally manipulate precise subsets of neurons, thus enabling a deeper understanding of the associated behavior circuits.

A recent study uncovered a subset of MPOA neurons expressing the neuropeptide galanin that are specifically activated during male and female parenting (Fig. 5A) (*34*). Specific ablation of MPOA galanin neurons in virgin females, mothers, and fathers results in a marked impairment of parental responses and induced pup-directed aggression in virgin females (Fig. 5, B and C). In contrast, optogenetic activation of these neurons in virgin males suppresses pup-directed aggression and induces pup grooming (Fig. 5D). These results suggest a direct role of MPOA galanin neurons in activating parental responses and confirm the suspected reciprocal inhibition between circuits activating and repressing parental behavior. The identification of MPOA galanin neurons as an essential regulatory node of male and female parenting behavior provides a precious entry point for further dissection of behavior circuits underlying parental care and their modulation by social experience.

Emerging evidence suggests that highly conserved circuits and modulatory mechanisms may exist across species and in both male and female brains to regulate parental interactions with offspring. Remarkably, the natural behavior of adults toward infants emerges as the mutually exclusive output of two highly regulated circuits driving affiliative versus aversive responses. Future studies should exploit the natural diversity of parental systems across animal species to gain mechanistic insights into the regulation of parental behavior in physiologically and ecologically relevant contexts. Such results are likely to shed new light on the complexity of human parental behavior and its susceptibility to mental illness.

## REFERENCES AND NOTES


1. K. L. Wisner *et al*., *JAMA Psychiatry* **70**, 490–498 (2013).
2. N. J. Royle, P. T. Smiseth, M. Kölliker, *The Evolution of Parental Care* (Oxford Univ. Press, Oxford, ed. 1, 2012).
3. D. Lukas, T. H. Clutton-Brock, *Science* **341**, 526–530 (2013).
4. J. S. Lonstein, G. J. De Vries, *Physiol. Behav.* **66**, 33–40 (1999).
5. C. S. Rosenfeld, S. A. Johnson, M. R. Ellersieck, R. M. Roberts, *PLOS ONE* **8**, e75725 (2013).
6. J. Malcolm, *Am. Zool.* **25**, 853–856 (1985).
7. S. Mendoza, W. Mason, *Anim. Behav.* **34**, 1336–1347 (1986).
8. M. Z. Wamboldt, R. E. Gelhard, T. R. Insel, *Dev. Psychobiol.* **21**, 187–202 (1988).
9. D. Oliveras, M. Novak, *Anim. Behav.* **34**, 519–526 (1986).
10. T. R. Insel, L. J. Young, *Nat. Rev. Neurosci.* **2**, 129–136 (2001).
11. K. J. Parker, T. M. Lee, *Horm. Behav.* **39**, 285–294 (2001).
12. S. Mihok, *Can. J. Zool.* **57**, 1520–1535 (1979).
13. B. McGuire, *J. Mammal.* **69**, 332–341 (1988).
14. J. D. Reynolds, N. B. Goodwin, R. P. Freckleton, *Philos. Trans. R. Soc. London Ser. B* **357**, 269–281 (2002).
15. J. Van Iersel, *Behavior* (suppl.), 1–159 (1953).
16. E. Ketterson, V. Nolan Jr., *Annu. Rev. Ecol. Syst.* **25**, 601–628 (1994).
17. H. Kokko, M. D. Jennions, in *The Evolution of Parental Care*, N. J. Royle, P. T. Smiseth, M. Kölliker, Eds. (Oxford Univ. Press, Oxford, 2012), pp. 101–112.
18. K. D. Wells, *The Ecology and Behavior of Amphibians* (Univ. of Chicago Press, Chicago, 2007).
19. L. Dalgetty, M. W. Kennedy, *Biol. Lett.* **6**, 293–296 (2010).
20. P. Weygoldt, *J. Zool. Syst. Evol. Res.* **25**, 51–67 (1987).
21. K. Summers, L. Weigt, P. Boag, E. Bermingham, *Herpetologica* **55**, 254–270 (1999).
22. N. Tinbergen, *The Study of Instinct* (Oxford Univ. Press, Oxford, 1951).
23. G. H. Brückner, *Z. Psychol.* **128**, 1–105 (1933).
24. F. A. Beach, J. Jaynes, *Behaviour* **10**, 104–124 (1956).
25. G. Ehret, C. Bernecker, *Anim. Behav.* **34**, 821–830 (1986).
26. G. Ehret, *Behav. Genet.* **35**, 19–29 (2005).
27. H.-X. Liu *et al*., *Nat. Commun.* **4**, 1346 (2013).
28. L. M. Schulte *et al*., *Anim. Behav.* **81**, 1147–1154 (2011).
29. F. Lévy, M. Keller, P. Poindron, *Horm. Behav.* **46**, 284–302 (2004).
30. J. S. Rosenblatt, *Science* **156**, 1512–1514 (1967).
31. J. A. Mennella, H. Moltz, *Physiol. Behav.* **42**, 303–306 (1988).
32. F. Lévy, M. Keller, *Behav. Brain Res.* **200**, 336–345 (2009).
33. K. S. Tachikawa, Y. Yoshihara, K. O. Kuroda, *J. Neurosci.* **33**, 5120–5126 (2013).
34. Z. Wu, A. E. Autry, J. F. Bergan, M. Watabe-Uchida, C. G. Dulac, *Nature* **509**, 325–330 (2014).
35. A. S. Fleming *et al*., *Dev. Psychobiol.* **26**, 115–132 (1993).
36. R. H. Porter, in *Smell and Taste in Health and Disease*, T. V. Getchell, Ed. (Raven, New York, 1991), pp. 429–442.
37. A. S. Fleming, M. Steiner, C. Corter, *Horm. Behav.* **32**, 85–98 (1997).
38. E. B. Keverne, F. Levy, P. Poindron, D. R. Lindsay, *Science* **219**, 81–83 (1983).
39. F. Levy, P. Poindron, P. Le Neindre, *Physiol. Behav.* **31**, 687–692 (1983).
40. W. P. Smotherman, R. W. Bell, J. Starzec, J. Elias, T. A. Zachman, *Behav. Biol.* **12**, 55–66 (1974).
41. J. T. Allin, E. M. Banks, *Anim. Behav.* **20**, 175–185 (1972).
42. R. C. Liu, J. F. Linden, C. E. Schreiner, *Eur. J. Neurosci.* **23**, 3087–3097 (2006).
43. R. C. Liu, C. E. Schreiner, *PLOS Biol.* **5**, e173 (2007).
44. L. Cohen, G. Rothschild, A. Mizrahi, *Neuron* **72**, 357–369 (2011).
45. G. Rothschild, L. Cohen, A. Mizrahi, I. Nelken, *J. Neurosci.* **33**, 12851–12861 (2013).
46. H. Kopel, E. Schechtman, M. Groysman, A. Mizrahi, *J. Neurosci.* **32**, 7519–7527 (2012).
47. K. M. Kendrick, F. Lévy, E. B. Keverne, *Science* **256**, 833–836 (1992).
48. S. B. Hrdy, *Ethol. Sociobiol.* **1**, 13–40 (1979).
49. B. Svare, M. Mann, *Physiol. Behav.* **27**, 921–927 (1981).
50. F. S. vom Saal, *Physiol. Behav.* **34**, 7–15 (1985).
51. R. Priestnall, S. Young, *Dev. Psychobiol.* **11**, 23–30 (1978).
52. M. M. McCarthy, F. S. vom Saal, *Physiol. Behav.* **35**, 843–849 (1985).
53. V. Soroker, J. Terkel, *Anim. Behav.* **36**, 1275–1281 (1988).
54. J. A. Mennella, H. Moltz, *Physiol. Behav.* **42**, 19–28 (1988).
55. R. W. Elwood, *J. Comp. Psychol.* **99**, 457–467 (1985).
56. J. B. Labov, *Behav. Ecol. Sociobiol.* **6**, 297–303 (1980).
57. R. Elwood, M. Ostermeyer, *Anim. Behav.* **32**, 293–294 (1984).
58. R. W. Elwood, *Behav. Processes* **33**, 15–24 (1994).
59. J. Terkel, J. S. Rosenblatt, *J. Comp. Physiol. Psychol.* **65**, 479–482 (1968).
60. H. Moltz, M. Lubin, M. Leon, M. Numan, *Physiol. Behav.* **5**, 1373–1377 (1970).
61. B. K. Lucas, C. J. Ormandy, N. Binart, R. S. Bridges, P. A. Kelly, *Endocrinology* **139**, 4102–4107 (1998).
62. F. Angelier, B. Moe, S. Blanc, O. Chastel, *Physiol. Biochem. Zool.* **82**, 590–602 (2009).
63. P. Tacon, J. F. Baroiller, P. Y. Le Bail, P. Prunet, B. Jalabert, *Gen. Comp. Endocrinol.* **117**, 54–65 (2000).
64. R. E. Brown, *Behav. Processes* **30**, 1–27 (1993).
65. L. T. Gettler, T. W. McDade, A. B. Feranil, C. W. Kuzawa, *Proc. Natl. Acad. Sci. U.S.A.* **108**, 16194–16199 (2011).
66. D. S. Townsend, W. H. Moger, *Horm. Behav.* **21**, 93–99 (1987).
67. L. A. O'Connell, B. J. Matthews, H. A. Hofmann, *Horm. Behav.* **61**, 725–733 (2012).
68. G. Perrigo, W. C. Bryant, F. S. vom Saal, *Physiol. Behav.* **46**, 121–128 (1989).
69. J. S. Schneider *et al*., *Proc. Natl. Acad. Sci. U.S.A.* **100**, 2951–2956 (2003).
70. D. E. Olazábal *et al*., *Neurosci. Biobehav. Rev.* **37**, 1875–1892 (2013).
71. M. Numan, D. S. Stolzenberg, *Front. Neuroendocrinol.* **30**, 46–64 (2009).
72. M. Numan, M. J. Numan, *J. Neuroendocrinol.* **9**, 369–384 (1997).
73. L. A. O'Connell, H. A. Hofmann, *J. Comp. Neurol.* **519**, 3599–3639 (2011).
74. B. Kirkpatrick, J. W. Kim, T. R. Insel, *Brain Res.* **658**, 112–118 (1994).
75. L. S. Demski, K. M. Knigge, *J. Comp. Neurol.* **143**, 1–16 (1971).
76. J. H. Werren, M. R. Gross, R. Shine, *J. Theor. Biol.* **82**, 619–631 (1980).
77. M. Numan, M. J. Numan, J. B. English, *Horm. Behav.* **27**, 56–81 (1993).
78. S. C. Motta *et al*., *Proc. Natl. Acad. Sci. U.S.A.* **106**, 4870–4875 (2009).
79. T. Sheehan, M. Paul, E. Amaral, M. J. Numan, M. Numan, *Neuroscience* **106**, 341–356 (2001).
80. M. Numan, *Dev. Psychobiol.* **49**, 12–21 (2007).
81. M. Numan, T. R. Insel, *The Neurobiology of Parental Behavior* (Springer, New York, 2003).
82. H. Hauser, R. Gandelman, *Horm. Behav.* **19**, 454–468 (1985).
83. A. Lee, S. Clancy, A. S. Fleming, *Behav. Brain Res.* **108**, 215–231 (2000).
84. M. Numan, D. S. Stolzenberg, A. A. Dellevigne, C. M. Correnti, M. J. Numan, *Behav. Neurosci.* **123**, 740–751 (2009).
85. S. Hansen, C. Harthon, E. Wallin, L. Löfberg, K. Svensson, *Behav. Neurosci.* **105**, 588–598 (1991).
86. S. Hansen, C. Harthon, E. Wallin, L. Löfberg, K. Svensson, *Pharmacol. Biochem. Behav.* **39**, 71–77 (1991).
87. S. A. Thomas, R. D. Palmiter, *Cell* **91**, 583–592 (1997).
88. S. D. Moffat, E. J. Suh, A. S. Fleming, *Physiol. Behav.* **53**, 805–811 (1993).
89. J. K. Lerch-Haner, D. Frierson, L. K. Crawford, S. G. Beck, E. S. Deneris, *Nat. Neurosci.* **11**, 1001–1003 (2008).
90. R. B. Simerly, L. W. Swanson, R. A. Gorski, *J. Comp. Neurol.* **225**, 151–166 (1984).
91. J. K. Rilling, *Science* **345**, 771 (2014).
92. K. Nishimori *et al*., *Proc. Natl. Acad. Sci. U.S.A.* **93**, 11699–11704 (1996).
93. A. H. Macbeth, J. E. Stepp, H. J. Lee, W. S. Young 3rd, H. K. Caldwell, *Behav. Neurosci.* **124**, 677–685 (2010).
94. M. E. Rich, E. J. deCárdenas, H.-J. Lee, H. K. Caldwell, *PLOS ONE* **9**, e98839 (2014).
95. D. Chokchaloemwong *et al*., *Horm. Behav.* **64**, 53–69 (2013).


## ACKNOWLEDGMENTS

We thank A. E. Autry and A. Bendesky for comments on the manuscript, and R. Hellmiss for assistance with figure artwork. Supported by the Howard Hughes Medical Institute (C.D., Z.W.), the National Institute on Deafness and Other Communication Disorders (C.D., Z.W.), and the William F. Milton Fund (L.A.O.). We apologize to colleagues whose work we could not cite because of space constraints.

10.1126/science.1253291

REVIEW

# The biology of mammalian parenting and its effect on offspring social development

James K. Rilling[1,2] and Larry J. Young[1]*

**Parents know the transformative nature of having and caring for a child. Among many mammals, giving birth leads from an aversion to infant stimuli to irresistible attraction. Here, we review the biological mechanisms governing this shift in parental motivation in mammals. Estrogen and progesterone prepare the uterus for embryo implantation and placental development. Prolactin stimulates milk production, whereas oxytocin initiates labor and triggers milk ejection during nursing. These same molecules, interacting with dopamine, also activate specific neural pathways to motivate parents to nurture, bond with, and protect their offspring. Parenting in turn shapes the neural development of the infant social brain. Recent work suggests that many of the principles governing parental behavior and its effect on infant development are conserved from rodent to humans.**

Giving birth is among the most transformative experiences in a parent's lifetime. Furthermore, from the offspring's perspective, the nurturing relationship between parent and infant profoundly affects the development of the brain systems regulating social behavior. Here, we explore the hormonal and neural regulation of mammalian parenting and its consequences for infant social development. The hormones of reproduction (i.e., estrogen, progesterone, oxytocin, and prolactin) create a hospitable intrauterine environment for fetal development, ensure timely birth, and provide sustenance for the infant through lactation, but also orchestrate a set of neural systems to ensure maternal nurturing, bonding, and protection of young. Similar systems along with vasopressin and testosterone influence paternal care in biparental species. Parental nurturing has long-term effects on these same neural systems in infants, resulting in nongenomic transmission of parenting and attachment styles. We review recent studies suggesting that the neural mechanisms regulating parental care and its effect on infant development are notably conserved from rodent to human.

[1]Silvio O. Conte Center for Oxytocin and Social Cognition, Center for Translational Social Neuroscience, Department of Psychiatry and Behavioral Sciences, Yerkes National Primate Research Center, Emory University, Atlanta, GA 30329, USA. [2]Department of Anthropology, Emory University, Atlanta, GA 30329, USA.
*Corresponding author. E-mail: lyoun03@emory.edu

## Hormonal synchronization of physiology, brain, and behavior in rodents

Virgin females and males of many species generally avoid infants, finding infant stimuli aversive. Yet parturient mothers typically find infants irresistible and display a suite of maternal nurturing behaviors to ensure survival of their offspring (Fig. 1). For example, virgin female rats avoid or attack pups, but postpartum dams will press a lever more than 100 times per hour to have a pup delivered into their nest box with each press, provided that the number of pups in the nest is maintained below 20. Thus, the onset of maternal care involves a switch in the valence of pup stimuli, resulting from inhibition of avoidance and activation of approach neural systems in response to infant stimuli (*1*). The power of humoral factors to induce maternal behavior was first illustrated by showing that blood transfusions from a pregnant rat to a virgin female elicited the simultaneous onset of maternal responsiveness in both. Subsequent research revealed that the rise in circulating estrogen and progesterone secreted by the ovaries during pregnancy, followed by the precipitous drop in progesterone at the end of pregnancy, signals that parturition is eminent and maximizes brain sensitivity to oxytocin and prolactin by increasing production of their receptors (Fig. 2).

The steroid receptor–rich medial preoptic area (MPOA) senses the course of pregnancy by monitoring changes in steroid hormone concentrations, and is likely the region responsible for the transition from pup aversion to attraction at parturition through suppressing amygdala to anterior hypothalamic and enhancing mesolimbic dopaminergic pathways. MPOA neurons are robustly activated by pup stimuli, and destruction of the MPOA abolishes maternal care. Depositing estrogen, oxytocin, prolactin, or dopamine into the MPOA of virgin female rats facilitates maternal responsiveness, demonstrating the pivotal role for this region in synchronizing the onset of maternal behavior with delivery and nursing (*2*). Elegant molecular genetic studies are beginning to dissect the contributions of specific

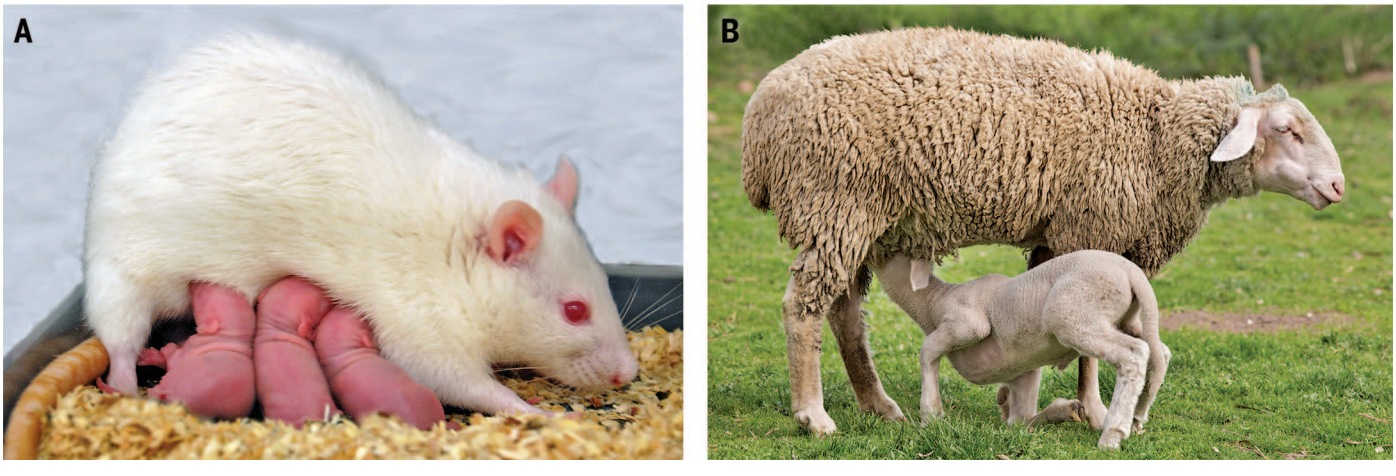


**Fig. 1. Giving birth in mammals leads to a transformation in maternal responsiveness toward infants.** In rats (**A**), this includes increases in nest building, pup retrieval, nursing, and defense of pups. Although many rodent mothers will care for any pup they encounter, sheep (**B**) develop selective bonds with their own lambs and reject lambs that are not their own. Experimental research using rodents and sheep have revealed some of the hormonal and neural mechanisms responsible for the onset of maternal behavior. (A) Photo courtesy of Doris Bayerl and Oliver Bosch.

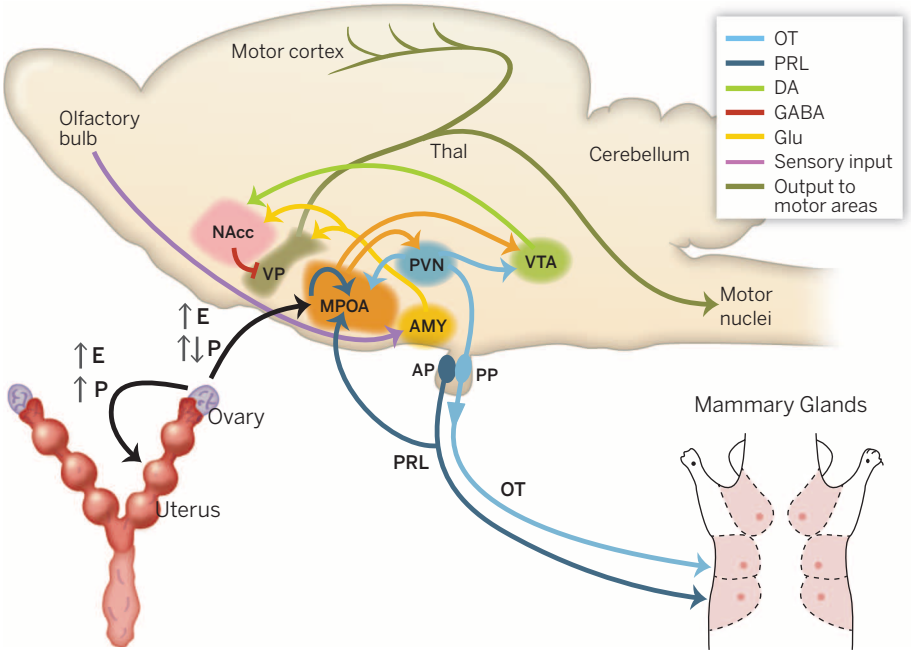


**Fig. 2. Schematic illustrating the hormonal and neural synchronization of reproductive physiology and maternal behavior in rodents.** Estrogen (E) and progesterone (P) secreted by the ovaries prepare the uterus for embryonic implantation, support placental development, and sensitize the MPOA to respond to oxytocin (OT) and prolactin (PRL). Prolactin released from anterior pituitary (AP) stimulates milk production in the mammary glands. Oxytocin released from the posterior pituitary (PP) stimulates uterine contractions during labor and milk letdown during nursing. OT, PRL, and dopamine (DA) signaling in the brain modulates communication between several neural pathways to initiate the onset of maternal behavior. GLU, glutamate; NAcc, nucleus accumbens; AMY, amygdala; PVN, paraventricular nucleus of the hypothalamus; VP, ventral pallidum; Thal, thalamus.

neural populations within the MPOA for initiating parental care (*1*).

## Dopamine and maternal care in rodents

Infusion of dopamine D1 receptor agonists into the MPOA in the absence of estrogen is sufficient to facilitate maternal behavior, suggesting an intra-MPOA interaction of estrogen and dopamine. However, it is the connection of the MPOA to the mesolimbic dopaminergic ventral tegmental area (VTA) that plays a pivotal role in maternal motivation. Like the MPOA, the VTA is activated by pup stimuli through direct MPOA-VTA connections, leading to increased extracellular dopamine in the nucleus accumbens during maternal care. Dopamine D1 agonists in the nucleus accumbens induce maternal responsiveness without hormonal stimulation. This elevated dopamine in the nucleus accumbens is mediated in part by oxytocin, because females that display higher levels of licking and grooming have higher densities of oxytocin projections to the VTA and elevated dopamine release in the nucleus accumbens in response to pups, which is diminished by oxytocin antagonist in the VTA (*2*). Thus, the MPOA is the master control region that senses the timing of parturition through the dynamic changes in estrogen, progesterone, oxytocin, and prolactin. At parturition, in response to pup stimuli, the MPOA activates the VTA directly and indirectly through the paraventricular nucleus of the hypothalamus via oxytocin, leading to elevated dopamine in the nucleus accumbens and activating dopamine D1 receptors. This releases the inhibitory control of the ventral pallidum by the nucleus accumbens, allowing excitatory input elicited by pup stimuli from the basolateral amygdala to activate the ventral pallidum. The ventral pallidum is a major output relay of the nucleus accumbens and modulates motor output in response to reinforcing stimuli via projections to the thalamus and cortical and mesencephalic motor nuclei, culminating in the expression of maternal nurturing responses toward pups (Fig. 2).

## Neural correlates of human parental care

In recent years, it has been possible to explore the biological correlates of human parenting through a variety of approaches, including brain imaging of the response to infant stimuli, endocrine studies, and gene association studies. Evidence to date suggests that similar mechanisms support animal and human parenting, with a shift to greater involvement of cortical systems in humans.

### *Neural response to infant and child visual stimuli*

Multiple functional magnetic resonance imaging (fMRI) studies report activation in the mesolimbic dopamine system (i.e., VTA, nucleus accumbens, and medial orbitofrontal cortex) as parents view pictures or videos of their children, and these activations are related to positive parenting behaviors (*3*) (Fig. 3A). For example, fathers who are more involved in instrumental caregiving show stronger VTA activation when viewing pictures of their children. In addition, mothers displaying more coordinated positive engagement and less intrusiveness with their infants more strongly activate the nucleus accumbens when viewing videos of their infants. Finally, mothers who exhibit more praise and positive affect while interacting with their child show stronger medial orbitofrontal cortex activation when viewing pictures of their children. Nonparents can also activate these regions when viewing children, and it may be the appealing facial features of children that drive these activations. In nulliparous women, activation of the nucleus accumbens scales to the degree of "baby schema" (i.e., cuteness) of the child stimuli, as well as with the reported motivation to care for the child. This implies that adult human attraction to infants is less tightly regulated by hormones compared with other species but does not rule out that the hormones of pregnancy intensify the attractiveness of infant stimuli (*3*–*6*).

### *Neural response to infant crying*

Infants solicit parental caregiving not only by their appearance but also through crying. Infant cries can also activate their parents' mesolimbic dopamine system. However, depressed mothers show attenuated activation to their own infant's cries in the nucleus accumbens, consistent with reduced caregiving motivation. Infant cries also reliably elicit activation in two other brain regions: the anterior insula and the prefrontal cortex. The insula is a visceral somatosensory cortex that represents not only the state of one's own body but also what others are feeling, and the right anterior insula may be where we become aware of those feelings. As such, the anterior insula is critically involved in emotional empathy, and more empathic mothers more strongly activate the anterior insula when viewing pictures of their children. Substance-using mothers show reduced anterior insula activation in response to infant cries, consistent with an attenuated empathic response. Although empathy is essential for parental care, empathic overarousal can lead to distress that interferes with compassionate behavior and effective parenting. For example, in high-risk mothers, stronger anterior insula responses to own-infant cries were related to more intrusive parenting. Fathers also show robust activation of the anterior insula to infant cries (Fig. 3B), and fathers with moderate anterior insula activation are the most involved in instrumental caregiving. Fathers with low and high insula activation may be less involved due to empathic under- and overarousal to cries (*3*) (*7*) (*8*).

The prefrontal cortex is thought to be involved in regulating the initial negative emotional response to infant crying. Frustration induced by inconsolable infant crying is a risk factor for infant abuse (*9*), highlighting the importance of

emotion regulation for sensitive parenting. Recruitment of prefrontal cortex during own-infant crying is associated with increased maternal sensitivity, decreased stress hormone responses to separation, and more secure child attachment behaviors upon reunion (*10*). Interestingly, depressed mothers and substance-using mothers are less able to engage the prefrontal cortex during infant crying and may therefore be less able to regulate their negative reactions to crying (*7*, *11*).

Fewer imaging studies support a role for the MPOA in human parenting, although hypothalamic activation in response to infant stimuli has been reported in a minority of studies (*12*). It is not clear whether this is due to a diminished role of the MPOA, technical issues with imaging, or because this region is not treated as a separate entity from the hypothalamus in human imaging studies. One possibility is that activation of subpopulations of MPOA neurons generates less fMRI signal as an output node than reflected in downstream targets such as the VTA and nucleus accumbens. In light of its pivotal role in regulating parental behavior in animals, we urge investigators to focus on MPOA/hypothalamus in their analyses.

## Oxytocin and parenting in rodents and sheep

Oxytocin has received considerable attention in recent years for modulating many aspects of social relationships, including parenting and social bonding. Disrupting brain oxytocin signaling pharmacologically or genetically disrupts maternal behavior (*13*). *CD38* knockout mice with impaired oxytocin secretion display disrupted maternal care, which is restored by subcutaneous injection of oxytocin (*13*). Whereas the role of peripheral oxytocin signaling in initiating maternal responsiveness has largely been unexplored, most, but not all, studies suggest that oxytocin signaling in the brain facilitates the onset—and to a lesser degree the maintenance of—maternal responsiveness in rodents. Oxytocin released centrally during parturition and nursing appears to play a role in the transition toward approach behaviors in mothers. Rodent mothers are promiscuously maternal, nurturing any pup they encounter; however, in herding animals like sheep, strong and selective mother-infant bonds are formed. Oxytocin signaling is necessary and sufficient to form a selective bond between a ewe and a lamb (*13*). Thus oxytocin affects not only maternal motivation but also the formation of mother-infant attachment where it exists. Oxytocin, along with the related peptide vasopressin, also elicits protective maternal aggression toward intruders (*14*). The essential roles of oxytocin in generating nurturing, bonding, and infant defense in mothers may be the evolutionary antecedent to the more generalized roles of this peptide in other social contexts, including pair-bonding behavior, empathy, trust and in-group favoritism.

## Oxytocin and human parenting

There is considerable evidence that oxytocin modulates human parenting from three experimental approaches. The first involves correlating parental behavior and peripheral oxytocin concentrations. Although peripheral oxytocin is less likely to be relevant to behavior than central measures, it is not feasible to measure central oxytocin levels noninvasively in humans. The degree to which peripheral oxytocin is correlated with oxytocin activity in the brain is a point of controversy, as are the methods for sample processing and the assays used. Nevertheless, we discuss studies relating peripheral oxytocin and behavior, with the caveat that little rigorous evidence supports a relationship between circulating plasma, salivary, or urinary oxytocin and brain oxytocin activity, although dynamic changes in peripheral oxytocin could possibly parallel central oxytocin release (*13*).

In both mothers and fathers, plasma oxytocin is positively correlated with affectionate contact (*15*) and coordinated positive engagement with infants during dyadic interactions (*16*). Both of these parental behaviors are important for healthy psychosocial development (*17*). Depressed mothers, who may be less responsive to their children, have lower salivary oxytocin than nondepressed mothers (*18*). Baseline plasma oxytocin concentrations in fathers, but not mothers, correlate with stimulatory parent-infant contact such as proprioceptive touch, stimulatory touch, and exploratory play (*16*). Thus, oxytocin may facilitate sexually differentiated styles of parent-infant interaction that could support different aspects of healthy child development.

Intranasal oxytocin administration has become popular for exploring the role of oxytocin on parenting. These studies should, however, be interpreted with caution with regard to brain mechanisms because nasally administered oxytocin elevates plasma oxytocin significantly, with only modest evidence for elevations within the brain (*19*–*21*). Most studies have been conducted in fathers due to concerns with administering oxytocin to lactating mothers. In fathers, intranasal oxytocin increases stimulatory and exploratory play with toddlers and increases the duration of episodes of father-infant touch and social reciprocity. These augmented paternal behaviors in turn increase the duration of episodes of infant gaze to the father and infant object manipulation, as well as infant salivary oxytocin (*16*). Notably, paternal head speed and acceleration during father-infant interactions are also increased by intranasal oxytocin and positively correlated with infant salivary oxytocin (*22*). Overall, oxytocin seems to motivate paternal behaviors that facilitate father-infant bonding. Intranasal oxytocin also decreases paternal hostility during interactions with toddlers and decreases frustration in response to infant cries among nulliparous women (*3*, *12*, *16*). Finally, in parallel with animal studies where oxytocin supports maternal aggression, intranasal oxytocin increases maternal protective responses in the presence of a socially intrusive stranger among women with postpartum depression (*23*).

Genetic evidence also supports a role for oxytocin in human parenting. Polymorphisms in genes encoding the oxytocin receptor (*OXTR*) and *CD38* have been reported to predict parenting behaviors. The G/G genotype of *OXTR* rs53576 is associated with increased maternal sensitivity toward toddlers at risk for externalizing behavior problems and with a more pronounced heart-rate response to infant cries (*24*). In another study, *OXTR* rs2254298 and rs1042778 and *CD38* rs3796863 risk alleles were each associated with lower plasma oxytocin. Reduced plasma oxytocin and both *OXTR* and *CD38* risk alleles were related to less parental touch (*16*). Moreover, a recent study showed that children with two A alleles at rs53576 tend to exhibit more negative emotionality, which in turn partially explains

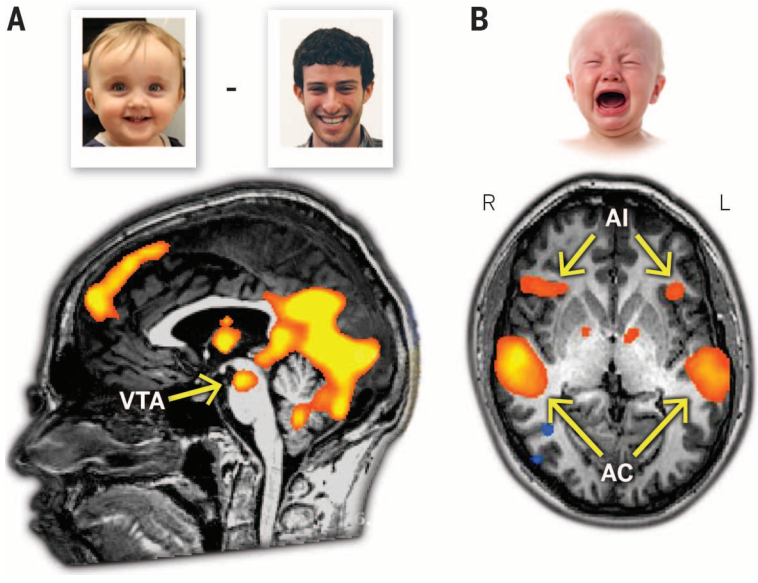


**Fig. 3. Paternal brain function in humans revealed by fMRI.** (**A**) The VTA in fathers is activated to a greater extent when viewing pictures of their own children compared with pictures of unknown adults. (**B**) The anterior insula in fathers is activated to a greater extent when listening to infant-cry stimuli compared with an auditory control tone. AC, auditory cortex.

some aspects of parental behavior (*25*). Thus, associations between rs53576 genotype and parental behavior could be partially mediated by genetically influenced child temperament and behavior. These genetic studies, although intriguing, have small samples and await replication.

### *Oxytocin modulation of the neural response to infants and children*

Research in animals suggests that oxytocin acts in the MPOA and VTA to activate the mesolimbic dopamine approach system and inhibit amygdala-based avoidance, rendering infant stimuli reinforcing rather than aversive. A similar mechanism may be operational in humans. Plasma oxytocin is positively correlated with nucleus accumbens response to viewing pictures or videos of one's own children. Intranasal oxytocin also attenuates the amygdala response to unknown infant cries among nulliparous women (*26*), consistent with inhibition of an avoidance pathway. The same study also found that intranasal oxytocin enhanced the anterior insula response to unknown infant cries, suggesting that oxytocin may also enhance empathic responses to unknown infant cries. Although animal research has emphasized the role of oxytocin in the onset of parental behavior, the human studies discussed above instead generally demonstrate a role for oxytocin in the maintenance of parental behavior. Two recent human studies suggest that peripartum exposure to oxytocin may alter maternal neural responses to infant stimuli. Compared with nonbreastfeeding mothers, breastfeeding mothers more strongly activate the insula and prefrontal cortex in response to own-infant cries, and mothers who deliver their babies vaginally have a stronger insula response to own-infant cries than do mothers who deliver by Caesarean section (*3*). Collectively, these neuroimaging data are consistent with the above findings, suggesting that oxytocin supports sensitive caregiving.

## Regulation of paternal care in rodents

The regulation of paternal care in mammals has received less attention than maternal care, primarily because of its rarity in rodent models, although there appear to be common elements with maternal care (*1*). In some species, testosterone is necessary for the maintenance of paternal care, perhaps by its conversion to estrogen in the brain (*27*). However, in several biparental rodent and primate species, the onset of paternal care is associated with a decrease in testosterone and an increase in prolactin. However, there is little evidence of a causal relationship between elevated prolactin concentrations and paternal behavior in any mammalian species (*28*).

The role of oxytocin in nonhuman mammalian paternal behavior has received little attention, although vasopressin appears to be involved. In monogamous male prairie voles, mating decreases vasopressin fiber content in the septum and increases vasopressin synthesis, consistent with intraseptal vasopressin release. Furthermore, infusion of a vasopressin V1a receptor antagonist into the septum disrupts paternal care in voles (*29*).

## Testosterone, testes size, and paternal caregiving in humans

In many species, testosterone supports mating effort at the expense of parenting effort. This may also be true of human males. Men with higher testosterone report less sympathy toward an unknown newborn infant cry, testosterone decreases when men become involved fathers, and fathers experiencing larger decreases in testosterone report less sexual intercourse (*30*). Moreover, among fathers, those with higher testosterone are less involved in paternal caregiving (*4*) and less responsive to infants (*31*). Low testosterone may facilitate paternal caregiving by allowing more empathy for the child, by increasing frustration tolerance, or by decreasing sexual motivation that could compete with parenting effort. Although married fathers have an attenuated nucleus accumbens response to visual sexual stimuli compared with unmarried nonfathers, this response was not correlated with testosterone levels. However, testosterone was negatively correlated with activation in face-emotion processing regions when viewing pictures of unknown children, consistent with a negative effect on neural systems involved with empathy (*32*).

Testes size is also correlated with increased investment in mating, both across and within nonhuman species (*4*). In human fathers, testes size has a weak but significant negative correlation with instrumental caregiving, such that men with smaller testes are more involved. Testes size also has a robust inverse correlation with the VTA activation in response to viewing pictures of one's own child (Fig. 4), implying stronger motivation to approach children in fathers with smaller testes (*4*).

The number of CAG repeats in exon 1 of the androgen receptor gene (*AR*) is inversely correlated with AR expression. Fathers with more CAG repeats, and presumably fewer AR, have stronger anterior insula response to infant cries (*8*). This suggests that fathers with less sensitivity to androgens have a more empathic response to infant cries.

## Effect of parenting on social development in rodents

Variation in parental nurturing affects the developing offspring's brain, affecting future social behaviors. Rat dams vary in the extent to which they lick and groom their pups. Notably, pups reared by low licking and grooming mothers display low licking and grooming when they become mothers, regardless of the maternal style of their biological mothers. This nongenomic transmission of maternal style is mediated by alterations in estrogen receptor and oxytocin receptor expression (*33*). High licking and grooming mothers have higher densities of estrogen receptor in the MPOA than low licking and grooming mothers as a result of differential methylation of the estrogen receptor (*ERα*) promoter. This lower estrogen receptor density leads to decreased sensitivity to estrogen and thus lower oxytocin receptor transcription in the MPOA. Being reared by a low licking and grooming mother also significantly alters several aspects of the mesolimbic dopamine system through adulthood (*34*). Parenting also has life-long effects on the oxytocin system in primates, as rhesus macaques raised by human caregivers have lower central oxytocin than mother-reared animals (*13*).

Variation in parental nurturing can affect other social behaviors as well. Repeated neonatal social isolations disrupt later-life pair bonding behaviors in monogamous voles (*35*). In contrast, pharmacologically stimulating oxytocin neurons with neonatal melanocortin agonists facilitates later-life pair bonding (*36*). Paternal care can also affect rodent social development and parenting style. Monogamous prairie vole pups of both sexes raised in the absence of the father show impairments in adult pair-bonding behavior and lower levels of licking and grooming compared with biparentally reared animals

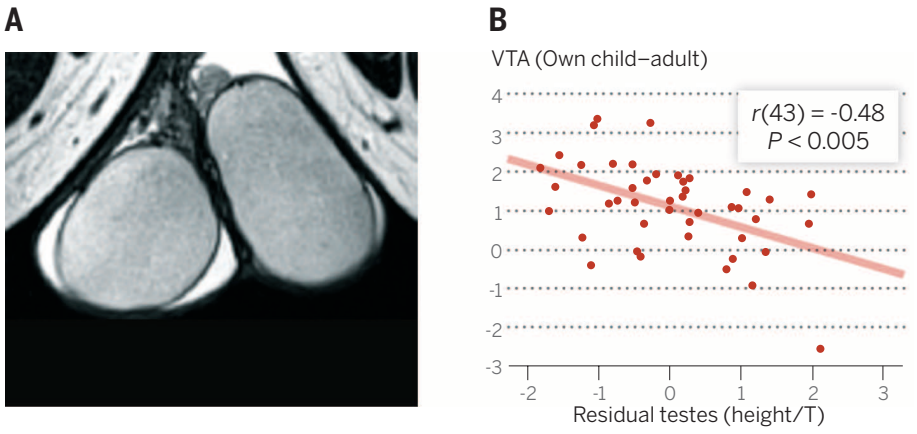


**Fig. 4. Relationship between testes volume and VTA fMRI signal in fathers in response to viewing pictures of their own children.** (**A**) Structural MRI was used to estimate testicular volume in fathers. (**B**) VTA activation in fathers while viewing pictures of their own children is negatively correlated with testicular volume, controlling for both height and testosterone level. Adapted from (*4*).

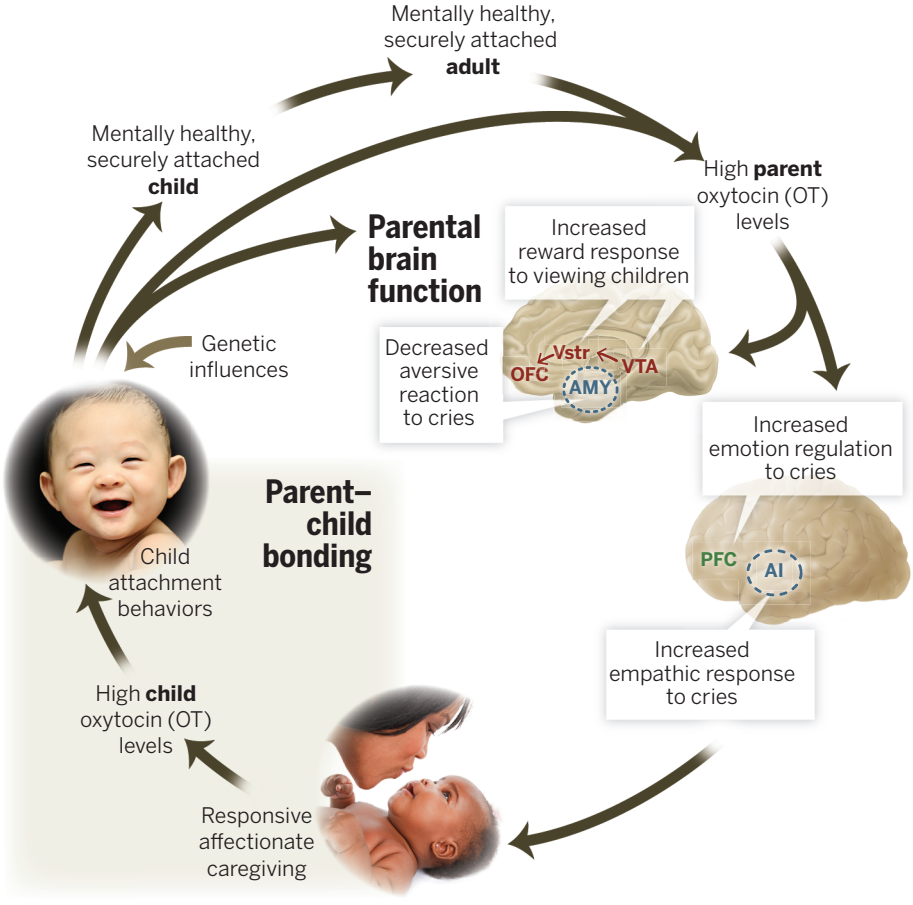


**Fig. 5. Postulated mechanisms supporting the intergenerational transmission of secure attachment in humans.** Securely attached parents have higher baseline oxytocin (OT) and a more pronounced OT response to interactions with their children. OT augments the mesolimbic DA system response to visual child stimuli, enhancing their reward value. It also inhibits AMY and augments anterior insula (AI) responses to infant-cry stimuli, facilitating a more empathic reaction. OT may also modulate prefrontal cortex activity to suppress negative emotional reactions to infant crying. These neurobiological influences promote responsive, affectionate caregiving, which in turn promotes OT activity in children, along with child attachment behaviors that further engage parental brain systems, resulting in a positive feedback cycle that culminates in a mentally healthy, securely attached child. Genetic influences of the child can also either support or interfere with child attachment behaviors and parent-offspring bonding. OFC, orbitofrontal cortex; PFC, prefrontal cortex.

(*37*). Likewise, paternal licking and grooming style is nongenomically transmitted from father to son in the monogamous, biparental California mouse (*27*).

## Effect of parenting on neural and social development in humans

A considerable body of work has investigated alterations in brain development in children initially raised without parents in orphanages who were subsequently adopted into stable families. The observed alterations have been focused on the amygdala and prefrontal cortex (*38*–*40*). Postinstitutionalized children have larger amygdala volumes than children not raised in orphanages, and amygdala volume is positively correlated with both anxiety symptoms and internalizing problems. Postinstitutionalized children also exhibit increased amygdala responses to fearful faces. Typically developing children have a stronger amygdala response to pictures of their mothers compared with female strangers, which presumably reflects the special affective salience of the mother. In contrast, amygdala response to strangers matches that to the mother among postinstitutionalized children, who have an increased tendency to approach unfamiliar adults. Finally, postinstitutionalized children show altered connectivity between the amygdala and medial prefrontal cortex, a key emotion-regulation pathway. We cannot be certain that parental deprivation is the primary contributor to these altered pathways, but the overlap with findings from experimental studies in rodents supports this possibility (*38*, *39*).

As described in rodents, the effect of variation in parenting on offspring development may be partially mediated by oxytocin in humans. For example, women experiencing childhood neglect or abuse have decreased oxytocin concentrations in cerebrospinal fluid as adults (*13*). Additionally, children previously raised in orphanages have an attenuated urinary oxytocin response to interactions with their mothers, although the caveats mentioned above regarding peripheral oxytocin and assay techniques must be considered (*41*). Furthermore, G/G genotype carriers at *OXTR* rs*53576* have a greater risk of displaying depressive symptomology and emotional dysregulation in response to childhood maltreatment but are also more likely to benefit from positive family environments than are A/A genotype carriers (*42*, *43*). Finally, attachment styles are often transmitted across generations, and oxytocin may be involved. Insecurely attached mothers have an attenuated plasma oxytocin response to interactions with their children (*12*), plasma oxytocin concentrations are positively correlated with parental affection toward infants (*18*), and infants respond to this affection with parent-directed behaviors that support parent-infant bonding (*44*). Thus, high levels of oxytocin in securely attached parents may facilitate greater affectionate behavior toward the child, who consequently becomes more securely attached to the parent (Fig. 5).

## Conclusion

The human parenting experience is likely to have some unique features relative to other mammals by virtue of the increased cortical complexity and control over emotion and behavior in our species. However, there is now strong evidence that human and animal parenting share many subcortical neural and neurochemical mechanisms. In rodents, the MPOA likely plays a primary role in the dramatic transformation of the maternal brain in response to hormonal changes though inhibiting avoidance pathways and activating mesolimbic dopamine-approach pathways. In humans, these mechanisms may modulate parental sensitivity, motivation, and drive, whereas higher-order cortical, hormone-independent mechanisms play a more prominent role in cognitively enriching the parental experience. As technology progresses, we will undoubtedly gain a deeper understanding of how neurochemistry and brain systems influence mammalian and human parenting, as well as how parental nurturing shapes the social neural systems of our offspring. We will likely discover even more parallels in the regulation of parenting and its consequences between rodents and humans. Perhaps this understanding will lead to new efforts to systematically improve parenting in all facets of society to benefit generations to come.

### REFERENCES AND NOTES


1. C. Dulac, L. A. O'Connell, Z. Wu, *Science* **345**, 765–770 (2014).
2. D. S. Stolzenberg, M. Numan, *Neurosci. Biobehav. Rev.* **35**, 826–847 (2011).
3. J. K. Rilling, *Neuropsychologia* **51**, 731–747 (2013).
4. J. S. Mascaro, P. D. Hackett, J. K. Rilling, *Proc. Natl. Acad. Sci. U.S.A.* **110**, 15746–15751 (2013).
5. K. J. Michalska *et al.*, *Front. Behav. Neurosci.* **8**, 21 (2014).
6. M. L. Glocker *et al.*, *Proc. Natl. Acad. Sci. U.S.A.* **106**, 9115–9119 (2009).

7. N. Landi *et al.*, *Front Psychiatry* **2**, 32 (2011).
8. J. S. Mascaro, P. D. Hackett, H. Gouzoules, A. Lori, J. K. Rilling, *Soc. Cogn. Affect. Neurosci.*, 10.1093/scan/nst166 (2013).
9. R. G. Barr, *Proc. Natl. Acad. Sci. U.S.A.* **109** (suppl. 2), 17294–17301 (2012).
10. H. K. Laurent, J. C. Ablow, *Infant Behav. Dev.* **35**, 761–772 (2012).
11. H. K. Laurent, J. C. Ablow, *Soc. Cogn. Affect. Neurosci.* **7**, 125–134 (2012).
12. L. Strathearn, P. Fonagy, J. Amico, P. R. Montague, *Neuropsychopharmacology* **34**, 2655–2666 (2009).
13. H. E. Ross, L. J. Young, *Front. Neuroendocrinol.* **30**, 534–547 (2009).
14. O. J. Bosch, I. D. Neumann, *Horm. Behav.* **61**, 293–303 (2012).
15. Y. Apter-Levi, O. Zagoory-Sharon, R. Feldman, *Brain Res.*, 10.1016/j.brainres.2013.10.052 (2013).
16. R. Feldman, *Horm. Behav.* **61**, 380–391 (2012).
17. R. Feldman, *J. Child Psychol. Psychiatry* **48**, 329–354 (2007).
18. Y. Apter-Levy, M. Feldman, A. Vakart, R. P. Ebstein, R. Feldman, *Am. J. Psychiatry* **170**, 1161–1168 (2013).
19. M. E. Modi, F. Connor-Stroud, R. Landgraf, L. J. Young, L. A. Parr, *Psychoneuroendocrinology* **45**, 49–57 (2014).
20. N. Striepens *et al.*, *Sci. Rep.* **3**, 3440 (2013).
21. I. D. Neumann, R. Maloumby, D. I. Beiderbeck, M. Lukas, R. Landgraf, *Psychoneuroendocrinology* **38**, 1985–1993 (2013).
22. O. Weisman *et al.*, *Biol. Lett.* **9**, 20130828 (2013).
23. B. L. Mah, M. J. Bakermans-Kranenburg, M. H. Van Ijzendoorn, R. Smith, *Depress. Anxiety*, 10.1002/da.22245 (2014).
24. M. M. Riem, S. Pieper, D. Out, M. J. Bakermans-Kranenburg, M. H. van Ijzendoorn, *Soc. Cogn. Affect. Neurosci.* **6**, 294–300 (2011).
25. K. R. Kryski, H. J. Smith, H. I. Sheikh, S. M. Singh, E. P. Hayden, *Pers. Individ. Dif.* **64**, 107–110 (2014).
26. M. M. Riem *et al.*, *Biol. Psychiatry* **70**, 291–297 (2011).
27. E. D. Gleason, C. A. Marler, *Proc. Biol. Sci.* **280**, 20130824 (2013).
28. T. E. Ziegler, S. L. Prudom, S. R. Zahed, A. F. Parlow, F. Wegner, *Horm. Behav.* **56**, 436–443 (2009).
29. Z. Wang, C. F. Ferris, G. J. De Vries, *Proc. Natl. Acad. Sci. U.S.A.* **91**, 400–404 (1994).
30. L. T. Gettler, T. W. McDade, S. S. Agustin, A. B. Feranil, C. W. Kuzawa, *Horm. Behav.* **64**, 755–763 (2013).
31. O. Weisman, O. Zagoory-Sharon, R. Feldman, *Prog. Neuropsychopharmacol. Biol. Psychiatry* **49**, 47–52 (2014).
32. J. S. Mascaro, P. D. Hackett, J. K. Rilling, *Psychoneuroendocrinology* **46**, 153–163 (2014).
33. F. A. Champagne, *Horm. Behav.* **60**, 4–11 (2011).
34. C. J. Peña, Y. D. Neugut, C. A. Calarco, F. A. Champagne, *Eur. J. Neurosci.* **39**, 946–956 (2014).
35. P. Yu *et al.*, *Psychoneuroendocrinology* **38**, 3128–3138 (2013).
36. C. E. Barrett *et al.*, *Neuropsychopharmacology* **85**, 357–366 (2013).
37. T. H. Ahern, E. A. Hammock, L. J. Young, *Dev. Psychobiol.* **53**, 118–131 (2011).
38. N. Tottenham, M. Shapiro, E. H. Telzer, K. L. Humphreys, *Dev. Sci.* **15**, 307–319 (2012).
39. D. G. Gee *et al.*, *Proc. Natl. Acad. Sci. U.S.A.* **110**, 15638–15643 (2013).
40. J. L. Hanson *et al.*, *Child Dev.* **84**, 1566–1578 (2013).
41. A. B. Wismer Fries, T. E. Ziegler, J. R. Kurian, S. Jacoris, S. D. Pollak, *Proc. Natl. Acad. Sci. U.S.A.* **102**, 17237–17240 (2005).
42. B. Bradley, T. A. Davis, A. P. Wingo, K. B. Mercer, K. J. Ressler, *Eur. J. Psychotraumatol.* **4**, 21659 (2013).
43. R. J. McQuaid, O. A. McInnis, J. D. Stead, K. Matheson, H. Anisman, *Front Neurosci* **7**, 128 (2013).
44. O. Weisman, O. Zagoory-Sharon, R. Feldman, *Biol. Psychiatry* **72**, 982–989 (2012).



**ACKNOWLEDGMENTS**

The authors acknowledge the support of a Positive Neuroscience Award from the John Templeton Foundation to J.K.R., National Institute of Mental Health (NIMH) R01MH096983 to L.J.Y., and NIMH 1P50MH100023 to J.K.R. and L.J.Y., as well as NIH OD P51OD11132 to the Yerkes National Primate Research Center during the writing of this manuscript.

10.1126/science.1252723


REVIEW

# The evolution of flexible parenting


**Nick J. Royle,* Andrew F. Russell, Alastair J. Wilson**



**Parenting behaviors, such as the provisioning of food by parents to offspring, are known to be highly responsive to changes in environment. However, we currently know little about how such flexibility affects the ways in which parenting is adapted and evolves in response to environmental variation. This is because few studies quantify how individuals vary in their response to changing environments, especially social environments created by other individuals with which parents interact. Social environmental factors differ from nonsocial factors, such as food availability, because parents and offspring both contribute and respond to the social environment they experience. This interdependence leads to the coevolution of flexible behaviors involved in parenting, which could, paradoxically, constrain the ability of individuals to rapidly adapt to changes in their nonsocial environment.**


Parents often have to deal with multiple, competing demands simultaneously, such as feeding and defending offspring. The costs and benefits of parental decisions at any given moment in time will be sensitive to a range of environmental factors. These include not only climatic (e.g., temperature and rainfall) and ecological (e.g., predation pressure, pathogen load, and food availability) factors, but also social factors, in the form of partner and/or offspring behavior. When individuals modify their behavior in response to environmental factors, this is known as plasticity of behavior (*1*–*4*). If plasticity improves the fitness of individuals, then it is adaptive (*5*–*7*). To understand how parenting evolves, it is essential to determine when and how individuals vary in their plastic responses to environments (*8*). However, individual variation in plasticity of parenting behaviors has rarely been quantified (*3*, *8*).

Here, we identify the gaps in our understanding and provide directions for future research. We will (i) outline the diversity of parenting behavior in animals, (ii) review the current evidence for adaptive plasticity, (iii) demonstrate the need for individual-based studies, and (iv) illustrate how evolving social environments can help us understand how plasticity contributes to adaptive evolution of parenting behaviors. To do this, we combine approaches from behavioral ecology and quantitative genetics. Our intention is to highlight how incorporating individual-level variation in parenting response to environments, particularly social environments, is essential for understanding the evolution of parenting. We demonstrate that parenting provides a particularly fertile context in which to investigate the role of plasticity in adaptation and evolutionary processes more generally.

## The diversity of parental care in animals

The extent of parenting, defined here as behavioral interactions directed toward improving the growth or survival of offspring after birth or hatching, varies across the animal kingdom (Fig. 1). For example, feeding offspring (hereafter referred to as "provisioning") occurs in only ~1% of insect species [all ants and some bees, wasps, termites, and beetles (*9*)] but is ubiquitous in mammals and nearly so in birds (*10*). Provisioning is not the only form of care, however. Parents also protect offspring from predators, and in many vertebrates they clean, carry, and provide warmth to offspring. Additionally, parental care occurs in ectothermic vertebrates: Various forms of parental care are found in fish (~30% of families), amphibians (e.g., 6 to 15% of anuran species, ~20% of salamander species), and reptiles (all crocodilians, ~1% of lizards, and 3% of snakes provide some form of care) (*10*). In ectothermic vertebrates, most forms of care are provided before offspring hatch or are born (e.g., egg guarding), but postnatal care also occurs (Fig. 1). Finally, care can be provided by the mother or father alone (uniparental care), both parents (biparental care), or parent(s) plus nonparents (cooperative care), with several species across different taxonomic groups showing more than one mode of care within a population [e.g., burying beetles (*Nicrophorus vespilloides*), acorn woodpecker (*Melanerpes formicivorus*), Galilee St. Peter's fish (*Sarotherodon galilaeus*), and gray wolf (*Canis lupus*) (*9*, *10*)].

## Parenting is complex and responsive to environmental factors

A parent spending more time foraging to provision offspring will have less time for offspring defense. Parents have to balance these competing demands when deciding how to allocate time to each activity. Parenting is therefore multidimensional [i.e., it is a multivariate trait (Fig. 2)]. The allocation of resources to these competing requirements is known to be sensitive to a host of environmental factors, both abiotic (e.g., rainfall and temperature) and biotic, with the latter further separable into nonsocial (e.g., food, predators, and pathogens) and social (e.g., offspring begging and partner contributions) categories. Figure 2 illustrates this idea for the simple case of two competing behaviors in two contrasting


Centre for Ecology and Conservation, College of Life and Environmental Sciences, University of Exeter, Cornwall Campus, Penryn TR10 9EZ, UK.
***Corresponding author. E-mail: n.j.royle@exeter.ac.uk**

**Fig. 1. Parenting behavior is found in diverse forms across a broad taxonomic spread.** Parent(s) commonly have to decide when and how much to allocate to distinct forms of behavior directed at or for offspring, including: defending and protecting (**A** to **D**), escorting and/or carrying (**E** and **F**), and provisioning (**G** to **I**) young. Parenting can be provided by a single parent, either the male (E) or, more commonly, the female (A, D, F, G, I); pairs (B, C, H); or cooperative groups (C and D). Not uncommonly, there is variation in parenting mode in the same species (C). (A) Female common earwig (*Forficula auricularia*) guarding nymphs [photo by Jöel Meunier]. (B) Male Gambel's quail (*Callipepla gambelii*) with chicks [photo © Alex Badyaev/www.tenbestphotos.com]. (C) White's skink (*Egernia whitii*) pair with offspring [photo by Geoffrey While]. (D) African elephants (*Loxodonta africana*) [photo by Nick Royle]. (E) Male *Hyloxalus nexipus* frog carrying tadpoles [photo by Jason Brown]. (F) Female red kangaroo (*Macropus rufus*) with joey [photo by Andy Russell]. (G) *Stegodyphus lineatus* spiderlings eating their mother (matriphagy) [photo by Trine Bilde]. (H) Wattled starling (*Creatophora cinerea*) feeding fledged young [photo by Nick Royle]. (I) Grey rhebok (*Pelea capreolus*) suckling young [photo by Nick Royle].

environments. For example, a parent experiencing an increased risk of nest predation would maximize fitness (reproductive success) by spending more time on nest defense, even though this must come at a cost to offspring provisioning. Consistent with this prediction, a recent study of 10 temperate and subtropical bird species from the Americas showed that parents provisioned offspring less when the perceived threat of nest depredation was raised by playing vocalizations of nest predators [Stellar's jays (*Cyanocitta stelleri*) in North America and plush-capped jays (*Cyanocorax chrysops*) in South America]. Parents were more responsive to the threat in those species with a higher natural risk of nest predation (*11*). Thus, whereas flexibility in behavior was found in all 10 species studied, the most responsive species were those with an evolutionary history of higher predation risk, providing evidence that behavioral plasticity has itself evolved under selection.

A defining feature of parenting behavior is that it involves repeated interactions with other individuals of the same species: The behavior of a mother blackbird feeding a brood of hungry nestlings will be affected by the behavior of her partner (e.g., how much food he provides to the nestlings or how much time he spends defending the nest) and that of her offspring (e.g., how much they beg). Consequently, one of the most important forms of environment that parents experience is the social environment provided by family members. Experimental studies have clearly established that individuals respond to changes in their social environment. For example, a recent meta-analysis of 54 bird studies showed that individuals generally responded by working harder when their partner's contributions were experimentally reduced (*12*). The average response differed between parental behaviors, with parents responding by increasing provisioning more than incubation and/or brooding. Additionally, females were more responsive than males to changes in partner contributions. It is currently unclear whether these results arise because individuals respond directly to changes in the contribution of their partner (*13*) or indirectly due to changes in offspring behavior (*14*). Importantly, however, these studies show that the social environment can induce changes in behavior and that such changes vary with the form of parental care, sex, and species involved.

## Studies of plasticity at the individual level are needed

As highlighted above, many studies of parental care have shown changes in mean levels of behavior across environments, suggesting that adaptive phenotypic plasticity has evolved. However, the question of how much plasticity varies among individuals within populations has been almost entirely overlooked in the context of parenting behavior (*8*). If we hope to understand the contribution of plasticity to parental care evolution, then this is an important omission, because selection acts on among-individual variation (*2*, *8*). Additionally, if this variation in plasticity is heritable, then plastic responses will themselves evolve (*2*, *7*). This evolution of phenotypic plasticity will contribute to the adaptation of parenting. Quantifying among-individual variation in plasticity requires repeated-measures studies, in which the behavior of individually identifiable animals is recorded multiple times across varying environments. Such repeated-measures data are routinely collected in both lab and field studies of parenting (see Box 1 for an example). It is therefore surprising that little is currently known about among-individual variation in the plasticity of parenting or plasticity in behavioral traits, more generally (*3*, *4*, *15*). Nonetheless, successful studies of individual plasticity in other fields of evolution and ecology provide a useful template to follow. For example, in a study of lay date in wild great tits (*Parus major*) (*16*), analysis of repeated-measures data showed that plastic responses to spring temperature were both under directional selection and genetically variable. This leads to the prediction that plasticity will evolve, contributing to an adaptive advance in lay date as spring temperatures increase as a consequence of climate change (*16*).

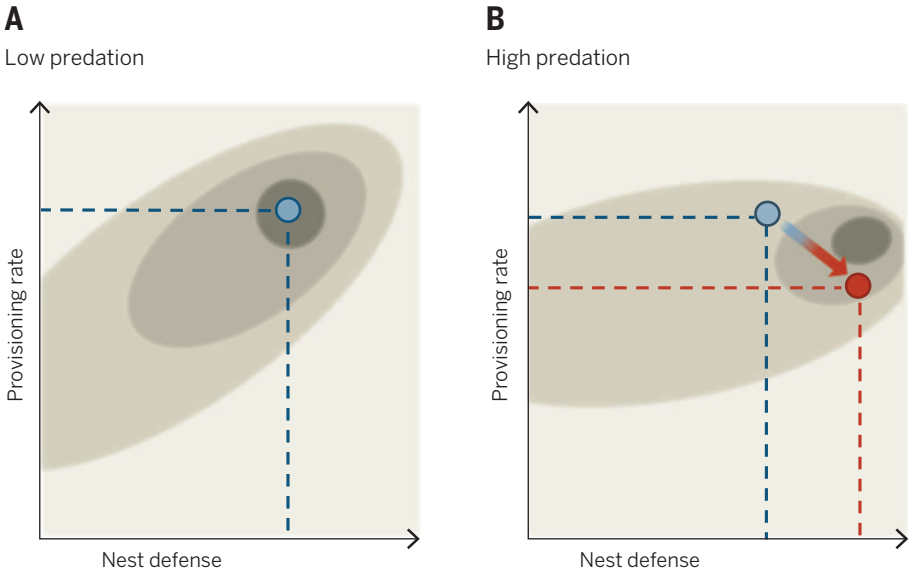


**Fig. 2. Parental fitness as a function of nest defense and offspring provisioning.** Darker shading denotes trait combinations yielding higher fitness. (**A**) Imagine a parent whose bivariate behavioral phenotype (blue circle) is optimal under low predation. (**B**) An increase in predation risk alters the fitness surface and also induces a plastic response (arrow) to a new phenotype (red circle) in which more time is spent in defense and less in provisioning. In this example, the plasticity is adaptive because fitness is greater than it would have been with no behavioral response. However, it is not optimal because higher-fitness trait combinations are possible. All else being equal, selection in the population should favor plastic responses that track the phenotypic optimum across environments.

## Behavioral reaction norms: A framework for studying individual-level plasticity

Variation in developmental plasticity has long been studied using the "reaction norm" approach (*6*, *17*). More recently, this approach has also been adopted by researchers studying flexible life history traits, such as body size (*1*) and behaviors (*3*). In the latter context, behavioral reaction norms (BRNs) can be used to describe an individual's behavior (e.g., the amount of food a parent provides to offspring) across an environment gradient, which may be nonsocial (e.g., food abundance) or social [e.g., offspring begging rate (*18*)]. Typically, though perhaps not always justifiably, a linear form of the BRN is assumed, which can be described by two parameters: a slope and an intercept (Fig. 3). The former describes plasticity, whereas mean-centering the $x$ axis ensures that the intercept, or elevation, of the line describes behavior in an average environment (Fig. 3A). For empiricists, a useful feature of the BRN concept is that reaction norms are readily incorporated into linear mixed-effect models to test for among-individual variance in plasticity [commonly referred to as an "individual-by-environment" interaction (IxE) (*2*) (Fig. 3B)]. Furthermore, if relationships among individuals in the population are known, then pedigree-based quantitative genetic methods can be used to test for and estimate any heritable variation in plasticity [that is, "genotype-by-environment" interaction (GxE)] (*2*). Although there are some important pitfalls of interpretation to avoid, there is now a mature literature on how to apply these statistical methods to evolutionary and ecological studies of phenotypic plasticity (*2*, *19*, *20*).

## Examples of BRN use in the study of parenting

Although the BRN approach has yet to be widely applied to studies of parenting, its utility has been demonstrated recently by Westneat *et al.* (*8*) in a study of provisioning behavior in house sparrows (*Passer domesticus*). In this study,

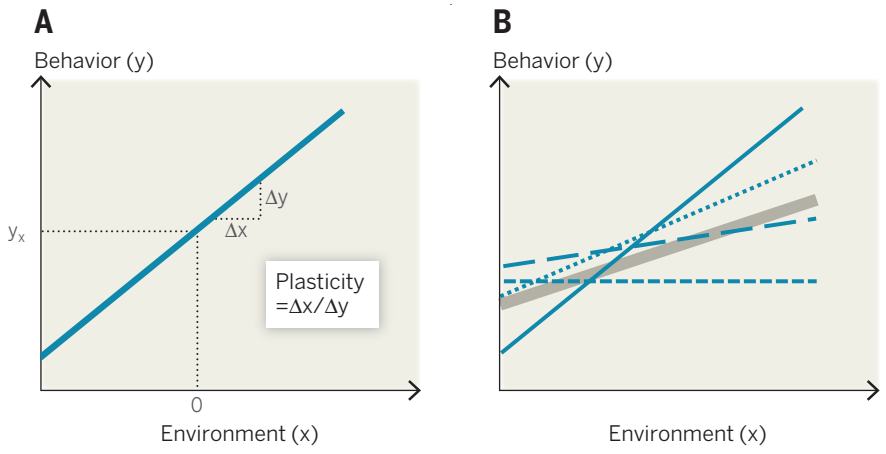


**Fig. 3. The BRN concept.** (**A**) Typically, BRN studies model an individual's behavior ($y$) as a straight-line function of environment ($x$) such that plasticity is determined as the slope of a reaction norm. (**B**) Although many studies of parenting have shown that population-average behavior changes with environment (gray line), few have quantified among-individual variation in plasticity (IxE) or tested for a genetic component to it (GxE). Such individual-level studies are required to understand the contribution of plasticity to adaptive parenting and its evolution.

Westneat *et al.* used a suite of different environmental variables to estimate population-level plasticity (that is, mean reaction norm slope across individuals) and quantify among-individual variation in reaction norm intercepts and slopes for provisioning [IxE (see Fig. 3B)]. The number of provisioning trips per hour made by a parent was significantly repeatable across days (brood age 2 to 14 days)—with differences among individuals accounting for ~11% of the observed variation—and did not differ between the sexes overall. IxE was present for the environmental variables of offspring age and partner visit rate, but not for brood size. There was a population-level response to brood size (foraging rates increased when there were more nestlings), but the lack of IxE meant that individuals all responded in a similar way to a change in brood size. In addition, males and females differed in their average plasticity of provisioning behavior: Females were less responsive than males to differences in brood size, but more responsive to changes in nestling age.

The above example clearly illustrates that parenting behaviors can be plastic with respect to multiple environmental variables, both social and nonsocial. However, responses to one variable will also depend on other variables. Figure 4 illustrates this for a hypothetical scenario in which mothers always forage for food to nourish offspring, but where fathers may or may not help [e.g., red-wing blackbirds (*Agelaius phoenicius*)]. From a mother's point of view, uniparental (maternal only) and biparental care represent two social environments, in each of which she needs to optimize foraging effort in relation to food abundance [i.e., a second, nonsocial environmental variable (Fig. 4)]. With no help from males, females will, on average, tend to decrease foraging effort as food abundance increases [solid gray line with slope $\beta_1 < 0$ (Fig. 4A)], but there is also some variation among individuals in their BRN elevations and slopes (that is, differences in plasticity). Under biparental care, the picture is different: On average, females forage less and have a weaker plastic response to food abundance [shown by $\mu_2 < \mu_1$ (where $\mu$ is the mean phenotype in the environment) and $|\beta_2| < |\beta_1|$ (Fig. 4B)]. This is because mothers and fathers now share the effort of finding food, as well as the savings that can be made when food is abundant.

However, it is also apparent that female BRNs are more variable under the biparental care scenario. We would expect this if females modify their behavior not only according to food abundance and the presence of a male partner, but also according to the level of foraging effort made by her partner. Variation in female BRNs will increase when mothers vary in their responses to a given male effort and/or when there is variation in effort among fathers partnered with different females. Of course, just as female behavior responds plastically to male effort, males typically alter their own behavior in response to female effort (*12*). Thus, how much care is provided, and by whom, will depend on reciprocal feedback between social partners (*13*). However, models of BRN evolution show that there is a cost to excessive plasticity in feedback between individuals (*21*). This is because unlimited feedback could lead to behavioral instability of the reaction norm, with individuals overreacting to behavioral change by their partners. Selection is therefore expected to favor reaction norms that allow behaviors to return to normal if there has been a temporary disturbance [for instance, when there has been an overreaction of one individual to another (*21*)].

## Integrating the social environment

More generally, the scenario depicted in Fig. 4 shows that variance in female behavior and its plasticity (for example, IxE of foraging effort with respect to food abundance) can depend on the social environment provided by the male phenotype. In an evolutionary context, social environments differ from nonsocial environments in one vital respect: they are able to evolve. This is because social environments are composed of the phenotypes (and, thus, genotypes) of interacting conspecifics, an idea that has led to the development of indirect genetic effect (IGE) theory (*22*, *23*). IGEs occur when characteristics (phenotype) of a focal individual (in this case, the parenting

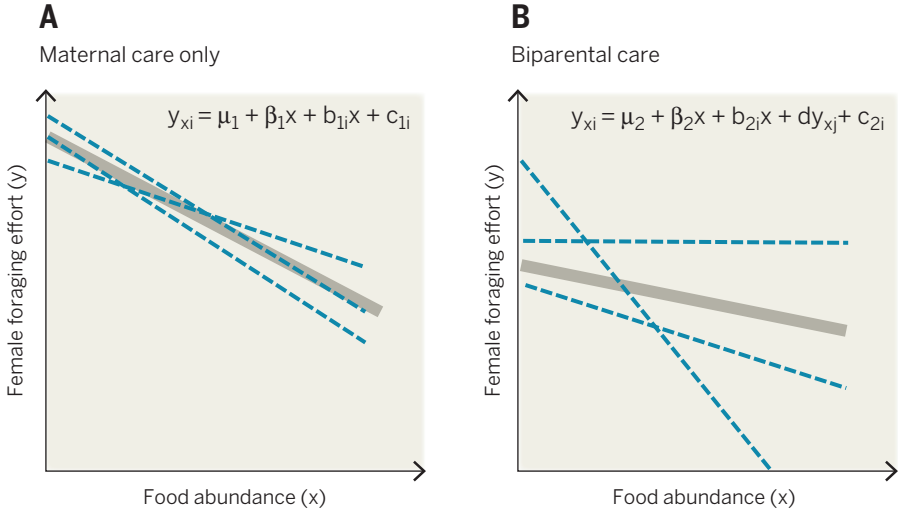


**Fig. 4. Parental plasticity across nonsocial and social environments.** Individual (blue dashed lines) and population-average (solid gray lines) behavioral reaction norms for female foraging effort ($y$) as a function of food abundance ($x$). (**A**) In the absence of a male partner, the behavior of a female $i$ at food abundance $x$ ($y_{ix}$) is specified by an elevation ($c_1$) and slope ($b_1$) expressed by convention as deviations from the population averages ($\mu_1$ and $\beta_1$, respectively). (**B**) With male partner $j$ present, female behavior will also depend on plastic response ($d_i$) to his foraging effort ($y_{jx}$). Except in the case that $d_i$ and $y_{jx}$ are both invariant across individuals, this leads to an expectation of more variable female BRNs under biparental care (see text for discussion).

behavior of the female) are causally influenced by genes being expressed in one or more interacting individuals (e.g., the parental effort provided by her partner). These are therefore distinct from the direct genetic effects (DGEs) of an individual's genes on its own phenotype. Thus, if there is genetic variation for female BRN elevations and slopes (i.e., plasticities), then during biparental care this will result from both DGEs (her own genetic makeup) and IGEs (arising from the genetic makeup of her partner).

The general importance of IGEs arising from social interactions has now been widely shown in laboratory and field studies (*23*–*27*), although field-based investigations of IGEs on parenting behaviors per se are limited. Nonetheless, in a study of wild common gulls (*Larus canus*), Brommer and Rattiste showed that variation in female lay date was subject to IGEs arising from their partners (*28*). In the same way that males and females can be a source of IGEs on each other, they will also be a source of IGEs on the offspring if parenting behavior is heritable. Maternal genetic effects on offspring development, morphology, and/or behavior have been widely demonstrated in captive animal populations (*29*) and a number of species in the wild, including red squirrels (*Tamiasciurus hudsonicus*) and soay sheep (*Ovis aries*) (*30*). Clearly, the scope for complexity is potentially enormous when individuals interact and respond plastically to each other's behavior. Exactly how IGEs will affect the evolutionary dynamics of the parenting BRN will depend on both the genetic covariance structure between DGEs and IGEs and the nature of selection acting, potentially antagonistically, through males and females (or parents and their offspring). Nonetheless, a key consequence of IGEs is that the evolution of parenting behaviors, and those phenotypes expressed by social partners to which they respond, will become coupled (that is, these behaviors will coevolve) (*31*, *32*). Thus, incorporating IGEs into the reaction norm framework outlined above [as, for example, in (*33*)] is a necessary step to model the coevolutionary dynamics of plasticity in parenting.

## Could coadaptation actually limit plasticity in parenting?

The presence of IGEs means that plasticity of parenting behaviors is expected to coevolve with traits expressed by partners (and their offspring) in their social environments. When selection favors particular combinations of parent and partner or parent and offspring behaviors, coadaptation will follow (*32*). Coadaptation occurs when the genetics underlying specific behaviors or other traits covaries between, for example, parents and offspring, and when this association is maintained over time via mechanisms that reinforce the associations and/or limit recombination between interrelated traits (*32*). As such, coadaptation is an evolutionary compromise in which conflicting fitness interests of parents and offspring impose limitations on the evolution of each other's behavior. The best evidence for such coadaptation of traits comes from cross-fostering studies of parent-offspring interactions, where offspring have higher fitness (are more likely to survive and/or reproduce) when matched with their genetic parents (usually the mother) than when mismatched with foster parents (*32*). Positive relationships between maternal feeding and offspring begging behaviors have been found for numerous species, including great tits (*P. major*) (*31*) and burying beetles (*N. vespilloides*) (*25*): Mothers that are good providers have offspring that beg most strongly. In contrast, negative correlations have been found for rhesus macaques (*Macacca mulatta*) (*34*) and burrower bugs (*Sehirus cinctus*) (*35*): Mothers that are the best providers have offspring that beg the least. In most species, males provide less care than females, and their reduced contact might limit the potential for coadaptation between fathers and offspring (*36*). In the only studies where this has been quantified, no coadaptation between fathers and their offspring was found [great tits (*P. major*) (*31*) and burying beetles (*N. vespilloides*) (*26*)]. Although collectively these studies reveal coadaptation in parent and offspring behaviors, they do not address the role of plasticity in the evolution of coadapted behaviors.

Coadaptation models that allow the slopes of the behavioral reaction norms to evolve suggest that the responsiveness of parents and offspring to each other leads to stability in the amount of parental care provided (*37*). This is because there are multiple parent-offspring behavior combinations that provide solutions to the same problem [obtaining food if you are an offspring and providing food if you are a parent (*37*)]. Although this means that individuals are highly responsive

**Box 1. Individual plasticity in parental care in burying beetles.**

*Nicrophorus vespilloides* burying beetles breed on the carcasses of small vertebrates (such as mice) that they process and bury underground as a source of food for their offspring (*40*). Parental care is complex and involves direct feeding of begging larvae and maintenance of the carcass to reduce competition from microbes (*25*, *26*, *36*, *40*). Both sexes care for their young, either as a pair or alone, but there is considerable variation in the amount of parental care provided by individuals (*36*, *40*). In the data presented below, individuals of both sexes reared offspring alone and in a pair in a repeated-measures, crossover-design experiment ($n$ = 40 individuals of each sex), with the amount of time spent providing parental care over a 30-min period as the response variable. (**A**) On average, females (red) provide more care than males (blue), regardless of which social environment they experience (error bars denote SEs on sex- and environment-specific means). Yet both sexes provide, on average, less time caring in a biparental context. Analyzed with a simple linear model, the main effects of sex ($P$ < 0.001) and social environment ($P$ < 0.004) are both significant. However, there is also a significant interaction between them, meaning that the average reaction norm slope differs between sexes ($P$ = 0.026).

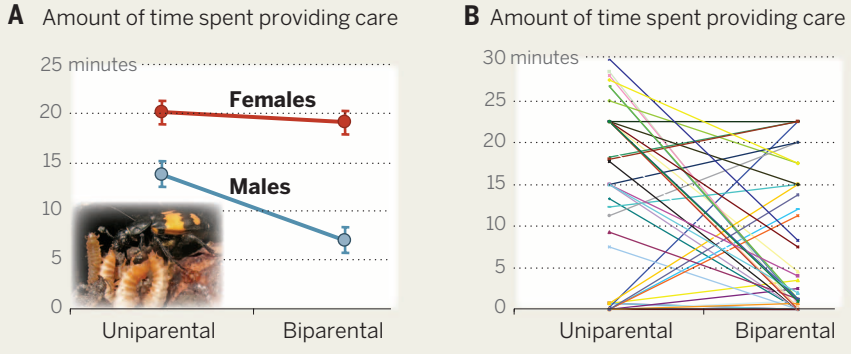


In fact, single-sex analysis shows that the mean reduction of female behavior associated with a switch between uniparental and biparental care is not significantly greater than zero. We might therefore conclude that, on average, males show plasticity but females do not. We know that the shift in mean male behavior must be due to plasticity, because the same individuals were observed in both social environments. However, we must also remember that population-level patterns only tell us what is happening on average. (**B**) Plotting individual reaction norms for the males reveals considerable among-individual variation around the average response. The correlation of care levels across environments for males is $r$ = 0.032 (95% confidence interval = −0.284, 0.348). The correlation coefficient is <1, which provides evidence of IxE (i.e., there is variation in reaction norms of individual males). The photograph in (A) shows wild female *N. vespilloides* feeding offspring [credit: Paul Hopwood].

to changes in the social environment, we hypothesize that coadaptation will actually limit the plasticity of parenting behaviors in response to nonsocial environments (for example, the threat of nest predation). This is because traits are genetically interdependent both within and between parents and offspring, meaning that behaviors are not free to evolve in the direction that always best serves the interests of the individuals involved.

Evolutionary interdependence of behaviors involved in social interactions stems from the presence of IGEs. Although IGEs can sometimes facilitate rapid evolutionary change (because the social environment can respond to behavioral change of individuals), they can also impose constraints on behavioral responses to other environments (*22*, *23*). If correlations between DGEs and IGEs on fitness are positive, more rapid evolutionary responses to selection are expected to occur; if correlations are negative, the opposite will be true. Empirical work on IGEs in parental care shows that DGEs are most often (strongly) negatively correlated with IGEs, regardless of whether the care is provided by mothers or fathers (*25*, *26*). This will limit the response of parenting behavior to selection on offspring and vice versa. As a result, IGEs and coadaptation traits involved in parenting are likely to be dynamic and responsive to changes in the social environment in which they have evolved, but this interdependence may limit adaptation to changes in nonsocial environments. An analogy can be drawn to organizations such as the United Nations (UN) responding to global crises, where the ability of the UN to respond effectively will be limited to some extent by compromises that have to be reached as a consequence of the often competing interests of member states: When behavior depends on others, the ability to respond to wider problems may be constrained.

## Suggestions for the future

Generating simple predictions about the contribution of plasticity to adaptive evolution of parenting behavior is difficult at this stage, primarily due to the lack of suitably analyzed data. However, studies of parenting to date, conducted primarily to test between sex or among-population differences, provide a robust foundation for the next step. For many species, we know both the key parenting behaviors that determine fitness and the environmental factors (abiotic and biotic) to which these behaviors should respond adaptively. By collecting repeated-measures data on individuals in many studies of parenting, we have learned that parents respond plastically to changes in their environment. We now need to adopt an individual-based analytical approach to analyzing these data (*2*). Only by doing so can we address the issue of among-individual variation in plastic responses to different environments, particularly social ones. In fact, many researchers will already have the necessary data to adopt the BRN approach to quantifying IxE that we outline (see Box 1 for an example). Additionally, investigating genetic variation for plasticity (i.e., GxE) currently requires breeding experiments [in the lab; for example, selection lines (*36*)] or building a pedigree [in wild populations (*30*)], although the growing feasibility of obtaining high-density single nucleotide polymorphisms means that pedigree-free quantitative genetic analyses (*38*) may soon dominate for nonmodel organisms. Regardless of methodology, the key point is that genetic studies must consider both direct and indirect genetic sources of variation in parenting behaviors. By integrating IGEs into the existing BRN framework, it will be possible to more realistically model the evolution of parenting behaviors.

The rewards for doing so are likely to be great, as such work will not only provide insights into the plasticity of parenting and the robustness of responses of parents and offspring to rapid changes in their environment, but may also provide insights into the evolution of between-individual characteristics (personality) and complex societies. If plasticity is costly (*3*, *4*), theoretical models demonstrate that this can favor the coexistence of plastic and nonplastic individuals within populations through frequency-dependent selection. This is because plastic individuals are good at responding to variation in their environment, which has the effect of reducing environmental variation experienced by others; nonplastic individuals can then exploit this environmental condition (*39*). This can lead to selection for between-individual differences in plasticity, which in turn, may have positive effects on population-level responses to environmental change because not all individuals will respond in the same way, maintaining variation in the population as a whole (*39*). Given the current rate of human-induced environmental change, we believe that it is important to address how plasticity, IGEs, and coadaptation interact to influence population responses to such perturbations. Consequently, to understand behavioral plasticity, we need to take a multidimensional view of both environmental and response variables. New theory and empirical tests of these questions and others we have highlighted are required if we are to understand variation in and the importance of plasticity in parenting and, more generally, the evolution of behavior.

### REFERENCES AND NOTES


1. T. Piersma, J. Drent, *Trends Ecol. Evol.* **18**, 228–233 (2003).
2. D. H. Nussey, A. J. Wilson, J. E. Brommer, *J. Evol. Biol.* **20**, 831–844 (2007).
3. N. J. Dingemanse, M. Wolf, *Anim. Behav.* **85**, 1031–1039 (2013).
4. S. A. Foster, *Anim. Behav.* **85**, 1061–1075 (2013).
5. T. J. DeWitt, S. M. Scheiner, in *Phenotypic Plasticity – Functional and Conceptual Approaches*, T. J. DeWitt, S. M. Scheiner, Eds. (Oxford Univ. Press, Oxford, 2004), pp. 1–9.
6. M. Pigliucci, *Trends Ecol. Evol.* **20**, 481–486 (2005).
7. I. Gomez-Mestre, R. Jovani, *Proc. Biol. Sci.* **280**, 20131869 (2013).
8. D. F. Westneat, M. I. Hatch, D. P. Wetzel, A. L. Ensminger, *Am. Nat.* **178**, 652–667 (2011).
9. J. T. Costa, *The Other Insect Societies* (Harvard Univ. Press, Cambridge, MA, 2006).
10. S. Balshine, in *The Evolution of Parental Care*, N. J. Royle, P. T. Smiseth, M. Kölliker, Eds. (Oxford Univ. Press, Oxford, 2012), pp. 62–80.
11. C. K. Ghalambor, S. I. Peluc, T. E. Martin, *Biol. Lett.* **9**, 20130154 (2013).
12. F. Harrison, Z. Barta, I. Cuthill, T. Székely, *J. Evol. Biol.* **22**, 1800–1812 (2009).
13. R. A. Johnstone *et al*., *Behav. Ecol.* **25**, 216–222 (2014).
14. R. M. Kilner, C. A. Hinde, in *The Evolution of Parental Care*, N. J. Royle, P. T. Smiseth, M. Kölliker, Eds. (Oxford Univ. Press, Oxford, 2012), pp. 119–132.
15. S. C. P. Renn, M. E. Schumer, *Anim. Behav.* **85**, 1012–1022 (2013).
16. D. H. Nussey, E. Postma, P. Gienapp, M. E. Visser, *Science* **310**, 304–306 (2005).
17. M. J. West-Eberhard, *Developmental Plasticity and Evolution* (Oxford Univ. Press, New York, 2003).
18. P. T. Smiseth, J. Wright, M. Kölliker, *Proc. Biol. Sci.* **275**, 1823–1830 (2008).
19. M. van de Pol, S. Verhulst, *Am. Nat.* **167**, 766–773 (2006).
20. J. G. A. Martin, D. H. Nussey, A. J. Wilson, D. Réale, *Methods Ecol. Evol.* **2**, 362–374 (2011).
21. R. Dobler, M. Kölliker, *Anim. Behav.* **77**, 1427–1434 (2009).
22. A. J. Moore, E. D. Brodie III, J. B. Wolf, *Evolution* **51**, 1352–1362 (1997).
23. J. B. Wolf, E. D. Brodie III, J. M. Cheverud, A. J. Moore, M. J. Wade, *Trends Ecol. Evol.* **13**, 64–69 (1998).
24. J. B. Wolf, *Proc. Natl. Acad. Sci. U.S.A.* **100**, 4655–4660 (2003).
25. J. E. Lock, P. T. Smiseth, A. J. Moore, *Am. Nat.* **164**, 13–24 (2004).
26. M. L. Head, L. K. Berry, N. J. Royle, A. J. Moore, *Evolution* **66**, 3570–3581 (2012).
27. A. J. Wilson, *Heredity* **112**, 70–78 (2014).
28. J. E. Brommer, K. Rattiste, *Evolution* **62**, 2326–2333 (2008).
29. A. J. Wilson, D. Réale, *Am. Nat.* **167**, E23–E38 (2006).
30. A. G. McAdam, D. Garant, A. J. Wilson, *Quantitative Genetics in the Wild*, A. Charmantier, D. Garant, L. E. B. Kruuk, Eds. (Oxford Univ. Press, Oxford, 2014).
31. M. Kölliker, M. W. G. Brinkhof, P. Heeb, P. S. Fitze, H. Richner, *Proc. Biol. Sci.* **267**, 2127–2132 (2000).
32. M. Kölliker, N. J. Royle, P. T. Smiseth, in *The Evolution of Parental Care*, N. J. Royle, P. T. Smiseth, M. Kölliker, Eds. (Oxford Univ. Press, Oxford, 2012), pp. 285–303.
33. A. J. Wilson *et al*., *PLOS Biol.* **4**, e216 (2006).
34. D. Maestripieri, *Behav. Ecol. Sociobiol.* **55**, 381–387 (2004).
35. A. F. Agrawal, E. D. Brodie III, J. Brown, *Science* **292**, 1710–1712 (2001).
36. M. L. Head, C. A. Hinde, A. J. Moore, N. J. Royle, *Ecol. Lett.* **17**, 803–810 (2014).
37. M. Kölliker, B. J. Ridenhour, S. Gaba, *PLOS ONE* **5**, e8606 (2010).
38. C. Bérénos, P. A. Ellis, J. G. Pilkington, J. M. Pemberton, *Mol. Ecol.* **23**, 3434–3451 (2014).
39. M. Wolf, G. S. van Doorn, F. J. Weissing, *Proc. Natl. Acad. Sci. U.S.A.* **105**, 15825–15830 (2008).
40. M. P. Scott, *Annu. Rev. Entomol.* **43**, 595–618 (1998).


### ACKNOWLEDGMENTS


We thank C. Hinde, M. Kölliker, H. Klug, A. Moore, and two anonymous reviewers for comments on a previous version of the manuscript. We also thank H. Fitzjohn for collecting the data presented in Box 1, which have been deposited in the Open Research Exeter (ORE) data repository and are freely available at http://hdl.handle.net/10871/15217. N.J.R. was funded by Natural Environment Research Council (NERC) grant NE/C002199/1, A.F.R. by NERC grant NE/K005766/1, and A.J.W. by a Biotechnology and Biological Sciences Research Council David Phillips Fellowship (BB/G022976/1).

10.1126/science.1253294

# RESEARCH

RAVE produces a map of a Diffuse Interstellar Band
*Kos* et al. *p. 791*

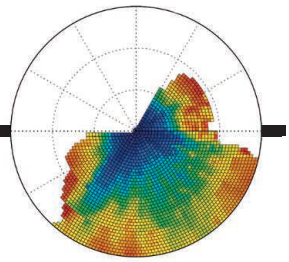

## IN *SCIENCE* JOURNALS

*Edited by* **Stella Hurtley**

A swarm of mini-robots on the move

ROBOTICS

### Large-scale robotic self-assembly

When individuals swarm, they must somehow communicate to direct collective motion. Swarms of robots need to deal with outliers, such as robots that move more slowly than the rest. Rubenstein *et al.* created a large swarm of programmed robots that can form collaborations using only local information. The robots could communicate only with nearby members, within about three times their diameter. They were able to assemble into complex preprogrammed shapes. If the robots' formation hit snags when they bumped into one another or because of an outlier, additional algorithms guided them to rectify their collective movements. — MSL

*Science*, this issue p. 795

PLACE CELLS

### Nerve cells displaying extra large spaces

Rats use brain cells called "place" cells to figure out where they are. Rich *et al.* used mazes or tracks many meters long—the size of rats' ranges in the wild— to investigate how rats represent a very large environment or extended experience in their brain. As novel environments became larger and larger, the rats' brains recruited new place cells. However, no matter how large the environment became, some cells always remained silent, perhaps as a reserve for other environments yet to be visited. — PRS

*Science*, this issue p. 814

INTERSTELLAR DUST

### Can you spot a speck of space dust?

NASA's Stardust spacecraft has been collecting cosmic dust: Aerogel tiles and aluminum foil sat for nearly 200 days in the interstellar dust stream before returning to Earth. Citizen scientists identified most of the 71 tracks where particles were caught in the aerogel, and scanning electron microscopy revealed 25 craterlike features where particles punched through the foil. By performing trajectory and composition analysis, Westphal *et al.* report that seven of the particles may have an interstellar origin. These dust particles have surprisingly diverse mineral content and structure as compared with models of interstellar dust based on previous astronomical observations. — MMM

*Science*, this issue p. 786

CANCER

### A potential target in a deadly brain cancer

A growth factor receptor called EGFR is often overactive in glioblastoma, a common and frequently lethal form of brain cancer. Kusne *et al.* found that the kinase aPKC was stimulated in glioblastoma cells not only by abnormally active EGFR but also in response to a cytokine called TNF-α released by immune cells that infiltrate the tumors. A drug that inhibited aPKC reduced tumor growth in a mouse model of glioblastoma, and glioblastoma patients with high aPKC levels had shorter survival times. Thus, two cancer-promoting pathways converge on aPKC, making it an attractive therapeutic target in glioblastoma. — WW

*Sci. Signal.* **7**, ra75 (2014).

PLANT SCIENCE

### Strangleweed shares too much information

Because RNA normally functions within an individual cell, we

Parasitic dodder plant strangles its host

Downloaded from www.sciencemag.org on August 15, 2014

CREDITS: (CLOCKWISE FROM TOP) KOS *ET AL.*; CURTIS CLARK/WIKIMEDIA COMMONS; MICHAEL RUBENSTEIN/HARVARD UNIVERSITY/WYSS INSTITUTE



Published by AAAS

generally think that we keep our RNAs to ourselves. Kim *et al.* now show that the parasitic dodder plant breaks that rule. When dodder attacks a host plant, it opens up a conduit through which messenger and perhaps other regulatory RNAs are exchanged between parasite and host. Because a single dodder plant can attack multiple hosts, such exchanges may underlie instances of genes transferring between species. — PJH

*Science*, this issue p. 808

CYSTIC FIBROSIS

## A breathtaking tale of sticky mucus

Patients with cystic fibrosis have difficulty breathing because their airways are clogged with thick mucus. Does this mucus accumulate because there is a defect in the way it is produced? Or does it accumulate because of other disease features, such as dehydration or airway wall remodeling? Distinguishing between these possibilities is important for future drug development. In a study of piglets with cystic fibrosis, Hoegger *et al*. identify mucus production as the primary defect (see the Perspective by Wine). The airway glands of the piglets synthesized strands of mucus normally, but the strands were never released and stayed tethered to the gland ducts. — PAK

*Science*, this issue p. 818; see also p. 730

CELL THERAPY

## A Swiss Army knife for treating sepsis

Sepsis is a complication of infection that kills ~7 million people a year, with no successful molecular therapy. But cells are more versatile than molecules: They make products and respond to their environments. Now, Fletcher *et al.* investigate whether cells are better equipped to battle this multifocal disease. One injection of anti-inflammatory cells derived from the lymph nodes dramatically increased survival in two mouse models of sepsis under conditions that mimic those in the clinic. These beneficial cells reduced the deadly "cytokine storm" associated with sepsis. — KL

*Sci. Transl. Med.* **6**, 249ra109 (2014).

RNA NANOSTRUCTURES

## The future of RNA origami writ large

Researchers have long fabricated intricate nanostructures from carefully linked DNA strands. Now they can use RNA made by gene expression, which avoids the costly strand synthesis and lengthy annealing steps necessary with DNA origami. Geary *et al.* used molecular modeling to extend the size of folded RNA origami structures (see the Perspective by Leontis and Westhof). The modeling revealed assembly patterns for linking single-stranded RNA into A-form helices. The authors created two-dimensional structures as large as 660 nucleotides on mica surfaces. — PDS

*Science*, this issue p. 799; see also p. 732

WATER ENGINEERING

## Sourcing corrosive sewer sulfides

Sewer systems are corroding at an alarming rate, costing governments billions of dollars to replace. Differences among water treatment systems make it difficult to track down the source of corrosive sulfide responsible for this damage. Pikaar *et al.* performed an extensive industry survey and sampling campaign across Australia (see the Perspective by Rauch and Kleidorfer). Aluminum sulfate added as a coagulant during drinking water treatment was the primary culprit in corroding sewer systems. Modifying this common treatment strategy to include sulfate-free coagulants could dramatically reduce sewer corrosion across the globe. — NW

*Science*, this issue p. 812; see also p. 734

# IN OTHER JOURNALS

*Edited by* **Kristen Mueller** *and* **Jesse Smith**

UNFOLDED PROTEINS

## Stitching mRNA back together again

Cells get rid of toxic, inappropriately folded proteins in a process called the unfolded protein response (UPR). The UPR occurs in the cell's endoplasmic reticulum, which folds and sorts proteins. It requires an unconventional type of RNA splicing: the removal of small pieces of genetic material called introns from messenger RNA (mRNA). But biologists weren't sure how the spliced mRNA got put back together. Lu *et al*. now report that the enzyme RtcB patches together the two halves of a spliced mRNA that codes for XBP1, an important regulator of the UPR. In the endoplasmic reticulum, RtcB bound another enzyme, IRE$\alpha$, which splices the intron out of the XBP1 mRNA. — GR

*Mol. Cell* **55**, 10.1016/j.molcel.2014.06.032 (2014).

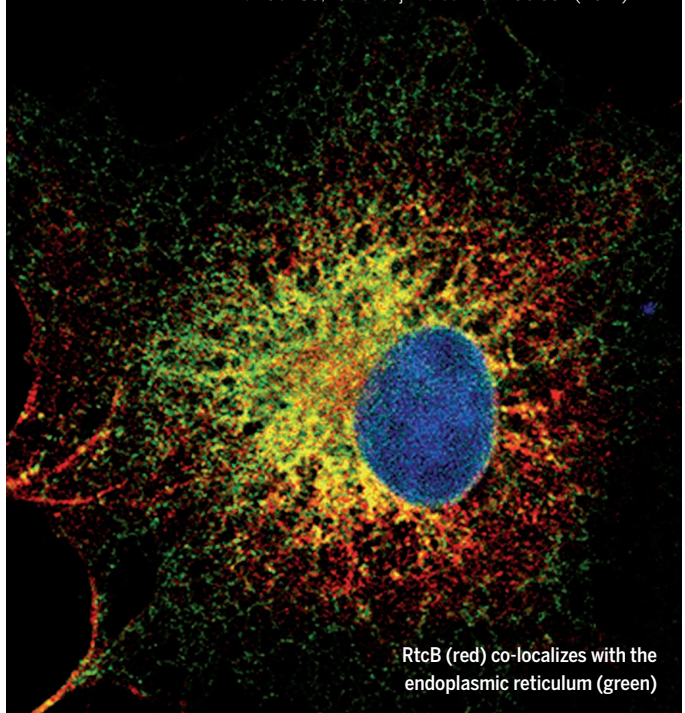

RtcB (red) co-localizes with the endoplasmic reticulum (green)

AGING

## A sweet decline for the aging fly brain

Our livers and muscles store glucose as glycogen, a branched polysaccharide. Glycogen is a major energy reserve, but it may play a more sinister role in the aging brain. Along with other components, glycogen forms aggregates in the brains of aging mice, humans, and flies that correlate with a decline in neuron function. To better understand this, Sinadinos *et al*. experimented with fruit flies. They used RNA interference to inhibit the flies' production of glycogen synthase, the enzyme that makes glycogen from glucose. Then the researchers measured how fast the flies could climb. As the flies aged, their neurons functioned better than those of controls. Treated male flies—but not females—lived longer. — LBR

*Aging Cell* 10.1111/acel.12254 (2014).

PHOTO: LU ET AL., *MOLECULAR CELL* (31 JULY 2014) © 2014 ELSEVIER INC.



*Published by AAAS*

Dalian, Liaoning Province, China

COASTAL ECOSYSTEMS

## The cost of economic growth

Anthropomorphic changes threaten the stability of coastal ecosystems, but whether economic growth contributes to such degradation is unknown. To find out, He *et al*. assessed the trends in coastal population, economy, and 15 different human impacts, including salt production, fishing, and marine freight transport, on 30,000 km of Chinese coastline both before and after economic reforms began in China in 1978. They found that all 15 human impacts increased after 1978, even though population growth remained constant, suggesting that economic growth contributed to coastal ecosystem decline. The authors highlight the need for a national policy of environmental management to protect the coupled human-ocean ecosystem. — AMS

*Sci. Rep.* **4**, 5995 (2014).

OPTICAL COMMUNICATION

## Steering an optical signal without wires

All wireless communications —radio, cell phones, wi-fi, or anything else—need reliable links between transmitters and receivers. In general, higher-frequency bands can convey more information than lower-frequency ones. Using a patterned array of tiny metallic nanoantennas, Dregely *et al.* show that they can steer an optical beam wirelessly from a transmitter to any one of a number of receivers. Because light has such high frequencies, these kinds of directed wireless optical channels should be able to transmit even greater amounts of information than devices using more traditional, longer-wavelength approaches. — ISO

*Nat. Commun.* 10.1038/ncomms5354 (2014).

CHEMISTRY

## Coatings keep gunk off nanoparticles

Nanoparticles have many potential therapeutic applications, such as delivering drugs. In untreated biological fluids such as plasma or serum, however, protein layers can cover the particles' surfaces, interfering with their intended function. Moyano *et al.* show that gold nanoparticles coated with zwitterionic ligands — neutral molecules with both positively and negatively charged regions — prevent protein coronas from forming around the particles. As a consequence, the nanoparticles can interact with cells as intended. Furthermore, the hydrophobicity of the nanoparticles can be tuned, which affects the cellular uptake of the particles. — MSL

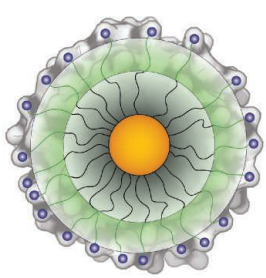

**A corona-free nanoparticle**

*ACS Nano* 10.1021/nn5006478 (2014).

VIRAL COMPETITION

## How infection rate determines virus spread

When a virus attacks a plant, it can damage cells locally or it can spread to the entire plant through the vasculature. Viral spread increases the odds that the virus could jump to other plants. To better understand this process, Rodrigo *et al*. mathematically modeled the timing and features that contribute to viral spead. They also watched viruses infect plants in experiments. A virus was sure to spread systemically when it infected many sites on the plant, and the most successful viruses were the ones that replicated the fastest, not the ones that spread quickly from cell to cell. But with a more moderate number of infection sites, rapid jumping between cells determined success. — PJH

*J. R. Soc. Interface* **11**, 20140555 (2014).

HYDROLOGY

## Looking beneath the drying surface

Groundwater is being depleted in the Colorado Basin region even faster than the rapid drawdown of Lakes Powell and Mead. Castle *et al.* determined groundwater depletion in the American Southwest by using data from the GRACE satellites, which measure minute variations in Earth's gravity field: in this case, ones associated with water movement below the surface. Looking at 9 years of results beginning at the end of 2004, 4 years after the current drought there began, they find that groundwater use makes up a much larger fraction of basin water use than previously recognized. Its continued depletion, they conclude, may pose a serious threat to the region's ability to meet future water needs. — HJS

*Geophys. Res. Lett.* 10.1002/2014GL061055 (2014).

OCEAN CHEMISTRY

## Mercury levels in surface ocean tripled

Human activities such as coal burning have tripled mercury in the surface ocean, posing a threat to human health, a study finds. Mercury emitted to the atmosphere rains out to the oceans, where it is converted to the neurotoxin methylmercury that bioaccumulates in fish. Lamborg *et al.* collected 8 years of water samples from four oceans and used databases of human-generated $CO_2$ from coal burning to scale up to worldwide pollution. The ocean contains 60,000 to 80,000 tons of pollution mercury, they found, two-thirds in water shallower than 1000 meters. In the top 100 meters, mercury has tripled compared to preindustrial times. — JY

*Nature*, 10.1038/nature13563(2014).

CREDITS: (TOP TO BOTTOM) © HENRY WESTHEIM PHOTOGRAPH /ALAMY; D. F. MOYANO *ET AL. ACS NANO* **8**, 7 ((27 JUNE 2014) © 2014 AMERICAN CHEMICAL SOCIETY



Published by AAAS

## ALSO IN *SCIENCE* JOURNALS

*Edited by* **Stella Hurtley**

IN UTERO EFFECTS

### The nutritional sins of the mother...

Prenatal exposures of a mother can affect the health of her offspring, but how? Radford *et al.* found that the male progeny of undernourished pregnant mice had altered DNA chemistry in their sperm. In addition, the offspring displayed compromised metabolic health. The specific affected genes not only lost DNA methylation but also lacked the normal sperm DNA packaging factors (protamines) and instead were enriched in nucleosomes. Thus, when subjected to a suboptimal prenatal environment, offspring feel the effects of the maternal assault. — BAP

*Science*, this issue p. 785

INTERSTELLAR DUST

### Clues to a mystery with RAVE results

An unknown interloper systematically picks off light from galactic sources, snatching at specific wavelengths ranging from the ultraviolet to the infrared. The cause of what astronomers term diffuse interstellar bands (DIBs) still evades identification. Kos *et al.* combined nearly 500,000 stellar spectra from the RAVE survey to make a telling map that may clue us in further. This pseudo–three-dimensional map shows the distribution of the carrier that absorbs light at 862 nm, and it closely follows a separate map of interstellar dust, but with a significantly larger scale height in the Galactic plane. Though this is only one DIB of many, this analysis sets a path for the future study of others. — MMM

*Science*, this issue p. 791

PHOTOSYNTHESIS

### Setting the stage for release of oxygen

Plants transform water into the oxygen we breathe using a protein-bound cluster of four manganese (Mn) ions and a calcium ion. Cox *et al.* now establish the precise electronic structure in that cluster immediately before formation of the O-O bond (see the Perspective by Britt and Oyala). Using the technique of electron paramagnetic resonance spectroscopy, they confirm a hypothesis that all four Mn ions are octahedrally coordinated and in the 4+ oxidation state. Such clues to the efficiency of the photosynthetic process, so essential to life on Earth, may also facilitate the development of artificial water-splitting catalysts. — JSY

*Science*, this issue p. 804; see also p. 736

CELL REPROGRAMMING

### Factor in oocyte assists reprogramming

Unfertilized eggs contain components that can dedifferentiate other cells that have gone down the path toward a specific cell fate. Gonzalez-Muñoz *et al.* show that the protein-folding factor ASF1A facilitates this reprogramming event and it acts at a particular phase of germ cell division termed metaphase II. ASF1A helps turn differentiated cells such as human adult dermal fibroblasts into undifferentiated pluripotent stem cells. — BAP

*Science*, this issue p. 826

TRANSDIFFERENTIATION

### Epigenetics direct transdifferentiation

To make an entire animal, many and varied cell types form and interact. Some of these differentiated cells take a U-turn and can de-differentiate or transdifferentiate to another cell fate. Although relatively rare in nature, Zuryn *et al.* followed such a program in the tiny roundworm *Caenorhabditis elegans,* where a rectal cell–to–motor neuron conversion is seen. Transcription factors with conserved roles in cell plasticity and terminal fate selection partner up with specific histone-modifying enzymes in discrete steps to specify separate sequential phases of cell identity. — BAP

*Science*, this issue p. 826

SYNTHETIC BIOLOGY

### Toward an "artificial cell" on a chip

Cell-free systems that reconstitute biochemical pathways have been critical for unraveling the inner workings of the cell. Karzbrun *et al.* created a highly miniaturized cell-free system on a silicon chip. A series of tiny linked compartments were fabricated on the chip, in which DNA-driven reactions occurred, with materials flowing into and diffusing between the compartments. The system recreated oscillating protein expression patterns and protein gradients, and provides a stepping stone to creating "artificial cells" on a chip. — GR

*Science*, this issue p. 829

PHOTO: CREDIT GOES HERE AS SHOWN; CREDIT GOES HERE AS SHOWN



Published by AAAS

RESEARCH ARTICLE SUMMARY

IN UTERO EFFECTS

# In utero undernourishment perturbs the adult sperm methylome and intergenerational metabolism

**Elizabeth J. Radford, Mitsuteru Ito, Hui Shi, Jennifer A. Corish, Kazuki Yamazawa, Elvira Isganaitis, Stefanie Seisenberger, Timothy A. Hore, Wolf Reik, Serap Erkek, Antoine H. F. M. Peters, Mary-Elizabeth Patti,* Anne C. Ferguson-Smith***

**INTRODUCTION:** The rapid global rise in metabolic disease suggests that nongenetic environmental factors contribute to disease risk. Early life represents a window of phenotypic plasticity important for adult metabolic health and that of future generations. Epigenetic inheritance has been implicated in the paternal transmission of environmentally induced phenotypes, but the mechanisms responsible remain unknown.

**RATIONALE:** We investigated the role of DNA methylation in epigenetic inheritance in an established murine model of intergenerational developmental programming. $F_1$ offspring of undernourished dams (UN) have low birth weight and multiple metabolic defects. Metabolic phenotypic inheritance to the $F_2$ generation is observed through the paternal line, even though the $F_1$ mice did not experience postnatal environmental perturbation. The timing of nutritional restriction coincides with methylation reacquisition in $F_1$ male primordial germ cells (PGCs). Therefore, we assessed $F_1$ sperm whole-genome methylation using immunoprecipitation of methylated DNA, combined with high-throughput sequencing, followed by independent validation. We characterized the regions susceptible to methylation change and investigated the legacy of such methylation change in the phenotypic development of the next generation.

**RESULTS:** In UN mice, 111 regions are hypomethylated relative to control sperm, and these changes are validated by bisulfite pyrosequencing. Methylation differences span multiple CpGs, with robust absolute changes of 10 to 30% (relative reduction ~50%). The absolute methylation level is consistent with differentially methylated regions (DMRs) being "low-methylated regions," known to be enriched in regulatory elements. Indeed, luciferase assays suggest a role for these DMRs in transcriptional regulation. Hypomethylated DMRs are significantly depleted from coding and repetitive regions and enriched in intergenic regions and CpG islands. They are also enriched in nucleosome-retaining regions, which suggests that, at some loci, paternal germline hypomethylation induced by in utero undernutrition is transmitted in a chromatin context. DMRs are late to regain methylation in normal male PGCs. This may render them particularly susceptible to environmental perturbations that delay or impair remethylation in late gestation.

Except for imprinted loci, gene-associated male germline methylation has generally been thought to be largely erased in the zygote, although recent studies suggest that resistance to reprogramming is more widespread. Indeed, 43% of hypomethylated DMRs persist and thus have the potential to affect development of the next generation. We show that differential methylation is lost in late-gestation $F_2$ tissues, but considerable tissue-specific differences in expression of metabolic genes neighboring DMRs are present. Thus, it is unlikely that these expression changes are directly mediated by altered methylation; rather, the cumulative effects of dysregulated epigenetic patterns earlier in development may yield sustained alterations in chromatin architecture, transcriptional regulatory networks, differentiation, or tissue structure.

ON OUR WEBSITE

Read the full article at http://dx.doi.org/10.1126/science.1255903

**CONCLUSION:** Prenatal undernutrition can compromise male germline epigenetic reprogramming and thus permanently alter DNA methylation in the sperm of adult offspring at regions resistant to zygotic reprogramming. However, persistence of altered DNA methylation into late-gestation somatic tissues of the subsequent generation is not observed. Nonetheless, alterations in gamete methylation may serve as a legacy of earlier developmental exposures and may contribute to the intergenerational transmission of environmentally induced disease. ■

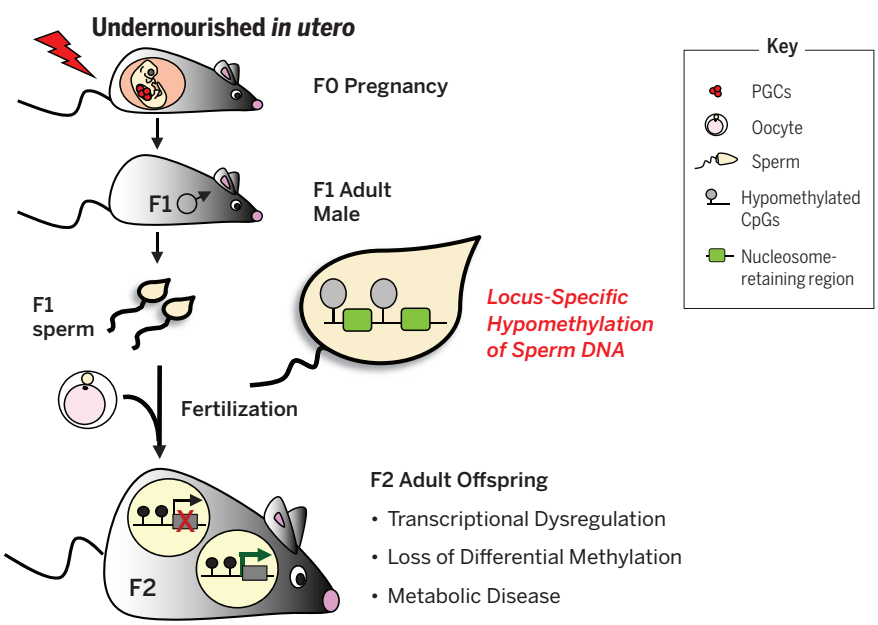


**In utero undernourishment alters the adult germ cell methylome.** Undernourishment during PGC reprogramming results in hypomethylation of discrete loci in adult sperm. These regions are enriched in nucleosomes and are low-methylated regions. Although partially resistant to blastocyst reprogramming, differential methylation does not persist in the next generation. However, dysregulated expression of genes neighboring DMRs is observed in $F_2$ offspring.

## RELATED ARTICLES

M. Susiarjo, M. S. Bartolomei, You are what you eat, but what about your DNA? *Science* **345**, 733–734 (2014).

The list of author affiliations is available in the full article online.
*Corresponding author. E-mail: afsmith@mole.bio.cam.ac.uk (A.C.F.-S.); mary.elizabeth.patti@joslin.harvard.edu (M.-E.P.)
Cite this article as E. J. Radford *et al.*, *Science* **345**, 1255903 (2014). DOI: 10.1126/science.1255903



Published by AAAS

RESEARCH ARTICLE

IN UTERO EFFECTS

# In utero undernourishment perturbs the adult sperm methylome and intergenerational metabolism

Elizabeth J. Radford,[1]* Mitsuteru Ito,[1]† Hui Shi,[1]† Jennifer A. Corish,[1] Kazuki Yamazawa,[1]§ Elvira Isganaitis,[2]§ Stefanie Seisenberger,[3] Timothy A. Hore,[3] Wolf Reik,[3] Serap Erkek,[4,5,6] Antoine H. F. M. Peters,[4,5] Mary-Elizabeth Patti,[2]‖ Anne C. Ferguson-Smith[1]‡‖

**Adverse prenatal environments can promote metabolic disease in offspring and subsequent generations. Animal models and epidemiological data implicate epigenetic inheritance, but the mechanisms remain unknown. In an intergenerational developmental programming model affecting $F_2$ mouse metabolism, we demonstrate that the in utero nutritional environment of $F_1$ embryos alters the germline DNA methylome of $F_1$ adult males in a locus-specific manner. Differentially methylated regions are hypomethylated and enriched in nucleosome-retaining regions. A substantial fraction is resistant to early embryo methylation reprogramming, which may have an impact on $F_2$ development. Differential methylation is not maintained in $F_2$ tissues, yet locus-specific expression is perturbed. Thus, in utero nutritional exposures during critical windows of germ cell development can impact the male germline methylome, associated with metabolic disease in offspring.**

The rapid global rise in the incidence of diabetes, obesity, and cardiovascular disease suggests that nongenetic environmental factors are major contributors to disease risk. Epidemiological data and animal models have demonstrated that early life represents a window of phenotypic plasticity critically important for later adult metabolic health (*1*). The impact of the early-life environment has been observed to extend over multiple generations in both human populations and animal models (*2*–*8*). There are at least two potential mechanisms mediating such non-Mendelian phenotypic inheritance: alterations in the parental metabolic milieu that induce fetal developmental exposures in the second generation and epigenetic inheritance. The latter is strongly implicated when paternal transmission of environmentally induced phenotypes is observed because rodent males, present solely at breeding, contribute to the future generation only through the sperm. Although a role for histone modifications and/or RNA has been proposed (*4*), the epigenetic mechanism(s) responsible for intergenerational inheritance of environmentally induced phenotypes remains unknown.

Paternal transgenerational epigenetic inheritance of altered DNA methylation has been demonstrated previously: for example, in rodents exposed to the endocrine disruptor vinclozolin (*9*) and in mice with variable methylation at the *Agouti viable yellow*, $A^{vy}$, and *Axin-Fused*, $Axin^{Fu}$, alleles formed by insertion of IAPs (intracisternal A particles) into or near endogenous genes (*10*). In addition to repeat-mediated cis-acting effects, other endogenous loci that have an inherent

[1]Department of Physiology, Development and Neuroscience, University of Cambridge, Downing Street, Cambridge CB2 3EG, UK. [2]Research Division, Joslin Diabetes Center and Harvard Medical School, 1 Joslin Place, Boston, MA 02215, USA. [3]The Babraham Institute, Babraham, Cambridge, and Wellcome Trust Sanger Institute, Hinxton, Cambridge, UK. [4]Friedrich Miescher Institute for Biomedical Research, Basel, Switzerland. [5]Faculty of Sciences, University of Basel, Basel, Switzerland. [6]Swiss Institute of Bioinformatics, Basel, Switzerland.
*Present address: Cambridge University Hospitals, NHS Foundation Trust, Cambridge CB2 0QQ, UK. †These authors contributed equally to this work. ‡Present address: Department of Genetics, University of Cambridge, Downing Street, Cambridge CB2 3EH, UK. §These authors contributed equally to this work.
‖Corresponding author. E-mail: afsmith@mole.bio.cam.ac.uk (A.C.F.-S.); mary.elizabeth.patti@joslin.harvard.edu (M.-E.P.)

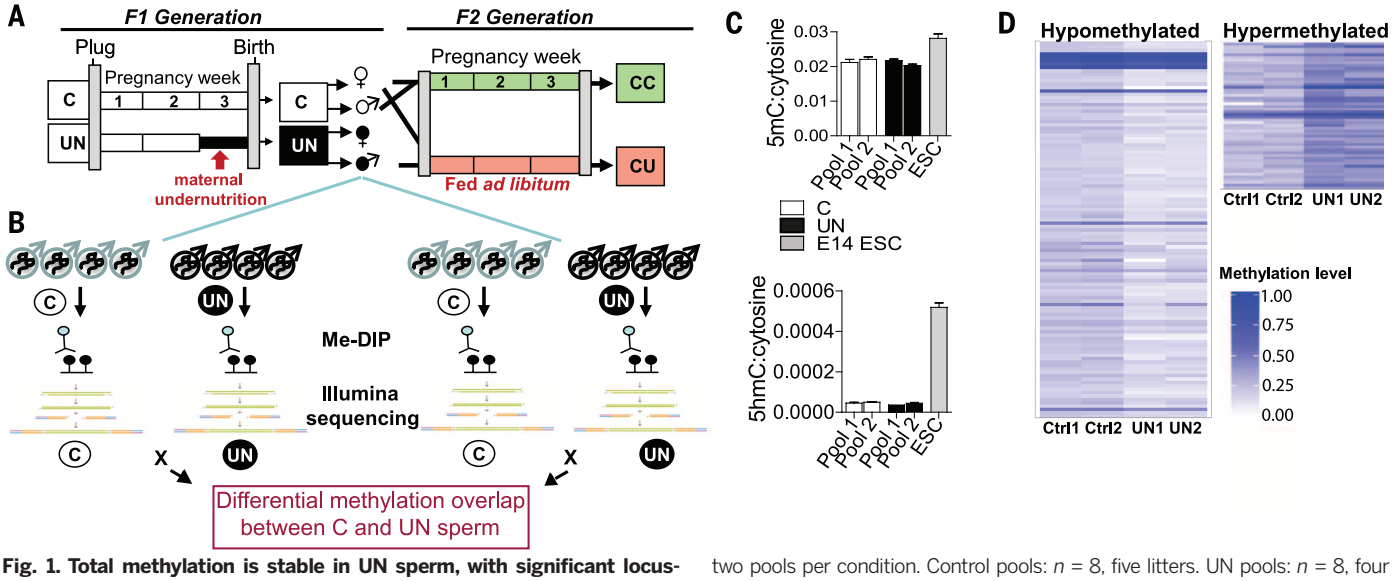


**Fig. 1. Total methylation is stable in UN sperm, with significant locus-specific changes.** (**A**) Experimental design. $F_1$ generation: Dams were randomized on pregnancy day 12.5 to control (C) or undernutrition (UN) groups, and UN food intake was restricted to 50%. Postnatal litters were equalized to eight pups, and animals were fed ad libitum. $F_2$ generation: Control $F_1$ females mated at age 2 months with nonsibling control or UN males and fed ad libitum to produce: CC, both parents controls; CU, control dam, UN sire. (**B**) Independent sperm DNA samples were quantified and pooled in equimolar ratios to generate two pools per condition. Control pools: $n = 8$, five litters. UN pools: $n = 8$, four litters. After MeDIP-seq, two independent C versus UN comparisons identified DMRs where methylation fold change >1.5× and binomial $P < 0.0001$ in both independent biological replicates. (**C**) Mass spectrometry quantification of control and UN sperm 5-methyl-cytosine (above) and 5-hydroxymethyl-cytosine (below). E14 embryonic stem cells (ESCs) are shown for comparison. (**D**) Heat map of 111 hypomethylated DMRs (left) and 55 hypermethylated DMRs (right). Hypermethylated DMRs did not validate.

epigenetic vulnerability to environmental conditions may contribute to intergenerational phenotypes and play an important role in the developmental origins of health and disease. Furthermore, recent studies have suggested that resistance to zygotic DNA methylation reprogramming extends beyond imprinted domains (*11*–*13*), which raises the possibility that gametic methylation may play a larger role than previously recognized in early development. A key unanswered question is whether an altered in utero environment or nutritional insult might affect the DNA methylation profile of adult germ cells.

Our aim was to investigate the role of DNA methylation in epigenetic inheritance in an established in utero murine model of intergenerational developmental programming (*3*). To produce the most robust phenotype, the maximum caloric restriction that does not cause significant fetal loss was chosen (Fig. 1A). This regime is largely incompatible with successful pregnancy in inbred mouse strains. Consequently, we used the outbred ICR strain, which also allowed us to better model the human population. In this model, $F_1$ offspring of undernourished dams have low birth weight as well as early-life adiposity, reduced muscle stem cell number and function, impaired pancreatic function, and progressive glucose intolerance (*14*–*16*). Inheritance of significantly reduced birth weight and glucose intolerance to the $F_2$ generation is observed through the paternal line in the absence of any further environmental perturbation (fig. S1, D to H) (*3*). The period of experimentally induced nutritional restriction in this model (day 12.5 to 18.5 of pregnancy) coincides with the reacquisition of methylation in male primordial germ cells as they are epigenetically reprogrammed (*17*). The dynamics of such methylation changes have been best studied at imprinting control regions (ICRs). However, we have already excluded a substantial perturbation of methylation at ICRs in this model (*18*). Thus, we now assess the whole-genome distribution of methylation in $F_1$ sperm, using immunoprecipitation of methylated DNA combined with high-throughput sequencing (MeDIP-seq) (*19*–*21*), followed by independent validation by bisulfite sequencing.

## Experimental design and metabolic phenotype

Mature sperm was isolated from $F_1$ male mice fed standard chow, ad libitum, at 3 months of age, before the onset of glucose intolerance or

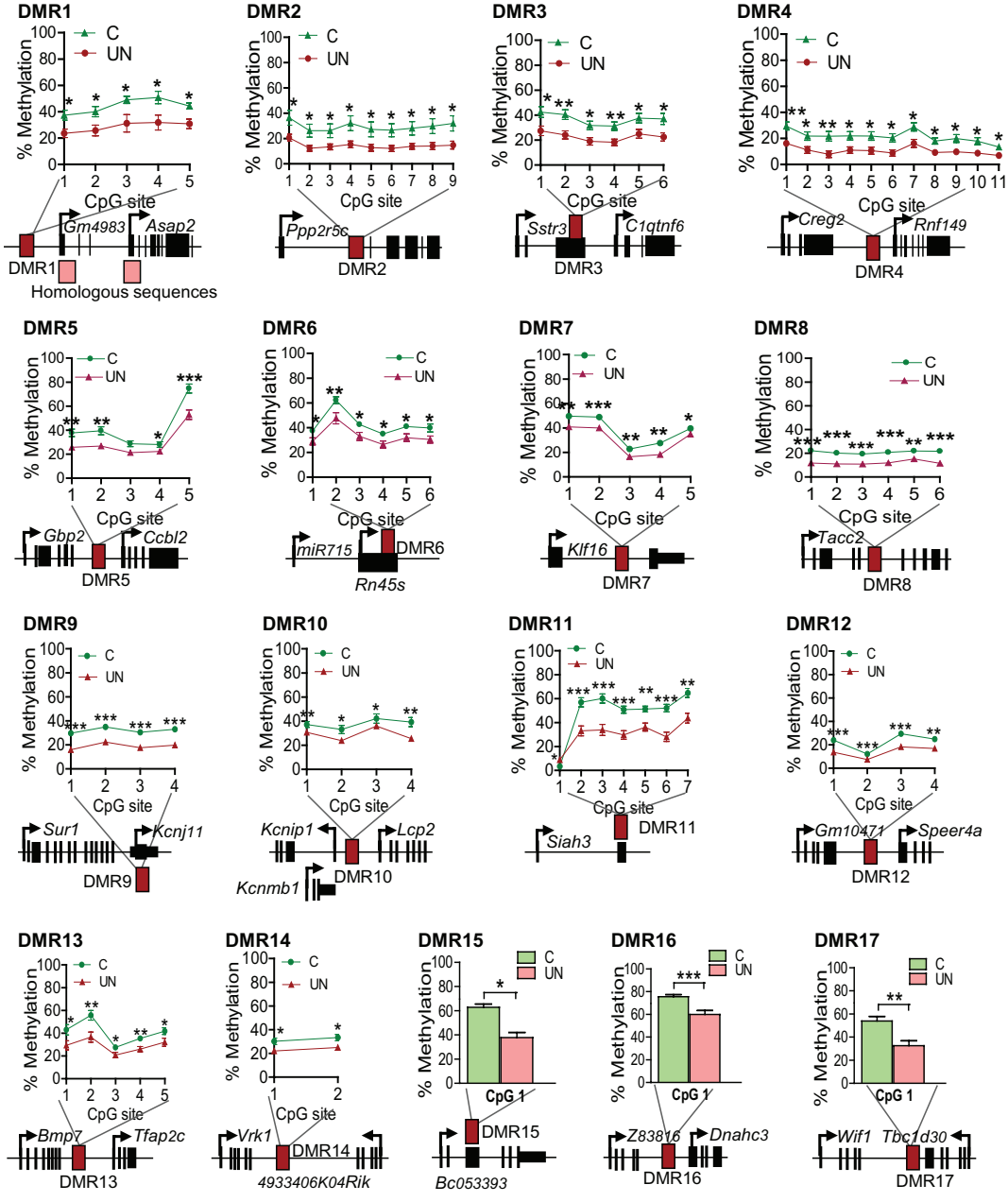


**Fig. 2. Bisulfite mutagenesis validation of hypomethylated DMRs in an expanded panel of $F_1$ males' sperm.** Seventeen genomic regions validated (Table 1). Data plotted: means ± SEM. C: $n$ = 12, five litters; UN: $n$ = 11, four litters. *$P$ < 0.05, **$P$ < 0.01, ***$P$ < 0.001; unpaired two-tailed $t$ test.

any discernible metabolic phenotypes (*14*). These $F_1$ males, previously exposed to experimental undernutrition in utero (UN), were smaller at birth (UN 1.34 ± 0.025 g, controls 1.65 ± 0.028 g, $P < 0.0001$) and at 3 months of age (UN 41.4 ± 0.82 g, controls 44.2 ± 0.94 g, $P = 0.04$) (fig. S1, B and C). Blood glucose and white adipose tissue mass at the time of sperm collection were not different between UN and control mice (fig. S1C). We bred $F_1$ control and UN males with control females before sperm isolation; offspring of these pregnancies were designated as CC ($F_2$ offspring of control males) and CU ($F_2$ offspring of UN males) (Fig. 1A). The $F_2$ offspring of $F_1$ sperm donors were harvested at embryonic day 16.5 (E16.5). A contemporaneous adult cohort of $F_2$ CU mice demonstrated, at 8 months of age, metabolic phenotypes similar to those previously observed (*3*), including reduced muscle mass and increased adiposity, with no difference in overall body or brain weight (fig. S1D). Furthermore, this CU cohort also showed glucose intolerance, particularly in the first-phase response to a glucose challenge (fig. S1E), as was previously observed. Pyruvate tolerance tests suggest that increased gluconeogenesis may contribute to this glucose intolerance (fig. S1F).

**Table 1. Validation of hypomethylated DMRs by bisulfite pyrosequencing.** Absolute methylation level calculated by bisulfite mutagenesis combined with pyrosequencing in C and UN $F_1$ sperm ($n \geq 11$, ≥4 litters), $F_2$ E16.5 brain and liver ($n \geq 12$, ≥3 litters) at hypomethylated DMRs. DMRs at nonrepetitive, distinct loci are indicated by an asterisk (*). Blastocyst methylation level was extracted from (*12*) and (*26*).

| DMR coordinates | Sperm methylation (%) | Blastocyst methylation (%) | $F_2$ E16.5 methylation (%) | |
|---|---|---|---|---|
| | | | Liver | Brain |
| **DMR1:** | Ctrl = 50 | 4 (12) | CC = 13 | CC = 10 |
| MMU12:19181482-19182200 | UN = 24 | 8 (26) | CU = 14 | CU = 10 |
| | $P < 0.0001$ | | | |
| **DMR2:** | Ctrl = 29 | 0 (12) | CC = 85 | CC = 82 |
| MMU12:111666100-111666400 | UN = 14 | 7 (26) | CU = 88 | CU = 83 |
| | $P < 0.0001$ | | | |
| **DMR3*:** | Ctrl = 37 | 0 (12) | CC = 81 | CC = 76 |
| MMU15:78370350-78370800 | UN = 23 | | CU = 81 | CU = 73 |
| | $P < 0.0001$ | | | |
| **DMR4*:** | Ctrl = 20 | 5 (12) | CC = 88 | CC = 88 |
| MMU1:39654450-39655100 | UN = 12 | | CU = 88 | CU = 87 |
| | $P < 0.0001$ | | | |
| **DMR5:** | Ctrl = 41 | 13 (12) | CC = 64 | CC = 62 |
| MMU3:142351001-142351500 | UN = 29 | 25 (26) | CU = 61 | CU = 56 |
| | $P = 0.0004$ | | | |
| **DMR6*:** | Ctrl = 43 | 7 (26) | CC = 30 | CC = 34 |
| MMU17:39984601-39985700 | UN = 33 | 26 (12) | CU = 26 | CU = 33 |
| | $P < 0.0001$ | | | |
| **DMR7*:** | Ctrl = 38 | 22 (26) | CC = 8 | CC = 8 |
| MMU10:80033801-80034300 | UN = 30 | 28 (12) | CU = 8 | CU = 9 |
| | $P = 0.001$ | | | |
| **DMR8*:** | Ctrl = 21 | 22 (26) | CC = 18 | CC = 20 |
| MMU7:137835001-137836500 | UN = 12 | 25 (12) | CU = 19 | CU = 20 |
| | $P < 0.0001$ | | | |
| **DMR9*:** | Ctrl = 18 | 0 (26) | CC = 78 | CC = 95 |
| MMU7:53354201-53354900 | UN = 11 | 9 (12) | CU = 80 | CU = 94 |
| | $P = 0.0003$ | | | |
| **DMR10:** | Ctrl = 39 | 16 (26) | CC = 38 | CC = 28 |
| MMU11:33922001-33922500 | UN = 29 | | CU = 38 | CU = 32 |
| | $P < 0.0001$ | | | |
| **DMR11*:** | Ctrl = 48 | 0 (26) | CC = 64 | CC = 78 |
| MMU14:75925601-75926100 | UN = 30 | 3 (26) | CU = 66 | CU = 83 |
| | $P < 0.0001$ | | | |
| **DMR12*:** | Ctrl = 23 | 24 (12, 26) | CC = 80 | CC = 85 |
| MMU5:26397201-26397700 | UN = 14 | | CU = 79 | CU = 85 |
| | $P < 0.0001$ | | | |
| **DMR13*:** | Ctrl = 41 | 6 (26) | CC = 74 | CC = 73 |
| MMU2:172688001-172688500 | UN = 29 | | CU = 72 | CU = 69 |
| | $P < 0.0001$ | | | |
| **DMR14:** | Ctrl = 32 | 27.6 (26) | CC = 54 | CC = 58 |
| MMU12:107752401-107752500 | UN = 24 | | CU = 55 | CU = 55 |
| | $P = 0.001$ | | | |
| **DMR15*:** | Ctrl = 63 | 4.2 (26) | CC = 59 | CC = 84 |
| MMU11:46390601-46391100 | UN = 38 | | CU = 57 | CU = 82 |
| | $P < 0.0001$ | | | |
| **DMR16:** | Ctrl = 75 | 56 (26) | CC = 70 | CC = 82 |
| MMU7:10836601-10837100 | UN = 54 | | CU = 71 | CU = 82 |
| | $P < 0.0001$ | | | |
| **DMR17:** | Ctrl = 54 | 12.3 (26) | CC = 70 | CC = 82 |
| MMU10:120699201-120699700 | UN = 33 | | CU = 73 | CU = 82 |
| | $P = 0.001$ | | | |

To assess whether a metabolic phenotype is discernible at E16.5 in the $F_2$ generation, we examined lipid metabolism. There is an overall trend toward increased lipid abundance, particularly for saturated fatty acid–conjugated triglycerides (fig. S1G). This is associated with a significant increase in expression of genes involved in lipid oxidation in E16.5 CU liver, such as *PPARα*, *Pgc1α*, and *Pgc1β*, and a trend toward down-regulation of genes involved in lipid synthesis, including *Scd1*, *Srebp1*, and *Dgat1* (fig. S1H), likely secondary to the increased hepatic lipid abundance at E16.5. Together, these data suggest that CU individuals have altered metabolism even in utero.

### Hypomethylation of discrete loci in $F_1$ adult sperm of males undernourished in utero

To confirm the purity of $F_1$ sperm samples, bisulfite sequencing of imprinting control regions was carried out (fig. S2A). Independent sperm DNA samples were pooled in equimolar ratios to make two pools for each condition, each pool comprising four individuals from four independent litters (Fig. 1B), which minimized outcomes that might be associated with interindividual genetic differences. Mass spectrometry analysis of $F_1$ sperm DNA demonstrates that in utero nutrition does not affect the total level of DNA methylation or hydroxymethylation (Fig. 1C). It is also notable that the level of hydroxymethylation in sperm is only 2.1% of that observed in embryonic stem cells (Fig. 1C). Consequently, only the genomic distribution of DNA methylation was analyzed further.

We assessed the genome-wide distribution of sperm methylation by MeDIP-seq (Fig. 1B). This approach is most suited to the detection of robust regional changes in DNA methylation, as it offers near-unbiased genome-wide coverage with underrepresentation of low-density mC/mCG (*22*), which minimizes the possible influence of single-nucleotide variants and allows identification of clusters of differentially methylated cytosines. Optimization of antibody specificity was carried out

to ensure that there was no cross-sampling of hydroxymethylated or unmethylated cytosine (fig. S2B) (see materials and methods). Sequencing of antibody-enriched samples generated a total of 322.6 million mappable reads for control and 301.8 million for UN libraries. We conducted two independent comparisons between the control and UN pools, using the MEDIPS package (*23*) (see materials and methods for more details). Loci with a methylation change >1.5-fold and a binomial $P < 0.0001$ in both of the independent comparisons were selected for further study and clustered into 166 differentially methylated regions (DMRs), of which 111 were hypomethylated and 55 hypermethylated in UN relative to control sperm (Fig. 1D).

### Bisulfite pyrosequencing validation of MeDIP-seq DMRs

To independently validate regions of altered methylation using a different technology, we used bisulfite pyrosequencing assays on 32 regions, using an expanded panel of sperm samples: 12 control males from five litters and 11 UN males from four litters. Twenty-four hypomethylated regions and eight hypermethylated regions were randomly chosen for validation, distributed throughout the range of fold change and *P* values. No significant difference in methylation was found at any hypermethylated DMR, which suggests that these regions may be false-positives (table S1). In contrast, significant loss of methylation was confirmed at 17 of the hypomethylated regions in the expanded panel of $F_1$ UN sperm samples (Fig. 2 and Table 1). The validation rate of the nonrepetitive, unique hypomethylated regions was 90%. Differences in methylation at these loci span multiple CpGs, with robust absolute changes of 10 to 30%, a relative reduction of up to 50% (Fig. 2). Moreover, these differences are remarkably consistent among individual animals from multiple independent litters, which indicates that they are unlikely to be caused by genetic variation (fig. S3). The bisulfite sequencing data show identical absolute levels of methylation in the two replicate pools assessed by MeDIP-seq (fig. S3). Furthermore, the absolute methylation level (generally, under 50% in both groups) is consistent with these DMRs being "low-methylated regions," previously shown to be enriched in regulatory elements (*24*). Together, these data demonstrate that discrete loci in the adult male germ line are susceptible to changes in methylation as a result of nutritional stress in utero.

### DMRs are not distributed randomly through the genome

We examined the distribution of unique and repetitive elements among DMRs. Hypomethylated DMRs are significantly depleted from coding regions but enriched in intergenic regions and CpG islands (Fig. 3). Repetitive elements are significantly depleted from hypomethylated DMRs ($\chi^2$ $P < 0.0001$) with underrepresentation of long interspersed nuclear elements (LINEs) ($\chi^2$ $P = 0.001$) and short interspersed nuclear elements (SINEs) ($\chi^2$ $P < 0.0001$) and no significant enrichment of IAPs (Fig. 3).

The predominance of hypomethylated DMRs is striking. This is consistent with in utero undernutrition during the final third of gestation impairing the reacquisition of methylation in developing $F_1$ male primordial germ cells (PGCs). The nutritional insult experienced by the fetus worsens with increasing gestation as maternal energy reserves are depleted. Therefore, we hypothesize that the likelihood of remethylation being disrupted by in utero undernutrition increases toward term. Analysis of the temporal dynamics of methylation reprogramming in normal PGCs (*25*) suggests that this is indeed the case. In normal male PGCs, whole-genome methylation is progressively reduced from E6.5 to E13.5, with evidence of remethylation by E16.5 (Fig. 4A, gray bars). In contrast, those DMRs found to be hypomethylated in adult UN sperm (green bars) exhibit a distinct temporal pattern of reprogramming. These DMRs have significantly lower methylation levels at E16.5 in normal male PGCs ($\chi^2$ $P < 0.0001$) (Fig. 4A), which suggests that these regions are late to remethylate and may be susceptible to environmental perturbations that delay or impair remethylation at this stage. In normal adult sperm, methylation has largely been regained, but a minority of regions retain low methylation levels (*26*). UN-associated hypomethylated DMRs are enriched in these low methylated regions ($\chi^2$ $P < 0.0001$) (Fig. 4A).

During spermiogenesis, 99% of histones are exchanged for protamines, but nucleosomes are particularly retained in regions of high CpG density and low DNA methylation (*27*). Given the low methylation level of our DMRs, we assessed whether these regions are also enriched in nucleosomes. In mature sperm, 23 out of 111 (21%) hypomethylated DMRs retain nucleosomes (Fig. 4B). Bootstrap resampling of randomly selected regions from the background methylome demonstrates that this is a significant enrichment, $P < 0.0001$, and a feature of low methylated regions (see fig. S4 for details). This suggests that, at some loci, paternal germline hypomethylation induced by in utero undernutrition is transmitted in a chromatin context.

### The developmental legacy of germline DMRs in late gestation of the $F_2$ generation

With the exception of imprints, it has been thought that gene-associated methylation in the male germ line is largely reprogrammed in the zygote by active DNA demethylation (*17*). However, recent studies suggest that resistance to DNA methylation reprogramming extends beyond imprinted domains (*11*–*13*). Indeed, 43% of our hypomethylated DMRs are resistant to zygotic reprogramming (*26*), which suggests that differential methylation in the paternal germ line may persist into the early embryo and may affect the development of the next generation (Table 2).

To determine whether altered $F_1$ sperm methylation persisted as a "memory" of sperm compromise in $F_2$ offspring, we bred $F_1$ control and UN males with control females. Offspring were designated as CC ($F_2$ offspring of control males) and CU ($F_2$ offspring of UN males) as noted above (Fig. 1A). Using liver and brain samples from late-gestation (E16.5) CC and CU embryos, we analyzed DNA methylation at validated germline DMRs. Differential methylation has been lost in $F_2$ E16.5 brain and liver (Table 1 and Fig. 5) and is therefore not a long-term heritable memory of a

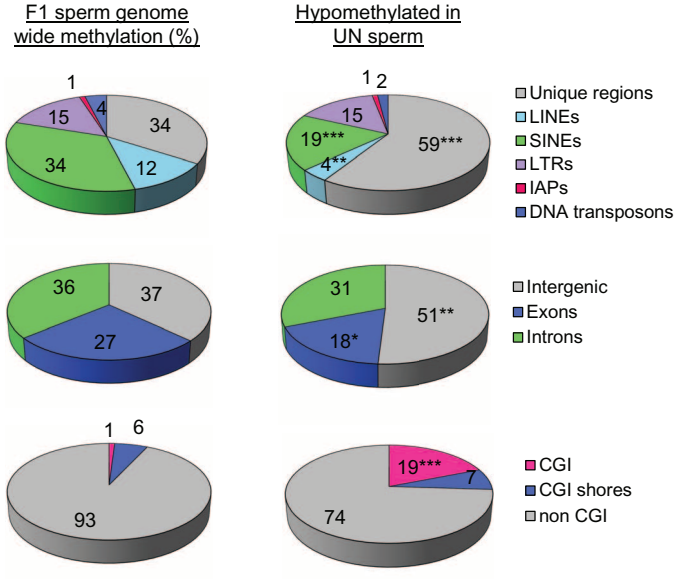


**Fig. 3. DMRs are enriched in intergenic nonrepetitive regions and CpG islands.** (**Top**) Relative distribution (%) of $F_1$ sperm methylated regions among distinct sequence and repetitive elements genome-wide (left) and among the $F_1$ UN sperm hypomethylated DMRs (right). Distinct regions are significantly enriched ($\chi 2$ $P < 0.0001$), whereas LINEs and SINEs are significantly depleted from hypomethylated DMRs ($\chi 2$ $P = 0.001$; $\chi 2$ $P < 0.0001$, respectively), relative to all methylated regions detected in $F_1$ sperm. (**Middle**) Relative distribution (%) of methylated regions among coding and noncoding sequences. Exons are significantly depleted ($\chi 2$ $P = 0.036$), and intergenic regions are significantly enriched ($\chi 2$ $P = 0.0012$) among hypomethylated DMRs. (**Bottom**) Relative distribution (%) of methylated regions detected by MeDIP-seq among CpG islands (CGI) and CGI shores. CGIs are significantly enriched among hypomethylated DMRs ($\chi 2$ $P < 0.0001$).

compromised germ line. These data indicate that any functional consequences of germline DMRs are likely to be established early in development and/or linked to associated, but currently unknown, regulatory effects that may persist despite DNA remethylation in later development.

Analysis of validated DMRs in publicly available data sets (*28*) indicates that these loci have cell type–specific enrichment of histone modifications and transcription factor binding, characteristic of a role in cis regulation of transcription (table S2). To assess the function of a randomly selected subset of six DMRs, we conducted luciferase reporter assays in neural stem cells (*29*) and NIH3T3 cells in culture, using methylation-stable regions (non-DMRs) validated by pyrosequencing as additional negative controls. No significant enhancer function could be attributed to any of the regions tested in either cell type. In contrast, in vectors designed to assess a negative influence on transcription, such as an enhancer blocking or silencer function, when inserted in both the forward and reverse orientation, five out of six regions showed significantly suppressed reporter activity in neural stem cells as did three out of six regions in NIH3T3 cells (Fig. 6A). Taken together, the data suggest that these germline DMRs may play cell-specific regulatory roles in the modulation of transcription.

To assess this possibility, we examined expression of genes neighboring the 17 germline DMRs, using quantitative polymerase chain reaction (qPCR) in liver and brain of $F_2$ CC and CU fetuses at E16.5. Genes associated with DMRs 15 and 16 were not expressed in these tissues. Eight DMRs showed significant tissue-specific differences in expression of neighboring genes (Fig. 6, B and C). In contrast, no change in expression was found at 12 genes not associated with DMRs (fig. S5). Because methylation differences are not observed in E16.5 tissues of these same $F_2$ offspring (Fig. 5), it is unlikely that these expression changes are directly mediated by alterations in methylation. Rather, the cumulative effects of dysregulated epigenetic patterns earlier in development may yield sustained alterations in chromatin architecture, transcriptional regulatory networks, cell type, or tissue structure.

Several affected genes, including *Sstr3*, *C1qntf6*, *Tbc1d30*, *Kcnj11*, and *Sur1*, are candidate contributors to the $F_2$ phenotypes, given their known roles in glucose tolerance and metabolism (*30*–*36*). For example, the DMR9 lies within the *Kcnj11* gene, immediately downstream of *Sur1*. These genes encode the two subunits of the pancreatic β-cell adenosine triphosphate (ATP)–dependent $K^+$ channel, which are necessary for the physiological control of insulin secretion (*34*, *36*). Furthermore, polymorphisms at these loci are associated with type 2 diabetes (*35*, *37*). In pancreatic islets isolated from 4-month-old CU mice ($F_2$ generation), expression of *Sur1* is reduced by 33% ($P < 0.05$) (Fig. 6D) (*3*). The function of β-cell ATP-dependent $K^+$ channels in controlling insulin secretion can be assessed by measuring the response to treatment with agents that inhibit and activate these channels, such as sulfonylureas and diazoxide, respectively, or through the insulin secretory response to a glucose challenge. Freshly isolated 4-month-old CU pancreatic islets demonstrate impaired insulin secretion in response to the sulfonylurea tolbutamide (Fig. 6E) and absence of suppression of insulin secretion to diazoxide (Fig. 6F) (*3*). Furthermore, basal insulin secretion before diazoxide challenge was significantly reduced (*3*) (Fig. 6F). Consistent with this, CU individuals secrete significantly less insulin during glucose tolerance testing (*3*) (Fig. 6G). These data strongly suggest impaired function of ATP-dependent $K^+$ channels in the adult CU pancreas and implicate this in the altered glucose tolerance observed in CU individuals (fig. S1E). Further work will be required to delineate the precise relation between compromised $F_1$ germline reprogramming at these loci and $F_2$ phenotypes.

## Discussion

Our data indicate that nutritional perturbations during in utero development can alter male germline methylation at discrete loci. In turn, some of these DMRs are associated with differential transcript expression during offspring embryonic life. Our findings contrast with the largely negative data of Carone *et al.* in which no significant changes were observed in sperm DNA methylation after dietary protein restriction in adult males (*4*). Disparities may be due to the use of caloric rather than protein restriction,

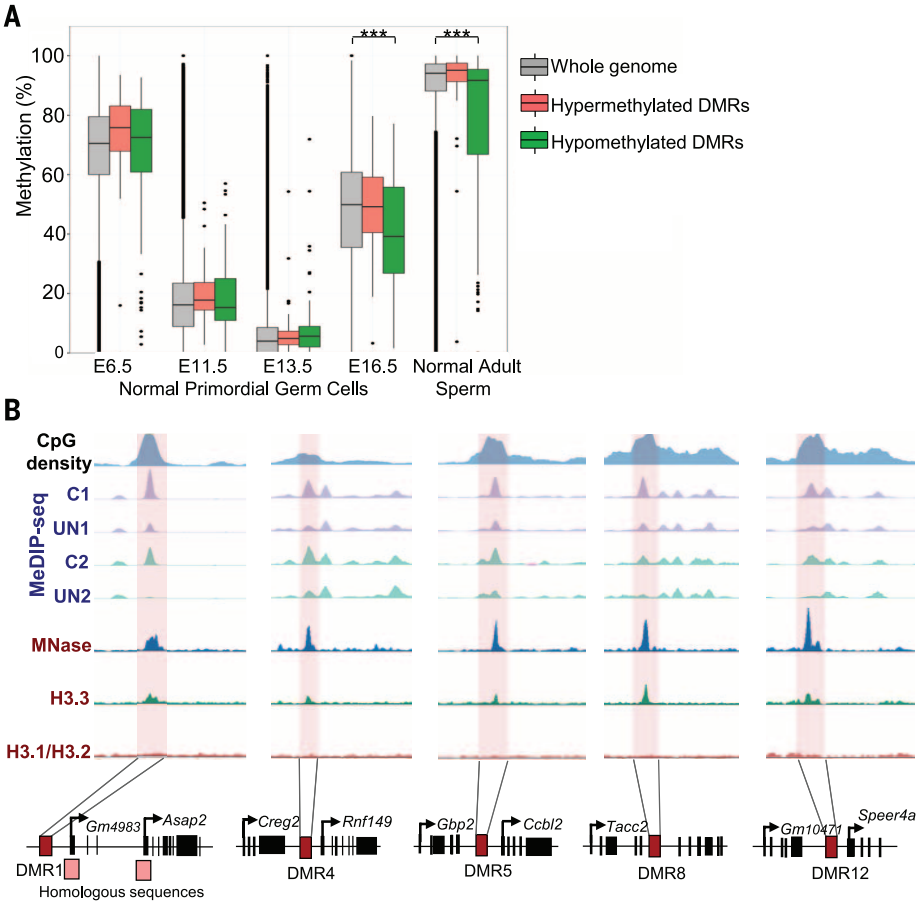


**Fig. 4. DMRs regain methylation late during PGC reprogramming and retain nucleosomes in mature sperm.** (**A**) Methylation level of hypomethylated (green) and hypermethylated (red) DMRs in our data set versus the whole genome (gray) in normal PGCs (*25*) and mature sperm from adult males (*26*). Hypermethylated DMRs act as an additional negative control because they did not validate. E13.5 and E16.5 are male PGCs. E6.5 and E11.5 are mixed-sex PGCs (*25*). (**B**) Nucleosome enrichment (*27*) at five representative hypomethylated DMRs.

**Table 2. Of hypomethylated DMRs, 43% are resistant to zygotic demethylation.** Hypomethylated DMRs susceptible (<20% methylation) or partially resistant (>20% methylation) to blastocyst reprogramming (*28*).

| | Number (%) of hypomethylated DMRs |
|---|---|
| Blastocyst methylation < 20% (26) | 63 (57) |
| Blastocyst methylation > 20% (26) | 48 (43) |

strain differences, or the greater number of individuals assessed in our analysis. Alternatively it may be due to differences in the timing of the nutritional insult, because of Carone and colleagues' imposed protein restriction during adult life. By contrast, the nutritional perturbation in our model occurs exclusively during late prenatal life, precisely when male PGCs in the developing embryo are undergoing reestablishment of their epigenetic profile. At this time, PGCs may be particularly vulnerable to epigenetic perturbation. It is notable that intergenerational phenotypic inheritance caused by endocrine disruptors associated with altered sperm DNA methylation also involves prenatal exposure (*9*, *38*). However, recent data have suggested that a high-fat diet during adult life might alter sperm DNA methylation, which indicates that the adult germline methylome may be more susceptible to environmental conditions than previously thought (*8*).

Our experiment was designed to minimize detection of single CpG methylation differences, which we a priori hypothesize to be more likely to be due to genetic differences. Our results indicate that robust germ cell methylation changes do occur after in utero undernourishment at regions partially resistant to zygotic reprogramming. However, persistence of altered DNA methylation into late-gestation somatic tissues of the subsequent generation was not observed. Nonetheless, gene expression is altered in these $F_2$ offspring at regions of $F_1$ germline differential methylation. Such differences in gene expression could reflect the impact of altered methylation during early development, with subsequent transcriptional patterns that persist despite DNA remethylation in later gestation. Alternatively, altered $F_2$ expression may be the cumulative result of multiple locus-specific defects in germline chromatin

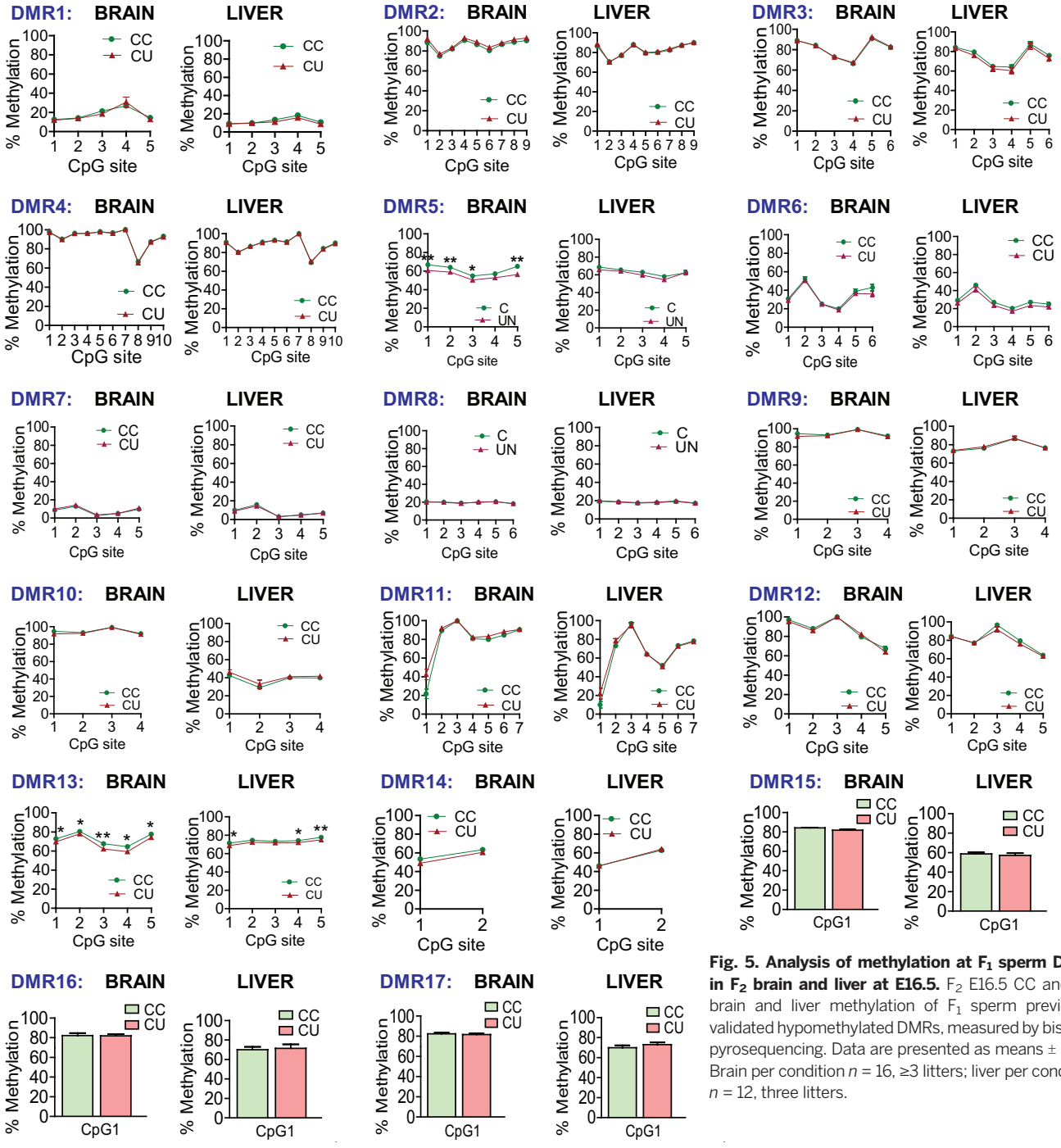


**Fig. 5. Analysis of methylation at $F_1$ sperm DMRs in $F_2$ brain and liver at E16.5.** $F_2$ E16.5 CC and CU brain and liver methylation of $F_1$ sperm previously validated hypomethylated DMRs, measured by bisulfite pyrosequencing. Data are presented as means ± SEM. Brain per condition $n = 16$, ≥3 litters; liver per condition $n = 12$, three litters.

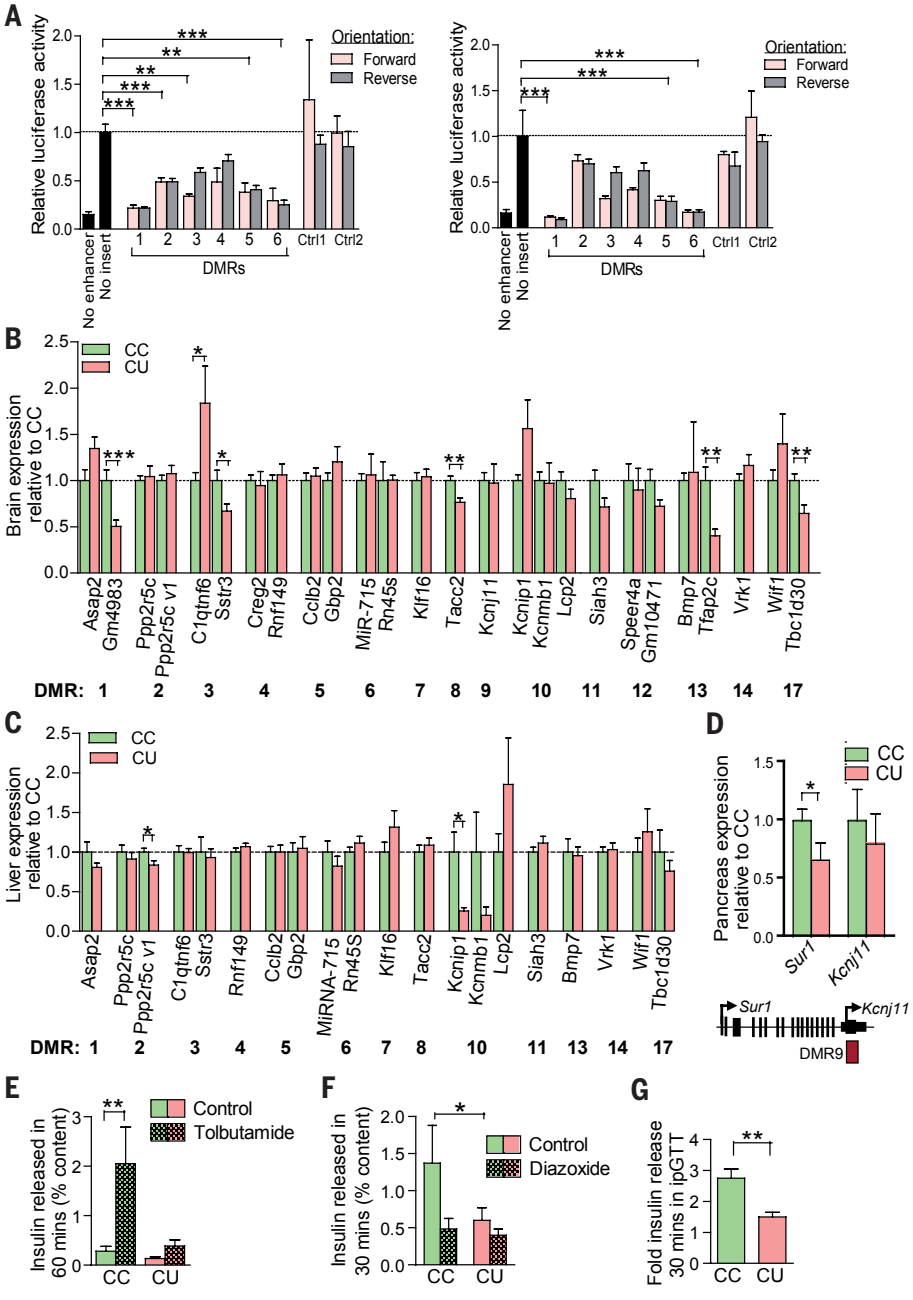


**Fig. 6. Developmental legacy of altered UN sperm methylation in the $F_2$ generation.** (**A**) Luciferase assay for a negative effect on transcription in 46C neural stem cells (*29*) (left) and NIH3T3 cells (right). Sequences were inserted between the promoter and enhancer of the control pGL3 vector. The pGL3 promoter vector (lacking an enhancer) was used as a positive control. Two regions validated by pyrosequencing as having unaffected $F_1$ sperm methylation were used as negative controls. Control 1: MMU2:77723600–77723900, control 2: MMU17:87639700-87640000. Data are plotted as means ± SEM, normalized to activity of the control pGL3 vector with no insert. One-way analysis of variance (ANOVA), Dunnett's post hoc test $^{**}P < 0.001$, $^{***}P < 0.0001$. (**B**) $F_2$ E16.5 brain expression of genes neighboring $F_1$ sperm DMRs. Data are plotted as means ± SEM. *MiR-715* expression normalized to *SnoRNA 202*; all other expression normalized to *Hprt*. *Hprt* and *SnoRNA202* were unaffected. Unpaired two-tailed *t* test: *Gmf4983*, $P = 0.0004$; *C1qtnf6*, $P = 0.049$; *Sstr3*, $P = 0.02$; *Tacc2*, $P = 0.0018$; *Tfap2c*, $P = 0.015$; and *Tbc1d30*, $P = 0.006$. Per condition $n = 16$, ≥3 litters. (**C**) $F_2$ E16.5 liver expression of genes neighboring $F_1$ sperm DMRs. Data are plotted as means ± SEM. Normalized as for (B). Unpaired two-tailed *t* test: *Ppp2r5c variant1*, $P = 0.03$; *Kcnip1*, $P = 0.011$. Per condition $n = 12$, three litters. (**D**) $F_2$ pancreatic expression at 4 months. Per condition $n \geq 5$, $^{*}P < 0.05$, unpaired two-tailed *t* test (*3*). (**E**) Tolbutamide (200 μM)–stimulated insulin secretion, freshly isolated 4-month-old islets; $n \geq 4$, ≥2 isolations. $^{**}P < 0.01$, unpaired two-tailed *t* test (*3*). (**F**) Diazoxide (250 μM) inhibition of insulin secretion, freshly isolated 4-month-old islets; $n = 4$ per group, ≥2 isolations. $^{*}P < 0.05$, unpaired two-tailed *t* test (*3*). (**G**) Fold change in serum insulin 30 min after intraperitoneal glucose bolus (1 mg/kg). $^{**}P < 0.01$, $n \geq 8$, unpaired two-tailed *t* test (*3*).

state. Further work will be required to explore these possibilities.

Recent work in cultured cells demonstrates that regional methylation levels can be a secondary consequence of changes in DNA binding factors (*24*). Thus, it is possible that the germline DMRs identified in our study are secondary to other chromatin perturbations. Consistent with this, we observed enrichment of nucleosome occupancy at DMRs. Further studies are required to examine whether these represent regions of vulnerability in the sperm genome. Histone modifications and small RNA molecules are known to be required for multigenerational gene-silencing effects in *Caenorhabditis elegans* (*39*, *40*), an animal that lacks DNA methylation, and such mechanistic processes may also be involved in mammals. Indeed, there is evidence that sperm-borne microRNAs play an important role in early mammalian development (*41*), and the early-life environment may have the potential to alter the abundance of some sperm microRNAs (*42*).

## Conclusion

Data presented here serve as a proof of principle that undernutrition during prenatal life, even when followed by normal postnatal nutrition, can compromise male germline development and epigenetic reprogramming and so permanently alter DNA methylation in the germ line of the adult offspring. Alterations in adult gamete methylation may serve as a legacy of earlier developmental exposures that may contribute to the intergenerational transmission of environmentally induced disease.

## REFERENCES AND NOTES


1. P. D. Gluckman, M. A. Hanson, C. Cooper, K. L. Thornburg, Effect of in utero and early-life conditions on adult health and disease. *N. Engl. J. Med.* **359**, 61–73 (2008). doi: 10.1056/NEJMra0708473; pmid: 18596274
2. A. J. Drake, B. R. Walker, The intergenerational effects of fetal programming: Non-genomic mechanisms for the inheritance of low birth weight and cardiovascular risk. *J. Endocrinol.* **180**, 1–16 (2004). doi: 10.1677/joe.0.1800001; pmid: 14709139
3. J. C. Jimenez-Chillaron *et al*., Intergenerational transmission of glucose intolerance and obesity by in utero undernutrition in mice. *Diabetes* **58**, 460–468 (2009). doi: 10.2337/db08-0490; pmid: 19017762
4. B. R. Carone *et al*., Paternally induced transgenerational environmental reprogramming of metabolic gene expression in mammals. *Cell* **143**, 1084–1096 (2010). doi: 10.1016/j.cell.2010.12.008; pmid: 21183072
5. S. F. Ng *et al*., Chronic high-fat diet in fathers programs β-cell dysfunction in female rat offspring. *Nature* **467**, 963–966 (2010). doi: 10.1038/nature09491; pmid: 20962845
6. M. E. Pembrey *et al*.ALSPAC Study Team, Sex-specific, male-line transgenerational responses in humans. *Eur. J. Hum. Genet.* **14**, 159–166 (2006). doi: 10.1038/sj.ejhg.5201538; pmid: 16391557
7. I. C. Weaver *et al*., Epigenetic programming by maternal behavior. *Nat. Neurosci.* **7**, 847–854 (2004). doi: 10.1038/nn1276; pmid: 15220929
8. Y. Wei *et al*., Paternally induced transgenerational inheritance of susceptibility to diabetes in mammals. *Proc. Natl. Acad. Sci. U.S.A.* **111**, 1873–1878 (2014). doi: 10.1073/pnas.1321195111; pmid: 24449870
9. M. D. Anway, A. S. Cupp, M. Uzumcu, M. K. Skinner, Epigenetic transgenerational actions of endocrine disruptors and male fertility. *Science* **308**, 1466–1469 (2005). doi: 10.1126/science.1108190; pmid: 15933200
10. V. K. Rakyan *et al*., Transgenerational inheritance of epigenetic states at the murine *Axin(Fu)* allele occurs after maternal and paternal transmission. *Proc. Natl. Acad. Sci. U.S.A.* **100**, 2538–2543 (2003). doi: 10.1073/pnas.0436776100; pmid: 12601169

11. J. Borgel *et al*., Targets and dynamics of promoter DNA methylation during early mouse development. *Nat. Genet.* **42**, 1093–1100 (2010). doi: 10.1038/ng.708; pmid: 21057502
12. S. A. Smallwood *et al*., Dynamic CpG island methylation landscape in oocytes and preimplantation embryos. *Nat. Genet.* **43**, 811–814 (2011). doi: 10.1038/ng.864; pmid: 21706000
13. Z. D. Smith *et al*., A unique regulatory phase of DNA methylation in the early mammalian embryo. *Nature* **484**, 339–344 (2012). doi: 10.1038/nature10960; pmid: 22456710
14. J. C. Jimenez-Chillaron *et al*., Beta-cell secretory dysfunction in the pathogenesis of low birth weight-associated diabetes: A murine model. *Diabetes* **54**, 702–711 (2005). doi: 10.2337/diabetes.54.3.702; pmid: 15734846
15. E. Isganaitis *et al*., Accelerated postnatal growth increases lipogenic gene expression and adipocyte size in low-birth weight mice. *Diabetes* **58**, 1192–1200 (2009). doi: 10.2337/db08-1266; pmid: 19208909
16. M. Woo *et al*., Early life nutrition modulates muscle stem cell number: Implications for muscle mass and repair. *Stem Cells Dev.* **20**, 1763–1769 (2011). doi: 10.1089/scd.2010.0349 pmid: 21247245
17. H. Sasaki, Y. Matsui, Epigenetic events in mammalian germ-cell development: Reprogramming and beyond. *Nat. Rev. Genet.* **9**, 129–140 (2008). doi: 10.1038/nrg2295; pmid: 18197165
18. E. J. Radford *et al*., An unbiased assessment of the role of imprinted genes in an intergenerational model of developmental programming. *PLOS Genet.* **8**, e1002605 (2012). doi: 10.1371/journal.pgen.1002605; pmid: 22511876
19. M. Weber *et al*., Chromosome-wide and promoter-specific analyses identify sites of differential DNA methylation in normal and transformed human cells. *Nat. Genet.* **37**, 853–862 (2005). doi: 10.1038/ng1598; pmid: 16007088
20. M. Weber *et al*., Distribution, silencing potential and evolutionary impact of promoter DNA methylation in the human genome. *Nat. Genet.* **39**, 457–466 (2007). doi: 10.1038/ng1990; pmid: 17334365
21. T. A. Down *et al*., A Bayesian deconvolution strategy for immunoprecipitation-based DNA methylome analysis. *Nat. Biotechnol.* **26**, 779–785 (2008). doi: 10.1038/nbt1414; pmid: 18612301
22. O. Taiwo *et al*., Methylome analysis using MeDIP-seq with low DNA concentrations. *Nat. Protoc.* **7**, 617–636 (2012). doi: 10.1038/nprot.2012.012; pmid: 22402632
23. L. Chavez *et al*., Computational analysis of genome-wide DNA methylation during the differentiation of human embryonic stem cells along the endodermal lineage. *Genome Res.* **20**, 1441–1450 (2010). doi: 10.1101/gr.110114.110; pmid: 20802089
24. M. B. Stadler *et al*., DNA-binding factors shape the mouse methylome at distal regulatory regions. *Nature* **480**, 490–495 (2011). pmid: 22170606
25. S. Seisenberger *et al*., The dynamics of genome-wide DNA methylation reprogramming in mouse primordial germ cells. *Mol. Cell* **48**, 849–862 (2012). doi: 10.1016/j.molcel.2012.11.001; pmid: 23219530
26. H. Kobayashi *et al*., Contribution of intragenic DNA methylation in mouse gametic DNA methylomes to establish oocyte-specific heritable marks. *PLOS Genet.* **8**, e1002440 (2012). doi: 10.1371/journal.pgen.1002440; pmid: 22242016
27. S. Erkek *et al*., Molecular determinants of nucleosome retention at CpG-rich sequences in mouse spermatozoa. *Nat. Struct. Mol. Biol.* **20**, 868–875 (2013). doi: 10.1038/nsmb.2599; pmid: 23770822
28. K. R. Rosenbloom *et al*., ENCODE whole-genome data in the UCSC Genome Browser: Update 2012. *Nucleic Acids Res.* **40** (D1), D912–D917 (2012). doi: 10.1093/nar/gkr1012; pmid: 22075998
29. Q. L. Ying, M. Stavridis, D. Griffiths, M. Li, A. Smith, Conversion of embryonic stem cells into neuroectodermal precursors in adherent monoculture. *Nat. Biotechnol.* **21**, 183–186 (2003). doi: 10.1038/nbt780; pmid: 12524553
30. T. Iwanaga, T. Miki, H. Takahashi-Iwanaga, Restricted expression of somatostatin receptor 3 to primary cilia in the pancreatic islets and adenohypophysis of mice. *Biomed. Res.* **32**, 73–81 (2011). doi: 10.2220/biomedres.32.73; pmid: 21383513
31. J. F. Bruno, Y. Xu, J. Song, M. Berelowitz, Pituitary and hypothalamic somatostatin receptor subtype messenger ribonucleic acid expression in the food-deprived and diabetic rat. *Endocrinology* **135**, 1787–1792 (1994). pmid: 7956902
32. T. Takeuchi, Y. Adachi, T. Nagayama, Expression of a secretory protein C1qTNF6, a C1qTNF family member, in hepatocellular carcinoma. *Anal. Cell. Pathol. (Amst.)* **34**, 113–121 (2011). pmid: 21508531
33. J. R. Huyghe *et al*., Exome array analysis identifies new loci and low-frequency variants influencing insulin processing and secretion. *Nat. Genet.* **45**, 197–201 (2013). doi: 10.1038/ng.2507; pmid: 23263489
34. A. P. Babenko *et al*., Activating mutations in the *ABCC8* gene in neonatal diabetes mellitus. *N. Engl. J. Med.* **355**, 456–466 (2006). doi: 10.1056/NEJMoa055068; pmid: 16885549
35. O. Laukkanen *et al*., Polymorphisms of the SUR1 (ABCC8) and Kir6.2 (KCNJ11) genes predict the conversion from impaired glucose tolerance to type 2 diabetes. The Finnish Diabetes Prevention Study. *J. Clin. Endocrinol. Metab.* **89**, 6286–6290 (2004). doi: 10.1210/jc.2004-1204; pmid: 15579791
36. A. L. Gloyn *et al*., Activating mutations in the gene encoding the ATP-sensitive potassium-channel subunit Kir6.2 and permanent neonatal diabetes. *N. Engl. J. Med.* **350**, 1838–1849 (2004). doi: 10.1056/NEJMoa032922; pmid: 15115830
37. K. E. Lohmueller, C. L. Pearce, M. Pike, E. S. Lander, J. N. Hirschhorn, Meta-analysis of genetic association studies supports a contribution of common variants to susceptibility to common disease. *Nat. Genet.* **33**, 177–182 (2003). doi: 10.1038/ng1071; pmid: 12524541
38. C. Guerrero-Bosagna, M. Settles, B. Lucker, M. K. Skinner, Epigenetic transgenerational actions of vinclozolin on promoter regions of the sperm epigenome. *PLOS ONE* **5**, e13100 (2010). doi: 10.1371/journal.pone.0013100; pmid: 20927350
39. A. Ashe *et al*., piRNAs can trigger a multigenerational epigenetic memory in the germline of *C. elegans*. *Cell* **150**, 88–99 (2012). doi: 10.1016/j.cell.2012.06.018; pmid: 22738725
40. M. Shirayama *et al*., piRNAs initiate an epigenetic memory of nonself RNA in the *C. elegans* germline. *Cell* **150**, 65–77 (2012). doi: 10.1016/j.cell.2012.06.015; pmid: 22738726
41. W. M. Liu *et al*., Sperm-borne microRNA-34c is required for the first cleavage division in mouse. *Proc. Natl. Acad. Sci. U.S.A.* **109**, 490–494 (2012). doi: 10.1073/pnas.1110368109; pmid: 22203953
42. K. Gapp *et al*., Implication of sperm RNAs in transgenerational inheritance of the effects of early trauma in mice. *Nat. Neurosci.* **17**, 667–669 (2014). doi: 10.1038/nn.3695; pmid: 24728267



## ACKNOWLEDGMENTS

We are grateful to members of the Ferguson-Smith and Patti labs for useful discussions of this work and to K. Tabbada and D. Oxley for expert technical assistance with Illumina sequencing and mass spectrometry. Work was supported by grants from the U.K. Medical Research Council; Wellcome Trust; and European Commission FP7, EpiGeneSys and EpiHealth (to A.C.F.-S.), from the Pediatric Endocrine Society and the Eunice Kennedy Shriver National Institute of Child Health and Human Development, NIH (to E.I.), and from the American Diabetes Association, the Graetz Foundation, and NIH P30DK036836 (to M.-E.P.). W.R. is a consultant for Cambridge Epigenetix. The MeDIP-Seq data sets have been deposited in GEO with accession number GSE58747. A.H.F.M.P. and S.E. are funded by the Novartis Research Foundation.


## SUPPLEMENTARY MATERIALS

www.sciencemag.org/content/345/6198/1255903/suppl/DC1
Materials and Methods
Figs. S1 to S5
Tables S1 to S6
References (*43*–*52*)


12 May 2014; accepted 27 June 2014
Published online 10 July 2014;
10.1126/science.1255903

RESEARCH ARTICLE

INTERSTELLAR DUST

# Evidence for interstellar origin of seven dust particles collected by the Stardust spacecraft

Andrew J. Westphal,[1]* Rhonda M. Stroud,[2] Hans A. Bechtel,[3] Frank E. Brenker,[4] Anna L. Butterworth,[1] George J. Flynn,[5] David R. Frank,[6] Zack Gainsforth,[1] Jon K. Hillier,[7] Frank Postberg,[7] Alexandre S. Simionovici,[8] Veerle J. Sterken,[9,10,11,12] Larry R. Nittler,[13] Carlton Allen,[14] David Anderson,[1] Asna Ansari,[15] Saša Bajt,[16] Ron K. Bastien,[6] Nabil Bassim,[2] John Bridges,[17] Donald E. Brownlee,[18] Mark Burchell,[19] Manfred Burghammer,[20] Hitesh Changela,[21] Peter Cloetens,[22] Andrew M. Davis,[23] Ryan Doll,[24] Christine Floss,[24] Eberhard Grün,[25] Philipp R. Heck,[12] Peter Hoppe,[26] Bruce Hudson,[27] Joachim Huth,[26] Anton Kearsley,[28] Ashley J. King,[23] Barry Lai,[29] Jan Leitner,[26] Laurence Lemelle,[30] Ariel Leonard,[24] Hugues Leroux,[31] Robert Lettieri,[1] William Marchant,[1] Ryan Ogliore,[32] Wei Jia Ong,[24] Mark C. Price,[19] Scott A. Sandford,[33] Juan-Angel Sans Tresseras,[22] Sylvia Schmitz,[4] Tom Schoonjans,[20] Kate Schreiber,[24] Geert Silversmit,[20] Vicente A. Solé,[22] Ralf Srama,[34] Frank Stadermann,[24]† Thomas Stephan,[23] Julien Stodolna,[1] Stephen Sutton,[29] Mario Trieloff,[7] Peter Tsou,[35] Tolek Tyliszczak,[3] Bart Vekemans,[20] Laszlo Vincze,[20] Joshua Von Korff,[1] Naomi Wordsworth,[36] Daniel Zevin,[1] Michael E. Zolensky,[14] 30714 Stardust@home dusters[37]

**Seven particles captured by the Stardust Interstellar Dust Collector and returned to Earth for laboratory analysis have features consistent with an origin in the contemporary interstellar dust stream. More than 50 spacecraft debris particles were also identified. The interstellar dust candidates are readily distinguished from debris impacts on the basis of elemental composition and/or impact trajectory. The seven candidate interstellar particles are diverse in elemental composition, crystal structure, and size. The presence of crystalline grains and multiple iron-bearing phases, including sulfide, in some particles indicates that individual interstellar particles diverge from any one representative model of interstellar dust inferred from astronomical observations and theory.**

Our understanding of the properties of contemporary interstellar dust (ISD) has been derived primarily from astronomical observations of the interstellar medium (ISM), including optical properties of the ISD and remote spectroscopy of the gas composition (*1*–*3*), and from in situ measurements by the dust analyzers on the Cassini, Ulysses, and Galileo spacecraft (*4*–*6*). The canonical picture of ISD is that it is dominated by ~0.2-μm-diameter (*7*) amorphous silicate grains, with or without carbonaceous mantles. However, the inferred properties of the particles, including size distribution, density, and composition, are heavily model dependent.

Direct, laboratory-based measurement of returned particles that may originate in the local ISM (LISM) offers an independent test of the assumptions on which the interpretation of spectroscopy and in situ dust measurements rest. Important questions to be addressed include: Is there one dominant dust phase, and if so, what is its composition? Is the dominant structure crystalline or amorphous? Is iron present in metal, oxide, carbide, and/or sulfide phases? Are the particles dense or fluffy? Is there evidence for particle mantles of either organic or silicate-like composition? We present here results from the Stardust Interstellar Preliminary Examination (ISPE) (*8*), in which we have identified seven dust particle impacts of probable interstellar origin, to address these and related questions. The identification of these seven impacts is the result of a massively distributed, volunteer-based, search of optical micrographs of the aerogel collectors, manual and automated searches of scanning electron micrographs of aluminum foils, extensive coordinated sample analyses, laboratory hypervelocity impact experiments, and numerical modeling of ISD propagation in the heliosphere. These are described in detail in a series of papers (*9*–*20*) published contemporaneously with this article; see also supplementary materials online (*21*).

The 0.1-$m^2$ Stardust Interstellar Dust Collector (SIDC) consisted of an Al frame holding ultralow-density silica aerogel tiles (*8*) that constitute 85% of the exposed area and Al foils that constitute the remaining 15%. The collector was exposed to the expected interstellar dust stream, approximately from the direction of Ophiuchus (*22*), for 195 days in two periods in 2000 and 2002. The low density of the silica aerogel enables capture of hypervelocity particles with mild deceleration as compared with other capture media, to limit the capture alteration effects, and simultaneously records particle trajectory in the form of a carrot-shaped track. The optical transparency of the aerogel allows for detection of tracks ≥2 μm in diameter (*9*). The Al foil is a collection medium that is complementary to the silica aerogel. Impact residues on the foils are localized to craters on the surface, which contain residue that is not mixed with silica aerogel. Scanning electron microscopy (SEM) of the foils can identify impact craters as small as 0.3 μm in diameter, corresponding to ~0.2-μm-diameter particles (*23*, *24*).

The criteria for identifying candidate interstellar particles (table S1) in the two collection media are slightly different. The first-order criteria (levels 0 to 2) are that the shape of the identified feature must be consistent with hypervelocity impact, and the captured particle or particle residue must have a composition that is consistent with formation in space, and inconsistent with spacecraft materials, or aerogel impurities. The trajectory of the particle is taken into consideration for the samples collected in aerogel, but not for the foils, because crater shapes depend strongly on the particle shape and composition, in addition to trajectory (*25*). The most definitive indication of an interstellar origin (level 3) for a particular particle would be an oxygen isotope composition inconsistent with solar system values. However, the converse is not true—an oxygen isotope composition within the range of solar system values does not uniquely constrain the origin to the solar system. All seven

[1]Space Sciences Laboratory, University of California at Berkeley, Berkeley, CA, USA. [2]Materials Science and Technology Division, Naval Research Laboratory, Washington, DC, USA. [3]Advanced Light Source, Lawrence Berkeley Laboratory, Berkeley, CA, USA. [4]Geoscience Institute, Goethe University Frankfurt, Frankfurt, Germany. [5]State University of New York at Plattsburgh, Plattsburgh, NY, USA. [6]Jacobs Technology/ESCG, NASA Johnson Space Center (JSC), Houston, TX, USA. [7]Institut für Geowissenschaften, University of Heidelberg, Germany. [8]Institut des Sciences de la Terre, Observatoire des Sciences de l'Univers de Grenoble, Grenoble, France. [9]Institut für Raumfahrtsysteme (IRS), University of Stuttgart, Stuttgart, Germany. [10]IGEP, TU Braunschweig, Braunschweig, Germany. [11]Max Planck Institut für Kernphysik, Heidelberg, Germany. [12]International Space Sciences Institute, Bern, Switzerland. [13]Carnegie Institution of Washington, Washington, DC, USA. [14]Astromaterials Research and Exploration Science, NASA JSC, Houston, TX, USA. [15]Field Museum of Natural History, Chicago, IL, USA. [16]Deutsches Elektronen-Synchrotron, Hamburg, Germany. [17]Space Research Centre, University of Leicester, Leicester, UK. [18]Department of Astronomy, University of Washington, Seattle, WA, USA. [19]University of Kent, Canterbury, Kent, UK. [20]University of Ghent, Ghent, Belgium. [21]University of New Mexico. [22]European Synchrotron Radiation Facility (ESRF), Grenoble, France. [23]University of Chicago, Chicago, IL, USA. [24]Washington University, St. Louis, MO, USA. [25]Max-Planck-Institut für Kernphysik, Heidelberg, Germany. [26]Max-Planck-Institut für Chemie, Mainz, Germany. [27]615 William Street, Apt 405, Midland, Ontario, Canada. [28]Natural History Museum, London, UK. [29]Advanced Photon Source, Argonne National Laboratory, Lemont, IL, USA. [30]Ecole Normale Superieure de Lyon, Lyon, France. [31]University Lille 1, France. [32]University of Hawai'i at Manoa, Honolulu, HI, USA. [33]NASA Ames Research Center, Moffett Field, CA, USA. [34]IRS, University Stuttgart, Stuttgart, Germany. [35]Jet Propulsion Laboratory, Pasadena, CA, USA. [36]Wexbury, Farthing Green Lane, Stoke Poges, South Buckinghamshire, UK. [37]Worldwide. List of individual dusters is at http://stardustathome.ssl.berkeley.edu/sciencedusters.
*Corresponding author. E-mail: westphal@ssl.berkeley.edu
†Deceased.

of the captured particles reported here are level 2 candidates, for which the oxygen isotope data are either not yet available, or are consistent with solar values. This means that although an interstellar origin cannot be definitively proven for the particles, other origins, including as interplanetary dust, have been determined to be statistically less likely than an interstellar origin. Three interstellar candidates were identified in a search of ~250 $cm^2$ of the exposed aerogel, and four interstellar candidates were identified in a search of ~5 $cm^2$ of the exposed Al foil.

## Identification and analysis of candidates in aerogel

We identified 71 tracks in an examination of slightly over half of the aerogel tiles in the SIDC. All but two were identified through the Stardust@home project (*9*, *10*), in which volunteers searched online for tracks in digital micrographs of the aerogel collector. We extracted a subset of these tracks in volumes of aerogel, called "picokeystones" (*10*, *26*), and mounted them between 70-nm-thick $Si_3N_4$ membranes to protect from loss and contamination. Picokeystones were subsequently analyzed at one or more of six synchrotrons with techniques including scanning transmission x-ray microscopy (STXM) (*12*), Fourier transform infrared spectroscopy (FTIR) (*11*), x-ray fluorescence spectroscopy (XRF) (*13*–*15*), and x-ray diffraction (XRD) (*16*). Forty-six of the tracks are consistent in their trajectories with an origin as secondary ejecta from impacts on the aft solar panels, and this origin was confirmed for four tracks (*12*–*15*) by the presence of cerium, a cosmically rare element present in the glass covering the spacecraft solar panels. The remaining 25 so-called midnight tracks have trajectories that are consistent with an origin either in the interstellar dust stream or as ejecta from impacts on the lid of the sample return capsule (*20*). The ambiguity in origin of these 25 tracks is due to the articulation of the collector on its arm during the exposure (*27*). Because of the extremely limited amount of sample, we analyzed only the first 13 midnight tracks identified. Six showed aluminum x-ray absorption near-edge structure (XANES) spectra consistent with Al metal. These tracks are consistent with Al ejected from the sample return capsule by micrometeoroid impacts. Three tracks showed heavy-element abundances that pointed away from an extraterrestrial origin, and one could not be analyzed because of unusually high aerogel density. We focus here on three midnight tracks that are consistent with an extraterrestrial origin.

I1043,1,30,0,0 ("Orion") (Fig. 1) is a multicomponent, low-density particle compositionally consistent (see Table 1 for all particle characteristics) with a mixture of forsteritic olivine, magnesium-spinel, and iron-bearing phases with minor elements calcium, chromium, manganese, and nickel. Further composition details and discussion of errors are available (*21*). XRD and STXM analyses show a good fit to polycrystalline olivine, with mosaiced domains showing broadening in x-ray diffraction extending over 20°, nanocrystalline spinel, two undetermined crystalline phases of unknown composition, and an amorphous magnesium, aluminum oxide phase. One of the unidentified crystalline phases is consistent with iron metal nanoparticles. We derived an average density of ~0.7 g $cm^{-3}$. Elemental abundances normalized to magnesium and the composition of CI meteorites, whose abundances of nonvolatile elements are nearly identical to those of the Sun, and hence the bulk solar system, show 10-fold enrichments in aluminum and the minor element copper; depletions for silicon and calcium; and near normal iron, chromium, manganese, and nickel. Magnesium was used for normalization rather than the more usual silicon because its abundance could be measured precisely by STXM, whereas the silicon abundance is less certain owing to the silica aerogel background. Comparison of the Orion track morphology with hypervelocity analog shots (*17*) indicates a capture speed <10 km $s^{-1}$.

I1047,1,34,0,0: ("Hylabrook") (Fig. 2) is a magnesium-, iron-, and silicon-rich ~4-pg particle with a mosaiced, partially amorphized, forsteritic olivine core. This core is surrounded by a low-density halo, compositionally modeled as disordered magnesium-silicate, amorphous oxidized aluminum, amorphous metal oxides, and an iron-bearing phase, which may include reduced iron nanoparticles. The overall density of the particle (as captured) was ~0.3 g $cm^{-3}$. The major elements magnesium, silicon, and iron are present in CI-like relative proportions; magnesium-normalized elemental abundances show depletions in calcium and nickel, and enrichments in chromium, manganese, and copper, relative to CI. XRD data provide a good match to mosaiced olivine with an internal strain field up to 0.3%. The magnesium XANES spectrum shows that magnesium is present both in Hylabrook's crystalline core and in a partially amorphized olivine shell. The morphology of the track indicates that Hylabrook was also captured at <10 km $s^{-1}$ (*17*).

Comparison of the morphology of track I1003,1,40,0,0 ("Sorok") with laboratory experiments (*17*) indicates that the capture speed was >15 km $s^{-1}$ and that the original projectile had a mass of ~3 pg (Fig. 3). Silicon and carbon were detected in the track walls, but it is not clear whether the carbon is projectile residue, or carbon indigenous to the compressed aerogel, because carbon contamination is known to be present in the Stardust aerogel collectors (*28*). Organic materials are below detection limits in an FTIR analysis (*11*). Magnesium and aluminum were below detection limits in STXM analysis. If this particle had iron contents similar to those of Orion or Hylabrook and the entire particle residue were retained in the track, iron should have been detectable with STXM in the track walls. The nondetection of iron implies that either the original projectile was relatively iron-poor compared to Orion and Hylabrook, or that relatively little of the original projectile was retained in the track.

## Identification and analysis of candidates on the aluminum foil

We identified 25 crater-like features after an automated SEM-based search of 13 individual Al foils (*19*). Elemental analysis, by either Auger electron spectroscopy or energy dispersive x-ray

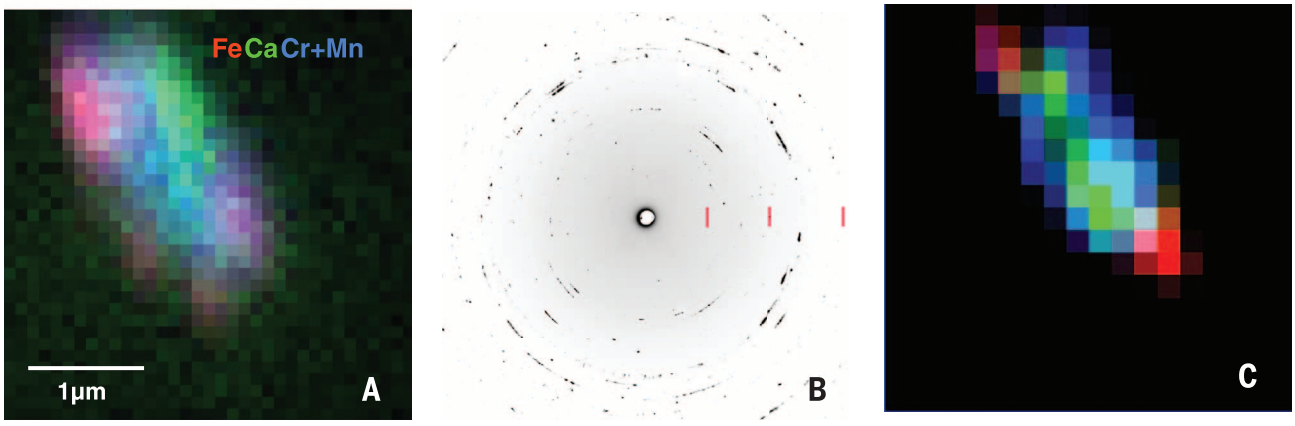


**Fig. 1. Track I1043,1,30,0,0 ("Orion").** (**A**) Tri-color iron, calcium, (chromium+manganese) elemental map derived from XRF data. Colors are scaled to span the entire range of each element. (**B**) XRD pattern taken at 13.9 keV. Tick marks at d-spacings of 6, 3, and 2 Å are indicated. (**C**) Phase map. Colors indicate olivine (green), spinel (red), and an unidentified phase (blue).

spectroscopy (EDS), indicates that most of these features are impacts from fragments of the spacecraft solar panels. These craters contain residues rich in elements that are associated with the solar panel cover glass (boron, cerium, zinc, and titanium) and antireflection coating (fluorine), and that are of low cosmic abundance. Five of the features are associated with native defects in the foil and are not impact craters. Four of the impact craters contain residues with compositions inconsistent with spacecraft origin or native foil defects. The diameter of these candidate interstellar craters ranges from 0.28 to 0.46 μm. The crater diameter ($D_c$) is a function of particle diameter ($D_p$), capture speed, and density (*23*, *24*), with $D_c \sim 1.6D_p$ for silica spheres impacting $Al_{1100}$ alloy at 6.1 km $s^{-1}$. Thus, the diameters of the particles that produced the craters range from ~0.2 to 0.3 μm. We extracted cross-sections of these craters with focused ion beam milling and then analyzed the cross-sections with scanning transmission electron microscopy (STEM) (*19*).

Dark-field STEM images and EDS maps (Fig. 4) of the cross-sections show the diversity of particle structure and composition. The residue in I1044N,3 is a silicate with a heterogeneous distribution of Mg, Si, and Fe, and no detectable sulfur. The residues in I1061N,3, I1061N,4, and I1061N,5 show both silicate and sulfide components. The shape of the crater provides an indication of the original distribution of the silicate and sulfide components, i.e, whether the impacting particle was a compact object with a single center of mass (1044N,3 and 1061N,3), or an aggregate with a few distinct centers of mass (I1061N,4 and I1061N,5). Quantitative individual element maps, including Ni, are shown in fig. S5.

Oxygen isotopic ratios were measured by secondary ion mass spectrometry on two of the crater cross-sections (*21*) and found to be consistent with solar system values within errors (Table 1). Oxygen isotope measurements of the two other craters were not possible owing to damage of the sections during transport between laboratories.

### Low probability of an interplanetary origin

The combination of the elemental compositions of the seven ISD candidates with their impact feature characteristics (i.e., track shape and direction, or crater morphology) demonstrates that they are extraterrestrial in origin. However, further information is needed to distinguish between a possible interplanetary origin and an interstellar origin. The determination of origin cannot be based on elemental composition alone, because of the similarity of the solar nebula and the LISM in gas composition, and the overlap in range of temperature and pressure conditions at which dust condenses. The products of gas-solid condensation in each environment will share some common phases, including amorphous and crystalline silicates, oxides, and potentially also sulfides. For example, a ubiquitous component of primitive, probably cometary, interplanetary dust particles (IDPs) consists of GEMS (glass with embedded metal and sulfides) particles, which are similar to the canonical ISD particle in size, composition, and lack of crystallinity in the silicate phase and thus have been argued to be preserved interstellar particles (*29*). However, the origin of GEMS remains highly controversial (*30*). Only a small fraction of GEMS particles have oxygen isotopic anomalies proving an origin outside the solar system, but particles formed in the ISM at the time of solar birth could have had solar isotopic signatures.

Three of the four crater ISD candidates show elemental compositions within the range reported for GEMS, and two of these have solar-system–like oxygen isotopic ratios. The lack of strong oxygen isotopic anomalies rules out an origin in stellar outflows as inferred for meteoritic presolar grains. However, as with GEMS, normal oxygen isotopic composition does not preclude an origin in the ISM, because the range of isotopic compositions measured in the present-day ISM overlaps solar system values (fig. S5). The fourth, I1044N,3, has a lower silicon and higher oxygen content than GEMS and is thus more consistent with average values for the ISM dust composition (*2*). Orion and Hylabrook are distinct from GEMS in size, composition, and/or degree of crystallinity, but both are composed of phases previously observed in interplanetary and circumstellar particles: Orion contains olivine and spinel-like amorphous oxide; the magnesium-rich amorphous content of Hylabrook appears to be a rim on an interior olivine, rather than a distinct amorphous silicate.

Because of the ambiguity in distinguishing interstellar and interplanetary origins on the basis of chemical and isotopic compositions, stronger constraints on the particle origin(s) come from the geometry of the Stardust interstellar collection. Modeling indicates that very few IDP impacts on the SIDC are expected to coincide with the

**Table 1. Summary of interstellar candidates.**

| ID | Mass or diameter | Composition | Structure | Capture speed (km $s^{-1}$) |
|---|---|---|---|---|
| I1043,1,30,0,0 ("Orion") | 3.1 ± 0.4 pg | Forsteritic olivine core ($Mg_2SiO_4$, 19 mol %), + nanocrystalline spinel + amorphous ($MgAl_2O_4$, 27 mol %) + Fe-bearing phase (47 mol %) with 7 mol % minor elements Cr, Mn, Ni, and Ca. | Low density (0.7 g $cm^{-3}$) | <<10 |
| I1047,1,34,0,0 ("Hylabrook") | 4.0 ± 0.7 pg | Forsteritic ($Fo_{>80}$) olivine core ($Mg_2SiO_4$ 30 mol %) surrounded by a low-density halo including amorphous Mg-silicate (1 mol %) + Al-, Cr-, Mn- (15 mol %), + Fe-bearing (54 mol %) phases. | Low density (<0.4 g $cm^{-3}$) | <<10 |
| I1003,1,40,0,0 ("Sorok") | ~3 pg | Possible Si + C | | > 15 |
| I1044N,3 | 0.28-μm crater | Mg, Fe-rich silicate (Mg+Fe)/Si = 3.3 | Single particle with chemical zoning | >10 |
| I1061N,3 | 0.37-μm crater | Silicate (Mg:Fe:Si = 0.58:0.22:1 atomic %) + FeS $\delta^{17}O = -13 \pm 30$‰, $\delta^{18}O = 11 \pm 13$‰, $^{18}O/^{17}O = 5.36 \pm 0.18$ (1σ errors) | Single particle or nanoscale aggregate | ~ 5 to 10 |
| I1061N,4 | 0.39-μm crater | Silicate (Mg:Fe:Si = 0.33:0.15:1 atomic%) + Fe, Ni metal and sulfide | Two-particle aggregate with zoning of metal and sulfide | ~ 5 to 10 |
| I1061N,5 | 0.46-μm crater | Silicate (Mg:Fe:Si 0.57:0.15:1 atomic %) + Fe metal and Fe, Ni sulfide $\delta^{17}O = -85 \pm 61$‰, $\delta^{18}O = -20 \pm 27$‰, $^{18}O/^{17}O = 5.61 \pm 0.36$ (1σ errors) | Nanoparticle aggregate | ~ 5 to 10 |

"midnight" direction where interstellar impacts occur (*10*, *19*), and we observed no tracks in the angular range where IDPs should have their maximum flux, indicating that the IDP background is small. Based on the observed angular distribution of captured particles, and model trajectories, the statistical likelihood of an interplanetary origin for all three interstellar dust candidates in aerogel is <0.03% (*10*, *20*). The ecliptic longitude of the interstellar dust radiant that best fits the observed trajectories of the three candidates in aerogel is somewhat larger than anticipated (*9*, *18*, *20*) based on observations from Ulysses and Galileo, but this may indicate a real long-term radiant shift, which is consistent with a long-term increase in radiant longitude in neutral helium, currently a topic of discussion (*22*, *31*).

Although the trajectories of the four foil interstellar candidates are unknown, statistical arguments based on trajectories still apply. We used the interplanetary micrometeoroid environment model (IMEM) (*21*, *32*) to estimate the fluence of IDPs >$10^{-14}$ g collected to be 0.17 $cm^{-2}$. The observed impact density of nonterrestrial materials on the foils is 0.8 $cm^{-2}$, and thus the fraction of impacts of interplanetary origin is estimated to be 0.17/0.8 = 0.2. This value is in good agreement with the preflight estimates of Landgraf *et al.* (*33*), who predicted a total collected particle count of 120 (80 <2 μm and 40 >2 μm diameter) interstellar particles and 20 IDPs. With the conservative assumption that all of the interplanetary dust is <2 μm, this equates to 100 small particles (80 interstellar and 20 interplanetary), of which 20% should be interplanetary. Based on the good agreement of these two model calculations, we take 20% to be the probability of an interplanetary origin for any one impact, and <0.16% to be the probability that all four craters are interplanetary in origin. The latter estimate assumes an uncorrelated origin for the impacting particles. A correlated origin as secondary ejecta from micrometeroid impacts on the sample capsule or solar cell array can be discounted: In the ejecta of such impacts, spacecraft material is expected to dominate over impactor material by about two orders of magnitude (*9*, *20*) and to have lower impact velocity and shallower impact depth than should be observed for interstellar candidate craters (*34*). This is inconsistent with the observed low ratio of target/projectile material in the impacts, even accounting for the low statistics (*35*), and the observed interstellar candidate crater morphologies. A correlated origin as fragments of asteroidal or other collisional products can also be discounted. Such an origin would require a mechanism for maintaining correlated particle trajectories over large distances, against the differential solar light pressure and Lorentz forces that act on this size of particles. We conclude that an interstellar origin is most likely for the four candidate impact craters.

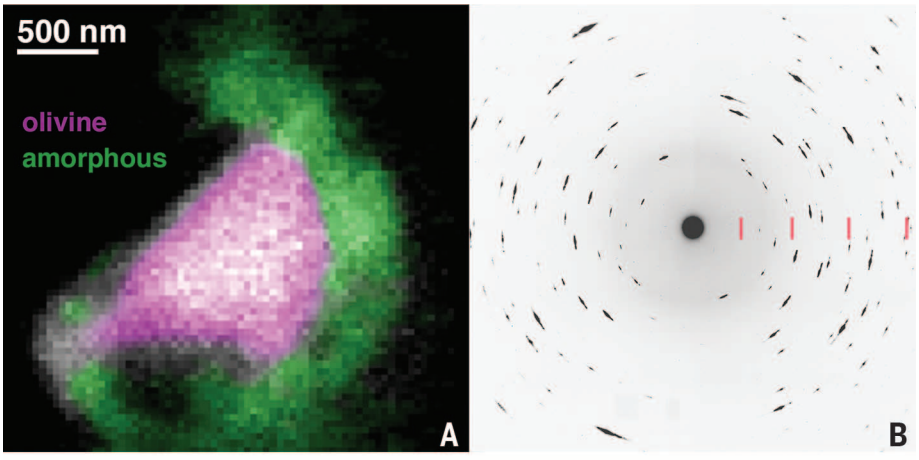


**Fig. 2. Track I1047,1,34,0,0 ("Hylabrook").** (**A**) Bi-color olivine + amorphous phase map derived from STXM Mg XANES data. (**B**) XRD pattern taken at 13.9 keV. Tick marks at d-spacings of 6, 3, 2, and 1.55 Å are indicated.

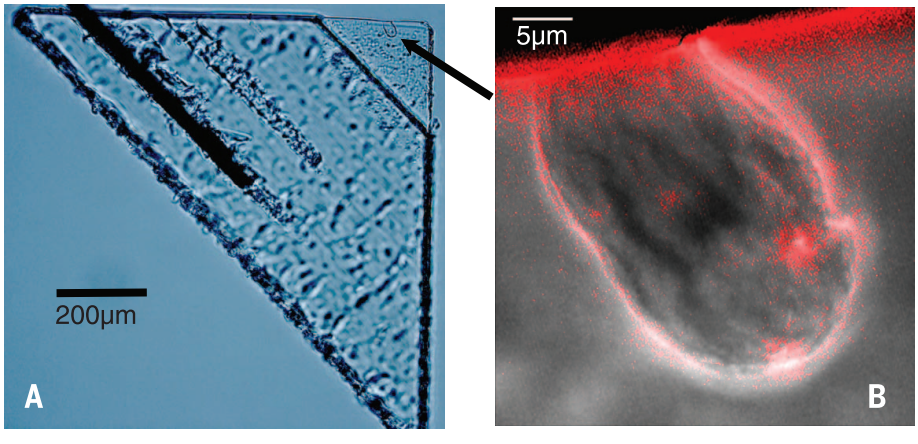


**Fig. 3. Track I1003,1,40,0,0 ("Sorok").** (**A**) Optical micrograph of Sorok in its picokeystone. (**B**) STXM absorption map at 280 eV with overlaid map of carbon (red).

## Implications for dust observations and modeling

Assuming that the captured particles are indeed all of interstellar origin, we can use their characteristics to address questions about the properties of contemporary interstellar dust. The particles in the aerogel and those in the foil represent two different size regimes. The particles captured in aerogel are >1 μm in diameter (~3 pg), which is consistent with the masswise dominant component of the dust sampled by in situ instruments on Ulysses and Galileo, but several hundred times more massive than the maximum dust size determined from observations of the ISM. The spectroscopic observations indicate a typical particle size of ~200 nm (~100 attograms for a density of ~2 g $cm^{-3}$). The particles captured in the Al foil are closer in size to that inferred for typical ISM particles by astronomical means. However, the in situ spacecraft data and models of heliospheric filtering (*18*) indicate that abundance of these particles is strongly reduced at 2 astronomical units compared to interstellar space than are the picogram-sized grains (*36*). Compared to the predictions prior to the Stardust sample return, we observed an order of magnitude fewer large particles (picogram-sized) and a factor of ~4 more small particles (attogram-sized) than expected from the in situ data.

The elemental compositions of the captured particles are generally consistent with expectations for ISD. Magnesium-rich silicates are common to all of the particles except Sorok, for which the actual particle composition could not be determined. In five of the particles (Orion, Hylabrook, and craters 1061N,3, 1061N,4, and 1061N,5), one or more distinct iron-rich phases were also observed. Some of the iron in Orion and Hylabrook may be in reduced form, and three of the particles captured in foil show FeS, and possibly metallic Fe. The chemical form of iron in ISD is uncertain. Estimates of the iron content of interstellar silicates vary widely [e.g., (*37*)], and the variation in Fe:Mg gas depletions in different regions of the ISM indicate that one or more iron-rich dust phases distinct from the magnesium-rich silicate are expected. The particular phase or phases are not known, because they do not provide distinct features in the ISM infrared (IR) spectra. Nanophase metallic Fe or FeS would be possible candidates, as both have broad, featureless IR spectra, and these phases are ubiquitous

components of primitive solar nebular materials and thus may also form as circumstellar and/or interstellar particles. The presence of a sulfide dust component in the ISM is a matter of debate. Most measurements of the ISM gas indicate little or no depletion of sulfur, compared to the solar abundance, which supports a lack of condensed sulfur-rich dust. However, uncertainty in determining the ISM gas-phase sulfur abundance and the difficulty of detecting nanophase sulfides with IR spectroscopy do not rule out the possibility that FeS nanoparticles are a component of ISM dust (*38*).

The crystallinity of the silicates in Orion and Hylabrook is unexpected. Spectroscopic measurements of interstellar silicates indicate that <2.2% are crystalline (*39*, *40*). Irradiation of the particles by gas accelerated by shockwaves in the diffuse intercloud medium are believed to effectively amorphize silicates in typical (~100 nm) ISD particles (*41*), but crystalline materials are probably preserved in the interiors of larger (>1 μm) particles. Crystalline silicates are observed in the outflows of oxygen-rich AGB stars (*42*) and observed as preserved presolar circumstellar particles in IDPs (*43*) and meteorites (*44*). Because the fraction of the mass contained in particles as large as Orion and Hylabrook (>3 pg) is <<1% of the condensed component of the ISM, the observation of crystalline material in them does not violate astronomical upper limits on silicate crystallinity (*39*, *40*). The mineralogical complexity of Orion may be consistent with assembly from small crystalline and amorphous components in a cold molecular cloud environment, whereas Hylabrook may be consistent with a single processed circumstellar condensate. This hypothesis may be testable by a future measurement of the isotopic composition of oxygen. The residues of the particles captured in the Al foil appear to be amorphous, but whether this is an original feature or an effect of hypervelocity capture alteration is unclear. Three of the four craters contain sulfides, whereas Orion contains only minor amounts of sulfur and Hylabrook has no appreciable sulfur content. This may be a further indication that larger particles sample a fundamentally different reservoir than small particles.

### Optical and mechanical properties inferred from dust dynamics and statistics

Our measured fluence of >1-μm-diameter particles is ~1/10 of the prelaunch estimate (*33*). Because we used control images to measure detection efficiency in the Stardust collector, we can be confident that the difference is not due to detection inefficiency of high-speed impacts. However, the dynamics of nanometer- and micrometer-size particles in the heliosphere are strongly affected by radiation pressure exerted by sunlight. To investigate whether repulsion of interstellar dust by sunlight might play a role in reducing the flux in the inner solar system, we compared our observations of the track diameter distribution for our interstellar candidates with predictions of a model of interstellar dust propagation based on the Ulysses and Galileo (U/G) observations. We used a standard model of the optical properties of interstellar dust as a function of particle size (*4*) and the high-speed laboratory calibrations of interstellar dust analogs carried out as part of the present effort (*17*). We observed a markedly lower flux of high-speed interstellar dust than predicted by this model (Fig. 5), but a model developed as part of the ISPE (*18*) in which the optical cross section of the dust is larger and which takes into account Lorentz forces, is consistent with the observations. Further, the standard model predicted that nearly all impacts would be at high speed (>>10 km $s^{-1}$), because the model of optical properties assumed relatively compact, high-density dust particles. However, two of the three candidate impacts >1 μm were captured with speeds <<10 km $s^{-1}$. These observations can be most easily understood if interstellar dust in this size range consists of low-density material with a wide distribution of β, the ratio of radiation pressure force to gravitational force. Canonical ISD structures (*2*) consistent with such

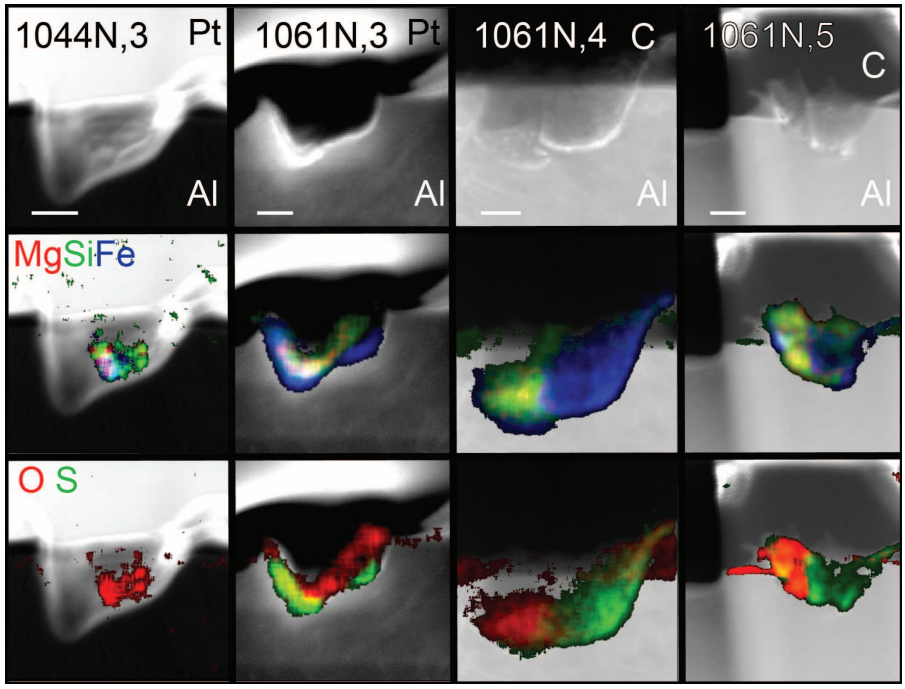


**Fig. 4. Candidate interstellar dust impacts in Al foil.** Dark-field STEM images (top row) and composite EDS element maps showing the Mg-Si-Fe and O-S distributions of the four candidate impacts. Pt and C refer to FIB-deposited protective masks. Scale bars: 100 nm.

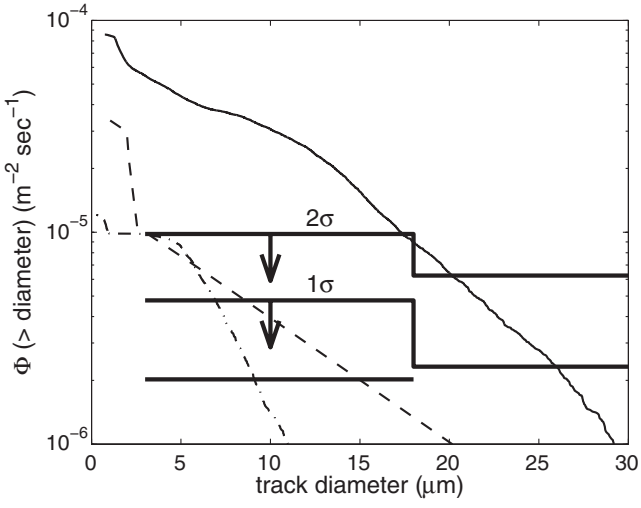


**Fig. 5. Observed and predicted interstellar dust fluence.** Comparison of the integral track areal density as a function of diameter observed in the Stardust aerogel collectors with the predictions of a model based on Ulysses and Galileo in situ observations (solid curve). The lower segment is the measured value, and stepped curves are 1σ and 2σ upper limits. For the prediction, we used an empirical model of track diameter versus particle diameter and capture speed derived from laboratory calibrations (*13*), and a standard model of β versus particle size (*4*). The dashed curve is a similar prediction based on work done under the ISPE (*18*), which includes a model of the optical properties of ISD with larger values of β, and includes Lorentz forces. The dot-dashed curve shows the same calculation, but with β taken to be three times the standard model of Landgraf *et al*. (*4*).

low-density particles include spheres with silicate cores and organic mantles, carbonaceous spheres, or aggregates of these. Of the seven candidate ISD particles, one is plausibly dominated by carbon and one is primarily a single silicate with a mantle-core structure, whereas the others are complex aggregates of various micrometer- to nanometer-size phases such as oxides, metal, and sulfides, in addition to silicate (Table 1).

The need for internal consistency leaves us with a twofold conclusion: If large interstellar dust particles consist of compact silicates with optical properties similar to those assumed by Landgraf *et al.* (*4*), then our results are in conflict with the U/G observations, and consistent with astronomical observations (*45*). By contrast, if large interstellar dust particles have low densities, which appears to be more likely based on trajectories, capture speeds, and compositions of our candidates, then our data can be consistent with the U/G observations, and possibly also with the astronomical observations, depending on the (currently unknown) wavelength dependence of the extinction cross sections of these particles. The latter conclusion is encouraging news for any future sample-return missions with the goal of capturing large numbers of relatively intact interstellar dust particles.

## REFERENCES AND NOTES


1. P. C. Frisch, J. D. Slavin, *Earth Planets Space* **65**, 175–182 (2013).
2. H. Kimura, I. Mann, E. K. Jessberger, *Astrophys. J.* **583**, 314–321 (2003).
3. B. T. Draine, *Annu. Rev. Astron. Astrophys.* **41**, 241–289 (2003).
4. M. Landgraf, W. J. Baggaley, E. Grun, H. Kruger, G. Linkert, *J. Geophys. Res. Space Phys.* **105**, 10343–10352 (2000).
5. E. Grün *et al.*, *Nature* **362**, 428–430 (1993).
6. H. Krüger *et al.*, *Planet. Space Sci.* **58**, 951–964 (2010).
7. All particle sizes heareafter are given in diameter, rather than radius.
8. D. Brownlee *et al.*, *Science* **314**, 1711–1716 (2006).
9. A. J. Westphal *et al.*, *Meteorit. Planet. Sci.* 10.1111/maps.12168 (2014).
10. D. R. Frank *et al.*, *Meteorit. Planet. Sci.* 10.1111/maps.12147 (2014).
11. H. A. Bechtel *et al.*, *Meteorit. Planet. Sci.* 10.1111/maps.12125 (2014).
12. A. L. Butterworth *et al.*, *Meteorit. Planet. Sci.* 10.1111/maps.12220 (2014).
13. F. E. Brenker *et al.*, *Meteorit. Planet. Sci.* 10.1111/maps.12206 (2014).
14. A. S. Simionovici *et al.*, *Meteorit. Planet. Sci.* 10.1111/maps.12208 (2014).
15. G. J. Flynn *et al.*, *Meteorit. Planet. Sci.* 10.1111/maps.12144 (2014).
16. Z. Gainsforth *et al.*, *Meteorit. Planet. Sci.* 10.1111/maps.12148 (2014).
17. F. Postberg *et al.*, *Meteorit. Planet. Sci.* 10.1111/maps.12173 (2014).
18. V. J. Sterken *et al.*, *Meteorit. Planet. Sci.* 10.1111/maps.12219 (2014).
19. R. M. Stroud *et al.*, *Meteorit. Planet. Sci.* 10.1111/maps.12136 (2014).
20. A. J. Westphal *et al.*, *Meteorit. Planet. Sci.* 10.1111/maps.12221 (2014).
21. Supplementary details are available on *Science* Online.
22. R. Lallement, J. L. Bertaux, *Astron. Astrophys.* **565**, A41 (2014).
23. M. C. Price *et al.*, *Meteorit. Planet. Sci.* **45**, 1409–1428 (2010).
24. M. C. Price *et al.*, *Meteorit. Planet. Sci.* **47**, 684–695 (2012).
25. A. T. Kearsley *et al.*, *Meteorit. Planet. Sci.* **43**, 41–73 (2008).
26. A. J. Westphal *et al.*, *Meteorit. Planet. Sci.* **39**, 1375–1386 (2004).
27. P. Tsou, D. E. Brownlee, S. A. Sandford, F. Horz, M. E. Zolensky, *J. Geophys. Res. Planets* **108**, 8113 (2003).
28. S. A. Sandford *et al.*, *Meteorit. Planet. Sci.* **45**, 406–433 (2010).
29. J. P. Bradley, *Science* **265**, 925–929 (1994).
30. L. P. Keller, S. Messenger, *Geochim. Cosmochim. Acta* **75**, 5336–5365 (2011).
31. P. C. Frisch *et al.*, *Science* **341**, 1080–1082 (2013).
32. V. Dikarev, E. Grün, M. Landgraf, W. J. Baggaley, D. P. Galligan, in *Proceedings of the Meteoroids 2001 Conference*, B. Warmbein, Ed. (2001), vol. 495, pp. 609–615.
33. M. Landgraf, M. Müller, E. Grün, *Planet. Space Sci.* **47**, 1029–1050 (1999).
34. M. J. Burchell, M. J. Cole, M. C. Price, A. T. Kearsley, *Meteorit. Planet. Sci.* **47**, 671–683 (2012).
35. N. Gehrels, *Astrophys. J.* **303**, 336–346 (1986).
36. H. Krüger, E. Grün, *Space Sci. Rev.* **143**, 347–356 (2009).
37. M. Min, J. W. Hovenier, L. B. F. M. Waters, A. de Koter, *Astron. Astrophys.* **489**, 135–141 (2008).
38. E. B. Jenkins, *Astrophys. J.* **700**, 1299–1348 (2009).
39. F. Kemper, W. J. Vriend, A. G. G. M. Tielens, *Astrophys. J.* **609**, 826–837 (2004).
40. F. Kemper, W. J. Vriend, A. Tielens, *Astrophys. J.* **633**, 534–534 (2005).
41. A. P. Jones, J. A. Nuth III, *Astron. Astrophys.* **530**, A44 (2011).
42. F. J. Molster, L. Waters, *Astromineralogy* **609**, 121–170 (2003).
43. S. Messenger, L. P. Keller, D. S. Lauretta, *Science* **309**, 737–741 (2005).
44. C. Vollmer, P. Hoppe, F. E. Brenker, C. Holzapfel, *Astrophys. J.* **666**, L49–L52 (2007).
45. B. T. Draine, *Space Sci. Rev.* **143**, 333–345 (2009).


## ACKNOWLEDGMENTS


We are deeply grateful to the Stardust@home dusters (list at http://stardustathome.ssl.berkeley.edu/sciencedusters), whose tremendous efforts were critically important to the success of this project. The ISPE consortium gratefully acknowledges the NASA Discovery Program for Stardust, the fourth NASA Discovery mission. NASA grants supported the following authors: NNX09AC36G—A.J.W., A.L.B., Z.G., R.L., D.Z., W.M., and J.V.K.; NNX09AC63G—C.F., R.D., A.L., W.J.O., K.S., and F.J.S.; NNH11AQ61I—R.M.S., H.C.G., and N.D.B.; NNX11AC21G—A.M.D., A.J.K., and T.S.; NNX11AE15G—G.J.F. The Advanced Light Source and the National Center for Electron Microscopy are supported by the Director, Office of Science, Office of Basic Energy Sciences, of the U.S. Department of Energy (DOE) under contract no. DE-AC02-05CH11231. Use of the National Synchrotron Light Source, Brookhaven National Laboratory, was supported by the U.S. DOE, Office of Science, Office of Basic Energy Sciences, under contract no. DE-AC02-98CH10886. Use of the Advanced Photon Source, an Office of Science User Facility operated for the U.S. DOE Office of Science by Argonne National Laboratory, was supported by the U.S. DOE under contract no. DE-AC02-06CH11357. M.T. and F.P. acknowledge support by Klaus Tschira foundation. A.A. and P.R.H. were supported by the Tawani Foundation. M.J.B. and M.C.P. are supported by Science and Technology Facilities Council (UK). F.E.B., J.K.H., P.H., J.L., F.P., S.S., R.S., and M.T. were supported by funding of the German Science Foundation (DFG) within SPP1385: the first ten million years of the solar system—a planetary materials approach. The ESRF ID13 measurements were performed in the framework of ESRF LTP EC337, with financial support by the Funds for Scientific Research (FWO), Flanders, Belgium (contract nr. G.0395.11, G.0257.12N and Big Science program G.0C12.13). G. Silversmit was postdoctoral fellow of the FWO during the ISPE investigations. Data presented in this paper are described in the supplementary materials and in references (*9*–*20*).


## SUPPLEMENTARY MATERIALS

www.sciencemag.org/content/345/6198/786/suppl/DC1
Materials and Methods
Supplementary Text
Figs. S1 to S8
Tables S1 to S3
References (*46*–*56*)


21 February 2014; accepted 9 July 2014
10.1126/science.1252496


REPORTS

INTERSTELLAR MEDIUM

# Pseudo–three-dimensional maps of the diffuse interstellar band at 862 nm


**Janez Kos,[1]* Tomaž Zwitter,[1] Rosemary Wyse,[2] Olivier Bienaymé,[3] James Binney,[4] Joss Bland-Hawthorn,[5] Kenneth Freeman,[6] Brad K. Gibson,[7] Gerry Gilmore,[8] Eva K. Grebel,[9] Amina Helmi,[10] Georges Kordopatis,[8] Ulisse Munari,[11] Julio Navarro,[12] Quentin Parker,[13,14,15] Warren A. Reid,[13,14] George Seabroke,[16] Sanjib Sharma,[5] Arnaud Siebert,[3] Alessandro Siviero,[17,18] Matthias Steinmetz,[18] Fred G. Watson,[15] Mary E. K. Williams[18]**



**The diffuse interstellar bands (DIBs) are absorption lines observed in visual and near-infrared spectra of stars. Understanding their origin in the interstellar medium is one of the oldest problems in astronomical spectroscopy, as DIBs have been known since 1922. In a completely new approach to understanding DIBs, we combined information from nearly 500,000 stellar spectra obtained by the massive spectroscopic survey RAVE (Radial Velocity Experiment) to produce the first pseudo–three-dimensional map of the strength of the DIB at 8620 angstroms covering the nearest 3 kiloparsecs from the Sun, and show that it follows our independently constructed spatial distribution of extinction by interstellar dust along the Galactic plane. Despite having a similar distribution in the Galactic plane, the DIB 8620 carrier has a significantly larger vertical scale height than the dust. Even if one DIB may not represent the general DIB population, our observations outline the future direction of DIB research.**


Diffuse instellar bands (DIBs) are wide and sometimes structured absorption lines in the optical and near-infrared (NIR) wavelengths that originate in the interstellar medium (ISM) and were discovered in 1922 (*1*, *2*); more than 400 are known today (*3*), but their physical carriers are still unidentified (*4*–*8*). Their abundances are correlated with interstellar extinction and with abundances of some simple molecules (*9*), so DIBs are probably

associated with carbon-based molecules (*2*). DIBs show no polarization effects (*1*) and are likely positively charged (*10*), as suggested by the relatively low energies of absorbed photons (*11*). No known transition of any molecule or atom has yet been found to match the central wavelengths of the DIBs (*2*). Their origin and chemistry are thus unknown, a unique situation given the distinctive family of many absorption lines within a limited spectral range. Like most molecules in the ISM that have an interlaced chemistry, DIBs may play an important role in the life-cycle of the ISM species and are the last step to fully understanding the basic components of the ISM. The problem of their identity is more intriguing given the possibility that the DIB carriers are organic molecules. DIBs remain a puzzle for astronomers studying the ISM, physicists interested in molecular spectra, and chemists studying possible carriers in the laboratories.

The maps presented here are based on data from the recently completed RAVE (Radial Velocity Experiment) spectroscopic survey (*12*) and are limited to one DIB. However, extensive surveys of Galactic stars (*13*–*17*) that are starting now will permit spatial mapping, the study of environmental constraints, and a comparison of the spatial distribution for over a dozen DIBs, interstellar molecules, and dust with techniques similar to the ones described here. Large spectroscopic surveys observing ~$10^5$ stars are a big leap forward from previous DIB-specific surveys, in which only a few thousand stars were observed at most (*18*, *19*), or only around a hundred stars, if weaker DIBs were observed (*20*).

Making a three-dimensional (3D) map of an ISM species from absorption lines in stellar spectra is a challenge, requiring a large number of observed lines of sight with measured abundances of the ISM species, as well as the distances to the observed stars. The DIB carrier can be found anywhere along the line of sight to the observed star, so the distance to the DIB carrier is uncertain, with only an upper limit from the distance to the star. It can only be established through the observations of many stars within a small solid angle but at different distances. To produce a map, such sets of observations must be achievable in any direction. The RAVE survey fulfills these requirements. In the pre-Gaia era, we have precise distances only to Hipparcos stars and a few others. For maps to be made at distances larger than the Hipparcos sample, spatial resolution must be sacrificed, as the distance measurements are less precise and errors in distance calculations will exceed the typical size of the ISM clumps.

DIBs are more numerous than absorption lines of other ISM species in the optical and NIR bands and are therefore ideal to be studied in general spectroscopic surveys, as they are present in almost any band observed by the surveys mentioned above. Having observations of multiple DIBs also allows the study of different parameters (*21*) of the ISM apart from observing the spatial distribution of a single species.

DIBs are traditionally observed in the spectra of hot stars, where interstellar lines rarely blend with stellar ones, but hot stars are intrinsically rare. With new analytical methods (*22*, *23*), it is possible to observe DIBs in the spectra of cool stars, which dominate in most spectroscopic surveys. In the (magnitude-limited) RAVE survey, only 1.1% of the stars have effective temperature above 8000 K. Our method makes use of a large database of RAVE spectra and requires neither knowledge of stellar parameters nor the use of synthetic spectra (*22*). For each spectrum, a number of most-similar stellar spectra were

[1]Faculty of Mathematics and Physics, University of Ljubljana, Jadranska 19, 1000 Ljubljana, Slovenia. [2]Johns Hopkins University, Homewood Campus, 3400 North Charles Street, Baltimore, MD 21218, USA. [3]Observatoire astronomique de Strasbourg, Université de Strasbourg, CNRS, 11 rue de l'Université, F-67000 Strasbourg, France. [4]Rudolf Peierls Centre for Theoretical Physics, Keble Road, Oxford OX1 3NP, UK. [5]Sydney Institute for Astronomy, School of Physics A28, University of Sydney, NSW 2008, Australia. [6]Research School of Astronomy and Astrophysics, Australian National University, Canberra, Australia. [7]Chair, Computational Astrophysics, Jeremiah Horrocks Institute, University of Central Lancashire, Preston PR1 2HE, UK. [9]Institute of Astronomy, Madingley Road, Cambridge CB3 0HA, UK. [9]Astronomisches Rechen-Institut, Zentrum für Astronomie der Universität Heidelberg, Mönchhofstraße 12–14, D-69120 Heidelberg, Germany. [10]Kapteyn Astronomical Institute, Post Office Box 800, NL-9700 AV Groningen, Netherlands. [11]Instituto Nazionale di Astrofisica Astronomical Observatory of Padova, 36012 Asiago (VI), Italy. [12]University of Victoria, Victoria BC, Canada V8P 5C2. [13]Department of Physics and Astronomy, Macquarie University, Sydney, NSW 2109, Australia. [14]Centre for Astronomy, Astrophysics and Astrophotonics, Macquarie University, Sydney, NSW 2109, Australia. [15]Australian Astronomical Observatory, Post Office Box 915, North Ryde, NSW 1670, Australia. [16]Mullard Space Science Laboratory, University College London, Holmbury St Mary, Dorking RH5 6NT, UK. [17]Department of Physics and Astronomy, Padova University, Vicolo dell'Osservatorio 2, I-35122 Padova, Italy. [18]Leibniz-Institut für Astrophysik Potsdam (AIP), An der Sternwarte 16, 14482 Potsdam, Germany.
***Corresponding author. E-mail: janez.kos@fmf.uni-lj.si**

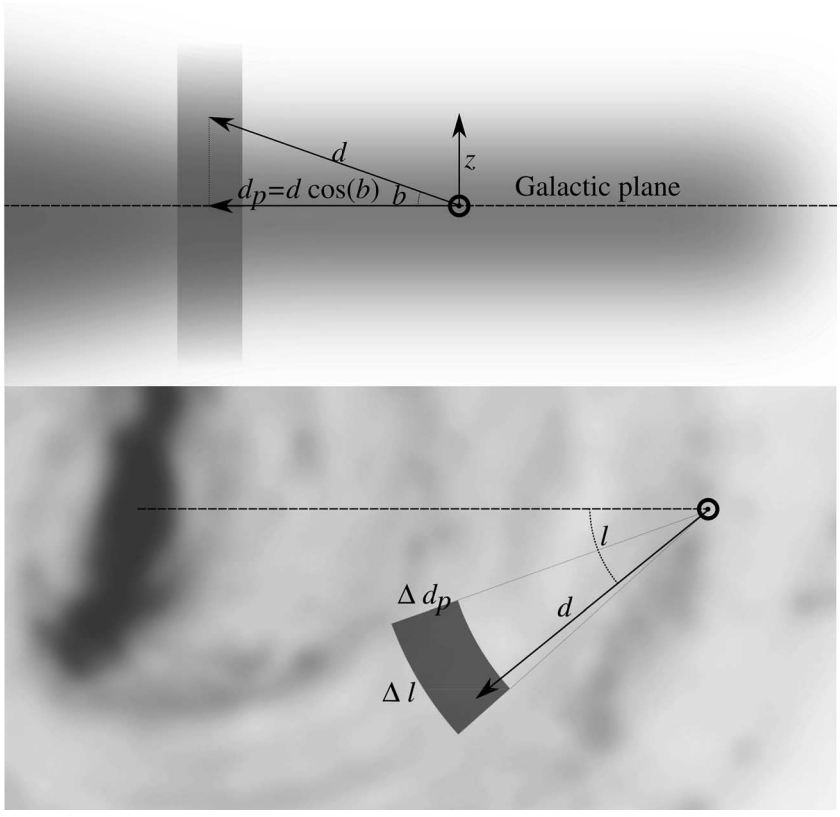


**Fig. 1. Coordinate system for spatial sampling of the DIB carrier and dust in the Galaxy. Top:** Side-view of two columns, representing two bins (one stretching from the Galactic plane in the positive *z* direction and one in the negative *z* direction), giving two data points, one for each Galactic hemisphere. The height of the column above (or below) the Galactic plane is limited to 1.5 kpc in *z* and 40° in Galactic latitude, primarily to avoid using any spectra that were normalized by a large factor, as the normalization enhances the noise. Because most of the gas and dust is located near the Galactic plane, this limitation should not influence the final results. **Bottom:** Face-on view of one column, representing one bin, giving one data point. The columns are segments of equally spaced cylindrical shells. In the first shell, there are three columns, and in each following shell there are $3(2n - 1)$ columns, where *n* is the number of the shell. All the columns thus have the same area of the cross-section and are as close to square as possible. To calculate the maps with different spatial resolutions, only the width of the shell is changed. *d* is the distance to a star, $d_p$ is the distance projected onto the Galactic plane, *b* and *l* are the Galactic latitude and longitude.

found in regions with very low extinction at high Galactic latitudes. From these spectra, we generated a stellar template to divide out the stellar contribution in the target spectrum. This leaves only the interstellar features in the spectrum: in this case, only the DIB at 862 nm. A detailed description of the DIB extraction method can be found in (*22*), which also shows that the RAVE data satisfy the prerequisities for the analysis of this paper: The DIB 8620 can be detected after the combination of several RAVE spectra; it can be detected at high Galactic latitudes; and the DIB strength correlates with the interstellar extinction. The DIB in (*22*) is measured more precisely than the extinction, as is reflected in the correlation plots.

Distances and extinctions are calculated jointly by a Bayesian algorithm (*24*). As input it takes photometric data and spectroscopic parameters of stellar atmospheres measured in RAVE survey, and it assumes asymptotic values of extinction from the SFD maps (*25*), corrected accordingly to known deviations. The value of the total V-band extinction, $A_V$, is the calculated parameter. [See (*26*) for a more detailed description.]

The number of observed stars in the RAVE proved to be high enough for this study only in the nearest 3 kpc of the Galaxy (*26*). The signal-to-noise (S/N) ratio of an individual RAVE spectrum is too low (the mode of the S/N values is 25) to detect the DIB in the spectrum of an individual star, so several spectra were combined to achieve a S/N ratio of ~300. The DIB is generally detectable in these combined spectra, and its strength can be measured with a precision of 10 to 20% [for details on combining spectra, see (*22*)]. This requirement to combine spectra is the limiting factor in the achievable spatial resolution. The resolution of a true 3D map would be low, so we produced a pseudo-3D map, where the distribution of the carrier in the $z$ direction (perpendicular to the Galactic plane) is described by an exponential law with a fixed scale height and a variable in-plane scaling factor, represented by a 2D map separately for the northern and the southern Galactic hemisphere (Fig. 1). Because of the highly variable star density in different volumes, the final maps vary in spatial resolution, between 75 and 400 pc. This allowed us to cover a wider volume of the Galaxy than we could with a better, but fixed, resolution. Combining spectra in a given bin also improved the distance value of each bin: Distance errors of 25% for individual stars are reduced when averaging over all stars in a bin, so that the error on the bin distance becomes smaller than the bin size.

An exponential law is a good approximation of the spatial distribution of the interstellar dust, as well as the strength of the DIB at 862 nm in the direction perpendicular to the Galactic plane (Fig. 2). The scale heights of the DIB and dust components differ significantly: 117.7 ± 4.7 pc

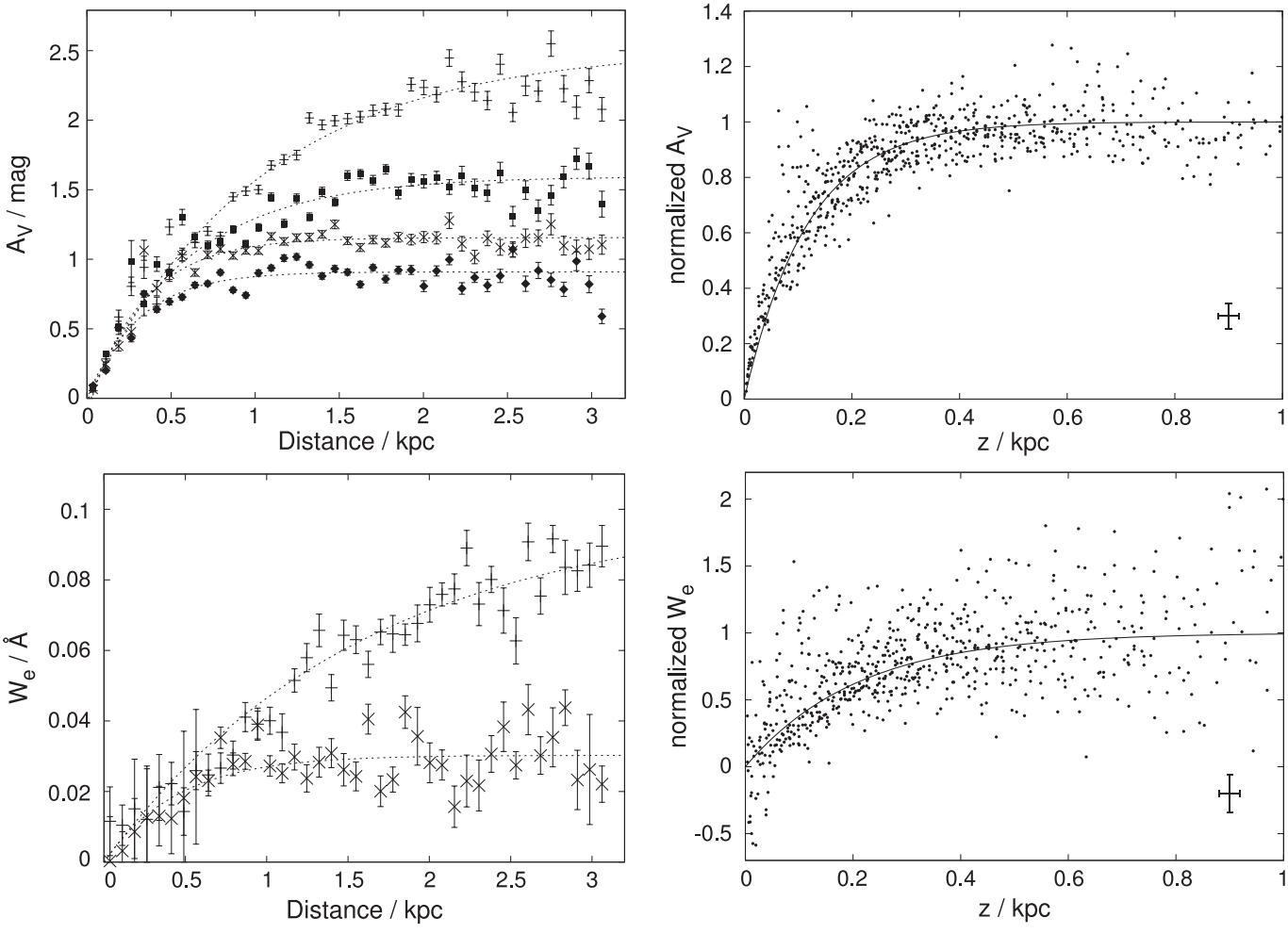


**Fig. 2. Determination of the scale height perpendicular to the Galactic plane.** The average extinction ($A_V$) was calculated by a Bayesian algorithm [top left (*26*)] and equivalent width ($W_e$) of the DIB (bottom left) of stars in 2° wide regions at different central Galactic latitudes ($b$) are shown as a function of distance. The averages extend over all longitudes in every region. Only four examples for the extinction (top to bottom: $b$ = −6°, $b$ = −10°, $b$ = −14°, $b$ = −18°) and two for the DIB (top to bottom: $b$ = −6°, $b$ = −14°) out of 20 regions are plotted here. Dashed curves are fitted exponential models. Data points from all 20 regions are represented in the same plot for the extinction (top right) and for the DIB (bottom right). Instead of the distances $d$, the distance from the Galactic plane $z = d \sin(|b|)$ was used, and each was normalized to unity to make the data at all Galactic latitudes comparable. The solid line is the fitted exponential model. Error bars in the bottom right corner represent a typical error of the data points.

for the dust and 209.0 ± 11.9 pc for the DIB-bearing gas. These two scale heights were used as constants uniformly through the whole region of the Galaxy included in this study. Some of the gas components, such as $H_2$ or CO (87 pc) (*27*, *28*) and probably Na I (<200 pc) (*29*), are consistent with the vertical distribution of the dust layer that we find, while a larger thickness of the DIB layer is similar to the one of Ca II (>200 pc) (*29*). H I has a profile of many components with an average half width at half maximum of 115 pc and large fluctuations (*30*). Massive stars, with a high ultraviolet luminosity, have a scale height even smaller than dust (*31*).

The strength of the DIB is measured as its equivalent width. The projected equivalent width has been normalized by an exponential law (*26*) and represents the equivalent width that would be measured if both the observer and the star were in the Galactic plane. The resulting maps show some distinctive features (Fig. 3). Most notable are large, narrow cavities, where the column density is low. In between these underdense regions lie clouds of the ISM, some with gentle increases in column density and some with well-defined boundaries. The smoother transitions are probably due to several less prominent clouds at different Galactic latitudes that collectively produce a gradient in that direction. We could recognize some known absorbing clouds (*26*), but the identification of other features is more difficult, as all the information in the $z$ direction is condensed into two data points, one for each hemisphere. Although spiral arms are elusive, a steeper rise in density is observed toward the longitudes between 320° and 60°, toward the Sagittarius arm and the Orion spur. We note that the projected equivalent width can decrease with distance. Different bins can represent stars at different Galactic latitudes, and the stars included in one bin can have more ISM in front of them than stars included in a more distant bin at the same Galactic longitude. However, the general rise that we find in the DIB equivalent width with distance increases confidence in the maps.

Because this work only studies one DIB, the detailed results should not be generalized to other DIBs. It is known, from other studies, that different DIBs show different behavior. The main difference that is expected among other DIBs is in the value of the vertical scale height and not so much in the projected equivalent width, because the former has little influence on the quite good correlation between DIBs and the interstellar extinction.

The projected distribution of the DIB-bearing gas (Fig. 3) is the first plot of its kind, as it is the

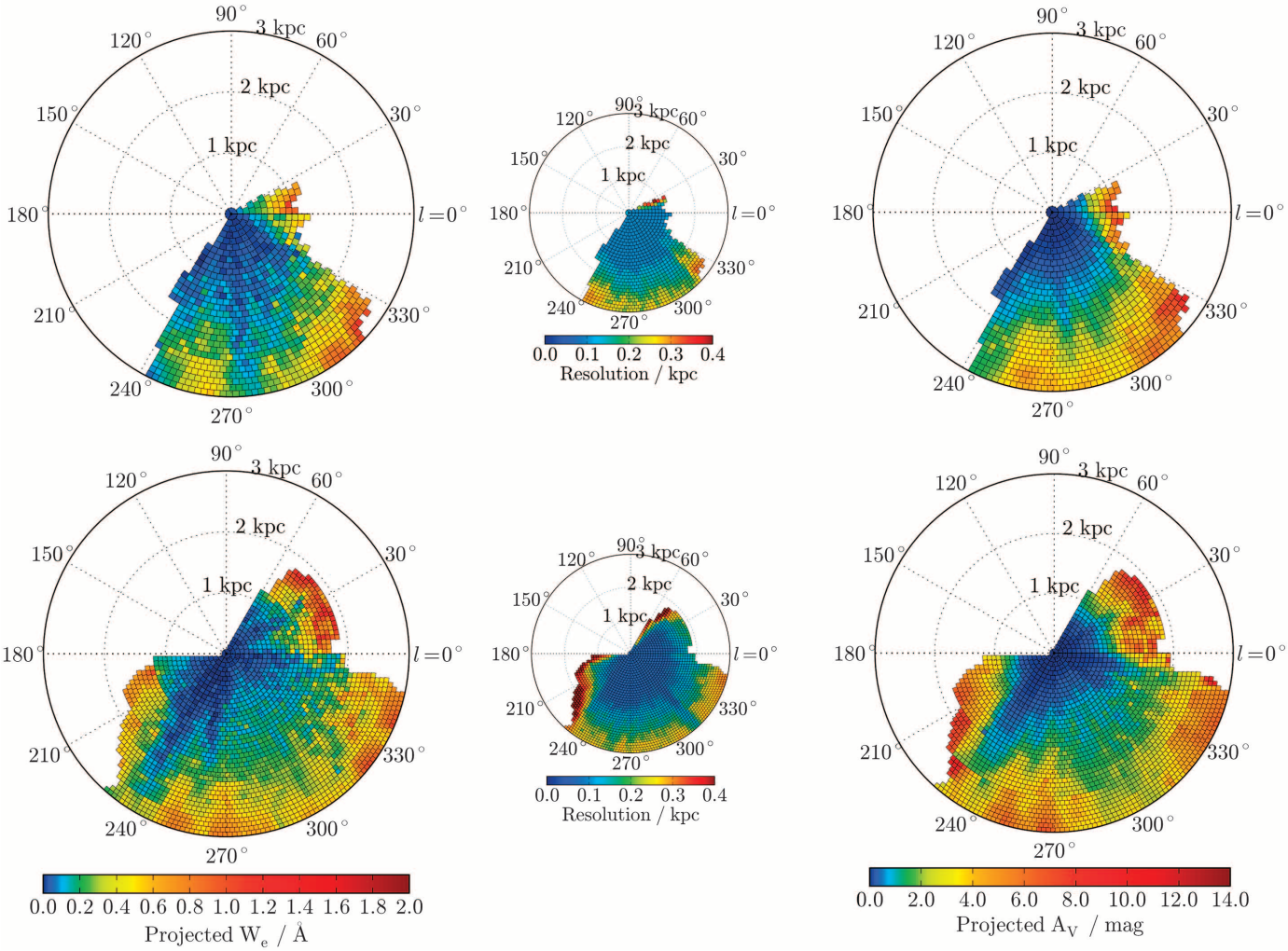


**Fig. 3. Projected equivalent width of the DIB at 862 nm, projected extinction, and the corresponding spatial resolution of the map.** The large maps show a color-coded projected equivalent width (left) and projected extinction (right). The small maps show the spatial resolution. Top and bottom three maps correspond to the northern and to the southern Galactic hemisphere, respectively. Notice the nonlinear color scale. Individual maps with spatial resolution between 0.8 and 0.075 kpc were used to make this combined result (*26*). The Sun is in the center of each map, with projected polar coordinates of the Galactic plane distance and the Galactic longitude. The stars analyzed in this study are located south of the celestial equator, which is why Galactic longitude and distance are incompletely sampled between the $l$ ~ 0° and $l$~ 210°. There are 1292 bins on the maps for the northern and 2212 bins on the maps for the southern Galactic hemisphere. The typical relative error of the extinction value in each bin is 14% and the relative error for the $W_e$ is 12%.

only map of any DIB carrier at this scale and the only one taking the distance information as a major parameter. Together with the measured scale height, this is the first 3D study of the spatial distribution of the DIB-bearing ISM clouds. The projected distribution of the extinction due to the interstellar dust is markedly similar to that of the DIB carrier [see (*26*) for the correlation analysis], confirming the strong correspondence between the two (*32*). The map of the extinction is itself an advance, as it maps the regions out of the Galactic plane and probes dust to greater distances than present maps (*33*) of these regions and is consistent with maps in the literature. Our success in producing the maps of the DIB carrier implies good prospects for future spectroscopic surveys (*14*–*16*) that will produce similar (*15*) or better quality (*14*, *16*) spectra and will also rely on DIBs to provide information about the ISM. Our work opens new possibilities in the study of DIBs and also offers a unique way of comparing DIBs with other interstellar species by studying their out-of-plane distribution. This can be translated into the study of physical and chemical properties of DIB carriers in the near future.

The measured 3D distribution, especially the unexpectedly high scale-height of the DIB 8620 carrier, calls for a theoretical explanation. There are two options—either the DIB carriers migrate to their observed distances from the Galactic plane, or they are created at these large distances, from components of the ISM having a similar distribution. The latter is simpler to discuss, as it does not require knowledge of the chemistry of the DIB carrier or processes in which the carriers are involved. Khoperskov and Shchekinov (*34*) showed that mechanisms responsible for dust migration to high altitudes above the Galactic plane segregate small dust particles from large ones, so the small ones form a thicker disk. This is also consistent with the observations of the extinction and reddening at high Galactic latitudes (*35*).

## REFERENCES AND NOTES


1. G. H. Herbig, *Annu. Rev. Astron. Astrophys.* **33**, 19–73 (1995).
2. P. J. Sarre, *J. Mol. Spectrosc.* **238**, 1–10 (2006).
3. L. M. Hobbs *et al.*, *Astrophys. J.* **705**, 32–45 (2009).
4. G. Galazutdinov, B.-C. Lee, I.-O. Song, M. Kazmierczak, J. Krełowski, *Mon. Not. R. Astron. Soc.* **412**, 1259 (2011).
5. J. Krełowski *et al.*, *Astrophys. J.* **714**, L64 (2010).
6. F. Salama, G. A. Galazutdinov, J. Krełowski, L. J. Allamandola, F. A. Musaev, *Astrophys. J.* **526**, 265–273 (1999).
7. S. Iglesias-Groth *et al.*, *Mon. Not. R. Astron. Soc.* **407**, 2157–2165 (2010).
8. J. P. Maier *et al.*, *Astrophys. J.* **726**, 41 (2011).
9. J. A. Thorburn *et al.*, *Astrophys. J.* **584**, 339–356 (2003).
10. D. Milisavljevic *et al.*, *Astrophys. J.* **782**, L5 (2014).
11. A. G. G. M. Tielens, *The Physics and Chemistry of the Interstellar Medium* (Cambridge Univ. Press, Cambridge, 2005).
12. G. Kordopatis *et al.*, *Astron. J.* **146**, 134 (2013).
13. D. J. Eisenstein *et al.*, *Astron. J.* **142**, 72 (2011).
14. G. Gilmore *et al.*, *Messenger* **147**, 25–31 (2012).
15. J. H. J. de Bruijne, *Astrophys. Space Sci.* **341**, 31–41 (2012).
16. K. C. Freeman, *Galactic Archaeology: Near-Field Cosmology and the Formation of the Milky Way*, W. Aoki, M. Ishigaki, T. Suda, T. Tsujimoto, N. Arimoto, Eds. (2012), vol. 458 of *Astronomical Society of the Pacific Conference Series*, p. 393.
17. L.-C. Deng *et al.*, *Res. Astron. Astrophys.* **12**, 735–754 (2012).
18. T. P. Snow Jr., D. G. York, D. E. Welty, *Astron. J.* **82**, 113 (1977).
19. J. T. van Loon *et al.*, *Astron. Astrophys.* **550**, A108 (2013).
20. S. D. Friedman *et al.*, *Astrophys. J.* **727**, 33 (2011).
21. J. Kos, T. Zwitter, *Astrophys. J.* **774**, 72 (2013).
22. J. Kos *et al.*, *Astrophys. J.* **778**, 86 (2013).
23. H.-C. Chen *et al.*, *Astron. Astrophys.* **550**, A62 (2013).
24. J. Binney *et al.*, *Mon. Not. R. Astron. Soc.* **437**, 351–370 (2014).
25. D. J. Schlegel, D. P. Finkbeiner, M. Davis, *Astrophys. J.* **500**, 525–553 (1998).
26. Supplementary materials are available on *Science* Online.
27. D. B. Sanders, P. M. Solomon, N. Z. Scoville, *Astrophys. J.* **276**, 182 (1984).
28. J. G. A. Wouterloot, J. Brand, W. B. Burton, K. K. Kwee, *Astron. Astrophys.* **230**, 21 (1990).
29. K. R. Sembach, A. C. Danks, *Astron. Astrophys.* **289**, 539 (1994).
30. J. M. Dickey, F. J. Lockman, *Annu. Rev. Astron. Astrophys.* **28**, 215–259 (1990).
31. S. Sharma, J. Bland-Hawthorn, K. V. Johnston, J. Binney, *Astrophys. J.* **730**, 3 (2011).
32. U. Munari *et al.*, *Astron. Astrophys.* **488**, 969–973 (2008).
33. G. A. Gontcharov, *Astron. Lett.* **36**, 584–595 (2010).
34. S. A. Khoperskov, Y. A. Shchekinov, Transport of charged dust grains into the galactic halo (2014); http://arxiv.org/abs/1403.7075 .
35. J. E. G. Peek, Ultraviolet extinction at high galactic latitudes II: The ultraviolet extinction function (2013); http://arxiv.org/abs/1311.2941.



## ACKNOWLEDGMENTS

We are grateful to the anonymous referees for valuable advice on the discussion of possible DIB origins. J.K. and T.Z. thank A. F. Kodre for a stimulating discussion of the topic. Funding for RAVE has been provided by the Anglo-Australian Observatory; the Leibniz-Institut für Astrophysik Potsdam; the Australian National University; the Australian Research Council; the French National Research Agency; the German Research Foundation (SFB 881); the Istituto Nazionale di Astrofisica at Padova; The Johns Hopkins University; the U.S. National Science Foundation (AST-0908326); the W. M. Keck foundation; the Macquarie University; the Netherlands Research School for Astronomy; the Natural Sciences and Engineering Research Council of Canada; the Slovenian Research Agency; Center of Excellence Space.si; the Swiss National Science Foundation; the Science and Technology Facilities Council of the UK; Opticon; Strasbourg Observatory; European Research Council; and the Universities of Groningen, Heidelberg, and Sydney. The RAVE Web site is at www.rave-survey.org.


## SUPPLEMENTARY MATERIALS

www.sciencemag.org/content/345/6198/791/suppl/DC1
Materials and Methods
Supplementary Text
Figs. S1 to S3
References

10 March 2014; accepted 19 June 2014
10.1126/science.1253171

ROBOTICS

# Programmable self-assembly in a thousand-robot swarm

**Michael Rubenstein,* Alejandro Cornejo, Radhika Nagpal**

**Self-assembly enables nature to build complex forms, from multicellular organisms to complex animal structures such as flocks of birds, through the interaction of vast numbers of limited and unreliable individuals. Creating this ability in engineered systems poses challenges in the design of both algorithms and physical systems that can operate at such scales. We report a system that demonstrates programmable self-assembly of complex two-dimensional shapes with a thousand-robot swarm. This was enabled by creating autonomous robots designed to operate in large groups and to cooperate through local interactions and by developing a collective algorithm for shape formation that is highly robust to the variability and error characteristic of large-scale decentralized systems. This work advances the aim of creating artificial swarms with the capabilities of natural ones.**

In nature, groups of thousands, millions, or trillions of individual elements can self-assemble into a wide variety of forms, purely through local interactions. Examples can be found across a wide range of physical scales and systems: at the molecular scale with self-assembly of crystals or rotary motors of bacterial flagella (*1*, *2*), at the cellular scale with the development of multicellular organisms (*3*, *4*), and at the colony level with ants creating structures such as rafts, chains, and nests (bivouacs) using only their interconnected bodies as building material (*5*, *6*). Through collective shape formation, a group can dramatically change how it interacts with its environment. For example, the evolution of multicellular body plans enabled organisms to rapidly fill many ecological niches (*7*), and self-assembly of bridges and bivouacs allows army ant colonies to traverse difficult terrain while providing security and environmental regulation for the queen and brood (*5*). These examples of collective intelligence are fascinating to scientists across disciplines, as much of the global complexity arises from interactions among individuals that are myopic, sensing and interacting at scales many orders of magnitude smaller than the phenomenon itself.

In the field of robotics, researchers use inspiration from collective intelligence in nature to create artificial systems with capabilities observed in natural swarms. Researchers have designed tiny robots, inspired by bees and ants, that are envisioned to work together in large groups, even assembling together to cross difficult terrains (*8*–*10*). Similarly, using inspiration from multicellular development, several groups have

School of Engineering and Applied Sciences and Wyss Institute for Biologically Inspired Engineering, Harvard University, Cambridge, MA 02138, USA.
***Corresponding author. E-mail: mrubenst@seas.harvard.edu**

developed self-assembling "cellular" robots that can reconfigure into many morphologies to complete different grasping or locomotion tasks (*11*), or can act as programmable matter that can rapidly assemble into user-specified tools such as a wrench or key (*12*, *13*). However, there still exists a substantial gap between the conceptual designs and the realized systems. Increasing the scale of autonomous robotic systems remains a significant challenge both for algorithm and hardware design. Current systems are on the order of 10 to 50 robots, with only a few exceeding 100 robots (*14*, *15*), in part because of cost and design choices that make manufacturing and operations difficult. This lack of large-scale physical systems has in turn hindered experimental investigation of algorithms for engineering self-assembly and other forms of complex collective intelligence. Although simulators are a valuable tool for systematically exploring algorithm behavior, they frequently involve simplifications for computational tractability. Such simulated systems can fail to faithfully reproduce the intricate physical interactions and variability that exist in real systems, and their fidelity to the real world is difficult to verify or improve without feedback from physical experiments.

We report a system that addresses both the physical and algorithmic challenges of robotic swarms. We demonstrate a thousand-robot swarm capable of large-scale, flexible self-assembly of two-dimensional shapes entirely through programmable local interactions and local sensing, achieving highly complex collective behavior. The approach involves the design of a collective algorithm that relies on the composition of basic collective behaviors and cooperative monitoring for errors to achieve versatile and robust group behavior, combined with an unconventional physical robot design that enabled the creation of more than 1000 autonomous robots.

In designing a large-scale robot swarm, the extent to which the robots can be fully autonomous (capable of computation, locomotion, sensing, and communication) must be balanced against the cost per robot. Mass production favors robots with fewer and cheaper components, resulting in lower cost but also reduced capabilities and reliability. Additionally, operations such as powering on/off, reprograming, and charging must be addressed; at the scale of a thousand robots, there is a substantial and practical need for group-level rather than individual-level operation (*16*). In general, how individual capabilities and reliability relate to collective capabilities and reliability remains an active theoretical question. Here, we demonstrate that the limited capabilities of our system are sufficient to permit the execution of a complex algorithm for self-assembly at the swarm level for a collective of 1024 robots (Fig. 1), both theoretically and experimentally.

We designed a simple low-cost robot called Kilobot, first presented in (*17*) with a small prototype swarm of 30 robots executing a suite of simple collective behaviors. Kilobot exploits several unconventional design choices, such as using vibration motors for sliding movement rather than traditional wheels (*18*) and reflecting infrared light off the table surface below for communication and distance sensing between robots. Vibration motors provide noisy locomotion without position feedback, preventing a single robot from traveling long distances with any precision. Robots can measure distance to a neighboring robot by sensing the infrared light intensity of received messages, although this measurement is noisy and provides no information about the relative angle between the two robots. In addition, the system as a whole is inherently decentralized and asynchronous; any collective behavior must be achieved purely through local interactions between neighboring robots. Some individual limitations can be overcome through cooperation; a robot can use distance measurements from a stationary neighbor as feedback to enable more precise motion, and errors in distance sensing can be reduced by comparing readings among neighbors.

We developed a collective algorithm that guarantees that a large group of robots, with limited capabilities and local communication, can cooperatively assemble into any 1-connected user-specified shape [with some restrictions (*19*)]. The self-assembly algorithm (Fig. 2) composes three primitive collective behaviors: (i) edge-following, where a robot can move along the edge of a group by measuring distances from robots on the edge; (ii) gradient formation, where a source robot can generate a gradient value message that increments as it propagates through the swarm, giving each robot a geodesic distance from the source; and (iii) localization, where robots can form a

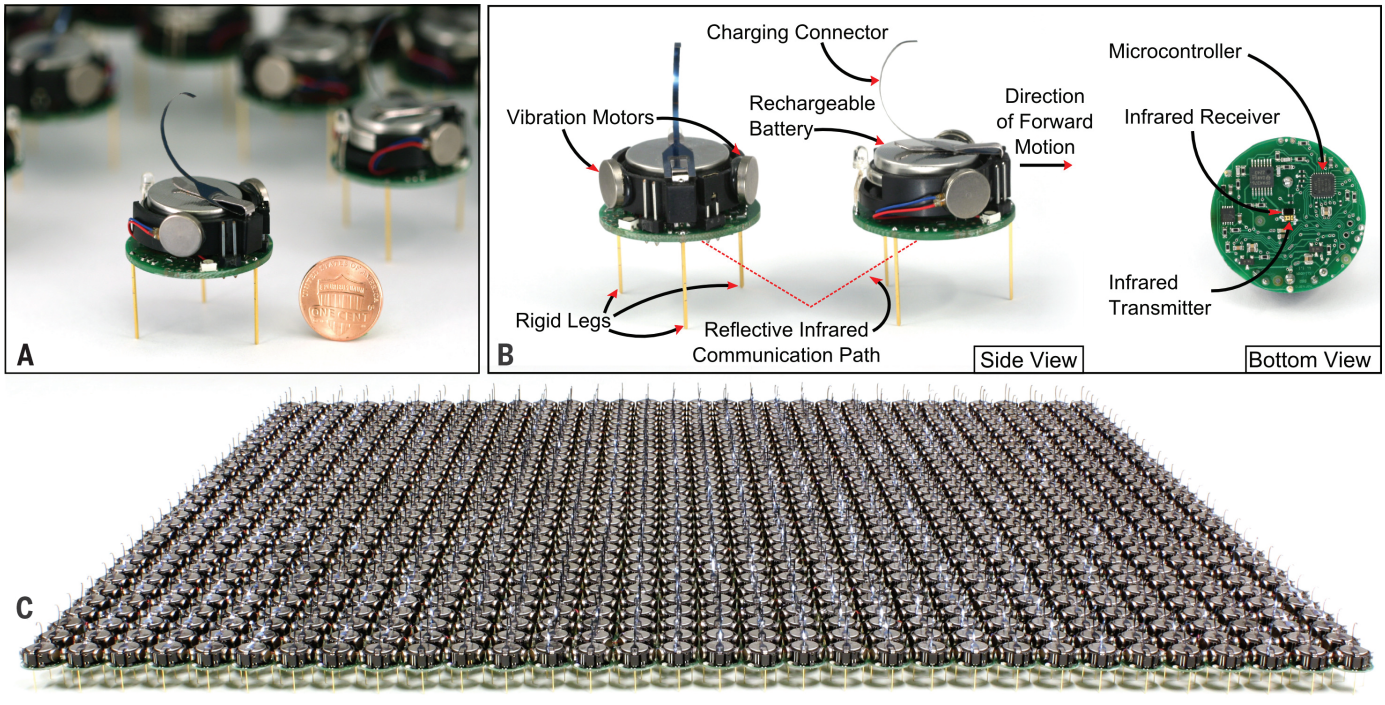


**Fig. 1. Kilobot swarm robot.** (**A**) A Kilobot robot, shown alongside a U.S. penny for scale. (**B**) Each Kilobot has an onboard microcontroller for executing programs autonomously, two vibration motors for moving straight or turning on a flat surface, and a downward-facing infrared transmitter and receiver. Robots communicate with others within a range of 10 cm (roughly three robot diameters) by reflecting infrared light off the table below. Communicating robots can evaluate relative distance by measuring the strength of the received infrared signal, but they cannot sense relative bearing (angle). (**C**) A $2^{10}$ Kilobot swarm. The Kilobot design allows for all operations on the entire swarm (charging, programming, etc.) to take a constant time to complete, independent of the number of robots in the swarm.

local coordinate system using communication with, and measured distances to, neighbors. The self-assembly algorithm links these three primitives with a finite-state automaton. We describe the algorithm at a high level here; see (*19*) for a detailed description of each aspect along with proofs of correctness and completion.

All robots are given an identical program that includes the fixed self-assembly algorithm and an image of the specific target shape and size. The robots are initially tightly packed into an arbitrarily shaped group without any knowledge about their location in the environment (Fig. 2). To start the self-assembly process, a user places four specially programmed seed robots next to the initial group, marking the position and orientation for where the shape should be formed in the environment. The seed robots become the source of a gradient formation that propagates through the initial group. Robots along the outer edge of the initial group are able to move without being physically blocked. They can determine that they are on the outer edge by comparing their gradient values to those of their neighbors. These robots can then use edge-following around the stationary initial group to reach the seed. To avoid congestion that would occur if all robots along the outer edge moved at once, randomness is used to allow only a subset to start motion at any one time. This method creates the effect of the initial group "dissolving" from the outer edge inward, with all robots eventually edge-following to the seed.

Robots have no direct information about their global position, only the distances to nearby neighbors. However, they can use this distance information to collectively construct a coordinate system. Initially, the stationary seed robots embody the origin of this coordinate system. As new robots arrive at the seed, they can use the localization primitive to determine their own position in this coordinate system; once this occurs, they can become reference points for the localization of additional robots. In this way, a coherent coordinate system can be built up through local interactions. The localization primitive works in the following way: Localized robots continually transmit messages that contain their $(x, y)$ position in the coordinate system. A new robot listens and measures distances to all previously localized neighbors; if it can observe at least three stationary and noncollinear localized robots, it can compute its own $(x, y)$ position using a distributed implementation of trilateration (Fig. 2) (*19*, *20*). Moving robots continually compute both their location and gradient value as they move.

Once a robot is localized, it can determine whether it is located inside the desired shape by comparing its position to the shape image. If it is not within the shape, the robot edge-follows the partially formed assembly until it detects that it has entered the shape. Once inside the shape, the robot continues to edge-follow until one of two conditions is met. If the robot is about to exit the shape, or if it is next to (less than a predefined distance from) a stationary robot that has the same gradient value as itself, it becomes stationary for the remainder of the process. This process of robots moving into and joining the assembly continues until the shape is filled with robots. The overall effect is that the shape builds up in successive layers (Fig. 2 and Fig. 3J).

This seed-initiated self-assembly algorithm can form a large class of shapes, relying only on local interactions of the robots [see (*19*) for proof]. The algorithm resembles previous lattice-based algorithms for collective construction and self-assembly of modular robots (*12*, *13*, *21*–*24*) and uses conceptual primitive behaviors found in previous work, such as edge-following (*23*–*25*), gradient formation (*23*, *26*) and localization (*22*, *23*). However, unlike most previous methods, our algorithm allows components to be positioned freely

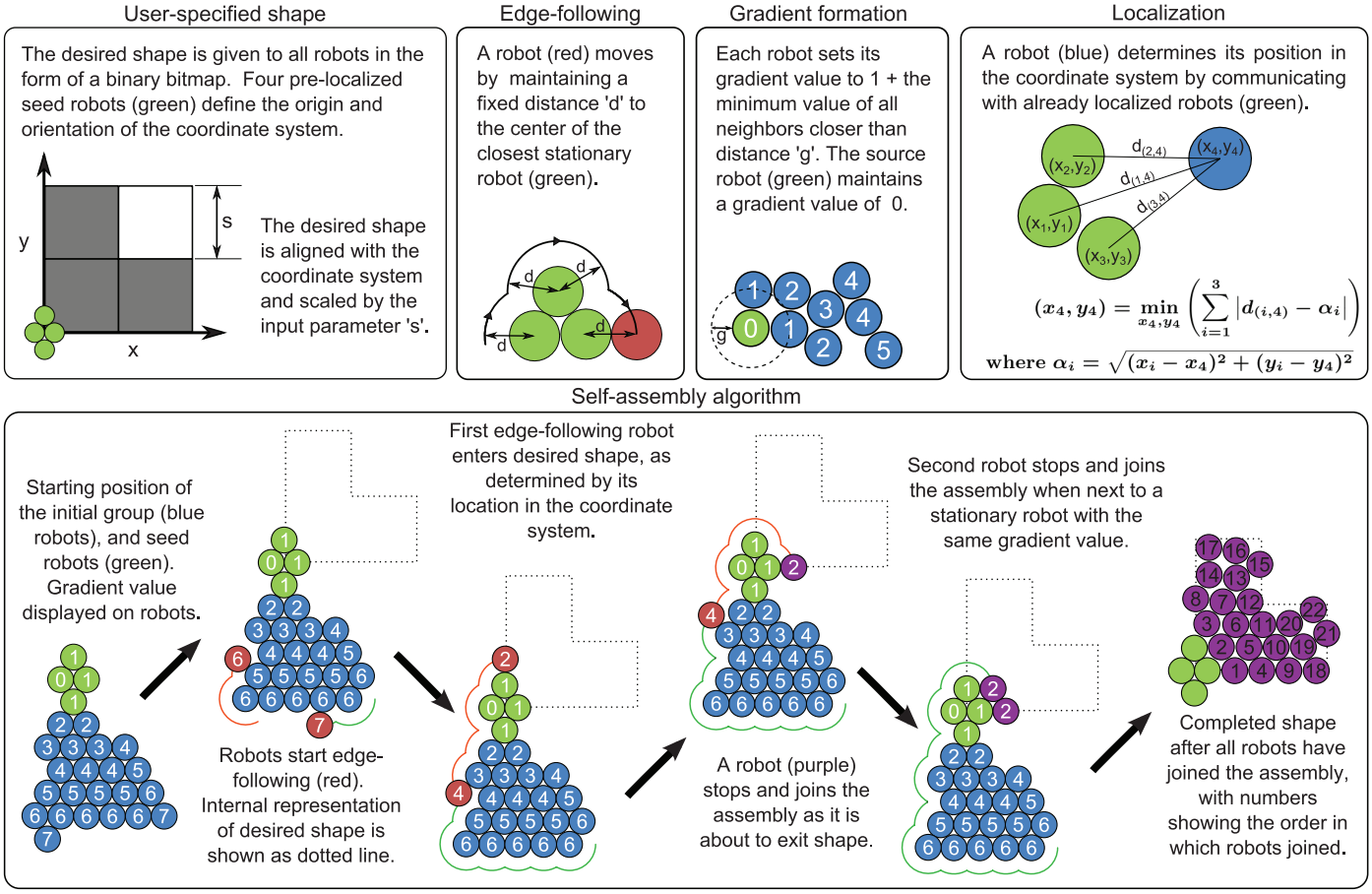


**Fig. 2. Collective self-assembly algorithm.** Top left: A user-specified shape is given to robots in the form of a picture. Top right: The algorithm relies on three primitive collective behaviors: edge-following, gradient formation, and localization. Bottom: The self-assembly process by which a group of robots forms the user-defined shape.

in continuous two-dimensional space and comes with a provable guarantee that the shape will form correctly. The use of continuous space implies that the implementations of the primitive behaviors are substantially different because of continuous and noisy sensing and motion, and proving correctness is more complex as the shape may be self-assembled differently each time because of differential packing of robots. However, avoiding grid restrictions allows for simpler robots and more robustness to imprecision in element positioning, which was instrumental in translating our algorithm onto a 1000-robot swarm.

Moving from abstract algorithms to physical robots requires solving several additional challenges. Mathematical models assume idealized behavior in order to achieve tractability; however, real robots exhibit much more complex behaviors. For example, robots often have imprecise locomotion, noisy distance sensing, and message loss. Moving from tens of robots to more than a thousand introduces additional nonideal behaviors that are not easily observed in smaller groups and are therefore rarely incorporated into simulators for modeling large robot swarms. These include systematic errors and high variability in robot locomotion and sensing, which can be manually detected and easily corrected in small groups but are too cumbersome and time-consuming to correct in larger groups, resulting in robots with statistically different variability. Increasing group size also increases the occurrence of statistically rare events, such as a robot becoming completely immobilized because of motor failure or a robot getting physically pushed by another. We observed that with a thousand physical robots running for tens of hours, high variability and rare errors are inevitable and capable of completely bringing such abstract algorithms to a halt.

To achieve robustness at the 1000-robot scale, we used several additional algorithmic strategies (*19*). For example, a continuous-space shape representation in our algorithm describes the desired shape as a boundary but does not dictate the exact location of robots within that shape. This enables the algorithm to tolerate a variety of packing patterns of robots within the shape, helping to prevent small position errors by the robots from propagating into large-scale self-assembly failures. One key technique for robustness was cooperative monitoring, in which a robot uses interactions with neighbors to detect and recover from faults that it cannot observe itself. For example, an immobilized robot can cause havoc in an edge-following algorithm by causing a permanent blockage. Similarly, localized robots can be physically pushed and therefore no longer have correct knowledge of their position in the swarm, and this error can then propagate through the rest of the assembling swarm. The robots lack the internal sensors to detect such rare events on their own; however, by using neighbor interaction, these faults can be detected. For example, both errors cause sensed distance between neighbors to change in predictable ways. This allows for autonomous recovery: An immobilized robot can reset its motors and try again, or it can signal to other robots that they should move around it; similarly, a pushed robot can selectively reevaluate its position and correct for the unintended movement. In general, many faults can be detected through information exchange with neighbors; this cooperative monitoring was essential to enable large-scale swarm experiments without human intervention.

Using this algorithmic approach, we conducted several large-scale experiments (Fig. 3 and movies S1 to S4). We programmed the full swarm of 1024 robots to self-assemble into two shapes, each taking roughly 12 hours of execution time. We performed 11 additional experiments with smaller collectives to analyze the accuracy of shape formation and to investigate the consistency of the collective behavior (*19*). All experimental trials fully assembled the desired shape without human intervention (such as charging batteries or reprogramming); hence, the collective behavior is remarkably robust. To quantitatively measure the accuracy of shape formation, we measured the mean square error between the true position of each robot (as measured from a calibrated camera) and each robot's internal localized position in the shared coordinate system (Fig. 3G). We observed that the final shape accuracy is high but not perfect; errors by individual robots during the assembly process can translate into global warping of the shape or small packing defects, but without halting the self-assembly process. To test consistency, we used approximately 100 robots to form the same rectangular shape 10 times. The results show that although the shape accuracy values are comparable between experiments, the packing pattern of robots can exhibit considerable variability, as is true in natural self-assemblages. These patterns are a manifestation of the natural variation in agent behavior in such large groups.

Experiments also revealed several interesting emergent behaviors that occur during the formation process (Fig. 3). For example, "traffic jams" of edge-following robots formed behind particularly slow robots, similar to vehicle traffic. Another observed behavior was the complex "erosion" of the initial group, caused by edge-following robots that would accidently push stationary

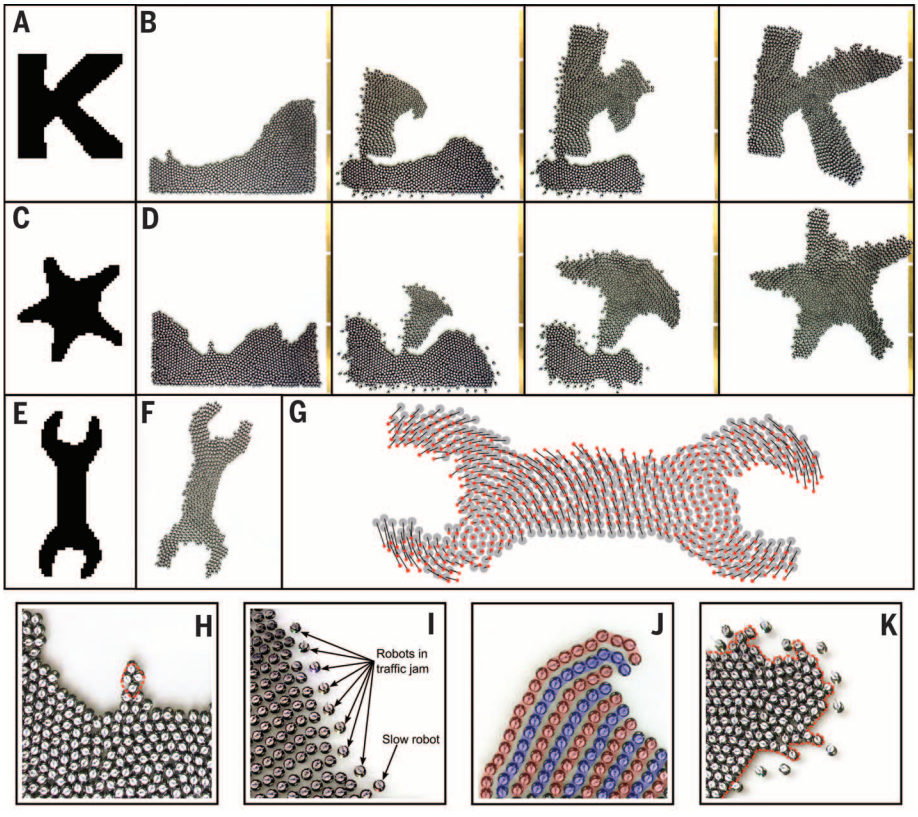


**Fig. 3. Self-assembly experiments using up to 1024 physical robots.** (**A**, **C**, and **E**) Desired shape provided to robots as part of their program. (**B** and **D**) Self-assembly from initial starting positions of robots (left) to final self-assembled shape (right). Robots are capable of forming any simply connected shape, subject to a few constraints to allow edge-following (*19*). (**F**) Completed assembly showing global warping of the shape due to individual robot errors. (**G**) Accuracy of shape formation is measured by comparing the true positions of each robot (red) and each robot's internal localized position (gray). (**H** to **K**) Close-up images of starting seed robots (H), traffic backup due to a slowly moving robot (I), banded patterns of robots with equal gradient values after joining the shape (robots in each highlighted row have the same gradient value) (J), and a complex boundary formed in the initial group (dashed red line) due to erosion caused by imprecise edge-following (K).

robots and create sharp edges; this resulted in a positive-feedback process where the sharp edges attracted more collisions, resulting in complex boundaries being formed as the initial group dissolved. Idealized mathematical models of robot swarms do not predict these phenomena.

Collective behavior in nature often involves large numbers of independent individuals interacting to produce complex assemblies. Engineered systems such as DNA-based self-assembly (*27*) have replicated this ability in synthesized chemical systems. We have demonstrated this ability in a robotic system by creating and programming a large-scale autonomous swarm to achieve complex global behavior from the cooperation of many limited and noisy individuals. The large-scale experiments advance our ability to engineer complex robotic systems. This motivates new investigations into advanced collective algorithms capable of detecting malfunctioning robots and recovering from large-scale external damages, as well as new robot designs that, like army ants, can physically attach to each other to form stable self-assemblages.

## REFERENCES AND NOTES


1. G. M. Whitesides, B. Grzybowski, *Science* **295**, 2418–2421 (2002).
2. H. C. Berg, *Annu. Rev. Biochem.* **72**, 19–54 (2003).
3. P. Lawrence, *The Making of a Fly: The Genetics of Animal Design* (Blackwell, Oxford, 1992).
4. S. Camazine *et al.*, *Self-Organization in Biological Systems* (Princeton Univ. Press, Princeton, NJ, 2003).
5. C. Anderson, G. Theraulaz, J. Deneubourg, *Insectes Soc.* **49**, 99–110 (2002).
6. N. J. Mlot, C. A. Tovey, D. L. Hu, *Proc. Natl. Acad. Sci. U.S.A.* **108**, 7669–7673 (2011).
7. M. Kirschner, J. Gerhart, *The Plausibility of Life: Resolving Darwin's Dilemma* (Yale Univ. Press, New Haven, CT, 2005).
8. R. Wood, R. Nagpal, G. Y. Wei, *Sci. Am.* **308**, 60–65 (March 2013).
9. R. Groß, M. Bonani, F. Mondada, M. Dorigo, *IEEE Trans. Robot.* **22**, 1115–1130 (2006).
10. E. William, G, Mermoud, A. Martinoli, in *Proceedings of the 2010 International Conference on Robotics and Automation* (Anchorage, AK, May 2010), pp. 1438–1445.
11. M. Yim *et al.*, *Robot. Automat. Mag.* **14**, 43–52 (2007).
12. S. Goldstein, J. Campbell, T. Mowry, *Computer* **38**, 99–101 (2005).
13. M. Tolley, H. Lipson, *Int. J. Robot. Res.* **30**, 1566–1584 (2011).
14. P. Wurman, R. D'Andrea, M. Mountz, *AI Mag.* **29**, 9–19 (2008).
15. K. Konolige *et al.*, *Exp. Robot.* **IX**, 131–140 (2006).
16. J. McLurkin *et al.*, in *AAAI Spring Symposium: To Boldly Go Where No Human-Robot Team Has Gone Before* (Stanford, CA, March 2006), pp. 72–75.
17. M. Rubenstein, C. Ahler, R. Nagpal, in *Proceedings of the 2012 IEEE International Conference on Robotics and Automation* (St. Paul, MN, May 2012), pp. 3293–3298.
18. P. Vartholomeos, E. Papadopoulos, in *Proceedings of the 2006 IEEE International Conference on Robotics and Automation* (Orlando, FL, May 2006), pp. 649–654.
19. See supplementary materials on *Science* Online.
20. D. Moore, J. Leonard, D. Rus, S. Teller, in *The 2nd International Conference on Embedded Networked Sensor Systems* (Baltimore, November 2004), pp. 50–61.
21. J. Werfel, Y. Bar-Yam, D. Rus, R. Nagpal, in *Proceedings of the 2006 IEEE International Conference on Robotics and Automation* (Orlando, FL, May 2006), pp. 2787–2794.
22. D. Arbuckle, A. Requicha, *Auton. Robots* **28**, 197–211 (2010).
23. K. Støy, *Robot. Auton. Syst.* **54**, 135–141 (2006).
24. K. Tomita, S. Murata, H. Kurokawa, E. Yoshida, S. Kokaji, *IEEE Trans. Robot. Autom.* **15**, 1035–1045 (1999).
25. M. De Rosa, S. Goldstein, P. Lee, J. Campbell, P. Pillai, in *Proceedings of the 2006 IEEE International Conference on Robotics and Automation* (Orlando, FL, May 2006), pp. 1462–1468.
26. R. Nagpal, H. Shrobe, J. Bachrach, in *Information Processing in Sensor Networks*, F. Zhao, L. Guibas, Eds. (Springer, Berlin, 2003), pp. 333–348.
27. P. W. Rothemund, *Nature* **440**, 297–302 (2006).



## ACKNOWLEDGMENTS

Supported by the Wyss Institute for Biologically Inspired Engineering and by NSF grants CCF-0926148 and CCF-0643898.


## SUPPLEMENTARY MATERIALS

www.sciencemag.org/content/345/6198/795/suppl/DC1
Materials and Methods
Figs. S1 to S10
Tables S1 and S2
Movies S1 to S4
References (*28*, *29*)

3 April 2014; accepted 18 June 2014
10.1126/science.1254295

RNA NANOSTRUCTURES

# A single-stranded architecture for cotranscriptional folding of RNA nanostructures

**Cody Geary,[1] Paul W. K. Rothemund,[2] Ebbe S. Andersen[1]***

**Artificial DNA and RNA structures have been used as scaffolds for a variety of nanoscale devices. In comparison to DNA structures, RNA structures have been limited in size, but they also have advantages: RNA can fold during transcription and thus can be genetically encoded and expressed in cells. We introduce an architecture for designing artificial RNA structures that fold from a single strand, in which arrays of antiparallel RNA helices are precisely organized by RNA tertiary motifs and a new type of crossover pattern. We constructed RNA tiles that assemble into hexagonal lattices and demonstrated that lattices can be made by annealing and/or cotranscriptional folding. Tiles can be scaled up to 660 nucleotides in length, reaching a size comparable to that of large natural ribozymes.**

Design methods for DNA (*1*, *2*) and RNA (*3*–*5*) nanostructures have been developing along parallel lines for more than a decade. Both allow the generation of a wide variety of structures, including polygons (*6*–*8*), three-dimensional (3D) shapes (*9*–*13*), 1D arrays (*3*, *14*), and 2D lattices (*15*, *16*). RNA structure design lags behind only in the size of structures created: Whereas RNA designs have been limited to 50 to 200 nucleotides (nt), DNA structures up to 45,000 nt have been achieved (*17*, *18*). The advantage of RNA structures lies in their greater potential to be cloned, genetically expressed in large quantities, and used for synthetic biology applications in vivo. DNA nanostructures built from single strands (*19*), or mostly single strands (*9*), have been synthesized or even cloned (*20*), but they variously require downstream purification or heat annealing, and none has yet been demonstrated to be folded isothermally as it is enzymatically produced.

RNA nanostructures have already been cotranscriptionally assembled from a mixture of numerous strands (*12*) and expressed in bacterial cells (*21*). Even if genetically encoded DNA structures are eventually achieved, other breakthroughs will have to be made, because existing DNA nanostructures lack the structural resolution and diversity of RNA tertiary motifs (*22*), such as kissing-loop interactions (KLs) (*23*), and they are currently unable to match the functional capacity of RNA to perform tasks such as scaffolding proteins (*21*, *24*), detecting ligands (*25*), or releasing small interfering RNAs in response to stimuli (*26*). But despite the potential for expressible RNA structures, a general architecture for designing them has yet to be achieved.

We present a method for designing single-stranded RNA (ssRNA) structures that can fold either by heat-annealing over mica or by cotranscriptional folding. Similar to the previously reported scaffolded DNA origami method (*17*), our ssRNA origami architecture is scalable and follows systematic design rules, in this case based on 3D modeling of the A-form helix. We demonstrated constructions up to six helices tall and 660 nt in length. We took inspiration from multistranded DNA double-crossover (DX) molecules (*27*) and their use as modular lattice-forming tiles (*16*). To turn multistranded DNA tiles into ssRNA ones, we developed an architecture that uses hairpins and programmable kissing loops. To extend the architecture to more than two helices, we introduced a new crossover pattern that we call a "dovetail seam, for creating arrays of coaxially stacked helices that are both sequence-specific and nontopologically linked.

Our design method used 3D modeling of RNA (Fig. 1A) to plan the interconnection of helices and RNA structural motifs to form compact structures and lattices (Fig. 1B). Outputs of 3D

[1]Center for DNA Nanotechnology, Interdisciplinary Nanoscience Center, and Department of Molecular Biology and Genetics, Aarhus University, 8000 Aarhus, Denmark. [2]Bioengineering, Computer Science, and Computation and Neural Systems, California Institute of Technology, Pasadena, CA 91125, USA.
***Corresponding author. E-mail: esa@inano.au.dk**

modeling were used to produce secondary structure blueprints (Fig. 1C), to which sequences were assigned by sequence design algorithms so that the structures could be synthesized and tested by one of two experimental protocols (Fig. 2, B and C). Figure 1D shows the vision that guided our design of RNA structures for cotranscriptional folding: RNA structures should contain stable hairpins that fold up in the order they are produced by the polymerase (Fig. 1D, 1 to 4). Next, the hairpins should condense in a sequential fashion dictated by long-range interactions (Fig. 1D, 5 to 7) to create a global fold. Finally, individual structures may assemble further into higher-order quaternary structures (Fig. 1D, 8). In all our designs, we specified the start of transcription (the 5′ end) to divide each structure into two independently and sequentially folding domains (Fig. 1D, inset).

RNA DX molecules were modeled by inserting crossovers between aligned computer-generated A-form RNA helices. By varying the spacing between the two antiparallel crossovers, we generated "antiparallel odd" (RNA-AO, Fig. 1A, top) or "antiparallel even" (RNA-AE, Fig. 1A, bottom) juxtapositions of the crossovers (*27*), where odd and even refer to the number of helical half-turns between crossovers. Similar to their DNA analogs (*16*), multistranded RNA-AE tiles comprise five different strands, whereas multistranded RNA-AO tiles comprise only four different strands. Unlike B-form DNA helices, which have only approximately –1° of base-pair inclination with respect to the helical axis (*28*), A-form RNA helices have approximately 19° of inclination (*29*) [fig. S1 (*30*)], accentuating a geometric difference between RNA-AE and RNA-AO tiles. In RNA-AE tiles, the base-pair inclinations of both helices align, and the base pairs between crossovers define a parallelogram (Fig. 1A, bottom). In contrast, in RNA-AO tiles the base-pair inclinations are opposed, so that the base pairs between crossovers define a trapezoid (Fig. 1A, top), and the number of base pairs between the crossovers on each helix is unequal.

Conversion of multistranded RNA DX tiles to ssRNA origami tiles (Fig. 1C) was accomplished by (i) connecting outer helix ends with hairpin loops and (ii) replacing one of the intercrossover helical domains with a 180° KL interaction. Depending on the sequence signature used [fig. S2 (*30*)], RNA KL interactions can define a wide variety of angles for construction, including ~180° connections (*31*) or ~120° bends (*32*) [Fig. 1B, insets; angles vary with sequence and exhibit some variation because of structural flexibility (*33*)]. The geometry of tile-tile interactions can be programmed by the choice of loops at the four corners of the tile. For example, by using six different 120° KL interactions, three different tiles can be programmed to form a hexagonal lattice (Fig. 1B). Alternatively, by using four different 180° KL interactions, two different tiles can be programmed to form a rectilinear lattice (Fig. 3D, top).

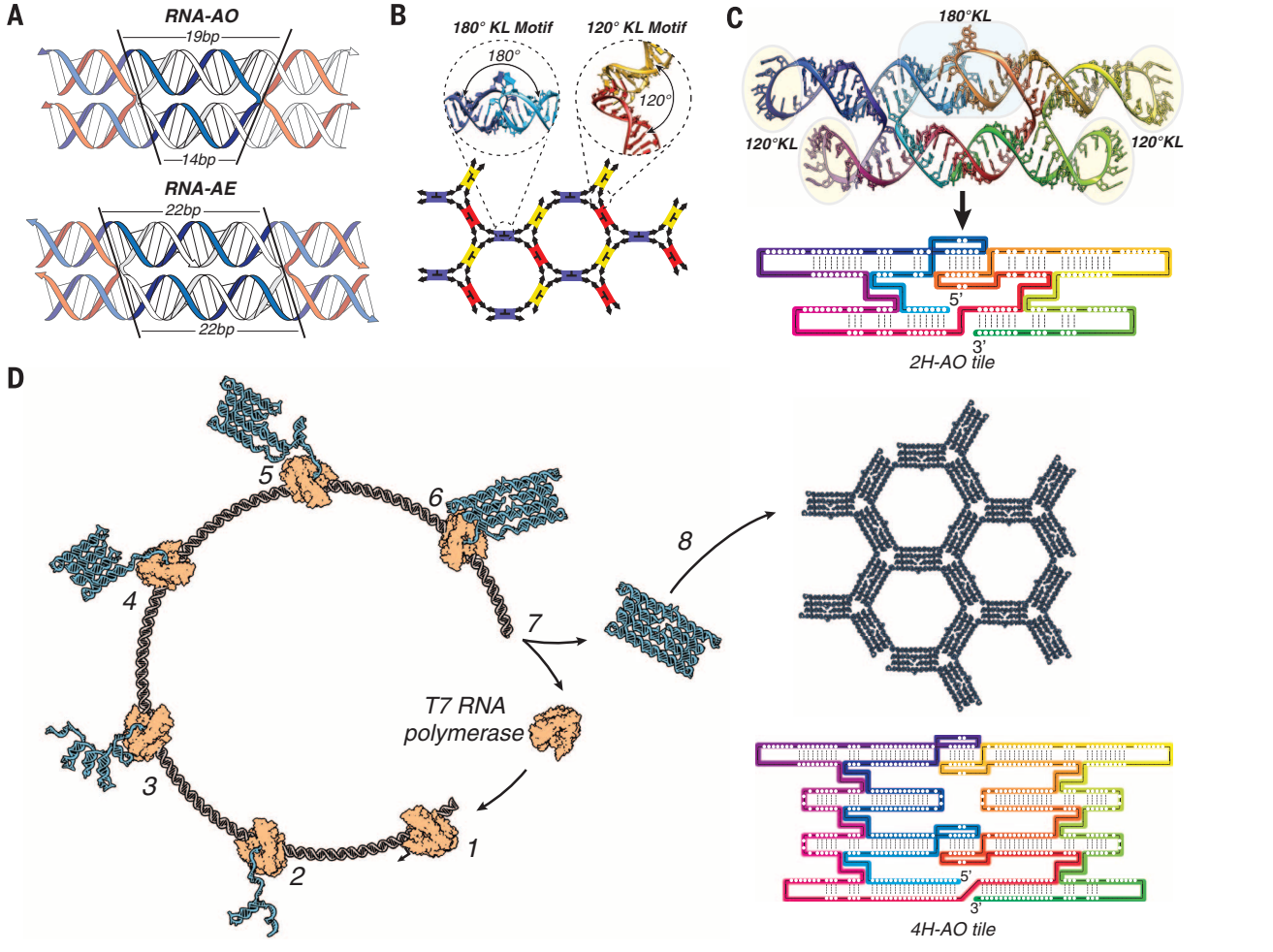


**Fig. 1. Design of ssRNA origami for tile assembly.** (**A**) Comparison of A-form antiparallel DX molecules: RNA-AO with an odd number of half-turns (three) between crossovers and RNA-AE with an even number (four). Base pairs between the crossovers of an RNA-AO define a trapezoid; those of an RNA-AE define a parallelogram. (**B**) Schematic shows how KL interactions of 180° (tile edges and left inset) and 120° (black arrows and right inset) can be used to specify a hexagonal lattice. (**C**) Design of a 2H-AO tile starts with 3D modeling from which a secondary structure blueprint is derived. The strand path is colored by a gradient that indicates the order of synthesis. (**D**) Schematic showing the cotranscriptional folding pathway for the 4H-AO tile. The T7 RNA polymerase binds to the template DNA (step 1) and the RNA folds as it is being synthesized (steps 2 to 6). By step 4, the 5′ half of the tile is fully synthesized and can fold into a domain composed of 11 helical subdomains. As the second domain is synthesized, the kissing loops can form in succession (steps 5 and 6). At the end of the synthesis (step 7), the tile is released and can form lattices (step 8).

Starting from the basic RNA-AO and RNA-AE geometries, tiles of different sizes were modeled using Assemble2 (*34*). Assemble2 generates A-RNA helices based on classical parameters (*35*) and helps to merge them with RNA tertiary motifs from the Protein Data Bank (PDB) [Fig. 2A, see materials and methods for details and PDB IDs (*30*)]. Two-helix structures (2H-AE and 2H-AO) were modeled on the initial RNA-AE and RNA-AO tiles shown in Fig. 1A. Taller four-helix (4H) and six-helix (6H) structures were generated, with an additional helical turn (11 base pairs) between crossovers that made them wider. Intra-tile 180° KLs were examined for steric clashes between AA bulges (a feature of the 180° KLs) and neighboring helices. Clashes predicted for 4H-AO and 6H-AO tiles motivated the omission of intra-tile KLs for every other helix. Inter-tile 120° KLs were

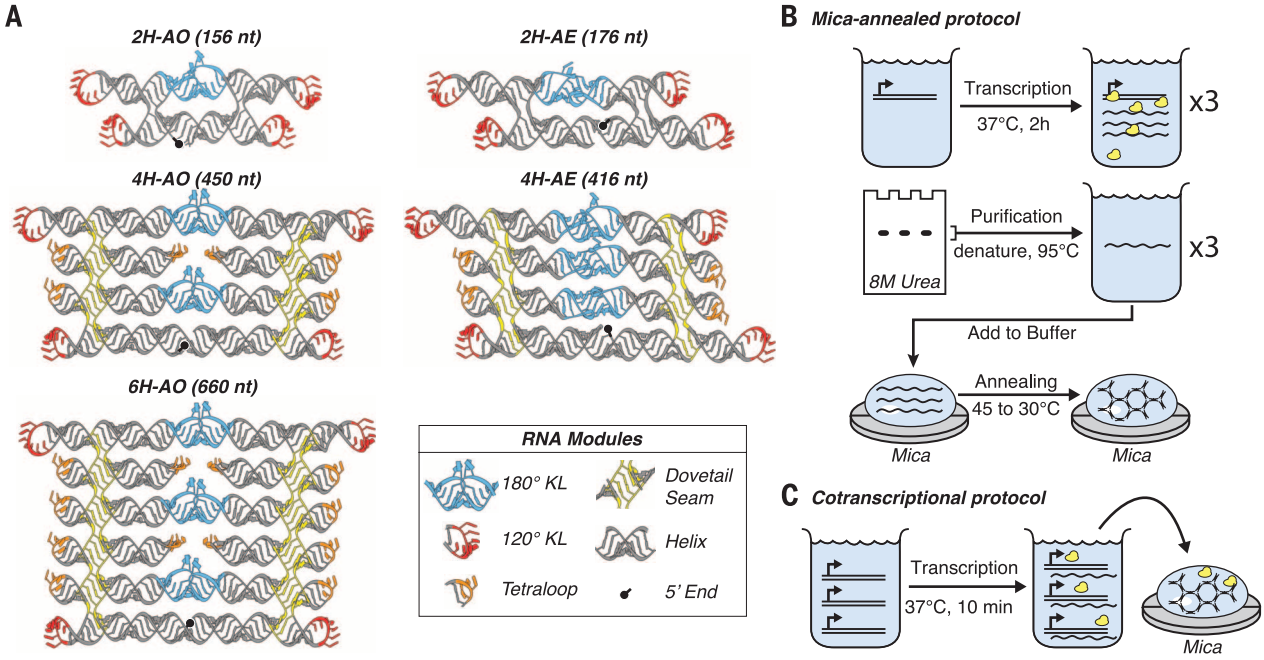


**Fig. 2. ssRNA origami tiles and preparation protocols.** (**A**) Renderings based on atomic models for RNA-AE and RNA-AO tiles that are two, four, and six helices tall. The legend shows structural modules. (**B**) Purification and annealing protocol showing DNA templates (double line), T7 promoter (bent arrows), T7 polymerase (yellow), RNA transcripts (wavy lines), and tile assembly. (**C**) Cotranscriptional folding protocol.

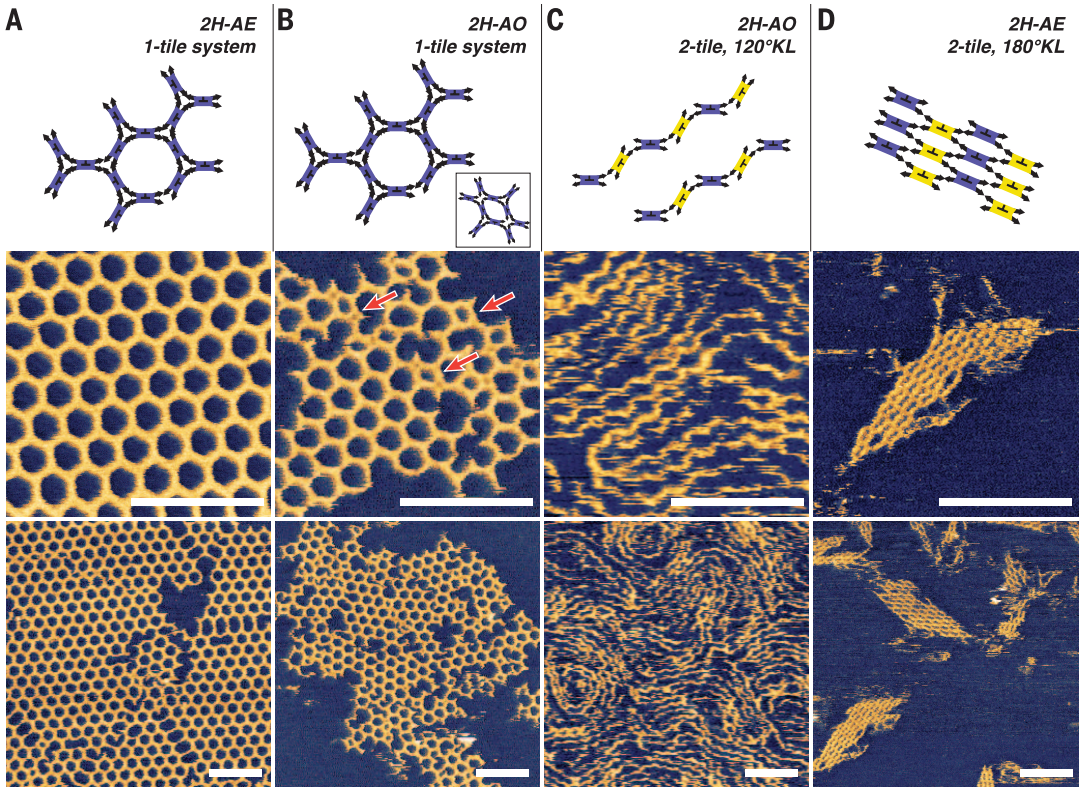


**Fig. 3. Programming RNA tile assembly with KL interactions.** (**A** to **D**, top) Schematics of different tile assemblies. (**A** to **D**, bottom) AFM images at two different zoom levels. (**A**) A single-tile 2H-AE system with 120° KLs forms hexagonal lattices. (**B**) A single-tile 2H-AO system with 120° KLs forms hexagonal lattices, but some defects are observed. (**C**) A two-tile 2H-AO system created by removing one of the tiles from a three-tile system (Fig. 1B) forms 1D zigzag arrays. (**D**) A two-tile 2H-AE system using 180° KLs forms rectilinear lattices. Samples were prepared as in Fig. 2B. Scale bars, 100 nm.

fit to tile corners (Fig. 2A, red module) by (i) rotating tiles (without corner KLs) using $D_3$ symmetry in UCSF Chimera molecular modeling software (*36*), (ii) arranging the tiles to form a planar structure, and (iii) aligning the nuclear magnetic resonance structure of the 120° KL between the tiles [materials and methods and fig. S3 (*30*)]. All helices not capped with KLs were terminated with GNRA or UNCG tetraloops (Fig. 2A, orange module) to increase thermostability (*37*).

For tiles more than two helices tall, crossovers form extended seams that the RNA backbone does not cross. Similar seams held together purely by stacking interactions have been created in DNA structures (*17*, *38*), but they are not sequence-specific. By analogy with dovetail joints from woodworking, we introduced "dovetail seams" (Fig. 2A, yellow module) in which 2 to 3 base pairs cross the seam at each helix, providing sequence specificity and potentially aiding in the folding of the tile. Further, the number of base pairs in the dovetail seam can, in principle, be used to control the geometry of the tile. In the 4H-AE tile, repeated use of a 2–base-pair dovetail should create slight curvature in the tile. In contrast, for the 4H-AO and 6H-AO tiles, 3–base-pair dovetails should cause each half of the tile to bend in opposite directions and impose a symmetry that tends to flatten the tile.

Secondary structures describing base pairing and strand paths were generated from 3D designs and represented in a simple text-based format. In principle, any position along the strand path could have been chosen as the start site for transcription. To avoid kinetic trapping (*39*), we positioned the 5′ start site and 3′ end to divide each tile into two domains, bridged by the 180° KLs [figs. S4 and S5 (*30*)]. In particular, this was intended to ensure that the folding of an entire domain precedes the formation of any KL interactions. Sequences for the RNA tiles were generated with NUPACK (*40*), aided by a Perl script [fig. S6 and note S2 (*30*)] that converts secondary structure into NUPACK's design format. Because secondary structure in the DNA template (from which an RNA tile is transcribed) can interfere with the synthesis of that template, we designed sequences that would have less structure in their DNA form by adding G-U wobbles to our RNA tile designs, with a frequency of one wobble pair per every eight base pairs of helix [figs. S6 and S7 (*30*)]. The sequences of the 120° and 180° KL interactions were chosen because they are highly sequence-specific (*8*, *13*) [fig. S8 and table S1 (*30*)].

To confirm the overall geometry of RNA-AO and RNA-AE DX tiles, we first explored them in the context of simple systems programmed to create hexagonal lattices from a single type of tile, which requires only two different KL interactions: The top left loop pairs with the bottom left loop and the top right loop pairs with the bottom right loop (Fig. 3, A and B, top). We first studied substrate-assisted lattice formation of purified tiles by annealing them over mica [materials and methods, Fig. 2B, and fig. S9 (*30*)], a process known to create micrometer-sized lattices of tiles that form only small lattices in solution (*41*, *42*). Atomic force microscopy (AFM) revealed high

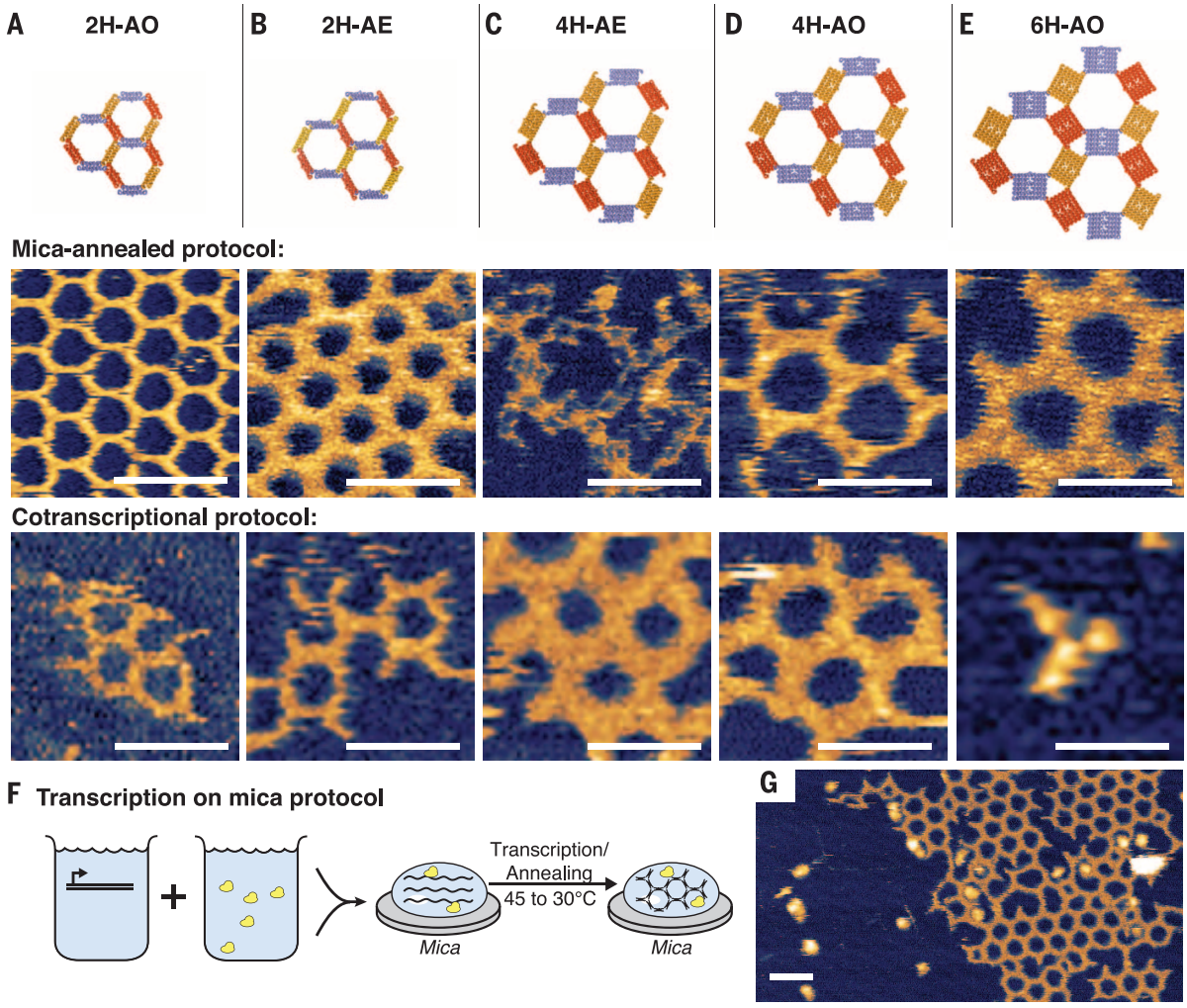


**Fig. 4. Scalability of ssRNA tile architecture.** (**A** to **E**) Three-tile hexagonal lattices shown in order of increasing tile size. (Top) 3D models displayed to scale. (Middle) AFM images of purified tiles annealed over mica as in Fig. 2B. (Bottom) AFM images of the same designs formed cotranscriptionally in solution and deposited on mica as in Fig. 2C. (**F**) Protocol for RNA transcription over mica, representing a combination of Fig. 2, B and C. (**G**) AFM images of 2H-AE tiles both transcribed and assembled directly over a mica surface. Scale bars, 50 nm.

surface coverage of the mica by 2H-AE and 2H-AO lattices (Fig. 3, A and B, bottom row), confirming that the basic geometry of these tiles and lattices was as designed. Defects in 2H-AE lattices, such as diamond-shaped cells or elongated eight-tile hexagons, occurred mainly at boundaries between ~300-nm crystal domains [Fig. 3A and fig. S10 (*30*)], whereas 2H-AO crystal domains were smaller (50 nm) and exhibited a number of nonhexagonal defects [Fig. 3B and fig. S11 (*30*)]. This result suggested that 2H-AO tiles have a slight distortion from the geometry predicted or may be more flexible than 2H-AE tiles. A control experiment in which two 2H-AO tiles were programmed to form 1D zigzag arrays (Fig. 3C) demonstrated that 120° KLs were at least successful in controlling the gross orientation of 2H-AO tiles. To demonstrate the geometric programmability of the tiles, we designed 2H-AE tiles of the same basic design demonstrated in Fig. 3A, but with 180° KLs for tile-tile connections [figs. S7 and S8 (*30*)]. As intended, these tiles formed rectilinear lattices (Fig. 3D) that were ~100 nm in size. We also examined the quality of solution-formed lattices by incubating a three-tile system 2H-AO at 37°C [materials and methods and fig. S9 (*30*)] and depositing the mixture over mica after assembly [fig. S12 (*30*)]. We observed fewer, smaller crystals than could be obtained by mica annealing of the same system (Fig. 4A, middle row).

To test the scalability of our architecture, we generated four-helix 4H-AO and 4H-AE tiles that are approximately 2.5 times greater in molecular weight than corresponding two-helix tiles, and six-helix 6H-AO tiles that are 4.2 times larger than corresponding two-helix tiles. Results from single-tile systems based on larger tiles (4H-AO and 4H-AE) were poor (a low yield of small lattices), but three-tile systems for all tile sizes (Fig. 4, top row) generated lattices by at least one of two different protocols: mica annealing (Fig. 4, middle row, and Fig. 2B) and cotranscriptional assembly at 37°C (Fig. 4, bottom row, and Fig. 2C). [See fig. S9 for protocols, fig. S13 for polyacrylamide gel electrophoresis gels, and figs. S14 to S21 for larger AFM views and height analysis showing that experimentally observed lattice spacings match predicted spacings within 2 nm, summarized in table S2 (*30*).]

Mica annealing yielded lattices in all cases except the 4H-AE system (Fig. 4C, middle row), which formed a disordered weblike structure. Gel electrophoresis of individual 4H-AE tiles solution-incubated at 37°C [fig. S13 (*30*)] showed that little or no monomer formed, and slower-migrating potentially misfolded species dominated. The sudden introduction of salt (upon which KL formation depends) to highly concentrated tiles occurs in both mica annealing and solution incubation protocols, and so in both cases 4H-AE tiles may have been kinetically trapped in multistranded structures, perhaps involving intermolecular binding of the strong 180° KLs intended as intramolecular contacts. However, cotranscriptional assembly of the 4H-AE system allowed small lattices to form (Fig. 4C, bottom row), and a substantial fraction of monomer was observed by gel electrophoresis of cotranscriptionally folded tiles [fig. S13 (*30*)].

Cotranscriptional assembly yielded lattices in all cases except the 6H-AO system (Fig. 4, A to E, bottom row). In this case, a substantial fraction of slower-migrating potentially misfolded tiles were observed by gel for both cotranscriptionally folded and solution-incubated tiles [fig. S13 (*30*)]. If all internal 180° KLs and the dovetail seams form as desired, a relatively flat tile would be created. However, given the symmetry and dovetail spacing used, the desired fold for the 6H-AO system may be highly strained, and it is possible for it to be trapped in more 3D distorted states of lower strain. This result is consistent with the increased height (~3.5 nm versus 2 to 2.5 nm for tiles in typical lattices) observed for cotranscriptionally assembled 6H-AO tiles [fig. S21 (*30*)]. In the case of mica annealing, the confinement and heating of 6H-AO tiles on the mica may have flattened tiles and allowed them to form lattices [Fig. 4E, middle row, and figs. S20 and S23 (*30*)]. This difference seems plausible because highly curved DNA tubes are slowly opened and flattened by interaction with mica surfaces (*43*). Combining the transcription of 2H-AE tiles with our mica annealing protocol (Fig. 4F) allowed the visualization of RNA polymerase in association with the tile lattice (Fig. 4G and fig. S22) and yielded our best cotranscriptional result.

We have shown that our ssRNA architecture is compatible with cotranscriptional folding and lattice assembly for four out of five tile designs tested. One design, the 4H-AE system, appeared to benefit from or perhaps require cotranscriptional folding. Figure 1D outlines how we envision how cotranscriptional folding proceeds for our architecture, diagrammed for the similar 4H-AO system. T7 RNA polymerase adds nucleotides quickly, in the range of 200 to 400 nt/s, and secondary structure forms two to three orders of magnitude more quickly, on the microsecond time scale (*44*, *45*). Thus, we expect that halfway through transcription, the 5′ half of the tile will already be folded and the left half of each intramolecular KL will be positioned at the end of a helical stem. As the 3′ half of the tile is synthesized, the remaining halves of each intramolecular KL are expected to be synthesized and bind their complementary halves in order. Without such a prescribed ordering of folding, hairpins that we intend to form intramolecular KLs might have the opportunity to form intermolecular KLs and thus unintended multimeric structures, as might happen for 4H-AE tiles when not cotranscriptionally folded, perhaps because of their three somewhat crowded intramolecular KL interactions.

The 6H-AO tile artificial RNA nanostructure produced as a single strand comprises 660 nt and 35 helical subdomains, which corresponds to a structural complexity (*4*) comparable to that of the group II intron [fig. S24 (*30*)]. Although the basic architecture we present only provides for 2D structures, the addition of RNA modules that can control helical stacking, such as the A-minor four-way junction (*46*), or control bending such as the kink turn (*47*), could extend the architecture to three dimensions. More generally, augmentation of the basic architecture with complex tertiary motifs will allow structures with different geometry, finer detail, and specific protein binding (*48*).

## REFERENCES AND NOTES


1. N. C. Seeman, *J. Theor. Biol.* **99**, 237–247 (1982).
2. A. V. Pinheiro, D. Han, W. M. Shih, H. Yan, *Nat. Nanotechnol.* **6**, 763–772 (2011).
3. L. Jaeger, N. B. Leontis, *Angew. Chem. Int. Ed. Engl.* **39**, 2521–2524 (2000).
4. W. Grabow, L. Jaeger, *F1000Prime Rep.* **5**, 46 (2013).
5. J. Lee *et al.*, *Proc. Natl. Acad. Sci. U.S.A.* **111**, 2122–2127 (2014).
6. I. Severcan, C. Geary, E. Verzemnieks, A. Chworos, L. Jaeger, *Nano Lett.* **9**, 1270–1277 (2009).
7. P. Guo, C. Zhang, C. Chen, K. Garver, M. Trottier, *Mol. Cell* **2**, 149–155 (1998).
8. W. W. Grabow *et al.*, *Nano Lett.* **11**, 878–887 (2011).
9. J. H. Chen, N. C. Seeman, *Nature* **350**, 631–633 (1991).
10. W. M. Shih, J. D. Quispe, G. F. Joyce, *Nature* **427**, 618–621 (2004).
11. E. S. Andersen *et al.*, *Nature* **459**, 73–76 (2009).
12. K. A. Afonin *et al.*, *Nat. Nanotechnol.* **5**, 676–682 (2010).
13. I. Severcan *et al.*, *Nat. Chem.* **2**, 772–779 (2010).
14. H. Yan, X. Zhang, Z. Shen, N. C. Seeman, *Nature* **415**, 62–65 (2002).
15. A. Chworos *et al.*, *Science* **306**, 2068–2072 (2004).
16. E. Winfree, F. Liu, L. A. Wenzler, N. C. Seeman, *Nature* **394**, 539–544 (1998).
17. P. W. K. Rothemund, *Nature* **440**, 297–302 (2006).
18. B. Wei, M. Dai, P. Yin, *Nature* **485**, 623–626 (2012).
19. Z. Li *et al.*, *J. Am. Chem. Soc.* **131**, 13093–13098 (2009).
20. C. Lin *et al.*, *Proc. Natl. Acad. Sci. U.S.A.* **105**, 17626–17631 (2008).
21. C. J. Delebecque, A. B. Lindner, P. A. Silver, F. A. Aldaye, *Science* **333**, 470–474 (2011).
22. L. Jaeger, A. Chworos, *Curr. Opin. Struct. Biol.* **16**, 531–543 (2006).
23. S. Horiya *et al.*, *Chem. Biol.* **10**, 645–654 (2003).
24. H. Ohno *et al.*, *Nat. Nanotechnol.* **6**, 116–120 (2011).
25. J. S. Paige, T. Nguyen-Duc, W. Song, S. R. Jaffrey, *Science* **335**, 1194 (2012).
26. L. M. Hochrein, M. Schwarzkopf, M. Shahgholi, P. Yin, N. A. Pierce, *J. Am. Chem. Soc.* **135**, 17322–17330 (2013).
27. T. J. Fu, N. C. Seeman, *Biochemistry* **32**, 3211–3220 (1993).
28. R. E. Dickerson *et al.*, *Science* **216**, 475–485 (1982).
29. Y. Tanaka *et al.*, *Nucleic Acids Res.* **27**, 949–955 (1999).
30. See the supplementary materials on *Science* Online.
31. E. Ennifar, P. Walter, B. Ehresmann, C. Ehresmann, P. Dumas, *Nat. Struct. Biol.* **8**, 1064–1068 (2001).
32. A. J. Lee, D. M. Crothers, *Structure* **6**, 993–1007 (1998).
33. W. Kasprzak, E. Bindewald, T. J. Kim, L. Jaeger, B. A. Shapiro, *Methods* **54**, 239–250 (2011).
34. S. Arnott, D. W. Hukins, S. D. Dover, W. Fuller, A. R. Hodgson, *J. Mol. Biol.* **81**, 107–122 (1973).
35. F. Jossinet, T. E. Ludwig, E. Westhof, *Bioinformatics* **26**, 2057–2059 (2010).
36. E. F. Pettersen *et al.*, *J. Comput. Chem.* **25**, 1605–1612 (2004).
37. M. Molinaro, I. Tinoco Jr., *Nucleic Acids Res.* **23**, 3056–3063 (1995).
38. X. C. Bai, T. G. Martin, S. H. Scheres, H. Dietz, *Proc. Natl. Acad. Sci. U.S.A.* **109**, 20012–20017 (2012).
39. H. Isambert, *Methods* **49**, 189–196 (2009).
40. J. N. Zadeh *et al.*, *J. Comput. Chem.* **32**, 170–173 (2011).
41. X. Sun, S. Hyeon Ko, C. Zhang, A. E. Ribbe, C. Mao, *J. Am. Chem. Soc.* **131**, 13248–13249 (2009).
42. S. Hamada, S. Murata, *Angew. Chem. Int. Ed. Eng.* **48**, 6820–6823 (2009).
43. P. W. K. Rothemund *et al.*, *J. Am. Chem. Soc.* **126**, 16344–16352 (2004).
44. S. L. Heilman-Miller, S. A. Woodson, *RNA* **9**, 722–733 (2003).
45. J. A. Cruz, E. Westhof, *Cell* **136**, 604–609 (2009).
46. C. Geary, A. Chworos, L. Jaeger, *Nucleic Acids Res.* **39**, 1066–1080 (2011).

47. D. J. Klein, T. M. Schmeing, P. B. Moore, T. A. Steitz, *EMBO J.* **20**, 4214–4221 (2001).
48. W. W. Grabow, L. Jaeger, *Acc. Chem. Res.* **47**, 1871–1880 (2014).

**ACKNOWLEDGMENTS**

The authors thank E. Winfree and M. Dong for use of their AFM facilities. We acknowledge financial support from the Danish Council for Independent Research (Sapere Aude Starting Grant DFF-0602-01772), the Danish National Research Foundation funding Centre for DNA Nanotechnology (grant DNRF81, http://cdna.au.dk/), the U.S. National Science Foundation for Expeditions in Computing funding for the Molecular Programming Project (grant nos. 0832824 and 1317694, http://molecular-programming.org), and Army Research Office award W911NF-11-1-0117. C.G., P.W.K.R., and E.S.A planned experiments and wrote the paper together. C.G. performed all experiments. The authors declare no competing financial interests.

**SUPPLEMENTARY MATERIALS**

www.sciencemag.org/content/345/6198/799/suppl/DC1
Materials and Methods
Figs. S1 to S24
Tables S1 and S2
Notes S1 and S2

25 March 2014; accepted 16 June 2014
10.1126/science.1253920

PHOTOSYNTHESIS

# Electronic structure of the oxygen-evolving complex in photosystem II prior to O-O bond formation

**Nicholas Cox,[1]* Marius Retegan,[1] Frank Neese,[1] Dimitrios A. Pantazis,[1] Alain Boussac,[2] Wolfgang Lubitz[1]***

**The photosynthetic protein complex photosystem II oxidizes water to molecular oxygen at an embedded tetramanganese-calcium cluster. Resolving the geometric and electronic structure of this cluster in its highest metastable catalytic state (designated $S_3$) is a prerequisite for understanding the mechanism of O-O bond formation. Here, multifrequency, multidimensional magnetic resonance spectroscopy reveals that all four manganese ions of the catalyst are structurally and electronically similar immediately before the final oxygen evolution step; they all exhibit a 4+ formal oxidation state and octahedral local geometry. Only one structural model derived from quantum chemical modeling is consistent with all magnetic resonance data; its formation requires the binding of an additional water molecule. O-O bond formation would then proceed by the coupling of two proximal manganese-bound oxygens in the transition state of the cofactor.**

In oxygenic photosynthesis, an inorganic $Mn_4O_5Ca$ cofactor embedded in photosystem II (PSII) (Fig. 1A) catalyzes water oxidation to $O_2$ with a high turnover number ($10^6$) and a maximal turnover frequency (TOF) of ≈500 $s^{-1}$ (*1*). In contrast, free $Mn_xO_yCa$ oxides display intrinsically slow water-splitting capacity, with TOFs six orders of magnitude lower (*2*). The cofactor's reaction cycle comprises five distinct redox intermediates, the $S_n$ states, where the subscript indicates the number of stored oxidizing equivalents ($n$ = 0 to 4) required to split two water molecules (Fig. 1B) (*3*). The cycle is sequentially driven by the photo-oxidant of PSII (P680), a multichlorophyll pigment assembly. The photochemistry of the reaction center is coupled to the reaction catalyzed by the $Mn_4O_5Ca$ cofactor via a nearby redox-active tyrosine residue $Y_Z$ ($D_1$-Y161), which acts as a single electron gate (Fig. 1B). Upon the last oxidation of $Y_Z$, (forming the $S_3Y_Z^{\bullet}$ state), the system rapidly decays to the $S_0$ state, with the concomitant release of molecular triplet oxygen and the rebinding of one substrate water molecule (*4*, *5*). The chemical steps involved in O-O bond formation in the transition state ($S_4$) remain uncertain.

The current molecular-level picture of the biological water-oxidizing catalyst extends only halfway through its reaction cycle, to the $S_2$ state. Here, the net oxidation states of the four manganese (Mn) ions are generally considered to be IV, IV, IV, and III (Fig. 1B); however, some researchers favor a net oxidation level two electrons lower: IV, III, III, and III [a discussion is available in (*1*)]. Theoretical models for the cofactor in the $S_2$ state (*6*), which combine structural (*7*, *8*) and spectroscopic data (*9*, *10*), suggest that the cofactor in this state is inherently flexible. The cofactor adopts two distinct but interconvertible Mn core topologies, an open and a closed cubane motif, which differ by the reorganization of a single μ-oxo bridge, O5 (*6*), rendering the $Mn^{III}$ ion five-coordinate.

Unlike the $S_2$ state, the structure of the $S_3$ state remains unresolved. Interpretation of x-ray spectroscopic data of $S_3$ is vigorously debated, with some researchers suggesting that its formation is accompanied by a Mn-centered oxidation, whereas others instead favor a ligand-centered oxidation, possibly of one of the substrate waters (Fig. 1B) (*11*, *12*). Similarly, there is little agreement on the coordination number of the four Mn ions, or the number of substrate waters (1 or 2) bound to the cofactor before the $S_3$ state (*4*, *5*, *13*). This ambiguity in the structure of the $S_3$ state translates into a lack of consensus about the O-O bond–formation mechanism. Pulse electron paramagnetic resonance (EPR) measurements presented here conclusively resolve the oxidation state of the cofactor in the $S_3$ state and thus constrain the oxidation states of all S states of the cycle. The data show that the cofactor does have an expanded core topology in $S_3$, with all Mn ions of the cluster in the 4+ oxidation state and coordinatively saturated (six-coordinate). These results demonstrate that all S-state transitions before $S_4$ represent Mn-centered oxidations and provide further evidence that the O-O bond formation step is best described in terms of the coupling of two proximal Mn-bound oxygen ligands attached to Mn1 and Mn4 in the $S_3$ and subsequent $S_4$ state.

EPR spectroscopy has been extensively used to characterize the structure of the $Mn_4O_5Ca$ cofactor and its catalytic (S state) cycle (*14*, *15*).

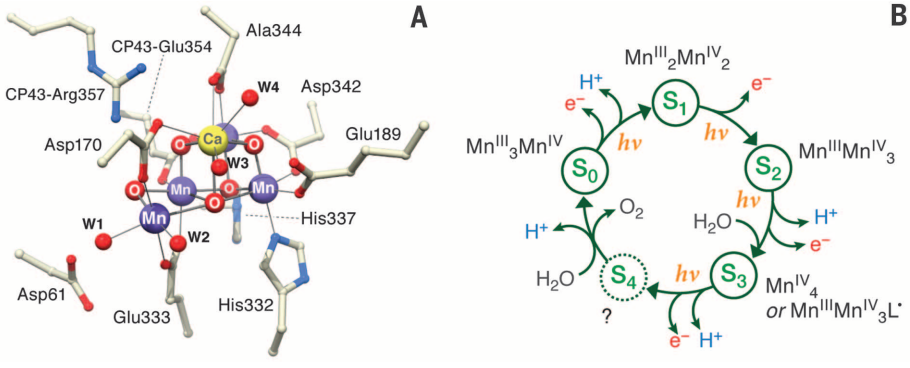


**Fig. 1. The water oxidation cofactor of PSII.** (**A**) X-ray crystallographic structure (*7*) of the oxygen-evolving complex, a $Mn_4O_5Ca$ cofactor. (**B**) The five intermediate "S" states of the reaction cycle (*1*, *3*, *33*), showing the sequence of electron- and proton-removal steps and the likely oxidation states of the Mn ions in each metastable state.

[1]Max Planck Institute for Chemical Energy Conversion, Stiftstrasse 34-36, D-45470 Mülheim an der Ruhr, Germany. [2]Institut de Biologie et de Technologies de Saclay, CNRS UMR 8221, Commissariat à l'Énergie Atomique (CEA) Saclay, 91191 Gif-sur-Yvette, France.
***Corresponding author. E-mail: nicholas.cox@cec.mpg.de (N.C.); wolfgang.lubitz@cec.mpg.de (W.L.)**

The four paramagnetic Mn ions that constitute the cofactor magnetically couple with each other so that the complex can be described in terms of a ladder of effective electronic spin states. Because each S state differs by a single-electron oxidation of the Mn cluster, the cluster's EPR activity oscillates. In the even-numbered S states ($S_0$, $S_2$), in which the cofactor carries an odd number of electrons, the cofactor is EPR active, with ground state (or states) of half integer spin ($S_G$ = 1/2, 5/2) (*10*, *16*–*20*). In the odd-numbered S states ($S_1$, $S_3$), the cofactor instead carries an even number of electrons. Depending on magnetic interactions within the complex, this can result in either an EPR-inactive ground state, as in the case of the $S_1$ state ($S_G$ = 0) (*21*, *22*), or an EPR-active ground state, as in the case of the $S_3$ state (*23*, *24*), with earlier CW-EPR measurements suggesting that the $S_3$ state has a ground spin state of three ($S_G$ = 3) (*23*, *24*).

The W-band EPR spectrum of the Mn cofactor poised in the $S_3$ state is shown in Fig. 2B. The spectrum is centered at 3.4 T [isotropic *g* value ($g$) ≈ 2] and consists of six evenly spaced lines separated by ≈0.4 T. The large spectral breadth of the EPR signal (1.8 T) indicates that it arises from an effective spin state with several unpaired electron spins. In such systems, electron spin-spin interactions lead to the spreading of the EPR spectrum across a large magnetic field range. The extent of this spreading scales with the magnitude of the electron spin interactions, termed "the fine-structure splitting" (*D*). Procedures used to generate and quantify the $S_3$ state population are described in the supplementary materials, section 3.1.

The ground spin state of the Mn cofactor in the $S_3$ state can be determined by using a pulse EPR technique called electron-spin nutation (Fig. 2A). In pulse EPR, the EPR signal is measured by applying a sequence of short nanosecond microwave pulses. The optimal length of these pulses is defined by the effective (total) spin state of the species being measured. Incrementing the length of the microwave pulse (or pulses) causes the EPR signal intensity to oscillate, with the period of the oscillation equal to twice the optimal pulse length. This experiment allows definitive assignment of the spin state of the $S_3$ to $S_G$ = 3, by calibration against an $S$ = 1/2 standard—in this instance, an organic radical species present in PSII, the $Y_D^{\bullet}$ radical (supplementary materials, section 2.3).

In a spin Hamiltonian simulation, we decomposed the EPR spectrum into six subspectra, corresponding to single-quantum spin transitions between adjacent ($m_S$) levels of the ground-state spin manifold (Fig. 2C). Fitting the simulation to the experimental spectrum by using three independent parameters yielded a fine-structure splitting of $D$ = −0.175 $cm^{-1}$, a rhombicity of the fine-structure splitting of $E/D$ = 0.27, and an isotropic *g* value of $g$ = 1.99. The relative Boltzmann populations of the different $m_S$ levels require $D$ to be negative. The same parameter set also reproduces EPR spectra measured at lower (X- and Q-band) microwave frequencies (fig. S6 and supplementary materials, section 3.5). The small fine-structure splitting that emerges from the fit is similar to that observed in biomimetic $Mn_3CaO_4$ cubane models (*25*). In these systems, the Mn ions are all in the 4+ oxidation state and are coordinatively saturated (six-coordinate). In the $S_G$ = 5/2 isomer of the $S_2$ state, which contains a $Mn^{III}$ ion, the $D$ value is almost threefold larger: $|D|$ = 0.45 $cm^{-1}$ (*20*).

The effective electron spin of the Mn complex also couples to the nuclear spins associated with each Mn ion [$I(^{55}Mn)$ = 5/2]. This interaction, termed "the hyperfine interaction," provides detailed information on the oxidation state, local electronic structure, and ligand environment of the individual Mn centers and the magnetic connectivity of the cofactor. Such metal-centered hyperfine interactions can be accurately assessed by using double-resonance EPR techniques, including electron-nuclear double resonance (ENDOR) and electron-electron double resonance–detected nuclear magnetic resonance (EDNMR). These techniques have been used to resolve the electronic and geometric structure of the $S_2$ state (*26*–*29*) and related synthetic Mn model complexes (*30*, *31*).

The spectral positions of nuclear transitions are defined by two parameters, the nuclear Larmor frequency ($\nu_n$), which is defined by the nuclear

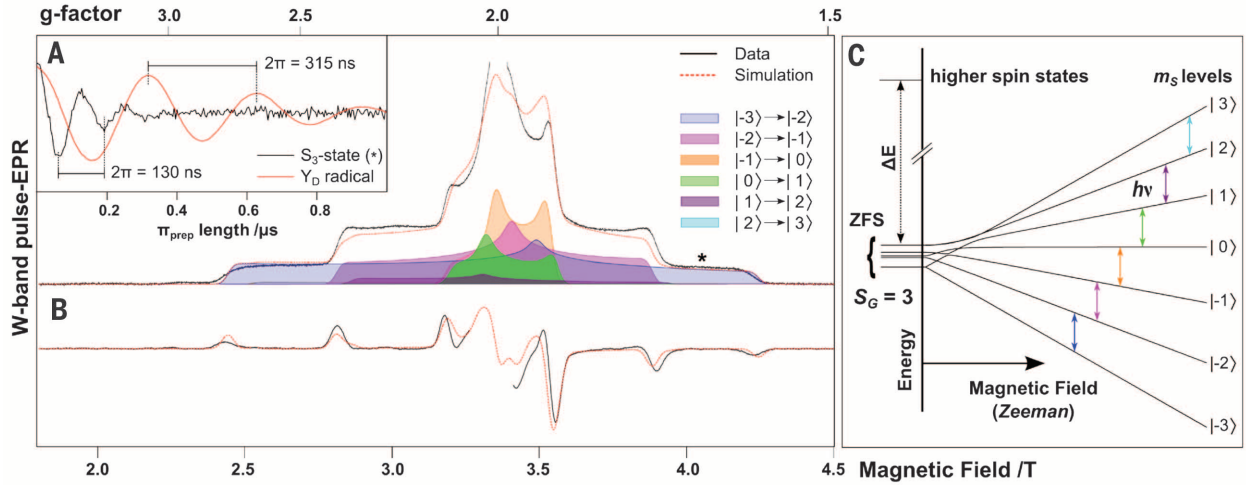


**Fig. 2. Measured and simulated EPR spectra of the $S_3$ state.** (**A**) Electron-spin nutation curves for the Mn cofactor as compared with a radical standard, the background tyrosine radical ($Y_D^{\bullet}$). (**B**) The EPR spectrum of the $S_3$ state measured at W-band (94 GHz). The procedures used to prepare PSII samples are given in the supplementary materials (materials and methods, section 3.2, and fig. S1). The spectrum represents the light-minus-dark difference between a sample poised in the $S_1$ state and one poised in the $S_3$ state. The red dashed line is the result of a simulation using the spin Hamiltonian $\hat{H} = g\beta\vec{S}\cdot\vec{B} + D[\vec{S}_Z^2 - \frac{1}{3}S(S+1) + E/D(\vec{S}_X^2 - \vec{S}_Y^2)]$, where $g$, $D$, and $E/D$ represent fitted parameters. The fitted $g$ value essentially defines the center of the EPR spectrum. The two fine-structure tensor parameters ($D$ and $E/D$) then define the width of the EPR spectrum and the spacing of the turning points. The shaded curves represent a decomposition of the simulation, showing the contribution of each allowed EPR transition to the powder spectrum. Owing to Boltzmann population of the levels at low temperatures (7 K), only the four lowest transitions substantially contribute to the overall spectral lineshape (C). The $m_S = |-3\rangle \rightarrow |-2\rangle$ component (light blue) is broadest and defines the low (2.40 T) and high (4.25 T) field edges of the spectrum, averaged over all powder orientations (fig. S3). The $m_S = |-2\rangle \rightarrow |-1\rangle$ component (pink) defines the next turning points at 2.80 T and 3.90 T, and the $m_S = |-1\rangle \rightarrow |0\rangle$ (orange) and $m_S = |0\rangle \rightarrow |1\rangle$ (green) components define the inner structure centered at 3.4 T. The bottom trace shows the pseudo-modulated (CW-EPR–like) $S_3$ state spectrum generated by convolution of the absorption spectrum with a Bessel function of the first kind. (**C**) The ground state spin ($S_G$ = 3) manifold of the Mn cofactor. Electron spin-spin interactions break the degeneracy of the ground state septet at zero magnetic field [zero-field splitting (ZFS)]. These levels further diverge because of the Zeeman interaction, scaling linearly with the applied field. The colored arrows represent allowed EPR transitions at W-band.

Zeeman interaction, and the hyperfine interaction ($A$). In the strong coupling limit ($A$ is large relative to $\nu_n$), as is typically seen for Mn complexes, spectral lines appear as pairs around multiples of $A$ and separated by twice $\nu_n$ (Fig. 3C). In contrast, in the weak coupling limit, spectral lines appear around $\nu_n$ separated by $A$ (Fig. 3D).

$^{55}$Mn-EDNMR spectra for the Mn cofactor poised in the $S_3$ state are shown in Fig. 3. Two classes of nuclear transitions are observed, representing the two coupling limits described above: Class 1 consists of a set of sharp transitions [full width at half maximum (FWHM) ≈ 10 MHz] in the range 50 to 300 MHz (Fig. 3, B and C); class 2 instead consists of a single, broader transition (FWHM ≈ 10 MHz) centered at the $^{55}$Mn nuclear Larmor frequency ($\nu_n$) (Fig. 3, B and D). The hyperfine coupling for class 1 represents the strong coupling limit, with a coupling of $|A| \approx 100$ MHz, whereas the hyperfine coupling for class 2 represents the weak coupling limit, with a coupling of $|A| < 30$ MHz. The two classes are easily distinguished by their magnetic-field dependence. The line positions of class 1 transitions shift dramatically depending on which EPR transition is pumped, whereas class 2 transitions all appear at approximately the same position (Fig. 3, C and D). Spin Hamiltonian simulations of the entire $^{55}$Mn-EDNMR data set are shown by the red dashed lines in Fig. 3B (figs. S7 and S9). The same parameter set reproduces concomitant $^{55}$Mn-ENDOR data collected at a lower microwave frequency (Q-band, (fig. S8, table S1, and supplementary materials, section 3.6).

The sharp spectral lines observed and the high level of symmetry seen for the $^{55}$Mn-EDNMR data set (the spectral pattern measured on the low and high field edges of the EPR spectrum are mirror images of each other) indicate that all hyperfine couplings of the complex are isotropic. The lack of large hyperfine anisotropy is a fingerprint for a particular motif, the all-octahedral, coordinatively saturated $Mn^{IV}$ ion, with its small hyperfine anisotropy stemming from its local quasi-spherical d-orbital configuration ($t_{2g}^3e_g^0$ for a perfect octahedron). Other possibilities—such as $Mn^{IV}$ complexes with tetrahedral (four-coordinate) or trigonal bipyramidal (five-coordinate) ligand fields, and all $Mn^{III}$ complexes—exhibit much larger hyperfine anisotropy (*26*). Thus, both the analysis of the EPR lineshape and $^{55}$Mn-EDNMR data support assignment of the $S_3$ state to an all-octahedral $(Mn^{IV})_4$ complex.

The observation that there are two classes of hyperfine couplings also places an important new restriction on the electronic structure of the $Mn_4O_5Ca$ cofactor. For simple monomeric $Mn^{III}$ and $Mn^{IV}$ complexes, the magnitude of the hyperfine interaction lies within a narrow range, 180 to 250 MHz (*26*). This situation becomes more complicated in systems containing more than one Mn ion, in which the magnitude of the measured hyperfine couplings is modified by two factors: (i) the total electronic spin state of the complex and (ii) the precise magnetic connectivity of the complex. Of these, the spin state is most important, with the measured hyperfine couplings scaling approximately with the inverse of the total electron spin. For example, in the all-$Mn^{IV}$ $Mn_3O_4Ca$ synthetic cubane complex mentioned above (*25*), which has a spin ground state of $S_G$ = 9/2, the observed $^{55}$Mn couplings are ≈60 MHz, which is 25 to 35% of monomeric complexes. The second factor, the magnetic connectivity of the complex, determines the contribution of each ion to the electronic spin state. In the case of the synthetic cubane complex, the three Mn ions interact so that each contributes equally to the electronic spin ground state. As such, the measured hyperfine coupling for each Mn is approximately the same. This is not a general result; for a system of arbitrary coupling topology, the contribution of one or more Mn ions can be diminished. In the case of the $Mn_4O_5Ca$ cofactor in the $S_3$ state, two of the Mn ions must have a small contribution to the ground spin state, whereas the other two ions have a large contribution, leading to two sets of measured hyperfine couplings. This result implies that the magnetic interactions within the cofactor are more complex than that seen for the symmetric model cubane complexes, essentially requiring a balancing of couplings to yield a dimer-of-dimers coupling topology (supplementary materials, section 3.7).

Density functional theory (DFT) models for the $Mn_4O_5Ca$ cofactor in the $S_3$ state were developed from the parent structural models of the $S_2$ state described above (Fig. 4, figs. S10 and S11, and supplementary materials, section 1.4) (*6*). Two possible scenarios can be envisaged to satisfy the requirement that all four Mn ions are six-coordinate in

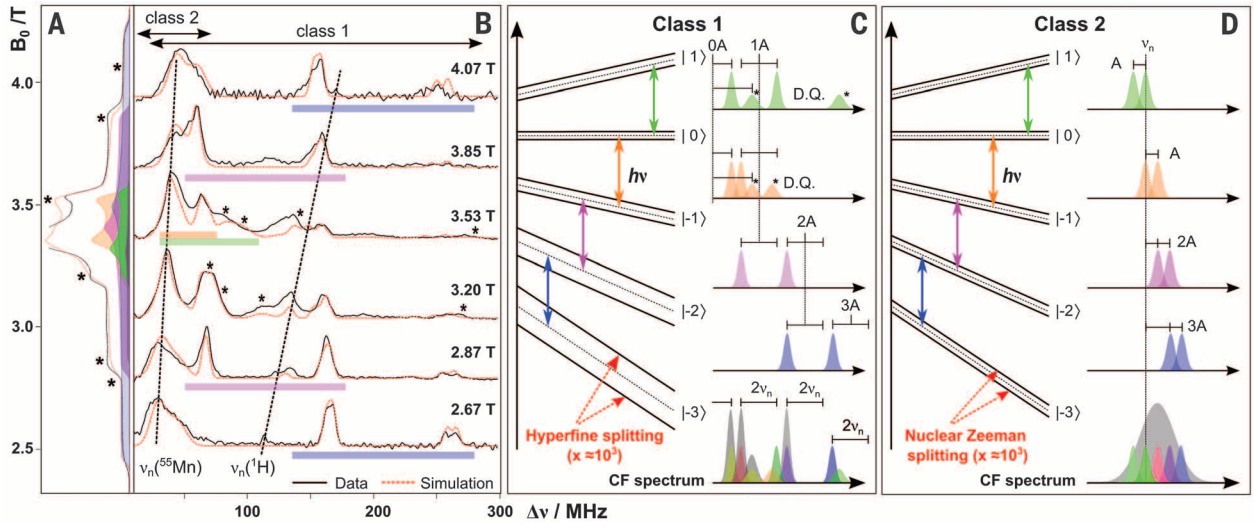


**Fig. 3. Measured and simulated $^{55}$Mn-EDNMR spectra of the $S_3$ state.** (**A**) EPR spectrum of the $S_3$ state measured at W-band showing the positions (asterisks) where the $^{55}$Mn-EDNMR spectra were collected. (**B**) W-band $^{55}$Mn-EDNMR spectra of $S_3$. The red dashed line is the result of a simulation using the spin Hamiltonian formalism. Double quantum transitions are marked with an asterisk. (**C**) Pictorial decomposition of the class 1–type nuclear transitions associated with each EPR transition of the ground-state spin manifold. These appear about multiples of the hyperfine coupling ($A \approx 100$ MHz) split by twice the $^{55}$Mn nuclear Larmor frequency [$\nu(^{55}Mn) = 35.8$ MHz at 3.4 T]. The color of each nuclear transition matches the EPR transition with which they are associated. Because the hyperfine splitting in the spectra scales with the electronic $m_S$ number, nuclear transitions associated with the $m_S = |-3\rangle \leftrightarrow |-2\rangle$ EPR transition define the high-frequency edge of the EDNMR spectra [(B), blue bars]. (**D**) Pictorial decomposition of the class 2–type nuclear transitions associated with each EPR transition of the ground-state spin manifold. These appear centered at the $^{55}$Mn nuclear Larmor frequency and split by the hyperfine coupling ($A < 20$ MHz). These transitions show a more modest magnetic field dependence and are located at ≈35 to 40 MHz. The composite center-field (CF) spectra shown at the bottom of (C) and (D) demonstrate the relative contributions of each transition to the measured spectra. Data processing and simulation details are given in the supplementary materials (materials and methods, section 3.4, and figs. S5, S7, and S9).

the $S_3$ state: (i) collapse of the inorganic core, rendering the O5 a $\mu_4$-oxo bridge; or (ii) core expansion, allowing the inclusion of an additional water-derived ligand. In a recent study, we examined the oxidation of the cofactor in the $S_2$ state using large models that included the redox active $Y_Z$ residue (*32*) and found that Mn oxidation does not occur in either of the $S_2$-state structures. Instead, the energetic minimum corresponds to the oxidation of the $Y_Z$ residue—the $S_2Y_Z^{\bullet}$ electronic configuration is obtained with no change in the structure of the inorganic core. These results are consistent with earlier experimental data that have suggested that $S_3$ formation is associated with a conformational change (*8*). Our next approach was to include an additional water-derived ligand within either the open or the closed cubane core, in the form of a hydroxyl group, so as to compensate for the net oxidation change of the cofactor—that is, proton release (*33*). In such models, the all-$Mn^{IV}$ electronic configuration, as established by the computed spin populations, is the energetic minimum, suggesting that one of the two oxidized $S_2$ state structures, with an additional OH ligand, indeed represents the $S_3$ state. Both structures broadly reproduce extended x-ray absorption fine structure (EXAFS) distance constraints (fig. S11) (*12*, *34*). From an energetic point of view, the open cubane form (Fig. 4) is 10 kcal $mol^{-1}$ lower in energy than is the closed cubane form, thus favoring it as the best candidate for the $S_3$ state structure. The open structure has a similar core connectivity to recent $S_3$ models proposed by Siegbahn (*35*). These calculations suggest that the structural flexibility seen in the $S_2$ state (*6*) is lost upon formation of the $S_3$ state.

The same structural model can readily rationalize the magnetic properties of the $S_3$ state presented above. The magnetism of the complex can be described in terms of pairwise exchange interactions between the four Mn ions, which are either ferromagnetic or antiferromagnetic. The coupling pathways within the open cubane subunit ($Mn_3O_4Ca$), which now only contains $Mn^{IV}$ ions, are dominantly ferromagnetic, rendering this fragment high-spin ($S = 9/2$) (*6*). This spin state is also a characteristic feature of $Mn^{IV}{}_3O_4Ca$ biomimetic models (*25*) because of the constrained $Mn^{IV}$-O-$Mn^{IV}$ bond angles (≈90°) within the cubane subunit, which essentially dampen all antiferromagnetic pathways (*36*). Antiferromagnetic coupling between the outer $Mn^{IV}$ (Mn4, $S = 3/2$) and the cubane subunit ($S = 9/2$), mediated by a more linear μ-oxo/μ-carboxylato bridging network, yields the experimentally observed ground spin state ($S_G = 3$) (Fig. 4 and fig. S11).

The open cubane model also reproduces the $^{55}$Mn hyperfine couplings. As indicated above, the hyperfine coupling constants measured with EPR for a magnetically coupled transition-metal complex depend on its electronic structure. The measured values can be expressed as the product of the site (hyperfine) couplings of the individual metal ions and a weighting factor that describes the contribution of each metal ion to the total electronic state. Because all four Mn ions have the same oxidation state (4+) and similar octahedral coordination geometries, the site hyperfine couplings are expected to be very similar. The calculated onsite hyperfine couplings for both structures fall in the range typically seen for synthetic monomeric $Mn^{IV}$ complexes (*26*), $A_{iso}$ = 170 to 250 MHz. In contrast, the individual metal ion contributions differ for the two structures. The Mn ions in the open cubane structure couple so that the four Mn ions have substantially different contributions. The weighting factors (spin-projection coefficients) for each of the metal ions fall into two classes: Mn1 and Mn2 carry a value of ≈0.5, whereas Mn3 and Mn4 carry a much smaller value of ≈0.1 to 0.2 (fig. S12, table S1, and supplementary materials, section 3.7). This yields the two distinct sets of hyperfine couplings, as seen in the experiment. The dimer-of-dimers coupling topology described above is a specific property of the open cubane motif that cannot be achieved in the closed cubane motif.

Recent spectroscopic studies have implicated O5 as representing the "early binding" substrate water molecule (*29*, *37*). In the $S_2$ state, the O5 ligand acts as either a bis-μ-oxo linkage between Mn4 and Mn3 (open structure) or a vertex of the cuboidal unit [closed structure (Fig. 4)]. The flexibility of this μ-oxo bridge is important for chemical function, presumably allowing the inclusion of the second substrate oxygen ligand along the Mn4-Mn1 axis upon $S_3$ formation seen here (Fig. 4). It remains to be determined whether this second substrate represents an additional water molecule binding from bulk solvent or a repositioned terminal oxygen ligand of Mn4 (that is, W2) or Ca (that is, W3). Regardless of its precise identity, O-O bond formation then most likely proceeds by coupling of the two proximal oxygens ligated to Mn1 and Mn4, as shown in Fig. 4 (*38*, *39*). After forming the all-$Mn^{IV}$ complex in the $S_3$ state, the last oxidation event is either substrate-centered (*40*), generating a $Mn^{IV}$-oxyl state in $S_4$ (*35*, *38*, *41*), or metal-centered, generating a $Mn^{V}$-oxo species (*42*). The predominance of ferromagnetic exchange interactions within the $Mn_3Ca$ cubane moiety, in conjunction with the antiferromagnetic exchange interaction between the outer Mn ($Mn_4$) and the cubane moiety, forces the Mn4 and Mn1 ions to carry opposite spin. In the context of a radical-coupling-type mechanism, this would lead to the development of opposite spin on the two substrate oxygens in

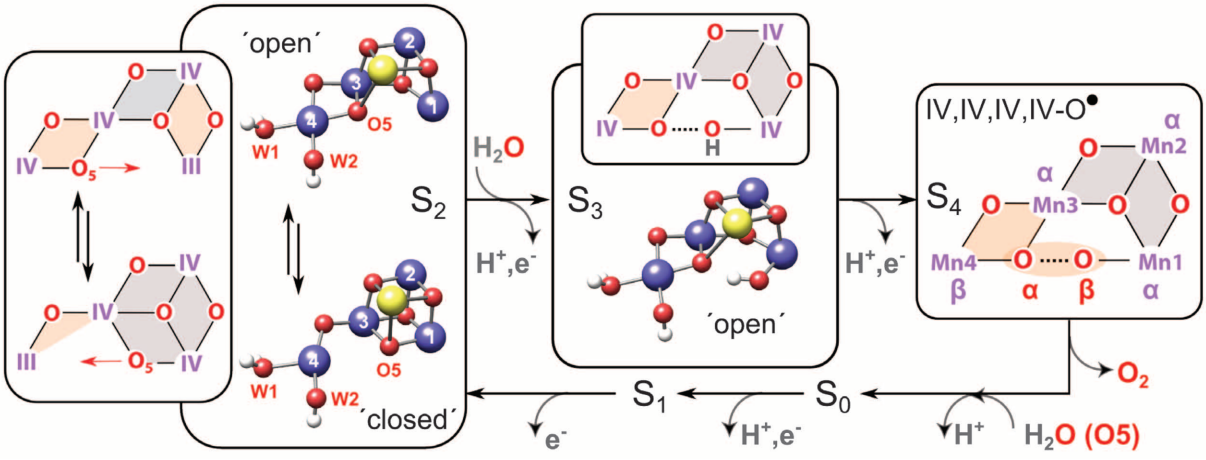


**Fig. 4. Theoretically calculated structures for the $S_2$ and $S_3$ states and the proposed mechanism of O-O bond formation**. Structures were developed from the x-ray crystal structure by using DFT as described in Pantazis *et al*. (*6*). The models presented were identified as candidates for the $S_2$ and $S_3$ structure of the cofactor on the basis of agreement of calculated geometric and spectroscopic parameters obtained from EXAFS and magnetic resonance data. Mn ions are depicted in violet, O in red, and Ca in yellow. Two-dimensional representations of the core connectivity and magnetic coupling pathways are also shown. Shaded boxes represent the antiferromagnetic (orange) and ferromagnetic (gray) interactions of the $Mn_4O_5Ca$ cofactor during the S-state cycle. Low-barrier O-O bond formation may be facilitated by antiparallel alignment of the spin on the two substrate oxygens in $S_4$, imparted by the Mn-Mn coupling topology of the $S_3$ ($S_4$) state (*35*, *38*, *41*).

the $S_4$ state—the $Mn^{IV}$-oxyl radical and the Mn ligated μ-oxo bridge (Fig. 4) (*29*)—facilitating low-barrier O-O bond formation (*35*, *38*, *41*).

This mechanistic framework provides a blueprint for the design of synthetic water-splitting catalysts. It is an all-$Mn^{IV}$ complex that proceeds to the O-O bond–forming transition state, with its formation coupled to the inclusion of the second substrate water at the open coordination site within the heterometallic cubane. This concerted process, oxidation coupled to substrate binding, may be of benefit in avoiding the binding/activation of both substrates in the resting state of the catalyst, "switching off" slow two-electron, catalase-like reactivity (*43*). Upon completion of the cycle, the heterometallic complex imposes the correct spin alignment for the two substrates in the transition state. This latter property can be exploited in heterogeneous $Mn_2O_2Ca$ oxide materials that form layered cuboidal-like structures (*2*) and may explain why a heterometallic MnCa complex evolved to perform the water-splitting reaction in the first place.

## REFERENCES AND NOTES


1. N. Cox, D. A. Pantazis, F. Neese, W. Lubitz, *Acc. Chem. Res.* **46**, 1588–1596 (2013).
2. M. Wiechen, I. Zaharieva, H. Dau, P. Kurz, *Chem. Sci.* **3**, 2330–2339 (2012).
3. B. Kok, B. Forbush, M. McGloin, *Photochem. Photobiol.* **11**, 457–475 (1970).
4. W. Hillier, J. Messinger, in *Photosystem II: The Light-Driven Water: Plastoquinone Oxidoreductase*, T. Wydrzynski, K. Satoh, Eds. (Springer, Dordrecht, Netherlands, 2005), vol. 22, pp. 567–608.
5. N. Cox, J. Messinger, *Biochim. Biophys. Acta* **1827**, 1020–1030 (2013).
6. D. A. Pantazis, W. Ames, N. Cox, W. Lubitz, F. Neese, *Angew. Chem. Int. Ed. Engl.* **51**, 9935–9940 (2012).
7. Y. Umena, K. Kawakami, J.-R. Shen, N. Kamiya, *Nature* **473**, 55–60 (2011).
8. Y. Pushkar, J. Yano, K. Sauer, A. Boussac, V. K. Yachandra, *Proc. Natl. Acad. Sci. U.S.A.* **105**, 1879–1884 (2008).
9. J. L. Zimmermann, A. W. Rutherford, *Biochim. Biophys. Acta* **767**, 160–167 (1984).
10. A. Boussac, J.-J. Girerd, A. W. Rutherford, *Biochemistry* **35**, 6984–6989 (1996).
11. J. Messinger *et al.*, *J. Am. Chem. Soc.* **123**, 7804–7820 (2001).
12. M. Haumann *et al.*, *Biochemistry* **44**, 1894–1908 (2005).
13. T. Noguchi, *Philos. Trans. R. Soc. B* **363**, 1189–1195 (2008).
14. A. Haddy, *Photosynth. Res.* **92**, 357–368 (2007).
15. T. Lohmiller, W. M. Ames, W. Lubitz, N. Cox, S. Misra, *Appl. Magn. Reson.* **44**, 691–720 (2013).
16. G. C. Dismukes, Y. Siderer, *Proc. Natl. Acad. Sci. U.S.A.* **78**, 274–278 (1981).
17. J. Messinger *et al.*, *J. Am. Chem. Soc.* **119**, 11349–11350 (1997).
18. K. A. Åhrling, S. Peterson, S. Styring, *Biochemistry* **36**, 13148–13152 (1997).
19. O. Horner *et al.*, *J. Am. Chem. Soc.* **120**, 7924–7928 (1998).
20. A. Haddy, K. V. Lakshmi, G. W. Brudvig, H. A. Frank, *Biophys. J.* **87**, 2885–2896 (2004).
21. S. L. Dexheimer, M. P. Klein, *J. Am. Chem. Soc.* **114**, 2821–2826 (1992).
22. T. Yamauchi, H. Mino, T. Matsukawa, A. Kawamori, T. Ono, *Biochemistry* **36**, 7520–7526 (1997).
23. A. Boussac, M. Sugiura, A. W. Rutherford, P. Dorlet, *J. Am. Chem. Soc.* **131**, 5050–5051 (2009).
24. Y. Sanakis, J. Sarrou, G. Zahariou, V. Petrouleas, in *Photosynthesis. Energy from the Sun. 14th International Congress on Photosynthesis*, J. F. Allen, E. Gantt, J. Golbeck, B. Osmond, Eds. (Springer, Dordrecht, Netherlands, 2008), p. 479.
25. S. Mukherjee *et al.*, *Proc. Natl. Acad. Sci. U.S.A.* **109**, 2257–2262 (2012).
26. N. Cox *et al.*, *J. Am. Chem. Soc.* **133**, 3635–3648 (2011).
27. J. M. Peloquin *et al.*, *J. Am. Chem. Soc.* **122**, 10926–10942 (2000).
28. L. V. Kulik, B. Epel, W. Lubitz, J. Messinger, *J. Am. Chem. Soc.* **129**, 13421–13435 (2007).
29. L. Rapatskiy *et al.*, *J. Am. Chem. Soc.* **134**, 16619–16634 (2012).
30. D. W. Randall *et al.*, *J. Am. Chem. Soc.* **117**, 11780–11789 (1995).
31. K. O. Schäfer *et al.*, *J. Am. Chem. Soc.* **120**, 13104–13120 (1998).
32. M. Retegan, N. Cox, W. Lubitz, F. Neese, D. A. Pantazis, *Phys. Chem. Chem. Phys.* **16**, 11901–11910 (2014).
33. A. Klauss, M. Haumann, H. Dau, *Proc. Natl. Acad. Sci. U.S.A.* **109**, 16035–16040 (2012).
34. C. Glöckner *et al.*, *J. Biol. Chem.* **288**, 22607–22620 (2013).
35. P. E. M. Siegbahn, *Biochim. Biophys. Acta* **1827**, 1003–1019 (2013).
36. V. Krewald, F. Neese, D. A. Pantazis, *J. Am. Chem. Soc.* **135**, 5726–5739 (2013).
37. M. Pérez Navarro *et al.*, *Proc. Natl. Acad. Sci. U.S.A.* **110**, 15561–15566 (2013).
38. P. E. M. Siegbahn, *Acc. Chem. Res.* **42**, 1871–1880 (2009).
39. K. Yamaguchi *et al.*, *Int. J. Quantum Chem.* **113**, 453–473 (2012).
40. M. Haumann *et al.*, *Science* **310**, 1019–1021 (2005).
41. P. E. M. Siegbahn, *Chem. Eur. J.* **12**, 9217–9227 (2006).
42. J. Limburg, V. A. Szalai, G. W. Brudvig, *J. Chem. Soc. Dalton Trans.* **1999**, 1353–1362 (1999).
43. A. W. Rutherford, *Trends Biochem. Sci.* **14**, 227–232 (1989).



## ACKNOWLEDGMENTS

The authors acknowledge A. Savitsky (Max-Planck-Institut für Chemische Energiekonversion Mülheim) for his assistance with the EPR measurements and M. Sugiura (Ehime University, Japan) for the gift of the *T. elongatus* strains. Financial support was provided by the Max-Planck-Gesellschaft, the "Bioénergie" program from the CEA, and by the French Infrastructure for Integrated Structural Biology (FRISBI) ANR-10-INSB-05-01.


## SUPPLEMENTARY MATERIALS

www.sciencemag.org/content/345/6198/804/suppl/DC1
Materials and Methods
Supplementary Text
Figs. S1 to S12
Tables S1 and S2
References (*44*–*76*)

17 April 2014; accepted 9 July 2014
10.1126/science.1254910

PLANT SCIENCE

# Genomic-scale exchange of mRNA between a parasitic plant and its hosts

**Gunjune Kim,[1] Megan L. LeBlanc,[1] Eric K. Wafula,[2] Claude W. dePamphilis,[2] James H. Westwood[1]***

**Movement of RNAs between cells of a single plant is well documented, but cross-species RNA transfer is largely unexplored. *Cuscuta pentagona* (dodder) is a parasitic plant that forms symplastic connections with its hosts and takes up host messenger RNAs (mRNAs). We sequenced transcriptomes of *Cuscuta* growing on *Arabidopsis* and tomato hosts to characterize mRNA transfer between species and found that mRNAs move in high numbers and in a bidirectional manner. The mobile transcripts represented thousands of different genes, and nearly half the expressed transcriptome of *Arabidopsis* was identified in *Cuscuta*. These findings demonstrate that parasitic plants can exchange large proportions of their transcriptomes with hosts, providing potential mechanisms for RNA-based interactions between species and horizontal gene transfer.**

*Cuscuta* species (dodders) are parasitic plants that obtain water and nutrients from their plant hosts by using specialized organs termed haustoria. The haustoria of *Cuscuta* develop from the stem of the parasite, where it coils around the host, penetrating host tissues and ultimately forming vascular connections (*1*, *2*). These connections allow transfer of not only water and nutrients into the parasite but macromolecules, including mRNAs (*3*–*5*) and proteins (*6*), and even pathogens, such as viruses (*7*, *8*), viroids (*9*), and phytoplasmas (*10*). Here, we characterize the scope and directionality of mRNA movement.

mRNA trafficking between cells regulates plant development (*11*, *12*), with potential for controlling processes such as leaf shape (*13*, *14*), time of flowering (*15*), tuber formation (*16*, *17*), and root growth (*18*). Small RNAs can also act systemically to influence plant development (*19*), and a construct encoding a silencing RNA and expressed in a host plant can silence a *Cuscuta* gene (*20*). Although this last example is from an artificial construct, it supports the idea that RNA movement between separate plant individuals can function as a type of organismal communication (*21*). We used transcriptomics to investigate the RNA transfer between *Cuscuta* and its hosts.

*Cuscuta* species parasitize a wide range of broad-leaved plants (often simultaneously) and are destructive to crops, such as tomato (*Solanum*

[1]Department of Plant Pathology, Physiology and Weed Science, Virginia Tech, Blacksburg, VA 24061, USA. [2]Department of Biology and the Huck Institutes of the Life Sciences, Pennsylvania State University, University Park, PA 16802, USA.
*Corresponding author. E-mail: westwood@vt.edu

*lycopersicum*) (*22*). We grew *Cuscuta* on *Arabidopsis thaliana* and tomato hosts because the sequenced genomes of these species facilitates confident identification of host and parasite transcripts from mixed RNA populations. We harvested three distinct regions for each parasite-host association for analysis (Fig. 1A). The *Cuscuta* haustorium grows toward the center of the host stem and does not spread systemically inside the host (*2*), so the tissues harvested did not risk inclusion of endophytic haustorial tissue that could lead to cross-contamination of samples. Furthermore, the growth habit of *Cuscuta* allows unattached stem regions to be easily collected separate from the interface regions where haustoria bind tightly to host tissues (Fig. 1A and fig. S1).

To identify host and parasite mobile transcriptomes, we sequenced cDNA libraries derived from each of the three tissues. The rate of RNA mobility was expected to be low, so the first libraries were sequenced with a full lane of Illumina GAIIx (Illumina, Incorporated, San Diego, CA) for one run each of *Cuscuta* growing on *Arabidopsis* and tomato hosts. Second and third biological replicates of *Cuscuta* with *Arabidopsis* were sequenced with a full lane and one-sixth lane of the higher output HiSeq 2000 (Illumina, Incorporated) platform, respectively. This yielded over 1.6 billion high-quality reads, which were subjected to various controls by which we filtered out contaminating reads and poor quality reads and trimmed away adapters and primers. Reads were then identified as host, parasite, or too highly conserved to assign (fig. S2). The parasite reads were used to reconstruct a *Cuscuta* transcriptome assembly.

Reads from each library were stringently mapped to host and parasite transcriptomes to estimate RNA movement between the species. *Arabidopsis* read proportions in parasite tissue averaged 1.1% of total mapped reads across the three sequencing runs, whereas host stems contained 0.6% *Cuscuta* reads (Fig. 1B). Read mapping in the tomato-*Cuscuta* association suggested somewhat lower rates of transfer, but the pattern was similar to that of *Arabidopsis* with the exception of interface tissue, where the greater mass of the tomato stem likely resulted in a higher proportion of reads. Bidirectional mobility in transcript movement is consistent with the long-established ability of *Cuscuta* to transmit viruses between plants bridged by the parasite (*7*) and suggests that *Cuscuta* is capable of transmitting mRNAs between different plants.

Independent confirmation of mobility was shown by reverse transcription polymerase chain reaction (RT-PCR) amplification and subsequent sequencing of selected transcripts. Mobility of 24 tomato transcripts into *Cuscuta* has been documented this way (*3*, *23*), so we analyzed *Arabidopsis* transcripts moving into *Cuscuta* and *Cuscuta* transcripts moving into *Arabidopsis* and tomato hosts (fig. S3). Such confirmation is not practical for all mobile transcripts, but the output of read mapping itself produced a compelling picture of RNA transfer (Fig. 2). The read sequences and coverage from parasite stem tissue closely matched those of the interface tissue, with the exception that mobile mRNAs in the parasite occurred in fully spliced mature form; introns were only found in libraries derived from host stem or interface tissues.

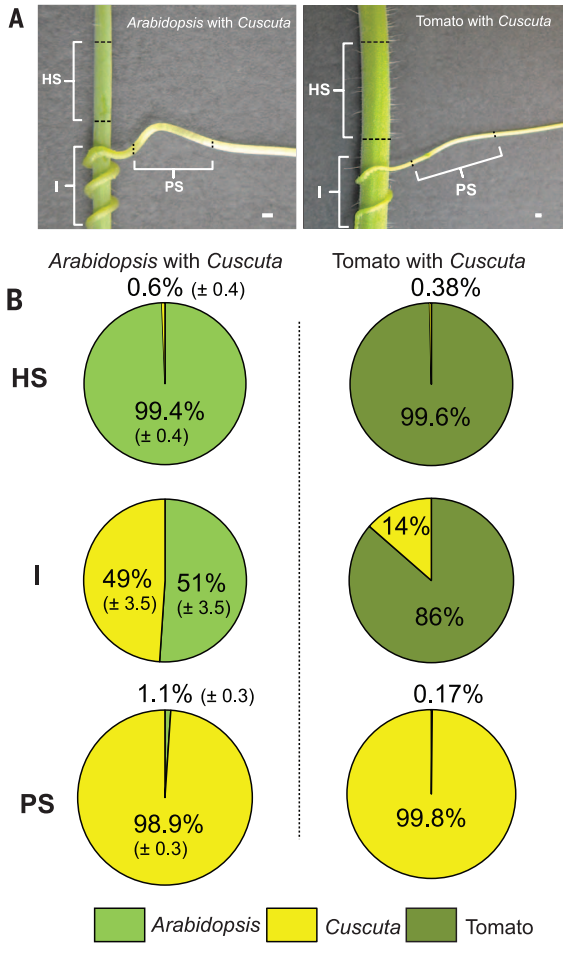


**Fig. 1. Transcriptome compositions of host and parasite tissues at and near the region of haustorial attachment.** (**A**) Tissues analyzed were the host stem above the region of attachment (HS), interface region where parasite is connected to the host (I), and the parasite stem near the region of attachment (PS). Scale bars represent 1 mm. (**B**) Pie charts show the proportions of reads mapped to host and parasite transcriptomes in each tissue. *Arabidopsis* with *Cuscuta* data are means (±SE) of three separate sequencing runs; tomato with *Cuscuta* data are from one run.

The diversity of transcripts represented by the mobile reads was determined by high-stringency mapping of reads from the three species (*Arabidopsis*, tomato, and *Cuscuta*) to their combined reference sequences. The criterion for transcript mobility was set by using fragment counts where one fragment represents either a matched pair of reads or a single unpaired read. The threshold for mobile transcripts was set at a mean of four fragments per transcript because this level was found to produce positive RT-PCR confirmation (fig. S3), whereas eight fragments per transcript was considered strong evidence of mobility. The greatest number of mobile transcripts originated from *Arabidopsis* hosts, with 45% (9518) of the genes in the expressed *Arabidopsis* transcriptome found in *Cuscuta*, and most of these (5983) showed strong evidence of mobility (Table 1). In contrast, tomato hosts produced substantially fewer mobile transcripts than *Arabidopsis*, with 347 (1.6% of total expressed) detected in the parasite. Part of the difference between tomato and *Arabidopsis* transcript mobility into *Cuscuta* may be attributed to the single sample of tomato-*Cuscuta* sequenced and the lack of deep sequencing from a full lane of HiSeq 2000 data, but even allowing for these differences there appear to be differences in RNA transfer to the parasite from different host species.

With respect to movement from parasite to host, 8655 *Cuscuta* unigenes were classified as mobile into *Arabidopsis* stem, and 5973 unigenes showed strong evidence of mobility (Table 1). This is 24% of the 35,614 unigenes expressed in *Cuscuta*. Tomato host uptake of *Cuscuta* transcripts was again lower than that of *Arabidopsis*, with 288 unigenes showing evidence of mobility. The rates of transcript movement between *Cuscuta* and the two hosts were consistent in both directions, with a much freer exchange occurring between *Cuscuta* and *Arabidopsis* than between *Cuscuta* and tomato, suggesting that mechanisms regulating haustorial selectivity may be host-specific.

We asked whether mobile and nonmobile RNAs have distinctive properties that provide insight into mechanisms of mobility. One characteristic common to mobile transcripts was high abundance, as measured by fragments per kilobase per million mapped reads (FPKM) in the interface region, and this was especially pronounced for the *Arabidopsis* interaction with *Cuscuta* (Fig. 3A). FPKM (*24*) was used because it normalizes fragment counts to transcript length and depth of transcriptome sequencing to better estimate transcript

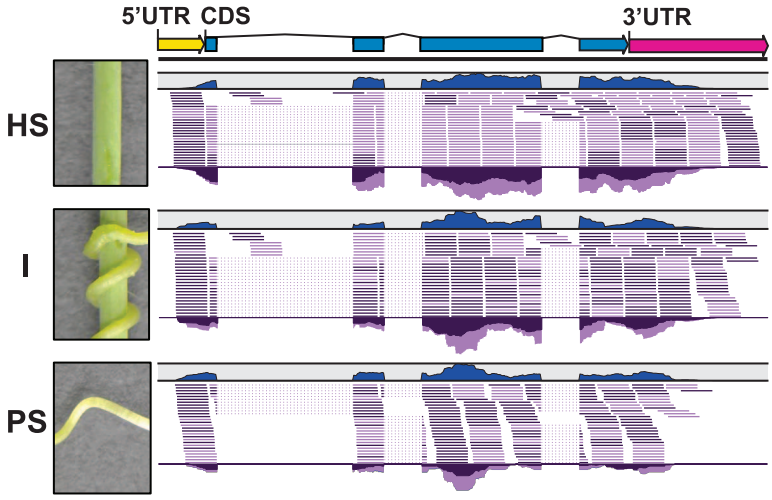


**Fig. 2. Example of read assemblies of an *Arabidopsis* gene, *TRANSLATIONALLY CONTROLLED TUMOR PROTEIN* (*AtTCTP*), in host stem (HS), interface (I), and parasite stem (PS) tissues.** Intron sequences were not found in sequences derived from parasite tissue. The gene model at top indicates coding sequence as blue bars and introns as line bridges. Dark and light purple lines indicate forward and reverse paired reads, respectively, as mapped to the gene model. UTR, untranslated region; CDS, coding sequence.

levels. The patterns were similar for mobile and nonmobile transcripts in the tomato-*Cuscuta* interaction, although tomato nonmobile transcripts spanned the spectrum from low to high abundance (Fig. 3B). This indicates that one aspect of transcript mobility is related to their high abundance in the cells near the host-parasite boundary, but it is not the only factor influencing mobility, as evidenced by the many transcripts with similar expression levels yet differing mobility.

To consider whether transcript mobility is associated with gene function, we used OrthoMCL software to generate orthologous clusters of mobile and nonmobile gene classes that were common to all three species (*25*) (Fig. 3C). Assigning genes from these clusters to gene ontology terms led to the identification of terms enriched among mobile and nonmobile classes (table S2). Restricting the list to those terms that were only enriched for multiple species (e.g., transcripts from both *Arabidopsis* and *Cuscuta*) yielded smaller sets of terms that may reflect core mobile and nonmobile categories (Fig. 3D). These results demonstrate that mobility can be correlated with gene function, but the mechanistic basis for such correlations remains obscure. For example, a large proportion of mobile transcripts are assigned to the response-to-stimulus term; it is possible that these transcripts are specifically targeted for intercellular mobility, but it is also possible that characteristics of transcript accumulation or localization in the cytoplasm makes them especially prone to host-parasite exchange.

Further evidence for selective mobility of RNAs comes from plots of transcript abundance in the interface region versus abundance of the same transcripts in the parasite stem (Fig. 4). The plot of *Arabidopsis* to *Cuscuta* mobile transcripts showed that levels of most transcripts in the parasite were about one-hundredth of those in the interface tissues, indicating that most transcripts follow the same dynamics of movement (Fig. 4A). However, some host RNAs appear to move more readily into the parasite and occurred at FPKM levels in the parasite nearly equal to those in the interface (seen as outliers above the main group in Fig. 4). The tomato-*Cuscuta* data showed a more-dispersed pattern of mobilities that supports the idea that dynamics of movement differ between tomato and *Arabidopsis* hosts (Fig. 4B).

**Table 1. Numbers of genes and unigenes with mobile transcripts from hosts into *Cuscuta* or *Cuscuta* into hosts.** The numbers represent transcript reference (the *Arabidopsis* Information Resource reference annotation TAIR 10/International Tomato Annotation Group annotation ITAG 2.4/*Cuscuta* unigenes) sequences as categorized by number of fragments detected in self and nonself tissues. A threshold of four fragments per gene was used to determine transcript detection, with four fragments detected in nonself tissues considered evidence for mobility and eight fragments providing strong evidence for mobility.

| Mobility category | *Arabidopsis-Cuscuta* | | *Tomato-Cuscuta* | |
|---|---|---|---|---|
| | *Arabidopsis* genes | *Cuscuta* unigenes | Tomato genes | *Cuscuta* unigenes |
| Total mobile | 9,518 | 8,655 | 347 | 288 |
| Mobile (>8 fragments) | 5,983 | 5,973 | 147 | 116 |
| Mobile (>4 fragments) | 3,535 | 2,682 | 200 | 172 |
| Nonmobile | 11,874 | 26,960 | 21,848 | 26,717 |
| Total expressed genes/unigenes | 21,392 | 35,614 | 22,194 | 27,005 |

An unresolved question regarding *Cuscuta* haustoria is the precise route used to acquire material from the host. Substantial physiological evidence points to symplastic connections consistent with direct transfer between phloem tissues of host and parasite [e.g., (*8*)], but no open phloem connections have been observed (*26*). Rather, *Cuscuta* haustorial cells share plasmodesmata with hosts across chimeric cell walls (*2*, *8*), and these have been implicated in host-parasite mobility of RNA (*4*). The long-distance movement of RNAs in the parasite suggest phloem involvement (*4*, *5*), but our data indicate that the situation is complex. We compared transcripts moving from *Arabidopsis* into *Cuscuta* to published phloem transcriptome data from *Arabidopsis* and four other species (*27*–*31*), finding significant associations between the data sets (table S3). Further analysis using the subset of *Arabidopsis* transcripts with especially high mobility into *Cuscuta* (i.e., those significantly above the mass of data points in Fig. 4A) indicated correlations with the more-robust data sets (*Arabidopsis* and ash) but did not demonstrate a linkage between phloem-associated transcripts and high mobility into *Cuscuta* (table S4). Our data also indicate that *Cuscuta* acquires transcripts such as the ribulose-1,5-bisphosphate carboxylase-oxygenase (RuBisCO) small subunit, which is not considered part of an authentic phloem transcriptome (*32*). Taken together, these data suggest that host-parasite RNA exchange includes RNAs known to occur in phloem but also many RNAs from other cells.

We can only speculate about the importance of large-scale mRNA movement between individuals of different species. For example, some specific mRNAs transmit information long distances in plants (*13*, *14*, *18*, *33*), and these same information molecules could help the parasite track host physiological status or, in the other direction, use its own mRNA to manipulate the host to facilitate parasitism. However, it is not known whether mobile mRNAs act through translation into protein or through another mechanism, so it is unclear whether mRNAs could even function across widely different species. Host mRNAs disappear within several hours inside *Cuscuta* (*5*), but this could be due to processes such as translation into protein or degradation for nucleotide recycling. In this regard, the question of whether *Cuscuta* can distinguish its own transcripts from those of its hosts is interesting.

This widespread exchange of mRNA raises the possibility of horizontal gene transfer (HGT).

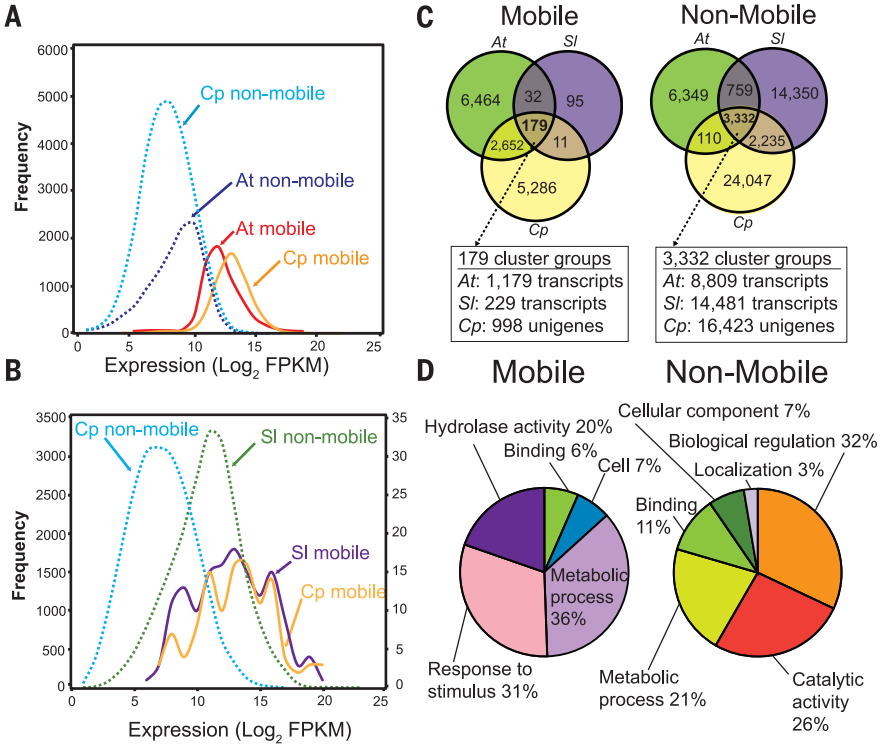


**Fig. 3. Properties of mobile and nonmobile RNAs.** (**A**) Distribution of transcript expression levels in interface tissue as related to mobility in *Arabidopsis-Cuscuta* associations. (**B**) Same as (A), but for mobility in tomato-*Cuscuta* associations. (**C**) Venn diagrams showing common sets of transcripts that were either mobile or nonmobile out of *Arabidopsis*, tomato, or *Cuscuta*. Numbers are orthologous clusters as determined by OrthoMCL. (**D**) Pie charts showing Gene Ontology (GO) slim terms as proportions of sets of 11 mobile and 23 nonmobile GO terms that were enriched for multiple species. The full lists of GO slim terms for these data sets and all terms significantly overrepresented and underrepresented in each of the three species are given in table S2.

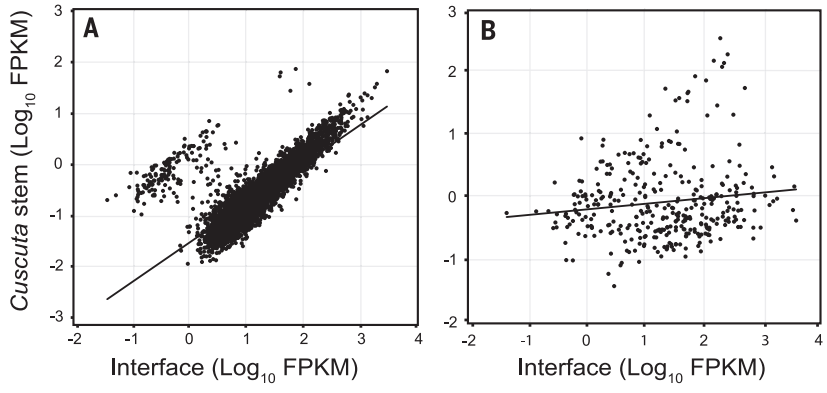


**Fig. 4. Scatter plots of transcript abundance (FPKM) in parasite stem versus host-parasite interface.** (**A**) A total of 9518 *Arabidopsis* transcripts identified as mobile into *Cuscuta* (Table 1). (**B**) A total of 347 tomato transcripts identified as mobile into *Cuscuta*. Lines are linear regressions of the data.

Given what appears to be a constant exchange of mRNA between *Cuscuta* and its hosts, the relative prevalence of cases of HGT involving *Cuscuta* is not surprising (*34*–*38*). Although most documented cases of HGT in parasitic plants suggest a mechanism involving direct transfer of DNA, at least one case of HGT into a parasitic plant (*Striga hermonthica*) exhibits evidence of an RNA intermediate in the mechanism (*39*). The ability of one *Cuscuta* plant to bridge many different host individuals raises the possibility that this parasite could mediate RNA exchange across different individuals and even across hosts of different species.

## REFERENCES AND NOTES


1. J. Dawson, L. Musselman, P. Wolswinkel, I. Dörr, *Rev. Weed Sci.* **6**, 265–317 (1994).
2. K. C. Vaughn, *Protoplasma* **220**, 189–200 (2003).
3. J. K. Roney, P. A. Khatibi, J. H. Westwood, *Plant Physiol.* **143**, 1037–1043 (2007).
4. R. David-Schwartz, S. Runo, B. Townsley, J. Machuka, N. Sinha, *New Phytol.* **179**, 1133–1141 (2008).
5. M. LeBlanc, G. Kim, B. Patel, V. Stromberg, J. Westwood, *New Phytol.* **200**, 1225–1233 (2013).
6. S. Haupt, K. J. Oparka, N. Sauer, S. Neumann, *J. Exp. Bot.* **52**, 173–177 (2001).
7. R. M. Hosford, *Bot. Rev.* **33**, 387–406 (1967).
8. M. Birschwilks, S. Haupt, D. Hofius, S. Neumann, *J. Exp. Bot.* **57**, 911–921 (2006).
9. H. J. M. van Dorst, D. Peters, *Eur. J. Plant Pathol.* **80**, 85–96 (1974).
10. M. Kamińska, M. Korbin, *Acta Physiol. Plant.* **21**, 21–26 (1999).
11. W. J. Lucas *et al.*, *J. Integr. Plant Biol.* **55**, 294–388 (2013).
12. C. G. N. Turnbull, R. M. Lopez-Cobollo, *New Phytol.* **198**, 33–51 (2013).
13. V. Haywood, T.-S. Yu, N.-C. Huang, W. J. Lucas, *Plant J.* **42**, 49–68 (2005).
14. M. Kim, W. Canio, S. Kessler, N. Sinha, *Science* **293**, 287–289 (2001).
15. C. Li *et al.*, *Sci. Rep.* **1**, 73 (2011).
16. A. K. Banerjee, T. Lin, D. J. Hannapel, *Plant Physiol.* **151**, 1831–1843 (2009).
17. D. J. Hannapel, *J. Integr. Plant Biol.* **52**, 40–52 (2010).
18. M. Notaguchi, S. Wolf, W. J. Lucas, *J. Integr. Plant Biol.* **54**, 760–772 (2012).
19. A. Molnar *et al.*, *Science* **328**, 872–875 (2010).
20. A. Alakonya *et al.*, *Plant Cell* **24**, 3153–3166 (2012).
21. P. Sarkies, E. A. Miska, *Science* **341**, 467–468 (2013).
22. Y. Goldwasser, W. T. Lanini, R. L. Wrobel, *Weed Sci.* **49**, 520–523 (2001).
23. J. H. Westwood, J. K. Roney, P. A. Khatibi, V. K. Stromberg, *Pest Manag. Sci.* **65**, 533–539 (2009).
24. C. Trapnell *et al.*, *Nat. Biotechnol.* **28**, 511–515 (2010).
25. F. Chen, A. J. Mackey, C. J. Stoeckert Jr., D. S. Roos, *Nucleic Acids Res.* **34**, D363–D368 (2006).
26. K. C. Vaughn, *Int. J. Plant Sci.* **167**, 1099–1114 (2006).
27. R. Deeken *et al.*, *Plant J.* **55**, 746–759 (2008).
28. X. Bai *et al.*, *PLOS ONE* **6**, e16368 (2011).
29. C. Doering-Saad, H. J. Newbury, C. E. Couldridge, J. S. Bale, J. Pritchard, *J. Exp. Bot.* **57**, 3183–3193 (2006).
30. S. Guo *et al.*, *Nat. Genet.* **45**, 51–58 (2013).
31. S. Huang *et al.*, *Nat. Genet.* **41**, 1275–1281 (2009).
32. R. Ruiz-Medrano, B. Xoconostle-Cázares, W. J. Lucas, *Development* **126**, 4405–4419 (1999).
33. D. J. Hannapel, P. Sharma, T. Lin, *Front. Plant Sci.* **4**, 10.3389/fpls.2013.00257 (2013).
34. J. P. Mower, S. Stefanović, G. J. Young, J. D. Palmer, *Nature* **432**, 165–166 (2004).
35. J. P. Mower *et al.*, *BMC Biol.* **8**, 150 (2010).
36. L. Jiang *et al.*, *PLOS ONE* **8**, e81389 (2013).
37. Y. Zhang *et al.*, *BMC Evol. Biol.* **13**, 48 (2013).
38. D. Zhang *et al.*, *BMC Plant Biol.* **14**, 19 (2014).
39. S. Yoshida, S. Maruyama, H. Nozaki, K. Shirasu, *Science* **328**, 1128 (2010).


## ACKNOWLEDGMENTS

Data are archived at National Center for Biotechnology Information BioProject ID PRJNA257158. This research was supported by NSF award IOS-0843372 to J.H.W. and NSF Plant Genome Research Program awards DBI-0701748 and IOS-1238057 to J.H.W. and C.W.D., with additional support to J.H.W. from the U.S. Department of Agriculture Hatch Project no. 135997. This work was facilitated by resources provided by the iPlant Collaborative. We are grateful to T. Lanini for supplying *C. pentagona* seeds. Additional data are in supplementary materials.

## SUPPLEMENTARY MATERIALS

www.sciencemag.org/content/345/6198/808/suppl/DC1
Materials and Methods
Figs. S1 to S4
Tables S1 to S5
References (*40*–*47*)

10 March 2014; accepted 3 July 2014
10.1126/science.1253122

WATER ENGINEERING

# Reducing sewer corrosion through integrated urban water management

Ilje Pikaar,* Keshab R. Sharma,* Shihu Hu, Wolfgang Gernjak, Jürg Keller, Zhiguo Yuan†

**Sewer systems are among the most critical infrastructure assets for modern urban societies and provide essential human health protection. Sulfide-induced concrete sewer corrosion costs billions of dollars annually and has been identified as a main cause of global sewer deterioration. We performed a 2-year sampling campaign in South East Queensland (Australia), an extensive industry survey across Australia, and a comprehensive model-based scenario analysis of the various sources of sulfide. Aluminum sulfate addition during drinking water production contributes substantially to the sulfate load in sewage and indirectly serves as the primary source of sulfide. This unintended consequence of urban water management structures could be avoided by switching to sulfate-free coagulants, with no or only marginal additional expenses compared with the large potential savings in sewer corrosion costs.**

Urban sewer networks collect and transport domestic and industrial wastewaters through underground pipelines to wastewater treatment plants for pollutant removal before environmental discharge. They protect our urban society against sewage-borne diseases, unhygienic conditions, and noxious odors and so allow us to live in ever larger and more densely populated cities. Today's underground sewer infrastructure is the result of an enormous investment over the last 100+ years with, for example, an estimated asset value of one trillion dollars in the USA (*1*). This equates to ~7% of its current gross domestic product. However, these assets are under serious threat with an estimated annual asset loss of around $14 billion in the United States alone (*1*). Sulfide-induced concrete corrosion is recognized as a main cause of sewer deterioration in most cases (*2*).

Under the anaerobic conditions common in sewage, sulfate is reduced to hydrogen sulfide by sulfate-reducing bacteria (*3*). The emission of hydrogen sulfide in gravity sewer sections, sewage pumping stations, and inlet structures of wastewater treatment plants induces sulfide oxidation to form corrosive sulfuric acid on concrete surfaces exposed to air (*4*, *5*). The presence of sulfate in wastewater and its conversion to sulfide in anaerobic sewers are generally considered unavoidable, and water utilities around the world have been focusing on the removal of sulfide after its formation (*3*, *5*–*7*), incurring mitigation costs comparable to the value of asset losses (*3*).

Sulfate in sewage can originate from three potential sources, namely, sulfate in source water used for drinking water production, sulfate added as the counter ions of aluminum or iron salts used as coagulants in the water treatment processes, and human and/or industrial wastes discharged. Coagulation plays an important role in drinking water treatment (*8*, *9*). It removes (colloidal) solids and natural organic matter (NOM), which can compromise disinfection and act as precursors for disinfection by-products. Sulfate- and chloride-based aluminum (Al) or iron (Fe) salts are most commonly used.

To reveal the relative contribution of each of the three sources, we conducted an extensive measurement campaign over 2 years (January 2009 to December 2010), during which we monitored sulfate levels in raw source water, drinking water, and sewage in a suburban area in South East Queensland, Australia (*10*), where aluminum sulfate is used as coagulant in the drinking water production. Sulfate concentrations in the source water supplying a water treatment plant, produced water from the plant, and sewage from a sewage pumping station collecting freshly discharged sewage from ~2900 households supplied by the plant were analyzed weekly. We subsequently conducted an extensive industry survey in Australia, comparing sulfate data in drinking water with and without sulfate addition during water treatment.

As much as 52% of the sulfate present in the sewage of the monitored area is contributed by the addition of aluminum sulfate as coagulant in the drinking water production, with a net contribution of 9.2 mg S/liter (Fig. 1 and fig. S1). This result is supported by the national industry survey (table S1). Among the 77 plants surveyed, 51 plants provided sulfate data in both the source and produced waters. The sulfate levels in the source and product waters are comparable in the 17 plants that do not use sulfate-containing coagulants (Fig. 2). In the remaining 34 plants, where sulfate-based coagulants are added, the average sulfate concentration in the produced drinking water is approximately four times that in the source water (Fig. 2). The average sulfate addition in the 34 plants is 10.1 mg S/liter, comparable to the 9.2 mg S/liter increase measured in our sampling campaign (Fig. 1). These results reveal the substantial contribution of sulfate-based coagulants to sulfate levels in drinking water. The dosing rates (1.9 to 20.3 mg S/liter) are in agreement with the practice in other countries (table S2) and are also consistent with the theoretical demand. The coagulant dosing rate is typically determined by the NOM concentration in the source water, with a theoretical dosing ratio of 1.0 mg Al/mg C (*11*). The NOM levels in source waters typically range between ~3 and 15 mg C/liter (*12*–*14*), which would lead to a sulfate addition of 5 to 27 mg S/liter.

Forty-three out of the 77 plants surveyed (56%) use aluminum sulfate as the coagulant, which confirmed its widespread application. This result is consistent with reports from other countries such as the United States, China, India, and the United Kingdom (table S2).

There is evidence that sewers are more seriously corroded in cities and regions with higher sulfate concentrations in drinking water (fig. S2). To assess the impact that sulfate-based coagulants can have on sewer corrosion, we performed extensive simulation studies using a virtual sewer network with average characteristics (*10*, *15*). To enable a robust and equitable comparison between the different simulation cases, we implemented chemical dosing in the model (*16*). Through the addition of ferric chloride, a commonly used chemical for corrosion mitigation (*7*), the dissolved sulfide concentration was maintained at low levels (mostly below 0.5 mg S/liter) in all cases. With the addition of sulfate at 5 to 15 mg S/liter in the drinking treatment, the predicted costs for sulfide mitigation in sewers increased by ~30 to 50% compared with the case

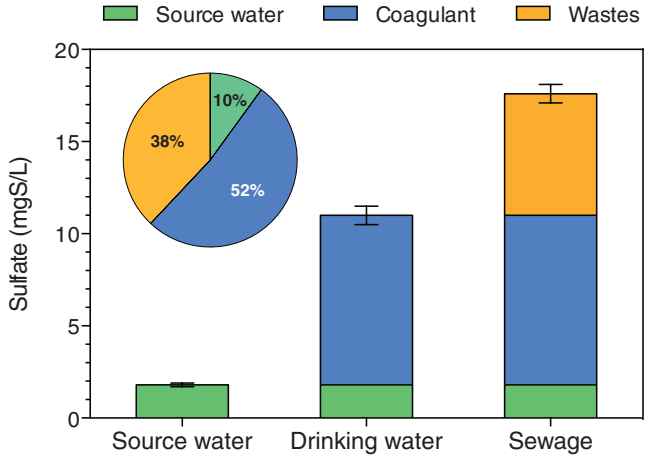


**Fig. 1. Sulfate concentrations in source water, drinking water, and sewage in the sampled suburban area in 2009–2010.** The sample sizes for the source water, drinking water, and sewage are 101, 104, and 92, respectively. Presented data are means ± SEM. The inset shows the relative contributions of the three sources.

The University of Queensland, Advanced Water Management Centre, Queensland 4072, Australia.
*These authors contributed equally to this work †Corresponding author. E-mail: z.yuan@awmc.uq.edu.au

without sulfate addition (Fig. 3). We performed 72 additional simulation runs with the source water sulfate concentration, hydraulic retention time, rising main fraction, and sewage temperature systematically varied within their typical ranges (*10*). The results reveal that substantial cost savings can be achieved by avoiding the use of sulfate-based coagulants in all cases except when the source water already contains a high level of sulfate (e.g., >10 mg S/liter) (fig. S4A). Sulfate concentration in source waters is dependent on geological conditions and varies substantially between regions. It varies between ~1 and 14 mg S/liter with a mean value of 3.4 mg S/liter and a median value of 2.2 mg S/liter in the surveyed Australian cities (Fig. 2). Wide concentration ranges have also been reported for other parts of the world from <1 to >300 mg S/liter, with typical values of 5 to 7 mg S/liter (*17*, *18*). These results imply that the majority of source waters have a sulfate concentration that is below the threshold values (10 to 15 mg S/liter) revealed by our simulation studies.

Our results highlight the benefits that could be attained by replacing sulfate-based coagulants with alternative, non–sulfate-based coagulants. Ferric chloride and polyaluminum chloride (PAC) are similarly effective coagulants and readily available and are indeed already used by some water utilities worldwide (*19*). The changeover costs are generally very low compared with the downstream saving potential, which may help water utilities, who are facing large, and still escalating, expenditures for the protection and rehabilitation of sewer assets (*20*, *21*).

In cases where source waters contain high levels of sulfate (e.g., > 10 to 15 mg S/liter), proactive sulfate removal could be considered. Nanofiltration or reverse osmosis, for example, typically removes 95% to >99% of sulfate but is associated with high capital and operational costs. Simulation results show, however, that substantial savings can be achieved in corrosion management by removing sulfate from source water (fig. S5), which could largely offset the cost for membrane filtration. For example, the addition of a nanofiltration step in a French water treatment plant resulted in an increase of only €0.045/$m^3$ in its operational costs (*22*). The filtration process also removes NOM, which would generate additional benefits such as the reduction of disinfection by-products, micropollutants, and microbial hazards, all of which are key considerations for public health protection (*23*, *24*). Similar benefits can be achieved by the use of "climate-independent" water sources, such as desalination or potable water reuse that typically incorporate similar membrane filtration processes. However, such advanced treatment methods are more energy- and cost-intensive compared with conventional drinking water treatment (*25*). Their potential application should be carefully assessed from a health, economic, and environmental perspective.

Many water utilities will need to upgrade both their water supply and wastewater service infrastructure over the next 10 to 15 years, which will require enormous capital investments (*21*, *23*, *26*). Our findings show that there are critically important connections between these two seemingly independent systems. Although integrated urban water management and total water-cycle planning are firmly anchored in many policies developed by various levels of governments, in reality, individual subsystems—such as drinking water production and sewer and/or wastewater management—are often considered separately and optimized to generate locally maximized benefits (or least cost) without taking into account the existing connections across the water cycle. Our results show that such a disconnected management strategy can generate negative impacts in other parts of the urban water infrastructure. Although the technical challenges of reducing sulfate in sewage seem simple, institutional barriers may prevent a shift toward a whole-of-water-cycle optimization strategy. Given the increasing complexity and interdependence of the urban water systems, including recent trends in local water reuse, water-sensitive urban design, and low-impact development, the development and consistent application of novel, system-wide integration tools are essential to an overall optimization strategy. Such advances will be crucial to encourage the water industry to fully embrace integrated urban water management processes and to reap the benefits of this valuable concept.

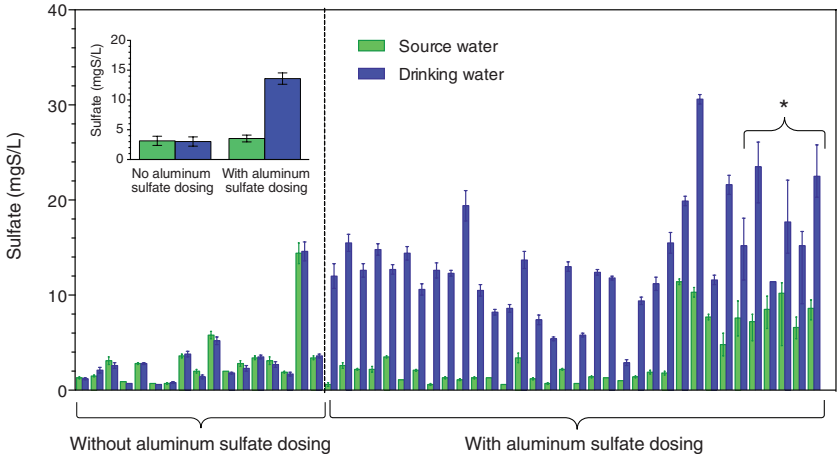


**Fig. 2. Sulfate concentrations in source water and drinking water.** (Inset) Average sulfate concentrations in source and drinking waters with and without aluminum sulfate addition in the treatment process. Presented data are means ± SEM, except for those under the asterisk (*), which show the mean, maximum, and minimum values. In the cases marked by the asterisk, data were provided in the form of mean, maximum, and minimum values.

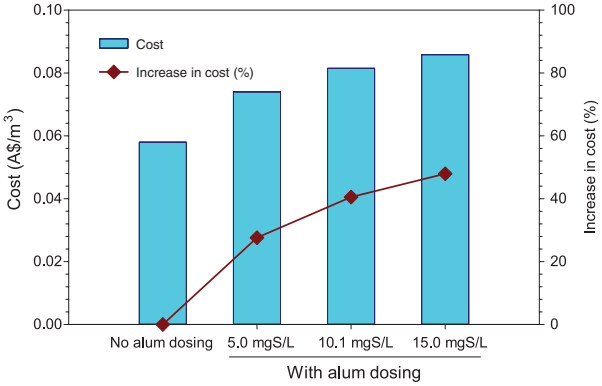


**Fig. 3. Predicted impact of the use of sulfate-based coagulants in drinking water treatment on sewer corrosion mitigation for average sewer and sewage conditions.** The relative sulfide mitigation cost increases were calculated by using the case without sulfate addition as the reference.

## REFERENCES AND NOTES


1. M. P. H. Brongers, P. Y. Virmani, J. H. Payer, "Drinking water and sewer systems in corrosion costs and preventative strategies in the United States" (Federal Highway Administration Publication FHWA-RD-01-156, U.S. Department of Transportation, Washington, DC, 2002).
2. U.S. Environmental Protection Agency, "Technical report: Hydrogen sulfide corrosion in wastewater collection and treatment systems" (publication 430/09-91-010, EPA, Washington, DC, 1991).
3. Water Environment Research Foundation, *Minimization of Odors and Corrosion in Collection Systems Phase 1* (WERF publication 04-CTS-1, WERF, Alexandria, VA, 2007).
4. C. D. Parker, *Aust. J. Exp. Biol. Med.* **23**, 81–90 (1945).
5. EPA, *Process Design Manual for Sulfide Control in Sanitary Sewerage Systems* (publication 625/1-74-005, EPA, Washington, DC, 1974).
6. L. Zhang *et al.*, *Water Res.* **42**, 1–12 (2008).
7. R. Ganigue, O. Gutierrez, R. Rootsey, Z. Yuan, *Water Res.* **45**, 6564–6574 (2011).
8. A. Matilainen, M. Vepsäläinen, M. Sillanpää, *Adv. Colloid Interface Sci.* **159**, 189–197 (2010).
9. C. Volk *et al.*, *Water Res.* **34**, 3247–3257 (2000).
10. Materials and methods are available as supplementary materials on *Science* online.
11. J. K. Edzwald, J. E. Tobiason, *Water Sci. Technol.* **40**, 63–70 (1999).
12. D. Wang, Y. Zhao, J. Xie, C. W. K. Chow, J. van Leeuwen, *Separ. Purif. Tech.* **110**, 188–195 (2013).
13. E. L. Sharp, S. A. Parsons, B. Jefferson, *Sci. Total Environ.* **363**, 183–194 (2006).
14. R. Fabris, C. W. K. Chow, M. Drikas, B. Eikebrokk, *Water Res.* **42**, 4188–4196 (2008).
15. K. R. Sharma *et al.*, *Water Res.* **42**, 2527–2538 (2008).
16. K. R. Sharma *et al.*, *Water* **35**, 132–137 (2008).

17. "Sulfate in drinking-water—Background document for development of WHO guidelines for drinking-water quality" (WHO/SDE/WSH/03.04/114, WHO, Geneva, 2004).
18. EPA, *Contaminant Candidate List Regulatory Determination Support Document for Sulfate* (publication 815-R-03-16, EPA, Washington, DC, 2003).
19. M. Edwards, P. Scardina, L. S. McNeill, "Enhanced coagulation impacts on water treatment plant infrastructure" [American Water Works Association (AWWA) Research Foundation, Denver, CO, 2004].
20. EPA, *State of Technology for Rehabilitation of Wastewater Collection Systems* (EPA/600/R-10/078, EPA, Washington, DC, 2011).
21. American Society of Civil Engineers, *Failure to Act: The Impact of Current Investment Trends in Water and Wastewater Treatment Infrastructure* (ASCE, Washington, DC, 2011).
22. B. Cyna, G. Chagneau, G. Bablon, N. Tanghe, *Desalination* **147**, 69–75 (2002).
23. S. D. Richardson, M. J. Plewa, E. D. Wagner, R. Schoeny, D. M. Demarini, *Mutat. Res.* **636**, 178–242 (2007).
24. D. L. Sedlak, U. von Gunten, *Science* **331**, 42–43 (2011).
25. M. Elimelech, W. A. Phillip, *Science* **333**, 712–717 (2011).
26. AWWA, *Dawn of the Replacement Era: Reinvesting in Drinking Water Infrastructure* (AWWA, Denver, CO, 2001).

**ACKNOWLEDGMENTS**

K.R.S., W.G., J.K., and Z.Y. are affiliated with CRC for Water Sensitive Cities Pty Ltd. Several Australian water utilities including South Australian Water Corporation participated in the industry survey and provided data reported in the paper. O. Hoegh-Guldberg, D. Sedlak, G. Daigger, and J. Metcalfe provided valuable comments. Raw data are provided in the supplementary materials.

**SUPPLEMENTARY MATERIALS**

www.sciencemag.org/content/345/6198/812/suppl/DC1
Materials and Methods
Figs. S1 to S5
Tables S1 and S2
References (*27*–*70*)

28 January 2014; accepted 27 June 2014
10.1126/science.1251418

PLACE CELLS

# Large environments reveal the statistical structure governing hippocampal representations

**P. Dylan Rich,[1,2]* Hua-Peng Liaw,[1] Albert K. Lee[1]***

**The rules governing the formation of spatial maps in the hippocampus have not been determined. We investigated the large-scale structure of place field activity by recording hippocampal neurons in rats exploring a previously unencountered 48-meter-long track. Single-cell and population activities were well described by a two-parameter stochastic model. Individual neurons had their own characteristic propensity for forming fields randomly along the track, with some cells expressing many fields and many exhibiting few or none. Because of the particular distribution of propensities across cells, the number of neurons with fields scaled logarithmically with track length over a wide, ethological range. These features constrain hippocampal memory mechanisms, may allow efficient encoding of environments and experiences of vastly different extents and durations, and could reflect general principles of population coding.**

The hippocampus is involved in encoding long-term memories of items and events from daily life in humans (*1*) and spatial environments in rodents (*2*). Each item (*3*), experience (*4*), or environment (*5*–*7*) is represented by a subset of active neurons among an often much larger number of inactive neurons. For spatial representations, the active subset consists of place cells, each of which fires when the animal is at specific locations in an environment (called the place fields of that cell) (*8*). The inactive neurons, which fire few or no spikes throughout the environment, are called silent cells (*5*). When an animal encounters another environment, a different subset of neurons becomes active, and this difference is believed to be the basis by which spatial contexts are distinguished (*7*, *9*). Within a given environment, the fields of different cells together cover the space and are thought to provide a cognitive map enabling flexible navigation (*2*).

In environments typically used to study spatial firing (total track length <5 m, or open arenas <1 $m^2$), ~20 to 50% of pyramidal neurons from the dorsal CA1 subregion of the rat hippocampus are recruited to be place cells (*5*, *6*, *10*), and most have a single place field. Wild rats have home ranges typically up to 50 m across, sometimes extending to hundreds of meters (*11*); in larger laboratory environments (up to 18 m long or 3 $m^2$), more neurons are recruited to be place

[1]Howard Hughes Medical Institute, Janelia Farm Research Campus, Ashburn, VA 20147, USA. [2]Department of Psychology, University of Cambridge, Cambridge CB2 3EB, UK.
*Corresponding author. E-mail: richp@janelia.hhmi.org (P.D.R.); leea@janelia.hhmi.org (A.K.L.)

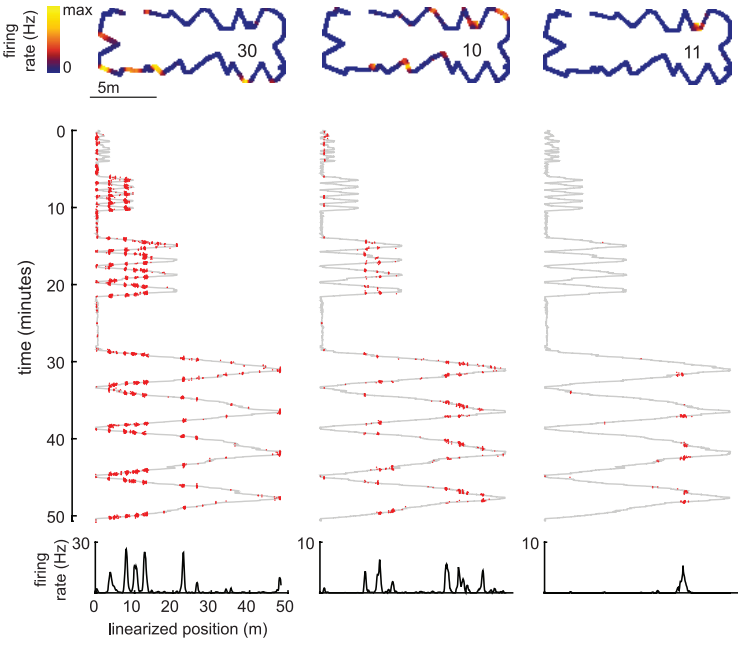


**Fig. 1. Place cells form multiple peaks in large environments.** From top to bottom, for three different neurons: firing rate on 48-m-long track, with peak rate noted; linearized position of animal (gray) and spikes (red); linearized firing rate. Spikes when an animal's speed was <5 cm/s are omitted.

cells, many cells have multiple fields, and place fields are wider (*12*–*14*).

However, far less is understood about the organizing principles of hippocampal spatial maps. Basic questions remain with implications for the underlying mechanisms and proposed functions of hippocampal representations. When fields are formed, which cells do they come from?

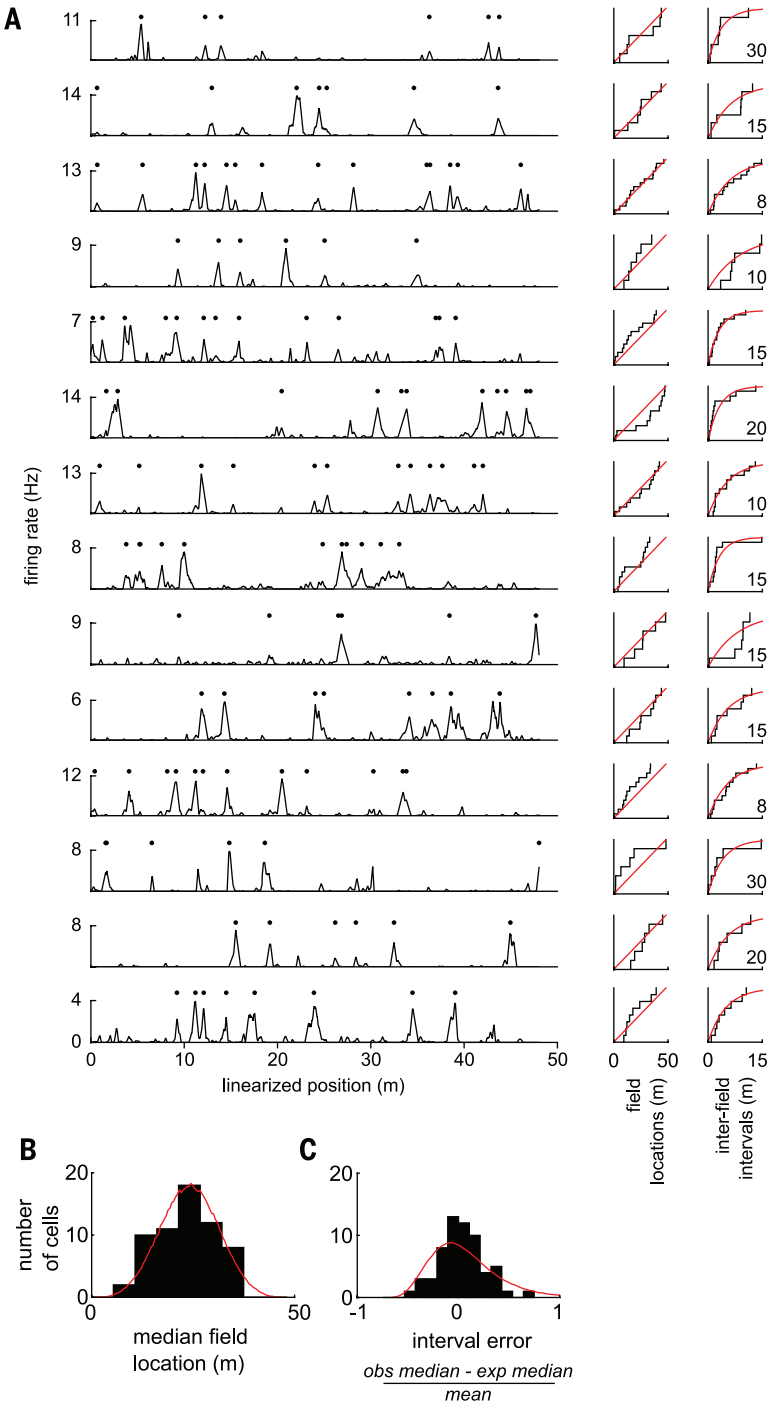


**Fig. 2. Place field formation in individual cells is well described as a spatial Poisson process.** (**A**) All cells with ≥6 place fields from a single animal; dots denote centers of detected fields. Cumulative distributions of field locations and interfield intervals are shown at the right (black), together with the uniform and exponential distributions expected for a Poisson process (red). (**B**) Distribution of median field location of all cells with ≥6 fields across animals ($n$ = 61 cells from 5 rats) versus distribution expected for cells with uniformly distributed fields (red curve). (**C**) Distribution of deviation from exponential of median interfield interval (normalized by the mean interval) for all cells with ≥6 fields versus distribution expected for cells with exponentially distributed fields (red curve).

Place fields are the units of spatial representation in CA1, and their distribution among cells determines how they code for location. Will every cell become a place cell if the environment is large enough? If all cells became place cells, the specificity of active subsets would disappear, requiring other mechanisms for retrieving the appropriate spatial context from memory.

To investigate such questions, we used a very large maze and quantified two key aspects of hippocampal maps—which cells fire and where they fire—as they were was being established in five rats. We recorded 253 putative pyramidal cells from dorsal CA1 (fig. S1) in the rats as they explored a 48-m-long track (fig. S2). The track and room were both entirely novel to the animal. To test whether there was a limit to recruitment, we challenged the representational capacities of the hippocampus by progressively extending the track in stages and making locations along the track as distinct as possible. In each epoch, an animal traversed the current total length of track three to five times, and between epochs it was confined to the original start location while the track was extended. Total track lengths in the four epochs were 3, 10, 22, and 48 m. Although animals traversed the entire available track during each epoch, we restricted analysis to periods when the animal explored the additional novel sections of track introduced in each epoch; this enabled us to focus on the initial recruitment of cells and fields. To ensure accurate counts of silent cells, we only analyzed neurons that could be isolated in sleep periods flanking behavioral periods (*5*, *6*).

In each new section of track, existing place cells formed additional fields and new place cells were recruited from the pool of silent cells (*12*) (Fig. 1 and figs. S3 to S5). The multiple fields of individual cells appeared to be irregularly spaced over the track (Fig. 2A). The simplest model of place field formation is that the locations of the fields of each cell follow a spatial Poisson process; that is, the locations are random and described only by a certain average rate. For cells with ≥6 fields (61/253), neither the spatial distributions of fields nor interfield interval distributions differed from the Poisson model (Anderson-Darling test, 0/61 cells with $P < 0.05$, adjusted for false discovery rate), where they are uniform and exponential, respectively (Fig. 2; see fig. S6 for cells with <6 fields).

We asked whether a correspondingly simple model could describe the population as a whole (Fig. 3A). Specifically, did each cell have the same Poisson rate of field formation? This model would capture the qualitative behavior observed as environments increase in size, i.e., additional fields are formed and previously silent cells are recruited to be place cells. Quantitatively, this model makes certain predictions. First, the observed number of fields per cell would follow a Poisson distribution. Second, the distribution of the location of each cell's field that is closest to the start of the track (called the recruitment curve, as it shows the fraction of the population that is recruited to be place cells as the track lengthens)

would follow an exponential distribution. However, the fits of both distributions to the data were poor (Fig. 3, B and C), indicating that such a model does not describe hippocampal population representations in novel environments.

Instead, the observed number of fields per cell was overdispersed relative to the equal-rate Poisson model (Fig. 3B and fig. S7A), indicating significant differences in the spatial rate of field formation between cells. That is, a few neurons had many fields, whereas many more than expected had few or no fields. The recruitment of neurons into the representation reached only ~65% at 48 m (range 46 to 77%, fig. S7B), greatly undershooting the equal-rate Poisson prediction. To see whether the ~35% of cells that remained silent were capable of forming fields at all, we later exposed the animal to a second novel environment and found that some of these cells formed clear place fields (fig. S8).

We next asked whether the differing propensity of cells to form fields across the population could be described by a particular distribution. The number of fields per cell was well fit with a negative binomial distribution (Fig. 3B, parameters $r$, $p$ = 0.57, 0.14), which can arise if each cell is an independent Poisson process with its rate drawn from a gamma distribution (fig. S9). Moreover, the recruitment curve under such a gamma-Poisson model would follow a Lomax, or Pareto type II (power law), distribution. The predicted recruitment curve matched the observed one well (Fig. 3C; Kolmogorov-Smirnov statistic = 0.05, $P$ = 0.48). The curve shows logarithmic-like recruitment over spatial scales spanning several orders of magnitude, including the range of distances traveled by wild rats (*11*), and its extrapolation predicts 90% recruitment at ~500 m.

We examined additional properties of the distribution of fields. As expected from independent Poisson processes, overall field density was uniform over the environment (Fig. 3D; Kolmogorov-Smirnov statistic = 0.03, $P$ = 0.36) and was uninfluenced by local track features or running speed (fig. S10), field propensities were stationary across the track (fig. S11), and field locations were uncorrelated between pairs of cells (fig. S12).

Memorylessness—being invariant with respect to the starting point or history—is a defining property of Poisson processes. We thus chose evenly spaced points on the track, ignored whether or not cells had been recruited before that point, and then determined the subsequent recruitment curve for the remainder of the track. These memoryless recruitment curves had the same shape regardless of the starting point (Fig. 3E and fig. S13).

The uniform field density at the single-cell and population levels, exponential interfield spacing, good match to the predicted recruitment curve, stable propensity distribution, uncorrelated field locations across cells, memorylessness of recruitment, and uncorrelated spatial and nonspatial field properties (fig. S14) demonstrate that the gamma-Poisson model is a good statistical description of place field formation in a novel environment. Different criteria for place field detection

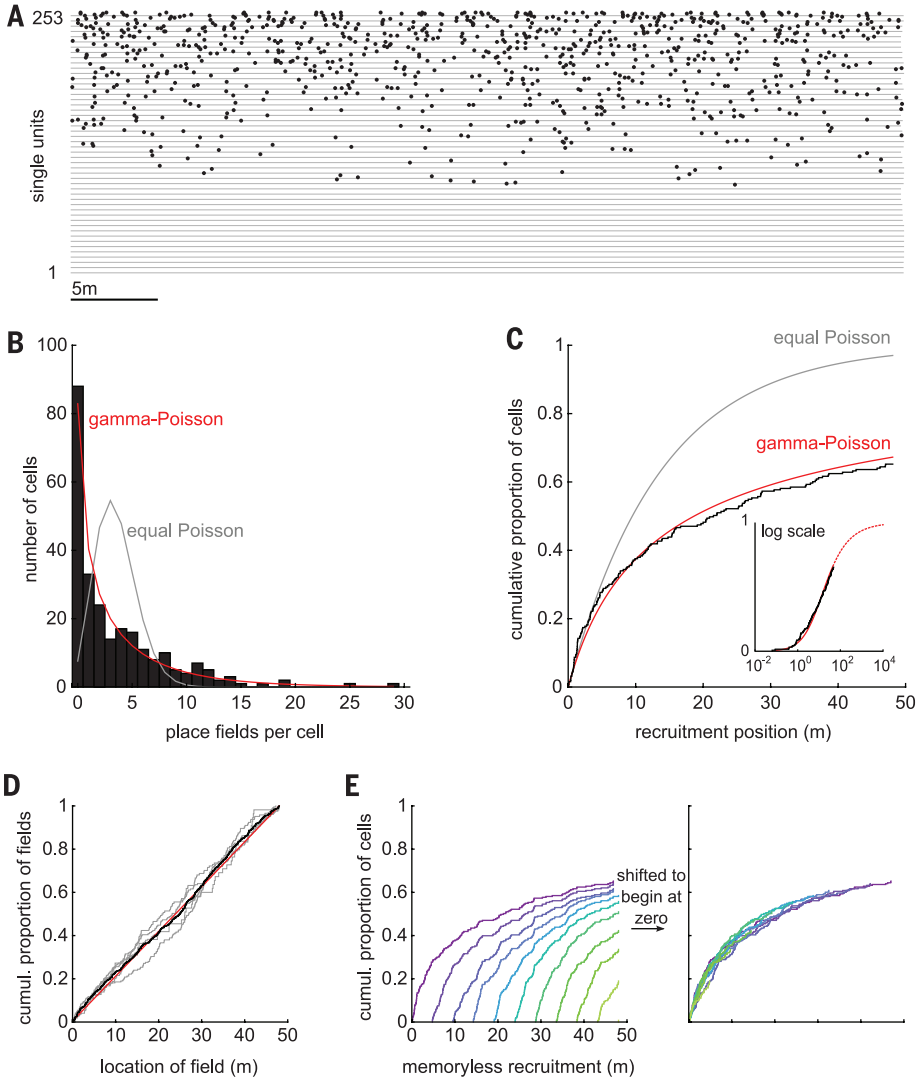


**Fig. 3. Statistical, population-level model of the formation of hippocampal spatial representations.** (**A**) Place field locations of all 253 recorded neurons. Lines show extent of the track every 5 cells. Cells sorted by number of fields. (**B**) Number of place fields per cell. Distribution assuming each cell has equal Poisson rate (given by the mean number of fields per cell) of forming place fields per unit length (gray). Fit of negative binomial distribution (red), which results from gamma-distributed Poisson rates (i.e., gamma-distributed field propensities). (**C**) Recruitment curve, derived from location of field closest to start (0 m) for each cell, representing the proportion of place cells in the entire population as function of track size. Predictions of equal-rate Poisson (gray) and gamma-Poisson (red) models, each using parameters estimated from (B). (**D**) Distribution of all fields across animals (black) along track versus constant-density uniform distribution (red). Individual animals (gray). (**E**) Memoryless recruitment curves constructed by starting at a point along track and then calculating subsequent recruitment regardless of activity in previous length of track. Same curves shifted to allow comparison of shapes (right).

did not change the results (fig. S15). Although the gamma-Poisson model was sufficient to explain the recruitment of cells and fields under our experimental conditions, other studies have shown increased field density around goals (*15*) and changing recruitment over time (*10*, *16*), indicating that other factors can modulate field propensity.

Our attempt to challenge the representational capacity of the hippocampus revealed neither a hard limit to recruitment nor completely random recruitment. Instead, a skewed distribution of field propensities across the population led to logarithmic-like recruitment over a wide range of ethologically relevant distances. What causes place cells to fire has been the subject of intense investigation for decades; this finding adds another dimension to that question: What causes a cell to have a particular rate of expressing place fields?

Two distinct mechanisms can give rise to the observed gamma-Poisson process (*17*): (i) preexisting differences between cells (*18*), or (ii) a

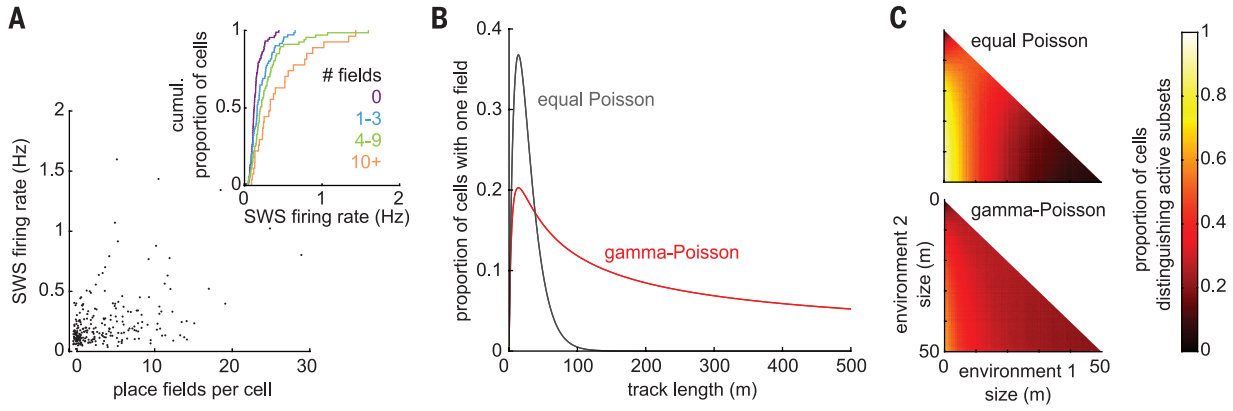


**Fig. 4. Origin and coding implications of the distribution of field propensities.** (**A**) Firing rates in slow-wave sleep (SWS) before exploration were correlated with subsequent number of fields per cell on track (jitter added for visualization). SWS firing rates separated into groups by number of fields (inset). (**B**) Proportion of cells with exactly one place field as a function of environment size under equal-rate Poisson and gamma-distributed models of field propensities. (**C**) Simulation of the expected proportion of neurons that are place cells in one environment and silent in another for environments of different sizes under the two models.

cumulative advantage mechanism during exploration (e.g., Polya-Eggenberger urn). Firing rates in slow-wave sleep (SWS) before the animal had experienced the maze were moderately correlated with the subsequent number of fields per cell (Fig. 4A; $r = 0.45$, $P < 10^{-13}$); this finding provides evidence that preexisting differences contribute to field propensities but does not rule out possible additional cumulative advantage mechanisms.

Preexisting differences between cells could result from differences in cellular excitability or network inputs. Future place cells are more excitable than future silent cells before exploration (*19*), and artificially increasing the excitability of silent cells can convert them to place cells (*20*), thereby linking preexisting intrinsic differences (*21*) with field propensity. Fixed cellular or network differences likely underlie the moderate variation in field propensity (*22*, *23*) (fig. S16) with anatomical location.

Place fields are ultimately derived from spatial information originating from external sensory or self-motion sources. Preexisting differences, whether cellular or network-based, could act as an additional element in existing models of place field origin (*24*–*26*) by modifying responses to spatial inputs (*20*). The gamma distribution of field propensities we observed provides a specific constraint on mechanisms and models of place cell firing. The link between preexisting differences and field propensity could also account for preplay of novel environments (*27*), as well as correlated firing rates (*28*) and correlated field propensities (fig. S17) across multiple environments.

What functions might a range of field propensities serve? Equal rates of random field formation would maximize the network's ability to uniquely encode distinct places. But with the observed gamma-distributed propensities, the proportion of cells with single fields would remain at ~5 to 10% over a wide range of environment sizes, potentially enabling a simple readout of location (Fig. 4B). Furthermore, equal propensities would lead to difficulties in distinguishing environments based on their active subsets, because large-enough environments would recruit all cells. Instead, the observed distribution of propensities allows environments with a wider range of sizes to be distinguished based on their active subsets, even if one assumes each cell's propensity to be permanently fixed (Fig. 4C and fig. S18). These features may also operate alongside the dorsoventrally modulated range of CA3 field sizes (*14*) to efficiently encode differently sized environments.

Loglike recruitment has been seen in motor (*29*) and sensory (*30*) systems, which suggests that it may be a general feature of neural population coding, along with other functions of skewed distributions (*28*). In the hippocampus, it could underlie a Weber-like perception of space. The quantitative description of spatial representations provides new insight into how the hippocampus may handle capacity for multiple items as well as single, extended experiences, and may have implications for representations and memory formation (*31*) in other systems.

## REFERENCES AND NOTES


1. W. B. Scoville, B. Milner, *J. Neurol. Neurosurg. Psychiatry* **20**, 11–21 (1957).
2. J. O'Keefe, L. Nadel, *The Hippocampus as a Cognitive Map* (Oxford Univ. Press, Oxford, 1978).
3. R. Q. Quiroga, L. Reddy, G. Kreiman, C. Koch, I. Fried, *Nature* **435**, 1102–1107 (2005).
4. H. Gelbard-Sagiv, R. Mukamel, M. Harel, R. Malach, I. Fried, *Science* **322**, 96–101 (2008).
5. L. T. Thompson, P. J. Best, *J. Neurosci.* **9**, 2382–2390 (1989).
6. M. A. Wilson, B. L. McNaughton, *Science* **261**, 1055–1058 (1993).
7. S. Leutgeb, J. K. Leutgeb, A. Treves, M.-B. Moser, E. I. Moser, *Science* **305**, 1295–1298 (2004).
8. J. O'Keefe, J. Dostrovsky, *Brain Res.* **34**, 171–175 (1971).
9. X. Liu *et al.*, *Nature* **484**, 381–385 (2012).
10. M. P. Karlsson, L. M. Frank, *J. Neurosci.* **28**, 14271–14281 (2008).
11. D. E. Davis, J. T. Emlen, A. W. Stokes, *J. Mammal.* **29**, 207–225 (1948).
12. A. A. Fenton *et al.*, *J. Neurosci.* **28**, 11250–11262 (2008).
13. T. J. Davidson, F. Kloosterman, M. A. Wilson, *Neuron* **63**, 497–507 (2009).
14. K. B. Kjelstrup *et al.*, *Science* **321**, 140–143 (2008).
15. S. A. Hollup, S. Molden, J. G. Donnett, M. B. Moser, E. I. Moser, *J. Neurosci.* **21**, 1635–1644 (2001).
16. Y. Ziv *et al.*, *Nat. Neurosci.* **16**, 264–266 (2013).
17. O. Lundberg, *On Random Processes and Their Application to Sickness and Accident Statistics* (Almqvist & Wiksells, Uppsala, 1940).
18. M. Greenwood, G. U. Yule, *J. R. Stat. Soc.* **83**, 255 (1920).
19. J. Epsztein, M. Brecht, A. K. Lee, *Neuron* **70**, 109–120 (2011).
20. D. Lee, B.-J. Lin, A. K. Lee, *Science* **337**, 849–853 (2012).
21. T. Jarsky, R. Mady, B. Kennedy, N. Spruston, *J. Comp. Neurol.* **506**, 535–547 (2008).
22. E. J. Henriksen *et al.*, *Neuron* **68**, 127–137 (2010).
23. K. Mizuseki, K. Diba, E. Pastalkova, G. Buzsáki, *Nat. Neurosci.* **14**, 1174–1181 (2011).
24. M. Tsodyks, T. Sejnowski, *Int. J. Neural Syst.* **6** (suppl.), 81–86 (1995).
25. T. Hartley, N. Burgess, C. Lever, F. Cacucci, J. O'Keefe, *Hippocampus* **10**, 369–379 (2000).
26. T. Solstad, E. I. Moser, G. T. Einevoll, *Hippocampus* **16**, 1026–1031 (2006).
27. G. Dragoi, S. Tonegawa, *Nature* **469**, 397–401 (2011).
28. G. Buzsáki, K. Mizuseki, *Nat. Rev. Neurosci.* **15**, 264–278 (2014).
29. H. S. Milner-Brown, R. B. Stein, R. Yemm, *J. Physiol.* **230**, 359–370 (1973).
30. M. A. Muniak, S. Ray, S. S. Hsiao, J. F. Dammann, S. J. Bensmaia, *J. Neurosci.* **27**, 11687–11699 (2007).
31. A. J. Silva, Y. Zhou, T. Rogerson, J. Shobe, J. Balaji, *Science* **326**, 391–395 (2009).


## ACKNOWLEDGMENTS

We thank M. Karlsson, J. Osborne, M. Copeland, and J. Cox and the Vivarium staff for technical assistance and S. Druckmann, J. Dudman, A. Hantman, J. Cohen, and D. Lee for valuable comments on the manuscript. All primary electrophysiological and behavioral data are archived at the Janelia Farm Research Campus. This work was supported by the Howard Hughes Medical Institute.

## SUPPLEMENTARY MATERIALS

www.sciencemag.org/content/345/6198/814/suppl/DC1
Materials and Methods
Supplementary Text
Figs. S1 to S18
References (*32*–*40*)

5 May 2014; accepted 4 July 2014
10.1126/science.1255635

CYSTIC FIBROSIS

# Impaired mucus detachment disrupts mucociliary transport in a piglet model of cystic fibrosis

Mark J. Hoegger,[1] Anthony J. Fischer,[2] James D. McMenimen,[3] Lynda S. Ostedgaard,[3] Alex J. Tucker,[3] Maged A. Awadalla,[3] Thomas O. Moninger,[4] Andrew S. Michalski,[3] Eric A. Hoffman,[3,5,6] Joseph Zabner,[3] David A. Stoltz,[1,3,6]* Michael J. Welsh[1,3,7]*

**Lung disease in people with cystic fibrosis (CF) is initiated by defective host defense that predisposes airways to bacterial infection. Advanced CF is characterized by a deficit in mucociliary transport (MCT), a process that traps and propels bacteria out of the lungs, but whether this deficit occurs first or is secondary to airway remodeling has been unclear. To assess MCT, we tracked movement of radiodense microdisks in airways of newborn piglets with CF. Cholinergic stimulation, which elicits mucus secretion, substantially reduced microdisk movement. Impaired MCT was not due to periciliary liquid depletion; rather, CF submucosal glands secreted mucus strands that remained tethered to gland ducts. Inhibiting anion secretion in non-CF airways replicated CF abnormalities. Thus, impaired MCT is a primary defect in CF, suggesting that submucosal glands and tethered mucus may be targets for early CF treatment.**

Cystic fibrosis (CF) is a hereditary disease caused by mutations in *CFTR*, a gene encoding an ion channel [cystic fibrosis transmembrane conductance regulator (CFTR)] that transports chloride and bicarbonate across epithelial cell membranes (*1*). Lung disease, the source of most mortality in people with CF, arises from defective host defense that predisposes airways to bacterial infection. Mucociliary transport (MCT) defends airways by trapping pathogens in mucus, and cilia propel them out of the lung (*2*–*4*). The observation that MCT is abnormal in advanced CF (*3*) and several in vitro studies (*5*) have led to the proposal that impaired MCT causes CF lung disease. Yet, in vivo data suggest that CF MCT defects may be secondary to inflammation and airway remodeling. For example, in some studies CF adults showed no MCT abnormality, and CF children exhibited no MCT defects (*3*, *6*, *7*). Moreover, MCT deficits increased as the severity of CF lung disease increased, and in other pulmonary diseases, airway inflammation is also linked to MCT defects (*8*). Until now, lack of both sensitive MCT assays and an animal model that replicates human CF prevented determination of whether MCT is impaired from the outset and thus contributes to pathogenesis or is a secondary defect.

A porcine CF model provides an opportunity to test MCT in vivo at the disease's origin (*9*). At birth, the airways of pigs with CF lack infection and inflammation but spontaneously develop hallmark CF features including infection, inflammation, mucus accumulation, and obstruction. To assay MCT in vivo with good spatial and temporal resolution, we developed an x-ray computed tomography–based assay to track movement of 350-μm diameter tantalum microdisks (*10*) (see supplementary materials and methods).

Most current MCT assays measure disappearance of radioactivity (clearance) after inhalation of radiolabeled particles (*3*, *6*, *7*). After insufflation into newborn piglet airways, a similar percentage of microdisks cleared CF and non-CF lungs in 10 min (Fig. 1, A and B, and fig. S1) (*10*). As microdisks were swept toward the larynx, they migrated to the ventral tracheal surface in both genotypes (Fig. 1C), consistent with our finding that ciliary orientation drives microdisks ventrally (*10*). Both genotypes propelled microdisks with similar maximal and mean speeds, and microdisks spent a similar percentage of time moving (Fig. 1, D to F). Thus, under basal conditions, CF MCT appeared intact.

Airway insults can elicit a cholinergic reflex, a protective response that increases cilia beating and generates copious submucosal gland mucus secretion (*4*, *11*, *12*). The cholinergic agonist methacholine raised cilia beat frequency in CF and non-CF lungs (fig. S2A). However, it tended to reduce the percentage of microdisks that cleared CF lungs (Fig. 1, A and B, and movie S1). Measurements of individual microdisk behavior revealed that methacholine accelerated maximal and mean microdisk speeds in piglets without CF, but not those with the disease (Fig. 1, D and E, and fig. S1, C to E). The most marked difference between genotypes was that in piglets with CF, methacholine reduced the percentage of time individual microdisks were in motion by ~40% (Fig. 1F). Thus, rather than enhancing MCT and airway defense, a cholinergic agonist impeded MCT in piglets with CF. One possible limitation of this in vivo study is that the piglets were supine, anesthetized, and did not cough; cholinergic stimulation might have produced a different response in awake animals.

Several studies of cultured airway epithelia reported that loss of the CFTR increased $Na^+$ channel activity, causing excess liquid absorption from airway surfaces; decreased periciliary liquid; impaired cilia function; and, thus, a reduction in MCT (*5*). However, culture models do not recapitulate the complexity of MCT because mucus cannot enter or escape cultures and the model lacks submucosal glands, which are estimated to produce ~95% of mucus in large airways (*4*). After infusing methacholine, we found that periciliary liquid depth did not differ by genotype (fig. S2B), consistent with previous studies in pigs and humans with CF (*13*, *14*). However, mucus overlying cilia was often dislodged during processing, and we could not assess potential effects of reduced volume secretion by CF submucosal glands (*15*, *16*). Together, the results suggested that MCT might be disrupted by a CF abnormality in glands rather than surface epithelia. To test this, we flooded tracheas from methacholine-treated piglets with saline in a volume >1000 times the periciliary liquid volume (Fig. 2A and movie S2). This intervention prevents airway surface epithelia from altering the volume or composition of liquid covering airways.

Microdisks added to submerged non-CF airways rarely stopped as they progressed to the cranial and ventral edges (Fig. 2B and movie S2, A and B). In CF tracheas, some microdisks traveled like those on non-CF tracheas. However, CF decreased the time that microdisks were in motion by ~50% (Fig. 2C), in good agreement with in vivo data (Fig. 1F). These results further excluded periciliary liquid depletion as the cause of impaired MCT. Moreover, on some occasions, we could see and remove CF mucus strands with attached microdisks (movie S2C).

To probe further for CF mucus abnormalities, we examined the response to methacholine because it elicited CF MCT defects in vivo and ex vivo (Figs. 1 and 2) and it stimulates submucosal gland secretion, consisting of liquid and proteins including mucins, which confer key structural properties to mucus (*11*, *12*). Cholinergic stimulation can also activate the CFTR, increase the driving force for anion secretion through the CFTR, and thereby enhance liquid secretion (*17*, *18*). To visualize mucus in real time, we covered excised tracheas with saline that contained a dilute suspension of fluorescent nanospheres (40-nm diameter) (Fig. 3A and movie S3).

When nanospheres attached to mucus, their increased local density highlighted strands and globules of mucus flowing over or linked to

[1]Department of Molecular Physiology and Biophysics, University of Iowa, Roy J. and Lucille A. Carver College of Medicine, Iowa City, IA 52242, USA. [2]Department of Pediatrics, University of Iowa, Roy J. and Lucille A. Carver College of Medicine, Iowa City, IA 52242, USA. [3]Department of Internal Medicine, University of Iowa, Roy J. and Lucille A. Carver College of Medicine, Iowa City, IA 52242, USA. [4]Central Microscopy Research Facility, University of Iowa, Roy J. and Lucille A. Carver College of Medicine, Iowa City, IA 52242, USA. [5]Department of Radiology, University of Iowa, Roy J. and Lucille A. Carver College of Medicine, Iowa City, IA 52242, USA. [6]Department of Biomedical Engineering, University of Iowa, Iowa City, IA 52242, USA. [7]Howard Hughes Medical Institute (HHMI), University of Iowa, Roy J. and Lucille A. Carver College of Medicine, Iowa City, IA 52242, USA.
*Corresponding author. E-mail: david-stoltz@uiowa.edu (D.A.S.); michael-welsh@uiowa.edu (M.J.W.)

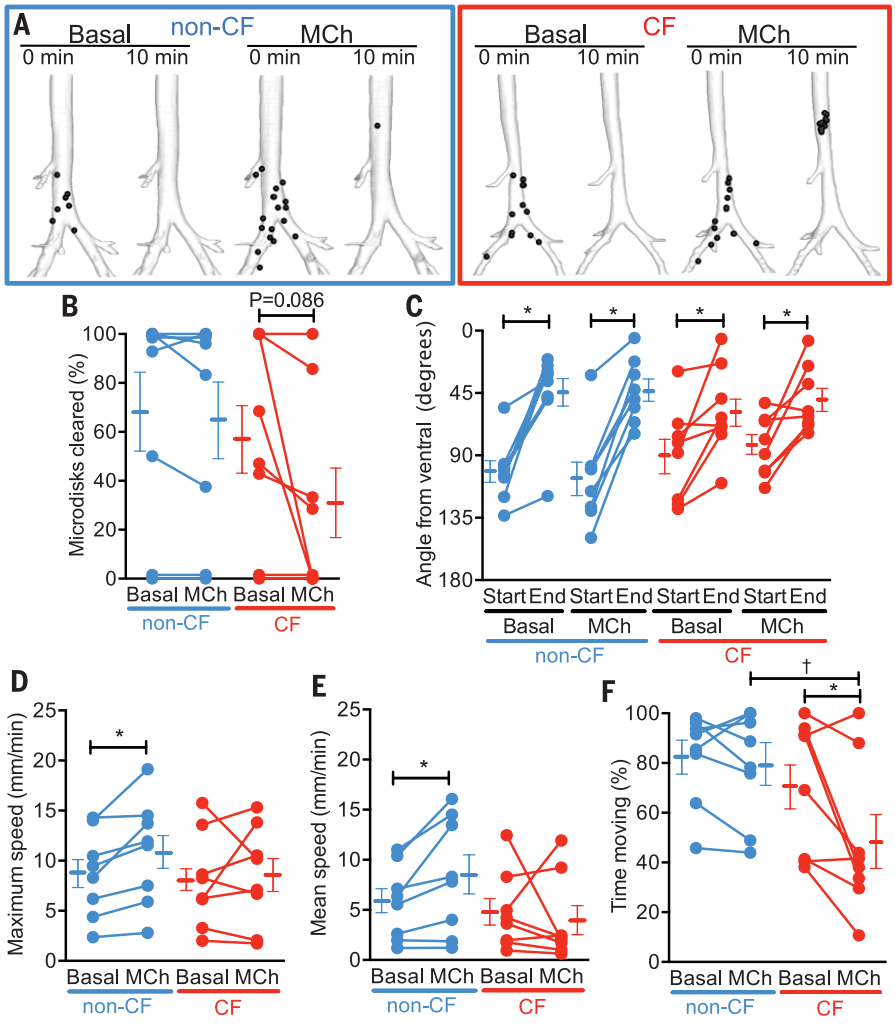


**Fig. 1. Loss of CFTR impairs MCT in vivo in newborn piglets treated with methacholine.** (**A**) Images are reconstructed ventral-dorsal views of non-CF and CF airways under basal conditions and after 1.28 × $10^{-7}$ mol/kg intravenous (IV) methacholine. Images are from the beginning and end of a 10-min tracking period (movie S1, A and B). Positions of microdisks are shown as spheres (enlarged ~40 times actual area). (**B** to **F**) Symbols indicate data from eight piglets without CF and eight animals with CF studied before and after 1.28 × $10^{-7}$ mol/kg IV methacholine. Each data point represents average behavior of individual microdisks in a piglet during a 10-min tracking run. Lines and whiskers beside individual data are mean ± SEM. *$P$ < 0.05; paired Student's $t$ test. (B) Percentage of microdisks that cleared the tracking field during the 10-min tracking period. (C) Radial position of microdisks at the start and end of the 10-min tracking period. Data are absolute values of angles relative to ventral (0°). (D and E) Maximum and mean speed of microdisks. (F) Percentage of time microdisks were moving during a tracking run. †$P$ < 0.05; unpaired Student's $t$ test. Analysis performed with a linear mixed effects model with random effect for pigs yielded a similar conclusion ($P$ = 0.024). Analysis in (F) was not adjusted for multiple comparisons.

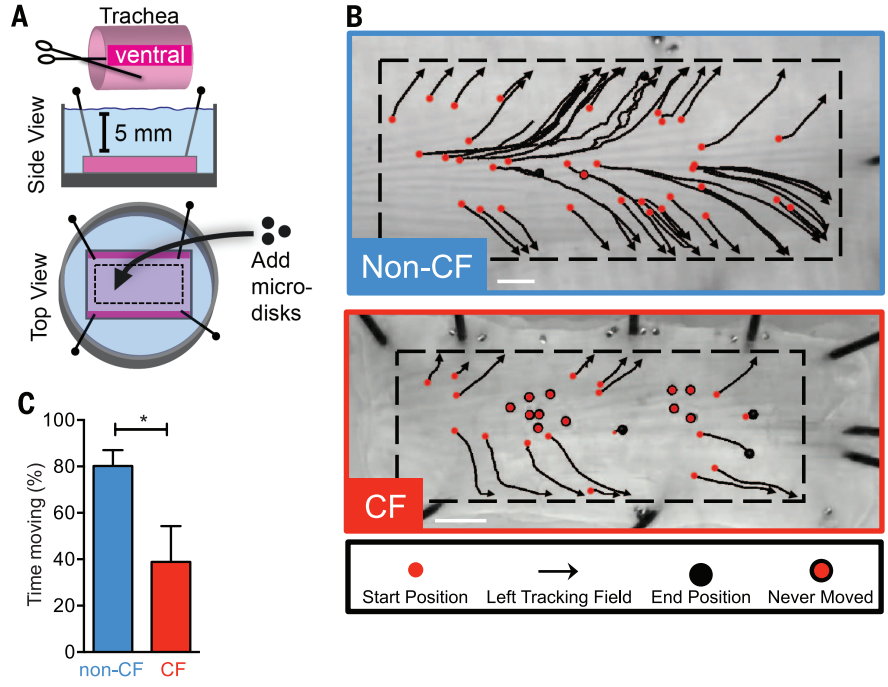


**Fig. 2. Loss of CFTR increases the percentage of nonmobile microdisks on ex vivo trachea submerged in saline.** (**A**) Schematic showing trachea removed from piglets treated with methacholine (1.28 × $10^{-5}$ mol/kg, IV), opening along the ventral surface, covering with saline, application of tantalum microdisks to the surface, and tracking of movement. Images in (B) are examples; data in (C) are averages. (**B**) Track of microdisks. Red circles indicate microdisk starting positions. Arrows indicate positions of tracking field exits. Black circles indicate end positions of microdisks that failed to clear the tracking field. Red circles with black outlines indicate disks that never moved. Dashed boxes indicate the tracking field. Scale bars, 2 mm. Images are compiled from a 10-min tracking period (movie S2, A and B). (**C**) Percentage of time microdisks were moving. $N$ = 4 tracheas from piglets without and with CF. *$P$ < 0.05; unpaired Student's $t$ test. Error bars denote SEM.

airways (movie S3A). Methacholine stimulated production of mucus strands that emanated from submucosal gland ducts and sometimes extended hundreds of micrometers from their anchor point (Fig. 3B and movie S3B). Strands grew in length from gland ducts (Fig. 3C). As mucus strands grew, they broke free and were carried up the airway (Fig. 3D and movie S3C). Mucus strands flowing over the surface sometimes attached to and stretched anchored strands. If the two strands separated, the strand attached to a submucosal gland often snapped back like a rubber band (Fig. 3E and movie S3D), indicating elasticity and tenacity, important properties of mucus. Reflected light studies (movie S3E), as well as scanning electron microscopy and immunocytochemistry studies (fig. S3, A and B), also revealed mucus strands emerging from submucosal gland ducts.

Because our preliminary observations suggested more mucus attached to CF airways, we developed a time-averaging procedure to preferentially visualize stationary mucus and provide panoramic views of entire tracheal segments (Fig. 4A, fig. S4, and movie S4). During a 15-min basal period, stationary mucus was rarely detected on non-CF airways (Fig. 4B and movie S4A). After adding methacholine, nanosphere-labeled mucus was mobile and therefore not visualized; it only became apparent after accumulation on ventral and cranial edges of airway segments. Under basal conditions, the surface of CF trachea revealed only small amounts of stationary mucus. However, methacholine stimulation generated a markedly different appearance, with many immobile mucus strands and globules failing to detach from submucosal gland ducts (or attaching to anchored strands) and not flowing across the airway (Fig. 4, C and E, fig. S5, and movie S4B).

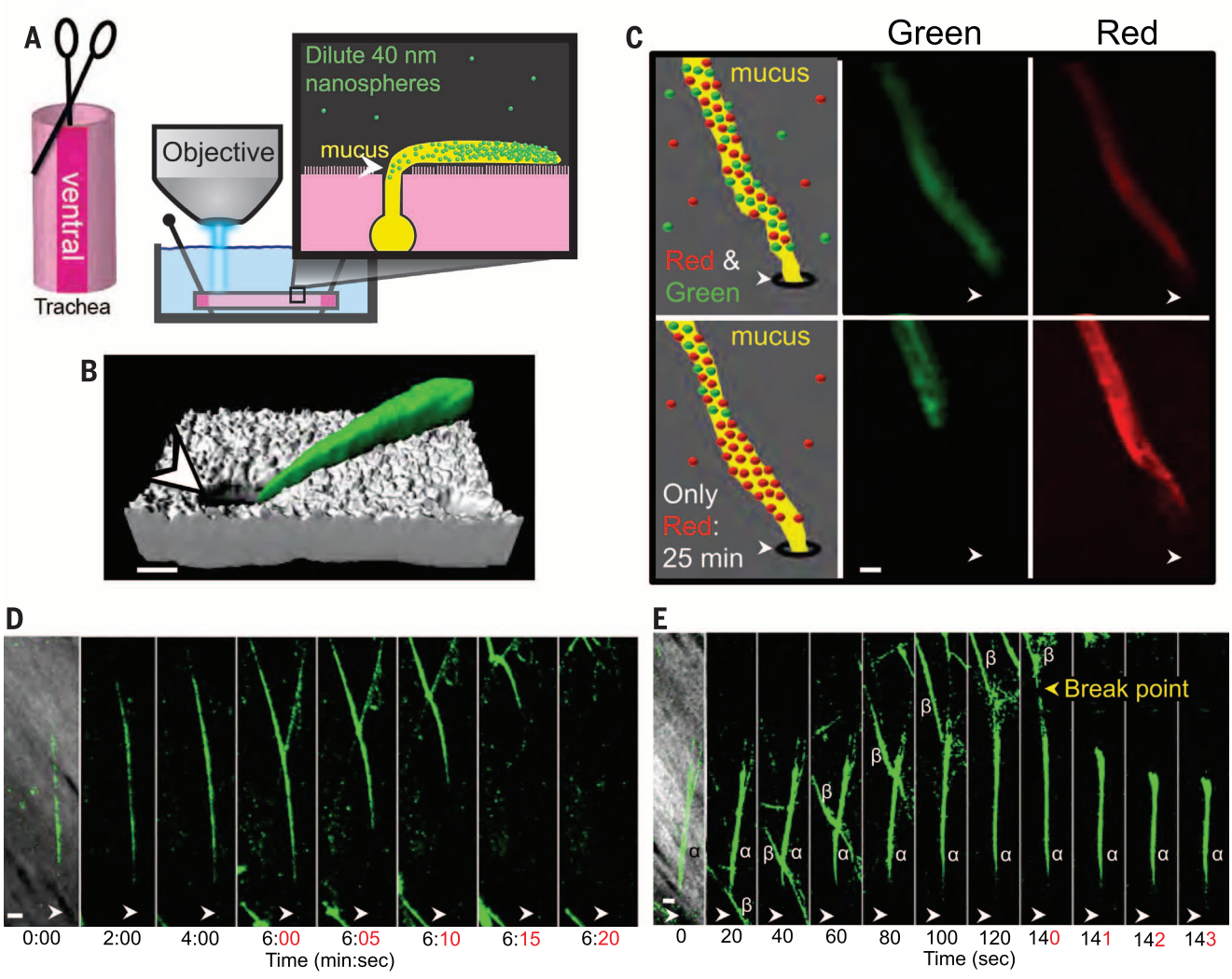


**Fig. 3. Strands of mucus emerge from submucosal gland ducts in methacholine-treated non-CF airways studied ex vivo.** Submucosal gland duct openings are indicated by arrowheads. (**A**) Schematic of imaging procedure. All experiments were repeated at least three times. Non-CF tracheas were removed from piglets, opened along the ventral surface, pinned flat, submerged in a $HCO_3^-$- and $CO_2$-buffered Ringer's solution, and treated with $1.28 \times 10^{-5}$ mol/liter methacholine. Tracheas were opened along the ventral surface so that cilia would propel mucus and nanospheres to lateral edges of the tracheal preparation (*10*). The solution bathing the trachea contained a dilute suspension of fluorescent 40-nm nanospheres. Images were obtained with a high-speed confocal microscope at the tracheal surface. Green indicates fluorescence from nanospheres (movie S3A). (**B**) Reconstruction of mucus (labeled with green nanospheres) emerging from a submucosal gland duct onto the airway surface (gray) (movie S3B). Scale bar, 50 μm. (**C**) Mucus strands grow in length from submucosal glands. (Top) Saline contained a dilute suspension of green and red nanospheres, and both labeled a mucus strand. Green nanospheres were then removed from saline, and the mucus strand continued to elongate from the gland duct, as indicated by labeling with red nanospheres 25 min later (bottom). Scale bar, 50 μm. (**D**) Mucus strand grew from the openings of submucosal gland ducts and then broke free and rapidly flowed out of the microscopic field (movie S3C). Time is shown at bottom. The gray background in the leftmost panel denotes a reflected light image. Scale bar, 50 μm. (**E**) Mucus strand "α," anchored at an arrowhead, temporarily captures another mucus strand ("β") flowing past. α stretches, and then the connection between α and β breaks at 140 s. Immediately after the break, β leaves the field, and α snaps back to its original length (movie S3D). The gray background in the leftmost panel denotes a reflected light image. Scale bar, 50 μm.

Failure of mucus to detach, despite being bathed in saline of controlled composition, indicates that CF mucus was abnormal before it emerged onto the airway surface. This result points to a defect in the submucosal glands; they express abundant CFTR (*19*, *20*) and conduct $Cl^-$ and $HCO_3^-$ (*21*) that contribute to liquid secretion (*11*, *17*, *22*, *23*). To test if the loss of anion transport might be responsible for altered mucus behavior in CF, we bathed non-CF trachea in $HCO_3^-$-free saline or saline containing bumetanide, which inhibits basolateral $Cl^-$ entry into epithelia (*23*). Neither alone caused a failure of mucus detachment (fig. S6). However, when combined, they reproduced the CF phenotype of tethered mucus strands and globules (Fig. 4, D and F, and movie S4C). Tracing mucus strands to their source revealed submucosal gland ducts as their origin (movie S4D). Because ion transport by epithelia lining airways would not alter the composition of liquid covering the surface, these changes can be attributed to reduced anion secretion into submucosal gland lumens. The results are also consistent with previous findings that inhibiting both $Cl^-$ and $HCO_3^-$ secretion altered viscoelastic properties of submucosal gland secretions (*4*, *24*).

To explore whether mucus impeded movement of the microdisks we used in vivo (Fig. 1), we applied them to non-CF epithelia in $HCO_3^-$-free saline plus bumetanide and found that they failed to move across the surface. Adding fluorescent nanospheres revealed microdisks attached to mucus (Fig. 4G and movie S4E). We obtained similar results in airways of piglets with CF (Fig. 4H and movie S4F).

Our findings identify impaired mucus detachment from CF submucosal glands as a primary defect that disrupts MCT. $Na^+$ hyperabsorption by airway surface epithelia and periciliary liquid depletion (*5*) do not explain the data. These in vivo and ex vivo results link the loss of CFTR and reduced anion secretion to altered mucus that has a reduced ability to break free after emerging from glands. Both reduced $Cl^-$- and $HCO_3^-$-dependent liquid secretion (*23*, *24*) and reduced $HCO_3^-$ secretion (or acidic pH) (*25*–*27*) have been proposed to alter CF mucus properties. Our data suggest that neither alone may be sufficient to generate abnormal CF mucus.

In combination with our earlier results (*28*), these findings reveal that the loss of CFTR disrupts two lung defense processes: MCT and secreted antimicrobial activity. Vertebrates and invertebrates employ these two defenses at the point of contact with environmental pathogens. CF does not eliminate either defense, but it does reduce their effectiveness. A vicious cycle caused

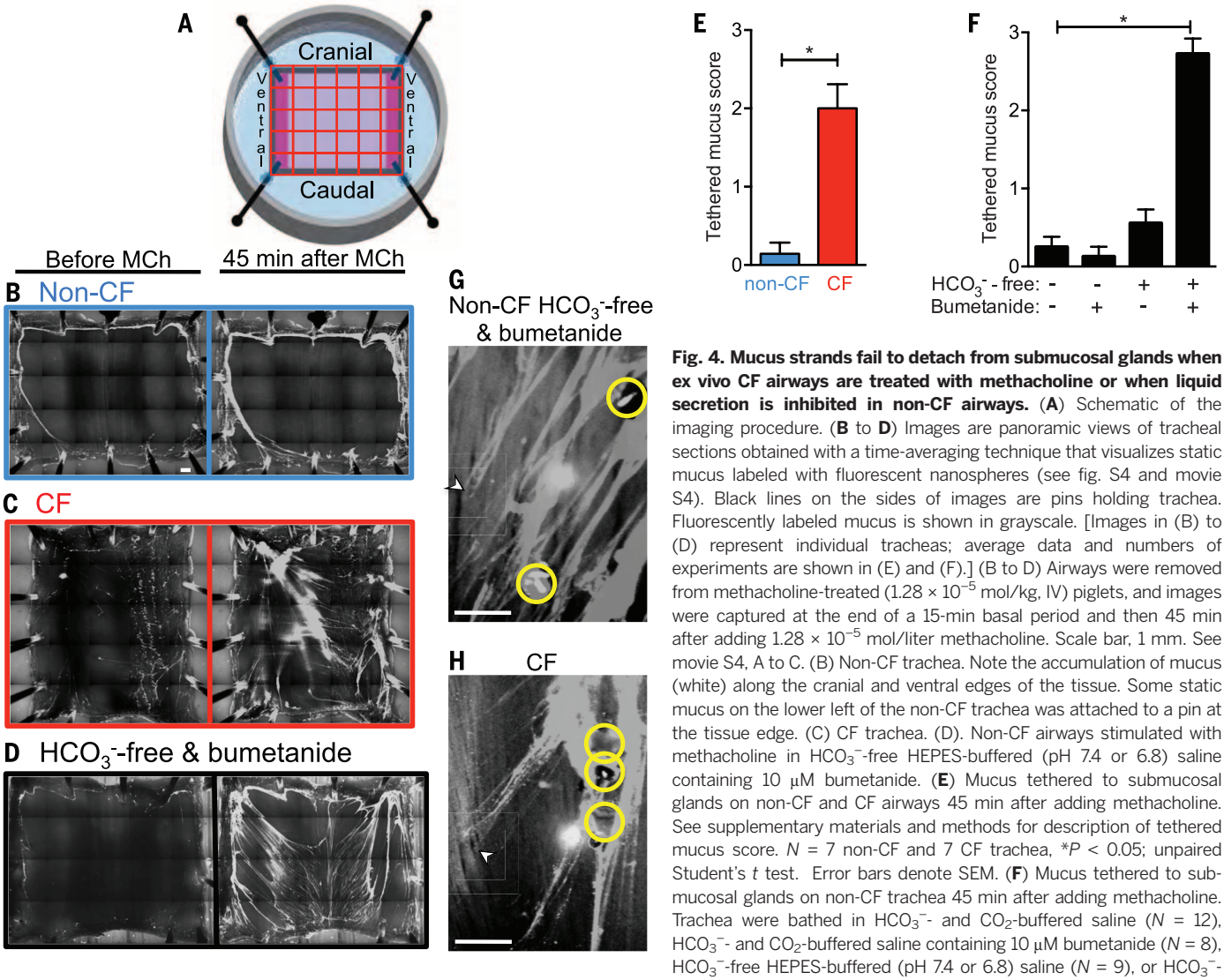


**Fig. 4. Mucus strands fail to detach from submucosal glands when ex vivo CF airways are treated with methacholine or when liquid secretion is inhibited in non-CF airways.** (**A**) Schematic of the imaging procedure. (**B** to **D**) Images are panoramic views of tracheal sections obtained with a time-averaging technique that visualizes static mucus labeled with fluorescent nanospheres (see fig. S4 and movie S4). Black lines on the sides of images are pins holding trachea. Fluorescently labeled mucus is shown in grayscale. [Images in (B) to (D) represent individual tracheas; average data and numbers of experiments are shown in (E) and (F).] (B to D) Airways were removed from methacholine-treated ($1.28 \times 10^{-5}$ mol/kg, IV) piglets, and images were captured at the end of a 15-min basal period and then 45 min after adding $1.28 \times 10^{-5}$ mol/liter methacholine. Scale bar, 1 mm. See movie S4, A to C. (B) Non-CF trachea. Note the accumulation of mucus (white) along the cranial and ventral edges of the tissue. Some static mucus on the lower left of the non-CF trachea was attached to a pin at the tissue edge. (C) CF trachea. (D). Non-CF airways stimulated with methacholine in $HCO_3^-$-free HEPES-buffered (pH 7.4 or 6.8) saline containing 10 μM bumetanide. (**E**) Mucus tethered to submucosal glands on non-CF and CF airways 45 min after adding methacholine. See supplementary materials and methods for description of tethered mucus score. $N$ = 7 non-CF and 7 CF trachea, $^*P < 0.05$; unpaired Student's $t$ test. Error bars denote SEM. (**F**) Mucus tethered to submucosal glands on non-CF trachea 45 min after adding methacholine. Trachea were bathed in $HCO_3^-$- and $CO_2$-buffered saline ($N$ = 12), $HCO_3^-$- and $CO_2$-buffered saline containing 10 μM bumetanide ($N$ = 8), $HCO_3^-$-free HEPES-buffered (pH 7.4 or 6.8) saline ($N$ = 9), or $HCO_3^-$-free saline containing bumetanide ($N$ = 11). $^*P < 0.05$ by one-way analysis of variance and Bonferroni post-test. (**G** and **H**) Combined reflected light and fluorescence images show the positions of tantalum microdisks (yellow circles) and mucus; mucus often wrapped around microdisks and partly obscured them. Microdisks were applied to non-CF trachea in $HCO_3^-$-free saline containing bumetanide (G) and to CF trachea (H). Subsequent addition of fluorescent nanospheres to saline revealed that all stationary microdisks were attached to mucus. These data also indicate that mucus strands formed independently of nanospheres. Arrowheads indicate submucosal gland ducts. Experiments were repeated at least three times. Scale bars, 1 mm. See movie S4, E and F.

by partial disruption of two processes may partly explain greater severity of lung disease in CF compared with primary ciliary dyskinesia, which obliterates MCT (*29*), because compromising one defense may accentuate the other defect. For example, mucus that fails to detach would impair MCT and provide a nidus for bacteria to grow under conditions that promote resistance to host defenses already weakened by CF (*28*, *30*). Conversely, reduced antibacterial activity could precipitate infection that triggers submucosal gland secretion, and defective mucus detachment would impair MCT. Inflammation resulting from both defects would evoke submucosal gland hypertrophy, further increasing the amount of static mucus. Because newborns are universally screened for CF in many countries, an opportunity for early intervention exists. Our data suggest that submucosal glands and the mucus tethered to them may be targets for early treatment and that MCT assays could report therapeutic efficacy.

## REFERENCES AND NOTES


1. M. J. Welsh, B. W. Ramsey, F. Accurso, G. R. Cutting, in *The Metabolic and Molecular Basis of Inherited Disease*, C. R. Scriver *et al*., Eds. (McGraw-Hill, New York, 2001), pp. 5121–5189.
2. A. Wanner, M. Salathe, T. G. O'Riordan, *Am. J. Respir. Crit. Care Med.* **154**, 1868–1902 (1996).
3. M. Robinson, P. T. Bye, *Pediatr. Pulmonol.* **33**, 293–306 (2002).
4. J. J. Wine, N. S. Joo, *Proc. Am. Thorac. Soc.* **1**, 47–53 (2004).
5. R. C. Boucher, *J. Intern. Med.* **261**, 5–16 (2007).
6. D. McShane *et al*., *Eur. Respir. J.* **24**, 95–100 (2004).
7. J. A. Regnis *et al*., *Am. J. Respir. Crit. Care Med.* **150**, 66–71 (1994).
8. J. V. Fahy, B. F. Dickey, *N. Engl. J. Med.* **363**, 2233–2247 (2010).
9. D. A. Stoltz *et al*., *Sci. Transl. Med.* **2**, 29ra31 (2010).
10. M. J. Hoegger *et al*., *Proc. Natl. Acad. Sci. U.S.A.* **111**, 2355–2360 (2014).
11. S. T. Ballard, D. Spadafora, *Respir. Physiol. Neurobiol.* **159**, 271–277 (2007).
12. J. J. Wine, *Auton. Neurosci.* **133**, 35–54 (2007).
13. J.-H. Chen *et al*., *Cell* **143**, 911–923 (2010).
14. U. Griesenbach *et al*., *Am. J. Respir. Cell Mol. Biol.* **44**, 309–315 (2011).
15. N. S. Joo, H. J. Cho, M. Khansaheb, J. J. Wine, *J. Clin. Invest.* **120**, 3161–3166 (2010).
16. D. X. Y. Wu *et al*., *Am. J. Physiol.* **274**, L388–L395 (1998).
17. A. Billet, J. W. Hanrahan, *J. Physiol.* **591**, 5273–5278 (2013).
18. R. J. Lee, J. K. Foskett, *J. Biol. Chem.* **287**, 38316–38326 (2012).
19. J. F. Engelhardt *et al*., *Nat. Genet.* **2**, 240–248 (1992).
20. R. J. Lee, J. M. Harlow, M. P. Limberis, J. M. Wilson, J. K. Foskett, *J. Gen. Physiol.* **132**, 161–183 (2008).
21. J. H. Poulsen, H. Fischer, B. Illek, T. E. Machen, *Proc. Natl. Acad. Sci. U.S.A.* **91**, 5340–5344 (1994).
22. S. Moon, M. Singh, M. E. Krouse, J. J. Wine, *Am. J. Physiol.* **273**, L1208–L1219 (1997).
23. L. Trout, J. T. Gatzy, S. T. Ballard, *Am. J. Physiol.* **275**, L1095–L1099 (1998).
24. S. T. Ballard, S. K. Inglis, *J. Physiol.* **556**, 1–10 (2004).
25. P. M. Quinton, *Lancet* **372**, 415–417 (2008).
26. P. M. Quinton, *Am. J. Physiol.* **299**, C1222–C1233 (2010).
27. J. K. Gustafsson *et al*., *J. Exp. Med.* **209**, 1263–1272 (2012).
28. A. A. Pezzulo *et al*., *Nature* **487**, 109–113 (2012).
29. M. Cohen-Cymberknoh *et al*., *Chest* **145**, 738–744 (2014).
30. B. J. Staudinger *et al*., *Am. J. Respir. Crit. Care Med.* **189**, 812–824 (2014).


## ACKNOWLEDGMENTS


We thank M. Abou Alaiwa, R. J. Adam, E. Allard, L. A. Askland, D. C. Bouzek, K. Chaloner, N. D. Gansemer, O. A. Itani, T. A. Mayhew, S. Mobberley, J. H. Morgan, L. R. Reznikov, J. Sieren, M. R. Stroik, P. J. Taft, and T. J. Wallen for valuable assistance and discussions. This work was supported by the NIH (HL051670, HL091842, DK054759), the Carver Foundation, and the Cystic Fibrosis Foundation (CFF). D.A.S. is supported by the Gilead Sciences Research Scholars Program in Cystic Fibrosis and the NIH (DP2 HL117744). A.J.F. is supported by a CFF Fellowship. M.J.W. is an Investigator of the HHMI. The University of Iowa Research Foundation has submitted patent applications for CF pigs and has licensed materials and technologies to Exemplar Genetics. M.J.W. was a cofounder of and holds equity in Exemplar Genetics. E.A.H. is a founder of and holds equity in VIDA Diagnostics, a company commercializing lung image analysis software.


## SUPPLEMENTARY MATERIALS

www.sciencemag.org/content/345/6198/818/suppl/DC1
Materials and Methods
Figs. S1 to S6
References (*31*–*36*)
Movies S1 to S4


8 May 2014; accepted 26 June 2014
10.1126/science.1255825


CELL REPROGRAMMING

# Histone chaperone ASF1A is required for maintenance of pluripotency and cellular reprogramming


**Elena Gonzalez-Muñoz,[1] Yohanna Arboleda-Estudillo,[1] Hasan H. Otu,[2,3] Jose B. Cibelli[1,4,5]***



**Unfertilized oocytes have the intrinsic capacity to remodel sperm and the nuclei of somatic cells. The discoveries that cells can change their phenotype from differentiated to embryonic state using oocytes or specific transcription factors have been recognized as two major breakthroughs in the biomedical field. Here, we show that ASF1A, a histone-remodeling chaperone specifically enriched in the metaphase II human oocyte, is necessary for reprogramming of human adult dermal fibroblasts (hADFs) into undifferentiated induced pluripotent stem cell. We also show that overexpression of just ASF1A and OCT4 in hADFs exposed to the oocyte-specific paracrine growth factor GDF9 can reprogram hADFs into pluripotent cells. Our Report underscores the importance of studying the unfertilized MII oocyte as a means to understand the molecular pathways governing somatic cell reprogramming.**


Two major breakthroughs in the biomedical field occurred with the discovery that either oocytes or specific transcription factors can radically change a cell's phenotype from a differentiated to an embryonic state (*1*–*3*). A clear understanding of how this cellular reprogramming process takes place remains incomplete. Growing evidence suggests that the reprogramming capacity of the mammalian metaphase II oocyte yields superior results—when looking at epigenetic marks of the resulting cells—to those of the factor-based reprogramming approaches (*4*–*8*). One hypothesis that accounts for this enhanced reprogramming capacity posits that the current induced pluripotent stem cell (iPSC) generation strategies lack specific factors that the oocyte possesses. We hypothesized that by understanding the functions of genes present in the MII oocyte, we will be able to identify intra- and extracellular oocyte factors responsible for the oocyte's reprogramming capacity that may also have a role in dedifferentiation events such as generation of iPSCs.

Histone chaperones regulate all facets of histone metabolism. One such gene, antisilencing function 1 (ASF1), the most conserved histone 3 and histone 4 chaperone, has been implicated in replication, transcription, and DNA repair [reviewed in (*9*)]. ASF1 has been identified as a single protein in yeast (*10*), whereas in most vertebrates, it exists as two paralogs, termed ASF1A and ASF1B in mammals.

ASF1A is specifically enriched in the metaphase II human oocyte (*11*), and recent research using cross-species global transcriptional analysis has singled it out as a potential oocyte reprogramming factor (*12*). Most of the information about ASF1A comes from the work done in yeast and *Drosophila* (*9*, *13*). It has been characterized as a histone-remodeling chaperone that cooperates with histone regulator A (HIRA) and with chromatin assembly factor 1 (CAF-1), which plays a key role in remodeling chromatin in pluripotent embryonic cells (*14*). ASF1A is specifically required for H3K56 acetylation, a histone state shown to reflect more accurately the epigenetic differences between human embryonic stem cells (hESCs) and somatic cells—more so than other active histone marks, such as H3K4 trimethylation and


[1]LARCEL, Laboratorio Andaluz de Reprogramación Celular, BIONAND, Centro Andaluz de Nanomedicina y Biotecnología Andalucía, 29590, Spain. [2]Department of Genetics and Bioengineering, Istanbul Bilgi University 34060, Istanbul, Turkey. [3]Department of Electrical Engineering, University of Nebraska-Lincoln, Lincoln, NE 68588, USA. [4]Department of Animal Science, Michigan State University, East Lansing, MI 48824, USA. [5]Department of Physiology, Michigan State University, East Lansing, MI 48824, USA.
***Corresponding author. E-mail: cibelli@msu.edu**

H3K9 acetylation—suggesting the involvement of K56Ac in the human core transcriptional network of pluripotency (*15*–*18*). However, little is known about the role of ASF1A in human cells and, more specifically, about its role in the pluripotency state of a cell. Here, we report that ASF1A is necessary for the cellular reprogramming of human adult dermal fibroblasts (hADFs) into undifferentiated iPSCs.

Furthermore, we show that overexpression of ASF1A and OCT4 alone in somatic cells exposed to oocyte-specific growth factor GDF9 can reprogram hADFs into pluripotent cells. In addition, we identify transcriptional networks activated by ASF1A, OCT4, and GDF9 involved in the reprogramming process. Our study suggests that studying the unfertilized MII oocyte offers an important opportunity to elucidate the molecular pathways governing somatic cell reprogramming.

To determine whether ASF1A has a role in pluripotent stem cells and pluripotency acquisition, we investigated its expression in hESCs during differentiation. Gene expression and protein analyses show that during spontaneous differentiation, ASF1A expression decreases, as does the expression of the pluripotency-related genes OCT3/4, NANOG, SOX2, and DNMT3B (Fig. 1A and fig. S1A). We found the highest ASF1A expression levels in hESCs and the lowest in hADFs (fig. S1B).

To further investigate the role of ASF1A in somatic and embryonic stem cells, we tested whether forced expression of ASF1A in hESCs and hADFs would affect their differentiated states. We engineered H9 hESCs or hADF to overexpress either ASF1A or green fluorescent protein (GFP) by transducing these cells with a lentiviral vector (pWPI). H9 hESCs overexpressing ASF1A showed a tenfold increase in OCT4, NANOG, SOX2, and DNMT3B expression (fig. S2B) 6 days after transduction. We found that hADFs overexpressing ASF1A also showed a similar relative increase in pluripotency marker expression compared with GFP-transduced cells (fig. S2A). When we cultured hESCs overexpressing ASF1A as embryo bodies and then plated them into 10% fetal bovine serum media to promote spontaneous differentiation into endoderm, mesoderm, and ectoderm cell derivatives, ASF1A-overexpressing hESCs showed a clear resistance to differentiation by delaying the down-regulation of pluripotency-related genes and the onset of expression of differentiation markers (fig. S3, A and B). These results indicate that constitutive expression of ASF1A favors the maintenance of pluripotency, suggesting its role in pluripotency acquisition.

To determine whether ASF1A expression is required during cellular dedifferentiation into iPSCs, we blocked ASF1A expression using short hairpin RNA (shRNA) (fig. S4A) and subsequently transduced hADF with the four Yamanaka factors: OCT3/4, SOX2, KLF4, and c-MYC (OSKM). We used two different ASF1A shRNAs (ASF1A shRNA-147 and ASF1A shRNA-1234) or control shRNA. Down-regulation of ASF1A did not alter cell proliferation rates of hADF (fig. S4B). When shRNA-147 was used, we found a significant decrease in the number of TRA-1-60$^+$ reprogrammed iPSCs colonies. However, when we used the most efficient of the two shRNAs (shRNA-1234), we completely precluded the appearance of TRA-1-60$^+$ reprogrammed iPSC colonies (Fig. 1B). When the same ASF1A-shRNA vector was used to down-regulate ASF1A expression in hESC-H9, we observed a reduction in the expression of pluripotency markers (Fig. 1C), along with a change in colony morphology (fig. S5) as ASF1A decreased. These experiments show that ASF1A expression is required for pluripotency maintenance and for reprogramming hADFs into iPSCs.

To further analyze the role of ASF1A in the pluripotent state of a cell and its possible interaction with the master reprogramming genes, we overexpressed ASF1A along with the Yamanaka factors individually (OCT4, SOX2, and KLF4) and together (OSKM). One week after transduction, we observed no difference in the pluripotent gene expression pattern among the different combinations (fig. S6). Three to four weeks after transfection, however, the combination of ASF1A and OCT4 alone generated pre-iPSC–like colonies. Dermal fibroblasts transduced with OSKM plus ASF1A resulted in a slight increase in TRA-1-60$^+$ iPSC-like colonies (fig. S7A) over fibroblasts transduced with OSKM alone.

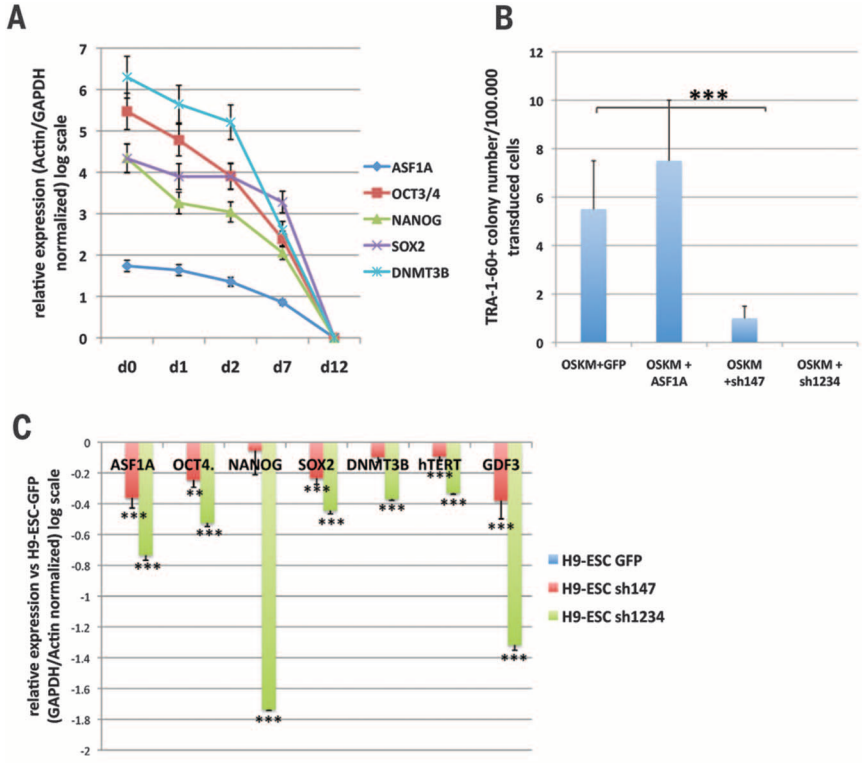


**Fig. 1. ASF1A role during cell reprogramming**. (**A**) H9 hESCs were cultured under conditions to promote spontaneous differentiation. ASF1A expression decreases as pluripotent cells differentiate. Quantitative reverse transcription polymerase chain reaction (qRT-PCR) data for genes characteristic of undifferentiated stem cells was performed as indicated on mRNA collected at days 0, 1, 2, 7 and 12 during differentiation. Mean values ± SEM are plotted, indicating expression of the specific gene normalized to glyceraldehyde-phosphate dehydrogenase (GAPDH)/Actin relative to the expression on day 12, which was arbitrarily assigned a value of 0, in a logarithmic scale (1 unit means 10-fold change). (**B**) In the absence of ASF1A, somatic cells cannot reprogram into pluripotent cells when using the Yamanaka factors. Seventy-two hours after hADFs lentiviral transduction with GFP, ASF1A or two different shRNAs against ASF1A, hADFs were transduced with retroviral supernatants encoding OSKM factors for reprogramming. The graph shows the number of Tra-1-60$^+$ colonies derived from 100,000 cells after OSKM overexpression in GFP (control), ASF1A, or the shRNAs 147 or 1234 expressing cells compared with control OSKM GFP-expressing fibroblasts. Mean values ± SEM. ***$P < 0.01$. (**C**) Down-regulation of ASF1A in H9-hESCs significantly decreases the expression of pluripotency-related genes. qRT-PCR data for ASF1A expression on mRNA were collected from H9-hESC cells expressing a lentivector encoding GFP or two different shRNAs against ASF1A (sh147 and sh1234). Mean values ± SEM are plotted indicating expression of the specific gene normalized to GAPDH/Actin relative to the expression of H9-hESC-GFP, which was arbitrarily assigned a value of 0, in a logarithmic scale. For all three panels, data correspond to the average of three independent experiments done in duplicate. ***$P < 0.001$, **$P < 0.05$, and *$P < 0.01$ compared with H9-hESC-GFP.

We hypothesized that other oocyte factors could be necessary to achieve complete iPSCs formation. We focused on paracrine factors secreted by the oocyte itself, which are known to have well-described signaling pathways in the mammalian MII oocyte. We tried seven different ligands in combination with the overexpression of ASF1A and OCT4 (table S1). Only GDF9, added during 48 hours after ASF1A/OCT4 transduction, could generate colonies with typical iPSC morphology ($5 \pm 2 \times 10^{-7}$% of transduced cells) (figs. S7, A and B, and S8). Overexpression of OCT4 alone or in the presence of GDF9 did not produce any reprogrammed colony. ASF1A-OCT4-GDF9 (AO9)–derived colonies were fully reprogrammed, showed normal karyotype (fig. S9) and expressed standard stem cell markers after culturing for six to ten passages (Fig. 2A and fig. S7B), and showed a gene expression profile similar to hESCs (Fig. 2B). We found no detectable expression of exogenous ASF1A/OCT4 from the retroviral vectors in the AO9-iPSC clones 65 days after transduction (fig. S10).

When induced to differentiate in vitro, fully reprogrammed AO9-iPSCs formed ecto-, endo-, and mesoderm cell lineages (figs. S11 and S12). Injection of AO9-iPSC lines into immunodeficient mice formed mature teratomas that had intestinal epithelium (endoderm), cartilage (mesoderm), and neural epithelium (ectoderm) (Fig. 2, C to E).

At the epigenetic level, overexpression of ASF1A on human dermal fibroblasts increased H3K56Ac significantly, and the acetylation was even higher when OCT4 was coexpressed in the same cells (Fig. 3A and fig. S13). We further confirmed the interaction between ASF1A and H3K56Ac in hADFs, hiPSCs, and hESCs (Fig. 3B), corroborating the findings described in yeast and drosophila (*19*, *20*). We analyzed hADF 72 hours after the overexpression of the ASF1A-OCT4 factors and observed that these two factors coimmunoprecipitate (Fig. 3C). Chromatin immunoprecipitation (ChIP) analysis confirmed that H3K56ac is found in regulatory regions of NANOG, OCT4, and SOX2 after overexpression of ASF1A (Fig. 3D and fig. S14). Our results strongly suggest that both ASF1 and OCT4 are capable of activating genes at the core of the pluripotency regulatory network, at least in part through the acetylation of H3K56.

In an effort to elucidate the signaling pathways involved in the AO9 reprogramming process, we analyzed global gene expression profiles of human dermal fibroblasts 48 hours after exposing cells to the individual factors both alone and all three combined—i.e., overexpression of just ASF1A, OCT4, or GDF9, or of AO9 (the three factors combined) (Fig. 4). Using Ingenuity Pathway Analysis (Redwood City, CA) (table S2), we found that AO9 overexpression regulates, among many other signaling pathways, p38 and interleukin-6 signaling. Our data show that GDF9 activates R-SMADs 2/3 phosphorylation on human dermal fibroblasts, but not extracellular signal–regulated kinase 1/2 (Fig. 4 and fig. S15). Detailed information of the specific comparisons can be found in the supplementary materials.

Our work has uncovered two specific factors present in the human oocyte, ASF1A and GDF9, which play crucial roles in somatic cell reprogramming. ASF1A expression is necessary for somatic cell reprogramming and maintenance of pluripotency. It functions by interacting with histone 3, promoting its acetylation at lysine 56. H3K56 acetylation mediated by ASF1A occurs mainly at the S phase in unstressed cells (*15*). The fact that H3K56ac is cell-cycle–dependent and marks less than 1% of total H3 (*17*, *20*) may explain why it was previously difficult to determine the role of ASF1A in mammalian cells. Here, our coimmunoprecipitation experiments show that this interaction is likely to be direct. H3K56ac presence correlates positively with binding of

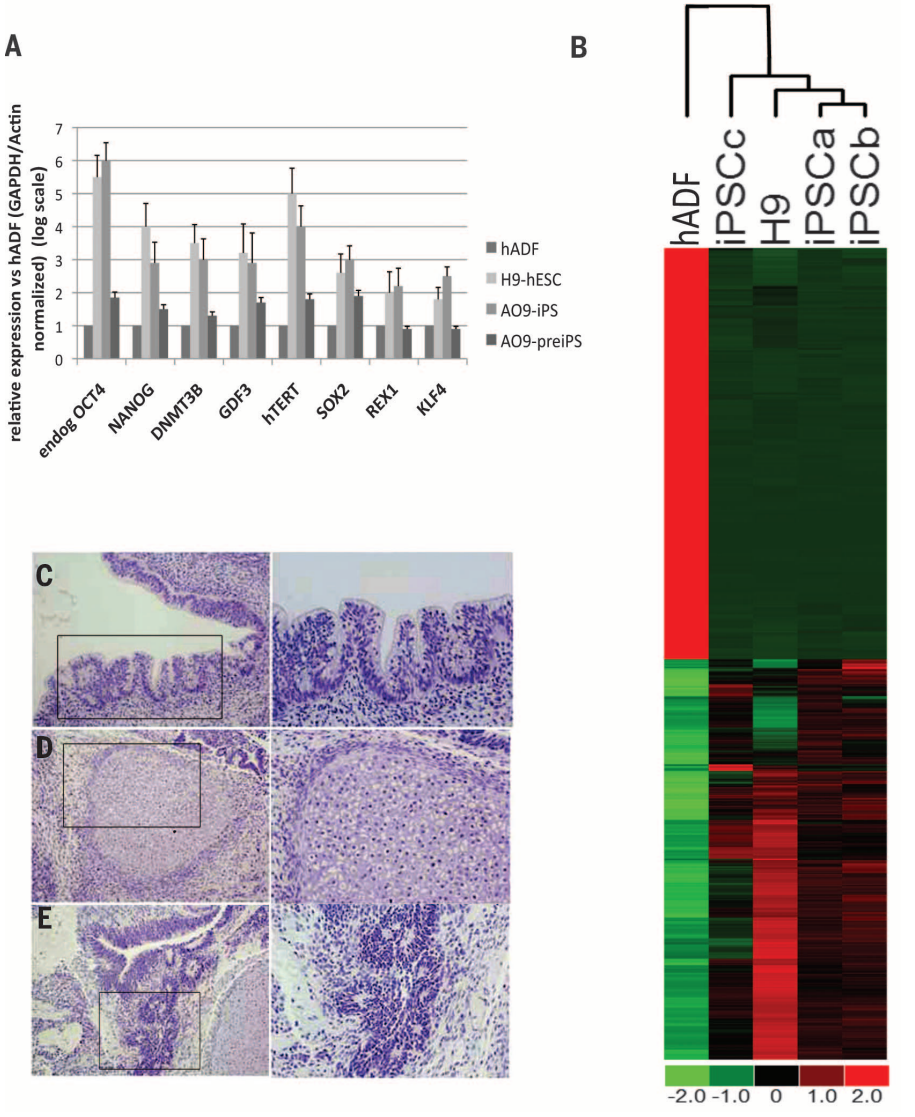


**Fig. 2. ASF1A, OCT4, and GDF9 (AO9) combination is sufficient for reprogramming hADF to pluripotency.** (**A**) qRT-PCR data for genes characteristic of pluripotent cells was performed as indicated on mRNA collected from hADF, H9 hESCs, and iPSCs obtained overexpressing ASF1A, OCT4 in the presence of GDF9 (AO9-iPSC). Values indicate expression of the specific gene normalized to GAPDH/Actin in a logarithmic scale relative to the hADF sample, which was arbitrarily assigned a value of 0. Data correspond to the average of three independent experiments done in duplicate. (**B**) Expression array data analysis of similarities between H9-ESCs and AO9-iPSCs (three independent lines: AO9-iPSCa, b, and c) compared with adult human dermal fibroblasts (hADF). Dendogram and heat map based on genes up- or down-regulated 10-fold or greater versus dermal fibroblasts to visualize similarly expressed group of genes. (**C** to **E**) AO9-iPSC differentiation capacity. Hematoxylin and eosin staining of representative matured AO9-iPS–derived teratomas exhibiting characteristic structure of (C) intestinal epithelium (endoderm), (D) cartilage (mesoderm), and (E) neural epithelium (ectoderm).

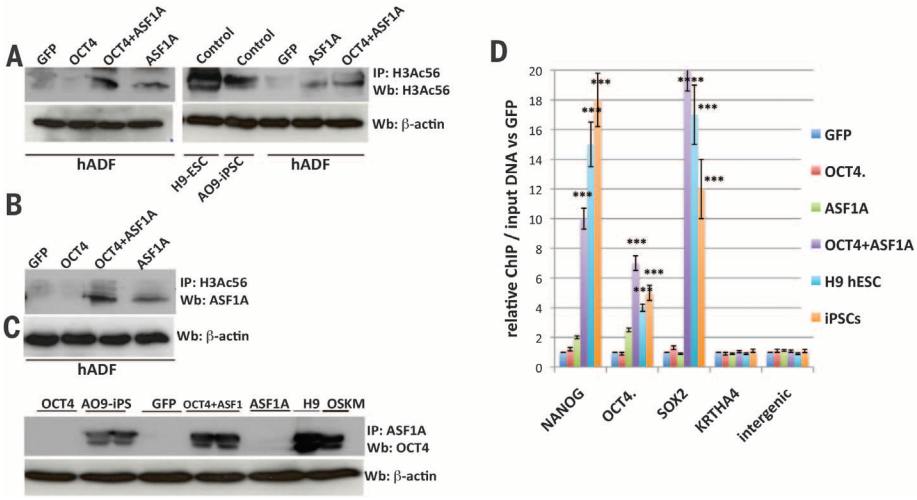


**Fig. 3. ASF1A, OCT4, and H3K56 acetylation.** (**A**) Retroviral-driven overexpression of ASF1A alone or ASF1A+OCT4 increases H3K56 acetylation in hADF shown by immunoprecipitation 72 hours after transduction using H3K56 antibodies (IP: H3Ac56) and gel blotted [Western blot (Wb)] with H3K56 antibody as well. H9-ESCs and AO9-iPSCs samples were used as positive control for immunoprecipitation. (**B**) IP and Wb using specific antibodies against H3K56ac (IP: H3Ac56) and ASF1A (Wb: ASF1A) demonstrate protein-protein interaction of ASF1A with acetylated H3K56 in transduced hADF. (**C**) Protein interaction is observed between ASF1A and OCT4 when ASF1A is immunoprecipitated in hADF overexpressing OCT4+ASF1A; in pluripotent cells H9-hESC; and in OSKM iPSCs and AO9-iPSC. Immunoprecipitated material was analyzed by Wb using the specified antibodies to detect OCT4 and ASF1A coimmunoprecipitation. Actin was used as a loading control. (**D**) ChIP assay in hADF overexpressing GFP, ASF1A, OCT4, both ASF1A and OCT4, and in H9 hESC and AO9-iPSCs using specific antibody against H3K56Ac. qRT-PCR was done using ChIP and input samples using the specific primers for NANOG, OCT4, and SOX2 promoters and two negative controls KRTHA4 (hypoacetylated gene) and an intergenic region primers. Mean values ± SEM are plotted indicating amplification of the specific gene region normalized to GFP sample, which was arbitrarily assigned a value of 1. Data correspond to the average of three independent experiments done in duplicate. Student's *t* test was applied for statistical significance. ***$P < 0.001$, **$P < 0.05$, and *$P < 0.01$ compared with ASF1A expressing hADF.

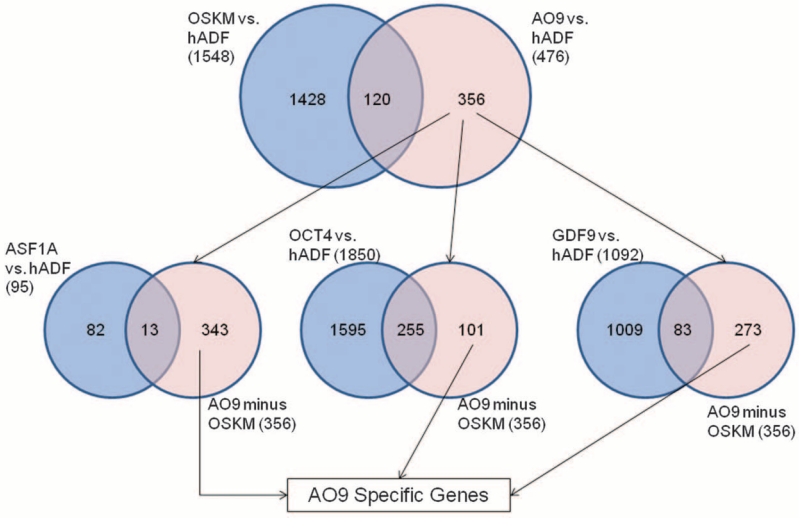


**Fig. 4. Comparisons of differentially expressed genes 48 hours after overexpression of different factors in human dermal fibroblasts.** Venn diagrams to select the genes that are differentially expressed in AO9 condition compared with OSKM (region II, upper diagram). Lower diagrams show three different comparison of previous region II with single-factor–specific up- or down-regulated genes.

NANOG, SOX2, and OCT4 transcription factors at their target gene promoters, and it binds specifically to these pluripotent factor promoters to increase their expression (*17*, *18*). ASF1A downregulation seems to mediate a reduction of histone 3 acetylation at lysine *56*, which in turn negatively impacts the expression of pluripotency-related markers and increases expression of differentiation-related ones (*18*).

In conclusion, we have identified two oocyte factors capable of—together with OCT4—reprogramming human dermal fibroblasts: ASF1A and GDF9. We found that GDF9 conditions somatic cells, activating SMAD 2/3 and likely making the cells more susceptible to reprogramming by OCT4 and ASF1A. We also found that ASF1A works by acetylating H3K*56*, affecting the expression of core pluripotency genes. It is quite possible that many other genes expressed in the MII oocyte are important for reaching and maintaining pluripotency. These genes may have a specific role during the first stages of the reprogramming process.

## REFERENCES AND NOTES


1. J. B. Gurdon, C. F. Graham, *Sci. Prog.* **55**, 259–277 (1967).
2. I. Wilmut, A. E. Schnieke, J. McWhir, A. J. Kind, K. H. Campbell, *Nature* **385**, 810–813 (1997).
3. K. Takahashi, S. Yamanaka, *Cell* **126**, 663–676 (2006).
4. S. Wakayama *et al.*, *Stem Cells* **24**, 2023–2033 (2006).
5. J. Hanna *et al.*, *Nature* **462**, 595–601 (2009).
6. S. Assou *et al.*, *BMC Genomics* **10**, 10 (2009).
7. K. Kim *et al.*, *Nature* **467**, 285–290 (2010).
8. K. Miyamoto *et al.*, *Science* **341**, 1002–1005 (2013).
9. F. Mousson, F. Ochsenbein, C. Mann, *Chromosoma* **116**, 79–93 (2007).
10. S. Le, C. Davis, J. B. Konopka, R. Sternglanz, *Yeast* **13**, 1029–1042 (1997).
11. A. M. Kocabas *et al.*, *Proc. Natl. Acad. Sci. U.S.A.* **103**, 14027–14032 (2006).
12. J. P. Awe, J. A. Byrne, *Cell Reprogram* **15**, 126–133 (2013).
13. A. Battu, A. Ray, A. A. Wani, *Nucleic Acids Res.* **39**, 7931–7945 (2011).
14. M. Houlard *et al.*, *PLOS Genet.* **2**, e181 (2006).
15. J. Yuan, M. Pu, Z. Zhang, Z. Lou, *Cell Cycle* **8**, 1747–1753 (2009).
16. F. Mousson *et al.*, *Proc. Natl. Acad. Sci. U.S.A.* **102**, 5975–5980 (2005).
17. W. Xie *et al.*, *Mol. Cell* **33**, 417–427 (2009).
18. Y. Tan, Y. Xue, C. Song, M. Grunstein, *Proc. Natl. Acad. Sci. U.S.A.* **110**, 11493–11498 (2013).
19. Q. Li *et al.*, *Cell* **134**, 244–255 (2008).
20. C. Das, M. S. Lucia, K. C. Hansen, J. K. Tyler, *Nature* **459**, 113–117 (2009).


## ACKNOWLEDGMENTS

We thank members of LARCEL laboratory for comments and support, A. Wittgreen and N. Lopez Corrales for intellectual input and discussion, and Biobanco del Sistema Sanitario Público de Andalucía for karyotyping and teratoma assay service. This work was supported by Fundacion Progreso y Salud, Sevilla, Andalucia, Spain; Michigan State University AgBioResearch, East Lansing, Michigan, USA; and the Naylor Family Foundation, York, Pennsylvania, USA. The Gene Expression Omnibus (GEO) accession number for the oocyte transcriptome is GSE12034. E.G.-M. and J.B.C. are listed as inventors on a patent application filed by Fundacion Progreso y Salud, Sevilla, Andalucia, Spain, and Michigan State University, East Lansing, Michigan, USA.

## SUPPLEMENTARY MATERIALS

www.sciencemag.org/content/345/6198/822/suppl/DC1
Materials and Methods
Supplementary Text
Figs. S1 to S17
Tables S1 to S3
References (*21*–*35*)

14 April 2014; accepted 7 July 2014
Published online 17 July 2014;
10.1126/science.1254745

TRANSDIFFERENTIATION

# Sequential histone-modifying activities determine the robustness of transdifferentiation

Steven Zuryn,[1] Arnaud Ahier,[1] Manuela Portoso,[2] Esther Redhouse White,[1]* Marie-Charlotte Morin,[1] Raphaël Margueron,[2] Sophie Jarriault[1]†

**Natural interconversions between distinct somatic cell types have been reported in species as diverse as jellyfish and mice. The efficiency and reproducibility of some reprogramming events represent unexploited avenues in which to probe mechanisms that ensure robust cell conversion. We report that a conserved H3K27me3/me2 demethylase, JMJD-3.1, and the H3K4 methyltransferase Set1 complex cooperate to ensure invariant transdifferentiation (Td) of postmitotic *Caenorhabditis elegans* hindgut cells into motor neurons. At single-cell resolution, robust conversion requires stepwise histone-modifying activities, functionally partitioned into discrete phases of Td through nuclear degradation of JMJD-3.1 and phase-specific interactions with transcription factors that have conserved roles in cell plasticity and terminal fate selection. Our results draw parallels between epigenetic mechanisms underlying robust Td in nature and efficient cell reprogramming in vitro.**

Tissue and organ regeneration occurs in multiple animal species and can originate from transdifferentiation (Td) of surrounding cell populations (*1*, *2*). Understanding how individual cells interconvert efficiently and precisely to contribute to or result in the robust regeneration of whole tissues is a major goal of regenerative medicine. To characterize these mechanisms in a physiological setting, we investigated a traceable and predictable Td event in *Caenorhabditis elegans*. The Y cell is a postmitotic hindgut cell that constitutes the half section of the third ring of the rectal tube. This cell exhibits a remarkable behavior by which it disengages from the tube and changes into a motor neuron called PDA during normal development (Fig. 1A) (*3*). We found that conversion between the two specialized cell types occurred with virtually invariant precision in each animal (100%, $n$ = 2209 animals). To identify those factors that endowed such precision, we chemically mutagenized worms, screened for low-penetrance mutants in which Td was no longer invariant (Td$^-$), and isolated several mutant alleles (*fp11*, *fp13*, *fp15*, and *fp25*) (Fig. 1B and fig. S1, A and B). Using deep-sequencing–based mapping (*4*), we cloned and confirmed that the causal genetic lesions of all mutants affected *jmjd-3.1* (fig. S1, C and D).

*jmjd-3.1* encodes an ortholog of human Jmjd3, which displays specificity for demethylating tri- and dimethylated histone H3 lysine 27 (H3K27) via a highly conserved Jumonji C terminus (JmjC) domain (*5*, *6*). In each *jmjd-3.1* mutant, the JmjC domain is either mutated, truncated, or absent, suggesting that H3K27me3/me2 demethylase activity mediates its Td role (Fig. 1C). Generating *jmjd-3.1(fp15)* strains harboring Cherry-tagged JMJD-3.1 forms, we found that nuclear JMJD-3.1 acted cell-autonomously [as well as nonredundantly (fig. S2)] and that disrupting its ability to demethylate lysine residues or recognize histone H3 tails abolished its activity during Td (Fig. 1C and figs. S3 and S4). Moreover, expressed and purified JMJD-3.1 mutant proteins mimicking *fp11*, *fp15*, and *fp25* had completely lost their capacity to demethylate H3K27me3 (fig. S5). This correlated with the Td$^-$ phenotypes and suggested that each allele encoded enzymatically null products. Last, deficiencies in the worm Polycomb Repressive Complex 1 component SPAT-3 (Ring1B) (*7*), which acts to fortify gene repression upon recruitment to trimethylated H3K27 residues (*8*), partially restored Td in *jmjd-3.1(fp15)* mutants (fig. S6). These data indicated that *jmjd-3.1* acts antagonistically to H3K27me3-mediated transcriptional repression during Td by demethylating H3K27me3.

Alongside H3K27, other histone tail residues can exist in several states of methylation, each of which can be modulated by specific enzymes. We performed RNA interference (RNAi) screens to determine whether other histone methyltransferases or demethylases, and hence other specific histone modifications, performed a role similar to *jmjd-3.1* in ensuring precise Td (fig. S7 and table S1). Only RNAi of the mammalian SET1A/SET1B ortholog, *set-2*, disrupted invariant Td. SET-2 is the catalytic subunit of the Set1 complex, a highly conserved multi-subunit ensemble that methylates H3K4 (*9*). Null deficiencies in *set-2*, as well as other Set1 complex subunits (*wdr-5.1*/WDR5, *ash-2*/ASH2L, *rbbp-5*/RbBP5,

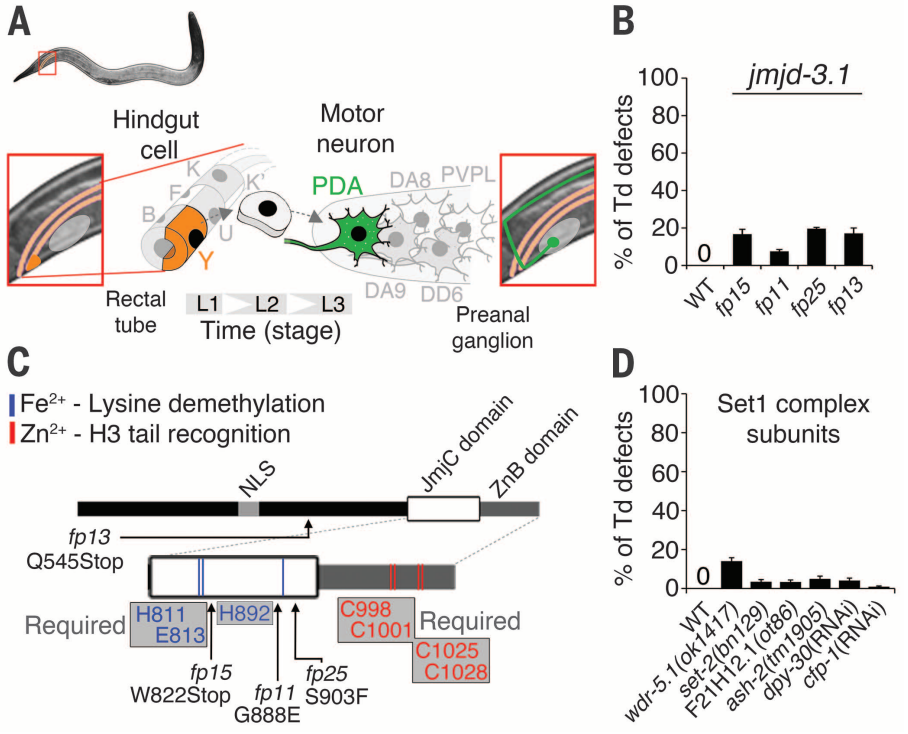


**Fig. 1. *jmjd-3.1* and the Set1 complex determine invariant Td.** (**A**) Schematic of Y-to-PDA Td. (**B**) *jmjd-3.1* mutations cause defects in Td. (**C**) Schematic of the JMJD-3.1 protein. NLS, nuclear localization signal; JmjC, Jumonji catalytic domain; ZnB, zinc-binding, H3 tail recognition domain. Amino acids highlighted in gray boxes were mutated in order to disrupt either lysine demethylation (blue) or H3 tail recognition (red). (**D**) Effect of deficiencies in Set1 complex subunits on Td.

[1]Department of Development and Stem Cells, Institut de Génétique et de Biologie Moléculaire et Cellulaire, CNRS UMR 7104/INSERM U964, Université de Strasbourg, 67404 Illkirch CU Strasbourg, France. [2]Institut Curie, INSERM U934, CNRS UMR3215, 26, Rue d'Ulm, 75005 Paris, France.
*Present address: Department of Cell and Developmental Biology, University College London, Gower Street, London WC1E 6BT, UK.
†Corresponding author. E-mail: sophie@igbmc.fr

*dpy-30*/DPY30, and *cfp-1*/CFP1), resulted in a low-penetrance Td⁻ phenotype, which again is not attributable to hypomorphism or redundancy (Fig. 1D and fig. S8). Set1 deficiencies could be phenocopied by overexpressing several functionally antagonistic enzymes (H3K4me3/me2 demethylases) in the Y cell in a demethylase-activity–dependent manner (fig. S9). The same effect was observed by overexpressing a K4 unmethylable replication-independent H3.3K4A in Y (fig. S9). Further implicating Set1 H3K4 methyltransferase activity in Td, only a catalytically active *set-2* transgene expressed in Y could rescue the defect in *set-2* mutants (discussed below). Thus, multiple specific histone-modifying activities acting on distinct lysines of histone H3 mediate invariant cell conversion in a natural setting.

How do specific histone methylation states elicit these effects? To answer this question, we investigated the progression of Td at the single-cell level in live mutant animals. Td⁻ cells in Set1 mutants, and in transgenic animals overexpressing Set1 antagonists or H3K4A in Y, could be broken into two distinct classes: Approximately half displayed a characteristic, hindgut fried-egg–shaped nuclear morphology, whereas the rest displayed speckled nuclear morphology (Fig. 2A and fig. S10A). In contrast, Td⁻ cells in *jmjd-3.1* mutants had exclusively speckled nuclei. These initial observations hinted that specific K4 and K27 methylation states mediated different transitions through successive stages of cell conversion, which became blocked in the absence of their respective modifiers. We have previously shown that Y-to-PDA proceeds through discrete phases: dedifferentiation and then redifferentiation into the new cell type (*10*), as observed in vertebrate examples of Td, such as newt lens regeneration (*1*). We thus tested whether *jmjd-3.1* and Set1 mediated distinct Td phases. Indeed, those Td⁻ cells with hindgut morphology in Set1 mutants persistently expressed hindgut molecular markers and remained attached to the rectal tube via intercellular adherens junctions (fig. S10, B and C), indicating a failure in dedifferentiation. In Td⁻ cells with speckled morphology in either *jmjd-3.1* or Set1 backgrounds, hindgut markers were correctly extinguished, and the cells disengaged from the rectal tube, but they did not properly activate a range of PDA neural markers (fig. S10B), indicating a failure to properly redifferentiate. In addition, timely rescue of *wdr-5.1* and *jmjd-3.1* mutant strains by heat shock–inducible rescue constructs demonstrated that the temporal requirements of each factor correlated precisely with their successive cellular roles (Fig. 2B). Therefore, Set1 acts dichotomously, mediating both dedifferentiation and redifferentiation, whereas *jmjd-3.1* mediates only redifferentiation. This suggests that stepwise modifications to distinct lysine residues on H3 mediate precise transition through distinct cellular phases of Td (Fig. 2C).

The model above implies a mechanism for efficient partitioning (temporally and functionally) of K4- and K27-modifying activities within a post-mitotic cell. To determine the mechanisms at play, we first addressed how each distinct requirement was established. Consistent with Set1's action at different steps of the process, functional, green fluorescent protein (GFP)–tagged Set1 subunits were nuclear-localized in Y/PDA throughout Td (fig. S11A). Contrastingly, Cherry-tagged JMJD-3.1 and a *jmjd-3.1* fosmid-based GFP construct were dynamically localized during Td (fig. S11, A to C). Both JMJD-3.1 reporters were detectable in the nucleus at all stages during, before, and after Td, except for a precise window when Y dedifferentiated. This pattern matched *jmjd-3.1*'s temporal requirements and exclusive redifferentiation role, suggesting that regulation of JMJD-3.1 levels may provide a mechanism to ensure stepwise K4 and K27 modification. Through the use of a photoconvertible JMJD-3.1::Dendra2 fusion protein, as well as artificial modulation of JMJD-3.1's nuclear localization, we determined that JMJD-3.1 levels were dynamically regulated through nuclear-dependent degradation during dedifferentiation (Fig. 2, D and E, and figs. S12). Moreover, precise temporal regulation of JMJD-3.1 levels, and hence stepwise histone modification, was critical for precise Y-to-PDA conversion because forced ectopic JMJD-3.1 expression during Y dedifferentiation induced a Td⁻ phenotype and resulted in cells displaying a mixture of abnormal identities (fig. S13). Catalytic inactivation of JMJD-3.1 largely mitigated these effects (fig. S13D). We conclude that regulation of nuclear JMJD-3.1 protein levels ensures partitioning of K27 demethylase activity into the redifferentiation phase of Td and that such control is critical for invariant Td.

We next turned our attention to the mechanism (or mechanisms) that partitioned Set1's K4 methylase activity into temporally separable, seemingly opposite cellular functions (dedifferentiation and redifferentiation). We reasoned that each distinct role might be segregated functionally through discrete temporal associations with coregulators. Using coimmunoprecipitation, we found that the core Set1 component WDR-5.1 associates with several subunits of the Nanog and Oct4 Deacetylase (NODE)–like complex (Fig. 3A) (*11*). We have previously found that the NODE-like complex is required for Y dedifferentiation (*12*) and is composed of factors that have conserved roles in the maintenance and induction of cell plasticity in a variety of species (*13*). Using Set1;NODE double mutants carrying catalytically active or inactive *set-2* rescue constructs, we found that the two complexes functionally cooperated—in a Set1-H3K4 methyltransferase–dependent manner—to specifically mediate Y dedifferentiation (Fig. 3B). This suggested that the NODE-like complex, which can bind DNA targets directly (*11*), provides dedifferentiation functional specificity to Set1.

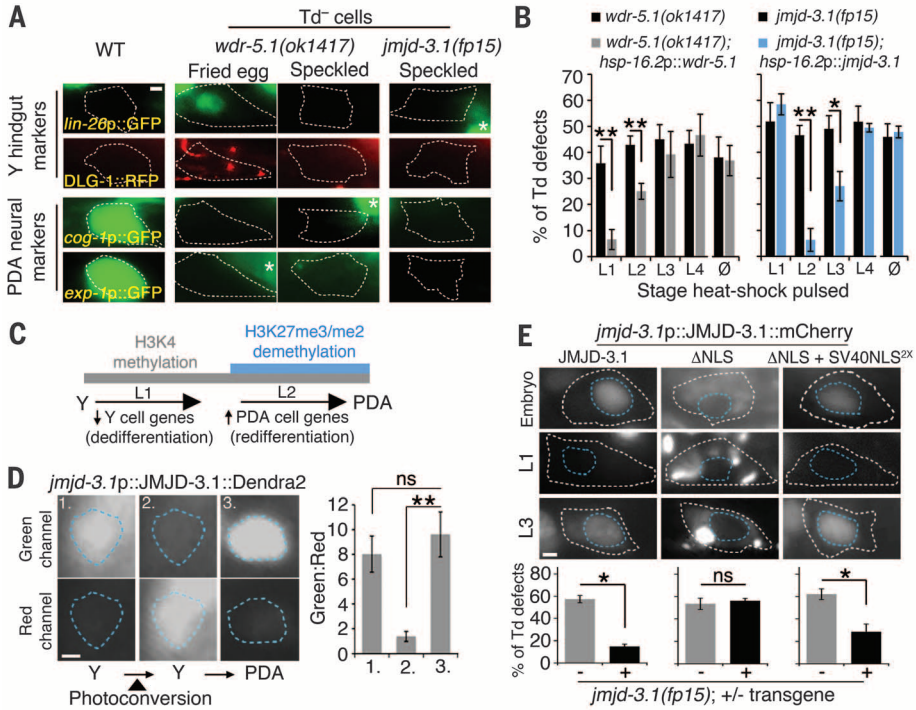


**Fig. 2. Set1 and *jmjd-3.1* mediate different Td phases.** (**A**) Fluorescent micrographs of cell fate markers in Td⁻ cells in live animals. Asterisk indicates signal from adjacent cell. (**B**) Timed heat shock pulses show that *wdr-5.1* and *jmjd-3.1* have distinct temporal requirements matching their successive cellular roles. Ø, no heat-shock. (**C**) Schematic showing requirements for histone-modifying activities. (**D**) Photoconversion of Dendra2 fused to JMJD-3.1 indicates that photoconverted protein is degraded during dedifferentiation and resynthesized during redifferentiation. (**E**) Modulation of JMJD-3.1 nuclear localization indicates that degradation is nuclear-dependent and that removal from the nucleus is sufficient for eliminating its activity. $^{**}P < 0.01$, $^{*}P < 0.05$; $n > 100$ animals.

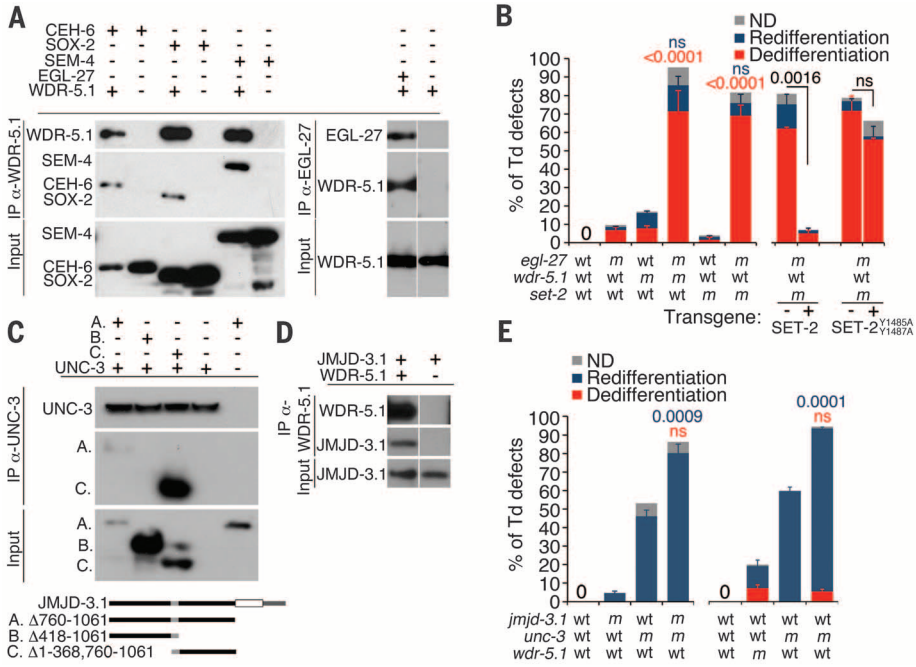


**Fig. 3. Phase-specific interactions specify Set1 and JMJD-3.1's Td roles.** (**A**) WDR-5.1 immunoprecipitates members of the *C. elegans* NODE complex, CEH-6(OCT), SOX-2(SOX2), SEM-4(SALL), and EGL-27(MTA). (**B**) Set1 functionally cooperates with the NODE-like complex to mediate hindgut dedifferentiation. *m*, mutant; wt, wild type. (**C** and **D**) JMJD-3.1 immunoprecipitates WDR-5.1 and UNC-3 via an N-terminal domain. (**E**) *unc-3* cooperates with *jmjd-3.1* and Set1 to mediate PDA redifferentiation. Red and blue *P* values correspond to dedifferentiation and redifferentiation, respectively. Error bars indicate SEM. ND, not determined; ns, not significant. Statistical significance was determined by using two-way analysis of variance.

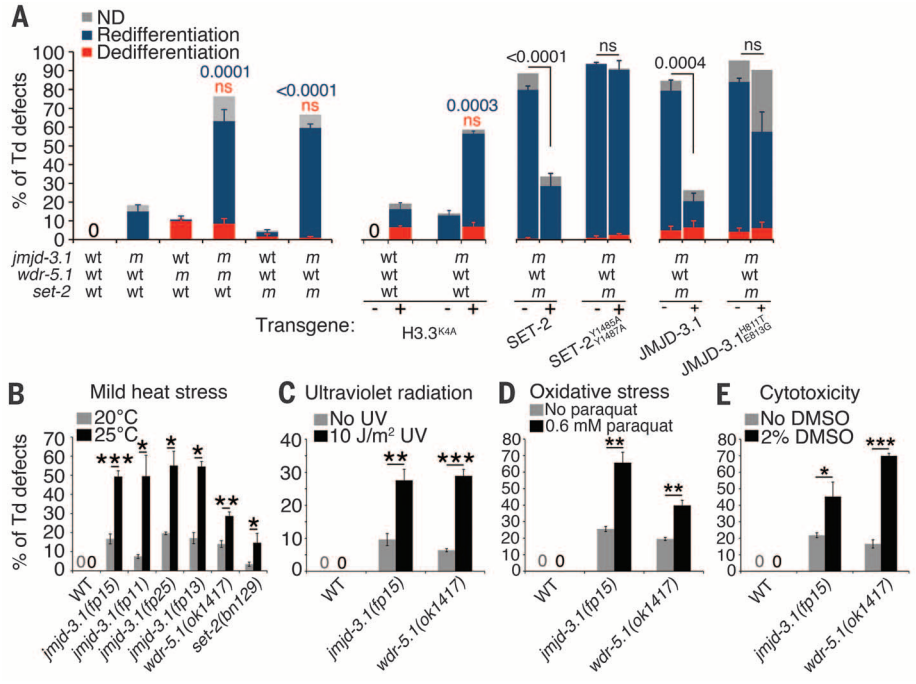


**Fig. 4. *jmjd-3.1* and Set1 cooperate to ensure robust Td against stress.** (**A**) *jmjd-3.1* and Set1 components exhibit synergistic genetic interactions in a H3K27 demethylase and H3K4 methyltransferase activity–dependent manner during redifferentiation. *m*, null mutant; wt, wild type. (**B** to **E**) Stressful environmental conditions enhance Td defects in *jmjd-3.1* and Set1 null mutants. Error bars indicate SEM. ND, not determined; ns, not significant. $n > 100$ animals; $^{***}P < 0.001$, $^{**}P < 0.01$, $^{*}P < 0.05$; $n > 100$ animals.

Next, we uncovered an alternative functional interaction network between WDR-5.1, JMJD-3.1, and the phylogenetically conserved COE (Collier, Olf, EBF)–type transcription factor (TF) UNC-3 that appeared to specify Set1's redifferentiation role. UNC-3 transcriptionally regulates batteries of genes that specify terminal features of motor neurons in *C. elegans* as well as chordates (*14*). We showed that UNC-3, which is required for PDA redifferentiation (*10*), interacts with a functionally important N-terminal region of JMJD-3.1. JMJD-3.1 in turn associates with WDR-5.1 (Fig. 3, C and D, and fig. S14), providing a mechanistic rationale for the precise regulation of JMJD-3.1 protein levels that we unraveled, one that may serve to prevent interaction with Set1 until redifferentiation, for which both activities are needed. Moreover, double *unc-3;jmjd-3.1* and *unc-3;wdr-5.1* mutants suggested that these three factors functionally cooperate specifically during the redifferentiation phase of Td and not during dedifferentiation (Fig. 3E). Thus, UNC-3 appears to act as an important regulatory hub for the redifferentiation phase of Td onto which chromatin modifiers may log their activities.

To gain deeper insight into SET1 and JMJD-3.1's mode of action, we analyzed double Set1;*jmjd-3.1* mutant strains carrying active or inactive *set-2* or *jmjd-3.1* transgenes, or *jmjd-3.1(fp15)* mutants overexpressing H3.3K4A (Fig. 4A). Our results suggested that K4 methylation and K27 demethylation (i) acted in parallel, rather than in a mutually dependent manner, and (ii) ultimately converged on a common downstream target (or targets) to specifically promote redifferentiation. One possibility—suggested by their physical association as well as data presented earlier indicating that Set1 and JMJD-3.1 cellular localizations and activities intersected precisely during redifferentiation—is that both activities act in a bifunctional K4/K27–modifying complex. Such complexes have been shown in other species (*6*, *15*–*17*) and have been predicted to resolve bivalent domains: nucleosomes containing both H3K4me3 and H3K27me3 signatures (*18*). Evidence suggests that such domains act to poise developmental loci for timely and efficient activation, representing an attractive mechanism for ensuring precise PDA redifferentiation (*19*). However, bivalency has only been reported thus far in vertebrates (*20*). Here, we demonstrate the co-occurrence of H3K4me3 and H3K27me3 marks on mononucleosomes purified from worms, pointing to the existence of bivalent domains in *C. elegans* (fig. S15) and opening the possibility that targets of Set1 and JMJD-3.1 may be bivalently marked.

Our results suggest a model in which Set1 and *jmjd-3.1*'s role is to ensure precise Td, whereas key TFs, which exhibit complete penetrance in null mutants (*3*, *10*, *12*), act as drivers. We found that histone modifications additionally are critically needed when the worm is exposed to adverse conditions. In absence of *jmjd-3.1* or Set1, Y-to-PDA Td was hypersensitive to a variety of stressful treatments, whereas Td remained unaffected in wild-type animals (Fig. 4, B to E). This suggests that both Set1-dependant H3K4 methylation and *jmjd-3.1*–dependent H3K27me3/me2

demethylation provide protection against variations that may be encountered in the worm's natural environment. These roles in ensuring the robustness of cell conversion in stressful circumstances may underlie invariant Td under normal conditions. Last, our in vivo results suggest that Set1 and *jmjd-3.1* perform highly conserved roles across phyla and cell types to reinforce TF-driven changes in identity. Indeed, modulation of H3K4 and H3K27 methylation state has been shown to regulate somatic reprogramming (*21*–*23*). Specifically, the core Set1 subunit, Wdr5, was recently shown to interact with and potentiate Oct4's roles in the initial phases of mammalian induced pluripotent stem (iPS) cell induction (*22*). Furthermore, Jmjd3 was found to specifically inhibit the initial stages of iPS reprogramming (*23*), drawing a distinct parallel to its disruption of the initial stages of Td we observed.

## REFERENCES AND NOTES


1. C. Jopling, S. Boue, J. C. Izpisua Belmonte, *Nat. Rev. Mol. Cell Biol.* **12**, 79–89 (2011).
2. E. M. Tanaka, P. W. Reddien, *Dev. Cell* **21**, 172–185 (2011).
3. S. Jarriault, Y. Schwab, I. Greenwald, *Proc. Natl. Acad. Sci. U.S.A.* **105**, 3790–3795 (2008).
4. S. Zuryn, S. Le Gras, K. Jamet, S. Jarriault, *Genetics* **186**, 427–430 (2010).
5. K. Agger *et al.*, *Nature* **449**, 731–734 (2007).
6. F. De Santa *et al.*, *Cell* **130**, 1083–1094 (2007).
7. O. Karakuzu, D. P. Wang, S. Cameron, *Development* **136**, 943–953 (2009).
8. N. J. Francis, R. E. Kingston, C. L. Woodcock, *Science* **306**, 1574–1577 (2004).
9. A. Shilatifard, *Annu. Rev. Biochem.* **81**, 65–95 (2012).
10. J. P. Richard *et al.*, *Development* **138**, 1483–1492 (2011).
11. J. Liang *et al.*, *Nat. Cell Biol.* **10**, 731–739 (2008).
12. K. Kagias, A. Ahier, N. Fischer, S. Jarriault, *Proc. Natl. Acad. Sci. U.S.A.* **109**, 6596–6601 (2012).
13. I. Chambers, S. R. Tomlinson, *Development* **136**, 2311–2322 (2009).
14. P. Kratsios, A. Stolfi, M. Levine, O. Hobert, *Nat. Neurosci.* **15**, 205–214 (2012).
15. I. Issaeva *et al.*, *Mol. Cell. Biol.* **27**, 1889–1903 (2007).
16. Y. W. Cho *et al.*, *J. Biol. Chem.* **282**, 20395–20406 (2007).
17. S. A. Miller, A. C. Huang, M. M. Miazgowicz, M. M. Brassil, A. S. Weinmann, *Genes Dev.* **22**, 2980–2993 (2008).
18. B. E. Bernstein *et al.*, *Cell* **125**, 315–326 (2006).
19. P. Voigt, W. W. Tee, D. Reinberg, *Genes Dev.* **27**, 1318–1338 (2013).
20. P. Voigt *et al.*, *Cell* **151**, 181–193 (2012).
21. A. A. Mansour *et al.*, *Nature* **488**, 409–413 (2012).
22. Y. S. Ang *et al.*, *Cell* **145**, 183–197 (2011).
23. W. Zhao *et al.*, *Cell* **152**, 1037–1050 (2013).


## ACKNOWLEDGMENTS

We are grateful to S. Gasser, R. Klose, M. Labouesse, B. Prud'homme, and R. Schneider for their comments on the manuscript. Work in R.M.'s laboratory is funded by a European Research Council–Stg (REPODDID) grant, an ATIP-Avenir grant, and a Fondation pour la Recherche Medicale (FRM) grant. Work in S.J.'s laboratory is funded by grants from FRM, the Fondation ARC pour la recherche sur le cancer, the Association Française contre les Myopathies (AFM), the Fondation Schlumberger pour l'Enseignement et la Recherche (FSER), and the European Molecular Biology Organization Young Investigator program (EMBO YIP). S.Z. is a FRM and ARC postdoctoral fellow, and S.J. is a Centre National de la Recherche Scientifique research director.

## SUPPLEMENTARY MATERIALS

www.sciencemag.org/content/345/6198/826/suppl/DC1
Materials and Methods
Figs. S1 to S16
Table S1
References (*24*–*42*)

12 May 2014; accepted 17 July 2014
10.1126/science.1255885

SYNTHETIC BIOLOGY

# Programmable on-chip DNA compartments as artificial cells

**Eyal Karzbrun,[1]* Alexandra M. Tayar,[1]* Vincent Noireaux,[2] Roy H. Bar-Ziv[1]†**

**The assembly of artificial cells capable of executing synthetic DNA programs has been an important goal for basic research and biotechnology. We assembled two-dimensional DNA compartments fabricated in silicon as artificial cells capable of metabolism, programmable protein synthesis, and communication. Metabolism is maintained by continuous diffusion of nutrients and products through a thin capillary, connecting protein synthesis in the DNA compartment with the environment. We programmed protein expression cycles, autoregulated protein levels, and a signaling expression gradient, equivalent to a morphogen, in an array of interconnected compartments at the scale of an embryo. Gene expression in the DNA compartment reveals a rich, dynamic system that is controlled by geometry, offering a means for studying biological networks outside a living cell.**

In the past decade, cell-free gene expression reactions have been used to design synthetic biological systems, including droplets for molecular evolution (*1*), a vesicle bioreactor toward an artificial cell (*2*), regulatory (*3*–*6*) and morphogenetic-like genetic circuits (*7*), as well as assembly of protein complexes (*8*–*10*). Thus far, the lack of efficient protein turnover has prevented the emergence of expression dynamic patterns, such as oscillations, in a continuous expression bioreactor or vesicle (*2*, *11*). Microfluidic chips containing switching valves and addressable fluidic chambers (*12*, *13*) have succeeded in implementing steady-state and dynamic protein synthesis reactions (*14*). However, micrometer-scale positional information encoded in diffusive concentration gradients of proteins and mRNA, as in a morphogenetic scenario (*15*), is washed away in flow-driven expression compartments. Here, we present a solid-state biochip approach for the assembly of an artificial cell, which enables protein turnover, materials exchange with the environment, a capacity to encode and express genes at high surface density within a controlled geometry, and the ability to maintain micrometer-scale positional information in diffusive molecular gradients.

Dense phases of end-attached, linear double-stranded DNA templates (DNA brushes) were assembled by chemical photolithography (*16*, *17*) on the surface of circular compartments carved in silicon with radius $R$ = 50 μm and depth $h$ = 1 to 3 μm (Fig. 1, A and B, and figs. S1 to S3). The DNA compartments were connected to a 30-μm-deep flow channel through thin capillaries of width $W$ = 20 μm and length $L$ = 50 to 300 μm. The device was sealed, and *Escherichia coli* cell extract (*18*, *19*) was continuously flown in the main channel. Reaction components were transported by diffusion into the DNA compartment because of the high resistance to flow through the capillary (fig. S4). Proteins were synthesized in the DNA compartment and diffused out to the flow channel through the capillary. A linear protein concentration gradient formed along the capillary, decaying from a maximal value in the DNA compartment, where its distribution was homogenous, down to zero at the channel junction (Fig. 1C). The protein linear gradient persisted throughout the duration of expression, which reached a steady-state concentration (fig. S5). The dilution through the capillary leads to an emergent effective protein lifetime, $\tau = \frac{\pi R^2}{WD} L$, that is obtained by solving the diffusion equation in the compartment geometry, where $D$ is the protein diffusion constant (supplementary materials).

The effective protein lifetime enabled us to observe gene expression dynamics, including steady states (Fig. 1D) and oscillations (Fig. 1E). Figure 1D shows expression of green fluorescent protein (GFP) through a positive feedback gene construct, which is self-activated by the AraC protein dimer in the presence of arabinose (*20*) (fig. S6). The kinetics was characterized by a sharp onset after a 2-hour delay and reached a steady-state level for over 8 hours. To implement an oscillatory gene expression dynamics, we used an activator-repressor network with sigma factor $\sigma^{28}$ for activation and the lambda phage cI repressor (fig. S6 and tables S1 to S3). The network exhibited emergent oscillations for many hours with a period of ~2.5 hours (Fig. 1E). Furthermore, the high concentration of regulatory proteins near the DNA brush enabled direct imaging of transcription regulation. We imaged repression of transcription by using a negative-feedback construct that codes for a fusion of a Cro repressor dimer and GFP, expressed under a Cro-regulated promoter (fig. S6). The synthesized fusion protein bound the repressor site adjacent to the promoter, thereby localized the GFP signal to the DNA brush (Fig. 1F) and led to a reduced self-regulated expression levels in steady state.

[1]Department of Materials and Interfaces, Weizmann Institute of Science, Rehovot 76100, Israel. [2]Department of Physics, University of Minnesota, Minneapolis, MN 55455, USA.
*These authors contributed equally to this work. †Corresponding author. E-mail: roy.bar-ziv@weizmann.ac.il

In order to investigate the effect of compartment geometry on the reaction-diffusion dynamics, we fabricated a device with varying capillary length and integrated up to 80 compartments on the chip. First, we studied three single-gene constructs as a function of the capillary length: unregulated, positive-feedback, and a negative-feedback construct (Fig. 2, A to C, and fig. S6). GFP appeared in the compartments in hierarchical

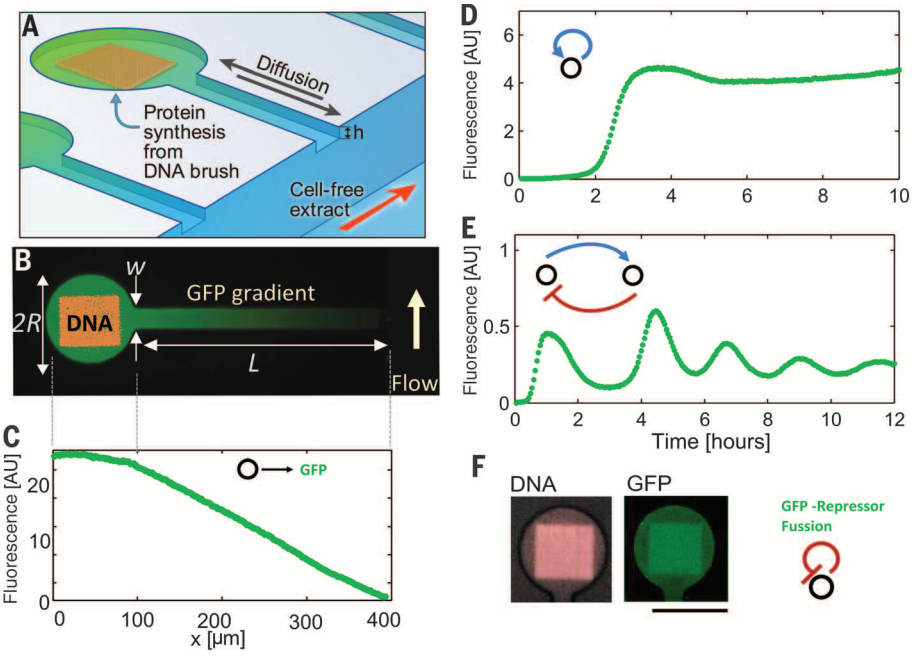


**Fig. 1. Two-dimensional DNA compartments and emergent gene network dynamics.** (**A**) DNA brushes patterned (red squares) in circular compartments ($h \approx 2$ μm), carved in silicon, and connected through a diffusive capillary to a channel flowing a cell-free expression reaction. (**B**) Overlay of expressed GFP in the compartment and end-labeled DNA brush images. (**C**) GFP intensity profile in arbitrary units (AU) of an unregulated construct along the capillary after 4 hours of expression. (**D**) Steady-state dynamics of a positive-feedback construct reported by GFP. (**E**) Emergent oscillation of an activator-repressor network. (**F**) Repressor-GFP fusion binding its own promoter during expression of a self-repressed DNA construct. Scale bar indicates 100 μm. GFP intensity was taken from single reactors and averaged over the compartment area with error bars the size of data points.

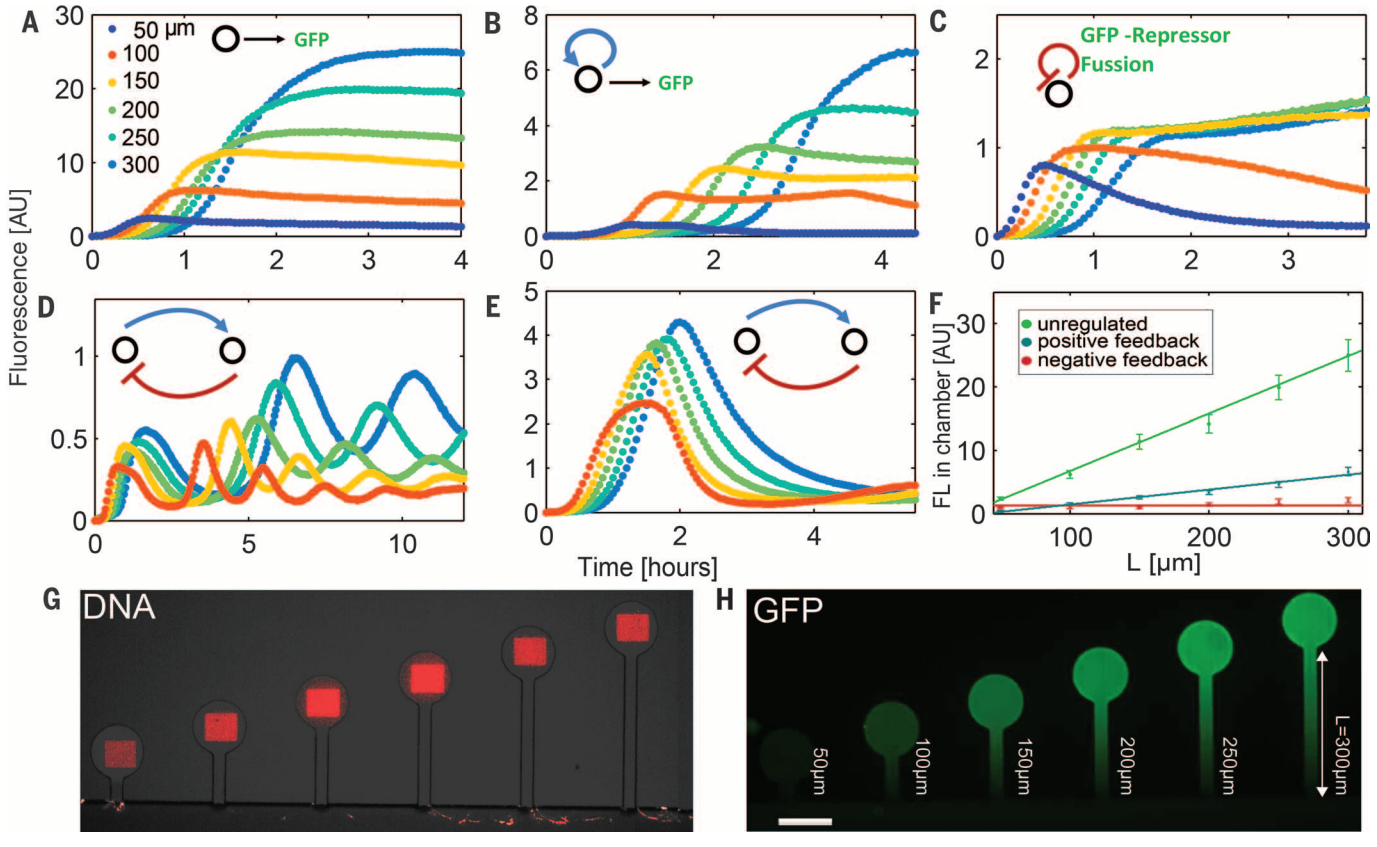


**Fig. 2. Gene network dynamics regulated by geometry.** Expression dynamics of GFP in the DNA compartment with $L$ = 50 to 300 μm as denoted and for five different constructs: (**A**) unregulated, (**B**) positive feedback, (**C**) negative feedback, (**D**) activator-repressor network with activator $\sigma^{28}$ and repressor cI, and (**E**) activator-repressor network with activator $\sigma^{38}$ and repressor cI. (**F**) Maximal GFP intensity as a function of the capillary length for the constructs in (A) to (C). Error bars represent standard variation over three repeats. Fluorescence images of (**G**) DNA brushes before expression and (**H**) GFP expression of the unregulated construct after 3 hours. Scale bar, 100 μm.

order, lighting up first in the short capillary (50 μm) and attaining low expression levels compared with longer capillaries (Fig. 2A and movie S1). The onset time, $\tau_{on}(L)$, was indeed linear in the capillary length for the three constructs, as predicted (fig. S7). In the positive-feedback construct, there was a long delay, 1 to 2.5 hours, before expression onset. The steady-state protein levels of the unregulated and positive-feedback constructs were proportional to $\tau$ and increased linearly with the capillary length over an order of magnitude (Fig. 2F), in accord with the solution to the diffusion equation (supplementary materials). The negative-feedback construct expression levels were low and independent of length for $L$ > 100 μm (Fig. 2F). For short capillaries, $L$ < 100 μm, steady state was not maintained because of rapid diffusion through the channel. All constructs showed a linear GFP profile along the capillary (fig. S8). Expression levels showed 10% variation between experiments (figs. S9 and S10).

We next explored the activator-repressor network, which exhibited oscillations and pulses of gene expression. In the first network (Fig. 2D), we used the sigma factor $\sigma^{28}$ for activation and the cI repressor (as in Fig. 1E). The network exhibited oscillations with a period linear in the capillary length (fig. S11). Oscillations were also obtained at a different activator:repressor DNA stoichiometry and with the addition of a Cro

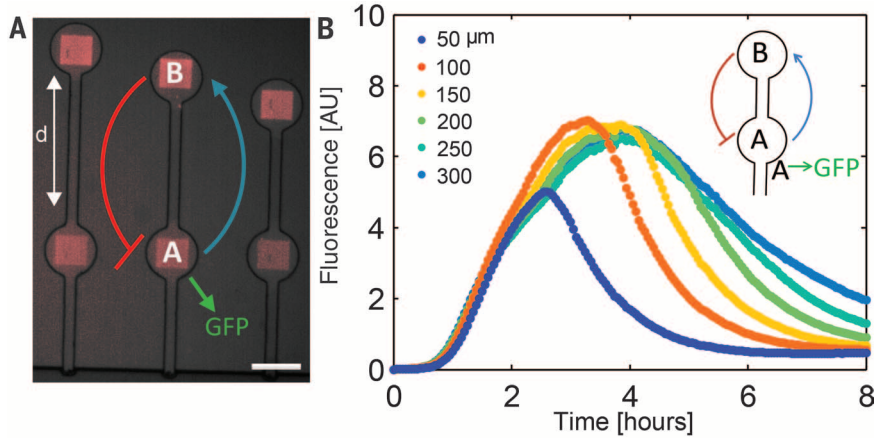


**Fig. 3. Communication between DNA compartments.** (**A**) Fluorescent image of DNA brush overlaid with the activator (denoted A)–repressor (denoted B) network scheme. The distance between compartments A and B varied, $d$ = 50 to 300 μm. Scale bar, 100 μm. (**B**) GFP expression kinetics at compartment A for different distances between compartments, as denoted.

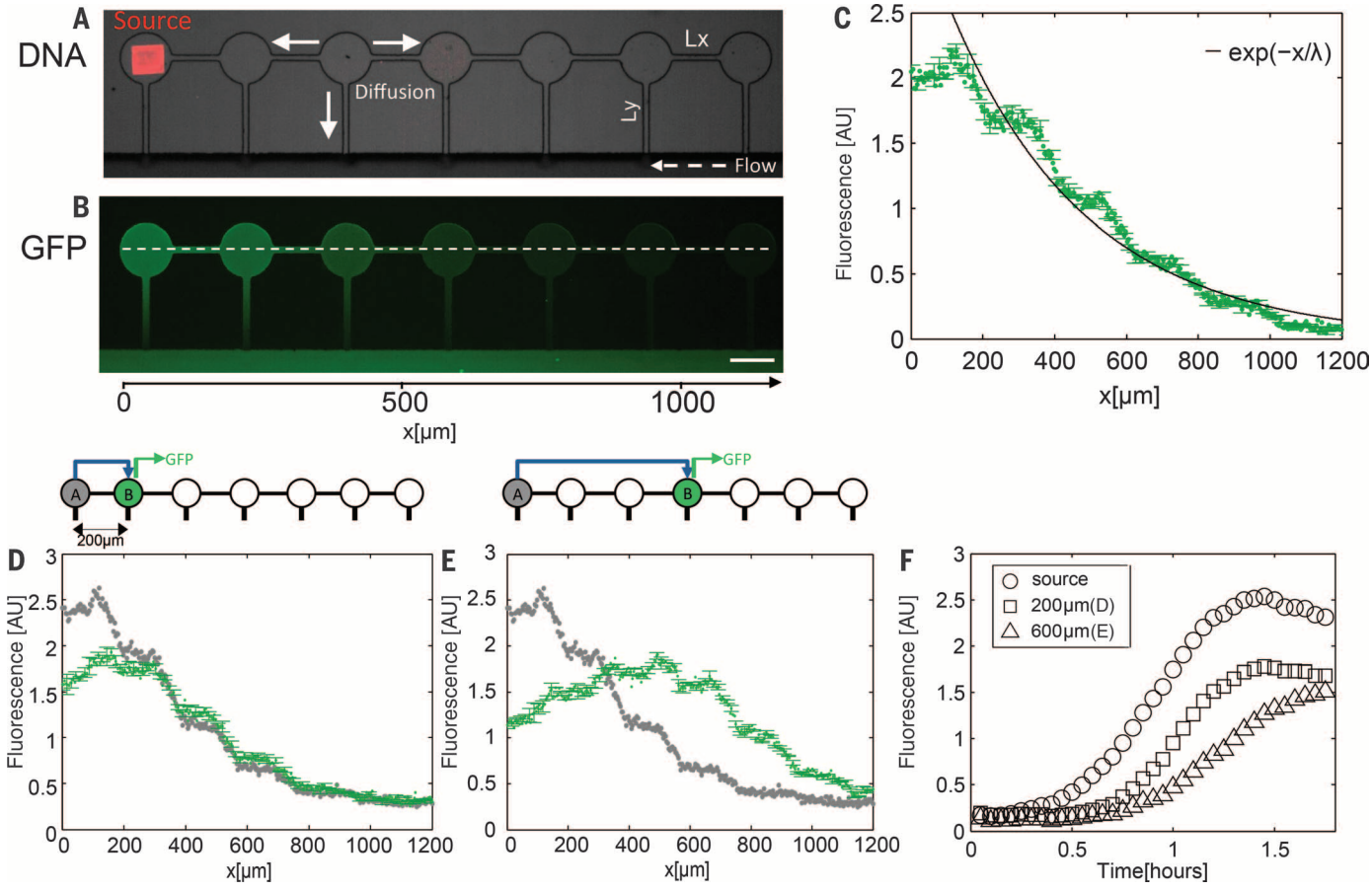


**Fig. 4. Protein gradients in one-dimensional arrays.** (**A**) DNA brush patterned in an array of seven connected compartments. (**B**) Image of GFP gradient after 3 hours of expression and (**C**) the resulting profile along the $x$ axis. Solid line is an exponential fit, $e^{-x/\lambda}$, with λ = 380 ± 40 μm averaged over three experiments. Scale bar, 100 μm. (**D** to **F**) A one-step gene expression cascade in the array: activator (denoted A) patterned in the first compartment and activated GFP (denoted B) patterned at the (D) second or (E) fourth compartment. In green is the GFP profile expressed from gene B. In gray, the activator profile, as measured in a parallel array on the same chip. Error bars in (C) to (E) represent standard deviation of fluorescence data in a single gradient. (F) Kinetics of GFP expressed from gene A (circles) and gene B at the second (squares) and fourth (triangles) compartments.

repressor protein (fig. S11). By replacing the activator with a weaker sigma factor, $\sigma^{38}$, we obtained a single pulse dynamics (Fig. 2E). Increasing the ratio of activator to repressor genes in the brush changed the dynamics from a pulse to a steady state of high expression levels (fig. S12). Targeting degradation of GFP fused to SsrA or YbaQ tags by the ClpXP complex endogenously present in the cell-free extract (*21*) showed no detectable difference in dynamics (fig. S13).

We next showed diffusion-based communication with the activator-repressor network separated into two connected compartments (Fig. 3 and movie S2). Compartment A was positioned 200 μm away from the feeding channel, and the distance to compartment B varied, $d$ = 50 to 300 μm. Compartment A was patterned with activator genes coding for the transcription initiation factor $\sigma^{38}$ and a GFP reporter (Fig. 3A). Compartment B encoded for the lambda phage repressor cI regulated by a $\sigma^{38}$ promoter. GFP appeared after 1 hour in compartment A for all capillary lengths and independently of $d$ (Fig. 3B and fig. S14). After expression in compartment A, the activator $\sigma^{38}$ diffused into compartment B and activated the cI repressor expression. In turn, the repressor diffused back to compartment A and shut down $\sigma^{38}$ expression, thereby creating a spatiotemporal pulse (Fig. 3B). The typical time at which expression shuts off varied from 4 to 8 hours and was linear with $d$ (fig. S14). In a related experiment, the positions of A and B were exchanged, resulting in a pulse with onset time and pulse width proportional to $d$ (fig. S15).

A one-dimensional array of seven compartments was assembled parallel to the flow channel (Fig. 4). The compartments, $d$ = 200 μm apart, were interconnected by capillaries of length $L_x$ = 100 μm and connected to dilution capillaries of length $L_y$ = 150 μm (Fig. 4A). A DNA brush coding for GFP was patterned in the first compartment of the array. A gradient of GFP appeared along the array with a maximum intensity at the DNA compartment, dropping in a series of linear steps between neighboring compartments, and with a constant intensity within the compartments (Fig. 4, B and C). The overall profile had an exponentially decaying envelope, $e^{-x/\lambda}$, with a decay length $\lambda = 380 \pm 40$ μm averaged over three experiments. By considering the diffusion equation in the array, we theoretically derived a similar value, $\lambda = d\sqrt{\frac{L_y}{L_x}} = 245$ μm, that is determined only by geometry and is independent of protein diffusion constant (supplementary materials).

To examine the response to a signaling molecule in the one-dimensional array, we used a gene expression cascade. The activator gene, coding for $\sigma^{28}$, was patterned in the first compartment of the array and a GFP under a $\sigma^{28}$ promoter in the second or fourth compartment (Fig. 4, D and E). The activator gene generated a protein concentration gradient along the array, and the reporter gene generated a profile that was maximal at the reporter compartment and decayed along the array in a piecewise linear profile. The reporter gene was activated with a delay that was dependent on its location along the array and distance from the source (Fig. 4F). The asymmetry in the GFP profile along the array (Fig. 4E) originated from residual flow between compartments (fig. S16).

The present approach for an artificial cell offers a means to program a variety of gene expression reactions and biological networks with a high degree of control that is amenable to prediction and theoretical modeling (*22*). The diffusion-based information transfer between adjacent compartments allows us to envisage a network of connected compartments with emergent spatial-temporal patterns as in morphogenesis.

## REFERENCES AND NOTES


1. D. S. Tawfik, A. D. Griffiths, *Nat. Biotechnol.* **16**, 652–656 (1998).
2. V. Noireaux, A. Libchaber, *Proc. Natl. Acad. Sci. U.S.A.* **101**, 17669–17674 (2004).
3. V. Noireaux, R. Bar-Ziv, A. Libchaber, *Proc. Natl. Acad. Sci. U.S.A.* **100**, 12672–12677 (2003).
4. J. Kim, K. S. White, E. Winfree, *Mol. Syst. Biol.* **2**, 68 (2006).
5. E. Franco *et al*., *Proc. Natl. Acad. Sci. U.S.A.* **108**, E784–E793 (2011).
6. A. J. Hockenberry, M. C. Jewett, *Curr. Opin. Chem. Biol.* **16**, 253–259 (2012).
7. M. Isalan, C. Lemerle, L. Serrano, *PLOS Biol.* **3**, e64 (2005).
8. D. Matthies *et al*., *J. Mol. Biol.* **413**, 593–603 (2011).
9. Y. Heyman, A. Buxboim, S. G. Wolf, S. S. Daube, R. H. Bar-Ziv, *Nat. Nanotechnol.* **7**, 374–378 (2012).
10. J. Shin, P. Jardine, V. Noireaux, *ACS Synth. Biol.* **1**, 408–413 (2012).
11. A. S. Spirin, V. I. Baranov, L. A. Ryabova, S. Y. Ovodov, Y. B. Alakhov, *Science* **242**, 1162–1164 (1988).
12. T. Thorsen, S. J. Maerkl, S. R. Quake, *Science* **298**, 580–584 (2002).
13. D. Gerber, S. J. Maerkl, S. R. Quake, *Nat. Methods* **6**, 71–74 (2009).
14. H. Niederholtmeyer, V. Stepanova, S. J. Maerkl, *Proc. Natl. Acad. Sci. U.S.A.* **110**, 15985–15990 (2013).
15. P. Müller, K. W. Rogers, S. R. Yu, M. Brand, A. F. Schier, *Development* **140**, 1621–1638 (2013).
16. A. Buxboim *et al*., *Small* **3**, 500–510 (2007).
17. D. Bracha, E. Karzbrun, S. S. Daube, R. H. Bar-Ziv, *Acc. Chem. Res.* **47**, 1912–1921 (2014).
18. J. Shin, V. Noireaux, *J. Biol. Eng.* **4**, 8 (2010).
19. J. Shin, V. Noireaux, *ACS Synth. Biol.* **1**, 29–41 (2012).
20. J. Stricker *et al*., *Nature* **456**, 516–519 (2008).
21. J. Shin, V. Noireaux, *J. Biol. Eng.* **4**, 9 (2010).
22. L. H. Hartwell, J. J. Hopfield, S. Leibler, A. W. Murray, *Nature* **402** (suppl.), C47–C52 (1999).


## ACKNOWLEDGMENTS

We thank A. Yoffe, S. Garussi, and Y. Barak of the Helen and Martin Kimmel Center for Nanoscale Science for guidance and assistance; I. Kaplan-Ashiri for scanning electron microscopy imaging; J. Hasty, University of California San Diego, for the generous gift of positive-feedback construct; and S. S. Daube and A. Libchaber for helpful discussions. This work was supported by the Israel Science Foundation (R.H.B.-Z.), the Minerva Foundation (R.H.B.-.Z), the U.S.-Israel Binational Science Foundation (R.H.B.-Z. and V.N.), NSF grant PHY-0750133 (V.N.), and the Azrieli Foundation (E.K.).

## SUPPLEMENTARY MATERIALS

www.sciencemag.org/content/345/6198/829/suppl/DC1
Materials and Methods
Supplementary Text
Figs. S1 to S16
Tables S1 to S3
References (*23*–*27*)
Movies S1 and S2

2 May 2014; accepted 16 July 2014
10.1126/science.1255550

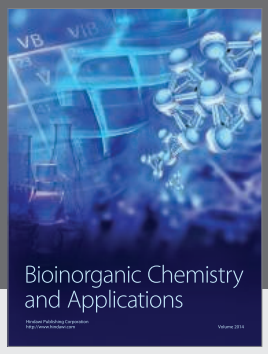

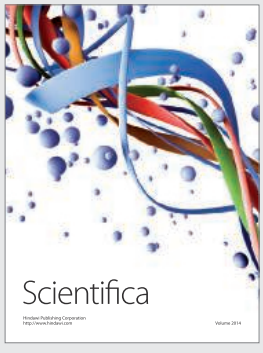

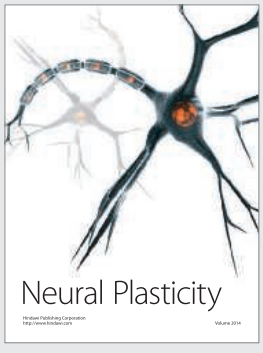

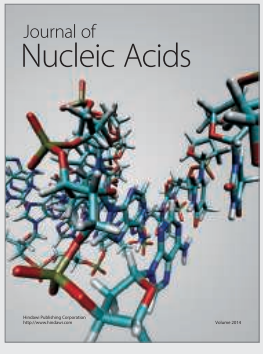

Hindawi
Submit your manuscripts at
http://www.hindawi.com

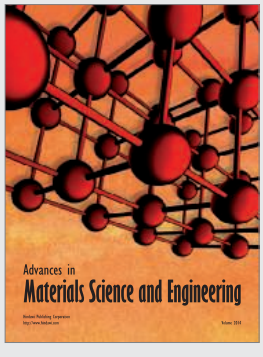

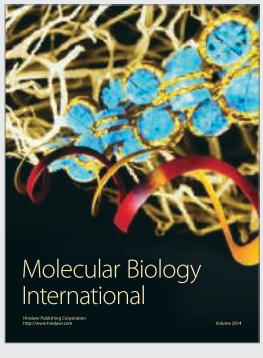

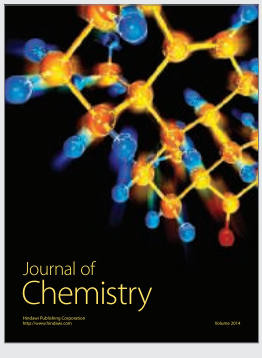

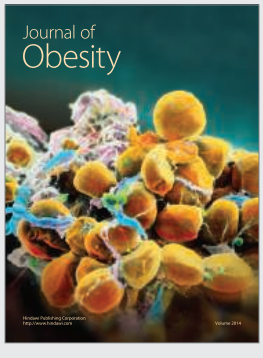

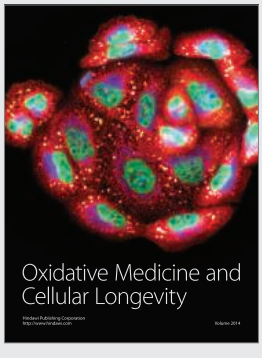

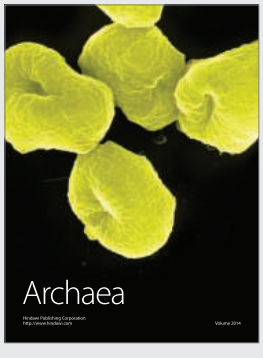

# AAAS 2015 ANNUAL MEETING

12–16 FEBRUARY • SAN JOSE, CA

INNOVATIONS, INFORMATION, AND IMAGING

## Join us in San Jose

Advance Registration is now open!
Register and reserve a room now for discounted rates.

Dear Colleagues:

On behalf of the AAAS Board of Directors, it is my honor to invite you to join us in San Jose, California, for the 2015 AAAS Annual Meeting, 12–16 February.

This year's theme—Innovations, Information, and Imaging—reflects on the information transformation happening in science and technology brought about by recent advances in organizing, visualizing, and analyzing data.

Attendees will have the opportunity to choose among a broad range of activities, including plenary and topical lectures by some of the world's leaders in science and technology, multidisciplinary symposia, networking and career development workshops, and an international exhibition hall, and Family Science Days.

We look forward to seeing you in San Jose. Registration and housing are now open.

Gerald R. Fink

AAAS President and Program Chair
Margaret and Herman Sokol Professor of Biology
Whitehead Institute, Massachusetts Institute of Technology

www.aaas.org/meetings

# immunogenomics 2014

## September 29 - October 1, 2014

## HudsonAlpha Biotechnology Campus
## Huntsville, Alabama, USA

***Join us at the intersection of Immunology and Genomics!***

**Keynote Speakers**

**Christophe Benoist**, Harvard Medical School
**Mary Ellen Conley**, University of Tennessee, College of Medicine, Memphis
**Mark Davis**, Howard Hughes Medical Institute;
Stanford University School of Medicine

**Session Chairs**

**Lou Bridges**, University of Alabama at Birmingham, AL, USA • **Jean-Laurent Casanova**, Howard Hughes Medical Institute, Rockefeller • **Alain Fischer**, Imagine Institute, Necker Hospital, Paris, France • **Dan Littman**, New York University, NY, USA • **Sara Marsal**, University of Barcelona, Spain • **Kristen Mueller**, *Science* • **Harlan Robins**, University of Washington/Fred Hutchinson Cancer Research Center

**Session Speakers**

**Scott Boyd**, Stanford University School of Medicine, CA • **Zhijian James Chen**, UT Southwestern, TX • **Yanick Crow**, University of Manchester, UK • **Malek Faham**, Sequenta, CA • **Wendy Garrett**, Harvard University School of Public Health, MA • **Peter Gregersen**, Feinstein Institute for Medical Research, NY • **Jian Han**, HudsonAlpha Institute for Biotechnology, AL • **Lionel Ivashkiv**, Hospital for Special Surgery, NY • **Thirumala-Devi Kanneganti**, St. Jude Children's Research Hosp. • **Julian Knight**, Merton College , University of Oxford, UK • **Mike Lenardo**, National Institutes of Health, Washington D.C. • **Xochitl Morgan**, Harvard University School of Public Health, MA • **Barbara Methe**, J. Craig Venter Institute, MD • **Kees Murre**, University of California, San Diego, CA • **Richard M. Myers**, HudsonAlpha Institute for Biotechnology, AL • **Soumya Raychaudhuri**, Broad Institute, MA • **Lars Steinmetz**, European Molecular Biology Laboratory, Germany • **Barbara Stranger**, University of Chicago, IL USA

**Platinum Sponsors**

BAY CITY CAPITAL

iRepertoire, Inc.

**Gold Sponsors**

UAB COMPREHENSIVE ARTHRITIS, MUSCULOSKELETAL, AND AUTOIMMUNITY CENTER

**Silver Sponsors**

GenapSys

illumina

**Bronze Sponsors**

SEQUENTA

follow @immunogenomics on twitter

## Register today at immunogenomics.com

*presented by*

HUDSONALPHA INSTITUTE FOR BIOTECHNOLOGY

Science AAAS

### Dying/Dead Cell Removal Device

ClioCell is an ex-vivo device for the removal of dying and dead cells, which improves viability and quality of cell populations and their subsequent productivity. The system comprises superparamagnetic nanoparticles, which have been coupled with proprietary elements that bind to dead and dying cells and cell debris. The resultant product selectively initiates dead-cell removal, emulating dead-cell clearance mechanisms, which operate in vivo to keep tissues functioning optimally. This technology is step-changing, providing new opportunities to optimize cell growth, culture, and storage. The ability to selectively remove inhibitory or toxic dead cells using a simple and rapid procedure results in radically improved cell populations; specifically, with regard to viability antibody/protein yield and consequent functional efficacy. ClioCell has been evaluated by several leading independent commercial and academic research institutions and has been successfully tested on many cell types, both human and mammalian.

**AMS Biotechnology**
For info: +44-(0)-1235-828200
www.amsbio.com/cliocell.aspx

### Serum-Free Medium

The new Xuri MSC Medium and Attachment Solution is designed for serum-free and xeno-free expansion of human mesenchymal stem cells. Xuri MSC Medium is a versatile and reliable cell culture product that enables the safe and efficient expansion of human mesenchymal stem cells (hMSC) without the use of animal-derived components or undefined serum. It can be used to culture hMSC from a range of sources, including bone marrow, umbilical cord, or adipose tissue. Compared with serum-facilitated cultivation, Xuri MSC Medium achieves a higher yield of multipotent cells in a single passage, thereby reaching the desired cell dose for patient treatment in a shorter timescale. Removing the need for lengthy batch validation and risk assessment associated with serum also enables a faster and more cost effective process. Xeno-Free Xuri MSC Attachment Solution is the recommended coating agent for the serum-free expansion of hMSC with Xuri MSC Medium and supports high reproducibility across batches.

**GE Life Sciences**
For info: 800-526-3593
www.gelifesciences.com

### Multiphoton Excitation System

The FluoView FVMPE-RS multiphoton excitation system enables high-precision, ultrafast scanning and stimulation, allowing researchers to see deep within specimens, take measurements at the highest speeds, and capture images, even when working under the most demanding conditions. The system has an unprecedented flexibility of customizable IX3 "open source" frames, where bespoke systems are effortlessly created by exchanging optical modules into an accessible infinite light path. Expanding the capabilities of the IX3, a range of accessories are available, and the high-end IX83 frame can be optimized for advanced live cell imaging with the cellVivo incubation system and cell^tirf laser module. Centered on workflow ergonomics, the modular and flexible cellVivo incubator is based on a "one size fits all" concept, with adaptors for various frame types. cellVivo is uniquely accessible with just one hand, enabling simultaneous handling of the incubator and specimens for swift usage, protecting samples from prolonged exposure to the external environment.

**Olympus**
For info: +49-402-3773-5913
www.olympus-europa.com/microscopy

### Chromatin Immunoprecipitation

The Zymo-Spin ChIP Kit streamlines chromatin immunoprecipitation (ChIP) with a protocol that has been optimized for efficient crosslinking, shearing, and immunoprecipitation of protein-chromatin complexes regardless of the mammalian cell type used. Features include high-sensitivity Protein A magnetic beads for rapid selection of targeted complexes and a unique microelution spin column for high-yield purification of ChIP DNA in ≥6 µL. The fast and highly reproducible procedure enriches DNA that is ideal for subsequent analysis including end point and quantitative polymerase chain reaction, ChIP-Seq library preparation, and next-gen sequencing-based applications.

**Zymo Research Corporation**
For info: 949-679-1190
www.zymoresearch.com

### HSP70 ELISA Kit

The Amp'd HSP70 High Sensitivity ELISA Kit enables detection of both baseline and upregulated levels of Hsp70 (Hsp72) and relies on small amounts of starting sample. Baseline levels (<20 pg/mL) of Hsp70, specifically the inducible form Hsp72, have been traditionally difficult to detect using current enzyme-linked immunosorbent assays (ELISAs). The Amp'd HSP70 High Sensitivity ELISA Kit has greatly improved sensitivity enabling detection of both baseline and upregulated/stressed level of Hsp70 (Hsp72). This increase in sensitivity allows less sample needed to obtain accurate quantification of very low levels of Hsp70 (Hsp72) concentrations. The Amp'd HSP70 High Sensitivity ELISA Kit can be used to quantify human, mouse, and rat Hsp70 (Hsp72) in serum and plasma samples. This ultrasensitive assay is fully quantitative, with the ability to detect as low as 7 pg/mL of Hsp70 (Hsp72). Negligible reactivity is detected of similar Hsp70 family members and assay results are obtained in 4.5 hours for up to 38 samples in duplicate.

**Enzo Life Sciences**
For info: 800-942-0430
www.enzolifesciences.com

Electronically submit your new product description or product literature information! Go to www.sciencemag.org/products/newproducts.dtl for more information.

Newly offered instrumentation, apparatus, and laboratory materials of interest to researchers in all disciplines in academic, industrial, and governmental organizations are featured in this space. Emphasis is given to purpose, chief characteristics, and availability of products and materials. Endorsement by *Science* or AAAS of any products or materials mentioned is not implied. Additional information may be obtained from the manufacturer or supplier.

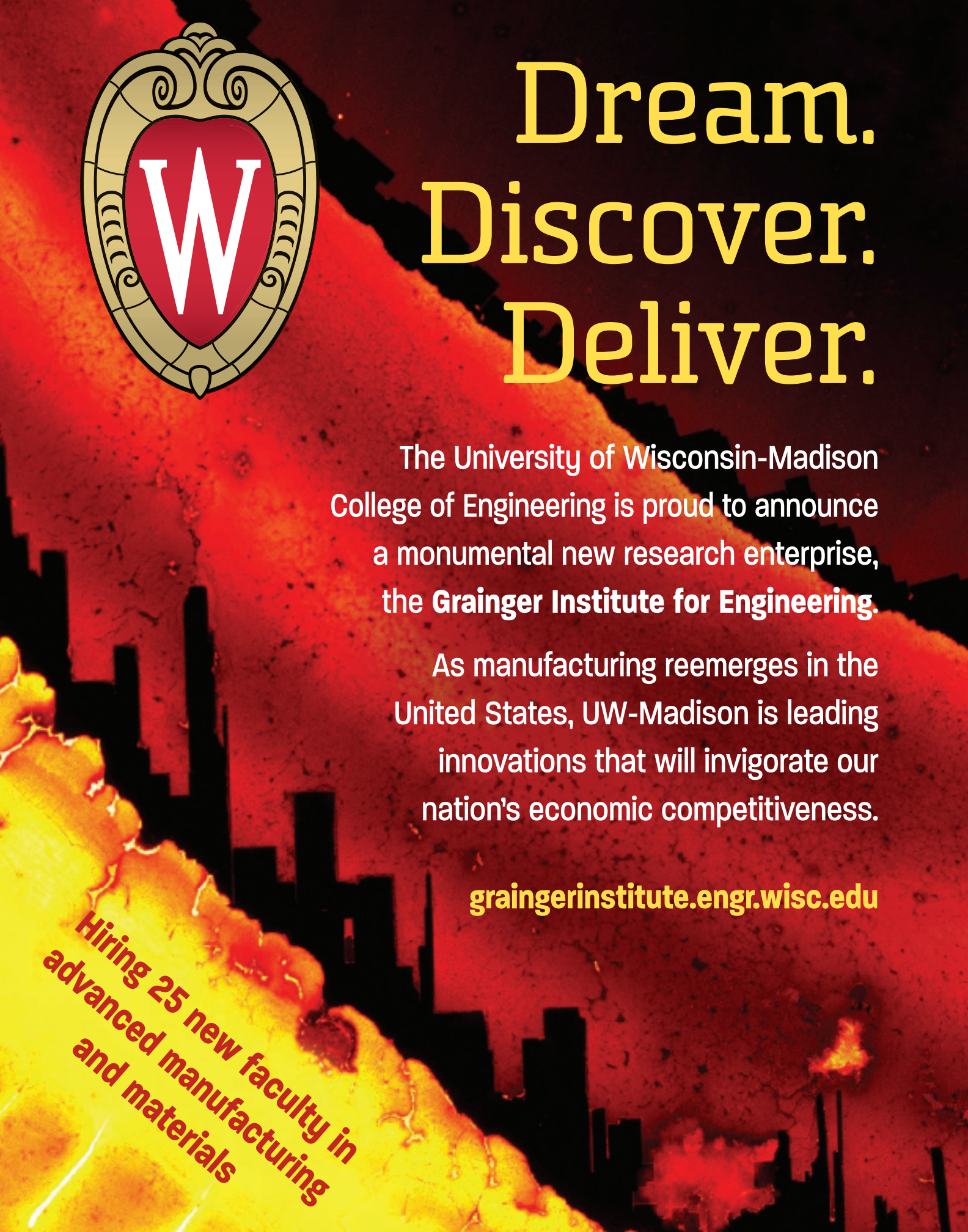
Dream.
Discover.
Deliver.
The University of Wisconsin-Madison College of Engineering is proud to announce a monumental new research enterprise, the **Grainger Institute for Engineering**.
As manufacturing reemerges in the United States, UW-Madison is leading innovations that will invigorate our nation's economic competitiveness.
graingerinstitute.engr.wisc.edu
Hiring 25 new faculty in advanced manufacturing and materials

# 10-fold higher transfection efficiency in difficult cells

> We were very happy and surprised to see Lipofectamine® 3000 reagent provide a more than 10-fold difference in transfection efficiency in our difficult-to-transfect cell line. There was even a reduction in cell death. Awesome results!
>
> **—Rui Eduardo Castro, PhD, University of Lisbon**

Discover the versatile reagent with the power to transfect your most difficult cells.

Find out more at **lifetechnologies.com/3000**

Join the conversation at #DiffCells

life technologies

A Thermo Fisher Scientific Brand

**For Research Use Only. Not for use in diagnostic procedures.** © 2014 Thermo Fisher Scientific Inc. All rights reserved.
All trademarks are the property of Thermo Fisher Scientific and its subsidiaries unless otherwise specified. **CO116925 0714**

## *Science* Careers Advertising

For full advertising details, go to ScienceCareers.org and click For Employers, or call one of our representatives.

**Tracy Holmes**
Worldwide Associate Director
*Science* Careers
Phone: +44 (0) 1223 326525

THE AMERICAS
E-mail: advertise@sciencecareers.org
Fax: 202-289-6742

**Tina Burks**
Phone: 202-326-6577

**Nancy Toema**
Phone: 202-326-6578

**Marci Gallun**
Sales Administrator
Phone: 202-326-6582

**Online Job Posting Questions**
Phone: 202-312-6375

EUROPE / JAPAN / INDIA / AUSTRALIA / NEW ZEALAND / REST OF WORLD
E-mail: ads@science-int.co.uk
Fax: +44 (0) 1223 326532

**Axel Gesatzki**
Phone: +44 (0)1223 326529

**Sarah Lelarge**
Phone: +44 (0) 1223 326527

**Kelly Grace**
Phone: +44 (0) 1223 326528

CHINA / KOREA / SINGAPORE / TAIWAN / THAILAND

**Ruolei Wu**
Phone: +86-186-0082-9345
E-mail: rwu@aaas.org

All ads submitted for publication must comply with applicable U.S. and non-U.S. laws. *Science* reserves the right to refuse any advertisement at its sole discretion for any reason, including without limitation for offensive language or inappropriate content, and all advertising is subject to publisher approval. *Science* encourages our readers to alert us to any ads that they feel may be discriminatory or offensive.

Science Careers
From the Journal Science AAAS

ScienceCareers.org

## POSITIONS OPEN

**ASSISTANT/ASSOCIATE PROFESSOR OF PHYSIOLOGY**
**Perelman School of Medicine**
**University of Pennsylvania**

The Department of Physiology at the Perelman School of Medicine at the University of Pennsylvania seeks candidates for an Assistant or Associate Professor position in the tenure track. Rank will be commensurate with experience. Responsibilities include establishing and conducting an independent research program, and supervising, mentoring, and teaching students. Applicants must have an M.D. or Ph.D or equivalent degree and have demonstrated excellent qualifications in research.

The successful candidate will have experience in any aspect of physiology or a related field, ranging from integrative to cell biological to molecular biophysical. Special attention will be given to investigators in the areas of signaling or membrane physiology. Emphasis will be placed on the novelty, importance, and impact of the research. Applicants at the Associate Professor level are expected to have funding and an internationally recognized track record of creative research productivity and excellence.

Highly competitive laboratory space and start-up funds are available. The Perelman School of Medicine is one of the top ranked medical schools in the nation for research and NIH funding. It is located on the campus of the University of Pennsylvania, a world-class institution located near the center of Philadelphia.

We seek candidates who embrace and reflect diversity in the broadest sense.

*The University of Pennsylvania is an Equal Opportunity Employer. Minorities/Women/Individuals with disabilities/Protected Veterans are encouraged to apply.*

Apply for this position online at **website: https://www.med.upenn.edu/apps/faculty_ad/index.php/g311/d3686.**

**UNIVERSITY OF ROCHESTER (NY)**

The Department of Chemistry invites applications for one position in the area of inorganic chemistry, broadly defined, and one position in the area of theoretical chemistry, broadly defined. This search is primarily for candidates at the junior level, but exceptional senior candidates can also be considered. Candidates are expected to establish an outstanding program of original research and to be effective teachers at the graduate and undergraduate levels. Application materials are to be submitted online at **website: https://www.rochester.edu/fort/chm/.** Materials to be submitted must include curriculum vitae indicating graduate and postdoctoral advisors, a statement of research plans, and a statement of teaching interests. Junior candidates will also enter the names and e-mail addresses of three references. The references will be notified by e-mail with instructions for online submission of letters. The department will solicit letters for senior candidates. Review of complete applications will begin on October 15, 2014. Questions may be sent to **e-mail: facrec@chem.rochester.edu.** *The University of Rochester has a strong commitment to diversity and actively encourages applications from groups underrepresented in higher education. The University is an Equal Opportunity Employer.*

Stop searching for a job; start your career.
**www.ScienceCareers.org**

## POSITIONS OPEN

**TENURE-TRACK POSITION in Animal Physiology**
**W.M. Keck Science Department of Claremont Mckenna, Pitzer, and Scripps Colleges**

The W.M. Keck Science Department of Claremont McKenna College, Pitzer College, and Scripps College invites applications for a tenure-track appointment in Animal Physiology at the **Assistant Professor** level to begin July 2015. The department, which houses the biology, chemistry, physics, and environmental analysis faculty for three of the five undergraduate Claremont Colleges, offers innovative and interdisciplinary programs in the natural sciences. Many faculty members participate in collaborative research projects, both within the department and with research groups at nearby colleges and universities in the greater Los Angeles area. We seek a broadly trained animal physiologist who is committed to excellence in teaching and who will develop a vibrant research program that incorporates quantitative and/or computational methods and fully engages undergraduate students. The position offers opportunities to teach an upper division physiology course with laboratory, introductory biology, biology courses for non-majors, and to design new courses in the candidate's field. Candidates should hold a Ph.D. degree with focus in physiology or a related field. Postdoctoral experience and a record of scholarly publication are preferred.

Please apply online at **website: https://webapps.cmc.edu/jobs/faculty/faculty_opening_detail.php?PostingID=14016.**

Uploaded materials should include a cover letter, curriculum vitae, a statement of teaching philosophy, a description of proposed research with equipment needs, and a diversity statement (of no more than 1 page) outlining the applicant's philosophy for fostering an educational environment that is inclusive of all students. Please also ensure that three reference letters be uploaded. Inquiries about the position should be addressed to **Dr. Patrick Ferree** at **e-mail: pferree@keckscl.claremont.edu.** Additional information about the department can be found at **website: http://www.keckscl.claremont.edu.** Review of applications will begin October 24, 2014, and the position will remain open until filled.

*The Keck Science Department of Claremont McKenna, Pitzer, and Scripps Colleges is an Equal Opportunity Employer. In a continuing effort to enrich its academic environment and provide equal educational and employment opportunities, the department actively encourages applications from women and members of other historically under-represented social groups in higher education.*

**DIVISION OF MATERIALS RESEARCH**

National Science Foundation, Arlington, Virginia. The Division of Materials Research (DMR) announces a nationwide search for senior-level researchers to serve as **Program Directors** in the Materials Research Science and Engineering Centers Program (MRSEC) and the Condensed Matter and Materials Theory Program.

For additional information and how to apply, please refer to the Materials Research Science and Engineering Centers Program and the Condensed Matter and Materials Theory Program Dear Colleague Letters at **website: http://www.nsf.gov/materials.**

Because NSF has a rotator program, there are often opportunities in diverse areas of materials research. Those interested are welcome to request further information from **e-mail: dmr-recruit@nsf.gov.**

For additional information on NSF's rotational programs, please visit **website: http://www.nsf.gov/about/career_opps/rotators/.**

*NSF is an Equal Opportunity Employer committed to employing a highly qualified staff that reflects the diversity of our nation.*

We deliver customized job alerts.
**www.ScienceCareers.org**

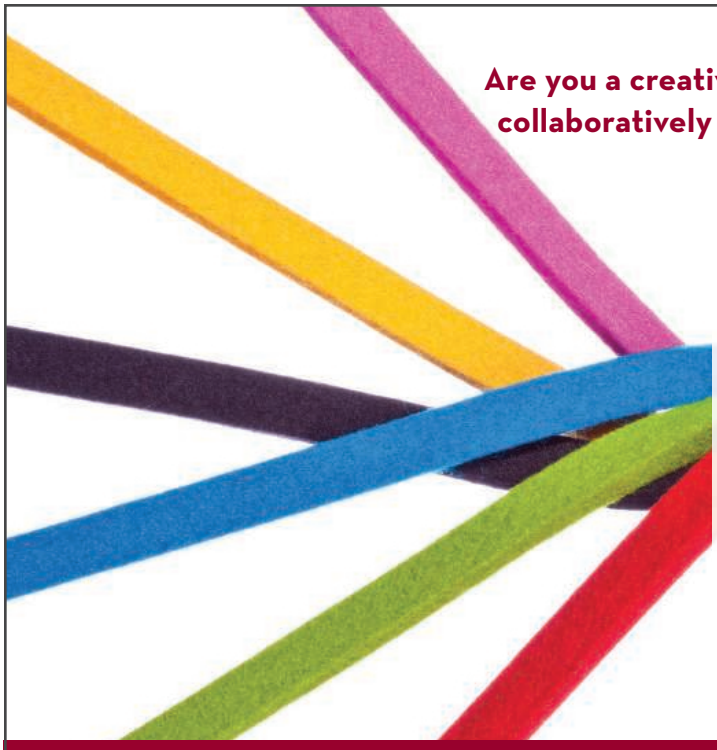

**Are you a creative investigator who excels at working collaboratively and pushing disciplinary boundaries?**

**Then we want to hear from you.**

The College of Biological Sciences at the University of Minnesota is hiring scientists for interdisciplinary research clusters in these emerging areas of biology:

- **biology education**
- **cellular biophysics**
- **computational and genome-enabled biology**
- **synthetic biology**

All positions are tenure track. Successful candidates will have expertise that complements current faculty and be committed to graduate and undergraduate education.

College of Biological Sciences
University of Minnesota
Driven to Discover℠

**Learn more about research cluster themes and specific positions at z.umn.edu/cbsclusterhiring**



ÉCOLE POLYTECHNIQUE FÉDÉRALE DE LAUSANNE

# Faculty Position in Clinical Neuroengineering and Human-Machine Interaction

## at the Center for Neuroprosthetics of the Ecole polytechnique fédérale de Lausanne (EPFL)

The School of Life Sciences and the School of Engineering at EPFL invite applications for a faculty position at the level of **associate professor or full professor** for the newly established **Center for Neuroprosthetics (http://cnp.epfl.ch/)**. The Center seeks outstanding individuals with strong expertise in translational research in behavioral neurology, clinical neuroengineering, or neurorehabilitation with the goal of testing novel technology- and neuroscience-based approaches in the clinical environment. Of particular relevance is previous experience in non-invasive brain stimulation, brain imaging (MRI, EEG, or BCI), and functional assessment of sensorimotor and cognitive functions in combination with approaches from virtual reality, robotics, rehabilitation medicine, and related neuroengineering approaches. Relevant clinical research fields – but not limited to – include sensorimotor and neuropsychological rehabilitation following vascular stroke, spinal cord injury, pain, and limb amputation.

EPFL seeks outstanding individuals with a medical degree, engineering degree, or equivalent degree. The sucessful candidate is expected to initiate an independent and competitive research program in a multidisciplinary environment, to lead the Center's activities at the Swiss Rehabilitation Clinic in Sion (SUVA), and to participate in graduate and undergraduate teaching.

Full access to all facilities at EPFL's Center for Neuroprosthetics and in Sion will be granted. Internationally competitive salaries, substantial start-up and on ongoing resources, and benefits are offered.

Applications should include a curriculum vitae with a list of publications, a concise statement of research and teaching interests, and the names and addresses (including e-mail) of at least five referees. Applications should be uploaded to:

https://academicjobsonline.org/ajo/jobs/4113

While the committee will start analyzing applications on **October 1st 2014** the search will remain open until the position is filled.

Enquiries may be addressed to:
**Prof. Olaf Blanke**
Chair of the search committee
Email: cnp@epfl.ch

For additional information on EPFL, the Schools of Engineering and Life Sciences, the Center for Neuroprosthetics, and the Swiss Rehabilitation Clinic (SUVA), please consult the following web sites: http://www.epfl.ch, http://sti.epfl.ch, http://sv.epfl.ch, http://cnp.epfl.ch, and http://www.crr-suva.ch/.

*EPFL aims to increase the presence of women amongst its faculty, and qualified female candidates are strongly encouraged to apply.*

Science Careers online @sciencecareers.org

UC San Diego
SKAGGS SCHOOL OF PHARMACY AND PHARMACEUTICAL SCIENCES

## Ladder-Rank (Tenure-Track) Assistant Professor

The Skaggs School of Pharmacy and Pharmaceutical Sciences (SSPPS) in the Division of Health Sciences at UC San Diego is committed to academic excellence and diversity within the faculty, staff, and student body. UC San Diego offers a superb environment for interdisciplinary research, and many SSPPS faculty members have joint appointments in other departments (e.g., Chemistry & Biochemistry, Pharmacology). The SSPPS has strong collaborations across the entire campus, including the Scripps Institution of Oceanography, the Moores Comprehensive Cancer Center, and the Departments of Chemistry & Biochemistry, Pharmacology, Cellular & Molecular Medicine, Medicine, Pediatrics, and Family & Preventive Medicine. Opportunities also abound for interactions with The Scripps Research Institute, The Salk Institute, The Sanford-Burnham Medical Institute, the Sanford Consortium for Regenerative Medicine, and the La Jolla Institute of Allergy and Immunology, as well as with hundreds of local pharmaceutical and biotechnology companies. State of the art facilities for chemical synthesis, high resolution nuclear magnetic resonance spectroscopy, and mass spectrometry, along with outstanding laboratory space, are available in the Pharmaceutical Sciences Building at UC San Diego. The UC San Diego Skaggs School of Pharmacy and Pharmaceutical Sciences (SSPPS) seeks a ladder-rank (tenure-track) Assistant Professor with a track record in identification and characterization of proteolytic enzymes associated with cancer, inflammation, and infectious diseases. He/she should also have a documented history of protease assay development using both fluorescent and mass spectrometric approaches that have direct application to identification of drug targets or disease biomarkers.

The candidate should have a Ph.D., a strong record of scientific achievement as demonstrated by publications and patents, a history of successful collaborations with basic scientists, clinicians, and industrial partners, and should be qualified for appointment as a tenure-track Assistant Professor at the UC San Diego SSPPS. The candidate will have ample opportunity to interface with an interdisciplinary team of biologists, biochemists, and medicinal chemists at the SSPPS. He/she will also contribute to team-taught courses for Doctor of Philosophy, Doctor of Pharmacy, and Doctor of Medicine students and will be expected to develop an extramurally funded research program. The ideal candidate will have strong demonstrated accomplishments in areas contributing to diversity, equity and inclusion, and a desire to play a leadership role in advancing UC San Diego's commitment to achieving excellence and diversity.

Salary and appointment level will be commensurate with qualifications and experience and based on published UC pay scales for Health Sciences.

Review of applications will begin **September 2, 2014** and continue until the position is filled.

The application should include detailed curriculum vitae; a statement of research interests and plans; a summary of teaching experience; and a separate statement describing past experience in activities that promote diversity and inclusion and/or plans to make future contributions. For further information about contributions to diversity statements, see **http://facultyequity.ucsd.edu/Faculty-Applicant-C2D-Info.asp**.

Applications should be submitted to the UCSD on-line application collection system, AP-On-Line Recruit, at: **https://apol-recruit.ucsd.edu/apply/JPF00592**.

*UCSD is an Equal Opportunity/Affirmative Action Employer with a strong institutional commitment to excellence and diversity (http://diversity.ucsd.edu).*

*The University of California is an Equal Opportunity/Affirmative Action Employer. All qualified applicants will receive consideration for employment without regard to race, color, religion, sex, national origin, disability, age or protected veteran status.*

CityU 30
香港城市大學
City University of Hong Kong
30th Anniversary

## *Worldwide Search for Talent*

**City University of Hong Kong** is a dynamic, fast-growing university that is pursuing excellence in research and professional education. As a publicly-funded institution, the University is committed to nurturing and developing students' talents and creating applicable knowledge to support social and economic advancement. The University has seven Colleges/Schools. As part of its pursuit of excellence, the University aims to recruit **outstanding scholars** from all over the world in various disciplines, including **business**, **creative media**, **energy**, **engineering**, **environment**, **humanities**, **law**, **science**, **social sciences**, **veterinary sciences** and other strategic growth areas.

Applications and nominations are invited for:

### Dean *[Ref. D/107/29]*
### School of Energy and Environment

**The Position**
Reporting to the Provost, the Dean will provide visionary, strategic leadership for the School, in alignment with the vision, mission and Strategic Plan of the University. In collaboration with the School's faculty and other academic units, the Dean will advance the School's academic excellence in research and professional education, and further its international standing.

**The Person**
The individual shall possess a doctorate degree and have strong academic and professional qualifications, a distinguished record of teaching, research and scholarship, and substantial relevant experience in academic leadership roles; the vision and capability to build on and expand the School's strengths; outstanding management effectiveness; commitment to interdisciplinary collaboration and teamwork; and strong communication and networking skills to build and nurture internal and external contacts to the benefit of the School and the University.

**Salary and Conditions of Service**
The appointee will be offered appointment to an academic rank commensurate with qualifications and experience. The deanship appointment will be on a concurrent basis for an initial period of three years. Remuneration package will be attractive and driven by market competitiveness and individual performance. Excellent fringe benefits include gratuity, leave, medical and dental schemes, and relocation assistance (where applicable).

**Information and Application**
Further information on the post and the University is available at http://www.cityu.edu.hk, or from the Human Resources Office, City University of Hong Kong, Tat Chee Avenue, Kowloon Tong, Hong Kong [Email : seesearch@cityu.edu.hk/Fax : (852) 2788 1154 or (852) 3442 0311].

To apply, please submit an online application at http://jobs.cityu.edu.hk, and include a current curriculum vitae and a statement on qualifications and vision to serve as Dean. Nominations can be sent directly to the Human Resources Office, or email to "seesearch@cityu.edu.hk". **Applications and nominations received before 31 October 2014 will receive full consideration.** The University's privacy policy is available on the homepage.

The University also offers a number of visiting positions for current graduate students, postdoctoral scholars, and for early-stage and established scholars, as described at http://www.cityu.edu.hk/provost/CityU_Visiting_Positions.htm.

City University of Hong Kong is an equal opportunity employer and we are committed to the principle of diversity. We encourage applications from all qualified candidates, especially those who will enhance the diversity of our staff.

**City University of Hong Kong was ranked 4th among the world's top 50 universities under the age of 50 in the *Quacquarelli Symonds* 2014 survey**
**http://www.cityu.edu.hk**

RADCLIFFE INSTITUTE
FOR ADVANCED STUDY
HARVARD UNIVERSITY

## Academic Fellowships

The Radcliffe Institute Fellowship Program at Harvard University welcomes fellowship applications in natural sciences and mathematics. The Radcliffe Institute for Advanced Study provides scientists the time and space to pursue their career's best work. At Radcliffe you will have the opportunity to challenge yourself. Meet and explore the work of colleagues in other fields. Take advantage of Harvard's many resources, including the extensive library system. Radcliffe Institute Fellowship Program invites applications from people of all genders, and from all countries. We seek to build a diverse fellowship program.

Scientists in any field who have a doctorate in the area of the proposed project (by December 2013) and at least two published articles or monographs are eligible to apply for a Radcliffe Institute fellowship. The stipend amount of $75,000 is meant to complement sabbatical leave salaries of faculty members. Residence in the Boston area and participation in the Institute community are required during the fellowship year.

Applications for 2015-2016 are due by **November 1, 2014**. For more information, please visit website: **www.radcliffe.harvard.edu** or email **sciencefellowships@radcliffe.harvard.edu**.

TEXAS STATE UNIVERSITY
*The rising STAR of Texas*

## Endowed Chair of Water Conservation

The Department of Biology (www.bio.txstate.edu) and the Meadows Center for Water and the Environment (www.meadowscenter.txstate.edu) at Texas State University (www.txstate.edu) invite applications for an Endowed Chair of Water Conservation.

The successful candidate will be expected to develop an externally funded, student-centered, research program that addresses the management and conservation of freshwater resources in the context of ecosystem and human needs. Applicants must have a Ph.D. in the natural sciences or engineering, an established externally-funded research program related to our fields of interest, be qualified for tenure in the Department of Biology at the rank of professor, and be an internationally-recognized authority in their field.

Preference will be given to individuals with experience working with government agencies and other groups on water management and conservation issues, a record of interdisciplinary collaboration, experience mentoring students, and the potential to collaborate widely with Texas State faculty members. Salary and start-up package are negotiable.

Inquiries or the letter of application, vitae, research prospectus, copies of five representative publications, and the names and contact information of five people willing to serve as references should be sent, preferred as a single PDF, to:
**Conservation@txstate.edu**

MORGRIDGE
INSTITUTE FOR RESEARCH

## METABOLISM INVESTIGATOR
## MADISON, WISCONSIN

The Morgridge Institute for Research, part of the dynamic research community at the University of Wisconsin-Madison, seeks a talented mid-career investigator to spearhead the development of a campuswide metabolism research initiative. We are particularly interested in attracting an energetic and talented researcher who will establish an innovative and collaborative research team to address key questions in metabolic processes, interactions and diseases. The Morgridge initiative will involve the recruitment of multiple investigators and will include both wet lab and computational approaches to metabolism research.

Candidates must have a proven track record of high quality research related to metabolism, be enthusiastic about engaging the public about the importance of research, and committed to helping recruit several other investigators into a collaborative and vibrant environment. The successful candidate can also be appointed to a tenure track or tenured position in an appropriate UW-Madison department, and will receive an attractive salary and benefits package plus generous start-up support.

The Morgridge Institute for Research is a private, nonprofit research institute affiliated with the University of Wisconsin-Madison. We serve as a collaborative hub for investigators across UW-Madison to work together on fundamental biomedical questions, and as such offer an extraordinary interdisciplinary work environment. For more information, please visit **www.morgridge.org**

**To Apply:** Written applications, including curriculum vitae, a concise description of research vision, future research plans, an explanation of why this opportunity attractive to you, and contact details for at least three referees who know you and your work well should be submitted by **October 1, 2014** to **metabolism@morgridge.org**.

*The Morgridge Institute for Research is an Equal Opportunity Employer.*

## Royal Society Professor for Public Engagement in Science

This prestigious new role is for a well-established scientist with exceptional communication skills and national media experience to support the Royal Society's aim to place science at the heart of our culture.

The ideal candidate will be able to:

- Stimulate greater public interest and enthusiasm for science
- Increase public awareness and understanding of scientific issues and their impact on policy
- Engage the public in strengthening the case for increased support for science

The appointment can be held part-time for five years. It offers a pro rata contribution to salary and up to £16,000 per year to support public engagement work.

**For full details visit:** royalsociety.org/grants/schemes/professorship-public-engagement

**Closing date: 16 September 2014**

THE ROYAL SOCIETY

# DIRECTOR
# AUTISM RESEARCH PROGRAM

## DEPARTMENT OF PEDIATRICS AND HUMAN DEVELOPMENT
## COLLEGE OF HUMAN MEDICINE, MICHIGAN STATE UNIVERSITY

The Department of Pediatrics and Human Development in the College of Human Medicine at Michigan State University is seeking a leader to develop and oversee an outstanding, interdisciplinary, nationally prominent research program in pediatric autism and related neurodevelopmental disorders. The research program will seek to identify the causes and genetic and environmental risk factors for autism and related disorders. It will emphasize early recognition of autism and related disorders, since early detection will likely be required for improved interventions to prevent, ameliorate and treat these conditions. An important focus of the program's research effort will be on genomic, epigenomic and transcriptomic factors in the development and severity of autism. A robust partnership with families, schools, providers and communities will be essential.

The program director will participate in recruitment of two additional investigators, one of whom should be a neurodevelopmental pediatrician. Thus documented strength in mentoring and development of young faculty to achieve their academic goals is essential. The research program will be developed in concert with ongoing and planned research in autism and related disorders at MSU taking place in at least five colleges and ten departments. The program director will work closely with the Chair of the Department of Pediatrics and Human Development to co-recruit faculty with other partnering departments and colleges in the university. The Program Director will encourage and facilitate collaborative research activities by program faculty across the entire MSU campus, and with community stakeholders, including pediatric colleagues in Lansing (Sparrow Hospital), Grand Rapids (Helen DeVos Children's Hospital), and Flint (Hurley Children's Hospital).

Successful candidates must hold a doctoral degree and should be eligible for appointment as Associate Professor or Professor of Pediatrics in the tenure system at Michigan State University. A well-developed research program and a strong track record of extramural funding are essential. Board certification in Pediatrics is not required, but will be viewed as an asset.

Applicants should apply on-line at **jobs.msu.edu** and search for posting **#9826**. Please attach a letter of application including a personal statement, curriculum vitae, and history of research funding, as well as contact information (address, e-mail and phone) for three potential references who will not be contacted without notice to the applicant. The personal statement should indicate, among other things, how this opportunity aligns with the applicant's current research emphases and career aspirations. To ensure full consideration, please submit application materials by October 2, 2014, although the position will remain open until filled.

For further information about the position, contact the search committee chair, Nigel Paneth, MD, MPH, University Distinguished Professor of Epidemiology & Biostatistics and Pediatrics & Human Development (**paneth@msu.edu**) or B. Keith English, MD, Professor and Chair, Department of Pediatrics and Human Development (**keith.english@hc.msu.edu**).

MICHIGAN STATE UNIVERSITY

MSU is committed to achieving excellence through cultural diversity. The University actively encourages applications and/or nominations of women, persons of color, veterans and persons with disabilities.

**MSU is an Affirmative Action, Equal Opportunity Employer.**

---

PENNSTATE University Park

## FACULTY POSITION IN PLANT BIOLOGY

The Biology Department at The Pennsylvania State University (Penn State) seeks candidates for a tenured or tenure-track faculty position in the area of plant biology. Candidates using genetics, genome-wide association studies (GWAS) or other big data approaches, functional genomics, or phenomics to study fundamental questions in plant biology are encouraged to apply. Candidates for the ranks of Associate Professor or Professor should have well-established research programs as well as strong records of teaching and service, and be widely recognized as leaders in their field. Candidates for the rank of Assistant Professor should have a strong record of research accomplishments.

Penn State has one of the top US graduate programs in the plant sciences, and a large, vibrant, and collaborative group of faculty in plant biology and the wider life sciences. Penn State`s flagship University Park campus is situated in a community consistently rated as among the most livable small cities in the US.

Applicants should prepare a cover letter, CV, and a third document containing a statement of research interests and a statement of teaching philosophy. Candidates for the rank of Assistant Professor should also include a fourth document with names and contact information for three professional references. Apply by submitting the requested documents at the Penn State employment website **www.psu.jobs** for **job #42967**. Review of applications will begin immediately and continue until a suitable candidate is found.

CAMPUS SECURITY CRIME STATISTICS: For more about safety at Penn State, and to review the Annual Security Report which contains information about crime statistics and other safety and security matters, please go to **http://www.police.psu.edu/clery/** , which will also provide you with detail on how to request a hard copy of the Annual Security Report.

*Penn State is an Equal Opportunity, Affirmative Action Employer, and is committed to providing employment opportunities to minorities, women, veterans, disabled individuals, and other protected groups.*

---

## Faculty Positions
## Tulane University School of Medicine

The Department of Biochemistry and Molecular Biology is seeking applicants for a tenure-track Assistant Professor position as part of a vigorous expansion of the department.The Tulane University School of Medicine (**http://tulane.edu/som**) offers a highly collaborative scientific environment with many multidisciplinary centers and state-of-the-art core facilities including transgenic, *in vivo* and *in vitro* imaging, genomic, and proteomic facilities. Applicants should be successful investigators with research interests that complement or strengthen existing research activities in the department (**http://tulane.edu/som/departments/biochemistry/**). Candidates who bring novel approaches and expertise in cancer signaling and metabolism, microRNA, epigenetics, cancer stem cells, medicinal chemistry, tumor immunology, and genetic/disease model systems are especially encouraged to apply. Successful applicants are expected to establish a strong and independent extramurally funded research program, and to participate in graduate and medical student teaching. The applicants will be provided with a highly competitive salary, significant start-up funds, and excellent laboratory space. Applicants for the position must have a Ph.D., M.D. or equivalent degree with several years of postdoctoral experience. The search committee will begin consideration of applications in September 2014 and continue until April 2015. The positions are expected to be filled by the fall of 2015.

Applicants should submit curriculum vitae, a brief summary of past accomplishments, future research plans, and the names and email addresses of three references to: **biochem@tulane.edu** or by mail to:

**The Faculty Search Committee**
**c/o Gilbert Estrada**
**Department of Biochemistry and Molecular Biology, #8543**
**Tulane University School of Medicine**
**1430 Tulane Avenue**
**New Orleans, LA 70112**

*Tulane University is an Affirmative Action/Equal Opportunity Employer and encourages applications from minorities, women, and other qualified persons.*

# State Key Lab of Respiratory Disease, China: seeking talents to lead research

**Employer**
State Key Lab of Respiratory Disease, Guangzhou Medical University, Guangzhou, China
**Location**
Guangzhou, China
**Research Discipline**
Focus on respiratory diseases, including but not limited to: infection, COPD, asthma, lung cancer, acute lung injury, lung stem cell and regeneration
**Job Type**
Professor, Associate Professor
**Salary**
Highly competitive salary and benefits will be provided depending on candidate's qualifications.

## Further information

The State Key Laboratory of Respiratory Disease (SKLRD), led by Director Prof. Nanshan ZHONG and Deputy Director Prof. Ling CHEN, is a leading research centre for respiratory diseases in China. SKLRD was jointly established by Guangzhou Institute of Respiratory Disease (GIRD)/Guangzhou Medical University,and Guangzhou Institute of Biomedicine and Health (GIBH)/Chinese Academy of Sciences. SKLRD aims to improve the quality of life by advancing the medical sciences in prevention and treatment of respiratory diseases. Current research areas include studying epidemiology and influencing factors, identifying the underlying mechanism of the diseases, exploring new treatment and prevention modalities, and management of chronic respiratory diseases.

SKLRD is committed to focus on translational research with the intention to identify the unmet medical needs to guide our research direction, and to take the discovery in basic research into more effective treatment and prevention of respiratory diseases. SKLRD published more than 100 SCI papers in 2012. Some of the research work represented the leading advancement in the field of respiratory diseases, such as the new etiology and management of COPD, the visualization of influenza virus infection in living mice, the new multiplex diagnostics for respiratory diseases. In the coming years, SKLRD will expand its current laboratory space. SKLRD is striving to become a world leading research laboratory in the field of respiratory diseases, with the goal of alleviating people's suffering from respiratory diseases in China and the world.

SKLRD is seeking highly qualified scientists to fill leading scientist positions. The candidates will need to apply for *"1000 Talent Program", "Young 1000 Talent Program", "Chinese NSF Distinguished Young Scholars", "Professor of Education Ministry Chang Jiang Scholar", or "Guangdong Province Universities and Colleges Pearl River Scholar".*

Successful candidates must possess a Ph.D or MD degree from top universities, have publications in internationally first class peer-reviewed journals in recent 5 years, and currently hold an Assistant professor or above in internationally renowned universities, institutes or hospitals. Preference will be given to those with a strong background and successful experiences in both clinical and basic research.

Applicants should send curriculum vitae, research proposal, publication list, PDF reprints of 5 representative publications, brief summary of past accomplishments to:

Ms. HE Shumin and copy to Dr. Ling CHEN

Email: lisaheshu@163.com; chen_ling@gibh.ac.cn

Science Careers online @sciencecareers.org
OPPORTUNITIES IN CHINA

# Science Careers

## CER

“《科学》职业” 已经与赛尔互联(CER)开展合作。中国大陆的高校可以直接联系CER进行国际人才招聘。

请访问 Sciencecareers.org/CER 点得联系信息。

招募学术精英，《科学》是您的不二之选 **Science**

**AAAS is here –**
helping scientists achieve career sucess.

Every month, over 400,000 students and scientists visit ScienceCareers.org in search of the information, advice, and opportunities they need to take the next step in their careers.

A complete career resource, free to the public, *Science* Careers offers hundreds of career development articles, webinars and downloadable booklets filled with practical advice, a community forum providing answers to career questions, and thousands of job listings in academia, government, and industry. As a AAAS member, your dues help AAAS make this service available to the scientific community. If you're not a member, join us. Together we can make a difference.

To learn more, visit
aaas.org/plusyou/sciencecareers

AAAS + U = Δ



**Temple University**
**Department of Chemistry**
**FULL/ASSOCIATE/ASSISTANT Professor**
**TENURE TRACK**
**Fall 2015**

The Department of Chemistry at Temple University invites applications and nominations for tenure-track faculty positions at the Full/Associate/Assistant Professor level in areas including Nanoparticle Plasmonics/Nanophotonics and Biochemistry/Chemical Biology. Applications for Assistant Professor level positions should include a CV, statement of teaching and research goals, a proposed research plan, and three letters of recommendation. Applications at the Associate or Full Professor level should provide a CV, names of at least five references, and selected reprints.

Applicants are expected to demonstrate a strong potential for establishing a vigorous research program funded by peer-reviewed research grants and for developing excellence in teaching.

Application materials should be sent to: **Dr. Robert J. Levis, Chair, Department of Chemistry, College of Science and Technology, Temple University, Beury Hall (016-00), 1901 North 13th Street, Philadelphia, PA 19122 or electronically on our department website at http://chem.cst.temple.edu/**. Review of applications will begin immediately and will continue until December 31, 2014. The Department specifically invites and encourages applications from women and minorities.

*Temple University is an Equal Opportunity, Equal Access, Affirmative Action Employer committed to achieving a diverse community (AA,EOE,M/F/D/V).*



**Staff Researcher opportunities in Systems Medicine and Bioinformatics at Stanford University**

The laboratory of Dr. Atul Butte at Stanford Medical School is seeking highly motivated investigators to develop and study novel approaches in data-driven biomedical research to discover new biomarkers, therapeutics, and to revolutionize health and health-care.

Ideal candidates will have an M.D. and/or Ph.D. and post-doctoral or industry experience with a strong background in bioinformatics, computational biology, biostatistics, and genomics, excellent communication and programming skills, and a great publication record.

Strong problem-solving skills, leadership, creative thinking, and the ability to build new software tools as needed are required. A dual background in both computation and molecular biology or medicine or pharmacology required. Prior experience with next generation sequencing, genotying, microarray, drug, or clinical databases, text-mining, knowledge representation, or parallel computing platforms is preferred.

Applicants must possess good communication skills and be fluent in both spoken and written English.This exciting work will be guided by multidisciplinary collaborations with top scientists in stem cell, immunology, diabetes, and cancer biology research at Stanford.

To apply, please send your CV, a brief statement of research interests, and contact information for three references.

**E-mail: butte-lab-jobs@lists.stanford.edu**

UCLA

## Integrative Biology and Physiology

The UCLA Department of Integrative Biology and Physiology invites applications for a tenure-track faculty position at the level of Assistant Professor or higher. We seek extraordinary applicants from any area of physiology, although we have particular interest in the general area of metabolism and molecular/cellular mechanisms that maintain homeostasis. The successful candidate will be expected to participate in undergraduate and graduate teaching and to establish a vigorous, externally funded research program.

Please submit CV and statements of research and teaching, before **October 1, 2014**, to **https://recruit.apo.ucla.edu/apply/JPF00317**. Faculty with a history and commitment to the mentoring of underrepresented minorities are encouraged to apply and state their experience in the cover letter.

**UCLA** is California's largest university, with an enrollment of nearly 38,000 undergraduate and graduate students. The Biosciences at UCLA has more than 300 faculty members, includes many top ten ranked departments, and is consistently in the top ten in NIH funding.

*The University of California is an Equal Opportunity/Affirmative Action Employer. All qualified applicants will receive consideration for employment without regard to race, color, religion, sex, national origin, disability, age or protected veteran status. For the complete University of California nondiscrimination and affirmative action policy see: UC Nondiscrimination and Affirmative Action Policy*

**Max Planck Institute for Dynamics and Self-Organization**

MAX-PLANCK-GESELLSCHAFT

## Nominations sought for the Position of Director

The **Max Planck Institute for Dynamics and Self-Organization** (MPIDS) invites nominations for the position of **Director of its Theory Department**. The MPIDS is a basic research institute with approximately 250 scientists. Research at the MPIDS is devoted to the study of self-organization in nature (see www.ds.mpg.de) and has a tradition of collaborative research within the institute and across the Campus Göttingen (see http://grc.uni-goettingen.de).

Nominees should work in theoretical physics as broadly applied to the field of dynamics and self-organization. The successful candidate will have established a record of original and creative research at the highest international level and can inspire and lead a substantial group of scientists. The nominee's research should preferably complement the collaborative research within the institute and the Campus Göttingen, but may also introduce new research directions.

Written nominations, which will be treated strictly confidentially, should be addressed to nomination@ds.mpg.de. They must include a short description of the nominee's background and most significant scientific accomplishments. Self-nominations will not be considered. The call for nominations willl remain active until the position is filled.

The Max Planck Society seeks to increase the number of women in those areas where they are underrepresented and explicitly encourages the nomination of women.

**MPI for Dynamics and Self-Organization**
**Am Faßberg 17**
**D-37077 Göttingen**
**Germany**

Zertifikat seit 2006 audit berufundfamilie

INDIANA UNIVERSITY
BLOOMINGTON

### Tenure-Track Faculty Position in Cell Biology Genomics, Cell and Developmental Biology (GCDB) Program Department of Biology http://www.bio.indiana.edu/index.shtml

The GCDB Program at Indiana University invites applications for a tenure-track position at the assistant professor level with a specific research emphasis in eukaryotic cell biology. We are especially interested in candidates whose research complements and/or extends our existing strengths in chromatin structure, genome replication, the DNA damage response, mitosis, meiosis, the cytoskeleton, and signal transduction. Exceptional scientists with a strong record of applying cutting-edge approaches to basic questions in eukaryotic cell biology are encouraged to apply. Successful candidates will receive a generous start-up package and lab space along with access to state-of-the-art facilities for light and electron microscopy, flow cytometry, structural biology, genomics and bioinformatics, protein analysis, and molecular biology. Our faculty members are expected to establish and maintain a vigorous well-funded research program and to participate in both undergraduate and graduate education.

Applicants should hold a Ph.D. or equivalent degree and have relevant postdoctoral experience with a strong record of research accomplishments. Please submit a cover letter, CV, research statement and three letters of references using the submission link at **http://indiana.peopleadmin.com/postings/952**. Please address inquires to **Jennifer Tarter jenjones@indiana.edu; 812-856-3984; 1001 E. Third Street, Bloomington, IN 47405-3700**. Applications received by **October 15, 2014** will be assured of full consideration.

*Indiana University is an Equal Employment and Affirmative Action Employer and a provider of ADA services. All qualified applicants will receive consideration for employment without regard to age, ethnicity, color, race, religion, sex, sexual orientation or identity, national origin, disability status or protected veteran status.*

INDIANA UNIVERSITY
BLOOMINGTON

### Faculty Position in Genomics

The Genome, Cell, and Developmental Biology Program at Indiana University invites applications for a tenured/tenure-track faculty position in **Genomics** at the level of assistant professor. Candidates should have well-developed research programs that apply cutting-edge genomic approaches to investigate the molecular mechanisms underlying important aspects of eukaryotic biology, including gene regulation, epigenetics, development, or evolution. More senior candidates with outstanding credentials in research and extramural funding may also be considered. The Department of Biology (http://www.bio.indiana.edu) and affiliated departments and programs represent more than 60 research labs housed in 3 adjacent buildings, providing ample opportunities for collaboration. The applicant will have access to outstanding resources including state-of-the-art facilities for genomics and bioinformatics, light and electron microscopy, flow cytometry, biophysical instrumentation, and computing.

Applicants must hold a Ph.D. degree and have relevant postdoctoral experience with a strong record of research accomplishments. Faculty members are expected to establish vigorous well-funded research programs and to participate in undergraduate/graduate education. Applications received by **October 15, 2014** will be assured of full consideration. Applicants should submit a cover letter, CV, research statement (past, present, and planned), up to three PDFs of re-prints/pre-prints, and arrange for three letters of references to be submitted at **http://indiana.peopleadmin.com/postings/957**. Please address inquires to **Jennifer Tarter at 812-856-3984; janjones@indiana.edu; 1001 E. Third Street, Bloomington, IN 47405-3700**.

*Indiana University is an Equal Employment and Affirmative Action Employer and a provider of ADA services. All qualified applicants will receive consideration for employment without regard to age, ethnicity, color, race, religion, sex, sexual orientation or identity, national origin, disability status or protected veteran status.*

*By* **Blaise J. Arena**

# *Outside my comfort zone*

Heat and sand. A restrictive culture. Saudi Arabia didn't seem to have much to offer compared with other countries I had visited. So, after decades spent happily working in laboratories, how did I end up in the Saudi desert, trying to do science at a petrochemical plant? ■ My long career with a developer of petrochemical processing technology began as a research chemist at its main research center near Chicago, Illinois. It was—is—a very fine laboratory. We were able to turn out accurate results quickly. An array of pilot plants ran smoothly, cranking out data 24/7. Complex experiments were designed, and definitive conclusions were drawn efficiently.

In time I took on a new role, helping develop collaborations with other companies in the United States and abroad. This was a fundamental shift for me: While I was still deeply involved in solving scientific problems, there was a new focus on building relationships. Then, a few years ago, someone got the bright idea that I should join a technical team to diagnose and solve performance problems at a customer's propane dehydrogenation facility, which my company had designed, while the plant remained up and running. It was a formidable challenge, and a lot was on the line.

In some ways, I was not an obvious choice. I knew little about the technology. I had never worked in the field, in a production unit. No one cared. Those encouraging me to join the team praised my "vast expertise and experience." They said my "fresh eyes" would be a benefit to the team. I fell for the flattery and signed on.

After a crash review of the technology, I embarked on the first of three 2-week site visits to Al Jubail on the Persian Gulf coast. Major culture shock. All women there wear full burqas; no faces are seen and no interaction permitted, so you are cut off from half of society. Everything is forced to close during prayer times. Inappropriate dress, even by men, results in a public reprimand from a local cop. I had been to Muslim countries before, but this was far more intense. It was jarring and isolating but also fascinating. And it was HOT.

You'd think that removing two little hydrogen atoms from propane to make propylene would be simple. It is not. Propane wants to keep them. The dehydrogenation facility is big and incredibly complicated: huge, hot catalytic reactors, multiple gas separation towers, gas purification units, and cooling systems, together covering four city blocks. It's loud and scary, and a lot different from the state-of-the-art laboratory I was used to.

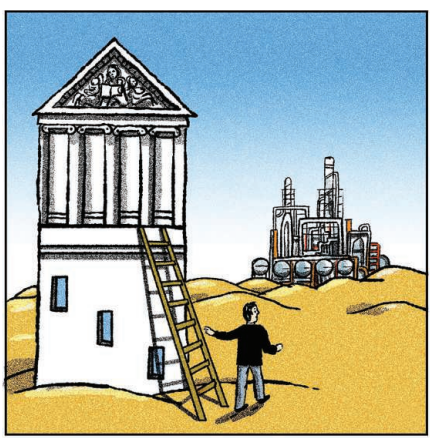

***"Things that are easy in the research lab ... are hard in the field."***

I knew going in that to succeed I must build respectful, somewhat personal, working relationships with the local staff. Pretending to know everything (or anything) would be a bad idea; it's much better to ask questions and dig for answers together. Cultural sensitivity was crucial. My first visit, during the fasting month of Ramadan, required some particularly difficult adaptations: If you must eat or drink water during the day, please be discrete.

Things that are easy in the research lab, I learned, are hard in the field. Reliable data are crucial in any investigation, but much harder to obtain in an operational industrial facility. A research pilot plant designed for liters per day is way different than a facility producing hundreds of tons per day. There is much you cannot do: You can't take samples from just any point in the process, or change operating conditions just to see what happens. Staff members may lack the experience necessary to avoid subtle problems in sampling and analysis. Data are often so uncertain, so clouded by events, that interpretation becomes more art than science, or impossible. I organized a series of conference calls with our analytical experts back home, reviewing and improving procedures alongside local staff. We made progress and improved relationships.

When troubleshooting complex systems—systems that encompass not just science and technology but also people and relationships—there may be many culprits. By addressing root causes of disparate problems, our team made important improvements. And I learned plenty. ■

*Blaise J. Arena is a retired research chemist and project manager. Read more on careers at http://www.sciencecareers.org.*

ILLUSTRATION: ROBERT NEUBECKER

Downloaded from www.sciencemag.org on August 15, 2014



Published by AAAS